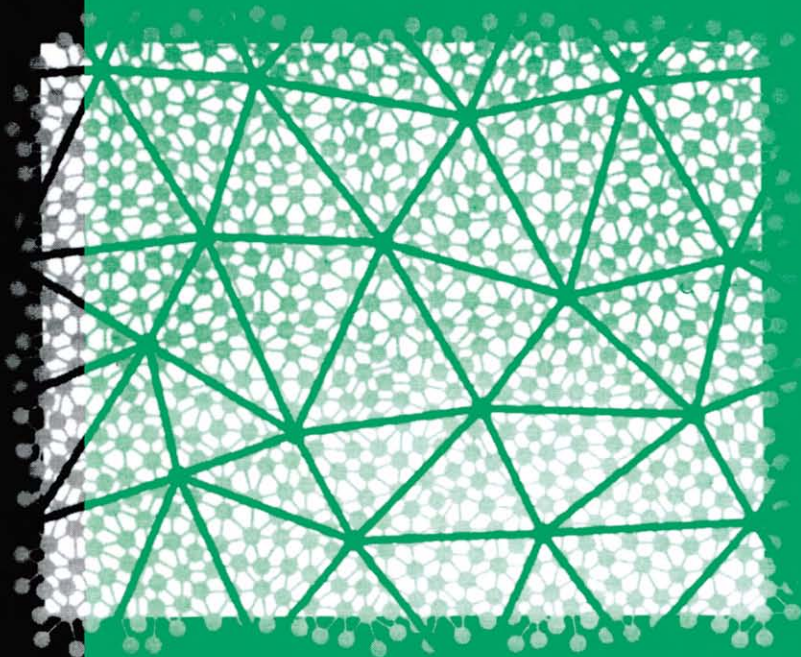


HANDBOOK
OF
BIOLOGICAL
PHYSICS
SERIES
EDITOR:
A.J. HOFF

VOLUME **1B**



Structure and Dynamics of Membranes

*Generic and
Specific Interactions*

VOLUME EDITORS:

R. LIPOWSKY

E. SACKMANN

NORTH-HOLLAND

HANDBOOK

OF

BIOLOGICAL

PHYSICS

VOLUME 1

Structure and Dynamics of Membranes

Generic and Specific Interactions

HANDBOOK
OF
BIOLOGICAL
PHYSICS

Series Editor: A.J. Hoff

Volume 1: Structure and Dynamics of Membranes
A: From Cells to Vesicles
B: Generic and Specific Interactions

HANDBOOK
OF
BIOLOGICAL
PHYSICS
VOLUME 1

Structure and Dynamics of Membranes

Generic and Specific Interactions

Editors:

R. Lipowsky

*Max-Planck-Institut für Kolloid- und
Grenzflächenforschung
Kantstrasse 55
14513 Teltow-Seehof, Germany*

E. Sackmann

*Biophysics Group
Technische Universität München
James Franckstrasse
D-85748 Garching, Germany*



1995

ELSEVIER

Amsterdam - Lausanne - New York - Oxford - Shannon - Tokyo

ELSEVIER SCIENCE B.V.
Sara Burgerhartstraat 25
P.O. Box 211, 1000 AE Amsterdam, The Netherlands

ISBN: 0 444 81975 4

© 1995 Elsevier Science B.V. All rights reserved.

No part of this publication may be reproduced, stored in a retrieval system or transmitted in any form or by any means, electronic, mechanical, photocopying, recording or otherwise, without the prior written permission of the publisher, Elsevier Science B.V., Copyright & Permissions Department, P.O. Box 521, 1000 AM Amsterdam, The Netherlands.

Special regulations for readers in the U.S.A. – This publication has been registered with the Copyright Clearance Center Inc. (CCC), Salem, Massachusetts. Information can be obtained from the CCC about conditions under which photocopies of parts of this publication may be made in the U.S.A. All other copyright questions, including photocopying outside of the U.S.A., should be referred to the copyright owner, Elsevier Science B.V., unless otherwise specified.

No responsibility is assumed by the publisher for any injury and/or damage to persons or property as a matter of products liability, negligence or otherwise, or from any use or operation of any methods, products, instructions or ideas contained in the material herein.

This book is printed on acid-free paper.

Printed in The Netherlands.

General Preface

What is Biological Physics?

A short definition of Biological Physics is “The physics of the life processes”. Aspects of the life processes are studied in light of the laws of nature, which are assumed to be equally valid for living and dead matter, with physical concepts and methods. A multidisciplinary approach brings together elements from biology – knowledge of the problem that is attacked – and from the physical sciences – the techniques and the methodology for solving the problem. Biological Physics is unlike any other physical (sub)discipline in one aspect: the observer and the examiner of the natural phenomena, as well as the conceptualizer are themselves object of study.

While this leads to interesting knowledge-theoretical problems in biophysical fields as the psychophysics of perception, normally this distinction is not important. In principle, Biological Physics covers the physics of all of biology, including medicine, and therefore its range is extremely broad. Hence, it is useful to classify research in biological physics according to the biological level of aggregation: molecular, cellular, supracellular and organismal. On every level one may further distinguish structural organization and function, and the relation between the two. In addition one may discriminate, even on a molecular level, processes of growth and structural differentiation, regulation of the energetic and material properties of the internal medium (thermodynamics, mass transport), sensory and neuro-motoric processes, etc.

Why a Handbook of Biological Physics?

It will be clear that even with the above ways of differentiating between its fields and subfields, Biological Physics is not a discipline that is easily covered by one or a few monographs. Yet, there is a need to bring order in the growing complexity of research in Biological Physics, to present the experimental results obtained in the manifold of its (sub)fields, and their interpretation, in a clear and concise manner, such that physicists with an interest in certain biological problems will find an in-depth and yet digestible coverage of a particular field, while biologists may learn to what extent the physical approach helps in solving problems in their respective fields. Furthermore, for appreciating the significance of the many branches of Biological Physics and to help guide the rapid evolution of the various subfields, it is necessary

to take time for assessing the results gathered over the past years, connect them to research in other, perhaps at first sight unrelated, fields and to reflect on the direction in which the field should, or is likely to move.

A good way to answer the need for assessment and reflection is setting up a series of interconnected volumes, each devoted to a certain subfield that is covered in depth and with great attention to the clarity of presentation. A series conceived in such a way that interrelations between fields and subfields are made clear, areas are identified in which a concentrated effort might solve a long-standing problem and, ideally, an evaluation is presented to which extent the application of physical concepts and methodologies, with often considerable effort in terms of personal and material input, has advanced our understanding of the biological process under study. The Handbook of Biological Physics, of which the present work is the first volume, is conceived to become such a series.

The Handbook of Biological Physics, an outline

Individual volumes of the Handbook are devoted to an entire “system” unless the field is very active or extended (as, e.g., for membranes or vision research), in which case the system will be broken down into two or more subsystems. A system can be a “membrane”, a cell, the peripheral part of a sensory or motor system, part of the brain, a complete perceptual system, a sensorimotor system, etc., as long as it has been studied using biophysical methods. Depending on the subject, there will be an emphasis on physical chemistry approaches (emphasis on structure at the molecular level) and biophysical approaches (emphasis on mechanisms).

The guiding principle of planning the individual volumes is that of going from simple, well-defined concepts and model systems on a molecular level, to the highly complex structures and working mechanisms of living matter. That is, every volume will be written in a bottom-up fashion. Each volume will contain an introductory chapter defining the place of each of the other chapters into this bottom-up approach. Ideally this introduction will define the “Black Box” and some of the sub-boxes constituting the system. This chapter will usually be followed by a morphological/structural chapter sufficiently detailed to form a basis for the later physiological and biophysical chapters. Generally the volume will end with a closing chapter indicating which parts of the black box have become somewhat “grey” or even “white”, and providing an outlook into the future.

Planned volumes

It goes without saying that the Handbook of Biological Physics as outlined above is an ambitious undertaking, which will take many years to complete. It is therefore not possible to present an exhaustive list of planned volume topics. The “bottom-up” approach adopted for individual volumes, is also the guideline for the entire series. This means that the Handbook starts with a number of volumes devoted to molecular and supramolecular systems, and will continue with several volumes on cellular and

supracellular systems. Finally, a number of volumes is planned on the biophysics of suborganismal systems and whole organisms.

Volumes presently completed, *in statu nascendi*, and tentatively planned are:

1. The Biophysics of Membranes I, Part 1 and 2.
2. The Biophysics of Membranes II, transport phenomena, signalling.
3. Vision I, molecular aspects and the retina.
4. Neuro-informatics I, neural modelling.
5. Neuro-informatics II, information processing.
6. Vision II, perception, pattern recognition, imaging.
7. Photosynthesis and electron transport.
8. Fluid dynamics and chaos.
9. Motion and contractile systems.
10. The vestibular system.
11. Hearing.
12. Electro-reception and magnetic field effects.

Of course, the above list is, apart from the first four or five volumes, tentative and subject to change, and must not be construed as providing a complete overview of research in Biological Physics. Further volumes will be added as the need arises.

In conceiving the Handbook of Biological Physics I have had help from many sides. It is a great pleasure to acknowledge the brainstorming sessions with Anita de Waard of Elsevier Science, who was instrumental in putting the idea of a Handbook of Biological Physics on a sure footing. Without the expertise and constructive help of Jos Eggermont in the initial stages of the project I doubt that the Handbook would ever have seen the light. The support of Elsevier Science and its staff was and continues to be, essential for the successful outcome of the enterprise. It is our hope that the Handbook will find a warm welcome in the Biological Physics Community, and that those who find occasion to read and peruse one of its volumes, will communicate to us their criticisms and suggestions for the future development of the project.

Leiden, Spring 1995
Arnold J. Hoff
Editor

This Page Intentionally Left Blank

Preface to Volume 1B

Generic and Specific Interactions: Introduction and Overview

All living matter is built up from cells. This has already been realized during the last century. However, the general principles underlying the structure and dynamics of these cells remained obscure for a long time. Recently, a combination of cell biology, genetics, biochemistry and biophysics has led to a new level of understanding and to the new discipline of molecular cell biology.

One general construction principle which has emerged from molecular cell biology is the use of membranes in order to organize space into different compartments. First of all, each biological cell is enclosed by its outer plasma membrane which controls the interaction between the cell and its environment. This applies both to the relatively small cells of bacteria or prokaryotes, which have no cell nucleus, and to the much larger cells of eucaryotes, which have such a nucleus. The latter class of organisms contains all animals and plants as well as single-celled microorganisms such as amoeba or yeast. In addition to the outer plasma membrane, all eucaryotic cells contain internal membranes which represent the boundaries of the internal organelles such as the nucleus, mitochondria, chloroplasts, etc.

On the molecular level, biomembranes are quite complex: they contain specific mixtures of molecules which reflect their diverse biological functions. However, in spite of this complex composition, all biomembranes exhibit an universal construction principle. Indeed, the basic structural element of all biomembranes appears to be a bilayer of lipid molecules which serves as a two-dimensional solvent for various proteins. Therefore, the simplest model systems for biomembranes are provided by lipid bilayers without any proteins. Such bilayers can be prepared in several ways and can then be studied by physical methods. When dissolved in water, these bilayers form closed vesicles which resemble the compartments formed by biomembranes.

The present volume on 'Structure and Dynamics of Membranes' covers various aspects of biomembranes and lipid bilayers from the biophysical point of view. An alternative title for this volume would be 'Biologically inspired physics of membranes'. The volume has two parts. Part A dealt with lipid water systems, the morphology of vesicles and the applications of liposomes. Part B about 'Generic and Specific interactions' covers membrane adhesion, membrane fusion and the interaction of biomembranes with the cytoskeleton. What follows is a brief summary of the contents of Part B.

The first two chapters of Part B discuss the generic interactions of membranes from the conceptual point of view. The first chapter by Lipowsky starts with an overview over the different experimental techniques for membrane adhesion and then focuses on the interplay between molecular forces and entropic interactions. The second chapter by Andelman gives a review of the electrostatic interactions of membranes.

The next two chapters summarize the experimental work on two different bilayer systems. In the chapter by Parsegian and Rand, lyotropic liquid crystals consisting of large stacks of interacting bilayers are studied using the osmotic stress method. In this latter approach, one applies an osmotic pressure to the membranes and measures their separation by X-ray diffraction. The second system consists of bunches of lipid bilayers which are observed in the light microscope. The behavior of these bunches is difficult to understand and may indicate that lipid bilayers have a 'hidden' reservoir of membrane area, see the chapter by Helfrich.

The adhesion of biomembranes is more complex than the adhesion of lipid bilayers. Plasma membranes, for example, are usually covered by many proteins which lead to specific adhesion mechanisms. The processes of contact formation, focal bounding and macroscopic contacts between cells are discussed in the chapter by Evans. Some representative models for cell adhesion are described in the chapter by Bongrand. In these systems, adhesion is controlled by specific adhesion molecules. For eucaryotic cells, these adhesion molecules are usually connected to the cytoskeleton inside the cells.

The cytoskeleton within eucaryotic cells consists of a network of relatively stiff filaments. Three different types of filaments have been identified: actin filaments, intermediate filaments and microtubuli. As explained in the chapter by Janmey, much has been recently learned about the interaction of these filaments with the cell membrane. This interaction is also crucial for cell shape, cell locomotion, and cell division.

The two final chapters of Part B deal with membrane fusion. Indeed, there are many biological processes in which membrane adhesion is the first step towards membrane fusion. One example is provided by the transport vesicles which shuttle between different compartments of eucaryotic cells. It seems that fusion can be induced in several ways. As discussed in the chapter by Dimitrov, one generic fusion mechanism which has recently become available is electrofusion induced by electroporation. Another more specific mechanism is based on the interactions with cations such as Ca^{2+} as described in the final chapter by Arnold.

We thank all authors of this handbook for their cooperation and Clarissa Jansen and Gudrun Conrad for their help with the editorial process.

Reinhard Lipowsky and Erich Sackmann

Contents of Volume 1B

<i>General Preface</i>	v
<i>Preface to Volume 1B</i>	ix
<i>Contents of Volume 1B</i>	xi
<i>General Contents</i>	xiii
<i>Contributors of Volume 1B</i>	xv
11. R. Lipowsky <i>Generic Interactions of Flexible Membranes</i>	521
12. D. Andelman <i>Electrostatic Properties of Membranes: The Poisson–Boltzmann Theory</i>	603
13. V.A. Parsegian and R.P. Rand <i>Interaction in Membrane Assemblies</i>	643
14. W. Helfrich <i>Tension-Induced Mutual Adhesion and a Conjectured Superstructure of Lipid Membranes</i>	691
15. E. Evans <i>Physical Actions in Biological Adhesion</i>	723
16. P. Bongrand <i>Adhesion of Cells</i>	755
17. P. Janmey <i>Cell Membranes and the Cytoskeleton</i>	805
18. D.S. Dimitrov <i>Electroporation and Electrofusion of Membranes</i>	851
19. K. Arnold <i>Cation-Induced Vesicle Fusion Modulated by Polymers and Proteins</i>	903
<i>Author Index</i>	959
<i>Subject Index</i>	1003

This Page Intentionally Left Blank

General Contents

1.	E. Sackmann <i>Biological Membranes Architecture and Function</i>	1
2.	M. Bloom and O.G. Mouritsen <i>The Evolution of Membranes</i>	65
3.	J.M. Seddon and R.H. Templer <i>Polymorphism of Lipid-Water Systems</i>	97
4.	H. Möhwald <i>Phospholipid Monolayers</i>	161
5.	E. Sackmann <i>Physical Basis of Self-Organization and Function of Membranes: Physics of Vesicles</i>	213
6.	P.F.F. Almeida and W.L.C. Vaz <i>Lateral Diffusion in Membranes</i>	305
7.	A. Ben-Shaul <i>Molecular Theory of Chain Packing, Elasticity and Lipid-Protein Interaction in Lipid Bilayers</i>	359
8.	U. Seifert and R. Lipowsky <i>Morphology of Vesicles</i>	403
9.	G. Ceve <i>Material Transport Across Permeability Barriers by Means of Lipid Vesicles</i>	465
10.	D.D. Lasic <i>Applications of Liposomes</i>	491
11.	R. Lipowsky <i>Generic Interactions of Flexible Membranes</i>	521
12.	D. Andelman <i>Electrostatic Properties of Membranes: The Poisson–Boltzmann Theory</i>	603
13.	V.A. Parsegian and R.P. Rand <i>Interaction in Membrane Assemblies</i>	643

14.	W. Helfrich <i>Tension-Induced Mutual Adhesion and a Conjectured Superstructure of Lipid Membranes</i>	691
15.	E. Evans <i>Physical Actions in Biological Adhesion</i>	723
16.	P. Bongrand <i>Adhesion of Cells</i>	755
17.	P. Janmey <i>Cell Membranes and the Cytoskeleton</i>	805
18.	D.S. Dimitrov <i>Electroporation and Electrofusion of Membranes</i>	851
19.	K. Arnold <i>Cation-Induced Vesicle Fusion Modulated by Polymers and Proteins</i>	903
	<i>Author Index</i>	959
	<i>Subject Index</i>	1003

Contributors to Volume 1B

- D. Andelman*, School of Physics and Astronomy, Tel Aviv University, Ramat Aviv 69978, Tel Aviv, Israel
- K. Arnold*, Institute of Medical Physics and Biophysics, Department of Medicine, University of Leipzig, Germany
- P. Bongrand*, Laboratoire d'Immunologie, Hôpital de Sainte-Marguerite, BP29, 13277 Marseille Cedex 09, France
- D.S. Dimitrov*, Section on Membrane Structure and Function, National Cancer Institute, National Institutes of Health, Bethesda, Maryland 20892, USA and Central Laboratory of Biophysics, Bulgarian Academy of Sciences, Sofia 1113, Bulgaria
- E. Evans*, Departments of Pathology and Physics, University of British Columbia, Vancouver, B.C., Canada V6T 2B5
- W. Helfrich*, Fachbereich Physik, Freie Universität Berlin, Arnimallee 14, 14195 Berlin, Germany
- P. Janmey*, Experimental Medicine Division, Brigham and Women's Hospital, Biomedical and Biological Sciences, Harvard Medical School, Boston MA 02115, USA
- R. Lipowsky*, Institut für Festkörperforschung, Forschungszentrum Jülich, D-52425 Jülich, Germany and Max-Planck-Institut für Kolloid- und Grenzflächenforschung, Kantstr. 55, D-14513 Teltow-Seehof, Germany
- V.A. Parsegian*, Division of Computer Research and Technology and National Institute of Diabetes, Digestive and Kidney Diseases, National Institutes of Health, Bethesda, MD 20892, USA
- R.P. Rand*, Department of Biological Sciences, Brock University, St Catharines, Ontario, Canada, L2S3A1

This Page Intentionally Left Blank

Generic Interactions of Flexible Membranes

R. LIPOWSKY

*Institut für Festkörperforschung,
Forschungszentrum Jülich, D-52425 Jülich, Germany
and
Max-Planck-Institut für Kolloid- und Grenzflächenforschung,
Kantstr. 55, D-14513 Teltow-Seehof, Germany*

Contents

1. Introduction	524
1.1. From biomembranes to bilayers	524
1.2. Molecular structure of lipid bilayers	525
1.3. Elastic properties of fluid membranes	526
2. Experiments on membrane adhesion	527
2.1. Surface force apparatus	527
2.2. Micropipet aspiration of giant vesicles	530
2.3. Reflection interference contrast microscopy	531
2.4. Multilayer systems under stress	533
2.5. Surface reflectivity of X-rays and neutrons	534
2.6. Optical microscopy of membrane bunches	534
3. Direct interaction between two rigid membranes	537
3.1. Hydration forces	537
3.2. Van der Waals forces	539
3.3. Electrostatic forces	540
3.4. Forces mediated by macromolecules	545
4. Bending undulations and fluctuation-induced interactions	546
4.1. Bending modes as an ideal gas of humps	547
4.2. From membranes to strings	548
4.3. Effect of lateral tension	549
4.4. Stretching versus bending modes	549
5. Renormalized interactions	550
5.1. Systematic theory for two membranes	551
5.2. Disjoining pressure from hard wall	552
5.3. Attractive interactions and unbinding transitions	555
5.4. Two-state model for unbinding transition	557
5.5. Unbinding transitions for realistic interactions	559
5.6. Direct interactions with a potential barrier	560
5.7. Tension-induced adhesion	564
6. Stacks and bunches of membranes	565
6.1. Model for many interacting membranes	566
6.2. One-membrane approximation	567
6.3. Two-membrane approximation	568
6.4. Hard-wall interaction	570
6.5. Cohesion of freely suspended bunches	572

6.6. Adhesion to a substrate or another interface	578
7. Hydration forces and protrusion modes	578
7.1. Single protrusion modes	579
7.2. Models for collective protrusion modes	580
7.3. Disjoining pressure from hard wall	582
7.4. Disjoining pressure from exponential hydration	582
7.5. Protrusions versus bending undulations	584
8. Related problems and outlook	586
8.1. Polymerized membranes	587
8.2. Random interactions	587
8.3. Perturbative renormalization	588
8.4. Dynamics of membranes	588
8.5. Membrane fusion	589
8.6. Experiments on model membranes	589
Appendices	591
A. Roughness of confined membranes	591
B. Limit of lyotropic liquid crystals	594
References	596

1. Introduction

The interaction of biomembranes and lipid bilayers is characterized by the interplay of energy and entropy [1]. The forces between the molecules lead to direct interactions which are already present for immobilized or rigid membranes. The membranes considered here are, however, not rigid but rather flexible and, thus, undergo thermally excited shape fluctuations which lead to fluctuation-induced interactions [2].

The competition between direct and fluctuation-induced interactions represents an interesting renormalization problem since it involves many length scales [3]. Indeed, the spectrum of shape fluctuations contains a wide range of length scales from about 1 nm for displacements of single molecules to about 10 μm for the flicker modes of vesicles and cells.

The renormalization arising from these shape fluctuations acts to increase the repulsive part of the direct interaction. In fact, sufficiently strong fluctuations overcome the attractive part of the direct interaction and lead to unbinding or adhesion transitions between bound and unbound states of the membranes [3–5]. Similar transitions occur for interfaces and polymers where they represent wetting and adsorption transitions, respectively [6].

This chapter is organized as follows. The basic properties of the model membranes considered here are briefly described in the remainder of this introductory section. Section 2 contains a short review of the experimental methods which have been used to study the adhesion and the cohesion of membranes. The direct interaction between two rigid membranes is discussed from a theoretical point of view in section 3. The effects of thermally excited fluctuations are first treated in a heuristic way in section 4. The systematic theory starts in section 5 where the renormalization of the interaction by bending undulations is described for the case of two membranes. Stacks and bunches of many membranes are considered in section 6. The renormalization of hydration forces by protrusion modes is studied in section 7.

1.1. From biomembranes to bilayers

Each biological cell is enclosed in an outer membrane which controls the interface between the cell and its environment. In addition, all eucaryotic cells, i.e. all cells of plants and animals, contain a large number of organelles such as the cell nucleus, mitochondria or chloroplasts etc. which are also bounded by membranes [7, 8]. The outer cell membrane can be observed through the light microscope. The peculiar form of the red blood cell, for example, was already discovered more than 300 years ago with this experimental technique. More recently, electron microscopy has revealed the amazing architecture of the interior membranes of the cell.

The total membrane area of an eucaryotic cell is relatively large. The membranes of a single liver cell, for example, have a total surface area of about $10^5 \mu\text{m}^2$ while its volume is about $5 \times 10^3 \mu\text{m}^3$. About 98 percent of this large area belong to the inner membranes and only 2 percent to the outer membrane of the cell.

The basic function of biomembranes is to provide different spatial compartments and to act as highly selective barriers for the exchange of molecules between the different compartments. In this way, they sustain the concentration gradients between these compartments. Because of this function, membranes must have been a crucial ingredient for the origin of life. Indeed, it is rather unlikely that a self-replicating mixture of macromolecules could survive without the enclosure by a membrane.

In addition, biomembranes have many other biological functions such as signal transduction or mechanical support for polymer networks. Because of their diverse biological functions, biomembranes are composed of specific mixtures of many lipids and (amphiphilic) proteins. However, in spite of these specific differences in their composition, all biomembranes have the same universal structure: The basic structural element is provided by a lipid bilayer to which the proteins are attached by their hydrophobic (or lipophobic) domains.

1.2. Molecular structure of lipid bilayers

Lipids are amphiphilic molecules with a hydrophilic head group and usually two lipophilic hydrocarbon chains. Single lipid molecules are essentially insoluble in water. More precisely, each lipid can be characterized by a critical concentration X_* [9]. For lipid concentrations $X < X_*$, one has a dilute solution consisting of single molecules or monomers. As soon as X exceeds X_* , the lipid molecules aggregate and form bilayers. Within these bilayers, the molecules are arranged in such a way that the hydrophilic head groups form the two lipid-water interfaces bounding the bilayer whereas the hydrocarbon chains are confined inside the bilayer and have essentially no contact with the water. These bilayers are essentially 2-dimensional systems: Their thickness is 4–5 nm whereas their lateral extension is usually of the order of μm 's.

The critical concentration X_* is very small and decreases with increasing length of the hydrocarbon chains. For lipids with two identical chains containing $2N_c$ carbon atoms, one has $X_* \sim \exp[-1.7N_c]$ at room temperature [10, 11]. This exponential dependence can be experimentally confirmed for small values of N_c . For DPPC (dipalmitoyl phosphatidyl choline) with $N_c = 16$, extrapolation leads to the estimate $X_* \sim 10^{-12}$, i.e. less than one molecule per $10 \mu\text{m}^3$ water. Such a small concentration cannot be measured directly.

For lipid concentrations $X > X_*$, the monomer concentration within the solution stays essentially constant and is given by X_* whereas the concentration of bilayers is proportional to X . Since X_* is so small, the exchange of molecules between the bilayers and the solution is very slow. As long as one considers phenomena which are fast compared to this rather slow exchange process, one may assume that the number of molecules within each bilayer is constant.

Since a lipid bilayer is an essentially two-dimensional system, it can exhibit distinct thermodynamic phases. Indeed, lipid bilayers always exhibit a fluid phase at high

temperatures and one or several gel or solid-like phases at low temperatures, see the chapter by Sackmann in this handbook. Within the fluid phase, the molecule can freely diffuse along the bilayer. The corresponding diffusion coefficients are usually 10^{-7} – 10^{-8} cm²/sec, see the chapter by Almeida and Vaz in this handbook. In this chapter, I will be primarily concerned with this *fluid state* of lipid bilayers.

1.3. Elastic properties of fluid membranes

Fluid membranes have rather special elastic properties. Since the shear modulus within a fluid membrane is zero, there are only two types of elastic deformations for such a membrane: stretching and bending [12–14].

The stretching of lipid bilayers is limited to rather small deformations since they start to rupture as soon as their area is changed by about one percent [15]. In this respect, they behave like a piece of paper. However, paper is not fluid but polymerized or solid-like, and one can bend it smoothly only in one direction since any other bending deformation necessarily implies a shearing deformation as well. In particular, it is not possible to deform a flat piece of paper into a spherical segment without creating folds and crinkles (this applies to any deformation which changes the Gaussian curvature of the paper surface). In contrast, a fluid membrane can undergo such a shape deformation in a smooth way: since there is no elastic response to applied shear forces, the molecules follow these forces and start to flow within the membrane.

Biomembranes also undergo complex shape transformations which imply that they must be in a fluid state. One example is the formation of small ‘satellite’ vesicles which bud off from a larger membrane, see chapter by Seifert and Lipowsky in this handbook (this process necessarily involves a change in the Gaussian curvature of the membrane). The fluidity of biomembranes is essential for many biological functions. Therefore, the cell adjusts the lipid composition of its membranes in such a way that they remain in a fluid state irrespective of the ambient temperature and of other external conditions.

In principle, a fluid surface which does not experience any lateral tension but undergoes thermally-excited fluctuations starts to behave as a random surface without any average orientation as soon as its size exceeds a certain length scale, the so-called persistence length ξ_p [16]. This length scale depends on the bending rigidity κ and on the temperature T , and is given by a molecular scale $a \times \exp[4\pi\kappa/cT]$ with a dimensionless coefficient c of order one [17, 18] (here and below, the temperature T has energy units, i.e. T is a short-hand notation for Boltzmann constant $k_B \times$ temperature in Kelvin).

For lipid bilayers, the bending rigidity has typical values $\kappa \simeq 10$ – $20 T$ [19, 20]. This implies that the persistence length is very large compared to the largest accessible size of the bilayers. Therefore, under normal circumstances, lipid bilayers (and biomembranes) do not behave as random surfaces with no average orientation. Nevertheless, they do exhibit thermally-excited fluctuations such as bending undulations or protrusion modes. As explained in this chapter, these shape fluctuations have a rather strong effect on the interaction between the membranes.

2. Experiments on membrane adhesion

There are several experimental methods by which one can probe the adhesion and cohesion of membranes. These methods will be briefly reviewed in the following section.

First, those methods will be discussed by which one can obtain information about the interaction of two surfaces:

- (i) With the surface force apparatus, one can measure the direct interaction between two rigid lipid bilayers which have been immobilized onto mica surfaces [21–24];
- (ii) The cohesion of two membranes can be controlled by micropipet aspiration. In this case, the flexibility of the membranes can be changed by varying the lateral tension [15, 25–27]; and
- (iii) The adhesion of one flexible membrane to a solid surface can be studied by reflection interference microscopy [28, 29].

In addition, several methods will be discussed which provide information about the interaction of two membranes within a stack or bunch of many membranes:

- (i) The osmotic stress method for bulk samples of lamellar phases [30–36];
- (ii) Surface reflectivity of X-rays [37, 38] or neutrons [39] for membranes bound to an interface; and
- (iii) Phase contrast microscopy of accidental adhesive contacts within bunches which contain a relatively small number of bilayers [40, 41].

It should be emphasized that this list of experimental methods is not complete. For example, useful structural information has also been obtained with nuclear magnetic resonance [42], a technique which is not described here.

2.1. Surface force apparatus

From a conceptual point of view, one would first like to know the interaction between two rigid membranes. To some extent, this interaction can be measured by the surface force apparatus [21–24]. This apparatus consists of two glass cylinders with a radius of the order of 1 cm. Curved layers of mica are glued onto these cylinders. The cylinders are mounted onto a spring system in such a way that the axes of the two cylinders are perpendicular. Thus, as the crossed cylinders are moved against each other via the spring system, they interact only over a relatively small area across the intermediate liquid solution. Within this interaction ‘zone’, the two mica surfaces are expected to be rather smooth down to molecular length scales. A first version of the surface force apparatus appeared in the work of Derjaguin and coworkers [43] and has been further developed during the last two decades, especially by Israelachvili and coworkers.

For two planar surfaces which are separated by a liquid layer of constant thickness l , the interaction free energy per unit area will be denoted by $V(l)$. This quantity will also be called the direct interaction since it directly reflects the forces between the molecules. The total interaction free energy \mathcal{H} is then given by

$$\mathcal{H} = \int d^2x V(l) \quad (2.1)$$

where the integration extends over the total area of the surfaces. This expression for \mathcal{H} can also be used for two curved surfaces with $l = l(\mathbf{x})$ provided

- (i) The curvature radii of the surfaces are large compared to the *minimal* separation l_m of the two surfaces, and
- (ii) The interaction $V(l)$ decays rapidly to zero and the integral in (2.1) is determined by those regions for which l is still of the same order of magnitude as l_m [44].

It is then appropriate to expand the separation $l(\mathbf{x})$ around $l(\mathbf{0}) = l_m$. For two crossed cylinders of radius R , this leads to

$$\mathcal{H} \approx 2\pi R \int_{l_m}^{\infty} dl V(l) \quad \text{for } R \gg l_m. \quad (2.2)$$

Now, the total force F between the two cylinders is given by

$$F(l_m) = -\partial\mathcal{H}/\partial l_m \approx 2\pi R V(l_m) \quad \text{for } R \gg l_m. \quad (2.3)$$

Therefore, if one measures the functional dependence of the force F on the minimal separation l_m , one also knows the direct interaction $V(l_m)$.

The force F between the crossed cylinders is measured via the deflection of the spring, and the shortest separation l_m of the two surfaces within the interaction ‘zone’ is determined via an optical technique using multiple-beam interference fringes.

The force F is balanced, within the surface force apparatus, by the spring system. If the spring is harmonic with spring constant K_s , stable force equilibrium is only possible if the gradient of the force satisfies

$$K_s > \partial F/\partial l \approx 2\pi R \partial V/\partial l. \quad (2.4)$$

In general, this inequality will not hold for a certain range of l -values. As soon as one reaches the boundaries of such an unstable l -range, the surfaces will jump closer together or further apart. Therefore, it is useful to vary the spring constant K_s in order to determine the quantity $\partial V/\partial l$ from the onset of these jumps [22, 23].

In principle, one has to immobilize a lipid bilayer on each mica surface in order to measure the direct interaction of these bilayers as a function of their separation. In practice, these immobilized bilayers have been built up by subsequent deposition of two monolayers. In order to avoid desorption of the lipid from the mica surfaces, the solution in the apparatus has to be presaturated with lipid monomers. On the other hand, one may also study the interaction of ‘partial bilayers’ for which some fraction of the lipid has desorped into the solution.

An example for the experimental data obtained in this way is shown in fig. 1 [22]. The data correspond to full and partial bilayers of DLPC (dilauroyl phosphatidyl choline) which are electrically neutral. In fig. 1, the quantity F/R and the direct interaction $V = F/2\pi R$ are plotted as a function of the bilayer separation l . At small separations, $V(l) \sim F(l)/R$ exhibits a strong repulsive part, the interpretation of which has led to some controversy, see section 7 below. At large separations, the direct interaction has an attractive part arising from Van der Waals forces. In

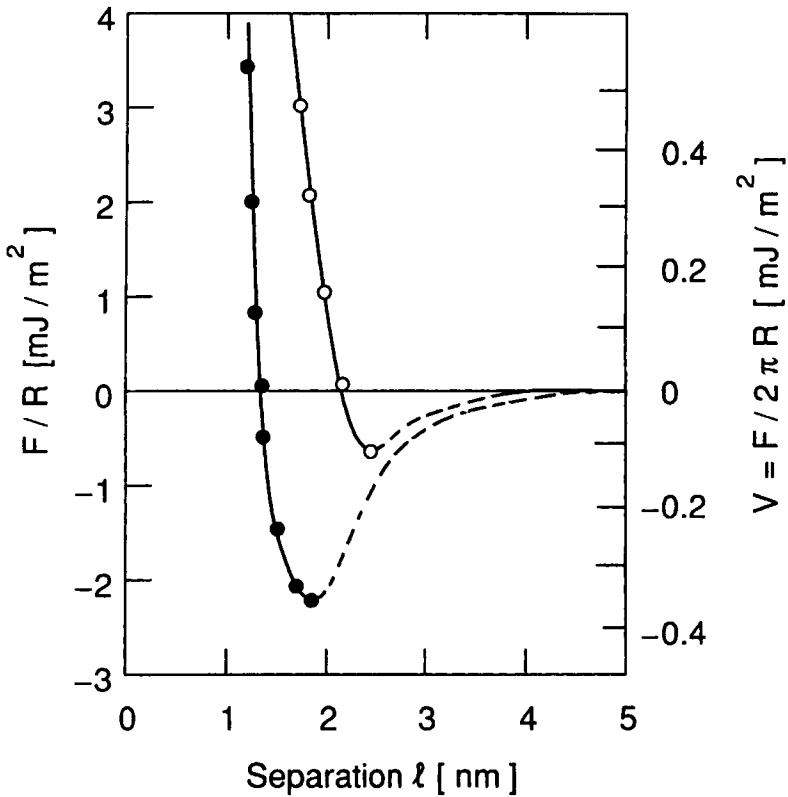


Fig. 1. Direct interaction $V = F/2\pi R$ between DLPC bilayers as measured by the surface force apparatus. The open circles correspond to full bilayers, the full circles to ‘partial’ bilayers where the two monolayers not in contact with the mica surfaces have been partially desorbed [22].

general, all electrically neutral bilayers lead to a functional dependence of the direct interaction $V \sim F/R$ on the bilayer separation l which is similar to the one shown in fig. 1.

If the force applied by the spring system vanishes, the two surfaces have a finite separation, see fig. 1. This separation is, however, different from the equilibrium separation of two *planar* bilayers. The latter separation is determined by

$$P = -\partial V/\partial l \approx \frac{1}{2\pi R} \frac{\partial F}{\partial l} \tag{2.5}$$

where P is the external pressure, i.e. force per unit area, acting on the membranes. For $P = 0$, the separation $l = l_0$ is determined by $\partial V/\partial l = 0$, i.e. by the minimum of $V(l)$.

For full DLPC bilayers, the data in fig. 1 imply that the pressure $P = -\partial V/\partial l$ grows rapidly to $10^6 \text{ Pa} \approx 10 \text{ atm}$ as the bilayers are further pushed to separations

$l < l_0 \simeq 2.5$ nm. In aqueous solution, these bilayers can sustain even much larger pressures of the order of 10^8 Pa $\simeq 10^3$ atm when their separation is reduced to a few monolayers of water [31, 35]. These latter pressures can be applied to multilayer systems as described below in section 2.4. Such high pressures are not accessible via the surface force apparatus since the mica layers start to deform elastically.

2.2. Micropipet aspiration of giant vesicles

Additional experimental information about the interaction of membranes can be obtained from the adhesion of vesicles in aqueous solution as controlled by micropipet aspiration [15, 25, 27]. The shape of these vesicles can be directly observed in the optical microscope, see fig. 2.

The vesicle is sucked into a pipet of radius R_{pip} by a suction pressure P_{pip} which is smaller than the pressure P_{out} of the aqueous medium outside of the pipet and of the vesicle. For a sufficiently large pressure difference $P_{\text{out}} - P_{\text{pip}}$, the vesicle consists of a capped cylinder of radius R_{pip} and of a spherical segment of radius R_{sp} . The cap of the cylinder has the curvature radius R_{pip} . It then follows from Laplace's law that $2\Sigma/R_{\text{pip}} = P_{\text{in}} - P_{\text{pip}}$ and $2\Sigma/R_{\text{sp}} = P_{\text{in}} - P_{\text{out}}$ where Σ and P_{in} are the lateral tension within the membrane and the pressure inside the vesicle, respectively. This implies

$$P_{\text{out}} - P_{\text{pip}} = 2\Sigma(R_{\text{pip}}^{-1} - R_{\text{sp}}^{-1}) > 0.$$

If such a pressurized vesicle is attracted towards another surface, it is pulled out of the pipet. As a result, a certain volume \mathcal{V} of water is transferred out of the pipet into the surrounding medium provided that the vesicle volume remains unchanged during this process. The corresponding work which has been performed on the system is

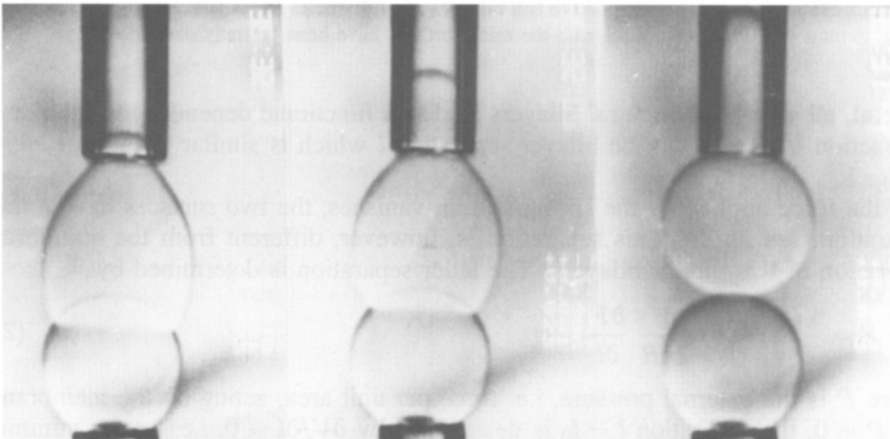


Fig. 2. Adhesion of two lipid vesicles which are brought into contact by two micropipettes. The vesicle radii are $\simeq 10$ μm . The vesicle at the bottom is almost spherical since it is exposed to a relatively large suction pressure. (Courtesy of E. Evans.)

equal to

$$\mathcal{V}(P_{\text{in}} - P_{\text{pip}}) + \mathcal{V}(P_{\text{out}} - P_{\text{in}}) = \mathcal{V}(P_{\text{out}} - P_{\text{pip}}).$$

On the other hand, the vesicle membrane now has a certain contact area \mathcal{A}_* with the second surface. Since the membrane within the contact region can still undergo some shape fluctuations, its separation from the second surface is not constant but will have a mean value $\ell = \langle l \rangle$ (which should be constant away from the boundary of the contact area). In addition, the shape fluctuations renormalize the direct interaction $V(l)$ and act to increase its repulsive part, see section 5 below. As a result, one has an effective interaction $V_{\text{eff}}(\ell)$ and, thus, the interaction free energy $\mathcal{A}_* V_{\text{eff}}(\ell) < 0$ (here and below, the interaction free energy for completely separated surfaces is taken to be zero, i.e. $V_{\text{eff}}(l = \infty) \equiv 0$). If this free energy is balanced against the work to transfer the water volume \mathcal{V} , one obtains the estimate

$$|V_{\text{eff}}(\ell)| \simeq \mathcal{V}(P_{\text{out}} - P_{\text{pip}})/\mathcal{A}_*. \quad (2.6)$$

In this way, one can determine the adhesion energy $|V_{\text{eff}}(\ell)|$ per unit area. So far, the mean separation ℓ has not been measured directly in these experiments.

Initial aspiration into a pipet with radius $R_{\text{pip}} \simeq 3 \mu\text{m}$ occurs at relatively small pressure differences $P_{\text{out}} - P_{\text{pip}} \simeq 10^{-1} \text{ Pa} \simeq 10^{-6} \text{ atm}$. Using Laplace's law, this leads to a lateral tension $\Sigma \simeq 10^{-4} \text{ mJ/m}^2$. This tension can be increased up to the tension of rupture, $\Sigma_{\text{max}} \simeq$ a few mJ/m^2 [15], which corresponds to the pressure difference $P_{\text{out}} - P_{\text{pip}} \simeq 10^{-2} \text{ atm}$. Since the lateral tension Σ reduces the shape fluctuations of the membranes, see section 4 and 5, the effective interaction $V_{\text{eff}}(l)$ becomes more similar to the direct interaction $V(l)$ with increasing tension Σ .

2.3. Reflection interference contrast microscopy

Vesicles in solution which are attracted towards a glass surface can be studied by reflection interference contrast microscopy [28, 29]. The vesicle, which is separated from the substrate by a liquid layer of variable thickness l , is illuminated through the glass surface (the same experimental technique has been used for a long time to study thin wetting films between gas bubbles and a solid substrate [45, 46]).

The light is reflected back both from the membrane and from the interface between the solid and the aqueous solution (it is useful to coat the glass by a thin layer of another solid material such as magnesium fluoride). The interference fringes arising from these two reflections are then observed in the optical microscope. Several examples of such interference patterns are shown in fig. 3.

The shape of the interference fringes already indicates if the vesicle is in a state of strong or weak adhesion. For relatively weak adhesion, the fringes undergo strong fluctuations which correspond to the thermally-excited fluctuations of the vesicle membrane. In addition, from a detailed analysis of the contrast of the interference fringes, one can obtain the separation l of the vesicle membrane from the solid substrate with a resolution of about 1 nm (the lateral resolution is about $0.2 \mu\text{m}$).

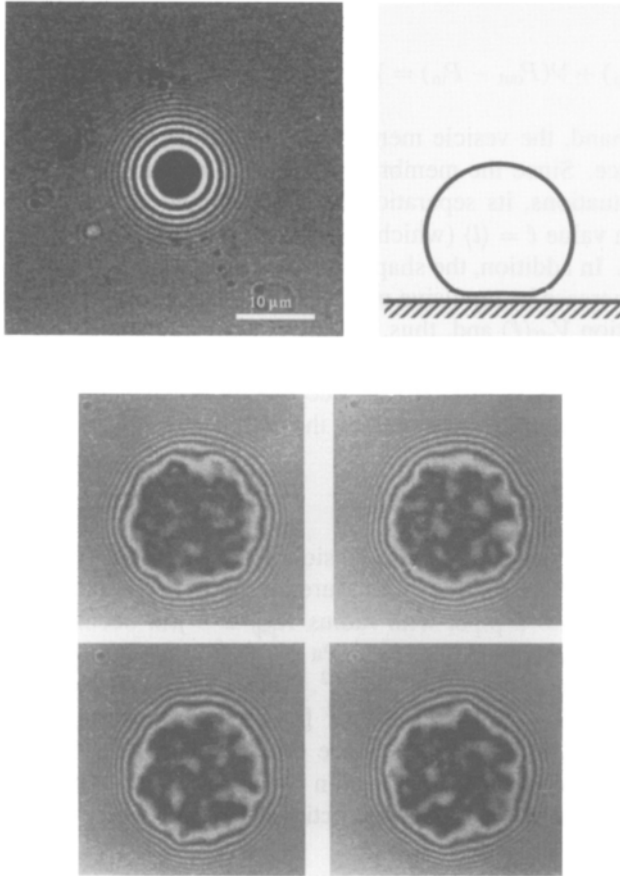


Fig. 3. Membrane of a bound vesicle as observed by reflection interference contrast microscopy. (a) Relatively large lateral tension which suppresses all shape fluctuations, and (b) Pronounced shape fluctuations for relatively small tension. (Courtesy of J. Rädler and E. Sackmann.)

So far, this experimental technique has not provided any quantitative information on the interaction free energy V . This could be achieved by a combination of reflection interference contrast microscopy and micropipet aspiration. In such an experiment, the vesicle is pushed towards or pulled from the solid surface by a micropipet, and the separation of the vesicle from the solid substrate is simultaneously measured by interference microscopy.

The analysis of the shape fluctuations as shown in fig. 3 indicates that the membrane of the vesicle experiences an effective lateral tension [47]. Since these vesicles contain sugar molecules which cannot penetrate the membrane, there is an osmotic pressure P_{os} between the inside and the outside of the vesicle. The corresponding tension is given by $\Sigma = RP_{os}/2 \approx RNT/2$ where N is the number of sugar molecules per unit volume inside the vesicle (it is assumed here that the solution

outside the vesicle does not contain sugar). This tension must not exceed the tension of rupture, Σ_{\max} , which is of the order of a few mJ/m^2 [15]. For a vesicle with radius $R \simeq 10 \mu\text{m}$ and $\Sigma_{\max} \simeq 5 \text{ mJ/m}^2$, for example, the sugar concentration must be smaller than $1 \text{ molecule}/(16 \text{ nm})^3$ or 0.4 mM .

2.4. Multilayer systems under stress

Most lipids form lamellar phases which consist of large stacks of lipid bilayers. If the membranes are in a fluid state as assumed here, these stacks represent smectic liquid crystals. A typical bulk sample contains several liquid crystal domains in equilibrium with excess water.

The bilayers within such a large stack are separated by thin layers of solvent and, thus, undergo some shape fluctuations. As mentioned, these fluctuations renormalize $V(l)$ into $V_{\text{eff}}(l)$. The mean separation l is now determined by

$$P = -\partial V_{\text{eff}}(l)/\partial l \tag{2.7}$$

where P represents the external pressure acting on the stack of membranes. The mean separation l can be measured by X-ray or neutron scattering. Since the pressure P

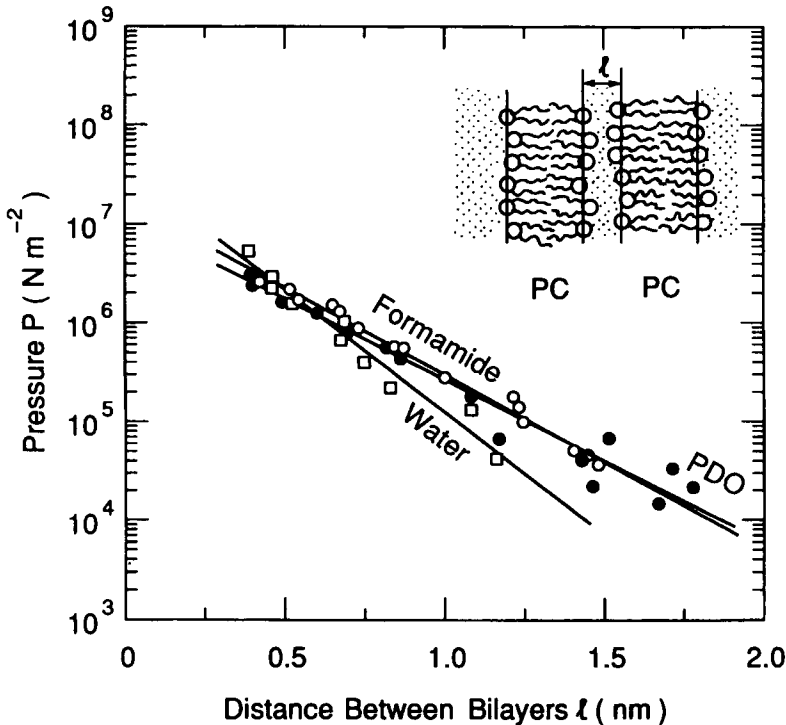


Fig. 4. Disjoining pressure P of PC bilayers as a function of the mean separation l for the three solvents water, formamide, and 1,3-propanediol [34].

can be varied over several decades, one can experimentally determine the functional dependence of ℓ on P [30–36]. Some experimental data obtained in this way are shown in fig. 4; in this case, the disjoining pressure of PC bilayers was measured for three different solvents.

By definition, $P = 0$ corresponds to a state in which the lamellar phase is in equilibrium with the reservoir of excess water. On the other hand, one may add some polymers such as dextran to the excess water which cannot enter the lamellar phase. This so-called osmotic stress method leads to the osmotic pressure $P_{\text{os}} \approx NT$ for small N where N is the number of polymers per unit volume of excess water. In practice, this osmotic pressure on the stack of membranes can be varied over several orders of magnitude from 10^2 to 10^6 Pa (or from 10^{-3} to 10 atm). One can extend this pressure range up to 10^8 Pa (or 10^3 atm) by using hydrodynamic pressure or by equilibrating the lamellar phase with a vapor phase which is in equilibrium with a saturated salt solution. These methods are described in more detail in the chapter by Parsegian and Rand in this handbook.

2.5. Surface reflectivity of X-rays and neutrons

Membranes which are attached to an interface or surface can be studied by surface reflectivity of X-rays [37, 38] or neutrons [39]. In these experiments, the incoming beam is reflected at an interface, and the intensity of the specularly reflected beam is measured as a function of the angle of incidence (or the momentum transfer perpendicular to the interface). One may then compare these data with the reflectivity as obtained from theoretical models for these profiles.

One example for this type of experiment is the recent observation of a stack of bilayers at the water-air interface [37, 38]. In this case, the surface of a suspension containing vesicles of DMPC (dimyristoyl phosphatidyl choline) was studied by X-ray reflectivity. The reflectivity data showed a strong dependence on temperature, see fig. 5. At relatively low temperatures, these data are consistent with the formation of a lipid monolayer at the water-air interface. As the temperature is increased, a series of sharp peaks is observed in the reflectivity which indicate the formation of bilayers adjacent to the monolayer. This could arise from the adhesion of the DMPC vesicles to the surface and from the subsequent fusion of these vesicles induced by the adhesion [48].

So far, this method has not been used to study the separation of the bilayers as a function of an external control parameter. It should be possible, however, to combine surface reflectivity methods with the osmotic stress method to obtain information about the effective interaction of the membranes close to the surface.

2.6. Optical microscopy of membrane bunches

Bunches of several lipid bilayers can be observed in swollen samples by optical microscopy [40, 41]. An example is shown in fig. 6. In this figure, horizontal bunches of membranes are connected by single bilayers. Inspection of fig. 6 shows that these bilayers are rather straight away from the bunches but are rounded close to

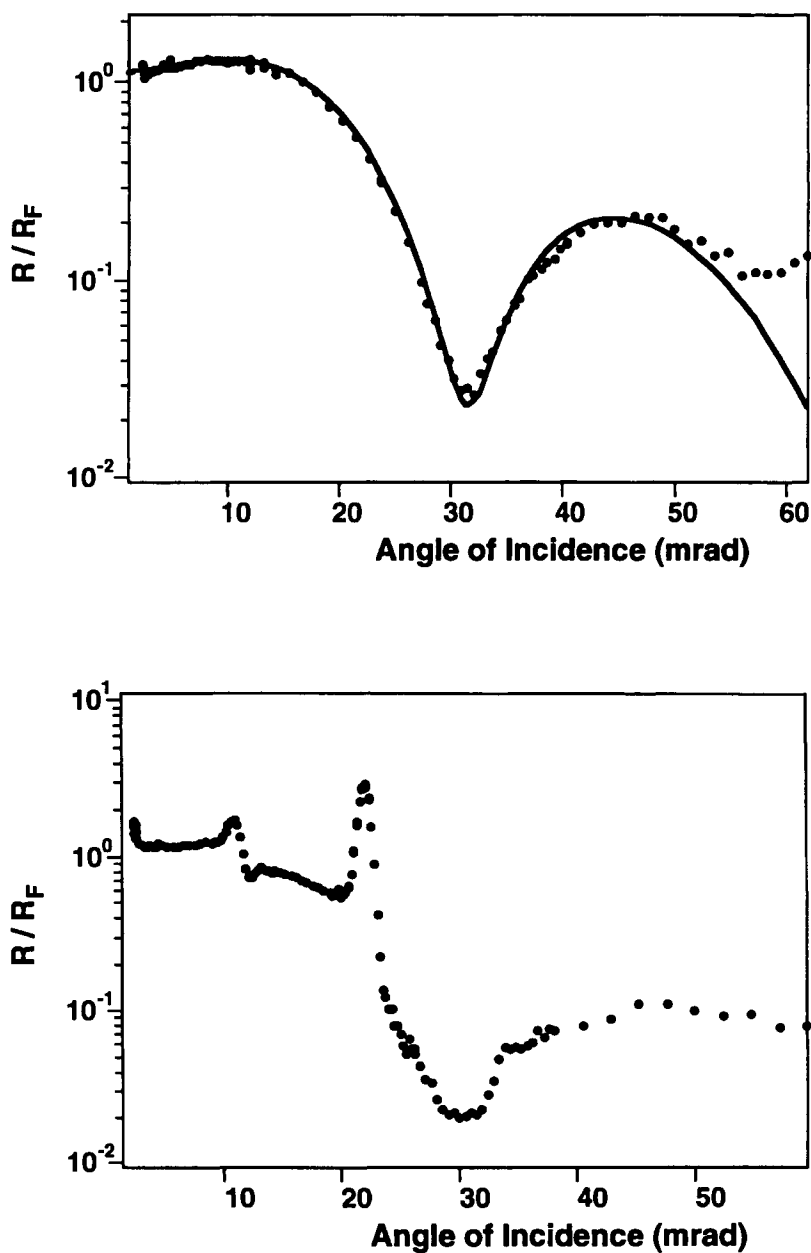


Fig. 5. X-ray reflectivity R from the surface of a suspension of DMPC vesicles. The reflectivity is normalized by the Fresnel reflectivity R_F . (a) At $T = 25^\circ\text{C}$, the data are well-fitted by the theoretical curve as calculated for a monolayer; and (b) At $T = 29^\circ\text{C}$, additional peaks appear after some hours which should arise from additional bilayers adjacent to the monolayer [38].

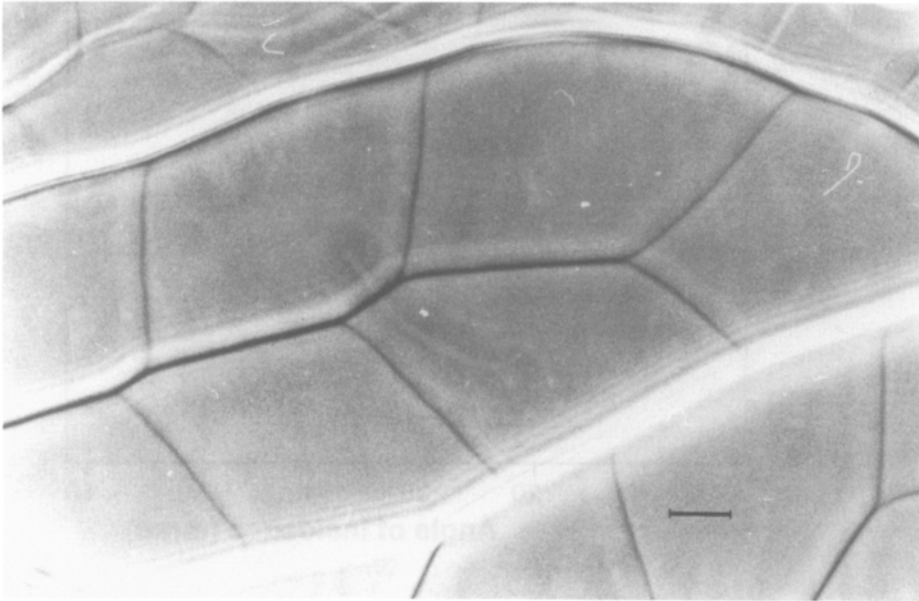


Fig. 6. Phase contrast micrograph of bunches of PC bilayers. The thick lines (which are roughly horizontal) represent bunches containing several bilayer, the thin lines (which are roughly vertical) are presumably single bilayers which form bridges between two neighboring bunches. (Courtesy of W. Helfrich).

these bunches. This geometry is discussed in more detail in the chapter by Helfrich in this handbook.

In general, a membrane which adheres to another, essentially flat surface exhibits the contact curvature radius [49, 50]

$$R_* = \sqrt{\kappa/2|V_{\text{eff}}(\ell)|} \quad (2.8)$$

where $V_{\text{eff}}(\ell)$ is the adhesion free energy per unit area as before. Thus, the measured value of R_* leads to a rough estimate for $|V_{\text{eff}}(\ell)|$ if one knows the bending rigidity κ .

As explained in section 5.6 below, the adhesion free energy $|V_{\text{eff}}(\ell)|$ increases with increasing lateral tension Σ since this tension acts to reduce the repulsion arising from shape fluctuations. Thus, the contact curvature radius R_* decreases with increasing Σ . In the limit of large Σ , the bilayer forms an effective contact angle ψ_{eff} with the membrane bunch which satisfies

$$|V_{\text{eff}}(\ell)| = \Sigma(1 - \cos \psi_{\text{eff}}). \quad (2.9)$$

From this relation, one can estimate the lateral tension Σ , using the experimentally determined contact angle ψ_{eff} and the estimate for $|V_{\text{eff}}(\ell)|$, as obtained from the measurement of the radius R_* of contact curvature. The lateral tensions deduced in this way lie in the range $3 \times 10^{-6} \text{ mJ/m}^2 \lesssim \Sigma \lesssim 10^{-3} \text{ mJ/m}^2$ [40, 41].

3. Direct interaction between two rigid membranes

In this section, the direct interaction between two rigid membranes will be discussed from the conceptual point of view. As explained before, an example is provided by two lipid bilayers which have been immobilized on mica surfaces. Here and below, it will be tacitly assumed that the membranes do not fuse and thus do not change their topology. In the absence of fusion, the membranes cannot penetrate each other, and their direct interaction contains the hard wall potential

$$V_{\text{hw}}(l) \equiv \begin{cases} \infty & \text{for } l < 0, \\ 0 & \text{for } l > 0. \end{cases} \quad (3.1)$$

Vanishing separation, $l = 0$, corresponds to direct contact between the lipid head groups of the two bilayers.

The hard wall potential V_{hw} represents a useful theoretical model since it contains no energy scale. In practice, the immobilized and planar membranes experience a variety of interactions arising from intermolecular forces. These interactions will be denoted by $\Delta V(l)$. Thus, the direct interaction between two planar membranes is taken to have the generic form

$$V(l) = V_{\text{hw}}(l) + \Delta V(l). \quad (3.2)$$

As explained before, one has $-\partial V/\partial l = P$, i.e. the disjoining pressure, $-\partial V/\partial l$, arising from the direct interaction is balanced against the external pressure P .

In general, there are several intermolecular forces which contribute to $V(l)$. First, consider the simplest case of two identical lipid bilayers which (i) are electrically neutral, and (ii) interact across a water layer which contains no macromolecules or colloids. In this case, the interaction potential $\Delta V(l)$ is composed of a repulsive hydration and an attractive Van der Waals interaction and has the schematic form as shown in fig. 1. These two contributions will be discussed in sections 3.1 and 3.2, respectively. The electrostatic interaction of charged membranes is considered in section 3.3, and the direct interaction mediated by macromolecules in section 3.4.

3.1. Hydration forces

For small separations of the order of 1 nm, lipid bilayers experience strong repulsive forces which have been originally discovered for multilayers under external stress [35]. In these multilayer systems, one has to exert a pressure of the order of $10^8 \text{ Pa} \simeq 10^3 \text{ atm}$ in order to obtain bilayer separations below 1 nm. For two bilayers immobilized on mica, one also finds a strong repulsive force at short separations [21, 33] but the pressure is limited to $P \lesssim 4 \times 10^6 \text{ Pa} \simeq 40 \text{ atm}$ since the mica surfaces are elastically deformed for higher pressures.

It was generally believed for some time that these hydration forces are governed by the intrinsic structure of the lipid water interfaces. An alternative explanation has been proposed, however, in which these forces arise from the protrusions of the lipid molecules [51]. These two explanations have led to some controversy [52, 53]. We

have recently argued that, in general, both hydration and protrusion will contribute towards the short-ranged repulsion between the bilayers [54, 55].

In this section on direct interactions, I will focus on the hydration forces between immobilized or rigid membranes which should arise from the intrinsic structure of the lipid water interfaces. This interface can be described by a density profile which represents the variation of an appropriate order parameter density with the distance y from the lipid surface. From the theoretical point of view, one would like to calculate this intrinsic structure of the lipid-water interface. There have been several attempts in this direction based on density functionals. However, since there is no satisfactory theory for water, the choice of the appropriate order parameter is not obvious. Various candidates have been proposed such as local water polarization [56, 57], orientation of hydrogen bonds [58] or electrostatic potentials [59–62].

If the lipid water interface were laterally smooth on the scale of the water molecules, the density profile would exhibit oscillations within the water which would represent the successive packing of water layers. However, the water molecules in front of the lipid surface ‘sees’ hills and valleys, the size of which is set by the lipid head groups. In a fluid bilayer, this corrugation exhibits no long-range order and the lateral average leads to a density profile for which the oscillatory part is strongly suppressed [54]. The profile should then be characterized by exponential tails $\sim \exp[-y/l_{\text{hy}}]$ which defines the hydration length l_{hy} . Such an exponentially decaying profile follows from the classical van der Waals theory for fluid-fluid interfaces and is also obtained from the more recent density functional theories mentioned above. One must note, however, that the hydration length l_{hy} is a phenomenological parameter in all of these theories.

Now, if two lipid water interfaces are brought into close contact across a water layer, their density tails become distorted which leads to an exponential *repulsion* between the two bilayers as described by the interaction

$$\Delta V(l) = V_{\text{hy}} \exp[-l/l_{\text{hy}}]. \quad (3.3)$$

The exponential form for $\Delta V(l)$ arising from the intrinsic structure of the lipid water interface was originally introduced in order to explain the experimental results obtained for multilayers under external stress. One must note, however, that the bilayers within a lamellar phase are not immobilized and thus undergo shape fluctuations which renormalize the direct interaction as given by (3.3). One type of shape fluctuations which change the hydration interaction are protrusion modes in which individual lipid molecules make small excursions perpendicular to the bilayer membrane, see section 7 below.

The total disjoining pressure observed for multilayers under applied stress is given by $P \approx P_{\text{t}} \exp[-\ell/l_{\text{t}}]$ where ℓ is the mean separation of the bilayers. The observed decay length l_{t} is not universal but varies from 0.1 to 0.3 nm and the measured pressure amplitude P_{t} is estimated to be in the range $4 \times 10^7 \text{ Pa} \lesssim P_{\text{t}} \lesssim 4 \times 10^9 \text{ Pa}$. The theory described in section 7 below predicts the general inequality $l_{\text{hy}} < l_{\text{t}}$.

3.2. Van der Waals forces

Water and lipid molecules have permanent dipole moments. If these dipoles have no average orientation, their interaction potential decays as $\sim 1/r^6$ for large separation r . In addition, these molecules possess induced dipole moments which are related to their spectrum of absorption frequencies. The corresponding interaction potentials also decay as $\sim 1/r^6$. These interactions between permanent and induced dipoles are collectively called Van der Waals forces, see, e.g., [63].

Now, consider two identical lipid bilayers separated by a solvent layer of thickness l . The bilayers have a typical thickness a_\perp of about 4 nm. For $l \ll a_\perp$, one may replace the two bilayers by two identical half spaces separated by the solvent layer. The Van der Waals interaction between two such half spaces is given by

$$\Delta V(l) = \frac{H}{12\pi} \frac{1}{l^2} \quad \text{with } H < 0. \quad (3.4)$$

The Hamaker constant H consists of two parts,

$$H = H_0(T, l_{\text{DH}}) + H_1, \quad (3.5)$$

arising from the static (or zero-frequency) polarizabilities of the molecules and from their polarizabilities at finite frequencies, respectively. The static part H_0 is proportional to temperature T and depends on the Debye–Hückel screening length l_{DH} . If the aqueous solution contains n_i ions of type i per unit volume and if each ion of type i has the electric charge q_i , the Debye–Hückel screening length is given by

$$l_{\text{DH}} \equiv \left[\varepsilon T / \sum n_i q_i^2 \right]^{1/2} \quad (3.6)$$

where ε is the dielectric constant of the solvent. In the SI units used here, one has $\varepsilon = \chi \varepsilon_0$ with the dimensionless coefficient χ and $\varepsilon_0 \simeq 8.85 \times 10^{-12} \text{ C}^2/\text{Jm}$; for water, $\chi \simeq 78.5$.

In the limit of small l_{DH}/l , i.e. if the Debye–Hückel screening length is small compared to the separation of the bilayers, one has [63]

$$H_0(T, l_{\text{DH}}) \sim H_0(T, \infty) e^{-2l/l_{\text{DH}}}. \quad (3.7)$$

Therefore, the static part of the Hamaker constant is strongly reduced in the presence of salt.

The Van der Waals interaction has been measured by the surface force apparatus for bilayer separations up to $l \simeq 6 \text{ nm}$ [22, 23]. It was found that the half space approximation which leads to $\Delta V(l) \sim 1/l^2$ as in (3.4) is appropriate (i) up to $l \simeq 5 \text{ nm}$ for pure water (for which $l_{\text{DH}} \simeq 1 \mu\text{m}$) and (ii) up to $l \simeq 4 \text{ nm}$ for a NaCl solution of 0.2 M (for which $l_{\text{DH}} \simeq 0.7 \text{ nm}$). For two composite bilayers, each consisting of one monolayer of DPPE (dipalmitoyl phosphatidyl ethanolamine) and one monolayer of DGDG (digalactosyl diglyceride), the Hamaker constants were

found to be (i) $H = (-7.5 \pm 1.0) \times 10^{-21}$ J for pure water, and (ii) $H \simeq H_1 = (-3.1 \pm 0.6) \times 10^{-21}$ J for the NaCl solution of 0.2 M.

In these experiments, the Hamaker constant H can be estimated both from measurements of the long-ranged attractive tail (as obtained by inward jumps in l using a variable spring constant K_S , see section 2.1) and from measurements of the direct interaction $V(l)$ close to its minimum (as obtained by outward jumps). For DGDG bilayers, both estimates were quite similar. Such an agreement was not found, however, for bilayers of DPPC and DPPE. For these phospholipids, the Hamaker constant estimated from the long-ranged attractive tail was about five times smaller than the one obtained from the minimum of the interaction potential. It has been argued that this difference arises from the correlations between the dipoles of the lipid head groups [64].

For membrane separations l large compared to the bilayer thickness a_\perp , the half space approximation is no longer appropriate and one must consider the corrections arising from the finite thickness a_\perp . For $l \gg a_\perp$, the bilayers represent essentially two-dimensional sheets which implies

$$\Delta V(l) \sim a_\perp^2/l^4 \quad \text{for large } l. \quad (3.8)$$

The value of the prefactor can be calculated if one applies the Lifshitz theory of Van der Waals forces to two planar and parallel films of hydrocarbon separated by water. The resulting expression for $\Delta V(l)$ which is somewhat complicated has been recently analyzed in detail [65].

In the absence of salt, the Van der Waals interaction is dominated by the zero-frequency part; the corresponding Hamaker constant H_0 is almost constant up to $l \simeq 10$ nm. On the other hand, if the Debye–Hückel length is sufficiently small, the zero-frequency part is completely suppressed, and the van der Waals interaction is approximately given by

$$\Delta V(l) \simeq \frac{H_1}{12\pi} \left[\frac{1}{l^2} - \frac{2}{(l + a_\perp)^2} + \frac{1}{(l + 2a_\perp)^2} \right] \quad (3.9)$$

with Hamaker constant $H_1 < 0$. This approximation applies as long as one can ignore retardation effects which lead to $\Delta V(l) \sim 1/l^5$ for sufficiently large l .

Note that the aqueous solution in biological systems is always ‘salty’ and characterized by a screening length l_{DH} of the order of 1 nm. Therefore, the zero-frequency part of the Van der Waals forces should play no role in these systems.

3.3. Electrostatic forces

Lipid bilayers may become charged by adsorption of ions from the solution or by dissociation of their head groups. They then exhibit electric double layers which usually lead to *repulsive* interactions between the surfaces as predicted by the classical Poisson–Boltzmann theory [66–68].

Within this continuum theory, each electric double layer is decomposed into a charged surface (which has no depth profile) and a diffuse layer of ions in front of

this surface. In general, one has both counterions and coions. The electric charges of the coions have the same sign as the surface charges whereas the counterions are oppositely charged. Therefore, the electrostatic potential acts to localize the counterions towards the surface. This is balanced by the entropy of mixing of these ions which acts to delocalize their density profile.

Now, consider two planar and parallel membranes which have the same surface charge Q per unit area (Q can be positive or negative). The coordinate perpendicular to these membranes is denoted by z . The two interacting lipid-solvent interfaces are located at $z = 0$ and $z = l$, respectively. The solution can contain several ions of type j with electric charges q_j . Between the two parallel surfaces, the ion densities depend only on z ; the corresponding density profiles will be denoted by $n_j(z)$.

Within mean-field theory, the electrostatic potential ψ satisfies the Poisson–Boltzmann equation

$$\frac{\partial^2 \psi}{\partial z^2} = \frac{\partial \Omega(\psi)}{\partial \psi} \tag{3.10}$$

with

$$\Omega(\psi) \equiv \frac{T}{\varepsilon} \sum_j n_j(z) = \frac{T}{\varepsilon} \sum_j \hat{n}_j e^{-q_j \psi / T}. \tag{3.11}$$

The summation over j runs over all types of ions. The densities \hat{n}_j are defined by $\hat{n}_j \equiv n_j(\hat{z})$ with $\psi(\hat{z}) = 0$. As before, T and ε are the temperature and the (average) dielectric constant of the solution. Note that the Poisson–Boltzmann equation has the same form as the equation of motion for a classical particle with ‘coordinate’ ψ which moves in the potential $-\Omega(\psi)$. This analogy is useful in order to classify the possible solutions of this equation.

Charge neutrality of each electric double layer leads to the boundary conditions

$$\partial \psi / \partial z|_0 = -Q / \varepsilon \quad \text{and} \quad \partial \psi / \partial z|_l = +Q / \varepsilon. \tag{3.12}$$

Because of the symmetric geometry, one has

$$\partial \psi / \partial z = 0 \quad \text{for} \quad \psi = \psi_m \equiv \psi(l/2) \tag{3.13}$$

at the midplane between the two charged surfaces. In the limit of large separation l , ψ_m attains the limiting value ψ_b with

$$\partial \Omega / \partial \psi = 0 \quad \text{at} \quad \psi = \psi_b. \tag{3.14}$$

The solution of these equations leads to the disjoining pressure

$$P = \varepsilon [\Omega(\psi_m) - \Omega(\psi_b)] = T \sum_j [n_j(l/2) - n_{jb}]. \tag{3.15}$$

Thus, the disjoining pressure is controlled by the excess densities $n_j(l/2) - n_{jb}$.

The relation (3.15) is useful since one may estimate $n_j(l/2)$ and thus P from the density profiles for a *single* electric double layer. In the latter case, one has the simple boundary condition

$$\psi(z = \infty) = \psi_b \tag{3.16}$$

for the electrostatic potential.

3.3.1. Small screening length

First, consider the situation in which the aqueous solution contains salt and the lipid-solvent interface is charged by the adsorption of ions from the solution. An example is provided by the adsorption of Ca^{2+} cations onto phospholipids from a solution of CaCl_2 .

If there are no counterions arising from the surface, the function $\Omega(\psi)$ consists of pairs of coions and counterions arising from the bulk solution. This implies that $\Omega(\psi)$ has its minimum at $\psi = \psi_b = 0$ and

$$\Omega(\psi) \approx \Omega(0) + \frac{1}{2} \psi^2 / l_{\text{DH}}^2 \quad (3.17)$$

for small ψ with the Debye–Hückel screening length

$$l_{\text{DH}} = \left(\varepsilon T / \sum_j n_{\text{jb}} q_j^2 \right)^{1/2}$$

as before. This harmonic approximation for $\Omega(\psi)$ leads to the linearized Poisson–Boltzmann equation. For a single lipid-solvent interface with surface charge density Q , the solution of the linearized equation is given by

$$\psi_1(z) = (Q l_{\text{DH}} / \varepsilon) e^{-z/l_{\text{DH}}}. \quad (3.18)$$

For two such interfaces interacting across a solvent layer of thickness l , one may use the estimate $\psi_m = \psi(l/2) \simeq 2\psi_1(l/2)$ which arises from the weak overlap of the two electric double layers. It then follows from (3.18) that

$$\begin{aligned} P &= \varepsilon [\Omega(\psi_m) - \Omega(\psi_b)] \simeq \varepsilon [\Omega(2\psi_1(l/2)) - \Omega(0)] \\ &\simeq (2Q^2 / \varepsilon) e^{-l/l_{\text{DH}}}. \end{aligned} \quad (3.19)$$

Since $P = -\partial \Delta V(l) / \partial l$, one obtains the electrostatic interaction

$$\Delta V(l) \simeq (2Q^2 l_{\text{DH}} / \varepsilon) e^{-l/l_{\text{DH}}} \quad (3.20)$$

which decays exponentially with the screening length l_{DH} . This exponential decay for large l is valid beyond the approximations used here. The amplitude of $\Delta V(l)$, on the other hand, should represent a reliable estimate

- (i) if the surface charge density Q is sufficiently small (which justifies the harmonic approximation to $\Omega(\psi)$) and
- (ii) if the bilayer separation l is larger than the screening length l_{DH} (which justifies the weak overlap approximation).

As an example, consider the adsorption of Ca^{2+} ions from a CaCl_2 solution onto DPPC (dipalmitoyl phosphatidyl choline). For a CaCl_2 solution of 1 mM, the surface charge density was estimated to be $Q \simeq 0.005 \text{ C/m}^2$ which corresponds to about one

adsorbed Ca^{2+} ion per 100 lipid head groups [22]. The screening length of the bulk solution is $l_{\text{DH}} \simeq 8$ nm. This implies the pressure amplitude $2Q^2/\epsilon \simeq 7.2 \times 10^4$ Pa and the interaction amplitude $2Q^2 l_{\text{DH}}/\epsilon \simeq 0.18$ mJ/m².

The electrostatic interaction has been measured using the surface force apparatus for PC (phosphatidyl cholin) and PE (phosphatidyl ethanolamine) bilayers in solutions of CaCl_2 or MgCl_2 [22]. These membranes are charged by the adsorption of Ca^{2+} or Mg^{2+} ions. For separations beyond a few nm, the experimental data confirm the exponential dependence $\Delta V(l) \sim \exp[-l/l_{\text{DH}}]$. Using the surface charge density Q as a fit parameter, quantitative agreement between experiment and theory has been obtained.

The interaction of phospholipid bilayers which are charged by the adsorption of divalent ions such as Ca^{2+} has also been studied for multilayers under osmotic stress [32]. As mentioned, these bilayers undergo shape fluctuations which renormalize the direct interaction $\Delta V(l)$. These effects will be discussed in sections 5 and 6.

3.3.2. Large screening length

Next, consider the situation in which the bulk solution contains very few ions and the screening length l_{DH} is very large. ‘Pure’ water, for example, is a 10^{-7} M solution of H_3O^+ and OH^- ions and has $l_{\text{DH}} \simeq 1$ μm . In the absence of ions in the bulk solution, surface charges and counterions arise by dissociation of surface groups.

If the solution contains only counterions of charge q , the charge density is given by

$$\rho = q\hat{n}e^{-q\psi/T}. \quad (3.21)$$

For a single lipid-solvent interface, the solution of the Poisson–Boltzmann equation leads to the counterion density

$$n_1(z) = \frac{2T\epsilon}{q^2} \frac{1}{(z + l_{\text{GC}})^2} \quad (3.22)$$

with the Gouy–Chapman length

$$l_{\text{GC}} \equiv -2T\epsilon/qQ = 2T\epsilon/|qQ|. \quad (3.23)$$

The latter length scale contains the whole dependence on the surface charge density.

For two lipid-solvent interfaces interacting across a solvent layer of thickness l , one may again use the weak overlap estimate $n(l/2) \simeq 2n_1(l/2)$ provided the separation l is sufficiently large. It then follows from (3.15) with $n_b = 0$ that the disjoining pressure is given by

$$P = Tn(l/2) \simeq 16T\epsilon/q^2 l^2. \quad (3.24)$$

The corresponding direct interaction is given by

$$\Delta V(l) \approx c\epsilon T^2/q^2 l \quad \text{for large } l. \quad (3.25)$$

The weak overlap estimate gives $c = 16$ whereas the solution of the Poisson–Boltzmann equation for the slab geometry leads to $c = 2\pi^2 \simeq 19.7$. Thus, in the limit of a large screening length, the electrostatic interaction decays as $\sim 1/l$ for large l .

The interaction of charged bilayers in pure water has been studied for multilayer systems under osmotic stress [30]. These bilayers were composed of a mixture of electrically neutral PC and negatively charged PG (phosphatidyl glycerol). The direct interaction should then decay as $\Delta V(l) \sim 1/l$ for separations l below the Debye–Hückel length $l_{DH} \simeq 1 \mu\text{m}$ of pure water. For such an interaction, the renormalization by the shape fluctuations is small, see section 5.2, and the effective interaction within the multilayer system should resemble the direct interaction $\Delta V(l)$. Indeed, the experimental data for the pressure as a function of separation could be well fitted with the theoretical form as given by (3.25) for $3 \text{ nm} < l < 10 \text{ nm}$ (the fitted surface charge density was $Q \simeq$ one elementary charge/ 14 nm^2 which corresponds to one elementary charge per two lipid head groups).

3.3.3. Small surface separations

As mentioned, the theoretical predictions for the electrostatic interaction $\Delta V(l)$ as given by (3.20) and (3.25) are in agreement with experimental observations provided the membrane separation l is sufficiently large. At small separations, on the other hand, there are various complications which will be briefly discussed in this subsection.

For small separations, the counterions with charge q will have an almost constant density given by $n \simeq 2|Q|/|q|l$. If this estimate is used in (3.15), one obtains the disjoining pressure

$$P = Tn(l/2) \simeq 2T|Q|/|q|l. \quad (3.26)$$

In practice, the behavior $P \sim 1/l$ is changed by two effects:

- (i) In general, the surface charge Q is not constant as the two surfaces approach each other. Instead, some of the counterions will recombine with the surface charges and, thus, Q will be reduced with decreasing separation l . This process is called charge regulation; and
- (ii) At small separations, the discrete nature of the molecules comes into play and provides some steric constraints. Sometimes, the finite size of the surface groups can be taken into account by separate ‘Stern layers’ in front of the surfaces which have a thickness of the order of 0.1–0.2 nm [66–68].

Within the Poisson–Boltzmann theory, the electrostatic interaction between equally charged surfaces is *repulsive* for all separations l . It turns out, however, that more refined theories which include correlations between the ions can lead to an *attractive* interaction between two equally charged surfaces. Such an attraction was first proposed in the context of interacting polyelectrolytes [69]. In the context of charged surfaces, such an attraction was observed in Monte Carlo simulations of two surfaces separated by a layer of divalent counterions [70]. It has also been obtained from an improved density functional theory (the so-called anisotropic hypernetted chain approximation) [71]. In these theoretical studies, the electrostatic interaction is found to be attractive for small separations of the order of 1 nm.

3.4. Forces mediated by macromolecules

Membranes within biological systems interact with many macromolecules [7, 8]. The outer surface of the plasma membrane, for example, is often covered by the glycocalix which consists of branched polysaccharides covalently bound to membrane proteins. On the inner surface, the plasma membrane is attached to networks of relatively stiff filaments which are part of the cytoskeleton inside the cell. In addition, the plasma membrane usually contains a large number of different adhesion molecules which play a crucial role in the specific adhesion between cells and between cells and the extracellular matrix. Cell adhesion molecules are relatively stiff rodlike molecules with a linear extension of the order of 20 nm. These molecules are embedded in the plasma membrane (and are usually connected to the cytoskeleton). In many cases, the adhesion of two adjacent plasma membranes is provided by bound pairs of such adhesion molecules which form bridges between the membranes.

A model system for these complex interactions is provided by systems containing lipid bilayers and polymers. From the physical point of view, polymers can be characterized by several length scales. First of all, they have a certain length, Na , where N and a are the number of monomers and the length of these monomers, respectively. Secondly, linear polymers are characterized by a certain persistence length, ξ_p : the polymer is hard and easy to bend on scales which are smaller and larger than ξ_p , respectively.

Many biopolymers seem to have a relatively large persistence length ξ_p which is comparable or exceeds its total length Na ; in this case, the polymer behaves as a worm-like chain which exhibits an average direction. On the other hand, if $Na \gg \xi_p$, polymers crumple or fold up in order to increase their configurational entropy. This leads to a more compact 3-dimensional structure with a gyration radius, $R_g \ll Na$. In good solvents, these structures are random coils and $R_g \sim N^\nu$ for large N with the Flory estimate $\nu \simeq 3/5$ (in 3-dimensional systems). In bad solvents, the polymers collapse and become densely packed with $R_G \sim N^{1/3}$.

A single lipid bilayer may attract or repel the monomers of the polymer leading to adsorption or desorption, respectively. These two situations lead to different types of interactions between two membranes across a polymer solution. First, consider the case in which the polymers do *not* adsorb onto the surfaces. Then, depletion layers build up in front of the membrane surfaces. It then follows from mean-field type theories that the polymer-induced interaction is *attractive* [72]. Such an attractive interaction has been observed in experiments on vesicle adhesion using micropipet aspiration [73].

Now, consider polymers which are *adsorbed* onto the two interacting surfaces. The size of the adsorbed polymer is set by the gyration radius, R_g , of the free polymer. Therefore, the polymer-induced interaction $\Delta V(l)$ must decay rapidly to zero for $l \gg R_g$. For smaller surface separations l , the interaction has been predicted to depend on the equilibration of the adsorption layers with the solution [74, 75]. First, assume that these adsorbed polymers are in chemical equilibrium with a polymer reservoir (which is characterized by a bulk chemical potential). Then, mean-field type theories again lead to an effective *attraction*, $\Delta V(l) < 0$, between two identical surfaces [75].

The effective interaction induced by adsorbed polymers has been experimentally studied using the surface force apparatus [76, 77]. The observed behavior is rather complex. It is found that equilibration between the adsorbed polymers and the bulk solution is difficult to attain. Instead, it seems that many experiments have been performed with essentially constant adsorption or coverage rather than constant chemical potential. Furthermore, the form of $\Delta V(l)$ was found to depend on the magnitude of the adsorption. For example, it was found for polyethylene oxide in aqueous solution (a good solvent system) that $\Delta V(l)$ exhibits a strong attraction with a minimum at $l \simeq 2R_g$ for low adsorption but becomes purely repulsive for high adsorption.

If the exchange of polymers between the adsorption layers and the bulk solution is blocked, there will be an osmotic pressure P_{os} between these two subsystems. The disjoining pressure between the two interacting surfaces can then be estimated from the osmotic pressure in the midplane. The simplest estimate is obtained if one assumes that the adsorbed polymer layers resemble a concentrated polymer solution with monomer density $n_{mo} \sim 1/l$. Mean-field theory gives the osmotic pressure $P_{os} \sim n_{mo}^2$ and thus $P \simeq P_{os} \sim 1/l^2$ [76]. This leads to a repulsive interaction $\Delta V(l) \sim 1/l$.

If one assumes that the adsorption layers correspond to a semi-dilute polymer solution, one has a self-similar density profile $n_{mo}(z) \sim 1/z^{(3\nu-1)/\nu}$ with $(3\nu-1)/\nu \simeq 3/4$ for good solvents [74, 78]. Scaling arguments give the osmotic pressure $P_{os}/T \sim n_{mo}^{3\nu/(3\nu-1)}$ in the semi-dilute regime. One then obtains the estimate $P \simeq P_{os} \simeq [n_{mo}(l/2)]^{3\nu/(3\nu-1)} \sim 1/l^3$ and thus the repulsive interaction $\Delta V(l) \sim 1/l^2$ [75]. The experimental data seem to be consistent with $\Delta V(l) \sim 1/l^2$ for intermediate values of l and with $\Delta V(l) \sim 1/l$ for small l [77].

4. Bending undulations and fluctuation-induced interactions

For bilayers immersed in a liquid solution, the direct interaction $V(l)$ as described in the previous section will be renormalized by thermally-excited fluctuations. Several types of fluctuations can be distinguished:

- (i) Bending modes or undulations in which the surface area of the membrane remains unchanged;
- (ii) Stretching modes for which the area per molecule is changed. Since the hydrocarbon film within the membrane is essentially incompressible, stretching of the bilayer area implies a thinning of the bilayer thickness; and
- (iii) Protrusion modes in which the lipid molecules are displaced perpendicular to the bilayer, and thus change the surface area of the lipid-solvent interface.

In this section and the two subsequent sections 5 and 6, I will focus on the effect of bending modes which should be the typical shape fluctuations on length scales large compared to the bilayer thickness. Stretching modes will be briefly considered in section 4.4. The effect of protrusion modes on the hydration force will be discussed in section 7.

4.1. Bending modes as an ideal gas of humps

Consider a large membrane segment which is confined by an external potential arising, e.g., from two walls as shown in fig. 7. The confined membrane has less configurational entropy than the free membrane. Indeed, all fluctuations of the free membrane which exceed a certain wavelength ξ_{\parallel} are strongly suppressed by the external potential. On the other hand, those fluctuations with a wavelength below ξ_{\parallel} are essentially not affected by the confinement. One is thus led to consider an ideal gas of uncorrelated membrane segments which have a longitudinal size ξ_{\parallel} .

Now, assume that the membrane is in the fluid state and undergoes bending undulations. As shown in appendix A, these fluctuations lead to a roughness of the membrane segment as given by

$$\xi_{\perp} \sim (T/\kappa)^{1/2} \xi_{\parallel} \tag{4.1}$$

with temperature T and bending rigidity κ . The bending rigidity κ has the dimensions of an energy. For phospholipid bilayers in their fluid state, it typically varies between 0.2×10^{-19} J and 4×10^{-19} J which implies $0.2 \gtrsim T/\kappa \gtrsim 0.01$ at room temperature $T \simeq 0.04 \times 10^{-19}$ J [19, 20].

Thus, each segment forms a hump of longitudinal and perpendicular extension ξ_{\parallel} and ξ_{\perp} , respectively, and thus of volume $\mathcal{V} \simeq \xi_{\parallel}^2 \xi_{\perp}$. Using the ideal gas law $P\mathcal{V} = T$ for a single degree of freedom and the relation (4.1), one then arrives at the pressure [2]

$$P \sim T^2/\kappa \xi_{\perp}^3. \tag{4.2}$$

Thus, the bending undulations lead to a disjoining pressure P which decays slowly with the roughness ξ_{\perp} .

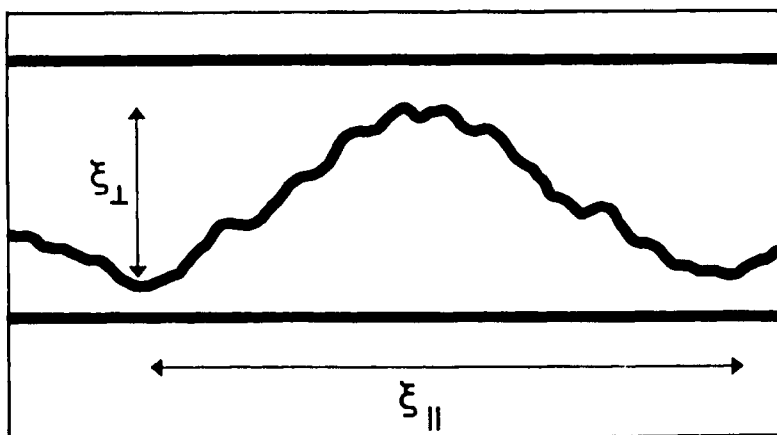


Fig. 7. A fluctuating membrane confined by two walls. The fluctuations consist of essentially uncorrelated humps with longitudinal extension ξ_{\parallel} and typical height ξ_{\perp} .

Alternatively, one may allude to the equipartition theorem and postulate that each such hump has a free energy $\Delta\mathcal{F} \sim T$. This implies that the hump free energy per unit (projected) area behaves as

$$V_{\text{fl}} \equiv \Delta\mathcal{F}/\xi_{\parallel}^2 \sim T/\xi_{\parallel}^2 \sim T^2/\kappa\xi_{\perp}^2 \quad \text{for large } \xi_{\perp}. \quad (4.3)$$

This free energy per unit area represents a fluctuation-induced interaction between the membrane and the confining potential. The disjoining pressure is now obtained from $P = -\partial V_{\text{fl}}/\partial\xi_{\perp}$.

For the confinement geometry as shown in fig. 7, the scale ξ_{\perp} is proportional to the spacing of the two walls. Likewise, two interacting membranes are usually characterized by a roughness which is proportional to their mean separation ℓ . It is then convenient to express the fluctuation-induced interaction V_{fl} between the surfaces in terms of ℓ and to write

$$V_{\text{fl}}(\ell) \approx c_{\text{fl}}T^2/\kappa\ell^2 \quad \text{for large } \ell. \quad (4.4)$$

The most precise value for the dimensionless coefficient c_{fl} has been obtained from Monte Carlo simulations [79–81] as described in section 5.2 below. For two identical membranes with bending rigidity κ_1 , one has $\kappa = \kappa_1/2$, and the Monte Carlo data lead to $V_{\text{fl}} \approx 2c_{\text{fl}}T^2/\kappa_1\ell^2$ with $2c_{\text{fl}} = 0.115 \pm 0.005 \simeq 3\pi^2/256$.

4.2. From membranes to strings

The scaling argument described in the previous subsection is not restricted to the case of fluid membranes which undergo bending undulations. It is useful to apply the same line of reasoning to 1-dimensional strings in two dimensions. In the context of condensed matter, the term string refers to a fluctuating line governed by a finite line tension σ . This tension represents the work (per unit length) which is necessary in order to increase the length of the string. One example is provided by stretched (or directed) polymers. For a string segment of linear size ξ_{\parallel} , the roughness ξ_{\perp} scales as

$$\xi_{\perp} \sim (T/\sigma)^{1/2}\xi_{\parallel}^{1/2}. \quad (4.5)$$

Thus, the string behaves as a (directed) random walk where the longitudinal scale ξ_{\parallel} plays the role of ‘time’.

In this case, the volume \mathcal{V} occupied by a ξ_{\parallel} -hump of the string is given by $\mathcal{V} \simeq \xi_{\parallel}\xi_{\perp}$. If one now repeats the above arguments, one arrives at the fluctuation-induced interaction

$$V_{\text{fl}}(\ell) \sim T^2/\sigma\ell^2. \quad (4.6)$$

Such an interaction was first derived in the context of commensurate-incommensurate transitions [82] and is implicit in some earlier work about steps on crystal surfaces [83]. Comparison with the relation (4.4) shows that the fluctuation-induced interaction V_{fl} for strings has the same functional dependence on the separation ℓ as for fluid membranes. Thus, one expects that the shape fluctuations of strings and of fluid membranes have a rather similar effect on the direct interaction of these objects. This expectation is indeed confirmed, see below.

4.3. Effect of lateral tension

It was tacitly assumed so far that the fluctuating membrane does not experience any lateral tension. Now, let us again consider the situation as shown in fig. 7, where the membrane is confined by two rigid walls, but let us now assume that it also experiences a lateral tension, Σ . Such a tension will act to reduce the membrane roughness [84, 85]. In fact, the membrane will now exhibit the same roughness as an interface governed by surface tension. As shown in appendix A, this roughness ξ_{\perp} is given by

$$\xi_{\perp} \approx (T/2\pi\Sigma)^{1/2} \sqrt{\ln(\xi_{\parallel}/a_{\parallel})} \quad (4.7)$$

where a_{\parallel} denotes the small-scale cutoff. The latter length scale is set by the size of the lipid head group. Thus, the dependence of ξ_{\perp} on ξ_{\parallel} becomes very weak: even a relatively large membrane segment with $\xi_{\parallel}/a_{\parallel} \simeq 10^4$ corresponding to a linear size of $\simeq 10 \mu\text{m}$ will only give a factor $\sqrt{\ln(\xi_{\parallel}/a_{\parallel})} \simeq 3$. Therefore, one has $\xi_{\perp} \simeq (T/\Sigma)^{1/2}$ and the size of ξ_{\perp} is primarily determined by the lateral tension Σ .

Repeating again the scaling arguments of section 4.1, one now obtains the fluctuation-induced interaction [86]

$$V_{\text{fl}}(\xi_{\perp}) \sim \exp[-2(\xi_{\perp}/l_{\Sigma})^2] \quad (4.8)$$

with the length scale

$$l_{\Sigma} \equiv (T/2\pi\Sigma)^{1/2}. \quad (4.9)$$

In this case, the membrane roughness ξ_{\perp} is not proportional to the mean separation ℓ of the membrane from the rigid walls or from another membrane. A systematic treatment shows that one now has $\ell \sim \xi_{\perp}^2$ and a hard wall interaction is renormalized into [87]

$$V_{\text{fl}}(\ell) \sim \exp[-\ell/l_{\Sigma}]. \quad (4.10)$$

Thus, when expressed in terms of the mean separation ℓ , the fluctuation-induced interaction decays exponentially for large ℓ . The amplitude of this interaction is discussed in appendix A.

4.4. Stretching versus bending modes

So far, pure bending modes have been considered. In this case, the excess area necessary for the elastic deformation is provided by the flow within the membrane. In principle, this excess area could also be provided by stretching the membrane.

Membrane stretching is governed by the modul K_A of the area compressibility. For a flat membrane segment of area A_0 , the lateral tension Σ leads to the area change ΔA with $\Sigma = K_A \Delta A/A_0$. This tension should not exceed the tension of rupture, Σ_{max} , at which the membrane breaks apart.

For lipid bilayers, the area compressibility modul K_A and the tension of rupture Σ_{\max} have been measured by micropipet aspiration techniques and were found to be of the order of $K_A \simeq 0.2 \text{ J/m}^2$ and $\Sigma_{\max} \simeq$ a few mJ/m^2 , respectively [15]. This implies that lipid bilayers rupture for relatively small area changes of the order of $\Delta A/A_0 \simeq 10^{-2}$.

Now, consider the extreme case in which a flat membrane is deformed into a bump and the whole excess area is created by stretching. If the segment has area $A_0 \simeq \xi_{\parallel}^2$ and the bump has height ξ_{\perp} , the change of area is $\Delta A \sim A_0(\xi_{\perp}/\xi_{\parallel})^2$ and the excitation energy is $\Delta E \sim K_A A_0 (\Delta A/A_0)^2 \sim K_A \xi_{\perp}^4 / \xi_{\parallel}^2$. In addition, this elastic deformation also involves some bending energy which is, however, always small compared to the stretching energy. If such a deformation is thermally excited, one must have $\Delta E \simeq T$ which implies

$$\xi_{\perp} \sim (T/K_A)^{1/4} \xi_{\parallel}^{1/2}. \quad (4.11)$$

This roughness arising from stretching modes must now be compared with the roughness arising from pure bending as given by (4.1). In this way, one finds the crossover length scales

$$\xi_{\perp*} \simeq (\kappa/K_A)^{1/2} \quad \text{and} \quad \xi_{\parallel*} \simeq \kappa/(TK_A)^{1/2}. \quad (4.12)$$

The roughness is dominated by stretching modes for wavelengths $\xi_{\parallel} \lesssim \xi_{\parallel*}$. Using the typical values, $\kappa \simeq 10^{-19} \text{ J}$ and $K_A \simeq 0.2 \text{ J/m}^2$, one obtains the roughness $\xi_{\perp*} \simeq 0.7 \text{ nm}$ and the wavelength $\xi_{\parallel*} \simeq 3.5 \text{ nm}$ which is of the order of the membrane thickness.

Similar estimates are obtained if one considers the fluctuation induced interaction arising from the stretching modes considered here. The latter interaction behaves as $V_{\text{fl}} \sim T^2/K_A \xi_{\perp}^4$ (the latter form also applies to peristaltic modes of the bilayer [53]). If this is compared with the fluctuation induced interaction $V_{\text{fl}} \sim T^2/\kappa \xi_{\perp}^2$ arising from pure bending modes, one again obtains the above crossover scales.

Thus, pure bending modes should be the dominant fluctuations on length scales which are large compared to the membrane thickness. Stretching modes, on the other hand, become important for wavelengths which are of the order of the membrane thickness. For these latter excitations, the continuum description used here is, however, no longer reliable. Instead, the discrete molecular structure of the membranes should be taken into account, see section 7.

5. Renormalized interactions

In the previous section, bending undulations have been treated in a heuristic manner. In this section, the interplay of these shape fluctuations with the direct interaction arising from molecular forces between two membranes will be studied in a systematic way.

If the attractive part of the direct interaction is sufficiently strong, or if the temperature is sufficiently low, the membranes form a bound state and the effect of the

bending undulations is rather small. However, as one decreases the strength of the direct attraction or increases the temperature, the bending undulations lead to a strong renormalization of the direct interaction. As a result, one finds a finite temperature T_* at which the membranes undergo an unbinding transition [3].

For $T > T_*$, the shape fluctuations drive the membranes apart even in the presence of the direct attraction. In this latter case, one can enforce a bound state by applying an external pressure or a lateral tension.

5.1. Systematic theory for two membranes

Now, let us consider two interacting membranes with bending rigidities κ_1 and κ_2 which are, on average, parallel. The separation (or relative displacement field) l of these two membranes is governed by the configurational energy (or effective Hamiltonian) [3, 88, 89]

$$\mathcal{H}\{l\} = \int d^2x \left\{ Pl + V(l) + \frac{1}{2} \kappa (\nabla^2 l)^2 \right\} \quad (5.1)$$

with the effective bending rigidity

$$\kappa = \kappa_1 \kappa_2 / (\kappa_1 + \kappa_2). \quad (5.2)$$

The limiting case in which the second membrane represents a rigid surface or wall with $\kappa_2 = \infty$, is included here since (5.2) reduces to $\kappa = \kappa_1$ in this limit.

The probability for a given configuration of l is governed by the Boltzmann weight, $\exp[-\mathcal{H}\{l\}/T]$. In principle, one now has to sum over all possible configurations in order to calculate the partition sum and other statistical quantities. In practise, one has to use some approximate methods which are briefly summarized in the following.

(i) *Superposition of direct and entropic interactions.* The simplest method is a superposition of direct and entropic interactions. Using such an approach, the excess free energy per unit area, ΔF , of two bound membranes with separation l can be estimated as

$$\Delta F(l) = \Delta E - T\Delta S \simeq V(l) + V_{\text{fl}}(l), \quad (5.3)$$

with the fluctuation-induced interaction $V_{\text{fl}}(l) \approx c_{\text{fl}} T^2 / \kappa l^2$.

The equilibrium value of the mean separation ℓ is now determined from $\partial\Delta F/\partial\ell = 0$. This method is reliable if $V(l)$ is purely repulsive, see section 5.2. It fails, however, if $V(l)$ has an attractive part which decays faster to zero than $1/l^2$ for large l .

(ii) *Functional renormalization.* A more systematic approach is based on the functional renormalization group (RG). Roughly speaking, the direct interaction $V(l)$ represents the interaction between two surface segments of linear size a where a

is the smallest wavelength available to the shape fluctuations. Within the RG approach, one then calculates the effective interaction, $V(l|t)$, between two segments of linear size $a_t \equiv a \exp(t)$ with $t > 0$. This interaction contains all fluctuations of wavelength L_{\parallel} with $a < L_{\parallel} < a_t$. As t is increased, one successively includes more and more shape fluctuations and thus obtains the effective interaction on larger and larger scales.

It is interesting to note that, when applied to interacting strings in two dimensions, one obtains essentially the same RG transformation as for fluid membranes [88]. Therefore, the functional RG also predicts that fluid membranes governed by bending rigidity and strings governed by tension behave in an analogous way.

(iii) *Renormalized interactions of strings.* Strings are 1-dimensional objects and, thus, are much easier to study theoretically than 2-dimensional membranes. In the continuum limit, the separation l of two interacting strings in $(1 + 1)$ dimensions is equivalent to the spatial coordinate of a quantum-mechanical particle in one dimension [90]. Since one has many tools to analyze the corresponding Hamilton operator, one can often obtain explicit results for the renormalized interaction of these strings.

(iv) *Two-state model.* The analogy with strings leads to a refined scaling picture which is based on a two-state model. In this model, adjacent membrane segments are ‘locally bound’ or ‘locally unbound’. The exact critical behavior is recovered if one makes plausible assumptions about the probability to form locally bound pairs, see section 5.4.

(v) *Computer simulations.* The methods described so far are quite powerful if one wants to determine the asymptotic behavior of the renormalized interactions for large separations of the surfaces. In real systems, one is often limited to a certain regime which is dominated by corrections to the asymptotic behavior. Such corrections arise, for example, from the molecular structure and usually lead to some ‘crossover’ behavior on intermediate length scales. In order to obtain information about these intermediate or even microscopic length scales, it is most effective to study the model by computer simulations, see section 5.5.

In the following subsections 5.2–5.5, I will consider interaction potentials $Pl + V(l)$ which have both a repulsive and an attractive part and which are characterized by a single minimum. Two cases will be explicitly discussed:

- (i) The direct interaction $V(l)$ is purely repulsive and the attractive part is provided by the pressure term Pl ; and
- (ii) The direct interaction $V(l)$ has both a repulsive and an attractive part and the membranes experience no external pressure, i.e. $P = 0$.

In general, the direct interaction can be more complicated and may exhibit a potential well at small values of l and a potential barrier at larger values of l . Such potentials will be discussed in section 5.6.

5.2. Disjoining pressure from hard wall

In order to compare the different theoretical methods, let us first consider the simple interaction

$$V_p(l) \equiv V_{hw}(l) + Pl \tag{5.4}$$

in which the membranes are pushed together by the external pressure P but are not allowed to cross because of the hard wall repulsion $V_{hw}(l)$.

Within the superposition approach, one now has the excess free energy

$$\Delta F(l) = V_{hw}(l) + c_{\text{fl}} T^2 / \kappa l^2 + Pl. \tag{5.5}$$

The mean separation ℓ now follows from $\partial \Delta F(\ell) / \partial \ell = 0$ which leads to

$$P = 2c_{\text{fl}} T^2 / \kappa \ell^3. \tag{5.6}$$

The same behavior is found within the functional RG approach. Under the RG transformation, the hard wall potential $V_{hw}(l)$ is mapped onto a completely repulsive fixed point, and the behavior as given by (5.6) follows from the renormalization of the pressure term, Pl , close to this fixed point. In fact, this RG flow can already be obtained from the simple scale transformation

$$x \rightarrow x' = x/b \quad \text{and} \quad l \rightarrow l' = l/b \tag{5.7}$$

which leaves the elastic part

$$\int d^2x \frac{1}{2} \kappa (\nabla^2 l)^2$$

of the effective Hamiltonian invariant. When this scale transformation is applied to $\int d^2x Pl$, one obtains

$$P \rightarrow P' = b^{\lambda_p} P \quad \text{with} \quad \lambda_p = 3. \tag{5.8}$$

In the language of the RG, P is a relevant perturbation with scaling index λ_p . Then, standard scaling arguments imply that the correlation length ξ_{\parallel} behaves as

$$\xi_{\parallel} \sim 1/P^{\nu_{\parallel}} \quad \text{with} \quad \nu_{\parallel} = 1/\lambda_p = 1/3 \tag{5.9}$$

for small P and that $\ell \sim \xi_{\perp} \sim \xi_{\parallel}$.

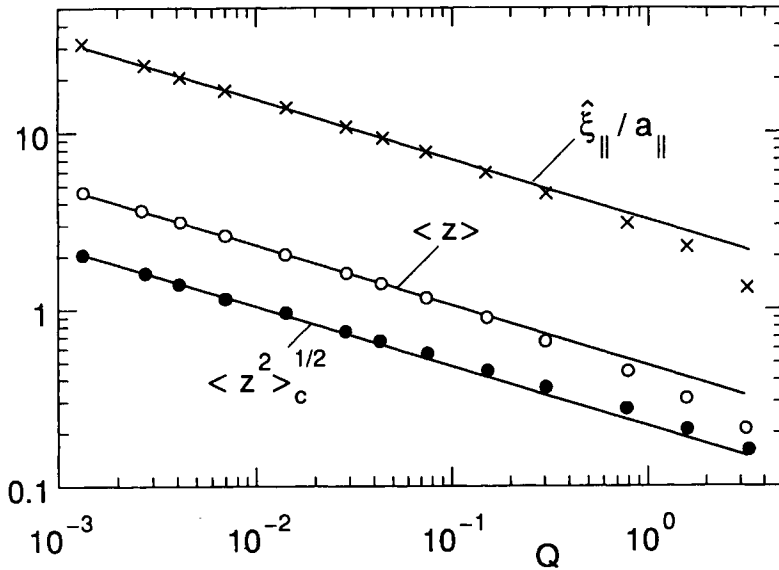


Fig. 8. The mean separation $\langle z \rangle = \ell/l_{sc}$ as a function of the pressure $Q = P/P_{sc}$ as obtained from MC simulations for the hard wall interaction. The length scale $\langle z^2 \rangle_c^{1/2}$ is the rescaled roughness, the length scale $\hat{\xi}_{\parallel}$ is proportional to the longitudinal correlation length. The pressure scale P_{sc} and the length scale l_{sc} are given by $P_{sc} = (T\kappa)^{1/2}/a_{\parallel}^3$ and $l_{sc} = a_{\parallel}(T/\kappa)^{1/2}$, respectively [79].

The critical behavior $\ell \sim \xi_{\perp} \sim \xi_{\parallel} \sim 1/P^{1/3}$ has also been confirmed by MC simulations which represents, in fact, the most reliable method to determine the coefficient c_{fl} .

The MC data for the rescaled variables $\langle z \rangle \sim \ell$, $\sqrt{\langle z^2 \rangle} \sim \xi_{\perp}$, and $Q \sim P$ are shown in fig. 8 [79]. In this double-logarithmic plot, the straight line represents the behavior $\ell \sim \xi_{\perp} \sim 1/P^{1/3}$ which is clearly confirmed by the data. The ratio ξ_{\perp}/ℓ approaches the constant value $c_{\perp} = 0.445 \pm 0.010$ for small P . The coefficient c_{fl} which governs the fluctuation-induced interaction V_{fl} and the corresponding disjoining pressure is found to be

$$2c_{fl} = 0.115 \pm 0.005. \tag{5.10}$$

For two identical membranes with bending rigidities $\kappa_2 = \kappa_1$, one has $\kappa = \kappa_1/2$ which implies $V_{fl}(l) \approx 2c_{fl}T^2/\kappa_1 l^2$. Thus, when expressed in terms of κ_1 , the coefficient of $V_{fl}(l)$ is equal to $2c_{fl}$. It is interesting to note that within the numerical accuracy, one has $2c_{fl} \approx 3\pi^2/256$ which is *half* the value as estimated in ref. [2] for a stack of many membranes, see also section 6.4 below.

It is instructive to study the corresponding behavior of two identical strings which interact with the same interaction as given by (5.4). If both strings have the same line tension $\sigma_1 = \sigma_2$, one finds that $V_{fl}(l) \approx 2c_{fl}T^2/\sigma_1 l^2$ with $2c_{fl} \approx 1.89$ [91].

Comparison with (5.10) shows that the amplitude of V_{fl} is much larger for strings than for membranes. On the other hand, the ratio ξ_{\perp}/ℓ approaches the constant value $c_{\perp} \simeq 0.447$ for two strings which is identical with the corresponding value for membranes.

Thus, for the hard wall interaction, the simple superposition of $V_{\text{hw}}(l) + Pl$ and $V_{\text{fl}}(l)$ represents a reasonable approximation. This is also true for a large class of direct interactions which are sufficiently long-ranged. In fact, this superposition approach is reliable as long as the attractive part of the interaction potential is sufficiently long-ranged and decays more slowly than $\sim 1/l^2$ for large l . These potentials belong to the so-called weak fluctuation regime [6]. In particular, the superposition approach may be used for unscreened electrostatic interactions $\Delta V(l) \sim 1/l$ as in (3.25). This leads to $\ell \sim 1/P^{1/2}$ [92, 93]. However, in the presence of short-ranged attractive forces, the simple superposition is no longer reliable.

5.3. Attractive interactions and unbinding transitions

Two identical membranes experience attractive interactions arising from Van der Waals forces. If the membranes carry no electric charges and the solvent contains no macromolecules, this van der Waals attraction dominates the direct interaction $V(l)$ for large membrane separations l .

The precise form of this Van der Waals interaction has been discussed in section 3.2. For large separations, the form as given by (3.9) leads to $\Delta V(l) \sim 1/l^4$. Since $\Delta V(l) \ll 1/l^2$ for large l , such an interaction belongs to the universality class of short-ranged interactions. The simplest example for this universality class is provided by the square-well potential with

$$\Delta V(l) = \begin{cases} U & \text{for } 0 < l < l_v, \\ 0 & \text{for } l_v < l, \end{cases} \quad (5.11)$$

which depends only on two parameters: the potential depth $U < 0$ and the potential range l_v . In general, any attractive interaction can be characterized by an effective potential depth and by an effective potential range. Such an interaction may then be approximated by a square-well potential with the appropriate values for U and l_v .

If one now considers the superposition, $\Delta F(l) = V_{\text{hw}}(l) + \Delta V(l) + V_{\text{fl}}(l)$, one finds that the qualitative form of $\Delta F(l)$ depends on the temperature T as schematically shown in fig. 9(a). For low T , the function $\Delta F(l)$ exhibits its global minimum at small l which represents the bound state of the two membranes. For high T , the global minimum of $\Delta F(l)$ is at $l = \infty$ which corresponds to the unbound state of the membranes. At the characteristic temperature $T_* = \sqrt{\kappa|U|l_v^2/c_{\text{fl}}}$, the bound and the unbound state have the same free energy. Therefore, the superposition predicts that the membranes undergo an unbinding transition at this temperature which proceeds in a *discontinuous* manner [3, 94].

The parameter dependence for T_* as obtained within the superposition approach is confirmed by more systematic methods. This approach fails, however, as far as the character of the transition is concerned since the unbinding transition proceeds, in fact, in a *continuous* fashion. This was first shown by renormalization group (RG)

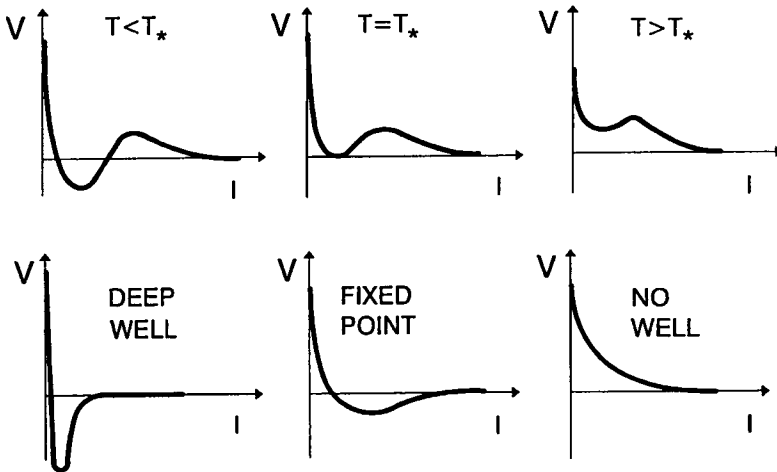


Fig. 9. Unbinding transition as obtained (top) from a simple superposition of fluctuation induced and direct forces, and (bottom) from functional renormalization. The unbinding temperature is denoted by T_* .

methods [3]. The corresponding RG transformations are displayed in fig. 9(b). As shown in this figure, the unbinding transition is governed by a critical fixed point of the RG transformation.

It is easy to understand the continuous character of the unbinding transition by analogy with strings in two dimensions. As mentioned, the separation of these strings corresponds to the spatial coordinate of a quantum-mechanical particle moving in the interaction potential $V(l)$. The probability distribution $\mathcal{P}(l)$ for the string separation l is governed by the ground state within this potential well. This ground state is localized at low temperature but becomes delocalized in a continuous manner as the unbinding temperature is approached from below.

The unbinding transition for square well potentials has also been studied by Monte Carlo simulations [79]. From these simulations, one finds that the unbinding temperature depends strongly on the small-scale cutoff for the bending undulations.

As an example, consider two relatively stiff membranes with $\kappa_1 = \kappa_2 = 2\kappa = 10^{-19}$ J which interact with a square well potential with the relatively small potential range $l_v = a_\perp/10$ where a_\perp denotes the membrane thickness as before. For a lipid bilayer, one typically has $a_\perp \simeq 4$ nm which implies the small potential range $l_v \simeq 0.4$ nm. In this case, the unbinding temperature T_* has been determined for several choices of the small-scale cutoff a_\parallel . As a result, one finds $T_*/T_{\text{room}} \simeq 0.7, 1$ and 1.5 for $a_\parallel/a_\perp = 1, 1.6$, and 2 , respectively [79]. Thus, the unbinding temperature T_* is roughly proportional to the small-scale cutoff a_\parallel for the bending undulations. Extrapolation to zero a_\parallel leads to the estimate $T_*/T_{\text{room}} = 0.4 \pm 0.1$ for this particular interaction potential.

As far as the critical behavior is concerned, RG calculations, MC simulations and the analogy with strings show that the mean separation ℓ and the roughness

$\xi_{\perp} = \sqrt{\langle(l - \ell)^2\rangle}$ scale as $\ell \sim \xi_{\perp} \sim (T/\kappa)^{1/2}\xi_{\parallel}$ and diverge as

$$\ell \sim 1/|T - T_*|^{\psi} \quad \text{with } \psi = 1 \tag{5.12}$$

as the transition temperature T_* is approached from below. The same critical behavior applies to all short-ranged interaction potentials $\Delta V(l)$ which decay faster to zero than $\sim 1/l^2$ for large l as follows from scaling arguments, RG calculations and the analogy with strings [86, 91]. These interactions belong to the so-called strong-fluctuation regime which is characterized by universal critical behavior at the unbinding transition [6]. On the other hand, interaction potentials $\Delta V(l)$ which decay as $\sim 1/l^2$ for large l belong to the so-called intermediate fluctuation regime which is characterized by rather complex critical behavior [6, 88, 89].

5.4. Two-state model for unbinding transition

The analogy with strings leads to a refined scaling picture for the unbinding transition from which one recovers the critical behavior as described in the previous subsection. This picture is based on the observation that two membranes which interact via a square-well potential can attain two different local states, see fig. 10: (i) They are ‘locally unbound’ if their separation exceeds the range of the potential; and (ii) They are ‘locally bound’ if their separation is smaller than this potential range. The probabilities for these two different local configurations will be denoted by \mathcal{P}_{ub} and \mathcal{P}_{2b} , respectively. In configuration (i), the strings still have a finite separation and then suffer a loss of entropy, ΔF_{ub} . For bending undulations as considered here, the entropy loss per unit area of ‘locally unbound’ membrane segments is given by (4.3) and thus $\Delta F_{ub} \sim T^2/\kappa \xi_{\perp}^2$.

The excess free energy per unit area of a bound pair will be denoted by ΔF_{2b} . Thus, the excess free energy per unit area of the two strings can be estimated as

$$\Delta F = \Delta F_{ub}\mathcal{P}_{ub} + \Delta F_{2b}\mathcal{P}_{2b}. \tag{5.13}$$

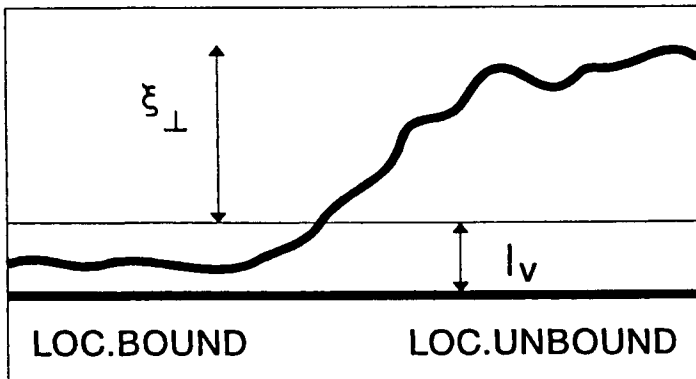


Fig. 10. Locally bound and locally unbound segments of the fluctuating membrane. The potential range is denoted by l_v .

If the unbinding transition is continuous, the roughness ξ_{\perp} will grow continuously. In such a situation, both the entropy loss $\Delta F_{\text{ub}} \sim 1/\xi_{\perp}^2$ of the ‘locally unbound’ configurations and the probability \mathcal{P}_{2b} for bound pairs must vanish in a continuous way, and $\mathcal{P}_{\text{ub}} = 1 - \mathcal{P}_{2b} \approx 1$ as the transition is approached. The excess free energy ΔF_{2b} for bound pairs, on the other hand, arises from configurations which have a separation of the order of the potential range l_v and, thus, will not depend on ξ_{\perp} . Therefore, the unbinding transition occurs when ΔF_{2b} vanishes.

For a square well potential of depth $|U|$, the excess free energy for bound pairs can be estimated as $\Delta F_{2b} \simeq -|U| + cT^2/\kappa l_v^2$ where the first and the second term represent the interaction energy and the entropy loss within the square well, respectively. Thus, one obtains $T_* = \sqrt{\kappa|U|l_v^2/c}$. This parameter dependence of T_* is certainly valid for strings as follows from explicit transfer matrix calculations and is in agreement with the results of Monte Carlo simulations for membranes.

In order to determine the critical behavior of ξ_{\perp} from the free energy ΔF as given by (5.13), one has to know how the probability \mathcal{P}_{2b} depends on this length scale. In the absence of any interactions, the probability distribution $\mathcal{P}(l)$ is a Gaussian distribution with width ξ_{\perp} and thus has the scaling form $\mathcal{P}(l) \approx \Omega(l/\xi_{\perp})/\xi_{\perp}$ with $\Omega(s) \approx \text{const}$ for small s . This implies $\mathcal{P}_{2b} \sim 1/\xi_{\perp}$ for large ξ_{\perp} . For two strings in two dimensions which attract each other by a short-ranged potential, one has the exponential distribution $\mathcal{P}(l) \sim \exp[-l/\xi_{\perp}]/\xi_{\perp}$ which also leads to $\mathcal{P}_{2b} \sim 1/\xi_{\perp}$. If one assumes that this property also applies to two fluid membranes which attract each other by a short-ranged potential, one obtains

$$\Delta F \approx c_1 T^2 / \kappa \xi_{\perp}^2 + c_2 (-|U| + cT^2 / \kappa l_v^2) / \xi_{\perp}. \quad (5.14)$$

Minimization of this expression for ΔF with respect to ξ_{\perp} leads to a continuous transition at $T = T_* \simeq \sqrt{\kappa|U|l_v^2/c}$ and to the critical behavior $\xi_{\perp} \sim 1/|T_* - T|^{\psi}$ with $\psi = 1$. Thus, one recovers the behavior as obtained by the other more systematic methods which have been discussed in the previous subsection.

In two dimensions, the scaling properties of two interacting strings are identical with the corresponding properties of the adsorption of ideal (or Gaussian) chain molecules [95]. In the latter context, a two-state model has been proposed some time ago [96]. A similar model has also been used by Helfrich who argued that ΔF_{2b} is determined by the reflections of the membrane at the hard wall and that this could lead to a discontinuous unbinding transition [97]. In contrast, the two-state model described here predicts a continuous transition; it has been generalized to bunches of N interacting membranes [98] as will be discussed in section 6.5.2 below.

It is important to note that the scaling relation $\mathcal{P}_{2b} \sim 1/\xi_{\perp}$ which seems to be rather natural does *not* hold in general as has been shown explicitly for interacting strings. For example, two strings which interact only via the hard wall interaction are characterized by the relation $\mathcal{P}_{2b} \sim 1/\xi_{\perp}^{2\zeta_0}$ with $\zeta_0 = 3/2$ [99, 100]. Another more complex example is provided by strings with direct interactions which behave as $\Delta V(l) \approx W/l^2$ for large l and thus belong to the intermediate fluctuation regime. Using the transfer matrix results of ref. [101–103], one obtains the contact probability

$\mathcal{P}_{2b} \sim 1/\xi_{\perp}^{2\zeta_0}$ with $\zeta_0 = 1 \pm (w + 1/4)^{1/2}$ and $w \equiv 2\sigma W/T^2$ where σ is the line tension as before. The plus and the minus sign correspond to effectively repulsive and effectively attractive interactions, respectively.

If one again assumes that strings and fluid membranes as considered here have analogous scaling properties, membranes with the hard wall interaction are characterized by $\mathcal{P}_{2b} \sim 1/\xi_{\perp}^{\zeta_0}$ with $\zeta_0 = 3$. Likewise, if the membrane interactions belong to the intermediate fluctuation regime, scaling implies $\mathcal{P}_{2b} \sim 1/\xi_{\perp}^{\zeta_0}$ with $\zeta_0 = 2 \pm (w + 1)^{1/2}$ and $w \equiv c_w \kappa W/T^2$. The small value of c_{fl} should lead to $c_w \gg 1$.

5.5. Unbinding transitions for realistic interactions

The direct interaction $V(l)$ for lipid bilayers without electric charges consists of the short-ranged repulsive hydration interaction and the long-ranged attractive van der Waals interaction; it has a single minimum at $l = l_0$ and decays to zero for large l . If the Debye–Hückel screening length is sufficiently small, the zero-frequency part of the Van der Waals interaction arising from the permanent dipol moments is strongly screened and the amplitude of this interaction is determined by the Hamaker constant $H \simeq H_1$, compare (3.9).

In the absence of shape fluctuations, the mean separation ℓ of the membranes is determined by $\partial V(\ell)/\partial \ell = 0$. If one applies an external pressure P , the minimum of $V(l)$ is shifted towards smaller values of l and the mean separation ℓ decreases. This leads to the functional dependence of P on ℓ as shown in the left part of fig. 11. The three sets of data shown in this part of the figure correspond to three different values of the Hamaker constant H . In the absence of shape fluctuations, the membranes are bound together as long as $|H| > 0$ and unbind only in the limit of zero H .

At finite temperature, the bending undulations act to increase the mean separation ℓ . This is shown in the right part of fig. 11 for two rather flexible membranes with bending rigidities $\kappa_1 = \kappa_2 = 0.2 \times 10^{-19}$ J at room temperature [48]. The same values of the Hamaker constant H have been chosen as in the left part of the figure. Comparison of the data in the left and in the right part shows that the effect of the shape fluctuations is more pronounced for smaller values of $|H|$.

In another set of simulations, the Hamaker constant was varied for zero pressure. Extrapolation of these data led to the critical Hamaker constant $|H_*| = (3.0 \pm 0.5) \times 10^{-21}$ J for $\kappa_1 = \kappa_2 = 0.2 \times 10^{-19}$ J at room temperature i.e. for the same temperature and for the same bending rigidities as in fig. 11 [48]. Likewise, one finds the critical value $|H_*| = (1.5 \pm 1.0) \times 10^{-21}$ J for the larger rigidities $\kappa_1 = \kappa_2 = 0.4 \times 10^{-19}$ J at room temperature. Thus, H_* is roughly proportional to the inverse bending rigidity.

For $|H| < |H_*|$ or $T > T_*$, the membranes fluctuate so strongly that the renormalized interaction is purely repulsive on large scales and the membranes are unbound. Within the functional renormalization group approach, this regime is governed by the same purely repulsive fixed point which also governs the hard wall interaction.

The numerical values for H_* just discussed are obtained for the special choice $a_{\parallel} = a_{\perp} = 4$ nm where a_{\parallel} is the small-scale cutoff and a_{\perp} is the membrane thickness as before. A change of the cutoff a_{\parallel} will have a strong effect on H_* (or on T_*). Indeed, for the square-well potential, the unbinding temperature T_* is roughly proportional to a_{\parallel} as discussed in the previous subsection.

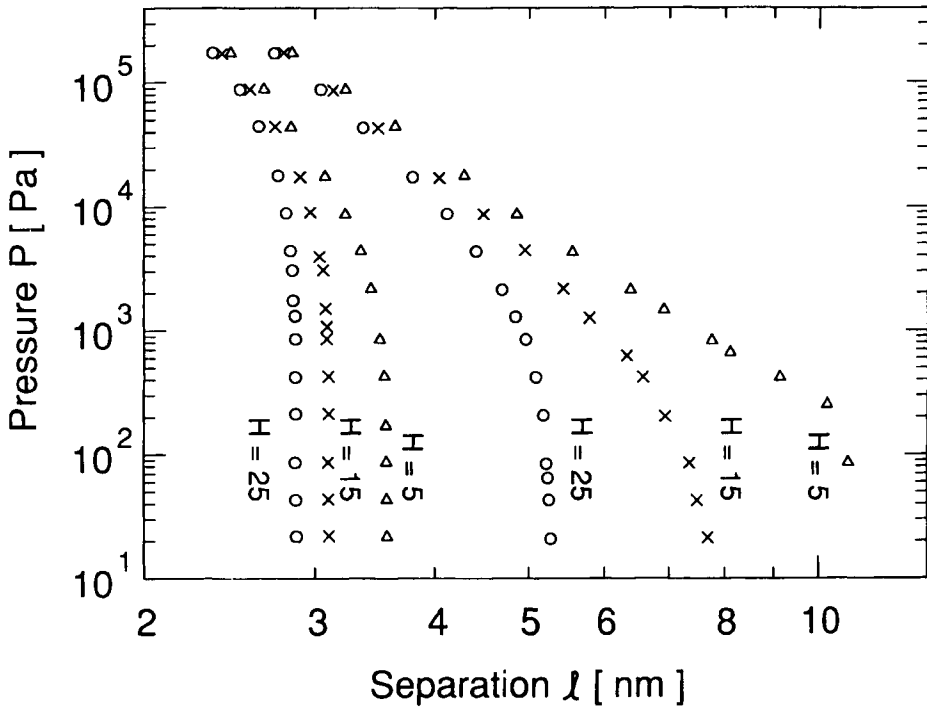


Fig. 11. Disjoining pressure P as a function of the separation l . The three curves on the right with Hamaker constants $|H| = 5, 15,$ and 25×10^{-21} J correspond to room temperature; the three curves on the left represent the behavior in the absence of shape fluctuations. The difference between these two sets of curves shows the strong renormalization of the direct interaction by bending undulations [50].

One must note, however, that this effect of the small-scale cutoff $a_{||}$ for the bending undulations was obtained under the tacit assumption that there are no other membrane fluctuations which act to renormalize the direct interaction. In fact, the direct interaction is also renormalized by protrusion modes as will be discussed in section 7. These protrusions also increase the repulsive part and thus decrease the attractive part of $V(l)$. Therefore, the effective interaction between membrane segments which have a lateral extension $a_{||} \simeq a_{\perp}$ will already be less attractive than $V(l)$.

5.6. Direct interactions with a potential barrier

So far, I have discussed direct interactions $V(l)$ which are (i) purely repulsive or (ii) are attractive for large l and repulsive for small l . In general, one may have more complicated interactions which exhibit an attractive potential well for small l and a repulsive potential barrier for larger l . Such an interaction can arise, for example, from the competition of Van der Waals and electrostatic interactions.

In the presence of such a potential barrier, the displacement field l of the interacting membrane can be trapped by the barrier. This happens if the shape fluctuations are

sufficiently weak or the barrier is sufficiently strong. One example is provided by barriers which decay more slowly than $\sim 1/l^2$ for large l (and thus belong to the weak-fluctuation regime). As the attractive part of the potential is decreased, the membrane will now undergo a *discontinuous* unbinding transition. This can be shown explicitly for strings in two dimensions [104] and must hold for membranes which are more easily trapped than strings.

Strings in two dimensions tunnel through any potential barrier which decays faster than $\sim 1/l^2$ for large l [104]. The latter interaction potentials belong to the strong-fluctuation regime. Therefore, in this regime, strings always undergo *continuous* unbinding transitions. Functional renormalization group calculations originally indicated that membranes can also tunnel through a potential barrier provided this barrier is sufficiently small [92]. In addition, a systematic study of the fixed point structure of the renormalization group transformation seemed to imply that fluid membranes can tunnel through any such a barrier [105–107]. However, this is not consistent with simple stability arguments as described in the following.

It is instructive to consider first a *symmetric* interaction potential $V(l)$ with two degenerate minima at finite values of l [105]. A simple example is provided by the direct interaction

$$V(l) = \begin{cases} \infty & \text{for } l < 0, \\ -|U_{we}| & \text{for } 0 < l < l_{we}, \\ U_{ba} & \text{for } l_{we} < l < l_{we} + l_{ba}, \\ -|U_{we}| & \text{for } l_{we} + l_{ba} < l < 2l_{we} + l_{ba}, \\ \infty & \text{for } 2l_{we} + l_{ba} < l, \end{cases} \quad (5.15)$$

which exhibits two attractive square-well potentials of depth $|U_{we}|$ and range l_{we} separated by a short-ranged potential barrier of height U_{ba} and thickness l_{ba} , see fig. 12(a).

Let us assume that the membrane is confined within one of these wells and let us see if such a state is stable with respect to thermal excitations in which a membrane segment is displaced into the other potential well. Such a conformation corresponds to an ‘island’ bounded by an edge where the edge goes through the potential barrier. This line of reasoning is completely analogous to the so-called Peierls argument for phase transitions in bulk systems.

The edge consists of membrane segments which go through the potential barrier of thickness l_{ba} . Therefore, this edge has an effective width $a_{\perp e} \sim (\kappa/T)^{1/2} l_{ba}$. The line tension σ of the edge can then be estimated as $\sigma \simeq U_{ba}^{\text{eff}} a_{\perp e}$ where the effective barrier height U_{ba}^{eff} is given by

$$U_{ba}^{\text{eff}} = U_{ba} + |U_{we}| - cT^2/\kappa l_{we}^2.$$

On small scales, the edge should behave as a string which implies that the small-scale cutoff $a_{\parallel e}$ for edge deformations is given by $a_{\parallel e} \simeq (\sigma/T)a_{\perp e}^2$.

For a displaced membrane segment or ‘island’ of linear size L_{\parallel} , one has the edge energy $\sim \sigma L_{\parallel}$ and the edge entropy $\sim \ln(3)L_{\parallel}/a_{\parallel e}$ arising from the different

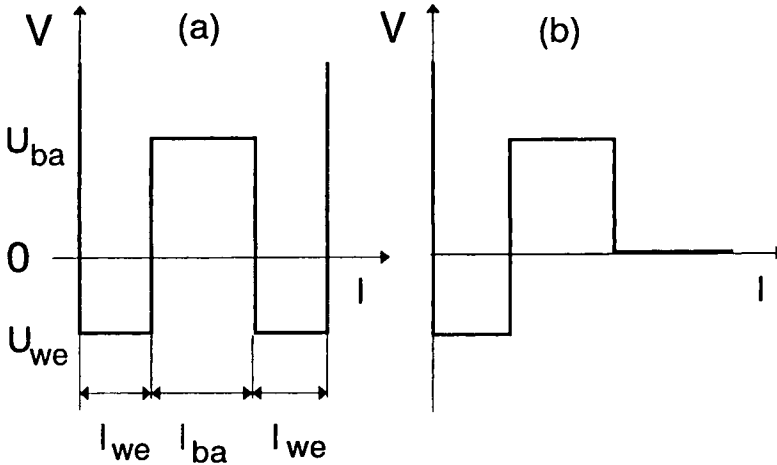


Fig. 12. Direct interactions $V(l)$ with a potential barrier: (a) Symmetric potential consisting of two wells with depth $|U_{we}|$ and range l_{we} separated by the barrier of height U_{ba} and thickness l_{ba} ; and (b) Asymmetric potential consisting of one well between the hard wall at $l = 0$ and the barrier.

shapes of the edge (in this estimate, the edge is viewed as a random walk with three possibilities at each step). This leads to the excess free energy of the edge as given by

$$\Delta F_e = [c_1\sigma - c_2T \ln(3)/a_{||e}]L_{||}. \quad (5.16)$$

This excess free energy is positive if $T < T_{ba}$ where T_{ba} satisfies

$$T_{ba} \sim (\kappa U_{ba}^{\text{eff}} l_{ba}^2)^{1/2} \quad (5.17)$$

as follows from the above estimates for σ and $a_{||e}$. In general, the effective barrier height U_{ba}^{eff} depends on T and the relation (5.17) represents an implicit equation for T_{ba} .

Thus, the membrane fluctuations experience an effective barrier and the original state should be stable for $T < T_{ba}$. The membrane then stays in one of the two wells and thus exhibits two degenerate states with two different mean separations $l_1 \simeq l_{we}/2$ and $l_2 \simeq l_{ba} + 3l_{we}/2$. This implies that the membrane *cannot tunnel* through the intermediate potential barrier and will undergo a discontinuous transition between the two different states for $T < T_{ba}$ [105]. Such a discontinuous transition has been recently observed in Monte Carlo simulations [108]. For $T > T_{ba}$, on the other hand, the edge entropy wins, the membrane feels no effective barrier and thus has a unique ground state.

Now, consider a membrane which experiences the asymmetric potential

$$V(l) = \begin{cases} \infty & \text{for } l < 0, \\ -|U_{we}| & \text{for } 0 < l < l_{we}, \\ U_{ba} & \text{for } l_{we} < l < l_{we} + l_{ba}, \\ 0 & \text{for } l_{we} + l_{ba} < l, \end{cases} \quad (5.18)$$

see fig. 12(b) as appropriate for unbinding from a potential well in the presence of a potential barrier.

Assume that the membrane is originally confined within the potential well. A segment of linear size L_{\parallel} then has the free energy

$$\Delta F_0 \simeq (-|U_{we}| + c_3 T^2 / \kappa l_{we}^2) L_{\parallel}^2.$$

If this segment is thermally excited to overcome the potential barrier, it will form a ‘hump’ with free energy $\Delta F_1 \simeq \Delta F_e + c_4 T$ where the first term represents the edge free energy (arising from the potential barrier) and the second term represents the entropy loss of the L_{\parallel} -hump. The excess free energy of the hump is given by $\Delta F \equiv \Delta F_1 - \Delta F_0$ and thus by

$$\Delta F \simeq (|U_{we}| - c_3 T^2 / \kappa l_{we}^2) L_{\parallel}^2 + [c_1 \sigma - c_2 T \ln(3) / a_{\parallel e}] L_{\parallel} + c_4 T. \quad (5.19)$$

The unbinding transition should occur when the coefficient of the L_{\parallel}^2 -term vanishes. In this case, the free energy of the membrane confined in the potential well is equal to the free energy of the unbound membrane. This leads to the estimate

$$T_{we} \sim (\kappa |U_{we}| l_{we}^2)^{1/2} \quad (5.20)$$

for the unbinding temperature.

However, this whole argument is only self-consistent as long as the membrane still feels an effective barrier at $T = T_{we}$. At the latter temperature, the effective barrier height $U_{ba}^{\text{eff}} = U_{ba}$ and the corresponding temperature $T_{ba} \sim (\kappa U_{ba} l_{ba}^2)^{1/2}$ as follows from (5.17). For $T < T_{ba}$, the membrane cannot tunnel through this effective barrier.

Therefore, the membrane will undergo a discontinuous unbinding transition from the potential well to infinity *provided* $T_{we} < T_{ba}$. For $T_{we} > T_{ba}$, on the other hand, there is no effective barrier at $T = T_{we}$ which implies that the unbinding transition should be continuous. If one expresses T_{ba} and T_{we} in terms of the parameters of the potential, one finds that the unbinding transition should be discontinuous for relatively large potential barriers with $U_{ba} l_{ba}^2 \gg |U_{we}| l_{we}^2$ but should be continuous for relatively small potential barriers with $U_{ba} l_{ba}^2 \ll |U_{we}| l_{we}^2$. Thus, the membrane tunnels through relatively weak barriers but is trapped by relatively strong ones.

These two types of transitions must be separated by a multicritical point. Within the functional renormalization group approach, such a multicritical transition should be described by a multicritical fixed point which has, however, not been found for fluid membranes as considered here [105–107]. This seems to be a deficiency of functional renormalization which remains to be clarified. A similar discrepancy has been recently pointed out for wetting transitions in d dimensions [109]. In this case, functional renormalization predicts that discontinuous transitions do not occur for $d < d_* \simeq 2.6$ whereas Peierls type arguments imply that such transitions can occur as soon as $d > 2$.

Thus, if the direct interaction contains a sufficiently high potential barrier, the membrane should unbind in a discontinuous way at zero pressure. By continuity, this implies discontinuous transitions at nonzero pressure, $P > 0$ [92]. Indeed, the interaction potential $V_P(l) = Pl + V(l)$ will then exhibit two local minima separated by a large barrier, and one will have discontinuous transitions between two different states which are both characterized by a finite value of the mean separation.

5.7. Tension-induced adhesion

As explained within the hump picture, lateral tension acts to suppress the bending undulations and thus to suppress the fluctuation-induced repulsion. In fact, this interaction now becomes short-ranged and cannot compete with the attraction arising from long-ranged Van der Waals forces. Therefore, if the direct interaction $V(l)$ is governed, for large l , by attractive Van der Waals forces, the membranes form a bound state in the presence of lateral tension [85]. An unbinding can only occur if the Hamaker constant $|H|$ or the lateral tension Σ go to zero. This situation is completely analogous to the behavior of wetting layers in fluid systems [110].

In the limit of small Σ , the fluctuation-induced interaction has the form

$$V_{\text{fl}}(\xi_{\perp}) \sim T\Sigma/\kappa(e^{2(\xi_{\perp}/l_{\Sigma})^2} - 1) \quad (5.21)$$

with the length scale $l_{\Sigma} = (T/2\pi\Sigma)^{1/2}$, see appendix A. Thus, the fluctuation-induced interaction is still governed by bending undulations as long as $\xi_{\perp} \ll l_{\Sigma}$.

If the shape fluctuations are governed by bending modes, the parallel correlation length ξ_{\parallel} satisfies $\xi_{\parallel} \approx (16\kappa/T)^{1/2}\xi_{\perp}$, see appendix A. This relation together with the inequality $\xi_{\perp} \ll l_{\Sigma}$ implies $\Sigma \ll 16\kappa/\xi_{\parallel}^2$. For a membrane segment of linear size $\xi_{\parallel} = 1 \mu\text{m}$ and bending rigidity $\kappa = 10^{-19} \text{ J}$, the bending undulations are not affected by the lateral tension Σ if $\Sigma \ll 10^{-4} \text{ mJ/m}^2$.

In the limit of zero Σ , the membranes must attain a bound state for $T < T_{*}$ or $|H| > |H_{*}|$, i.e. if the Van der Waals attraction is sufficiently strong. On the other hand, they will continuously unbind for $T > T_{*}$ or $|H| < |H_{*}|$, i.e. if the Van der Waals attraction is sufficiently weak. In the latter case, one may estimate the behavior of the mean separation ℓ by superimposing $V(l)$ and $V_{\text{fl}}(\xi_{\perp})$ as given by (5.15). One then finds that

$$\ell \sim \xi_{\perp} \simeq l_{\Sigma} = (T/2\pi\Sigma)^{1/2} \quad (5.22)$$

for small Σ and $T > T_{*}$ (or $|H| < |H_{*}|$).

The scaling relation $\ell \sim 1/\Sigma^{1/2}$ has been obtained in ref. [41] from a superposition of the fluctuation-induced interaction V_{fl} and the direct interaction $\Delta V(l) \sim H/l^2$ as obtained from the half space approximation for the Van der Waals forces, see (3.4). The same scaling relation is obtained if one treats the tension term,

$$\int d^2x \frac{1}{2} \Sigma (\nabla l)^2,$$

as a perturbation of the completely repulsive hard wall fixed point of the RG transformation [50]. The rescaling transformation $x \rightarrow x' = x/b$ and $l \rightarrow l' = l/b$ now leads to

$$\Sigma \rightarrow \Sigma' = b^{\lambda_{\Sigma}} \Sigma \quad \text{with } \lambda_{\Sigma} = 2, \quad (5.23)$$

which implies

$$\ell \sim \xi_{\perp} \sim \xi_{\parallel} \sim 1/\Sigma^{\nu_{\parallel}} \quad \text{with } \nu_{\parallel} = 1/\lambda_{\Sigma} = 1/2 \tag{5.24}$$

for small Σ and $T > T_*$. Since the hard wall fixed point governs all direct interactions with $|H| < |H_*|$, the asymptotic behavior of ℓ should be given by $\ell \approx c\ell_{\Sigma} = c(T/2\pi\Sigma)^{1/2}$ where the dimensionless coefficient c does *not* involve the Hamaker constant H . The same behavior will apply to all interactions within the strong fluctuation regime. On the other hand, interactions within the intermediate fluctuation regime will again lead to nonuniversal behavior.

6. Stacks and bunches of membranes

Lipid bilayers in solution often form stacks or bunches (or multilayers or lamellar states) in which several membranes are, on average, parallel to each other. Large oriented stacks corresponding to lyotropic liquid crystals have been studied for a long time by X-ray and neutron scattering methods. On the other hand, bunches containing only a relatively small number of membranes are also accessible to experiments: freely suspended bunches can be directly observed in the light microscope whereas multilayers attached to a fluid-vapor interface can be investigated by surface reflectivity measurements. Likewise, stacks of bilayers spread on a solid substrate such as a glass slide are often used in order to prepare lipid vesicles.

Thus, consider such a stack of many membranes which has been prepared by deposition of lipid onto a planar solid substrate. Far from this surface, the membranes will attain a constant mean separation ℓ . As in the case of two interacting membranes, the mean separation ℓ within the stack is determined by the interplay of direct interactions and undulations.

As far as the membrane roughness arising from these undulations is concerned, it is now important to distinguish several length scales. On scales which are smaller or comparable with the membrane separation ℓ , the membranes exhibit the humps of lateral size ξ_{\parallel} and roughness ξ_{\perp} as discussed previously. On length scales which are larger than ℓ , one must distinguish the case of a finite stack from the case of an infinite stack.

An infinite stack of membranes corresponds to a lyotropic liquid crystal. In this case, a single ‘tracer’ membrane within the stack exhibits the logarithmic roughness

$$L_{\perp} \sim \ell \sqrt{\ln(L_{\parallel}/\xi_{\parallel})} \quad \text{for } L_{\parallel} \gg \xi_{\parallel}. \tag{6.1}$$

This behavior is derived in appendix B from a harmonic model for the lyotropic liquid crystal. Thus, a single membrane within the infinite stack is almost but not quite flat on large scales.

If the stack contains a finite number of membranes and if it is free, i.e. not attached to another interface or wall, its ‘center-of-mass’ coordinate will also undulate. As shown in the next subsection the roughness of this coordinate scales as

$$L_{0\perp} \sim \sqrt{T/(N+1)\kappa_1} L_{\parallel} \quad \text{for large } L_{\parallel} \tag{6.2}$$

for a stack consisting of $(N + 1)$ identical membranes with bending rigidity κ_1 . For small N , the regime described by (6.1) is not accessible and the roughness of a single membrane is governed by the roughness $L_{0\perp}$ as soon as $L_{\parallel} \gg \xi_{\parallel}$. For large N , one has the additional crossover length

$$L_* \simeq \ell \left\{ [(N + 1)\kappa_1/T] \ln [(N + 1)\kappa_1/T] \right\}^{1/2} \sim \xi_{\parallel} \sqrt{N \ln N}. \quad (6.3)$$

Thus, on length scales L_{\parallel} with $\xi_{\parallel} \ll L_{\parallel} \ll L_*$, a single membrane exhibits the same logarithmic roughness as in the infinite stack. For $L_{\parallel} \gg L_*$, on the other hand, the roughness is governed by $L_{0\perp}$ as given by (6.2).

In the following, I will focus on length scales which are smaller or comparable to ξ_{\parallel} . The bending undulations on these length scales determine, together with the direct interaction, the mean separation of the membranes within the stack.

6.1. Model for many interacting membranes

Consider a bunch of $(N + 1)$ membranes which are, on average, parallel to a reference plane. The distance of membrane (n) from this reference plane is denoted by the height variable h_n with $n = 0, 1, \dots, N$.

The configurational energy (or effective Hamiltonian) for this bunch is given by

$$\begin{aligned} \mathcal{H}\{\underline{h}\} = \int d^2x \left\{ \sum_{n=1}^N V_n(h_n - h_{n-1}) + P \sum_{n=1}^N (h_n - h_{n-1}) \right. \\ \left. + \frac{1}{2} \sum_{n=0}^N \kappa_n (\nabla^2 h_n)^2 \right\}. \end{aligned} \quad (6.4)$$

Note that

$$\sum_{n=1}^N (h_n - h_{n-1}) = h_N - h_0.$$

The asymmetric stack corresponds to $\kappa_0 = \infty$ and $\kappa_n = \kappa_1$ for $n \geq 1$.

Even though the membrane positions within the stack are described by $(N + 1)$ fields h_n , only N of these variables are coupled by the direct interactions $V_n(l)$. This is obvious for the asymmetric stack on top of a rigid wall since the position of this wall does not fluctuate and $h_0 = \text{const}$. In general, one has a 'center-of-mass' coordinate l_0 which decouples from the N relative displacement fields $l_n = h_n - h_{n-1}$ with $n \geq 1$.

For $(N + 1)$ identical membranes with bending rigidity κ_1 , the 'center-of-mass' coordinate is given by

$$l_0 = \frac{1}{N + 1} \sum_{n=0}^N h_n. \quad (6.5)$$

It is not difficult to find an orthogonal transformation from the variables h_0, \dots, h_N to new variables y_0, \dots, y_N for which $y_0 = \sqrt{N+1} l_0$ and the remaining variables y_1, \dots, y_N are linear combinations of the relative displacement fields l_1, \dots, l_N . In this way, one can show that the ‘center-of-mass’ coordinate l_0 is decoupled from the relative displacement fields l_n and is governed by the effective Hamiltonian

$$\mathcal{H}_0\{l_0\} = \int d^2x \frac{1}{2} (N+1)\kappa_1 (\nabla^2 l_0)^2. \quad (6.6)$$

Thus, the corresponding bending rigidity is $(N+1)\kappa_1$. It then follows from the scaling properties of bending undulations that the ‘center-of-mass’ roughness $L_{0\perp} \equiv [(\langle l_0 - \langle l_0 \rangle \rangle^2)]^{1/2}$ scales as

$$L_{0\perp} \sim \sqrt{T/(N+1)\kappa_1} L_{\parallel} \quad (6.7)$$

for a bunch of lateral size L_{\parallel} . This roughness decays to zero as $1/\sqrt{N+1}$ with increasing N .

The separation of the membranes within the stack are determined by the mutual interactions or forces. In the absence of shape fluctuations, the balance of forces within the stack implies

$$P = P_n = -\partial V_n(l_n)/\partial l_n \quad \text{for } l_n = \ell_n. \quad (6.8)$$

More precisely, the disjoining force per unit area which membrane $(n-1)$ exerts onto membrane (n) is given by $P_n \hat{e}_z$ where \hat{e}_z is the unit vector perpendicular to the membranes which points from $(n-1)$ to (n) . Likewise, membrane (n) exerts the force density $-P_n \hat{e}_z$ onto membrane $(n-1)$.

In the presence of shape fluctuations, the direct interaction $V_n(l)$ becomes renormalized into $V_n^R(l)$, and the balance of forces becomes

$$P = P_n = -\partial V_n^R(l_n)/\partial l_n \quad \text{for } l_n = \ell_n. \quad (6.9)$$

This equation may be regarded as a definition of the renormalized interaction between the membranes.

6.2. One-membrane approximation

Now, consider a stack of $(N+1)$ identical membranes interacting with identical pair potentials, $V_n(l) = V(l)$. In the limit of large N , the membrane stack corresponds to a lyotropic liquid crystal. Far from the boundaries of such a crystal, all relative displacement fields $l_n = h_n - h_{n-1}$ will have the same mean value, $\langle l_n \rangle = \ell$. On length scales which are large compared to the correlation length ξ_{\parallel} , a single ‘tracer’ membrane makes arbitrarily large excursions from its average position, see (6.1). In the one- and two-membrane approximations discussed below, the corresponding

roughness which grows only logarithmically with the membrane size will be ignored. One may then assume that, each membrane feels an effective potential

$$U^{\text{eff}}(h_n) \approx U_0^{\text{eff}} + \frac{1}{2} U_2^{\text{eff}} (h_n - \langle h_n \rangle)^2 \quad (6.10)$$

which is harmonic for small fluctuations of h_n around its mean value $\langle h_n \rangle$.

The one-membrane approximation is obtained if one ignores the fluctuations of the two nearest neighbor membranes and treats them as two rigid walls at positions $h_{n-1} = \langle h_n \rangle - \ell$ and $h_{n+1} = \langle h_n \rangle + \ell$, respectively. This geometry was first used by Helfrich in order to estimate the excess free energy (or loss of entropy) of the membrane confined in the stack [2]. As mentioned by de Gennes and Taupin, [16] this approximation represents the analogue of the Einstein model for lattice vibrations or phonons of solids.

Several authors have used this geometry in an attempt to determine the effective potential $U^{\text{eff}}(h_n)$ starting from the direct interactions $V(l)$ between nearest neighbor membranes [111–115]. In this work, the mean separation ℓ was treated as an independent parameter even though its value is determined by the interaction potential $V(l)$. In some cases, the bare potential acting on the membrane was taken to be [111, 113, 115]

$$U^{\text{eff}}(h_n) = V(\ell + h_n - \langle h_n \rangle) + V(\ell - h_n + \langle h_n \rangle). \quad (6.11)$$

This latter approach has two additional problems:

- (i) Since one has $l_n + l_{n+1} = 2\ell$, the two independent degrees of freedom l_n and l_{n+1} have been reduced to a single degree of freedom. In fact, if the separation l_n increases, the separation $l_{n+1} = 2\ell - l_n$ must decrease. Thus, *all fluctuations in which l_n and l_{n+1} are displaced in the same direction are suppressed*. In the context of lattice vibrations of solids, this is a well-known defect of the Einstein model: it gives an approximate description of optical phonons in which neighboring atoms move against each other but fails to describe acoustical phonons in which neighboring atoms move in phase. In the limit of long wavelengths, the energy of acoustical phonons goes to zero whereas the energy of optical phonons attains a finite limit. Thus, thermal fluctuations will primarily excite acoustical phonons which are not contained in the Einstein model; and
- (ii) If the direct interaction $V(l)$ has an attractive part and thus a minimum, the superposition potential as in (6.11) may have two (degenerate) minima. If the membrane experienced such a potential, its position could attain two possible values as explained in section 5.6 [105]. However, such a spontaneous symmetry breaking would be an artefact of the approximation used to obtain (6.11).

6.3. Two-membrane approximation

In order to overcome the limitations of the one-membrane approximation, one may focus on a *pair* of nearest-neighbor membranes within the stack with $n = a$ and

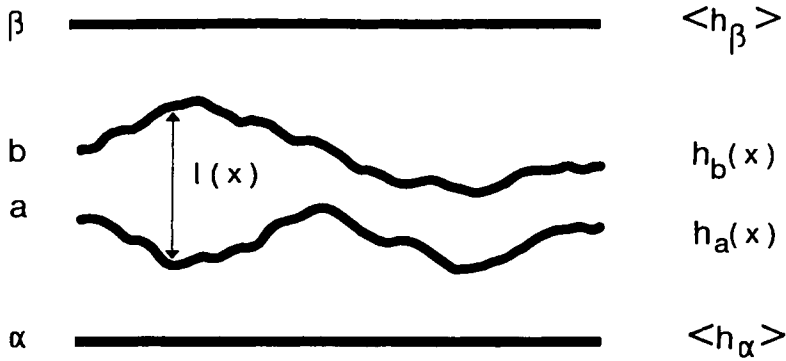


Fig. 13. Geometry of two-membrane approximation for a bunch of membranes. The outer membranes α and β are replaced by rigid walls at positions $\langle h_\alpha \rangle$ and $\langle h_\beta \rangle$, respectively.

$n = a + 1 \equiv b$, see fig. 13. These two membranes interact with each other and with the two adjacent membranes with $n = a - 1 \equiv \alpha$ and $n = b + 1 \equiv \beta$, see fig. 13.

Within such a two-membrane approximation which is of the mean-field type, the two membranes with $n = \alpha$ and $n = \beta$ are replaced by rigid walls with positions $\langle h_\alpha \rangle = \langle h_a \rangle - \ell_a$ and $\langle h_\beta \rangle = \langle h_b \rangle + \ell_\beta$, respectively. In addition, the two-membrane interactions $V_\alpha(h_a - h_\alpha)$ and $V_\beta(h_\beta - h_b)$ are approximated by the renormalized interactions $V_\alpha^R(h_a - \langle h_\alpha \rangle)$ and by $V_\beta^R(\langle h_\beta \rangle - h_b)$, respectively. If one now expands these interaction energies in powers of $h_a - \langle h_a \rangle$ and $h_b - \langle h_b \rangle$, one obtains

$$\begin{aligned}
 &V_\alpha^R(h_a - \langle h_\alpha \rangle) + V_\beta^R(\langle h_\beta \rangle - h_b) \\
 &\approx V_\alpha^R(\ell_a) + V_\beta^R(\ell_\beta) - P\ell_b + P(h_b - h_a)
 \end{aligned}
 \tag{6.12}$$

for small fluctuation amplitudes. If the last term is combined with all terms of $\mathcal{H}\{\underline{h}\}$ as given by (6.4) which depend explicitly on h_a and h_b , one obtains the same effective Hamiltonian $\mathcal{H}\{h_a, h_b\}$ as for two interacting membranes which are subject to the external pressure P . Therefore, the relative displacement field $l = h_b - h_a$ is governed by

$$\mathcal{H}\{l\} = \int d^2x \left\{ Pl + V(l) + \frac{1}{2} \kappa (\nabla^2 l)^2 \right\}
 \tag{6.13}$$

with the effective bending rigidity $\kappa = \kappa_1/2$. This model was the starting point for the systematic theory in section 5, see (5.1). Therefore, within this approximation, the renormalized potential of two membranes within the bunch is identical with the renormalized potential of two isolated membranes. This reduction of a stack of membranes to two membranes was introduced by us in refs [3, 92] and [93].

Within this two-membrane approximation, one can determine the mean separation ℓ as a function of the external pressure P . On the other hand, if ℓ is fixed by external

constraints such as the lipid-solvent composition, one may choose P in such a way that it leads to the required value for ℓ .

Even though the geometry shown in fig. 13 does not include all configurations of the two membranes in the stack, these two membranes can fluctuate more freely than the single membrane between two rigid walls as used in the one-membrane approximation. In particular, the two-membrane approximation includes those configurations in which these two membranes are displaced in the same direction. Finally, no spurious symmetry breaking can occur within the two-membrane approximation if the direct interaction $V(l)$ has only a single minimum.

6.4. Hard-wall interaction

The simplest pair potential for the membranes in the stack is again provided by

$$V_P(l) = V_{hw}(l) + Pl, \quad (6.14)$$

i.e. by the competition between the repulsive hard wall interaction and the attractive pressure term. *Two* identical membranes interacting with such a potential have been discussed in section 5.2. As explained in this latter section, this potential is renormalized into

$$V^{\text{eff}}(l) = 2c_{\text{fl}}T^2/\kappa_1l^2 + Pl$$

with $2c_{\text{fl}} = 0.115 \pm 0.005 \simeq 3\pi^2/256$ where κ_1 is the bending rigidity of each membrane.

In the case of $(N + 1)$ identical membranes with bending rigidity κ_1 , the renormalized pair potential should have the form

$$V^{\text{eff}}(l) \approx 2c_{\text{fl}}(N + 1)T^2/\kappa_1l^2 + Pl \quad (6.15)$$

in the limit of small P where, a priori, the coefficient $c_{\text{fl}}(N + 1)$ is expected to depend on N . However, extensive Monte Carlo simulations for a stack of three and of four membranes strongly indicate, that the coefficient c_{fl} is in fact independent of N [80, 81].

The MC data for three membranes are shown in fig. 14. These data lead to the numerical estimate $2c_{\text{fl}}(3) = 0.113 \pm 0.005$. Likewise, the MC simulations for four membranes show that all three separation variables l_1 , l_2 , and l_3 have the same asymptotic behavior governed by $2c_{\text{fl}}(4) = 0.113 \pm 0.005$. Within the numerical accuracy of these estimates which is of the order of one percent, the three values for c_{fl} are identical.

This asymptotic separability is not restricted to stacks of identical membranes. It has also been confirmed for asymmetric stacks in which membrane (0) at the bottom of the stack has infinite rigidity and thus corresponds to a rigid wall. In this case, the membrane pair (01) which contains membrane (0) is governed by $\kappa_{\text{eff}} = \kappa_1$ whereas all other pairs are governed by $\kappa_{\text{eff}} = \kappa_1/2$. Therefore, the effective pair potential

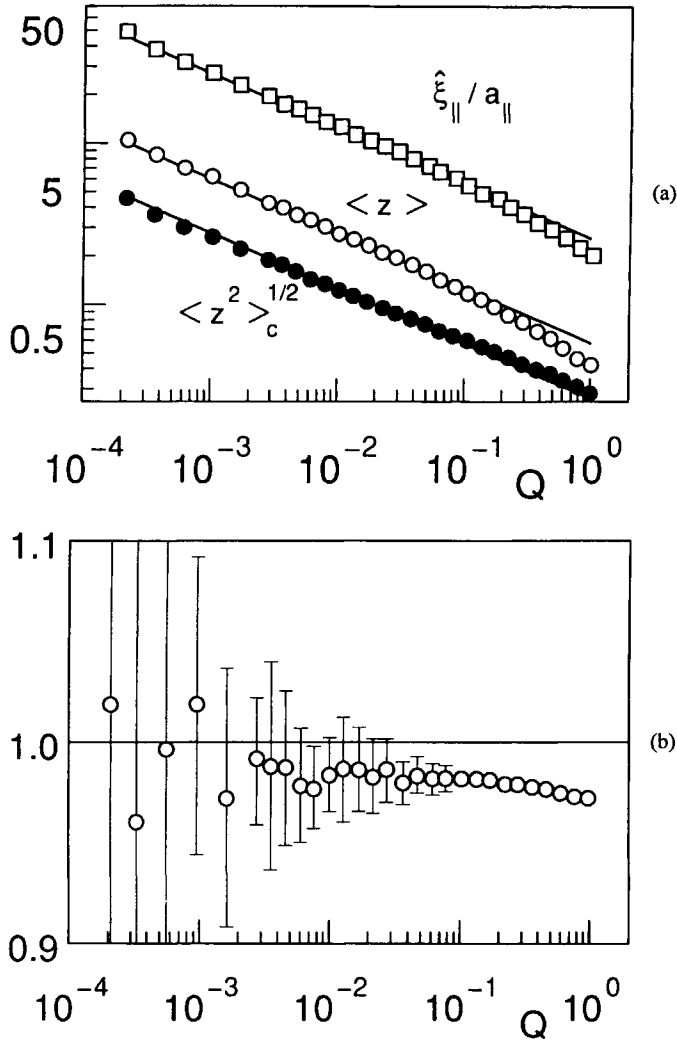


Fig. 14. Monte Carlo data for three membranes which repel each other by hard wall interactions: (a) The mean separation $\langle z \rangle$, the roughness $\langle z^2 \rangle_c^{1/2}$ and the longitudinal correlation length $\hat{\xi}_{\parallel}$ as a function of the pressure $Q = P/P_{sc}$ as in fig. 8; and (b) The ratio of the mean separation for the three-membrane system and of the mean separation for the two-membrane system seems to approach unity for small Q [80].

should be $V^{eff}(l) \approx c_{fl} T^2 / \kappa_1 l^2$ for the (01) pair and $V^{eff}(l) \approx 2c_{fl} T^2 / \kappa_1 l^2$ for all other pairs. This is exactly what is observed in the MC simulations.

As mentioned before, the value $2c_{fl} = 0.115 \pm 0.005$ is very close to $3\pi^2/256$ which is exactly half the value proposed originally [2] and deduced experimentally by X-ray scattering on lamellar phases in oil-water-surfactant mixtures, see appendix B. The value of the coefficient c_{fl} has also been estimated, in the limit of large N , using

functional renormalization [116]. As a result, one obtains the estimate $2c_\infty \simeq 0.081$ which is somewhat too small.

Another geometry which has been studied by MC simulations are N identical membranes with bending rigidity κ_1 confined between two rigid walls [117, 118]. The separation of these two rigid walls was taken to be $(N + 1)\ell$ so that the mean separation of all nearest neighbor surfaces is close to ℓ . The excess free energy density $\Delta f_N(\ell)$ per membrane was determined via the internal energy density which can be measured directly in the MC simulations. The MC data were well fitted by the asymptotic form $\Delta f_N(\ell) \approx 2c_N T^2 / \kappa_1 \ell^2$ with $2c_1 \simeq 0.080$, $2c_3 \simeq 0.093$, and $2c_5 \simeq 0.097$ for $N = 1, 3$ and 5 membranes [117]. Extrapolation of these data to large N gave the estimate $2c_\infty \simeq 0.106$ which is somewhat smaller than the value $2c_{\text{fl}} = 0.115 \simeq 3\pi^2/256$ as obtained in the pressure ensemble. The latter value should be more reliable, however, since it is independent of N and thus involves no extrapolation procedure.

Thus, for the competition of the hard wall interaction and the external pressure, the two-membrane approximation becomes presumably exact in the limit of small P , i.e. as the membranes unbind, provided one studies those scaling properties which involve only pairs of nearest-neighbor membranes. In other words: each pair of neighboring membranes behaves asymptotically as if it were not affected by the presence of the other membranes within the stack. This implies that the contact probability \mathcal{P}_{2b} for two membranes within the bunch should satisfy $\mathcal{P}_{2b} \sim 1/\xi_\perp^{\zeta_0}$ with $\zeta_0 = 3$ as for two isolated membranes.

If one considers the behavior of more than two membranes, more subtle critical effects are expected by analogy with strings. Indeed, bundles of strings which interact via hard wall interactions are characterized by the contact probabilities $\mathcal{P}_{nb} \sim 1/\xi_\perp^{2\zeta_0(n)}$ with $\zeta_0(n) = (n^2 - 1)/2$ where \mathcal{P}_{nb} describes the probability to find a locally bound bundle of n strings [119, 120]. Therefore, one expects the analogous scaling relation $\mathcal{P}_{nb} \sim 1/\xi_\perp^{\zeta_0(n)}$ with $\zeta_0(n) = n^2 - 1$ for the probabilities \mathcal{P}_{nb} to find locally bound bunches of n membranes within the larger stack of N membranes.

Scaling and renormalization group arguments imply that these scaling properties are valid as long as the direct interactions between two nearest-neighbor membranes are short-ranged and effectively repulsive (and one does not include next-nearest neighbor interactions or n -membrane interactions with $n > 2$). For this class of direct interactions, the mean separation of two adjacent membranes should asymptotically behave as in the case of two isolated membranes. It is not obvious, however, that this asymptotic separability also applies in the presence of *attractive* forces between the membranes.

6.5. Cohesion of freely suspended bunches

Bunches of identical lipid membranes in aqueous solution have been experimentally studied by phase contrast microscopy. For membranes composed of the sugarlipid DGDG, Helfrich and Mutz observed unbinding transitions for bunches between two and twenty membranes, see fig. 15 [4]. The transitions showed no hysteresis and

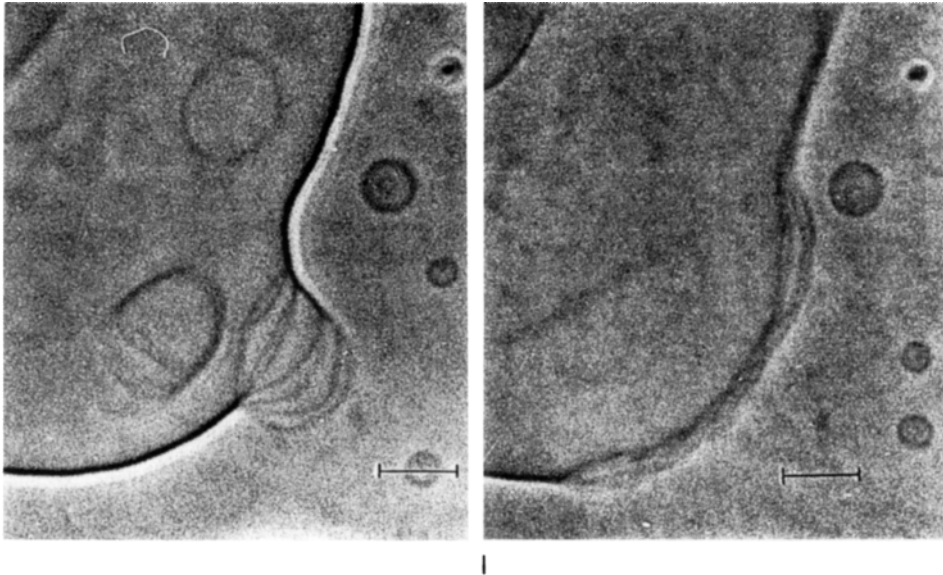


Fig. 15. Unbinding transition of a bunch of DGDG bilayers as observed by phase contrast microscopy. (right) For $T \approx 22.4^\circ\text{C}$, the membranes undulate very strongly and then appear as thick fuzzy lines; and (left) For $T \approx 22.1^\circ\text{C}$, the membranes form a bound state which corresponds to the sharp dark line. The water between the membranes has been squeezed into the large water pocket. The bars represent $10 \mu\text{m}$. (Courtesy of W. Helfrich.)

thus appeared to be continuous. The bilayers within the bunch should attract each other by Van der Waals forces and thus should experience direct interactions with a single minimum. Now, one would like to know if the critical phenomena at these unbinding transitions depend on the number of membranes contained in the bunch. It turns out that the transition temperature is independent of the number of membranes but that the critical behavior depends on this number.

6.5.1. Computer simulations of three membranes

In order to be more specific, consider the case of three membranes with identical bending rigidities $\kappa_1 = \kappa_2 = \kappa_3$. The configuration of membrane (n) is described by the height variable h_n with $n = 0, 1$ and 2 . The two nearest neighbor pairs experience, apart from the hard wall repulsion, a direct interaction of the square well form as given by

$$\Delta V(l) = \begin{cases} U & \text{for } 0 < l < l_v, \\ 0 & \text{for } l_v < l, \end{cases} \tag{6.16}$$

with $U < 0$.

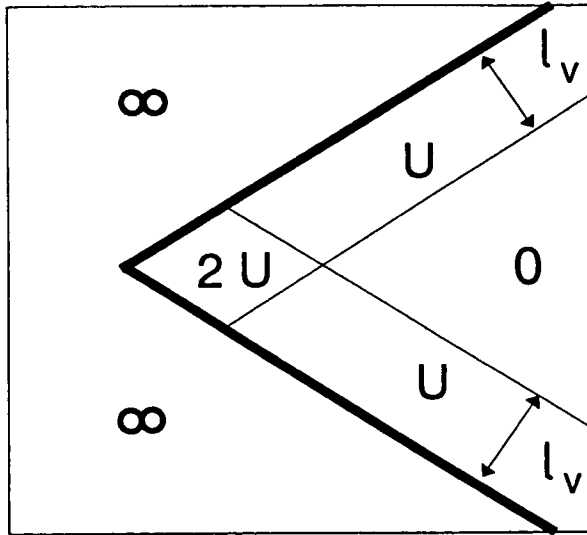


Fig. 16. Effective interaction potential of three membranes. Neighboring membranes interact via repulsive hard wall and attractive square well interactions with potential depth $U < 0$ and potential range l_v .

It is convenient to introduce new coordinates y_0 , y_1 , and y_2 via the orthogonal transformation

$$\begin{aligned}
 y_0 &\equiv (h_0 + h_1 + h_2)/\sqrt{3} = \sqrt{3}l_0, \\
 y_1 &\equiv (h_1 - h_0)/\sqrt{2} = l_1/\sqrt{2}, \quad \text{and} \\
 y_2 &\equiv \sqrt{2}(h_2 - h_1)/\sqrt{3} + (h_1 - h_0)/\sqrt{6} = \sqrt{2}l_2/\sqrt{3} + l_1/\sqrt{6}.
 \end{aligned}
 \tag{6.17}$$

In this way, the ‘center-of-mass’ coordinate $l_0 = y_0/\sqrt{3}$ is separated off from the two coordinates y_1 and y_2 which are linear combinations of the relative displacement fields $l_1 = h_1 - h_0$ and $l_2 = h_2 - h_1$. The two fields y_1 and y_2 are governed by the effective Hamiltonian [121, 122]

$$\mathcal{H}\{y_1, y_2\} = \int d^2x \left\{ V(y_1, y_2) + \frac{1}{2} \kappa_1 \sum_{n=0}^2 (\nabla^2 y_n)^2 \right\}
 \tag{6.18}$$

with the effective potential

$$V(y_1, y_2) = V(\sqrt{2}y_1) + V((\sqrt{3}y_2 - y_1)/\sqrt{2}).
 \tag{6.19}$$

This two-dimensional potential is shown in fig. 16. It consists of two hard walls which form a wedge with angle $\theta = \pi/3$. The attractive potential well lies in front of these walls. In the corner of the wedge, the depth of the potential is $2|U|$; otherwise, it is $|U|$.

The bunch considered here is up-down symmetric in the sense that it is invariant under an exchange of the two outer membranes. This symmetry implies that these two outer membranes must unbind *simultaneously* at the unbinding temperature $T_* = T_*^s(3)$ (where the superscript s indicates that the bunch is symmetric).

The above model for three membranes has been studied by extensive Monte Carlo simulations [5, 121]. Over the accessible range of length scales, the membranes undergo a continuous unbinding transition but the observed critical behavior is clearly different from the case of two membranes. The best fit for the mean separation $\ell = \langle l_1 \rangle = \langle l_2 \rangle$ leads to the power law $\ell \sim 1/|T - T_*^s(3)|^\psi$ with the effective critical exponent $\psi = 0.91 \pm 0.04$ which differs from the presumably exact value $\psi = 1$ for two membranes. The critical unbinding temperature $T_*^s(3)$, on the other hand, was found to be *identical* with the corresponding temperature $T_*^s(2)$ for two membranes [5].

The range of length scales which is accessible in the MC simulations of three membranes is limited by finite size effects and rather long equilibration times. Much more accurate data can be obtained by numerical transfer matrix calculations for three strings in two dimensions. Analysis of these data shows that the critical behavior of three strings is again very similar to the one of three membranes [5, 122, 123]. For three identical strings, interacting with the same pair potentials, the mean separation $\ell_1 = \langle l_1 \rangle = \ell_2 = \langle l_2 \rangle$ of two neighboring strings within the bundle diverges as $\ell_1 \sim 1/|T - T_*^s(3)|^\psi$ with $\psi \simeq 0.94$ over the accessible range of length scales which is again different from the exact value $\psi = 1$ for two strings. In contrast, the unbinding temperature $T_*^s(3)$ for three strings is again found to be identical with the corresponding temperature $T_*^s(2)$ for two strings within the numerical accuracy.

Originally, we thought that the observed N -dependence of the critical behavior could be understood in terms of an effective repulsion between the two outer membranes which arises from the loss of entropy of the confined membrane in the middle [121, 122, 124]. Such a mechanism is present in the so-called necklace model for interacting strings [125–127]. However, the necklace model predicts a discontinuous unbinding transition for three identical strings whereas the transfer matrix results clearly showed that the transition is continuous. In addition, the necklace model does not provide any clue why the unbinding temperature T_*^s should not depend on the number of membranes (or strings).

On the other hand, continuous transitions but with N -independent critical exponents were subsequently found

- (i) within two mean-field theories [128, 129], and
- (ii) by solving the string problem via Bethe Ansatz methods in which one essentially ignores the precise value of the potential energy of bound string triplets (i.e. the depth of the potential in the corner of the wedge, see fig. 16) [100, 130, 131].

The latter energy is effectively determined by 3-membrane interactions. The influence of these interactions has been studied in a systematic way by field-theoretic renormalization which predicts that this interaction leads to a pronounced crossover on intermediate scales but that it is irrelevant on sufficiently large scales [120]. Thus, the critical exponent for the asymptotic behavior is presumably $\psi = 1$ for

all N but the approach to asymptotic exhibits an intermediate scaling regime with an effective N -dependent exponent $\psi < 1$. The asymptotic critical behavior will be difficult to see in real systems whereas the intermediate scaling regime observed in the simulations might also be accessible to experiments.

6.5.2. N -state model for unbinding transition

The fact that the unbinding temperature T_*^s does not depend on N can be understood within the following scaling theory [98] which represents an extension of the two-state model described in section 5.4. Locally, three membranes (or strings) which interact via square well potentials can attain three different types of configurations, compare fig. 17:

- (i) All three membranes are ‘locally unbound’ if their separation exceeds the range of the interaction potential;
- (ii) two of the three membranes form a bound pair whereas the third one is ‘locally unbound’; and
- (iii) all three membranes form a bound triplet.

The probabilities for these three different local configurations will be denoted by \mathcal{P}_{ub} , \mathcal{P}_{2b} , and \mathcal{P}_{3b} , respectively.

For configuration (i), the loss of entropy per unit area will be denoted by ΔF_{ub} for each separation variable. On the other hand, the excess free energy per unit area for a bound pair and a bound triplet will be denoted by ΔF_{2b} and ΔF_{3b} , respectively. For interactions between nearest-neighbor pairs of membranes, one has $\Delta F_{3b} \simeq 2\Delta F_{2b}$. Thus, the excess free energy per unit area of the bunch can be estimated as [98]

$$\Delta F \simeq 2\Delta F_{ub}\mathcal{P}_{ub} + (\Delta F_{2b} + \Delta F_{ub})\mathcal{P}_{2b} + 2\Delta F_{2b}\mathcal{P}_{3b}. \quad (6.20)$$

If the unbinding transition is continuous, the probabilities \mathcal{P}_{2b} and \mathcal{P}_{3b} must vanish in a continuous way whereas $\mathcal{P}_{ub} \approx 1$ as the transition is approached. In addition, the scaling properties at such a transition will be governed by the single length scale ξ_{\perp} which determines the roughness of the separation variables l_1 and l_2 .

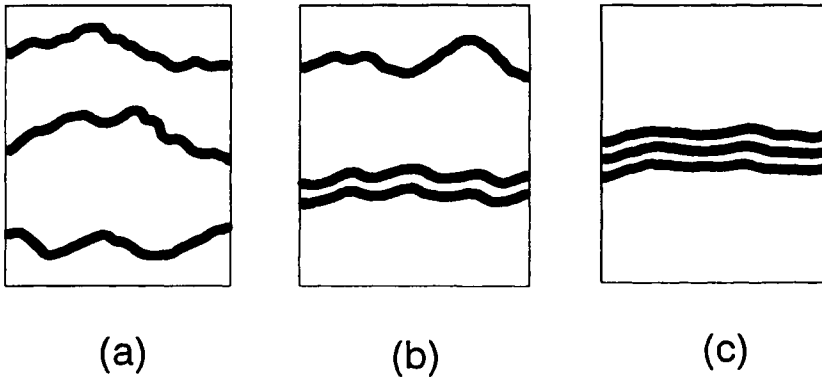


Fig. 17. Three-state model for unbinding transition of three identical membranes: (a) Locally unbound segments, (b) locally bound pairs, and (c) locally bound triplets.

So far, these arguments are rather general and apply to any kind of shape fluctuations (in particular, these arguments would also apply if the membranes exhibit an additional microroughness as proposed in ref. [132]). If the membranes undergo bending undulations, the entropy loss per unit area of ‘locally unbound’ membrane segments is given by $\Delta F_{\text{ub}} \sim T^2/\kappa\xi_{\perp}^2$. In order to determine ξ_{\perp} from this free energy, one has to know how the probabilities \mathcal{P}_{2b} and \mathcal{P}_{3b} depend on this length scale.

At a continuous transition, the probability distribution $\mathcal{P}(l_1, l_2)$ for the two separation variables l_1 and l_2 will exhibit the general scaling form

$$\mathcal{P}(l_1, l_2) \approx (l_v/\xi_{\perp})^2 \Omega(l_1/\xi_{\perp}, l_2/\xi_{\perp})$$

where l_v is the range of the square well potential. If the scaling function $\Omega(s_1, s_2)$ is finite for small arguments s_1 and s_2 , one has $\mathcal{P}_{2b} \sim (l_v/\xi_{\perp})$ and $\mathcal{P}_{3b} \sim (l_v/\xi_{\perp})^2 \sim \mathcal{P}_{2b}^2$. In general, one will have $\mathcal{P}_{3b} \ll \mathcal{P}_{2b}$ as long as one considers only two-membrane forces which act between nearest-neighbor pairs of membranes.

The behavior of ξ_{\perp} can now be determined by minimizing the excess free energy ΔF with respect to ξ_{\perp} . *The unbinding transition occurs when ΔF_{2b} vanishes.* Therefore, the transition of three membranes occurs at the same temperature T_*^s as the transition of two. For a square well potential of depth $|U|$, one has $\Delta F_{2b} \simeq -|U| + cT^2/\kappa l_v^2$ where the first and the second term represent the interaction energy and the entropy loss within the square well, respectively. Thus, one has $T_*^s \simeq \sqrt{\kappa|U|l_v^2/c}$.

The minimization of ΔF leads to a continuous unbinding transition at $T = T_*^s$ with $\xi_{\perp} \sim 1/|T_*^s - T|^{\psi}$. The critical exponent ψ has the universal value $\psi = 1$ if the probability for bound pairs behaves as $\mathcal{P}_{2b} \sim 1/\xi_{\perp}$. On the other hand, if the probability distribution $\mathcal{P}(l_1, l_2)$ appeared to be singular for small arguments over a certain range of length scales, one would have $\mathcal{P}_{2b} \sim 1/\xi_{\perp}^{1-b}$ for these scales. This would lead to the same unbinding temperature T_*^s but to the effective critical exponent $\psi = 1/(1 + b)$.

The scaling arguments just described can be directly extended to symmetric bunches containing an arbitrary number N of membranes. One again finds the N -independent unbinding temperature T_*^s whereas the critical behavior of ξ_{\perp} depends on the behavior of the probability distribution for small values of the separation variables. Furthermore, the behavior discussed here is not restricted to the case of square well potentials but also applies to realistic Van der Waals interactions and to all other attractive interactions within the strong-fluctuation regime.

The N -state model described here implies that the unbinding transition of N membranes is continuous for all values of N provided the direct interaction potential of adjacent membranes has a single minimum and no potential barrier. In contrast, it has been argued in ref. [94] that the unbinding transition of a membrane stack becomes discontinuous as a result of balloon-type fluctuations. For two-membrane forces, these latter fluctuations should be very exceptional compared to the bending modes considered here and thus should not determine the nature of the unbinding transition.

On the other hand, if the direct interaction between two adjacent membranes has a sufficiently high potential barrier, two different states can coexist as explained in section 5.6. If one changes the temperature and the lipid-solvent composition (or an effective external pressure), the phase diagram should then exhibit two-phase coexistence regions where two lamellar phases with two different spacings coexist as has been observed in some experimental systems.

6.6. Adhesion to a substrate or another interface

As mentioned, many preparation methods lead to bunches of membranes which stick to a solid substrate or another interface. Thus, let us consider a bunch of N identical membranes with bending rigidity κ_1 which adheres to another surface. This represents the limiting case of the model as given by (6.4) in which the bottom membrane with $n = 0$ has infinite rigidity. In general, the interaction $V_1(l) \equiv V_s(l)$ between the substrate and the membrane with $n = 1$ will differ from the mutual interaction $V(l)$ between two membranes within the bunch.

If the interaction potential V_s is relatively weak compared to the mutual interaction potential V , the separation of the two outer membranes of the bunch will stay finite while the whole bunch unbinds from the substrate at a critical temperature $T_*^a < T_*^s$ [100, 131]. In this case, the bunch has the effective bending rigidity $\kappa_{\text{eff}} = N\kappa_1$. If the substrate potential $V_s(l)$ is taken to be a square well potential with depth $|U_s|$ and range l_v , the unbinding temperature T_*^a is proportional to $\sqrt{N\kappa_1|U_s|l_v^2}$ which must be smaller than $T_*^s \sim \sqrt{\kappa_1|U|l_v^2}$.

On the other hand, if V_s is comparable with or stronger than V , the stack undergoes a *sequence of unbinding transitions* at successive temperatures $T_*^a(n)$ with $T_*^s \leq T_*^a(n) \leq T_*^a(1)$ [5, 122]. Thus, all unbinding transitions occur in a finite temperature range, and the last membrane unbinds at the temperature $T_*^a(1)$. At all of these transitions, the critical behavior is universal and the critical exponent $\psi = 1$. For large n , the unbinding temperatures $T_*^a(n)$ attain the limiting value T_*^s . In this limit, one expects $T_*^a(n) - T_*^s \sim 1/n^\lambda$. Extrapolation of the numerical data obtained for $n \leq 3$ gives the rough estimate $\lambda \simeq 2$ [5]. On the other hand, the analytical solution for strings via the Bethe ansatz leads to $\lambda = 1$ [100, 131].

In real systems, this sequence of unbinding transitions corresponds to a stack on top of a substrate from which the utter most membranes peel off one after another.

7. Hydration forces and protrusion modes

The shape fluctuations which have been considered in the previous sections represent bending undulations. These should be the typical excitations on length scales which are large compared to the membrane thickness. However, the concept of a bending mode is no longer well-defined as soon as the wavelength becomes of the order of the membrane thickness. On these latter length scales, the molecular structure of the lipid-water interface should be taken into account. This interface is roughened by the relative displacements or protrusions of the lipid molecules as has been observed in computer simulations [133, 134] and in scattering experiments [36, 135, 136]. In

contrast to bending modes, protrusions change the surface area of the lipid-water interface [51, 54] and are thus governed by an effective interfacial tension.

Protrusion modes must be distinguished from ‘blisters’ [137] which have been proposed in order to explain the hydration interaction between bilayers attached to mica surfaces. Such a blister consists of a curved bilayer domain which is not attached to the mica surface and which is governed by its bending energy. Therefore, in contrast to protrusions, blisters are special bending modes.

In this section, the effect of protrusion modes on the membrane interactions will be discussed. First, pure protrusions will be considered in which the molecules are displaced but not tilted [51]. These protrusions renormalize the direct hydration forces [54, 55]. The tilts of the molecules determine the membrane curvature. The interplay of protrusion and bending will be discussed in the last section 7.5.

7.1. Single protrusion modes

As explained in section 3.1, two rigid bilayers immobilized onto mica surfaces experience a strong repulsion for small separations of the order of 1 nm. It is believed that these hydration forces between the bilayers arise from the intrinsic structure of the lipid water interfaces. Phenomenological theories predict that this perturbed water structure leads to the direct interaction

$$\Delta V(l) = V_{\text{hy}} \exp[-l/l_{\text{hy}}]. \quad (7.1)$$

The hydration length l_{hy} should be given by an appropriate correlation length within the water, see section 3.1.

Now, consider a single protrusion mode in which one lipid molecule pulls out from one of the rigid membranes and bridges the intermediate water gap of size l [51]. The lipid molecule is taken to have the shape of a small column with constant cross-section and circumference a_0 . Such a protrusion has energy $\Delta E = \Sigma_0 a_0 l$ where Σ_0 represents the free energy of the interface between the nonpolar part of the molecule and the water (or another polar solvent). Now, the probability for such a fluctuation can be estimated by the Boltzmann weight, $\exp(-\Delta E/T) = \exp(-l/l_{\text{sc}})$ with the length scale

$$l_{\text{sc}} = T/a_0 \Sigma_0. \quad (7.2)$$

For a molecule with circumference $a_0 \simeq 3$ nm and interfacial free energy $\Sigma_0 \simeq 0.02$ J/m², this length scale is $l_{\text{sc}} \simeq 0.07$ nm at room temperature with $T = 4.12 \times 10^{-21}$ J.

Thus, the protrusions of the lipid water interface introduce another length scale, the protrusion length l_{pr} . Within the single mode picture, this scale is in fact equal to l_{sc} . In general, one has $l_{\text{pr}} = z_{\text{pr}} l_{\text{sc}}$ with a dimensionless coefficient $z_{\text{pr}} > 1$ as will be shown below. Thus, the interplay between hydration forces and protrusion modes can be understood in terms of two length scales, the hydration length l_{hy} and the protrusion length l_{pr} .

There is one obvious problem with a picture based on single protrusion modes. Since l_{sc} is of the order of 0.1 nm, a protrusion of a single molecule which bridges a water gap of about 1 nm is very unlikely. In real systems there are, however, two different effects which act to increase the effective range of protrusions [54, 55]:

- (i) The molecules protrude *collectively*. If several molecules protrude in a coherent fashion, they can form, e.g., transient roof-like ripples. In this way, collective protrusions can bridge a water layer of 1 nm even though the relative displacements of neighboring molecules are only of the order of 0.1 nm; and
- (ii) The profile of the water structure in front of the lipid surface is shifted by the protrusions.

These two effects will now be taken into account.

7.2. Models for collective protrusion modes

In order to go beyond the single mode picture, let us consider a rough membrane in which all molecules can be displaced with respect to the flat state. A snapshot of such a membrane is shown in fig. 18. In addition, we will include the direct hydration interaction between the membranes as given by (7.1). The separation of the protruding molecule i from the other membrane is now described by the local displacement field l_i which varies along the membrane surface. Each molecule interacts with n nearest neighbors. All molecules have the same cross-sectional

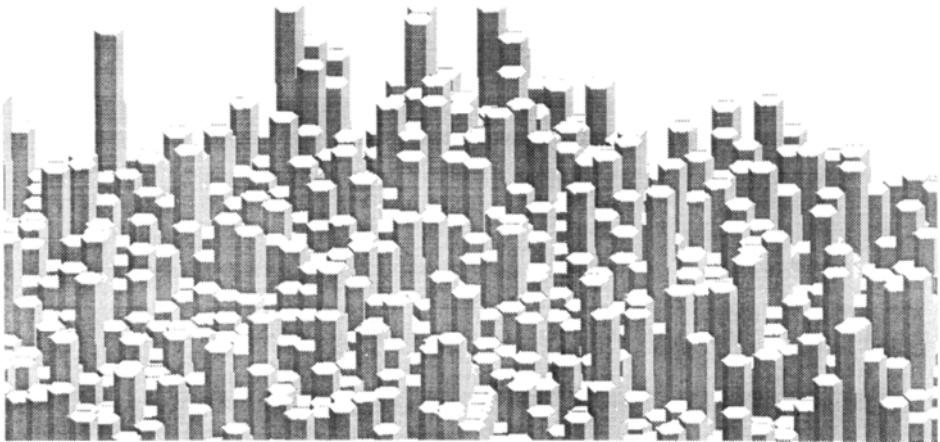


Fig. 18. Snapshot of membrane segment which is roughened by collective protrusion modes. Note that the vertical and the horizontal scale of this figure are different: Relative displacements of two neighboring molecules are typically of the order of 0.1 nm whereas the diameter of the molecules is about 0.8 nm [55].

area A_0 . The energy of such a membrane configuration is given by [54, 55]

$$\mathcal{H}\{l\}/T = \sum_{\langle ij \rangle} (a_0 \Sigma_0 / T n) |l_i - l_j| + \sum_i A_0 V(l_i) / T \quad (7.3)$$

and its statistical weight is given by the Boltzmann factor $\sim \exp[-\mathcal{H}\{l\}/T]$.

Protrusions change the area of the lipid water interface. Therefore, these fluctuations are governed, on large scales, by an effective interfacial tension, Σ_{pr} , which must be distinguished from the microscopic tension, Σ_0 , of the hydrocarbon solvent interface. The solvent layer between two such interfaces resembles a thin wetting layer.

Extensive Monte Carlo simulations and renormalization group calculations have shown that the discrete model defined by (7.3) belongs to the same universality class as the so-called Gaussian model

$$\mathcal{H}\{l\}/T = \int d^2x \left\{ \frac{1}{2} (\Sigma_{\text{pr}}/T) (\nabla l)^2 + V(l) \right\} \quad (7.4)$$

for which the discrete sites i are replaced by a continuous coordinate and the term $(a_0 \Sigma_{\text{pr}} / T n) |l_i - l_j|$ is replaced by $(\Sigma_{\text{pr}} / 2T) (\nabla l)^2$. The effective interfacial tension Σ_{pr} is related to Σ_0 via [54]

$$\Sigma_{\text{pr}} = c_{\Sigma} (a_0 \Sigma_0)^2 / T = c_{\Sigma} T / l_{\text{sc}}^2. \quad (7.5)$$

The dimensionless coefficient c_{Σ} can be estimated from the Monte Carlo simulations and is found to be $c_{\Sigma} \simeq 0.067$. Using the above estimate for l_{sc} , one then has $\Sigma_{\text{pr}} \simeq 0.056 \text{ J/m}^2$.

The discrete model as given by (7.3) describes the interaction of one protruding and one flat lipid solvent interface belonging to two different lipid bilayers. For the interaction between two flexible bilayers, there are two changes.

First of all, each bilayer is bounded by two lipid solvent interfaces. The protrusion of one bilayer will, in general, involve both interfaces of this bilayer in order to avoid bilayer cavities which would cost a lot of energy. If the bilayer were incompressible, the two lipid solvent interfaces would have constant separation which would imply that the interfacial free energy Σ_0 for its protrusions is *increased* by a factor of two.

On the other hand, if both bilayers exhibit protrusions, the effective interfacial tension Σ_{pr} for their *relative* displacement field is *decreased* by a factor of two. Since $\Sigma_{\text{pr}} \sim \Sigma_0^2$, these two effects compensate each other to a certain extent and lead to an overall increase of Σ_0 by a factor of $\sqrt{2}$. The finite area compressibility of the bilayer will act to reduce this factor.

As mentioned, these models for collective protrusions have been studied by Monte Carlo simulations and renormalization group methods [54, 55]. The results of these calculations are briefly summarized in the following subsections.

7.3. Disjoining pressure from hard wall

It is again instructive to consider the simple interaction

$$V_P(l) = V_{hw}(l) + Pl \quad (7.6)$$

which describes the interplay of the hard wall repulsion and the external pressure P . In the limit of small pressure, one obtains the exponential dependence

$$P \approx P_{hw} e^{-\ell/l_{pr}} (l_{pr}/\ell)^{1/4} \quad (7.7)$$

on the mean separation $\ell = \langle l \rangle$, and the Gaussian dependence

$$P \approx P_{hw\perp} e^{-2(\xi_\perp/l_{pr})^2} \quad (7.8)$$

on the roughness $\xi_\perp = \langle (l - \ell)^2 \rangle^{1/2}$. The protrusion length l_{pr} is found to be

$$l_{pr} \equiv (T/2\pi\Sigma_{pr})^{1/2} = z_{pr}T/a_0\Sigma_0 \quad (7.9)$$

with the dimensionless coefficient $z_{pr} \simeq 1.5$. Thus, the collective protrusions increase the value of this length scale by about 50 percent.

The pressure amplitudes P_{hw} and $P_{hw\perp}$ are obtained from the Monte Carlo simulations as

$$P_{hw}/P_{sc} = Q_{hw} \simeq 0.5 \quad \text{and} \quad P_{hw\perp}/P_{sc} = Q_{hw\perp} \simeq 0.9 \quad (7.10)$$

with the pressure scale

$$P_{sc} \equiv a_0\Sigma_0/A_0. \quad (7.11)$$

For $a_0 = 3$ nm, $A_0 = 0.7$ nm², and $\Sigma_0 = 0.02$ J/m², one has $P_{sc} \simeq 8.6 \times 10^7$ J/m³ which lies within the range of the experimentally observed values for the disjoining pressure.

7.4. Disjoining pressure from exponential hydration

Now, let us consider the exponential hydration interaction $\Delta V(l) = V_{hy} \exp[-l/l_{hy}]$ as in (7.1). The bilayer interaction is now given by

$$V_P(l) = V_{hw}(l) + V_{hy} \exp[-l/l_{hy}] + Pl. \quad (7.12)$$

In this case, one finds two different scaling regimes depending on the relative size of the hydration length l_{hy} and the protrusion length l_{pr} .

The *protrusion-dominated* regime is defined by $l_{pr} > 2l_{hy}$. In this case, one obtains the same ℓ -dependence or ξ_\perp -dependence for the disjoining pressure P as for the hard wall case. Thus, the two relations (7.7) and (7.8) are still valid with the protrusion length l_{pr} as given by (7.9).

The *hydration-dominated* regime, on the other hand, is defined by $l_{\text{pr}} < 2l_{\text{hy}}$. In this case, one has a nontrivial competition between the direct hydration and the collective protrusions. In the limit of small pressure, this competition leads to the exponential dependence

$$P \approx P_2 e^{-\ell/l_t} \quad (7.13)$$

on the mean separation ℓ with the decay length

$$l_t = [1 + (l_{\text{pr}}/2l_{\text{hy}})^2] l_{\text{hy}}. \quad (7.14)$$

The amplitude P_2 is given by

$$P_2 = (\Sigma_{\text{pr}}/a_{\parallel}^2)^{\rho} V_{\text{hy}}^{1-\rho} l_{\text{hy}}^{2\rho-1} \quad (7.15)$$

where a_{\parallel} is the diameter of the lipid molecule and

$$\rho \equiv (l_{\text{pr}}/l_{\text{hy}})^2 / [(l_{\text{pr}}/l_{\text{hy}})^2 + 4]. \quad (7.16)$$

This functional dependence for l_t and P_2 has been obtained by renormalization group calculations and confirmed by Monte Carlo simulations, see fig. 19. Within the hydration-dominated regime, the roughness ξ_{\perp} is related to the pressure P via

$$P \approx P_{2\perp} e^{-2(\xi_{\perp}/l_{\text{pr}})^2}. \quad (7.17)$$

The Gaussian dependence on ξ_{\perp} is the same as in the protrusion-dominated regime but the amplitude $P_{2\perp}$ depends on the hydration length. For $l_{\text{hy}}/l_{\text{sc}} = 1.5$ and 3, one obtains $P_{2\perp}/P_{\text{sc}} \simeq 1.4$ and 2.5, respectively.

As shown in fig. 20, the roughness ξ_{\perp} is always small compared to the mean separation ℓ for the collective protrusion modes studied here, and the relative displacements of the lipid molecules are only of the order of a few Å.

In summary, the disjoining pressure P depends exponentially on the mean separation ℓ as $P \sim \exp[-\ell/l_t]$ in both regimes but with a *non-universal* decay length l_t . In the protrusion-dominated regime with $l_{\text{pr}} > 2l_{\text{hy}}$, one has

$$l_t = l_{\text{pr}} = z_{\text{pr}} T / a_0 \Sigma_0 \quad \text{with } z_{\text{pr}} \simeq 1.5. \quad (7.18)$$

In the hydration-dominated regime with $l_{\text{pr}} < 2l_{\text{hy}}$, this length scale is given by

$$l_t = l_{\text{hy}} + z_{\text{pr}}^2 T^2 / 4(a_0 \Sigma_0)^2 l_{\text{hy}} \quad (7.19)$$

as follows from (7.14). Thus, the length scale l_t depends, in general, on temperature T , on the parameter combination $a_0 \Sigma_0$ (which represents an effective edge tension of the lipid molecule), and on the hydration length l_{hy} .

At fixed temperature T , the repulsive interaction will be dominated by protrusion and by direct hydration forces for small and for large values of the parameter $a_0 \Sigma_0$, respectively. Likewise, protrusion and hydration forces dominate for small and for large values of the hydration length, respectively. Thus, depending on the lipid and on the solvent, a real system may belong to either of both interaction regimes.

For fixed lipid and solvent, on the other hand, one will have a transition at a characteristic temperature $T = T_*$ which is implicitly given by $l_{\text{pr}}(T_*) = 2l_{\text{hy}}(T_*)$. It follows from the above expressions for these length scales that $T_* = 2a_0 \Sigma_0 l_{\text{hy}} / z_{\text{pr}}$ if one ignores the T -dependence of the interfacial free energy Σ_0 and of the hydration length l_{hy} . For the hydration-dominated regime at low temperatures $T < T_*$, the physical decay length l_t increases quadratically with increasing T , while it increases linearly with T for the protrusion-dominated regime at $T > T_*$.

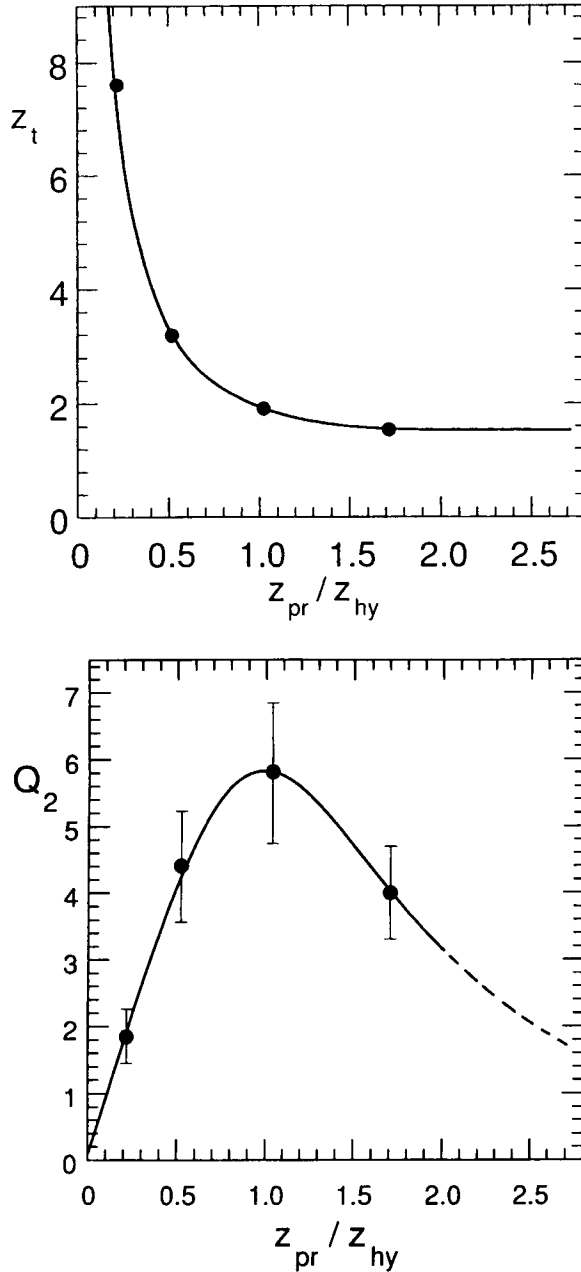


Fig. 19. (a) The decay length $z_t \equiv l_t/l_{sc}$ and (b) The pressure amplitude $Q_2 \equiv P_2/P_{sc}$ as a function of the ratio l_{pr}/l_{hy} . The length scale l_{sc} and the pressure scale P_{sc} are defined in (7.2) and (7.11), respectively. The four dots represent the best fits to the Monte Carlo data; the error bars for Q_2 are relatively large while the error bars for z_t are smaller than the size of the symbols. The solid curves represent the functional dependence in (7.14) and (7.15) [54].

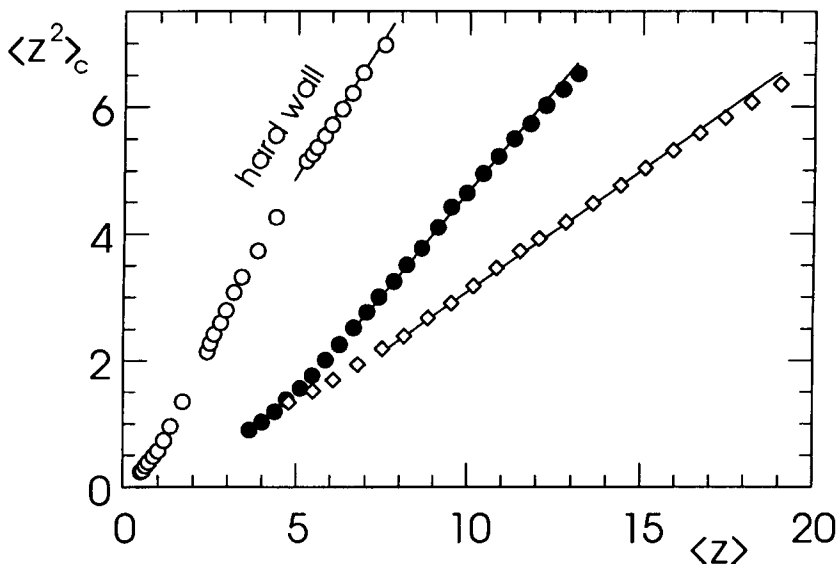


Fig. 20. The squared roughness $\langle z^2 \rangle_c \equiv (\xi_{\perp}/l_{sc})^2$ as a function of the mean separation $\langle z \rangle \equiv \ell/l_{sc}$. The three sets of data correspond to the hard wall (\circ) and to exponential hydration interactions with $l_{hy}/l_{sc} = 1.5$ (\bullet) and $l_{hy}/l_{sc} = 3$ (\diamond). The roughness is always small compared to the mean separation [55].

7.5. Protrusions versus bending undulations

Protrusions are excitations of the lipid solvent interfaces which change the interfacial area and are thus governed by an effective interfacial tension. These excitations should be dominant on length scales which are smaller than or comparable with the bilayer thickness. On the other hand, for larger length scales, the typical fluctuations are expected to be bending modes governed by bending rigidity as discussed in previous sections.

Protrusions act to reduce the bending rigidity. If a single molecule protrudes from the bilayer, it is easier to bend this membrane away from this protrusion. This effect can be studied within a simple model in which one considers protrusions on top of a curved membrane [55]. More precisely, the membrane has a neutral surface which is taken to be incompressible and characterized by a bare bending rigidity κ_0 . The position of the two lipid-solvent interfaces is then described by two additional displacement fields.

Within this model, one finds that the bare bending rigidity κ_0 is decreased by the protrusions. Explicit summation of all protrusion modes (on the harmonic level) leads to the effective bending rigidity [55]

$$\kappa = \kappa_0 / (1 + \Delta) \quad (7.20)$$

with

$$\Delta \approx (2c_{\Sigma}T / \kappa_0 g_{\max}^2 l_{sc}^2) (e^{4(\xi_{\perp}/l_{pr})^2} - 1) \quad (7.21)$$

in the limit of large wavelengths. The parameter $q_{\max} \simeq 2\sqrt{\pi}/a_{\parallel}$ represents the high-momentum cutoff where a_{\parallel} is the diameter of the lipid molecule. The length scale ξ_{\perp} is the roughness of the lipid-solvent interfaces arising from protrusions.

Thus, as soon as this roughness becomes comparable to the protrusion length l_{pr} , the effective bending rigidity κ becomes significantly smaller than the bare bending rigidity κ_0 . This effective bending rigidity should be identified with the bending rigidity measured experimentally via the shape fluctuations of vesicles. As mentioned, one typically finds $\kappa \simeq 10\text{--}20T$. This implies that the bare bending rigidity κ_0 on microscopic scales should be significantly larger than κ .

Finally, it is instructive to compare the disjoining pressure arising from protrusions with the disjoining pressure arising from bending undulations. First, consider the hard wall case. For a membrane interacting with a hard wall, protrusions lead to the disjoining pressure $P \approx F_{\text{hw}}e^{-\ell/l_{\text{pr}}}(l_{\text{pr}}/\ell)^{1/4}$ as in (7.7). Bending undulations, on the other hand, lead to $P \approx 2c_{\text{fl}}T^2/\kappa\ell^3$ with $2c_{\text{fl}} \simeq 3\pi^2/256$. Thus, the exponential dependence of P on ℓ becomes algebraic when ℓ becomes comparable to the crossover scale ℓ_* with

$$e^{-\ell_*/l_{\text{pr}}}(l_*/l_{\text{pr}})^{11/4} = 2c_{\text{fl}}T^2/F_{\text{hw}}l_{\text{pr}}^3\kappa \simeq 0.062T^2/P_{\text{sc}}l_{\text{sc}}^3\kappa. \quad (7.22)$$

The previous estimates for P_{sc} and l_{sc} lead to $P_{\text{sc}}l_{\text{sc}}^3 \simeq 2.9 \times 10^{-23}$ J. For bending rigidity $\kappa \simeq 10^{-19}$ J, one then obtains the crossover scale $\ell_* \simeq 9.1l_{\text{sc}}$ at room temperature. For $\ell < \ell_*$, the disjoining pressure arises primarily from the collective protrusions.

In the presence of a direct hydration interaction, $V_{\text{hy}} \exp[-\ell/l_{\text{hy}}]$, the crossover scale ℓ_* is increased. For $l_{\text{hy}} \simeq l_{\text{pr}}$, for example, one finds that ℓ_* is of the order of 2 nm. Likewise, this length scale is increased if one takes into account that, as a result of the protrusions, the bending rigidity κ_0 on small scales should be larger than κ .

8. Related problems and outlook

In this final section, some extensions and some open problems will be briefly discussed. First of all, the concepts described in this review are also useful for other types of membranes, such as solid-like or polymerized membranes. Likewise, one may incorporate random interactions between the membranes arising, for example, from domain formation within the membranes. Both for fluid and for other types of membranes, one would like to develop a systematic renormalization group method in which the renormalized interactions can be calculated perturbatively in a controlled way.

This review has focused on static properties. Interacting membranes also exhibit interesting dynamic, i.e. time-dependent phenomena. For example, one may study the time-dependent relaxation of their bending undulations which is often governed by hydrodynamics. Another dynamic process which is crucial for biology is membrane fusion.

Finally, I will discuss some general difficulties which one encounters in experimental studies of these phenomena in model systems.

8.1. Polymerized membranes

Throughout this review, the interacting membranes were taken to be lipid bilayers in their fluid state since these bilayers represent the most important class of biological model membranes. However, biological membranes often contain 2-dimensional protein networks which are attached via anchor proteins onto the fluid bilayer; one example is provided by the spectrin network which is part of the plasma membrane of red blood cells [7, 8]. These networks resemble fishnets of fixed connectivity and represent polymerized membranes with a finite shear modulus.

The meshsize of protein networks is typically large and of the order of 100 nm. Polymerized membranes with a much smaller meshsize can be obtained from bilayers of polymerizable lipids [138, 139]. Polymerisation of these molecules can often be accomplished by irradiation with ultraviolet light. In this way, one usually obtains partially polymerized membranes containing domains of crosslinked lipids.

On length scales which are large compared to the meshsize of the network, a polymerized membrane can be regarded as a thin elastic sheet. The bending of such a sheet leads, in general, to a change in the Gaussian curvature which necessarily implies some stretching and shearing of the sheet as well [140]. This coupling between bending and stretching acts to reduce the membrane roughness: a membrane segment of linear size ξ_{\parallel} now makes transverse excursions of size $\xi_{\perp} \sim \xi_{\parallel}^{\zeta}$ with a roughness exponent $\zeta < 1$ [141]. Computer simulations gave a range of values between $\zeta = 1/2$ and $\zeta \simeq 2/3$ [142, 143, 144, 145]. The best analytical estimate seems to be $\zeta \simeq 0.59$ [146].

The reduced roughness implies a reduced fluctuation-induced interaction $V_{\text{fl}}(\ell) \sim 1/\ell^{\tau}$ with $\tau = 2/\zeta > 2$ and, thus, a reduced renormalization of the direct interaction which has been studied by functional renormalization [88, 89]. In the presence of attractive forces, polymerized membranes again exhibit a critical unbinding temperature $T = T_*$ at which the mean separation ℓ of the membranes diverges as $\ell \sim 1/|T - T_*|^{\psi}$; functional renormalization leads to the estimates $\psi \simeq 0.68$ and $\psi \simeq 0.8$ for $\zeta = 1/2$ and $\zeta = 2/3$, respectively [88]. Molecular dynamics simulations of polymerized membranes led to folding transitions which seem to be intimately related to unbinding transitions [147].

As for fluid membranes, the unbinding temperature for a bunch of N polymerized membranes should be independent of N as follows from the N -state model discussed above. This property should also hold for other types of membranes (or of shape fluctuations) characterized by a different roughness exponent ζ .

8.2. Random interactions

The direct interaction between membranes may contain a random component arising from inhomogeneities within the membranes. For example, these membranes may contain several types of lipid molecules and thus may form intramembrane domains or clusters. Likewise, one may study the interaction of a flexible membrane with another interface or surface which is laterally inhomogeneous. In these systems, the direct interaction $V(l(x), x)$ depends both on the local separation $l(x)$ and on the lateral coordinate x .

Two types of randomness must be distinguished. If the lateral composition of the surfaces is in thermal equilibrium with the rest of the system, one will have an appropriate Boltzmann weight which governs both the composition of the surfaces and their displacement fields. This represents the case of ‘annealed’ randomness. On the other hand, if the lateral composition does not change on the typical time scales for the shape fluctuations, the randomness contained in the interaction is ‘frozen’ or ‘quenched’.

The effect of quenched disorder on the unbinding transition can be estimated by a simple scaling argument [50]. As a result, one finds that the critical behavior remains unchanged provided the unbinding exponent ψ and the roughness exponent ζ satisfy the inequality $\psi > \zeta$ in the absence of quenched disorder. For polymerized membranes, this inequality is satisfied and quenched disorder will not affect the asymptotic critical behavior. For fluid membranes, on the other hand, one has a marginal case since $\psi = \zeta$.

It is again instructive to consider interacting strings in two dimensions. In this latter case, short-ranged interactions with quenched disorder represent marginally relevant perturbations [159]. Therefore, the asymptotic critical behavior for strings could be changed by quenched disorder on sufficiently large scales. By analogy, this could also apply to fluid membranes.

8.3. *Perturbative renormalization*

As explained in this review, our theoretical understanding of interacting membranes relies on a combination of scaling arguments, functional renormalization, and computer simulations. Scaling arguments are very useful but it is often difficult to estimate their reliability. Computer simulations are necessarily limited to relatively small membrane segments and to relatively short relaxation times. The most systematic method which has been used so far is functional renormalization but this method involves several approximations which cannot be easily improved.

A perturbative renormalization group procedure has been recently developed for interfaces governed by interfacial tension (or for membranes which experience a lateral tension) [99, 119]. This procedure is based on an expansion of the direct interaction $V(l)$ in terms of the distribution $\delta(l)$ and its derivatives $\partial^n \delta(l)/\partial l^n$. These short-ranged interactions form a so-called operator algebra which can be used to renormalize the interaction in a perturbative and, thus, in a controlled way. It is highly desirable to extend this approach to (tensionless) membranes.

8.4. *Dynamics of membranes*

The conformational changes of membranes in solution are coupled to different dissipative mechanisms. In general, some energy will be dissipated in the viscous solvent surrounding the membranes [84]. In addition, the shape fluctuations of bilayers can be damped by the friction between the two monolayers [148].

The damping of bending undulations by these two mechanisms has been recently studied theoretically. For free membranes, the relaxation time (or inverse damping rate) increases with the wavelength q of the undulations: for small and large q ,

the damping is dominated by the dissipation in the surrounding solvent and by the friction between the monolayers, respectively [149]. For interacting membranes, the dependence of the relaxation time on the wavenumber q is rather complex and depends on the relative size of q , the mean separation ℓ and the correlation length ξ_{\parallel} [150, 151].

Another dynamical process which is closely related to the relaxation of the bending modes is the dynamic coarsening of these modes. Thus, consider a membrane which is initially stretched by a large lateral tension and thus is prepared in an essentially flat state. When this tension is switched off, the membrane starts to roughen. Scaling implies that the membrane roughness ξ_{\perp} will increase as $\xi_{\perp} \sim t^{\zeta/(1+2\zeta)}$ with time t when the dominant dissipation is provided by the viscous damping of the surrounding solvent [152]. For fluid membranes, one has $\zeta = 1$ and thus $\xi_{\perp} \sim t^{1/3}$.

8.5. Membrane fusion

As explained in the section on hydration forces, lipid bilayers tend to repel each other by a huge pressure of the order of $10^8 \text{ Pa} \simeq 10^3 \text{ atm}$ at small separations below 1 nm. This pressure prevents direct contact of the bilayers and thus usually prevents their fusion. Biomembranes, on the other hand, frequently fuse after they have made an adhesive contact. The transport vesicles, for example, which shuttle between different compartments of the cell always fuse with their target membranes [7, 8].

The fusion of two membranes is presumably initiated by the nucleation of a small neck or passage which connects the two adjacent membranes. From a physical point of view, one must then ask which intermediate structures are involved during such a nucleation process. Several such structures have been proposed. The activation energy associated with these structures has been estimated in terms of the bending energy of the monolayers and of the energy of the hydrophobic interstices (or defects) which are created as the monolayers are peeled apart [153].

For lipid bilayers, the experimentally determined fusion rates are increased by lateral tension, by the adsorption of Ca^{2+} ions, and by electroporation. The latter process is described in the chapter by Dimitrov in this handbook. The fusion of biomembranes is believed to be induced by various proteins, see the chapter by Arnold in this handbook. It remains to be seen if one can develop a conceptual framework for membrane fusion which has some predictive power and which can be applied both to lipid bilayers and to biomembranes.

8.6. Experiments on model membranes

As explained in section 2, several experimental methods are available in order to probe the interaction of flexible membranes. Indeed, the theoretical concepts reviewed here have been developed in order to understand and to explain the experimental observations, at least qualitatively. In some cases, even quantitative agreement between theory and experiment has been achieved.

However, there is one general obstacle which one encounters in this relatively young research field, and this consists of the experimental difficulties to *prepare*

the membranes in a well-characterized state. Some of the major difficulties are as follows:

- (i) Lipid bilayers usually represent a multi-component system: they always contain small amounts of other lipids which differ in their head groups or in their chain lengths; some hydrocarbon chains are saturated and some are unsaturated; in general, lipid molecules are not very robust and may degrade, i.e. change their chemical structure. On the other hand, relatively small changes in the composition can lead to large changes in the cooperative behavior of the membranes. One example is provided by the extreme sensitivity of vesicle shapes to small differences in the lipid composition of the two monolayers [154].
- (ii) The bilayer composition is also affected by the composition of the solution. The aqueous solution usually contains various ions which may adsorb onto the bilayer. Likewise, organic molecules with a hydrophobic part have a tendency to become concentrated within the bilayer. Molecules adsorbed onto the lipid bilayer change the structure of the lipid water interfaces. In addition, the membrane may become charged by the ions. In such a situation, the lipid water interfaces will contain clouds of counterions. Any change in the molecular structure of the lipid bilayer or of the lipid water interfaces will, in general, affect its elastic properties and its bending energy; and
- (iii) As explained in previous sections, even a small lateral tension has a strong effect on the interaction of flexible membranes. There are several mechanisms which induce such a tension but cannot be controlled experimentally. It can be induced, for instance, by an osmotic pressure arising from the presence of large molecules which cannot penetrate the membrane. If the membrane adheres to the container walls, it will often be pulled into different directions and thus will experience a lateral tension. Furthermore, nonequilibrium effects such as hydrodynamic flow and temperature gradients will often lead to lateral tension.

In summary, the cooperative behavior of membranes is strongly affected (i) by small changes in their composition and (ii) by small lateral tensions, both of which are difficult to control experimentally. This implies that lipid bilayers prepared in different laboratories will often exhibit small differences in their composition and will often experience small but different tensions. This explains, at least to some extent, why it is often difficult to obtain quantitative agreement between the measurements of different experimental groups.

On the other hand, it is also possible that our conceptual framework for the structure of lipid bilayers is still incomplete. For example, it has been suggested that tensionless lipid bilayers can possess a hidden reservoir for membrane area which is provided by a superstructure of the bilayer, see the chapter by Helfrich in this handbook. It is also conceivable that the internal structure of lipid bilayers undergoes a phase transformation as one varies the lateral tension, i.e. that there is a low-tension and a high-tension phase. More experimental work is certainly needed in order to clarify these issues.

Appendices

A. Roughness of confined membranes

Consider a membrane with bending rigidity κ which is subject both to the confining potential $V(l)$ and to the lateral tension Σ . The confining potential is taken to have the simple form

$$V(l) = \frac{1}{2} v_2 l^2.$$

For a general interaction potential $V(l)$ which has a minimum at $l = l_m$, one has $v_2 = (\partial^2 V / \partial l^2)$ at $l = l_m$.

The effective Hamiltonian of the confined membrane then has the form

$$\mathcal{H}\{l\} = \int d^2x \left\{ \frac{1}{2} v_2 l^2 + \frac{1}{2} \Sigma (\nabla l)^2 + \frac{1}{2} \kappa (\nabla^2 l)^2 \right\}. \quad (\text{A.1})$$

The membrane roughness ξ_{\perp} is now given by

$$\xi_{\perp}^2 = \langle (l - \langle l \rangle)^2 \rangle = T \int \frac{d^2p}{(2\pi)^2} \frac{1}{v_2 + \Sigma p^2 + \kappa p^4}. \quad (\text{A.2})$$

In general, one has to include a high-momentum cutoff, $p_{\max} \simeq \pi/a_{\parallel}$, where the length scale a_{\parallel} is of the order of the membrane thickness. The corrections arising from this cutoff are small as long as $\Sigma a_{\parallel}^2 / \kappa \ll 1$. For lipid bilayers with $a_{\parallel} \simeq 1$ nm and $\kappa \simeq 10^{-10}$ J, this implies $\Sigma \ll 10^2$ mJ/m². This inequality will be implicitly assumed in the following discussion.

An explicit evaluation of the integral in (A.2) (with $a = 0$) leads to

$$\xi_{\perp}^2 = (T/2\pi\Sigma)\Omega(\Sigma/\Sigma_*) \quad (\text{A.3})$$

with the crossover tension

$$\Sigma_* \equiv \sqrt{4\kappa v_2} \quad (\text{A.4})$$

and

$$\Omega(y) \equiv \begin{cases} \arctan(\sqrt{y^{-2}-1})/\sqrt{y^{-2}-1} & \text{for } y < 1, \\ \operatorname{arctanh}(\sqrt{1-y^{-2}})/\sqrt{1-y^{-2}} & \text{for } y > 1. \end{cases} \quad (\text{A.5})$$

Thus, one has two regimes: (i) a tension-dominated regime with $y > 1$ or $\Sigma > \Sigma_*$; and (ii) a rigidity-dominated regime with $y < 1$ or $\Sigma < \Sigma_*$.

Within the tension-dominated regime, the roughness behaves as

$$\xi_{\perp}^2 \approx (T/2\pi\Sigma) \ln(2\Sigma/\Sigma_*) \quad (\text{A.6})$$

for large Σ/Σ_* . It is instructive to express this ratio in terms of the crossover length

$$\xi_* \equiv (4\kappa/\Sigma)^{1/2} \quad (\text{A.7})$$

and the longitudinal correlation length

$$\xi_{\parallel} = \xi_{\Sigma} \equiv (\Sigma/v_2)^{1/2}. \quad (\text{A.8})$$

The latter length scale governs the exponential decay of the correlation function $\langle l(x)l(0) \rangle$ (in the limit of weak confinement, i.e. of small v_2). One then has

$$\xi_{\perp}^2 \approx (T/2\pi\Sigma) \ln(2\xi_{\parallel}/\xi_*) \quad (\text{A.9})$$

as used in section 4.3.

Within the rigidity-dominated regime, the roughness behaves as

$$\xi_{\perp}^2 \approx (T/2\pi\Sigma)(\pi\Sigma/2\Sigma_*) = (T/8\kappa)(\kappa/v_2)^{1/2} \quad (\text{A.10})$$

for small Σ/Σ_* . In this limit, the longitudinal correlation length which governs the exponential decay of the correlation function $\langle l(x)l(0) \rangle$ is given by

$$\xi_{\parallel} = \xi_{\kappa} \equiv (4\kappa/v_2)^{1/4}. \quad (\text{A.11})$$

It now follows from (A.10) that the roughness scales as

$$\xi_{\perp}^2 \approx (T/16\kappa)\xi_{\parallel}^2 \quad (\text{A.12})$$

within the rigidity-dominated regime.

The three scales ξ_* , ξ_{Σ} and ξ_{κ} as introduced above are the three length scales which can be obtained from the three parameters κ , Σ , and v_2 . Note that these scales satisfy the inequalities $\xi_* < \xi_{\kappa} < \xi_{\Sigma}$ in the tension-dominated regime, and $\xi_{\Sigma} < \xi_{\kappa} < \xi_*$ in the rigidity-dominated regime.

The relation between the roughness ξ_{\perp} and the correlation length ξ_{\parallel} can be obtained in a more transparent way if one treats one ξ_{\parallel} -hump of the confined membrane as a free membrane segment of linear size ξ_{\parallel} . The effective Hamiltonian for this segment is again given by (A.1) but with $v_2 = 0$ and with the x -integration restricted to the finite segment area, ξ_{\parallel}^2 . This leads to the roughness

$$\xi_{\perp}^2 = T \int' \frac{d^2p}{(2\pi)^2} \frac{1}{\Sigma p^2 + \kappa p^4} \quad (\text{A.13})$$

where the prime indicates the low-momentum cutoff $p_{\min} \sim 1/\xi_{\parallel}$ (as before, the effects of the high-momentum cutoff p_{\max} will be ignored). This leads to

$$\xi_{\perp}^2 = \frac{1}{2} l_{\Sigma}^2 \ln(1 + \Sigma/\kappa p_{\min}^2) \quad (\text{A.14})$$

with the length scale

$$l_\Sigma \equiv (T/2\pi\Sigma)^{1/2}. \tag{A.15}$$

If these expressions are used with $p_{\min} = c/\xi_{\parallel}$, one obtains

$$\xi_{\perp}^2 \approx \begin{cases} (T/2\pi\Sigma) \ln(2\xi_{\parallel}/c\xi_*) & \text{for large } \Sigma, \\ (T/4\pi c^2\kappa)\xi_{\parallel}^2 & \text{for small } \Sigma. \end{cases} \tag{A.16}$$

The dimensionless coefficient c can now be chosen in such a way that one recovers the true asymptotic behavior of the confined membrane as given by (A.9) and (A.12). This choice is given by $c = 1$ for large Σ and by $c = \sqrt{4/\pi} \simeq 1.1$ for small Σ . Thus, if one chooses $c = \sqrt{4/\pi}$ for all values of Σ , one obtains an approximation which differs from the full expression (A.3) by about 10 percent for large values of Σ .

The expression (A.14) is useful since it can be easily inverted in order to express $p_{\min} = c/\xi_{\parallel}$ in terms of ξ_{\perp} . If the resulting expression is inserted into the fluctuation-induced interaction $V_{\text{fl}} \approx bT/\xi_{\parallel}^2$, one obtains

$$V_{\text{fl}} \approx bT\Sigma/c^2\kappa(e^{2(\xi_{\perp}/l_\Sigma)^2} - 1). \tag{A.17}$$

The dimensionless coefficient b can be determined in the following way.

The interaction (A.17) represents the effective repulsion arising from the renormalization of the hard wall interaction (i) between one flexible membrane with bending rigidity κ and a rigid wall (with infinite rigidity) or (ii) between two flexible membranes which both have the bending rigidity $\kappa_1 = 2\kappa$. The mean separation of the two interacting surfaces is denoted by ℓ . For the rigidity-dominated regime, extensive Monte Carlo simulations have shown that the hard wall interaction is renormalized into the fluctuation-induced interaction $V_{\text{fl}}(\ell) \approx c_{\text{fl}}T^2/\kappa\ell^2$ with $c_{\text{fl}} \simeq 0.0578$, and that the roughness behaves as $\xi_{\perp} \approx c_{\perp}\ell$ with $c_{\perp} \simeq 0.447$ for large ℓ . One may now choose the dimensionless coefficient b in such a way that this behavior is recovered from (A.17) for small values of ξ_{\perp}/l_Σ . This choice is given by $b \simeq 0.185$.

In the tension-dominated regime, i.e. for large values of ξ_{\perp}/l_Σ , the length scales ξ_{\perp} and ℓ satisfy

$$2(\xi_{\perp}/l_\Sigma)^2 \approx \ell/l_\Sigma + \frac{1}{4} \ln(\ell/l_\Sigma) \tag{A.18}$$

as follows from functional renormalization of the hard wall interaction [54]. When this relation is combined with (A.17), one obtains the fluctuation-induced interaction

$$V_{\text{fl}}(\ell) \approx 0.185(T\Sigma/\kappa)e^{-\ell/l_\Sigma}(l_\Sigma/\ell)^{1/4} \tag{A.19}$$

for the tension-dominated regime with l_Σ as in (A.15).

B. Limit of lyotropic liquid crystals

In this appendix, an effective harmonic model for a large stack is derived starting from the two-membrane approximation. Thus, consider a stack of a large number of identical membranes with bending rigidity κ_1 interacting with the pair potential $V(l)$. Within the two-membrane approximation described in section 6.3, the renormalization of $V(l)$ can be studied in the same way as for two membranes.

Let us focus on the simplest possible interaction given by $V_{\text{hw}}(l) + Pl$, i.e. the competition between the repulsive hard wall interaction and the attractive pressure term. Taking into account all bending modes with wavelengths up to ξ_{\parallel} , this potential is renormalized into the effective potential

$$V^{\text{eff}}(l) = 2c_{\text{fl}}T^2/\kappa_1l^2 + Pl \quad (\text{B.1})$$

with $2c_{\text{fl}} \simeq 0.115$.

The mean separation ℓ follows from $\partial V^{\text{eff}}(\ell)/\partial \ell = 0$ and the fluctuations on the scale of ξ_{\parallel} are governed by the harmonic potential

$$V^{\text{eff}}(l) \approx V^{\text{eff}}(\ell) + \frac{1}{2} v_2(l - \ell)^2 \quad (\text{B.2})$$

with

$$v_2 = 12c_{\text{fl}}T^2/\kappa_1\ell^4. \quad (\text{B.3})$$

The renormalized potential V^{eff} will now be used for the pair interactions in the membrane stack. Within this stack, the position of the membrane is described by the height variables h_n , and the relative displacement fields are given by $l_n = h_n - h_{n-1}$. If one uses the harmonic potential (B.2) for each l_n and ignores constant terms, one obtains

$$\mathcal{H}\{\underline{h}\} = \int d^2x \sum_{n=1}^N \frac{1}{2} v_2(h_n - h_{n-1} - \ell)^2 + \sum_{n=0}^N \frac{1}{2} \kappa_1 (\nabla^2 h_n)^2. \quad (\text{B.4})$$

This is the effective Hamiltonian which governs the bending undulations on length scales comparable with or larger than ξ_{\parallel} . The mean separation ℓ now plays the role of the small-scale cutoff.

It will be convenient to introduce a coarse-grained displacement field $u(x, z)$ where z is the Cartesian coordinate perpendicular to the membranes. Thus, one has

$$u(x, z = \langle h_n \rangle) = h_n(x) - \langle h_n \rangle$$

which implies

$$h_n - h_{n-1} - \ell = u(x, z = \langle h_n \rangle) - u(x, z = \langle h_n \rangle - \ell) \simeq \ell(\partial u/\partial z)$$

at $z = \langle h_n \rangle$.

If one now performs the continuum limit and replaces \sum_n by $\int dz/\ell$, the effective Hamiltonian (B.4) becomes [92, 93]

$$\mathcal{H}\{u\} = \int d^2x \int dz \left\{ \frac{1}{2} B (\partial u / \partial z)^2 + \frac{1}{2} K (\nabla^2 u)^2 \right\} \tag{B.5}$$

with

$$B = v_2 \ell = 12c_{\text{fl}} T^2 / \kappa_1 \ell^3 \quad \text{and} \quad K = \kappa_1 / \ell. \tag{B.6}$$

This is the harmonic model for smectic liquid crystals. In general, one should include higher-order anharmonic terms the form of which is dictated by symmetry. It has been shown for smectic liquid crystals that these anharmonic terms become important on scales which are large compared to a certain crossover length $L_{\parallel*}$ [155]. This length scale $L_{\parallel*}$ is equal to the small-scale cutoff times $\exp(64\pi/5w)$ with the dimensionless coefficient $w \equiv TB^{1/2}/K^{3/2}$. Using the expression in (B.6), one obtains

$$L_{\parallel*} \simeq \xi_{\parallel} e^{c_* (\kappa_1/T)^2} \quad \text{with} \quad c_* = 64\pi/5 \sqrt{12c_{\text{fl}}} \simeq 48.3 \tag{B.7}$$

for $2c_{\text{fl}} \simeq 3\pi^2/256$. Even if the bending rigidity were rather small and κ_1/T were of the order of one, this length scale is astronomical since $\exp[c_*] \simeq 10^{21}$. Thus, anharmonic terms can be safely ignored.

Within the harmonic model, the roughness L_{\perp} of a single membrane of lateral size L_{\perp} is given by

$$L_{\perp}^2 = \langle u^2 \rangle' = \int' \frac{d^2q_x}{(2\pi)^2} \int \frac{dq_z}{(2\pi)} \frac{T}{Bq_z^2 + Kq_x^4} \tag{B.8}$$

where the prime indicates that the q_x -integration involves the large-scale cutoff L_{\parallel} and the small-scale cutoff ξ_{\parallel} . This integral can be performed in closed form and leads to

$$L_{\perp}^2 \sim (T/\sqrt{BK}) \ln(L_{\parallel}/\xi_{\parallel}). \tag{B.9}$$

If one inserts the effective elastic constants B and K as given by (B.6), one obtains

$$L_{\perp} \sim \ell \sqrt{\ln(L_{\parallel}/\xi_{\parallel})}. \tag{B.10}$$

Thus, the roughness of a single ‘tracer’ membrane increases very slowly with the lateral size L_{\parallel} .

The harmonic model as given by (B.5) and (B.6) also leads to the prediction of quasi-long range translational order of the membrane stack characterized by an algebraic decay of correlations.

In reciprocal space, the scattering intensity $S(q)$ exhibits the power-law behavior [156]

$$S(q) \sim (q_z - q_m)^{-(2-X_m)} \quad (\text{B.11})$$

along the q_z -direction close to $q_z = q_m = 2\pi m/\ell$ with $m = 1, 2, \dots$. These power-law peaks are known as Landau–Peierls singularities and are governed by the exponents

$$X_m = Tq_m^2/8\pi\sqrt{BK}. \quad (\text{B.12})$$

If q_m , B , and K are expressed in terms of T , κ_1 , and ℓ via (B.6), one obtains the simple expression

$$X_m = \pi m^2/2\sqrt{12c_{\text{fl}}} \quad (\text{B.13})$$

which does not depend on any material parameters of the membranes.

Several attempts have been made to study these Landau–Peierls singularities by scattering experiments on lamellar phases of oil-water-surfactant mixtures [157, 158]. Using X-ray scattering, Roux, Safinya and coworkers measured $X_1 \simeq 4/3$ which implies $2c_{\text{fl}} \simeq 3\pi^2/128$. Helfrich had previously obtained three different estimates from heuristic arguments applied to the harmonic model (B.5). One of these estimates was in fact $2c_{\text{fl}} = 3\pi^2/128$. Thus, the X-ray work seems to be in very good agreement with this prediction for $2c_{\text{fl}}$. However, the precise theoretical estimate of $2c_{\text{fl}}$ as obtained from MC simulations gives $2c_{\text{fl}} \simeq 0.115$ which is very close to $3\pi^2/256$, see section 5.2 and section 6.4. Using this value for c_{fl} , one obtains

$$X_m = (4\sqrt{2}/3)m^2. \quad (\text{B.14})$$

References

1. Lipowsky, R., 1991, The confirmation of membranes, *Nature* **349**, 475–481.
2. Helfrich, W., 1978, Steric interaction of fluid membranes in multilayer systems, *Z. Naturforsch.* **33a**, 305–315.
3. Lipowsky, R. and S. Leibler, 1986, Unbinding transitions of interacting membranes, *Phys. Rev. Lett.* **56**, 2541–2544.
4. Mutz, M. and W. Helfrich, 1989, Unbinding transition of a biological model membrane, *Phys. Rev. Lett.* **62**, 2881–2884.
5. Netz, R.R. and R. Lipowsky, 1993, Unbinding of symmetric and asymmetric stacks of membranes, *Phys. Rev. Lett.* **71**, 3596–3599.
6. Lipowsky, R., 1989, Renormalized interactions of interfaces, membranes and polymers, *Phys. Scr. T* **29**, 259–264.
7. Alberts, B., D. Bray, J. Lewis, M. Raff, K. Roberts and J.D. Watson, 1989, *Molecular Biology of the Cell*, 2nd edition (Garland, New York).
8. Darnell, J., H. Lodish and D. Baltimore, 1990, *Molecular Cell Biology*, Scientific American Books (Freeman, New York).
9. Tanford, C., 1980, *The Hydrophobic Effect* (Wiley, New York).
10. Cevc, G. and D. Marsh, 1987, *Phospholipid Bilayers: Physical Principles and Models* (Wiley, New York).
11. Marsh, D., 1990, *Handbook of Lipid Bilayers* (CRC Press, Florida).

12. Canham, P.B., 1970, The minimum energy of bending as a possible explanation of the biconcave shape of the human red blood cell, *J. Theoret. Biol.* **26**, 61–81.
13. Helfrich, W., 1973, Elastic properties of lipid bilayers: Theory and possible experiments, *Z. Naturforsch.* **28c**, 693–703.
14. Evans, E.A., 1974, Bending resistance and chemically induced moments in membrane bilayers, *Biophys. J.* **14**, 923–931.
15. Evans, E. and D. Needham, 1987, Physical properties of surfactant bilayer membranes: Thermal transitions, elasticity, rigidity, cohesion, and colloidal interactions, *J. Phys. Chem.* **91**, 4219–4228.
16. de Gennes, P.-G. and C. Taupin, 1982, Microemulsions and the flexibility of oil/water interfaces, *J. Phys. Chem.* **86**, 2294–2304.
17. Helfrich, W., 1985, Effect of thermal undulations on the rigidity of fluid membranes and interfaces, *J. Physique* **46**, 1263–1268.
18. Peliti, L. and S. Leibler, 1985, Effects of thermal fluctuations on systems with small surface tension, *Phys. Rev. Lett.* **54**, 1690–1693.
19. Duwe, H.P., J. Käs and E. Sackmann, 1990, Bending elastic moduli of lipid bilayers: Modulation by solutes, *J. Phys. France* **51**, 945–962.
20. Mutz, M. and W. Helfrich, 1990, Bending rigidities of some biological model membranes as obtained from the Fourier analysis of contour sections, *J. Phys. France* **51**, 991–1002.
21. Horn, R.G., 1984, Direct measurement of the force between two lipid bilayers and observation of their fusion, *Biophys. Acta* **778**, 224–228.
22. Marra, J. and J.N. Israelachvili, 1985, Direct measurement of the force between phosphatidylcholine and phosphatidylethanolamine bilayers in aqueous electrolyte solutions, *Biochemistry* **24**, 4608–4618.
23. Marra, J., 1986, Direct measurement of attractive Van der Waals and adhesion forces between uncharged lipid bilayers in aqueous solutions, *J. Colloid Interface Sci.* **109**, 11–20.
24. Afshar-Rad, T., A. Bailey and P. Luckham, 1986, Direct measurement of forces between lipid bilayers, *Faraday Discuss. Chem. Soc.* **81**, 239–248.
25. Evans, E.A., 1980, Analysis of adhesion of large vesicles to surfaces, *Biophys. J.* **31**, 425–432.
26. Evans, E.A., 1985, Detailed mechanics of membrane–membrane adhesion and separation, I. Continuum of molecular cross-bridges, *Biophys. J.* **48**, 175–183.
27. Evans, E.A., 1990, Adhesion of surfactant-membrane covered droplets: Special features and curvatures elasticity effects, *Coll. Surf.* **43**, 327–347.
28. Rädler, J. and E. Sackmann, 1992, Vesicle-substrate interaction studied by reflection interference contrast microscopy, in: *The Structure and Conformation of Amphiphilic Membranes*, eds R. Lipowsky, D. Richter and K. Kremer (Springer, Berlin).
29. Rädler, J. and E. Sackmann, 1993, Imaging optical thicknesses and separation distances of phospholipid vesicles at solid surfaces, *J. Phys. II France* **3**, 727–748.
30. Cowley, A.C., N.L. Fuller, R.P. Rand and V.A. Parsegian, 1978, Measurement of repulsive forces between charged phospholipid bilayers, *Biochemistry* **17**, 3163–3168.
31. Parsegian, V.A., N. Fuller and R.P. Rand, 1979, Measured work of deformation and repulsion of lecithin bilayers, *Proc. Nat. Acad. Sci. USA* **76**, 2750–2754.
32. Lis, L.J., W.T. Lis, V.A. Parsegian and R.P. Rand, 1981, Adsorption of divalent cations to a variety of phosphatidylcholine bilayers, *Biochemistry* **20**, 1771–1777.
33. Horn, R.G., J.N. Israelachvili, J. Marra, V.A. Parsegian and R.P. Rand, 1988, Comparison of forces measured between phosphatidylcholine bilayers, *Biophys. J.* **54**, 1185–1187.
34. McIntosh, T.J., A.D. Magid and S.A. Simon, 1989, Range of the solvation pressure between lipid membranes: Dependence on the packing density of solvent molecules, *Biochemistry* **28**, 7904–7912.
35. Rand, R.P. and V.A. Parsegian, 1989, Hydration forces between phospholipid bilayers, *Biochim. Biophys. Acta* **988**, 351–376.
36. McIntosh, T.J. and S.A. Simon, 1993, Contributions of hydration and steric (entropic) pressures to the interactions between phosphatidylcholine bilayers: Experiments with the subgel phase, *Biochemistry* **32**, 8374–8384.

37. Cevc, G., W. Fenzl and L. Sigl, 1990, Surface-induced X-ray reflection visualization of membrane orientation and fusion into multibilayers, *Science* **249**, 1161–1163.
38. Cevc, G., W. Fenzl and L. Sigl, 1992, Surface induced fusion of vesicles into planar bilayer, in: *The Structure and Conformation of Amphiphilic Membranes*. Springer Proceedings in Physics, Vol. 66, eds R. Lipowsky, D. Richter and K. Kremer (Springer, Berlin) pp. 162–165.
39. Johnson, S.J., T.M. Bayerl, D.C. McDermott, G.W. Adam, A.R. Rennie, R.K. Thomas and E. Sackmann, 1991, Structure of an adsorbed dimyristoylphosphatidylcholine bilayer measured with specular reflection of neutrons, *Biophys. J.* **59**, 289–294.
40. Servuss, R.-M. and W. Helfrich, 1989, Mutual adhesion of lecithin membranes at ultralow tensions, *J. Phys. France* **50**, 809–827.
41. Harbich, W. and W. Helfrich, 1990, Adhesion in egg lecithin multilayer systems produced by cooling, *J. Phys. France* **51**, 1027–1048.
42. Bayerl, T.M. and M. Bloom, 1990, Physical properties of single phospholipid bilayers adsorbed to micro glass beads, *Biophys. J.* **58**, 357–362.
43. Derjaguin, B.V., A.S. Titijevskaia, I.I. Abricossova and A.D. Malkina, 1954, Investigations of the forces of interaction of surfaces in different media and their application to the problem of colloid stability, *Faraday Discuss. Chem. Soc.* **18**, 24–41.
44. Derjaguin, B.V., 1934, Untersuchungen über die Reibung und Adhäsion, IV, *Kolloid Z.* **69**, 155–164.
45. Derjaguin, B.V. and M. Kussakov, 1939, Anomalous properties of thin polymolecular films, *Acta Physicochem. URSS* **10**, 25–44.
46. Blake, T.D., 1975, Investigation of equilibrium wetting films on n-alkanes on α -alumina, *J. Chem. Soc. Faraday Trans. I* **71**, 192–208.
47. Rädler, J., T.J. Feder, H.H. Strey and E. Sackmann. Fluctuation analysis of tension-controlled undulation forces between giant vesicles and solid substrates.
48. Lipowsky, R. and U. Seifert, 1991, Adhesion of vesicles and membranes, *Mol. Cryst. Liq. Cryst.* **202**, 17–25.
49. Seifert, U. and R. Lipowsky, 1990, Adhesion of vesicles, *Phys. Rev. A* **42**, 4768–4771.
50. Lipowsky, R. and U. Seifert, 1991, Adhesion of membranes: A theoretical perspective, *Langmuir* **7**, 1867–1873.
51. Israelachvili, J.N. and H. Wennerström, 1990, Hydration or steric forces between amphiphilic surfaces?, *Langmuir* **6**, 873–876.
52. Parsegian, V.A. and R.P. Rand, 1991, On molecular protrusion as the source of hydration forces, *Langmuir* **7**, 1299.
53. Israelachvili, J.N. and H. Wennerström, 1992, Entropic forces between amphiphilic surfaces in liquids, *J. Phys. Chem.* **96**, 520–531.
54. Lipowsky, R. and S. Grotehans, 1993, Hydration vs. protrusion forces between lipid bilayers, *Europhys. Lett.* **23**, 599–604.
55. Lipowsky, R. and S. Grotehans, 1994, Renormalization of hydration forces by collective protrusion modes, *Biophys. Chem.* **49**, 27–37.
56. Marcelja, S. and N. Radic, 1976, Repulsion of interfaces due to boundary water, *Chem. Phys. Lett.* **42**, 129–130.
57. Gruen, D.W.R. and S. Marcelja, 1983, Spatially varying polarization in water, *J. Chem. Soc. Faraday Trans. 2* **79**, 225–242.
58. Kjellander, R. and S. Marcelja, 1985, Perturbation of hydrogen bonding in water near polar surfaces, *Chem. Phys. Lett.* **120**, 393–396.
59. Cevc, G., 1985, Molecular force theory of solvation of the polar solutes: The mean-field solvation model, *Chem. Scr.* **25**, 96–107.
60. Kornyshev, A.A., 1985, Non-local dielectric response of a polar solvent, *Chem. Scr.* **25**, 63–66.
61. Belaya, M.L., V.G. Levadnyl and M.V. Feigel'man, 1986, Non-local polarizability of water and hydration interaction between lipid membranes, *Sov. Phys. JETP* **64**, 787–792.
62. Cevc, G., M. Hauser and A.A. Kornyshev, *Interfacial Structure Effects on Hydration Forces: Laterally Uniform Surfaces*, Preprint.
63. Mahanty, J. and B.W. Ninham, 1976, *Dispersion Forces* (Academic Press, London).

64. Atiard, P., D.J. Mitchell and B.W. Ninham, 1988, The attractive forces between polar lipid bilayers, *Biophys. J.* **53**, 457–460.
65. Fenzl, W., Van der Waals Interactions of Membranes, Preprint.
66. Verwey, E.J.W. and J.Th.G. Overbeek, 1948, *Theory of the Stability of Lyophobic Colloids* (Elsevier, Amsterdam).
67. Derjaguin, B.V., N.V. Churaev and V.M. Muller, 1987, *Surface Forces* (Consultants Bureau, New York).
68. Israelachvili, J.N., 1991, *Intermolecular and Surface Forces*, 2nd edition (Academic Press, London).
69. Oosawa, F., 1968, Interaction between parallel rodlike macroions, *Biopolymers* **6**, 1633–1647.
70. Guldbbrand, L., B. Jönsson, H. Wennerström and P. Linse, 1980, Electrical double layer forces, a Monte Carlo study, *J. Chem. Phys.* **80**, 2221–2228.
71. Kjellander, R. and S. Marcelja, 1988, Surface interactions in simple electrolytes, *J. Phys. France* **49**, 1009–1015.
72. Joanny, J.F., L. Leibler and P.-G. de Gennes, 1979, Effects of polymer solutions on colloid stability, *J. Polym. Sci.* **17**, 1073–1084.
73. Evans, E. and D. Needham, 1987, Long range interactions between lipid bilayers in salt solutions and solutions of non-adsorbant polymers, in: *Physics of Amphiphilic Layers*. Springer Proceedings in Physics, Vol. 21, eds J. Meunier, D. Langevin and N. Boccaro (Springer, Berlin) pp. 178–198.
74. de Gennes, P.-G., 1981, Polymer solutions near an interface, 1. Adsorption and depletion layers, *Macromolecules* **14**, 1637–1644.
75. de Gennes, P.-G., 1982, Polymers at an interface, 2. Interaction between two plates carrying adsorbed polymers layers, *Macromolecules* **15**, 492–500.
76. Klein, J. and P.F. Luckham, 1984, Forces between two adsorbed poly(ethylene oxide) layers in a good aqueous solvent in the range 0–150 nm, *Macromolecules* **17**, 1041–1048.
77. Luckham, P.F. and J. Klein, 1985, Interactions between smooth solid surfaces in solutions of adsorbing and nonadsorbing polymers in good solvent conditions, *Macromolecules* **18**, 721–728.
78. de Gennes, P.-G., 1987, Polymers at an interface; a simplified view, *Adv. Colloid Interface Sci.* **27**, 189–209.
79. Lipowsky, R. and B. Zielinska, 1989, Binding and unbinding of lipid membranes: A Monte Carlo study, *Phys. Rev. Lett.* **62**, 1572–1575.
80. Netz, R.R., 1994, *Membranenstapel und Fadenbündel*, PhD thesis, Universität zu Köln.
81. Netz, R.R. and R. Lipowsky, In preparation.
82. Pokrovskii, V.L. and A.L. Talapov, 1980, The theory of two-dimensional incommensurate crystals, *Sov. Phys. JETP* **51**, 269–295.
83. Gruber, E.E. and W.W. Mullins, 1967, On the theory of anisotropy of crystalline surface tension, *J. Phys. Chem. Solids* **28**, 875–887.
84. Brochard, F. and J.F. Lennon, 1975, Frequency spectrum of the flicker phenomenon in erythrocytes, *J. Physique* **36**, 1035–1047.
85. Helfrich, W. and R.-M. Servuss, 1984, Undulations, steric interaction and cohesion of fluid membranes, *Il Nuovo Cimento* **3D**, 137–151.
86. Lipowsky, R. and M.E. Fisher, 1987, Scaling regimes and functional renormalization for wetting transitions, *Phys. Rev. B* **36**, 2126–2141.
87. Lipowsky, R., 1988, Scaling properties of interfaces and membranes, in: *Random Fluctuations and Growth*, eds G. Stanley and N. Ostrowsky (Kluwer Academic Publ., Dordrecht) pp. 227–246.
88. Lipowsky, R., 1988, Lines of renormalization group fixed points for fluid and crystalline membranes, *Europhys. Lett.* **7**, 255–261.
89. Lipowsky, R., 1989, Parabolic renormalization-group flow for interfaces and membranes, *Phys. Rev. Lett.* **62**, 704–707.
90. Feynman, R.P. and A.R. Hibbs, 1965, *Quantum Mechanics and Path Integrals* (McGraw-Hill, New York).
91. Lipowsky, R., 1987, *Critical Behavior of Interfaces: Wetting, Surface Melting and Related Phenomena*, Habilitation-thesis (University of Munich, publ. by KFA Jülich).
92. Leibler, S. and R. Lipowsky, 1987, Complete unbinding and quasi-long-range order in lamellar phases, *Phys. Rev. B* **35**, 7004–7009.

93. Lipowsky, R. and S. Leibler, 1987, Unbinding of membranes, in: *Physics of Amphiphilic Layers*. Springer Proceedings in Physics, Vol. 21, eds J. Meunier, D. Langevin and N. Boccara (Springer, Berlin) pp. 98–105.
94. Wennerström, H., 1990, The unbinding transition and lamellar phase-lamellar phase coexistence, *Langmuir* **6**, 834–838.
95. Lipowsky, R. and A. Baumgärtner, 1989, Adsorption transitions of polymers and crumpled membranes, *Phys. Rev. A* **40**, 2078–2081.
96. de Gennes, P.-G., 1976, Scaling theory of polymer adsorption, *J. Phys.* **37**, 1445–1452.
97. Helfrich, W., 1989, Spontaneous and induced adhesion of fluid membranes, in: *Phase Transition in Soft Condensed Matter*, eds T. Riste and D. Sherrington (Plenum, New York).
98. Lipowsky, R., 1994, Stacks and bunches of fluid membranes, *J. Phys.: Cond. Mat.* **6**, A409–A413.
99. Lässig, M. and R. Lipowsky, 1993, Critical roughening of interfaces: A new class of renormalizable field theories, *Phys. Rev. Lett.* **70**, 1131–1134.
100. Hiergeist, C., 1994, *Aufrauungs- und Ablösungsübergänge in zwei-Dimensionalen Systemen*, Diplomarbeit, Universität su Köln.
101. Lipowsky, R. and T.M. Nieuwenhuizen, 1988, Intermediate fluctuation regime for wetting transitions in two dimensions, *J. Phys. A* **21**, L89–L94.
102. Jülicher, F., R. Lipowsky and H. Müller-Krumbhaar, 1990, Exact functional renormalization group for wetting transitions in $1 + 1$ dimensions, *Europhys. Lett.* **11**, 657–662.
103. Lipowsky, R., 1991, Typical and exceptional shape fluctuations of interacting strings, *Europhys. Lett.* **15**, 703–708.
104. Zia, R.K.P., R. Lipowsky and D.M. Kroll, 1988, Quantum unbinding in potentials with $1/r^p$ tails, *Am. J. Phys.* **56**, 160–163.
105. Grotehans, S. and R. Lipowsky, 1990, Absence of first-order unbinding transitions of fluid and polymerized membranes, *Phys. Rev. A* **41**, 4574–4577.
106. David, F. and S. Leibler, 1990, Multicritical unbinding phenomena and non-linear functional renormalization group, *Phys. Rev. B* **41**, 12926–12929.
107. Grotehans, S. and R. Lipowsky, 1993, The order of the unbinding transition for membranes, in: *Dynamical Phenomena at Interfaces, Surfaces and Membranes*, eds D. Beysens, N. Boccara and G. Forgacz (Nova Science, New York) pp. 267–279.
108. Ammann, A. and R. Lipowsky, In preparation.
109. Bausch, R. and R. Blosser, 1992, Private communication, *Z. Phys. B* **86**, 273.
110. Lipowsky, R., 1984, Upper critical dimension for wetting in systems with long-range forces, *Phys. Rev. Lett.* **52**, 1429–1432.
111. Evans, E.A. and V.A. Parsegian, 1986, Thermal-mechanical fluctuations enhance repulsion between bimolecular layers, *Proc. Nat. Acad. Sci. USA* **83**, 7132–7136.
112. Pincus, P., J.-F. Joanny and D. Andelman, 1990, Electrostatic interactions, curvature elasticity, and steric repulsion in multimembrane systems, *Europhys. Lett.* **11**, 763–768.
113. Evans, E. and J. Ipsen, 1991, Entropy-driven expansion of electric double layer repulsion between highly flexible membranes, *Electrochim. Acta* **36**, 1735–1741.
114. Odijk, T., 1992, Self-consistent theory of a charged multimembrane system, *Langmuir* **8**, 1690–1691.
115. Podgornik, R. and V.A. Parsegian, 1992, Thermal-mechanical fluctuations of fluid membranes in confined geometries: The case of soft confinement, *Langmuir*, pp. 557–562.
116. David, F., 1990, Renormalization group treatment of entropic interactions in lamellar phases, *Colloque de Physique* **51**, C7–115.
117. Gompper, G. and D.M. Kroll, 1989, Steric interactions in multimembrane systems: A Monte Carlo study, *Europhys. Lett.* **9**, 59–64.
118. Janke, W., H. Kleinert and M. Meinhart, 1989, Monte Carlo Study of a stack of self-avoiding surfaces with extrinsic curvature stiffness, *Phys. Lett. B* **217**, 525.
119. Lässig, M. and R. Lipowsky, 1994, Universal aspects of interacting lines and surfaces, in: *Fundamental Problems in Statistical Mechanics VIII*, ed. H. van Beijeren (North-Holland, Amsterdam).
120. Lässig, M., 1994, New criticality of 1d fermions, *Phys. Rev. Lett.* **73**, 561–564.

121. Cook-Röder, J. and R. Lipowsky, 1992, Adhesion and unbinding for bunches of fluid membranes, *Europhys. Lett.* **18**, 433–438.
122. Netz, R.R. and R. Lipowsky, 1993, Critical behavior of three interacting strings, *Phys. Rev. E* **47**, 3039–3042.
123. Netz, R.R. and R. Lipowsky, 1994, Three interacting strings in two dimensions: Non-universal and multiple unbinding transitions, *J. Phys. I France* **4**, 47–75.
124. Lipowsky, R., 1993, Statistical physics of flexible membranes, *Physica A* **194**, 114–127.
125. Huse, D.A. and M.E. Fisher, 1984, Commensurate melting, domain walls, and dislocations, *Phys. Rev. B* **29**, 239–270.
126. Fisher, M.E., 1984, Walks, walls, wetting, and melting, *J. Stat. Phys.* **34**, 667–729.
127. Fisher, M.E. and M. Gelfand, 1988, The reunions of three dissimilar visious walkers, *J. Stat. Phys.* **53**, 175.
128. Helfrich, W., 1993. Mean field theory of n-layer unbinding, *J. Phys. II France* **3**, 385–393.
129. Milner, S.T. and D. Roux, 1992, Flory theory of the unbinding transition, *J. Phys. I France* **2**, 1741–1754.
130. Burkhardt, T.W. and P. Schlottmann, 1993, Unbinding transition in a many-string system, *J. Phys. A* **26**, L501.
131. Hiergeist, C., M. Lässig and R. Lipowsky, 1994, Bundles of interacting strings in two dimensions, *Europhys. Lett.* **28**, 103.
132. Helfrich, W., 1989, Hats and saddles in liquid membranes, *Liq. Cryst.* **5**, 1647–1658.
133. Egberts, E. and H.J.C. Berendsen, 1988, Molecular dynamics simulation of a smectic liquid crystal with atomic detail, *J. Chem. Phys.* **89**, 3718–3732.
134. Marrink, S.J., M. Berkowitz and H.J.C. Berendsen, Molecular Dynamics Simulation of a Membrane-Water Interface: The Ordering of Water and Its Relation to the Hydration Force, Preprint.
135. König, S., W. Pfeiffer, T. Bayerl, D. Richter and E. Sackmann, 1992, Molecular dynamics of lipid bilayers studied by incoherent quasi-elastic neutron scattering, *J. Phys. II France* **2**, 1589–1615.
136. Wiener, M.C. and S.H. White, 1992, Structure of a fluid dioleoylphosphatidylcholine bilayer determined by joint refinement of X-ray and neutron diffraction data, *Biophys. J.* **61**, 434–447.
137. de Gennes, P.-G. and P. Pincus, 1990, Hydration forces: The blister model, *C.R. Acad. Sci.* **319**, 697–700.
138. Bader, H., K. Dorn, B. Hupfer and H. Ringsdorf, 1985, Polymeric monolayers and liposomes as models for biomembranes; how to bridge the gap between polymer science and membrane biology?, *Adv. Polym. Sci.* **64**, 1–62.
139. Sackmann, E., P. Eggl, C. Fahn, H. Bader, H. Ringsdorf and M. Schollmeier, 1985, Compound membranes of linearly polymerized and cross-linked macrolipids with phospholipids: Preparation, microstructure and applications, *Ber. Bunsenges. Phys. Chem.* **89**, 1198–1208.
140. Landau, L.D. and E.M. Lifshitz, 1989, *Elastizitätstheorie* (Akademie-Verlag, Berlin).
141. Nelson, D.R. and L. Peliti, 1987, Fluctuations in membranes with crystalline and hexatic order, *J. Phys. France* **48**, 1085–1092.
142. Lipowsky, R. and M. Girardet, 1990. shape fluctuations of polymerized or solidlike membranes, *Phys. Rev. Lett.* **65**, 2893–2896.
143. Abraham, F.F., 1991, Comment on “shape fluctuations of polymerized or solidlike membranes”, *Phys. Rev. Lett.* **67**, 1669.
144. Petsche, I.B. and G.S. Grest, 1993. Molecular dynamics simulations of the structure of closed tethered membranes, *J. Phys. I France* **1**, 1741–1754.
145. Gompper, G. and D.M. Kroll, 1991, Fluctuations of a polymerized membrane between walls, *J. Phys. I France* **1**, 1411–1432.
146. Le Doussal, P. and L. Radzihovsky, 1992, Self-consistent theory of polymerized membranes, *Phys. Rev. Lett.* **69**, 1209–1212.
147. Abraham, F.F. and M. Kardar, 1991, Folding and unbinding transitions in tethered membranes, *Science* **252**, 419–421.
148. Evans, E., A. Yeung, R. Waugh and J. Song, 1991, Dynamic coupling and nonlocal curvature elasticity in bilayer membranes, in: *The Structure and Conformation of Amphiphilic Membranes.*

- Springer Proceedings in Physics, Vol. 66, eds R. Lipowsky, D. Richter and K. Kremer (Springer, Berlin) pp. 148–153.
149. Seifert, U. and S.A. Langer, 1993, Viscous modes of fluid bilayer membranes, *Europhys. Lett.* **23**, 71–76.
 150. Seifert, U. and S.A. Langer, 1994, Hydrodynamics of membranes: The bilayer aspect and adhesion, *Biophys. Chem.* **49**, 13–22.
 151. Kraus, M. and U. Seifert, 1994, Relaxation modes of an adhering bilayer membrane, *J. Phys. II France* **4**, 1117–1134.
 152. Lipowsky, R., 1992, The physics of flexible membranes, in: *Festkörperprobleme. Advances in Solid State Physics*, Vol. 32, ed. U. Rössler, pp. 19–44.
 153. Siegel, D.P., 1993, Energetics of intermediates in membrane fusion: Comparison of stalk and inverted micellar intermediate mechanisms, *Biophys. J.* **65**, 2124–2140.
 154. Berndt, K., J. Käs, R. Lipowsky, E. Sackmann and U. Seifert, 1990, Shape transformations of giant vesicles: Extreme sensitivity to bilayer asymmetry, *Europhys. Lett.* **13**, 659–664.
 155. Grinstein, G. and R.A. Pelcovits, 1982, Non-linear elastic theory of smectic liquid crystals, *Phys. Rev. A* **26**, 915–925.
 156. Caillé and M.A. Guinier, 1972, Remarques sur la diffusion des rayons X dans les smectiques, *C.R. Acad. Sci.* **274B**, 891.
 157. Roux, D. and C.R. Safinya, 1987, Interactions in lyotropic lamellar phases: A high resolution X-ray study, in: *Physics of Amphiphilic Layers. Springer Proceedings in Physics*, Vol. 21, eds J. Meunier, D. Langevin and N. Boccara (Springer, Berlin) pp. 138–144.
 158. Porte, G., P. Bassereau, J. Marignan and R. May, 1987, Stability of brine swollen lamellar phases, in: *Physics of Amphiphilic Layers. Springer Proceedings in Physics*, Vol. 21, eds J. Meunier, D. Langevin and N. Boccara (Springer, Berlin) pp. 145–152.
 159. Kallabis, H. and M. Lässig, In preparation.

Electrostatic Properties of Membranes: The Poisson–Boltzmann Theory

D. ANDELMAN

*School of Physics and Astronomy, Tel Aviv University,
Ramat Aviv 69978, Tel Aviv, Israel*

Contents

1. Introduction	605
2. Charged surfaces in liquids: general considerations	607
2.1. Poisson–Boltzmann equation	608
2.2. Electrostatic free energy and electrostatic pressure	610
2.3. Beyond Poisson–Boltzmann: recent theory and experiment	611
3. A single flat and charged membrane	612
3.1. No added electrolyte	612
3.2. Added electrolyte	613
4. Two flat charged membranes	614
4.1. No added electrolyte	615
4.2. Added electrolyte	617
5. Flexible and charged membranes: general considerations	622
6. A single charged and flexible membrane	623
6.1. Electrostatic boundary conditions for bilayer membranes	624
6.2. One curved (spherical or cylindrical) charged membrane	625
6.3. One undulating membrane	627
6.4. Membranes with variable surface charge density	628
7. A stack of charged lamellae	629
7.1. Suppression of Helfrich interactions by electrostatics	630
7.2. Rigidity of charged lamellae	633
8. Conclusions and future prospects	639
Acknowledgments	640
References	640

1. Introduction

Biological membranes are complex and heterogeneous objects separating living cells from their extra-cellular surroundings. Many of the membrane structural properties depend substantially on electrostatic interactions [1, 2], e.g., rigidity, structural stability, lateral phase transitions (the ‘main’ transition), and dynamics. Furthermore, electric charges have a very important role in processes involving more than one membrane such as membrane adhesion and cell-cell interaction, as well as the overall interaction of the membrane with other intra- and extra-cellular molecules.

The delicate interplay between charged membranes and their surrounding ionic solution can simply be explained as following. As any charged object immersed in an ionic solution, the membrane attracts a cloud of opposite charges forming a *diffusive* ‘electric double layer’ [1–5]. The exact distribution of the charges is given by the competition between the electrostatic interactions and the entropy of the ions in the solution which tends to disperse them. This diffusive electric double layer in turn influences the overall electrostatic interactions of the membrane with its environment as well as the ‘internal’ membrane properties.

Electrostatic interactions constitute a key component in understanding interactions *between* charged bodies in ionic solutions. For example, the stability of colloidal particles dispersed in a solvent [1, 2] can be explained by considering the competition between repulsive electrostatic interactions and attractive Van der Waals interactions. Electrostatic interactions are also of importance when considering interactions and adhesion between membranes. Furthermore, strong (unscreened) electrostatic interactions tend to rigidify flexible objects such as membranes and charged polymers (polyelectrolytes). Another characteristic of ions in solutions is that due to entropic effects, temperature is an important parameter controlling equilibrium properties.

The aim of this chapter is to review some of the basic considerations underlying the behavior of charged membranes in aqueous solutions. Due to the tremendous complexity of *real* biological membranes, we will restrict ourselves to very simple *model* charged membranes and will rely on the following assumptions and simplifications:

- We will mainly be concerned with the interplay between electrostatic interactions and the structure of the membrane *as a whole*. The membrane will be treated in the *continuum limit* as an interface with some degree of flexibility and with a given surface charge distribution. Equipotential membranes (of a given surface potential) will also be mentioned in some of the cases. We will not discuss special function regions within real heterogeneous membranes such as ion channels which have a specific biological function.
- This review will present in detail only theoretical results. Some experimental results will be mentioned. The reader should look at the chapter by Parsegian

and Rand for more details on experiments. The calculations are limited to solutions of the Poisson–Boltzmann equation (mean field theory). The finite size of the ions in the solution and within the membrane is ignored. The electric potential and the charge densities of the various ions are described by continuous variables (using the continuum hypothesis). For theoretical results which go beyond the continuum approach, we provide a few references and a short summary in the next section.

- We will not discuss the effect of electrostatics on dynamic properties of membranes and restrict ourselves to the static ones (in thermodynamical equilibrium) as well as fluctuations. These are the properties which are presently better understood. In addition, we will not consider the important interplay between electrostatics and other interactions (Van der Waals, hydration, etc.).

This review is organized in the following way: after some general considerations of charged surfaces in liquids and the derivation of the Poisson–Boltzmann equation (section 2), we present specific solutions of several electrostatic problems starting with a single flat and rigid membrane in section 3, and generalizing it to two flat membranes in section 4. Then, we consider the possibility of having a flexible membrane in various situations: a single membrane (section 6), two membranes, a stack of membranes, etc. (section 7). Special emphasis is given to the coupling between the electrostatic and the elastic properties. Some concluding remarks are presented in section 8.

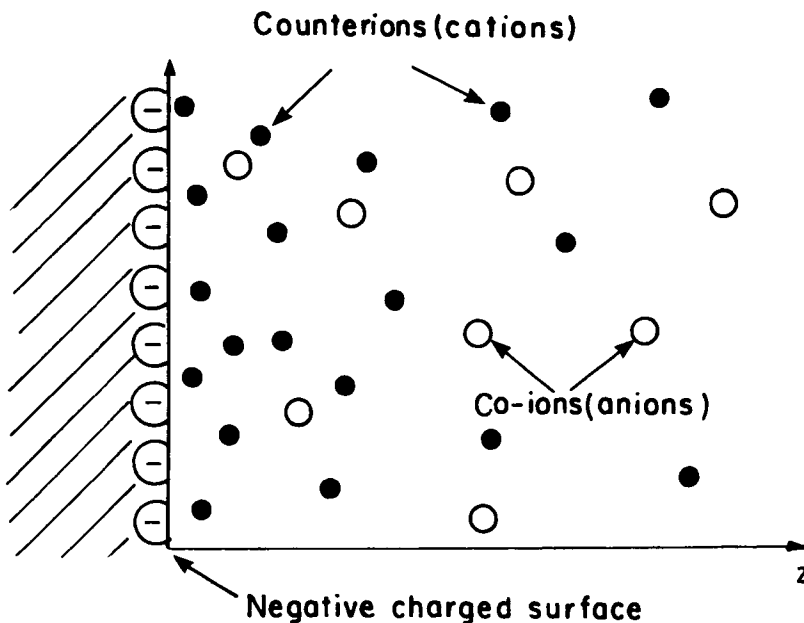


Fig. 1. Schematic illustration of the electric double layer problem. A surface which is negatively charged and immersed in an aqueous solution is attracting (positive) counterions and creates a depletion zone of the (negative) co-ions. The z axis denotes the distance from the surface. Adapted from ref. [2].

2. Charged surfaces in liquids: general considerations

Consider a charged and flat surface as displayed in fig. 1. In an ideal situation, this is a sharp boundary (located at $z = 0$) which limits the ionic solution to the half space $z > 0$. The ionic solution contains, in general, both anions and cations and is characterized by a dielectric constant ϵ_w assumed to be the dielectric constant of the water throughout the fluid. The boundary has two effects on the electrostatics of the system: (i) In the case of a charged boundary (equipotential boundary), the surface is characterized by a surface charge distribution (a surface potential). (ii) Even in the absence of surface charges, the boundary represents a discontinuous jump of the dielectric constant between the ionic solution and a different dielectric medium.

In fig. 2, a schematic view of a charged amphiphilic membrane is presented. The membrane of thickness t is composed of two monomolecular layers. The constituting molecules are amphiphiles having a charged moiety ('head') and an aliphatic moiety (hydrocarbon 'tail'). For phospholipid membranes, the molecules have a double tail (not drawn). We will model the membrane as a medium of thickness t having a dielectric constant ϵ_{oil} coming essentially from the closely packed hydrocarbon ('oily') tails. The molecular heads contribute to the surface charges and the entire membrane is immersed in an aqueous solution with a dielectric constant ϵ_w .

The surface charge can have two origins: Either a charge group (e.g., proton) dissociates from the polar head group into the aqueous solution leaving behind a charged surface, or an ion from the solution (e.g., Ca^{++}) binds to a neutral membrane. These processes are highly sensitive to the ionic strength and pH of the aqueous

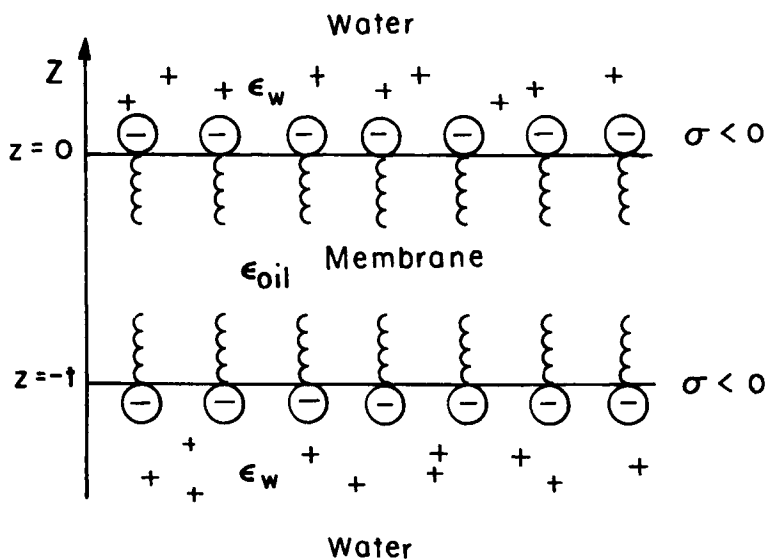


Fig. 2. A closer look at a bilayer membrane composed of two negatively charged surfaces, each of surface charge density σ . The membrane thickness is t and the 'inside' (hydrocarbon) dielectric constant is ϵ_{oil} . The water dielectric constant is $\epsilon_w \simeq 80$. The z axis denotes the distance from the membrane and its origin ($z = 0$) is chosen on the upper layer of the membrane.

solution. In many situations the finite thickness of the membrane can be safely taken to be zero and then the membrane surface is modeled like in fig. 1 – a single charged surface in contact with an ionic solution. We will see later in what conditions this frequently used limit is valid.

Without loss of generality, we assume that the membrane is negatively charged and take the surface charge density (per unit area) as a negative constant, $\sigma < 0$. In terms of the ionic solution itself, two different electrostatic situations will be distinguished throughout this review:

- (i) no electrolyte is added to the water, and the only ions in the solution are the counterions balancing exactly the charges within the membrane due to charge neutrality. Within the continuum hypothesis, the (positive) counterions in the solution at a point \vec{r} are described by a charge distribution $\rho_+(\vec{r}) = ez_+n_+(\vec{r})$, where the valency $z_+ = 1$ for monovalent ions, $e > 0$ is the electron unit charge and n_+ is the number density (per unit volume) of the counterions. Note, however, that even in pure water there is a finite concentration of H^+ and OH^- ions of about 10^{-7} M, due to a finite degree of dissociation of the water molecules themselves, making even pure water a very weak electrolyte.
- (ii) The solution is in contact with an electrolyte (salt) reservoir of fixed concentration n_0 . Two types of charge carries are present in the solution: co-ions and counterions and both types are in thermal equilibrium with the reservoir. We will not further differentiate between the activities of different ionic groups with the same charge. We assume for simplicity only one type of co-ions and one of counterions. The total charge density $\rho(\vec{r})$ at each point \vec{r} is the sum of the two ionic densities: $\rho(\vec{r}) = ez_+n_+(\vec{r}) + ez_-n_-(\vec{r})$, where z_+ (z_-) is the valency of the counterions (co-ions).

2.1. Poisson–Boltzmann equation

The relation between the electric potential $\psi(\vec{r})$ and the charge distribution $\rho(\vec{r})$ at any point \vec{r} is given by the Poisson equation

$$\nabla^2\psi = -\frac{4\pi}{\epsilon_w}\rho(\vec{r}) = -\frac{4\pi e}{\epsilon_w}(z_-n_- + z_+n_+) \quad (2.1)$$

where $\epsilon_w \simeq 80$ is the dielectric constant of the aqueous solution taken as a constant within the fluid.

In principal, ψ and all other electrostatic properties can be evaluated for a given surface charge distribution (so-called Neumann boundary condition) or surface potential (so-called Dirichlet boundary condition). In this review we will mainly consider the Neumann boundary condition of fixed surface charge distribution, but it is rather straightforward to repeat the calculations for the constant surface potential case. (See also ref. [6] for another type of boundary condition where the degree of dissociation was allowed to be a variable chosen by the system.)

The Poisson equation (2.1) determines the electric potential for a given spatial charge distribution $\rho(\vec{r})$. However, even for a fixed *surface* charge distribution σ , the ions in the solution are mobile and can adjust their positions. In thermal equilibrium,

and using the continuum hypothesis, the ‘smeared out’ local density distributions of the two ions $n_{\pm}(\vec{r})$ (in units of number per unit volume) adjust to the presence of the electric potential. The electro-chemical potential μ_i of the i th ion is defined as $\mu_i = ez_i\psi + T \ln n_i$, where the first term is the electrostatic contribution and the second one comes from the (ideal) entropy of the ions in the weak solution limit. In thermal equilibrium μ_i remains constant throughout the system. Consequently, each ion density in the solution obeys a Boltzmann distribution according to the electric potential it feels:

$$n_i = n_0^{(i)} e^{-ez_i\psi/T}. \quad (2.2)$$

Note that we adopt the convention of expressing T in units of energy (setting the Boltzmann constant to unity). Combining eqs (2.1) and (2.2), we get the *Poisson–Boltzmann equation* which determines the potential ψ self-consistently

$$\nabla^2\psi(\vec{r}) = -\frac{4\pi e}{\epsilon_w} \left(z_+ n_0^{(+)} e^{-ez_+\psi(\vec{r})/T} + z_- n_0^{(-)} e^{-ez_-\psi(\vec{r})/T} \right). \quad (2.3)$$

Generally speaking, the Poisson–Boltzmann theory is a good approximation in most physiological conditions, especially for monovalent ions and for surface potentials which are not too large. Close to the charged surface, the finite size of the surface ionic groups and that of the counterions leads to deviations from the Poisson–Boltzmann results. In section 2.3 we mention a few results which are going beyond the Poisson–Boltzmann theory.

We discuss now separately the two electrostatic cases which were introduced in section 1. In the first case, no electrolyte is added, and the only ions in the solution are the counterions. Hence, $n_0^{(-)} = 0$ and we define $n_0 \equiv n_0^{(+)}$ as the reference density for which $\psi = 0$. The Poisson–Boltzmann equation (2.3) is then reduced to:

$$\nabla^2\psi(\vec{r}) = -\frac{4\pi en_0}{\epsilon_w} e^{-e\psi(\vec{r})/T}. \quad (2.4)$$

In the other situation where the system is in contact with a 1:1 electrolyte reservoir (e.g., Na^+Cl^-), $n_0^{(\pm)} = n_0$ is the electrolyte concentration in the reservoir and

$$\nabla^2\psi(\vec{r}) = \frac{8\pi en_0}{\epsilon_w} \sinh(e\psi(\vec{r})/T). \quad (2.5)$$

Note that although eq. (2.3) holds for any valencies z_{\pm} , in eqs (2.4)–(2.5) we inserted explicitly $z_{\pm} = \pm 1$. Only this case of monovalent ions will be discussed hereafter since it makes the mathematical derivation easier to follow. Divalent ions such as Ca^{++} have important consequences on the electrostatics of membranes [7]. Most of those consequences go beyond the continuum approach of the Poisson–Boltzmann theory.

Equations (2.4) and (2.5) are non-linear equations in the electric potential ψ . For some boundary conditions they can be solved analytically. However, in general, one

has to rely on numerical or perturbative solutions. Whereas the classical works in this field date from the beginning of the century with the works of Gouy [3] and Chapman [4] for the case of flat boundary conditions, application to flexible and charged membranes is a rather recent development.

A useful and quite tractable approximation to the full Poisson–Boltzmann equation (2.5) is its linearized version. This can be justified for surface potentials which are smaller than 25 mV at room temperature. Expanding the righthand side of eq. (2.5) to first order in ψ we get

$$\nabla^2\psi(\vec{r}) = \lambda_D^{-2}\psi \quad (2.6)$$

where $\lambda_D = (8\pi n_0 e^2 / \epsilon_w T)^{-1/2} \sim n_0^{-1/2}$ is called the *Debye–Hückel screening length*. It varies from about 3 Å for a 1 M of 1:1 electrolyte like NaCl to about 1 μm for pure water (due to the ever presence of H⁺ and OH⁻ ions even in pure water with an ionic strength of about 10⁻⁷ M). In the presence of a relatively strong electrolyte, the electrostatic interactions are exponentially screened and can be effectively neglected for lengths larger than the Debye–Hückel screening length, λ_D . This is further explained in section 3.1.

2.2. Electrostatic free energy and electrostatic pressure

Up to now we discussed the Poisson–Boltzmann equation for the electric potential. It is also useful to evaluate the electrostatic *free energy* of the electric double layer problem as it will give us the electrostatic pressure between two charged surfaces in a liquid as well as the contribution to the membrane bending constant.

Two equivalent methods of calculating the electrostatic free energy are discussed at length by Verwey and Overbeek [1] leading to the following expression for the free energy per unit area

$$f_{el}[\sigma] = \int_0^\sigma \psi_s(\sigma') d\sigma' \quad (2.7)$$

where $\psi_s(\sigma')$ is the surface potential calculated for a fixed surface charge distribution σ' . The total free energy is obtained by integrating (2.7) over the entire charged surfaces. In the linear regime (eq. (2.6)), the free energy (2.7) simply reduces to $\frac{1}{2}\psi_s\sigma$ since the surface potential ψ_s is linear in the surface charge density σ .

Equation (2.7) can also be derived by considering the excess *bulk* free energy over that of the homogeneous electrolyte reservoir of concentration n_0 and with $\psi = 0$.

$$F_{el} = \frac{\epsilon_w}{8\pi} \int (\nabla\psi)^2 dV + T \int (n_+ \ln(n_+/n_0) + n_- \ln(n_-/n_0) - (n_+ + n_- - 2n_0)) dV \quad (2.8)$$

where the first term is the electrostatic internal energy, and the second accounts for the entropy of (monovalent) ions in the solution. Using the Poisson–Boltzmann equation and Green's theorem, eq. (2.8) can be transformed into the surface integral, eq. (2.7). For the boundary condition of constant surface potential, a similar expression to (2.7) can be derived [8].

The electrostatic pressure can be calculated in several different ways [1, 2]. It is defined as the force per unit area felt by the two charged membranes (boundaries) separated by a distance d in the aqueous solution. One straightforward way of calculating the pressure $P(d)$ is to take the variation of the free energy with respect to the inter-membrane distance d : $P(d) = -\partial f_{el}/\partial d$. This is discussed in more detail in sections 4 and 7.

2.3. Beyond Poisson–Boltzmann: recent theory and experiment

As this review deals exclusively with the Poisson–Boltzmann theory, we mention here some recent theoretical results and experiments which go beyond the simpler Poisson–Boltzmann theory.

The assumptions which led to the derivation of the Poisson–Boltzmann equation (2.3) [3–5] can be summarized as follows: the ionic charge distributions are smeared out and are represented as smoothly varying functions. The discrete nature of the ions is not taken into account and no other molecular interaction between the ions and solvent molecules (water) is considered. See the chapters by Parsegian and Rand, Lipowsky, Helfrich and Evans in this Handbook and refs. [1, 2, 9–11] for a detailed discussion of Van der Waals, hydration and other forces occurring between surfaces in water.

Moreover, the Poisson–Boltzmann theory does not take into account any charge-charge correlations. Physical observables like the charge distributions are replaced by their thermal averages and, in this sense, resemble mean-field results. An extension of the Poisson–Boltzmann theory including effects of charge images and ion correlations has been developed for counterions (no-added electrolyte) [12] and for symmetric electrolytes [13]. At large separations the corrections to the Poisson–Boltzmann theory appear as an effective surface charge.

Another approach was used by Kjellander and Marcelja [14, 15]. The hard-core repulsion between ions for inhomogeneous Coulomb fluids with long range correlation has been formulated. This method relies on numerical solutions of the integral equations for the charge profiles between two boundaries using the *hypernetted chain* closure relation. In a more recent study [16] the hypernetted chain approach was compared with Monte Carlo simulations for 1:1, 1:2, and 2:2 electrolyte solutions. The agreement is good except for very short separation between the two boundaries.

Interesting behavior was observed for 2:1 electrolytes (e.g., Ca^{++}) [7] using the force machine apparatus to measure forces between charged surfaces immersed in aqueous calcium solutions. It was found that at small separation, the forces between the two surfaces can be attractive due to the presence of the calcium ions. This is in agreement with the anisotropic hypernetted chain calculations [7]. The consequences of those attractive forces at small separation on membrane adhesion are discussed in ref. [17]. See, for example, refs [14, 18, 19] for more details on recent experiments.

Finally, we mention an older attempt to improve upon the Poisson–Boltzmann theory close to the charge surface [1, 2, 20]. The Poisson–Boltzmann potential is used up to a distance δ from the surface. There, it is matched with a proximity potential which takes into account the finite size of the various ionic groups. This is the so-called *Stern* and *Helmholtz layer* effect and the thickness δ is of order one to two angstroms [21].

3. A single flat and charged membrane

The simplest problem to be solved using the Poisson–Boltzmann equation is for one *single-sided* flat membrane. The membrane surface occupies the $z = 0$ plane, and has a constant surface charge density σ (see figs. 1 and 2). The aqueous solution occupies the positive half space, $z > 0$. The electric field vanishes for large z , is taken as zero for $z < 0$, and is related to the surface charge density σ by the electrostatic boundary conditions at $z = 0$

$$\left. \frac{\partial \psi}{\partial z} \right|_{z=0} = -\frac{4\pi}{\epsilon_w} \sigma > 0. \quad (3.1)$$

The simplifying assumption that the electric field does not penetrate inside the ‘oily’ part of the membrane, namely, where the aliphatic ‘tails’ are packed, can be justified [22, 23] for typical values of membrane thickness and $\epsilon_{\text{oil}}/\epsilon_w$. It is valid as long as the ratio of the two dielectric constants, $\epsilon_{\text{oil}}/\epsilon_w$, is much smaller than the ratio t/λ_D , where t is the membrane thickness and λ_D is the Debye–Hückel screening length (see fig. 2). All our results for one and two *flat* membranes (sections 3–4) rely on this decoupled limit where the two sides (monolayers) of the membrane are completely decoupled and the electric field inside the membrane is zero. However, we will return to this point in a more quantitative way in section 6.

3.1. No added electrolyte

When no electrolyte is added, there is only one type of ions in the solution $n_+(z) = n(z)$ and the Poisson–Boltzmann equation (2.4) can be integrated exactly using the boundary condition (3.1). The potential and the counterion density distribution in the aqueous solution ($z > 0$) are given by

$$\begin{aligned} \psi(z) &= \frac{2T}{e} \ln(z + b) + \psi_0, \\ n(z) &= \frac{1}{2\pi l} \frac{1}{(z + b)^2}, \end{aligned} \quad (3.2)$$

where ψ_0 is a reference potential. Two useful lengths are introduced in eq. (3.2): the *Bjerrum length*, $l = e^2/(\epsilon_w T)$, and the so-called *Gouy–Chapman length*,

$$b = e/(2\pi|\sigma|l) = \epsilon_w T/(2\pi e|\sigma|).$$

Whereas the Bjerrum length is a constant length of about 7 Å for aqueous solutions at room temperature, the Gouy–Chapman length characterizes the thickness of the diffusive counterion layer close to the membrane (only when *no electrolyte is added* to the solution as in eq. (3.2)). Although the counterion profile decays slower than an exponential, the integrated amount of counterions (per unit area) attracted to the surface from $z = 0$ to $z = b$ is exactly $-\sigma/2$. Namely, it balances half of the surface charge. Note that the potential in eq. (3.2) has a logarithmic divergence at large z . This weak divergence is a consequence of the infinite lateral extent of the charged boundary (membrane) used to obtain eq. (3.2). The divergence will disappear for any membrane with finite dimensions.

3.2. Added electrolyte

In many biological situations, the charged membrane is in contact with a reservoir of electrolyte. Taking the bulk electrolyte concentration as n_0 , eq. (2.5) can be solved with the boundary condition (3.1) in addition to having a vanishing potential and electric field at infinity with $n_{\pm}(\infty) = n_0$. The resulting potential is

$$\psi(z) = -\frac{2T}{e} \ln \frac{1 + \gamma e^{-z/\lambda_D}}{1 - \gamma e^{-z/\lambda_D}} \quad (3.3)$$

where the parameter γ is the positive root of the quadratic equation:

$$\gamma^2 + \frac{2b}{\lambda_D} \cdot \gamma - 1 = 0. \quad (3.4)$$

The surface potential $\psi_s = \psi(0)$ is related to γ and hence to b/λ_D by

$$\psi_s = -\frac{4T}{e} \operatorname{arctanh}(\gamma). \quad (3.5)$$

Typical profiles of the potential $\psi(z)$ and the ion densities in the solution $n_{\pm}(z)$ are shown in fig. 3. Since the surface charge was taken as negative, one can see from eq. (3.1) that the potential tends to zero from below at large z . Hence, it is negative for all z values. At larger z , both densities n_{\pm} tend to the reservoir (bulk) value n_0 , where the potential is zero. However, their distributions are quite different close to $z = 0$ since the counterions are attracted to the charged surface whereas the co-ions are repelled from it.

In the limit of a strong electrolyte, the surface potential ψ_s is small enough so a linearization of the Poisson–Boltzmann equation can be justified. By either solving directly the linear Poisson–Boltzmann equation (2.6), or substituting the small ψ_s limit in eqs. (3.3)–(3.5) one obtains

$$\psi(z) = \psi_s e^{-z/\lambda_D} = -\frac{4\gamma T}{e} e^{-z/\lambda_D}. \quad (3.6)$$

One readily sees from (3.6) and fig. 3 that the electrostatic properties (e.g., electric potential, ionic concentration profiles) are strongly screened and decay exponentially in the Debye–Hückel limit of strong electrolytes. The ‘diffusive layer’ of ions in the solution is characterized by a ‘thickness’ λ_D . This thickness is quite different from the no-added electrolyte case, eq. (3.2). There, the algebraically decaying profile of counterions is characterized by the thickness b .

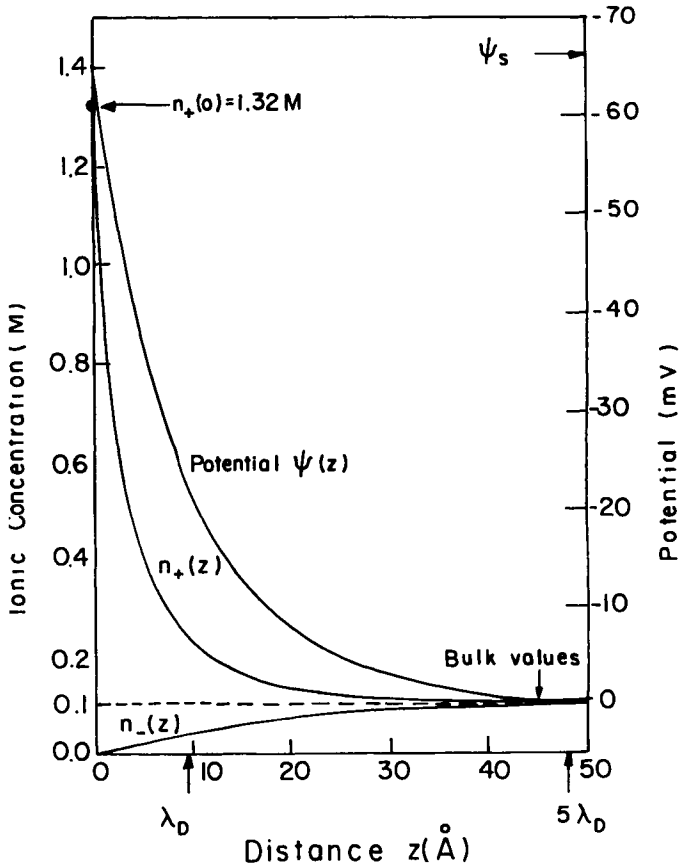


Fig. 3. Typical electric potential $\psi(z)$, counterion concentration $n_+(z)$ and co-ions concentration $n_-(z)$ profiles as function of the distance z from *one* charged surface. The electrolyte is monovalent with a bulk concentration of $n_0 = 0.1$ M. The surface charge is $\sigma = -0.0385$ electronic charge per \AA^2 , corresponding to about one charge per area of 26\AA^2 and the surface potential is $\psi_s = -62.2$ mV. Distances corresponding to $\lambda_D \simeq 9.5 \text{\AA}$ and $5\lambda_D \simeq 47.5 \text{\AA}$ are denoted by arrows on the z axis. Adapted from ref. [2].

4. Two flat charged membranes

The results for a *single* flat membrane can be extended to include the case of *two* identically charged planar membranes [24] at a separation d , immersed in an aqueous solution as is illustrated in fig. 4. One membrane is located at $z = -d/2$ while the other is at $z = d/2$. The surface potential on both membranes is denoted by $\psi_s = \psi(z = \pm d/2)$, and the midplane one by $\psi_m = \psi(z = 0)$. Again two cases will be considered: (i) no electrolyte is added and the total amount of counterions in the solution exactly balances the surface charge. (ii) The aqueous solution is in contact with an electrolyte reservoir of concentration n_0 .

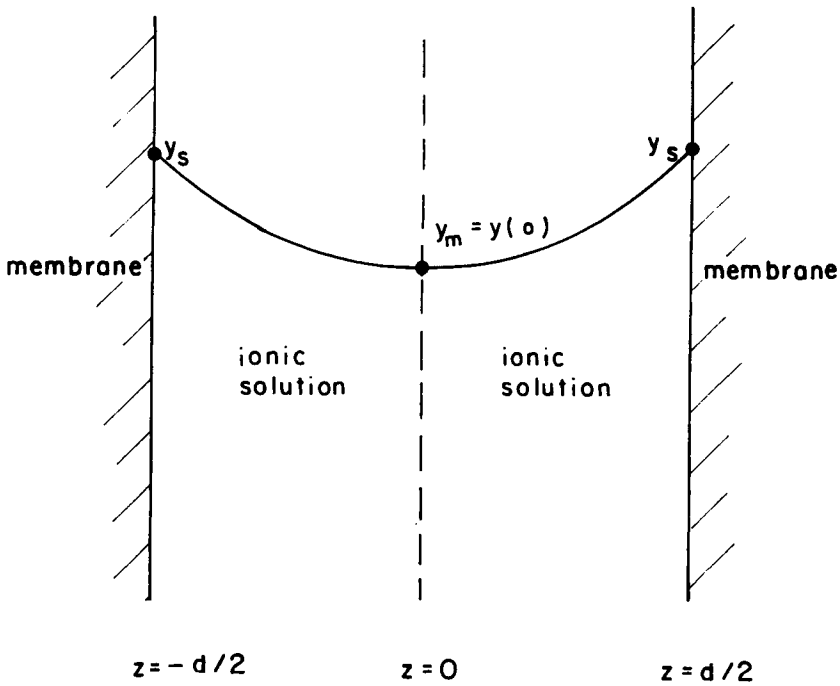


Fig. 4. Schematic drawing of a potential profile $y(z)$ (in rescaled units) between two membranes with the same negative charge separated by a distance d . The surface potential in rescaled units is $y_s = -e\psi_s/T$ and the midplane potential (where the electric field vanishes) is $y_m = -e\psi_m/T$.

One of the interesting and measurable physical quantities is the electrostatic pressure P felt by the membranes. It is equal (up to a sign) to the variation of the free energy density with respect to the inter-membrane distance d , eq. (2.7), $P(d) = -\partial f_{el}/\partial d$. For two flat boundaries, it can be shown [1, 2] that P is directly proportional to the increase in the concentration of ions at the midplane. Namely, $P(d)$ is the excess in osmotic pressure of the ions at the midplane over the bulk pressure

$$P(d) = T \sum_{i=\pm 1} (n_i(z=0) - n_0^{(i)}) \tag{4.1}$$

where $\sum_i n_i(z=0)$ is the total ionic concentration at the midplane and $\sum_i n_0^{(i)}$ is known from the electrolyte reservoir concentration.

4.1. No added electrolyte

In this case the Poisson–Boltzmann equation (2.4) can be solved analytically [2, 25, 26]. Since the two boundaries at $z = \pm d/2$ are symmetric about $z = 0$ (fig. 4), it is

sufficient to solve the Poisson–Boltzmann equation only in the interval $[0, d/2]$. The appropriate boundary conditions are $\partial\psi/\partial z|_{z=d/2} = (4\pi/\epsilon_w)\sigma < 0$ on the membrane; and from symmetry, a vanishing electric field at the midplane: $\partial\psi/\partial z|_{z=0} = 0$. Combining these boundary conditions with the differential equation, eq. (2.4), results in analytical expressions for $\psi(z)$ and $n(z)$:

$$\begin{aligned}\psi(z) &= \frac{T}{e} \ln(\cos^2 Kz) < 0, \\ n(z) &= n_m e^{-e\psi(z)/T} = \frac{n_m}{\cos^2 Kz}.\end{aligned}\tag{4.2}$$

Note that the midplane potential ψ_m is taken as the reference potential, and $n_m = n(z=0)$ is the midplane ionic concentration. The length K^{-1} (to be distinguished from the Debye–Hückel screening length λ_D) is related to n_m via

$$K^2 = \frac{2\pi e^2}{\epsilon_w T} n_m\tag{4.3}$$

and in turn can be related to the surface charge density σ using the membrane boundary condition

$$Kd \tan(Kd/2) = -\frac{2\pi e\sigma}{\epsilon_w T} d = \frac{d}{b}\tag{4.4}$$

where the Gouy–Chapman length $b = -\epsilon_w T / (2\pi e\sigma) \sim \sigma^{-1}$ was defined already after eq. (3.2).

The pressure (4.1) in the case of no-added electrolyte [25, 26] is simply $P(d) = Tn_m$ or in terms of K from eq. (4.3)

$$P(d) = \frac{\epsilon_w T^2}{2\pi e^2} K^2 = \frac{T}{2\pi l} K^2.\tag{4.5}$$

Two limits can now be discussed depending on the ratio d/b in eq. (4.4): (i) small surface charge density, $d/b \ll 1$, called the ideal-gas regime; and (ii) large surface charge density, $d/b \gg 1$, called the Gouy–Chapman regime. These two limits will be discussed in more detail in the next section when we consider the added electrolyte case. The former case, $d/b \ll 1$, yields from (4.4) $Kd \ll 1$ and $K^2 = 2/(bd)$. This is the case where the variation of the potential profile and ion concentration between the plates is minimal. The pressure varies like $1/d$, and essentially comes from the entropy of a homogeneous *ideal gas* of ions in solution

$$P(d) = -\frac{T}{d} \frac{2\sigma}{e} = \frac{T}{\pi l b} \frac{1}{d}\tag{4.6}$$

since $-2\sigma/ed$ is the average density of counterions needed to neutralize the two surfaces of surface charge σ each.

In the other limit of large surface charge density $d/b \gg 1$, one can see from eq. (4.4) that $Kd/2$ approaches a limiting value of $\pi/2$. The pressure varies as $1/d^2$

$$P(d) = \frac{\pi T}{2l} \frac{1}{d^2} = \frac{\pi \epsilon_w T^2}{2e^2} \frac{1}{d^2} \quad (4.7)$$

and is independent of the surface charge density σ . The last equation is closely related to the *Langmuir equation* [27] which describes the electrostatic contribution to the disjoining pressure of wetting films. This is the region where the electrostatic interactions are long range and unscreened. Of course, even in pure water the effective Debye–Hückel screening length is about $1 \mu\text{m}$ and the electrostatic interactions will always be screened for larger distances.

The electrostatic free energy can be evaluated either directly from (2.7) or as the integral over the pressure: $f(d) - f_\infty = \int P(d) \delta d$. In the ideal-gas limit ($b \gg d$) it varies as $\ln d$, whereas in the strong surface charge limit ($b \ll d$) it varies as $1/d$.

We turn now to the added electrolyte case. Note that the no-added electrolyte case discussed above can be obtained formally as the limit of vanishing electrolyte strength (very large λ_D). This will be shown in the next section.

4.2. Added electrolyte

When an aqueous solution between the two membranes is in contact with an electrolyte reservoir, the appropriate Poisson–Boltzmann equation to solve is eq. (2.5) as was explained in section 2. For a single membrane, the potential can be evaluated analytically as in eq. (3.3). However, for two charged membranes, ψ can only be expressed as an elliptic integral [1].

In terms of a dimensionless potential $y(z) \equiv -e\psi(z)/T$, eq. (2.5) and the boundary conditions are written as

$$\begin{aligned} \frac{\partial^2 y}{\partial z^2} &= \lambda_D^{-2} \sinh y, \\ \frac{\partial y}{\partial z} \Big|_{z=d/2} &= \frac{2}{b}, \quad \frac{\partial y}{\partial z} \Big|_{z=0} = 0. \end{aligned} \quad (4.8)$$

Using the notation $y_s \equiv y(d/2)$ on the membrane and $y_m \equiv y(0)$ on the midplane (see fig. 4) the first integration of eq. (4.8) yields

$$\lambda_D \frac{\partial y}{\partial z} = \sqrt{2 \cosh y(z) - 2 \cosh y_m}. \quad (4.9)$$

Note that $y(z) > 0$ (since it is proportional to $-\psi(z)$) for the entire interval $[0, d/2]$ and $y_s > y_m > 0$. A second integration of eq. (4.9) results in an elliptic integral which determines the potential y at any point of space z

$$z = \lambda_D \int_{y_m}^y (2 \cosh y' - 2 \cosh y_m)^{-1/2} dy'. \quad (4.10)$$

The boundary condition (4.8) combined with eq. (4.9) gives one relation between y_m and y_s

$$\frac{2}{b^2} \lambda_D^2 = \cosh y_s - \cosh y_m \quad (4.11)$$

whereas a second relation is obtained by substituting $z = d/2$ in eq. (4.10). Thus, up to performing the elliptical integration in (4.10), the profile $y(z)$ is uniquely determined and depends only on the three parameters in our problem: the spacing d , the surface charge σ and the reservoir concentration n_0 .

The general expression for the pressure $P(d)$ is obtained from (4.1) where the midplane ionic concentration for each charge is $n_m^{(\pm)} = n^{(\pm)}|_{z=0} = n_0 \exp(\pm y_m)$. Then

$$P(d) = T(n_m^{(-)} + n_m^{(+)} - 2n_0) = 2Tn_0(\cosh y_m - 1). \quad (4.12)$$

Since the elliptical integral in (4.10) can be solved only numerically, it is useful to separate the general solution of eq. (4.10) into several limits where approximate potentials and free energies can be calculated analytically. We will define these limits in terms of the three introduced lengths: the spacing between the two membranes d , the Debye–Hückel screening length $\lambda_D \sim n_0^{-1/2}$, and the Gouy–Chapman length $b \sim \sigma^{-1}$. As can be seen from fig. 5, the parameter space $(b/d, \lambda_D/d)$ is divided into four regions: the ideal-gas region; the Gouy–Chapman region; the Intermediate region and the Debye–Hückel region. The ideal-gas and Gouy–Chapman regions are limiting cases of no-added electrolyte (discussed in section 4.1) as will be demonstrated below.

4.2.1. Ideal-gas region

The elliptic integral (4.10) can be evaluated in the limit of large potential $y(z) \gg 1$ ($|e\psi(z)| \gg T$) and small membrane separation $d \ll \lambda_D$. Substituting $z = d/2$ in eq. (4.10) yields a relation between y_s and y_m :

$$e^{-(y_s - y_m)/2} = \cos \left(\frac{d}{4\lambda_D} e^{y_m/2} \right). \quad (4.13)$$

Another relation between y_s and y_m is obtained from the boundary condition (4.11) in the same limit of large $y(z)$

$$\frac{4\lambda_D^2}{b^2} = e^{y_s} - e^{y_m}. \quad (4.14)$$

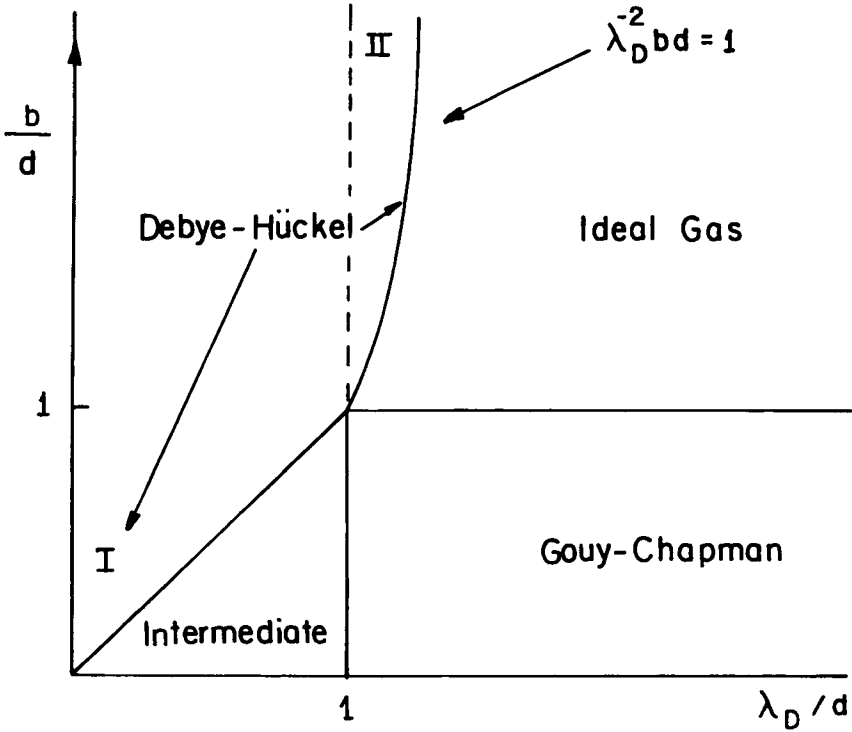


Fig. 5. Schematic representation of various limits of the full Poisson–Boltzmann equation for two flat charged surfaces. The diagram is plotted in terms of two dimensionless ratios: b/d and λ_D/d where b is the Gouy–Chapman length (appeared first in eq. (3.2)), d is the inter-membrane spacing and λ_D is the Debye–Hückel screening length. The four regions discussed in the text are: the linear Debye–Hückel regime, the ideal-gas regime, the Gouy–Chapman regime and the Intermediate regime. Apart from the line $\lambda_D^{-2}bd = 1$ separating the ideal-gas and Debye–Hückel regions, all crossover loci are straight lines. At those lines, the limiting solutions both for the potential $\psi(z)$ and the pressure $P(d)$ crossover smoothly from one regime to another. This diagram also applies to the different regimes used in section 7 in calculating the electrostatic contribution to the bending modulus, $\delta\kappa^e$, with one exception. Namely, the Debye–Hückel region is divided in two: the large-spacing Debye–Hückel (marked as region I) and the small-spacing one (marked as region II). Adapted from ref. [60].

The above expressions for y_m and y_s hold for both the ideal-gas and Gouy–Chapman regions of fig. 5 where the separation d is small and the potential is large. The difference between the two regions is that $\lambda_D^{-1}d \exp(y_m/2) \ll 1$ for the ideal-gas case, whereas for the Gouy–Chapman case $\lambda_D^{-1}d \exp(y_m/2) \simeq \pi$. Identifying $\lambda_D^{-1} \exp(y_m/2)$ with K of section 4.1 (no added electrolyte), we recover the no-added electrolyte limit of large λ_D .

The pressure for the ideal-gas region is just $P(d) = Tn_0 \exp(y_m)$ using the large y_m limit of (4.12). From eqs (4.12)–(4.14) one obtains

$$\begin{aligned}
 P(d) &= -\frac{2T\sigma}{e} \frac{1}{d} = \frac{T}{\pi lb} \frac{1}{d}, \\
 f_{\text{el}} &= \frac{2T\sigma}{e} \ln d = -\frac{T}{\pi lb} \ln d.
 \end{aligned}
 \tag{4.15}$$

The above expression coincides exactly with the no-added electrolyte limit, eq. (4.6), in the same limit of weak surface charges, and is independent of the Debye–Hückel screening length, λ_D . The limits of validity of the ideal-gas region are, hence, $\lambda_D \gg d$; $y_m, y_s \gg 1$; and $d \exp(y_m/2) \ll \lambda_D$. In fig. 5 they correspond to the region

$$b/d \gg 1 \quad \text{and} \quad (\lambda_D/d)^2 \gg b/d. \tag{4.16}$$

As both the surface charge density and the electrolyte strength are small in the ideal-gas region, the main contribution to the electrostatic pressure comes just from the entropy of mixing of the ions and not from their charges. The potential as well as the ionic density are almost constant throughout the region between the membranes.

4.2.2. Gouy–Chapman region

Repeating the above calculation for the limit $\lambda_D^{-1} d \exp(y_m/2) \simeq \pi$; $\lambda_D \gg d$, and $y_s \gg y_m \gg 1$, yields a different limiting value of the pressure. This is the limit of a strong surface charge density and weak electrolyte. It coincides exactly with the previous obtained results for the Gouy–Chapman regime (strong charges) for the no-added electrolyte case, eq. (4.7)

$$\begin{aligned}
 P(d) &= \frac{\pi T}{2l} \frac{1}{d^2}, \\
 f_{\text{el}} &= \frac{\pi T}{2l} \frac{1}{d} = \frac{\pi \varepsilon_w T^2}{2e^2} \frac{1}{d}.
 \end{aligned}
 \tag{4.17}$$

In the Gouy–Chapman region the electrostatic interactions are the strongest and the least screened. In fig. 5, the limits of validity for this region are shown as

$$b/d \ll 1 \quad \text{and} \quad \lambda_D/d \gg 1. \tag{4.18}$$

4.2.3. Intermediate region

When the separation between the membranes is large compared to λ_D , the potential at the midplane is always small, $y_m \ll 1$, and the coupling between the two membranes is weak even when the surface potential y_s on each surface is large. Thus, y_m is obtained by a linear superposition of the midplane potentials of two *non-interacting* membranes. Using the previously obtained potential for a single flat membrane, eq. (3.3), yields

$$y_m = 8\gamma e^{-d/2\lambda_D} \quad \text{and} \quad \gamma = \tanh(y_s/4) \approx 1. \tag{4.19}$$

The pressure expression (4.12) can be linearized since y_m is small, leading to

$$P(d) = Tn_0y_m^2 = 64\gamma^2Tn_0e^{-d/\lambda_D}. \quad (4.20)$$

Since $\gamma \approx 1$ and $\lambda_D^2 = 1/(8\pi n_0 l)$, the pressure for the Intermediate region can be expressed as

$$P(d) = \frac{8T}{\pi l \lambda_D^2} e^{-d/\lambda_D}, \quad (4.21)$$

$$f_{el} = \frac{8T}{\pi l \lambda_D} e^{-d/\lambda_D} = \frac{8\varepsilon_w T^2}{\pi e^2 \lambda_D} e^{-d/\lambda_D}.$$

Since the distance between the two membranes is large ($d \gg \lambda_D$), the interaction and the exerted pressure on the membranes fall off exponentially with the inter-membrane distance d . Note that unlike the expression for the pressure, the Poisson–Boltzmann equation itself *cannot* be linearized since the surface potential y_s is large.

The limits of validity of this region are (see fig. 5)

$$\lambda_D \gg b \quad \text{and} \quad \lambda_D/d \ll 1. \quad (4.22)$$

4.2.4. Debye–Hückel region

When the potential value on the membrane surface is small (less than 25 mV at room temperature), the Poisson–Boltzmann equation can be linearized. This is the Debye–Hückel region. Solving the linear equation for the two membrane problem, we get

$$\begin{cases} y_s = \frac{2\lambda_D}{b} \coth(d/2\lambda_D), \\ y_m = \frac{y_s}{\cosh(d/2\lambda_D)}. \end{cases} \quad (4.23)$$

As in the Intermediate region, the pressure and the free energy excess depend linearly on y_m yielding

$$P(d) = \frac{T}{2\pi l b^2} \frac{1}{\sinh^2(d/2\lambda_D)}, \quad (4.24)$$

$$f_{el} = \frac{T\lambda_D}{\pi l b^2} (\coth(d/2\lambda_D) - 1) = \frac{4\pi\sigma^2\lambda_D}{\varepsilon_w} (\coth(d/2\lambda_D) - 1).$$

Note that the limits of validity of the Debye–Hückel region extend all the way from large inter-membrane spacing and weak overlap ($\lambda_D/d \ll 1$ denoted as region I

on fig. 5) to small spacing and strong overlap ($\lambda_D/d \gg 1$ denoted as region II on fig. 5). For small d (region II), the Debye–Hückel region satisfies the conditions

$$(\lambda_D/d)^2 \ll b/d \quad \text{and} \quad \lambda_D/d \gg 1 \quad (4.25)$$

and the line $b/d \simeq (\lambda_D/d)^2$ indicates the crossover into the ideal-gas region. On the other hand, for large d (region I) the Debye–Hückel region crosses over into the Intermediate region on the line $\lambda_D \simeq b$. The Debye–Hückel region there is valid for

$$\lambda_D \ll b \quad \text{and} \quad \lambda_D/d \ll 1. \quad (4.26)$$

We remark that the crossover lines are not lines of singularities. They are rather lines where the expressions for the pressure $P(d)$ and potential profiles $\psi(z)$ crossover smoothly from one regime to another. The agreement between those approximations and the exact numerical integration of the full Poisson–Boltzmann equation is rather satisfactory [28].

This concludes our discussion on the electric double layer problem of *flat* membranes. As was mentioned in section 1, the profiles $\psi(z)$ and $n(z)$ as well as the electrostatic free energy and pressure are used extensively in analyzing experimental data of charged membranes. For monovalent ions, the Poisson–Boltzmann theory agrees quite well with experiments. Even within the simplifying approximations used in this review, we presented a few electrostatic regimes with different behavior for planar and rigid membranes. In the remainder of this review we will consider an even more complicated situation where the membranes are allowed to have some flexibility and curvature.

5. Flexible and charged membranes: general considerations

In many cases, amphiphilic membranes (as opposed to polymerized membranes) have a certain amount of ‘fluidity’. The fluidity depends crucially on the temperature as well as on other system parameters. Fluid membranes can be thought of as interfaces with a liquid-like response to inplane shear and elastic response to out-of-plane deformation [29, 30]. For many biological systems the elastic constants characteristic of the bending modes, vary between few dozens T (rigid membranes) to as low as one T (very flexible membranes).

When the membranes are flexible, they can be easily deformed and will have structural changes due to thermal fluctuations. The entire electrostatic problem for flat and rigid membranes, as was done in the previous sections, has to be reformulated in order to apply to more complicated geometries. Other examples of inherent deviations of membrane shapes from flat geometries are ‘rippled’ phases ($P_{\beta'}$) of lipid membranes where the ripples are believed to be equilibrium structures resulting from various competing membrane interactions [31–36].

Understanding the delicate coupling between the electric double layer problem and membrane shape, deformation and instabilities has been an active field of research in recent years. However, this problem turned out to be extremely complex. The

main difficulty is related to solving the full (non-linear) Poisson–Boltzmann equation together with complicated electric boundary conditions. A further complication is the effect of the charges on the boundary conditions themselves. Unlike solid objects with fixed charge distributions, the membrane shape can adjust to some degree in response to external forces such as the electric field. Thus, the membrane shape and electrostatics are coupled and need to be considered together.

Similar problems of comparable difficulty arise in the theory of polyelectrolytes [37, 38] – charged flexible polymers in aqueous solutions – as well as charged ‘worm-like’ cylindrical micelles [38, 39]. In these cases the shape conformation, stiffness and electrostatics are intimately related. The statistics of the polyelectrolyte chains depends on the local electric field and counterion distribution, which in turn depend on the polyelectrolyte chain configuration.

Lacking a global picture of the interplay between electrostatics and membrane shape, we will review in the following theoretical results which address only specific aspects of the coupling between electrostatic and structural properties as reflected in the membrane elastic constants. We will explain the interplay between electrostatics and entropically induced repulsive forces (the so-called Helfrich interactions [40]), but will neglect, for simplicity, all other inter-membrane interactions like hydration and Van der Waals interactions.

6. A single charged and flexible membrane

How do the charges affect the elastic properties of fluid-like membranes? To address this issue let us first mention the continuum model for the elastic energy of fluid-like membranes. This model was proposed by Helfrich in analogy to *smectic* phases of liquid crystals [29]. The phenomenological elastic energy is expressed as an integral over the membrane area

$$f_{\text{bend}} = \frac{1}{2} \kappa \int (c_1 + c_2 - c_0)^2 dS + \kappa_G \int c_1 c_2 dS \quad (6.1)$$

where κ and κ_G are the mean and Gaussian elastic moduli, respectively. The two principal curvatures are c_1 and c_2 whereas c_0 is the *spontaneous curvature*. For a single amphiphilic layer c_0 expresses the internal tendency of the layer to curve towards the water, $c_0 > 0$, or away from the water, $c_0 < 0$. The tendency to curve is a result of the different molecular structure and interactions of the head and tail moieties of the amphiphiles. For bilayer membranes composed of two identical layers $c_0 = 0$ from symmetry reasons. But c_0 can be non-zero if the composition of the two layers of the membrane differs. The membrane also is assumed to be incompressible. Hence, all the contributions to the surface tension (including those arising from electrostatics) vanish [41, 42].

The electrostatic contribution to κ and to κ_G are denoted, respectively, as $\delta\kappa^{\text{el}}$ and $\delta\kappa_G^{\text{el}}$. It has been calculated for a variety of geometries: cylinders, spheres and sinusoidal undulating membranes. The electrostatic contribution to the bending moduli can be identified by expanding the electrostatic free energy up to second order

in the local curvatures c_1 and c_2 , and comparing the expansion with the elastic energy per unit area, eq. (6.1), of the same object: a sphere of radius R , a cylinder of radius R , or an sinusoidal undulating membrane with wavelength $2\pi/q$ and amplitude u

$$\begin{aligned} f_{\text{bend}} &= \frac{1}{2} \kappa \left(\frac{2}{R} - c_0 \right)^2 + \kappa_G \left(\frac{1}{R} \right)^2, & \text{sphere,} \\ f_{\text{bend}} &= \frac{1}{2} \kappa \left(\frac{1}{R} - c_0 \right)^2, & \text{cylinder,} \\ f_{\text{bend}} &= \frac{1}{4} \kappa q^4 u^2, & \text{sinusoidal undulation } (c_0 = 0). \end{aligned} \quad (6.2)$$

Before presenting the electrostatic contributions to the bending moduli, we would like to explain the different ways the electrostatic boundary conditions can be formulated as one considers a *bilayer* membrane of finite thickness t . Namely, in what way are the two sides of the bilayer coupled electrically.

6.1. Electrostatic boundary conditions for bilayer membranes

Is the finite thickness of the membrane (denoted t in figs 2 and 6) of importance for the electrostatics properties of the membrane? Can one safely take the limit of membrane thickness to zero? Those questions have already arose in sections 3 and 4 for flat bilayer membranes. The answer is that there are two limiting behaviors as the thickness of the membrane becomes very small. The first is a limit of a bilayer which is composed of two (electrically) *completely decoupled* monolayers. In this case no electric energy is stored inside the membrane. This limit is sometimes called the ‘opaque’ or ‘adsorbing’ limit [43]. It corresponds to a vanishing membrane thickness t but with $t/\lambda_D \gg \varepsilon_{\text{oil}}/\varepsilon_w$ (figs 2 and 6). For this decoupled limit, $\delta\kappa^{\text{el}}$ of the bilayer is equal to twice the contribution of a single monolayer. When the ratio $\varepsilon_{\text{oil}}/\varepsilon_w$ is small, e.g., as in physiological conditions where this ratio is about 1/40, this limit is quite reasonable and it is used quite often in calculations. This is also the limit used throughout sections 3 and 4 for flat membranes. The other limit of $t/\lambda_D \ll \varepsilon_{\text{oil}}/\varepsilon_w$ (sometimes called the ‘transparent’ limit [43]) occurs when the two monolayers are *completely coupled* electrically. It is further discussed in refs [44, 45].

It is also possible to address the full (albeit more difficult) problem [22, 45] of an arbitrary electrostatic coupling between the two sides of the membrane. It is useful then to define the parameter $s \equiv (\lambda_D/t)(\varepsilon_{\text{oil}}/\varepsilon_w)$ and to consider its range of possible values. For typical values of water and oil dielectric constants, $\varepsilon_w = 80$ and $\varepsilon_{\text{oil}} \simeq 2$, we get $s \simeq \lambda_D/(40t)$. The small and large s limits correspond, respectively, to the fully decoupled and coupled limits introduced above.

Another possible boundary condition is to take the membrane as a surface of an electric conductor. The membrane is characterized by a fixed surface potential (Dirichlet boundary conditions). This different electrostatic problem was treated

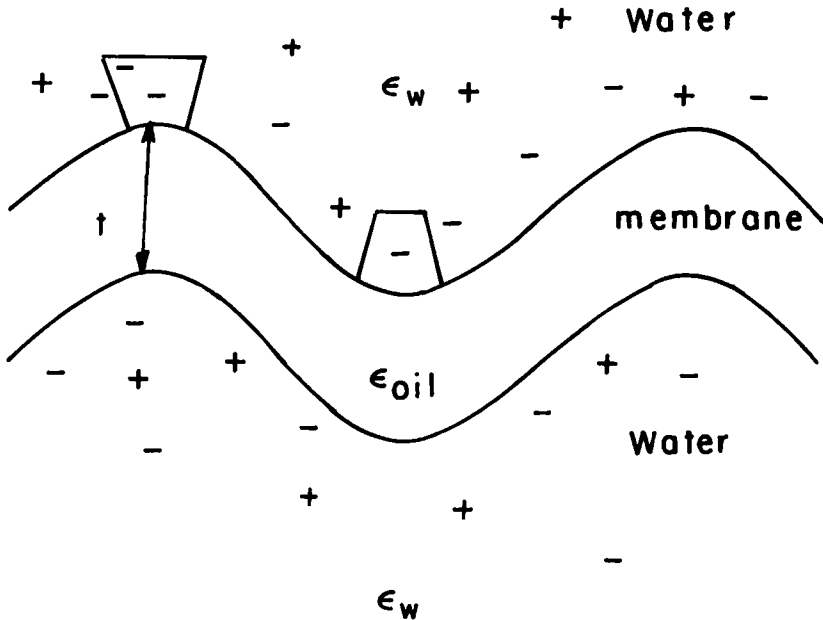


Fig. 6. A bilayer membrane of thickness t and surface charge density σ as in fig. 2 but here the flexible membrane is undulating in an aqueous solution. Notice the larger volume per unit surface area, accessible to the ions in the solution, in the convex parts as compared with to the concave parts.

separately in some works [8, 43, 44]. However, most of the results we will present are for the fixed surface charge densities.

We note that ‘real’ membranes do not satisfy any of those boundary conditions exactly. In a real membrane the charges are not frozen as on a perfect insulator, since they have an inplane mobility. In addition they can dissociate with different rates from different regions of the membrane. These two factors contribute to the redistribution of charges within the membrane. However, the membrane is not an equipotential surface either (like a metallic conductor). The motivation of studying those model systems with simplified electrostatic boundary conditions is that hopefully one can elucidate the more complex behavior of biological membranes.

6.2. One curved (spherical or cylindrical) charged membrane

6.2.1. Debye–Hückel limit of one decoupled bilayer

Winterhalter and Helfrich [46] calculated the free energy, eq. (2.7), of a single charged cylindrical membrane by solving the Poisson–Boltzmann equation in cylindrical coordinates. The calculation was also repeated for a sphere. They treated only the linearized Poisson–Boltzmann equation (strong electrolytes). Expanding the electrostatic free energy to order $1/R^2$, the electrostatic contribution to the bending modulus

$\delta\kappa^{\text{el}}$ per each monolayer of the bilayer membrane is obtained

$$\delta\kappa^{\text{el}} = \frac{3\pi}{2} \frac{\sigma^2 \lambda_{\text{D}}^3}{\epsilon_{\text{w}}} = \frac{3T}{8\pi l} \frac{\lambda_{\text{D}}^3}{b^2}, \quad (6.3)$$

$$\delta\kappa_{\text{G}}^{\text{el}} = -\frac{\pi\sigma^2 \lambda_{\text{D}}^3}{\epsilon_{\text{w}}} (1 + \lambda_{\text{D}}^{-1}t).$$

Note that in some works, $\delta\kappa^{\text{el}}$ is defined *per bilayer* which gives an extra factor of two. The above result are obtained in the decoupled limit of the bilayer (zero s). Since the results are obtained for a *single* bilayer, they correspond to taking *first* the limit of large inter-membrane separation d and then looking at region I (close to the origin) of the Debye–Hückel regime in fig. 5, where $b/\lambda_{\text{D}} \gg 1$ and $d/\lambda_{\text{D}} \gg 1$. As is apparent from eq. (6.3), electrostatics stiffen the membrane since $\delta\kappa^{\text{el}} > 0$. The other effect is a negative contribution to κ_{G} which will make saddle points less favorable. As long as $2\kappa + \kappa_{\text{G}} > 0$, the flat membrane is stable with respect to shape fluctuations. Hence, the electrostatic contribution, eq. (6.3), tends to stabilize the flat membrane, but the overall stability of the membrane depends also on the contribution to κ and κ_{G} coming from the aliphatic tails of the amphiphiles. We remark that in some more special situations (discussed below), the electrostatic contribution to the bending moduli can destabilize a flat membrane, which then transforms into, e.g., a vesicle [46].

6.2.2. Debye–Hückel limit: generalization to one coupled bilayer

Kiometzis and Kleinert [22] generalized the results of Winterhalter and Helfrich [46] for the decoupled limit. They considered the more general case of a coupled bilayer with any value of $s = (\lambda_{\text{D}}/t)(\epsilon_{\text{oil}}/\epsilon_{\text{w}})$ (see figs. 2 and 6), while still working in the linear Debye–Hückel limit of the Poisson–Boltzmann equation for a single bilayer of thickness t . Here, the electric field is not zero inside the membrane but satisfies the two boundary conditions on the two sides of the membrane. Their result for the bending moduli read

$$\delta\kappa^{\text{el}} = \frac{\pi\sigma^2 \lambda_{\text{D}}^3}{2\epsilon_{\text{w}}} \left(1 + \frac{2}{1 + 2s} \right), \quad (6.4)$$

$$\delta\kappa_{\text{G}}^{\text{el}} = -\frac{\pi\sigma^2 \lambda_{\text{D}}^3}{\epsilon_{\text{w}}} \left(1 + \lambda_{\text{D}}^{-1}t - \frac{1}{2} (\lambda_{\text{D}}^{-1}t)^2 \right).$$

Note that eq. (6.3) is recovered in the limit of zero s (the decoupled limit), whereas the other limit of completely coupled bilayer (large s) leads to a reduction of $\delta\kappa^{\text{el}}$ by a factor of three. On the other hand, the value of $\delta\kappa_{\text{G}}^{\text{el}}$ stays the same as it is independent of s .

6.2.3. Intermediate regime: weak electrolyte

Lekkerkerker [47] and Ninham and Mitchell [48] extended the linear Poisson–Boltzmann results (strong electrolyte) to the general electrolyte case. They solved the non-linear Poisson–Boltzmann equation for a single charged cylinder or sphere immersed in an electrolyte. It is convenient to express the Poisson–Boltzmann equation in cylindrical or spherical coordinates:

$$\begin{aligned}\nabla^2 y &= \frac{d^2 y}{dr^2} + \frac{1}{r} \frac{dy}{dr} = \lambda_D^{-2} \sinh y \quad (\text{cylindrical coordinates}), \\ \nabla^2 y &= \frac{d^2 y}{dr^2} + \frac{2}{r} \frac{dy}{dr} = \lambda_D^{-2} \sinh y \quad (\text{spherical coordinates}).\end{aligned}\tag{6.5}$$

The contribution to the bending moduli was calculated from the electrostatic free energy in the completely decoupled limit (zero s). For simplicity, we quote here only their results in the limit of a weak electrolyte and high surface charge density corresponding to the Intermediate region of fig. 5, $b \ll \lambda_D$ and $\lambda_D/d \ll 1$. More details can be found in refs [47, 48].

$$\begin{aligned}\delta\kappa^{\text{el}} &= \frac{\varepsilon_w \lambda_D}{2\pi} \left(\frac{T}{e}\right)^2 = \frac{T}{2\pi l} \lambda_D, \\ \delta\kappa_G^{\text{el}} &= -\frac{\pi \varepsilon_w \lambda_D}{6} \left(\frac{T}{e}\right)^2 = -\frac{\pi T}{6l} \lambda_D.\end{aligned}\tag{6.6}$$

Taking $\sigma = 0.15$ Coulomb per m^{-2} (about one charge per typical amphiphile compact area) and electrolyte strength of 0.4 M to 0.01 M, $\delta\kappa^{\text{el}}$ and $\delta\kappa_G^{\text{el}}$ vary from about 0.1 T to 1 T . Hence, electrostatic interactions have a significant effect on the elastic properties only if the uncharged (bare) membrane is flexible enough with bending moduli of order of T . In experiments, such flexible membranes have been realized by introducing a co-surfactant (short chain alcohol) which reduces substantially the ‘tail’ part of the bending moduli [49, 50]. Checking the overall electrostatic contribution to the bending (for zero spontaneous curvature, $c_0 = 0$), one can see from (6.6) that $2\delta\kappa^{\text{el}} + \delta\kappa_G^{\text{el}} < 0$. Hence, electrostatic interactions will tend to destabilize a flat membrane in this unscreened limit.

6.3. One undulating membrane

Results for electrostatic corrections to the bending moduli have been obtained by several authors [8, 43–45, 51] for a *single* sinusoidally undulating membrane. Taking the membrane height profile about a flat reference plane to be $u(x) = u \sin(qx)$, $\delta\kappa^{\text{el}}$ is obtained by expanding the Poisson–Boltzmann equation about the flat reference plane, for small u and q . In refs [8, 43, 44] only the linearized Debye–Hückel regime is investigated, but refs [45, 51] considered the full non-linear Poisson–Boltzmann equation.

6.3.1. Debye–Hückel limit: strong electrolyte

Calculations have been done in the decoupled (small s) and completely coupled (large s) limits [8, 43, 44]. The results coincide with the ones done in the cylindrical geometry:

$$\begin{aligned} \delta\kappa^{\text{el}} &= \frac{3\pi}{2} \frac{\sigma^2 \lambda_D^3}{\epsilon_w}, & \delta\kappa_G^{\text{el}} &= -\frac{\pi\sigma^2 \lambda_D^3}{\epsilon_w}, & \text{decoupled,} \\ \delta\kappa^{\text{el}} &= \frac{\pi}{2} \frac{\sigma^2 \lambda_D^3}{\epsilon_w}, & \delta\kappa_G^{\text{el}} &= -\frac{\pi\sigma^2 \lambda_D^3}{\epsilon_w}, & \text{completely coupled.} \end{aligned} \quad (6.7)$$

It was shown [45], then, that eq. (6.4) also describes the general s behavior of $\delta\kappa^{\text{el}}$ for the sinusoidally undulating membrane in the long wavelength limit of $q\lambda_D \ll 1$.

6.3.2. Intermediate regime: weak electrolyte

The full (non-linear) Poisson–Boltzmann equation with one sinusoidally undulating membrane was considered by Fogden et al. in the decoupled limit [51]. They have shown that $\delta\kappa^{\text{el}}$ in the long wavelength limit has the same expression as the one calculated [48] in the non-linear (but decoupled) regime for the cylindrical geometry, eq. (6.6). More recently, the decoupled limit as well as the completely coupled limit have been calculated [45]. For long wavelength, $q\lambda_D \ll 1$, $\delta\kappa^{\text{el}}$ has the following form:

$$\begin{aligned} \delta\kappa^{\text{el}} &= \frac{\epsilon_w T^2 \lambda_D}{2\pi e^2} \left(1 - 2(\lambda_D^{-1} b)^2 + \frac{2(\lambda_D^{-1} b)^3}{\sqrt{1 + (\lambda_D^{-1} b)^2}} \right), & \text{decoupled,} \\ \delta\kappa^{\text{el}} &= \frac{\pi\sigma^2 \lambda_D^3}{2\epsilon_w} \left(\frac{2\lambda_D^{-1} b}{\lambda_D^{-1} b + \sqrt{1 + (\lambda_D^{-1} b)^2}} \right)^2, & \text{completely coupled.} \end{aligned} \quad (6.8)$$

Both expressions of eq. (6.8) have the correct limits for $\lambda_D^{-1} b \gg 1$ (the Debye–Hückel region) as in eq. (6.3); and $\lambda_D^{-1} b \ll 1$ (the Intermediate region) as in eq. (6.6). The decoupled limit agrees with the one obtained in cylindrical geometry [48].

6.4. Membranes with variable surface charge density

Finally let us briefly mention the case where the surface charge density is not a constant but varies throughout the membrane. Membranes with variable surface charge density can be formed when a charged (cationic, anionic) amphiphile is mixed with a non-charged (zwitterionic) one. For example, a mixed system of phosphatidyl choline (non-charged) and phosphatidyl glycerol sodium salt (charged) [52, 53]. We discuss here electrostatic interactions only within the (simpler) linear Debye–Hückel regime.

When the charges within the membrane have a spatial distribution, two different limits can be distinguished depending on the lateral ion mobility [54]. First, for a quenched (immobile) surface charge density, $\sigma(x) = \sum \sigma_n \cos nqx$, of a membrane with one undulation mode $u(x) = u \cos qx$, the contribution to the bending modulus $\delta\kappa^{\text{el}}$ was calculated. It includes contributions from all the modes of the charge density, σ_n . For several simple $\sigma(x)$, the electrostatic interactions can be shown to rigidify the membrane since $\delta\kappa^{\text{el}} > 0$. This is a generalization of a constant surface charge distribution $\sigma(x) = \sigma_0$.

Second, for mobile charges on a flexible membrane, it has been shown [45] that the optimal surface charge density which minimizes the electrostatic free energy (in presence of an electrolyte) is identical to a membrane with an *equipotential* surface. This result assumes that the only degrees of freedoms present are the electrostatic ones. More generally, competition between electrostatic interactions and short-range inplane interactions lead to an optimal $\sigma(x)$. In this case the membrane is not anymore an equipotential surface. For asymmetric membranes, the contribution of the electrostatic interaction to the spontaneous curvature, c_0 in eq. (6.1), can be calculated. The asymmetry of the bilayer membrane can be a result of two different solvents on the two sides of the membrane, or an internal asymmetry which has to do with different structure and/or composition of the two monolayers. More details can be found in ref. [54].

Depending on the lateral diffusivity of the two components, a real membrane show a more complex and *dynamical* behavior in which the charge distribution is neither annealed nor quenched. So the quenched and annealed charge distribution should be regarded as the two extreme limits of, respectively, very slow and very fast relaxation times within the membrane. Note that the ions in solutions are always assumed to be in thermodynamical equilibrium and will adjust their distribution according to the charge distribution on the membrane.

7. A stack of charged lamellae

Natural phospholipids or artificial surfactants dissolved in water can form lamellar phases consisting of a stack of alternating amphiphilic bilayers and water regions [50, 55, 56]. The repeated periodicity of the stack can vary from as low as a few Angstroms to as high as several thousand angstroms [49, 57, 58].

The stability of the lamellar phase with respect to other ‘disordered’ phases (e.g., spherical or cylindrical micelles, isotropic ‘sponge’ L_3 phase), or other, liquid crystalline, phases (e.g., hexagonal, cubic) depends on several system parameters: specific short range interactions, controlled by the chemistry of the amphiphiles (size and structure of the aliphatic chain), as well as on thermodynamic and electrostatic parameters (temperature, membrane surface charge, ionic strength of the aqueous solution, and relative concentrations of the various components). In some cases, the stability depends crucially on the type and amount of an added co-surfactant (usually a short chain alcohol like pentanol [57]).

These parameters change the relative importance of intra- and inter-layer interactions. For layer separation below 20 Å, Van der Waals attraction is compensated

by repulsive hydration forces [11]. Hydration force plays an important role in preventing the phenomenon of *adhesion* of vesicles and membranes. These forces are reviewed elsewhere in this Handbook (Helfrich, Lipowsky, Parsegian and Rand). For large inter-membrane separations (roughly larger than a few dozens angstroms), the important interactions are attractive Van der Waals and repulsive electrostatic interactions. As was previously explained, electrostatic interactions strongly depend on the ionic strength of the solution. They can be completely screened, say for ionic strength of about 1.0 M, or only weakly screened for pure water.

7.1. Suppression of Helfrich interactions by electrostatics

Lamellar phases composed of a stack of membranes show quite universal behavior when the membrane are flexible with κ of order T . Entropically induced out-of-plane fluctuations of the stack cause an effective *long range* repulsion between adjacent membranes called the *undulation force* and have a pure entropic origin. This important idea was predicted by Helfrich in 1978 [40] and has been checked experimentally [57–59] in recent years, using high resolution X-ray scattering and dynamic light scattering. Helfrich's prediction takes into account the loss of entropy due to the constraint that each membrane is bounded between its two adjacent neighboring membranes.

The repulsive undulation interactions between the membranes (per unit area) have the form [40]

$$f_u \simeq \frac{T^2}{\kappa} \frac{1}{d^2} \quad (7.1)$$

or equivalently the disjoining pressure $P(d) = -\partial f_u / \partial d \sim 1/d^3$, where d is the average inter-membrane separation. As is clear from eq. (7.1), the undulation interaction is dominant only when the membrane is quite flexible, $\kappa \simeq T$. In the absence of charges (for lamellar phases diluted in oil) or for a strongly screened case (strong electrolyte solution), experiments verified the functional form of the predicted $P(d)$ for a range of spacings, d [49]. In other experiments, done for strongly charged and unscreened systems (no electrolyte), the dominant repulsion comes from the electrostatic interactions between completely flat and rigid stack membranes [57].

In what follows we will consider the interplay between the electrostatics and fluctuations of a stack of membranes [60–64]. We do not include Van der Waals and hydration forces. The excess free energy (per unit area) of one lamella fluctuating about its average position $z = 0$ over a flat reference lamella is

$$f_u = f_{\text{bend}} + \Delta f_{\text{el}} \quad (7.2)$$

where f_{bend} is the inplane bending free energy, eq. (6.1), for one undulating membrane. In the limit of small fluctuations f_{bend} can be conveniently estimated as $f_{\text{bend}} \simeq \frac{1}{2} \kappa (\nabla^2 u)^2$, where $u(\vec{r})$ is the displacement field of the membrane at a point \vec{r} . The second term is the excess in electrostatic free energy due to the undulation.

Within a local Deryagin-like approximation [2], Δf_{el} can be estimated by expanding the electrostatic free energy of a stack of flat membranes with separation d to second order in u ,

$$\Delta f_{\text{el}} = \frac{1}{2} \frac{\partial^2 f_{\text{el}}}{\partial d^2} u^2. \quad (7.3)$$

More formally, Δf_{el} can be expanded up to second order in u and forth order in q in the limit of large wavelengths and small amplitudes. Equation (7.3) is the zero q contribution to the u^2 term. The two other terms: $q^2 u^2$ and $q^4 u^2$ are correction to surface tension and bending modulus. Whereas the first can be dropped out for incompressible membranes, the second will be discussed later.

Substituting eq. (7.3) in (7.2) and expressing f_u as a sum over all q -modes, we obtain

$$f_u = \frac{1}{2} \kappa \sum_q u_q^2 (q^4 + \xi^{-4}) \quad (7.4)$$

where $\xi^{-4} = \kappa^{-1} \partial^2 f_{\text{el}} / \partial d^2$, or equivalently $\xi^{-4} = -\kappa^{-1} \partial P(d) / \partial d$, ξ is the in-plane electrostatic correlation length, and u_q is the q -mode of $u(x)$. This introduces a new cutoff for the undulation modes in the small q limit [42, 60]. For strong electrostatic interactions this new cutoff can dominate over the cutoff introduced by Helfrich for the uncharged case (the inter-membrane distance d) in order to preserve the lamellar order of the stack. We will estimate ξ by looking at the various limits for f_{el} for two flat and charged membranes (see section 4 and fig. 5).

Assuming that we are in the small fluctuation limit, the root-mean-square fluctuation $\sqrt{\langle u^2 \rangle}$ is much smaller than d . We later will check which of the electrostatic limits satisfies this condition: $\langle u^2 \rangle \ll d^2$. Using the equipartition theorem for the energy modes we get

$$\langle u^2 \rangle = \frac{T}{\kappa} \sum_q \frac{1}{q^4 + \xi^{-4}} = \frac{T}{8\kappa} \xi^2. \quad (7.5)$$

In the Gouy–Chapman region, the electrostatic interactions are almost unscreened since $d/\lambda_D \ll 1$. Using eq. (4.17) for the free energy of the two flat membranes, ξ is calculated to be [60, 61],

$$\xi = d \left(\frac{\kappa l}{\pi T d} \right)^{1/4} \sim d^{3/4} \quad (7.6)$$

leading to an estimate for $\langle u^2 \rangle$:

$$\langle u^2 \rangle = \left(\frac{T}{\kappa} \frac{l}{\pi d} \right)^{1/2} \frac{d^2}{8}. \quad (7.7)$$

We see from the above equation that for flexible membranes in a dilute lamellar phase $\kappa \simeq T$ and $d \gg l \simeq 7 \text{ \AA}$, indeed $\langle u^2 \rangle \ll d^2$, as is expected in the strong electrostatic regime since electrostatic interactions suppress the small q fluctuations. In addition, we can estimate the ratio f_u/f_{el} of the electrostatic and undulatory parts of the free energy: $f_{el} = \pi T/2ld$ and $f_u = T/8\xi^2$

$$f_u/f_{el} = \frac{1}{4\pi} \frac{ld}{\xi^2} \simeq \left(\frac{Tl}{\kappa d} \right)^{1/2} \ll 1. \quad (7.8)$$

Therefore, in the Gouy–Chapman regime because of strong and unscreened electrostatic interactions, the steric repulsion between neighboring membranes is small compared with the electrostatic contribution which suppresses the spectrum of out-of-plane fluctuations to values below the inter-membrane separation d [60, 61]. This is in agreement with the experimental findings which found that in the strong electrostatic regime, the data did not show any influence of the Helfrich steric interactions. Electrostatic interactions by themselves gave the best fit [57]. Note that in eqs (7.6)–(7.8) above we did not insert explicitly the electrostatic contribution to the bending modulus, $\delta\kappa^{el}$. This contribution in lamellar phases will be discussed in the next section.

In the other (weaker) electrostatic regimes, fig. 5, the suppression of the fluctuations is less drastic and in some cases, the screened electrostatic interactions can be completely neglected. Using eqs (4.24), (4.21) and (4.15) for the Debye–Hückel, Intermediate and ideal-gas regions, respectively, we obtain [60]:

$$\begin{aligned} \xi &= \left(\frac{\pi l \kappa \lambda_D^3}{8T} \right)^{1/4} e^{d/4\lambda_D} \quad \text{Debye–Hückel,} \\ \xi &= \left(\frac{\pi l b^2 \kappa \lambda_D}{2T} \right)^{1/4} e^{d/4\lambda_D} \quad \text{Intermediate,} \\ \xi &= \left(\frac{\pi \kappa b l}{T} \right)^{1/4} d^{1/2} \quad \text{ideal-gas.} \end{aligned} \quad (7.9)$$

Clearly for $d/\lambda_D \gg 1$, the Debye–Hückel and Intermediate results for ξ depend exponentially on d/λ_D leading to $\xi \gg d$. Hence, for these weak electrostatic cases, the new electrostatic cutoff will not suppress substantially the out-of-plane fluctuations. It does play only a minor role in reducing the Helfrich steric repulsion between adjacent membranes as compared with the uncharged case. Imposing the constraint $\langle u^2 \rangle \simeq d^2$ we get the following expression for f_u :

$$f_u \simeq \frac{T^2}{\kappa(d - 2\lambda_D)^2} \left[1 - \text{const} \left(\frac{\kappa}{T} \right)^2 \left(\frac{d}{\xi} \right)^4 \right] \quad (7.10)$$

where the prefactor of the second term is a constant depending on the details of the approximation employed. Thus, as long as $d/\lambda_D \gg 1$, the electrostatic interactions only slightly modify the Helfrich steric interactions. The main correction is that the effective distance between adjacent membranes is reduced to $d - 2\lambda_D$ instead of d . This is the conclusion for both the Debye–Hückel and Intermediate regimes. The ideal-gas regime is somewhat more delicate. As long as $bl < d^2$ but $b > d$, ξ is smaller than d and fluctuations are suppressed.

7.2. Rigidity of charged lamellae

Another important issue to consider for a stack of charged lamellae is how much electrostatic interactions affect the bending rigidity. In the previous section we reviewed the effect of electrostatic interactions on the spectrum of out-of-plane fluctuations of the membrane and its relation to the Helfrich interactions. An electrostatic contribution to the bending modulus κ will also have an effect on the spectrum of fluctuations and on structural properties. This contribution can, in principle, be measured experimentally [49, 59].

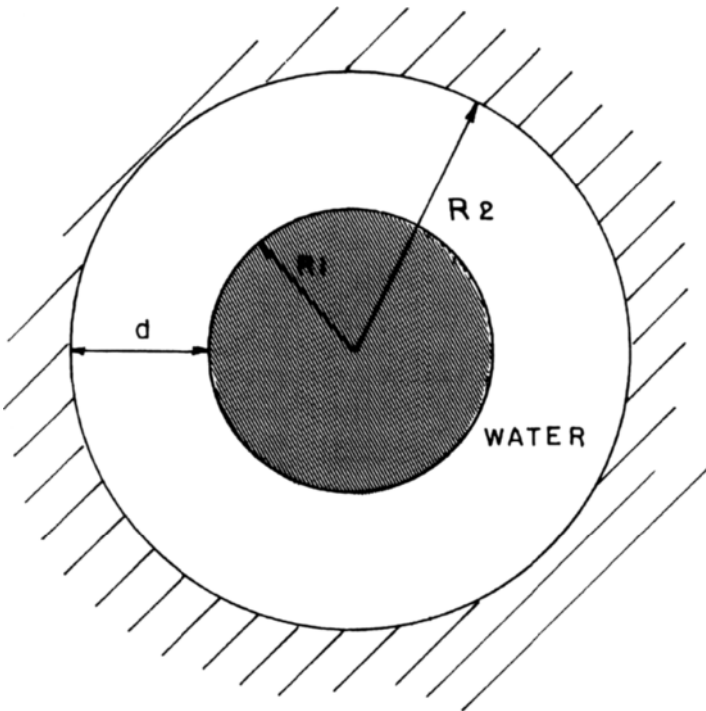


Fig. 7. Schematic drawing of a cross-section through two concentric cylindrical membranes of radii R_1 and R_2 . The aqueous solution fills the spacing of thickness $d = R_2 - R_1$ between the two membrane. This geometry is used to calculate $\delta\kappa^{el}$ in the limit of $R_1/d \gg 1$ and $R_2/d \gg 1$. Notice that an added complication as compared with two flat surfaces (fig. 4) is that the electric field is not zero at the midplane $(R_1 + R_2)/2$, due to the overall curvature of the cylinders.

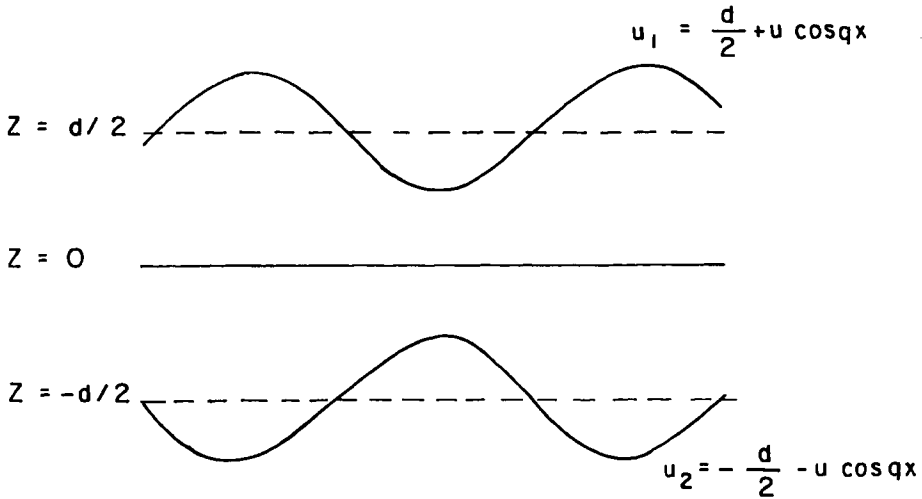


Fig. 8. Schematic drawing of two membranes u_1 and $u_2 = -u_1$, undulating out-of-phase about $z = d/2$ and $z = -d/2$, respectively. The wavenumber and amplitude of the undulations are q and u , respectively.

We recall that the electrostatic contribution to the bending modulus, $\delta\kappa^{el}$, has been presented in section 6 for a single lamella (one membrane). For a stack of membranes this applies in the limit where the inter-lamella spacing d is very large compared with the other electrostatic lengths: b and λ_D . When d is not that large, the electrostatic contribution to the bending modulus, $\delta\kappa^{el}$, depends also on d . We will present calculations of $\delta\kappa^{el}$ in the different electrostatic limits corresponding to the regions of fig. 5, since the full calculation of $\delta\kappa^{el}$ is extremely complex and not available at present.

Most of the calculations for $\delta\kappa^{el}$ have been done in the decoupled electrostatic limit (see section 6 for more details). Three types of geometries have been considered:

- (i) Two concentric cylinders (or spheres) in the limit of large radii of curvature, R_1 and R_2 , and small separation, $d/R_1 \ll 1$, and $d/R_2 \ll 1$ where $d = R_2 - R_1$ as in fig. 7.
- (ii) Two undulating membranes with an average separation d and a relative phase shift θ , each undulating with an amplitude u and a wavenumber q :

$$u_1 = \frac{d}{2} + u \cos qx \quad \text{and} \quad u_2 = -\frac{d}{2} + \cos(qx + \theta). \tag{7.11}$$

The two extreme phase shifts between the two membranes are either an in-phase ‘capillary mode’ with $\theta = 0$, or an out-of-phase ‘breathing mode’ with $\theta = \pi$ as in fig. 8.

- (iii) In analogy to smectic liquid crystals, a continuum approximation for the layered lamellar phase where the density of the lamellae is assumed to be a

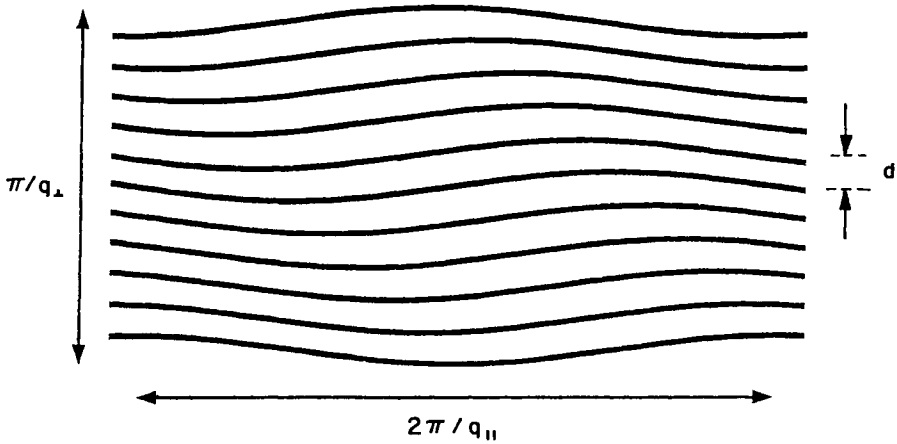


Fig. 9. Sketch of a stack of undulating charged membranes. Membranes are assumed to have average inter-membrane separation d , and undulations of wavelength $2\pi/q_{\parallel}$ and relative phase dq_{\perp} . Undulation amplitudes are shown exaggerated for effect; actual membranes are assumed to have low amplitude ($u \ll d$), long wavelength fluctuations ($q_{\parallel}d \ll 1$) with small inter-membrane phase angle ($q_{\perp}d \ll 1$).

slowly varying and periodic function both in the x direction (parallel to the lamellae), and in the z direction (perpendicular to the lamellae) as is seen in fig. 9.

7.2.1. Membrane rigidity in the Gouy–Chapman region

In terms of the regions of fig. 5, the single membrane calculations of section 6 gave us the contribution $\delta\kappa^{\text{el}}$ for the large-spacing Debye–Hückel regime (region I), eq. (6.4), and in the non-linear Intermediate regime, eq. (6.8). In the Gouy–Chapman regime of strong surface charge, large-spacing and no screening: $bd \ll 1$, and $d/\lambda_D \ll 1$, the effect of electrostatics is expected to be the largest. The scaling form for $\delta\kappa^{\text{el}}$ was conjectured by Pincus et al. [60] and later calculated by Higgs and Joanny [65]. The scaling form can be easily obtained by requiring a smooth crossover between the Intermediate and Gouy–Chapman regions on the crossover line $\lambda_D = d$. Since $\delta\kappa^{\text{el}} \sim \lambda_D$ in the Intermediate region, eq. (6.8), this implies $\delta\kappa^{\text{el}} \simeq Td/l$. Note that the expression for the pressure $P(d)$ also crosses over smoothly from the intermediate region, eq. (4.21), to the Gouy–Chapman one, eq. (4.17) on the same line, $d/\lambda_D \simeq 1$.

Higgs and Joanny [65] calculated $\delta\kappa^{\text{el}}$ using two different systems. In the first, two weakly undulating membranes with an out-of-phase phase shift of $\theta = \pi$ are considered (fig. 8). The non-linear Poisson–Boltzmann equation (2.4) in the limit of no-added electrolyte is solved with two undulating boundaries: $u_1 = d/2 + u \cos qx$ and $u_2 = -d/2 - u \cos qx$ while requiring $u \ll d$. Because of the symmetry about the midplane, $z = 0$, for the out-of-plane mode, it is enough to solve the Poisson–Boltzmann equation in the interval $[0, d/2]$ with a constant surface charge density σ at $z = d/2$ and a vanishing electric field at $z = 0$. The pressure $P(d)$ is calculated

by taking the variation of the free energy f_{el} with respect to d , eq. (2.8), in the limit of no-added electrolyte

$$P(d) = \int \left(Tn(0) + \frac{\epsilon_w}{4\pi} \psi(0, x) \frac{\partial E_x(0, x)}{\partial d} \right) dx \quad (7.12)$$

where the integral is performed along the midplane $z = 0$, and E_x is the x component of the electric field. Expanding the potential ψ and the pressure $P(d)$ up to order $u^2 q^4$ for the Gouy–Chapman region ($b \ll d$), the contribution to the bending modulus has been shown to scale as

$$\delta\kappa^{el} \simeq \text{const } T \frac{d}{l} \quad \text{for } b \ll d \ll \lambda_D. \quad (7.13)$$

The prefactor in (7.13) was not calculated for two undulating membranes due to mathematical complexity. However, this prefactor was calculated by the same authors [65] in a different geometry of two concentric cylindrical membranes of radii R_1 and R_2 , respectively (fig. 7). Note that here the midplane of an average radius $R = (R_1 + R_2)/2$ is not a plane of vanishing electric field due to the overall curvature. The electric potential of the double layer problem between two concentric cylinders was calculated some time ago in a seminal paper by Fuoss et al. [66] in relation to their model of polyelectrolytes. This expression for ψ was used in ref. [65] to calculate the pressure $P(d)$, eq. (7.12), as an expansion to second order in $1/R$. In the limit of $d/R \ll 1$, the bending constant can be deduced from this expansion

$$\delta\kappa^{el} = T \left(\frac{1}{\pi} - \frac{\pi}{12} \right) \frac{d}{l} \simeq 0.06 T \frac{d}{l}. \quad (7.14)$$

Again, eq. (7.14) is valid only in the limit of no-added electrolyte, $d/\lambda_D \ll 1$, and strong surface charge, $b \ll d$, which exists as a limit of the Gouy–Chapman region, fig. 5.

7.2.2. Membrane rigidity in the ideal-gas region

We turn now to ideal-gas region which is a region of weakly charged membranes but also with weak electrolytes. Harden et al. [67] calculated $\delta\kappa^{el}$ in this case for two concentric cylinders very much along the lines described in the previous section for the Gouy–Chapman region. The difference is that for the ideal-gas case $b/d \gg 1$, although the same limit of no-added electrolyte is taken (very large λ_D). The result in the ideal-gas regime is:

$$\delta\kappa^{el} = \frac{1}{30\pi} \frac{T}{b^2 l} d^3. \quad (7.15)$$

Note that the scaling behavior of $\delta\kappa^{el} \sim d^3/b^2$ in the ideal-gas region crosses over smoothly to the result for the Gouy–Chapman region, $\delta\kappa^{el} \sim d$ from eq. (7.14), on the boundary line $b = d$.

7.2.3. Membrane rigidity in the small-spacing Debye–Hückel region

Since the Debye–Hückel limit is the linear limit of the Poisson–Boltzmann equation, the free energy can be handled easier in a variety of boundary conditions. The contribution to $\delta\kappa^{\text{el}}$ in this Debye–Hückel limit for *one* single membrane have been described in section 6 with the result: $\delta\kappa^{\text{el}} = 3T\lambda_D^3/(4\pi lb^2)$ (taking into account the *two* sides of the membrane). This scaling corresponds to the large-spacing Debye–Hückel region (marked as region I in fig. 5) where $\lambda_D/d \ll 1$ and $b/\lambda_D \gg 1$.

The small-spacing Debye–Hückel regime is defined in the wedge $\lambda_D/d \gg 1$ but $b/d \gg (\lambda_D/d)^2$ (marked as region II in fig. 5). The first inequality is the condition on the short distance region, whereas the second is the condition on the linearity of the Poisson–Boltzmann equation. Pincus et al. [60] have studied the general Debye–Hückel case for two membranes, $u_1 = d/2 + u \cos qx$ and $u_2 = -d/2 - u \cos qx$ which fluctuate out-of-phase one with respect to the other in a breathing mode (so-called *peristaltic mode*) as shown on fig. 8). It is important to note that the membranes are taken to have a frozen spatial configuration; namely, q and u are both fixed. In the limit of small-spacing Debye–Hückel, [$\lambda_D/d \gg 1$; $b/d \gg (\lambda_D/d)^2$], $\delta\kappa^{\text{el}}$ is found to be

$$\delta\kappa^{\text{el}} \simeq \frac{T\lambda_D^3}{lb^2} \left(\frac{\lambda_D}{d} \right)^3 \quad (7.16)$$

which scales with an extra factor of $(\lambda_D/d)^3$ than the result for the large-spacing Debye–Hückel, eq. (6.3). We discuss below the limitations of this approach [67] when applied to a stack of undulating lamellae.

The bending constant was also calculated for a different electrostatic boundary condition of *constant surface potential* [8]. The free energy is calculated for two equipotential surfaces (membranes with a constant surface potential ψ_s) undulating with a fixed q -mode and with a general phase shift θ between them. The calculations are restricted to the linear Debye–Hückel regime. In the small-spacing Debye–Hückel limit, $\delta\kappa^{\text{el}}$ can be evaluated from their result to be

$$\delta\kappa^{\text{el}} = \frac{\varepsilon_w \psi_s^2 \lambda_D}{90} \left(\frac{d}{2\lambda_D} \right)^5 (16 - 7 \cos \theta) \quad (7.17)$$

where ψ_s is the fixed surface potential.

Although the above results, eqs (7.16) and (7.17) are valid for two membranes of a fixed spatial undulation, it was pointed out [67] that the connection to a stack of lamellae – as is measured in experiments – *is not precise especially in the small-spacing limit*. The reason is that taking a configuration of charged membranes undulating out-of-phase contributes to the bulk modulus in addition to the bending terms.

The way $\delta\kappa^{\text{el}}$ was calculated for a stack of membranes (lamellar phase) [67] was to consider the stack in the long wavelength and small amplitude limit. The spatial undulation field is written as $u(x, z) = u \cos(q_{\parallel}x + q_{\perp}z)$, where both $q_{\parallel}d \ll 1$ and $q_{\perp}d \ll 1$ as can be seen in fig. 9. Calculating the electrostatic free energy and

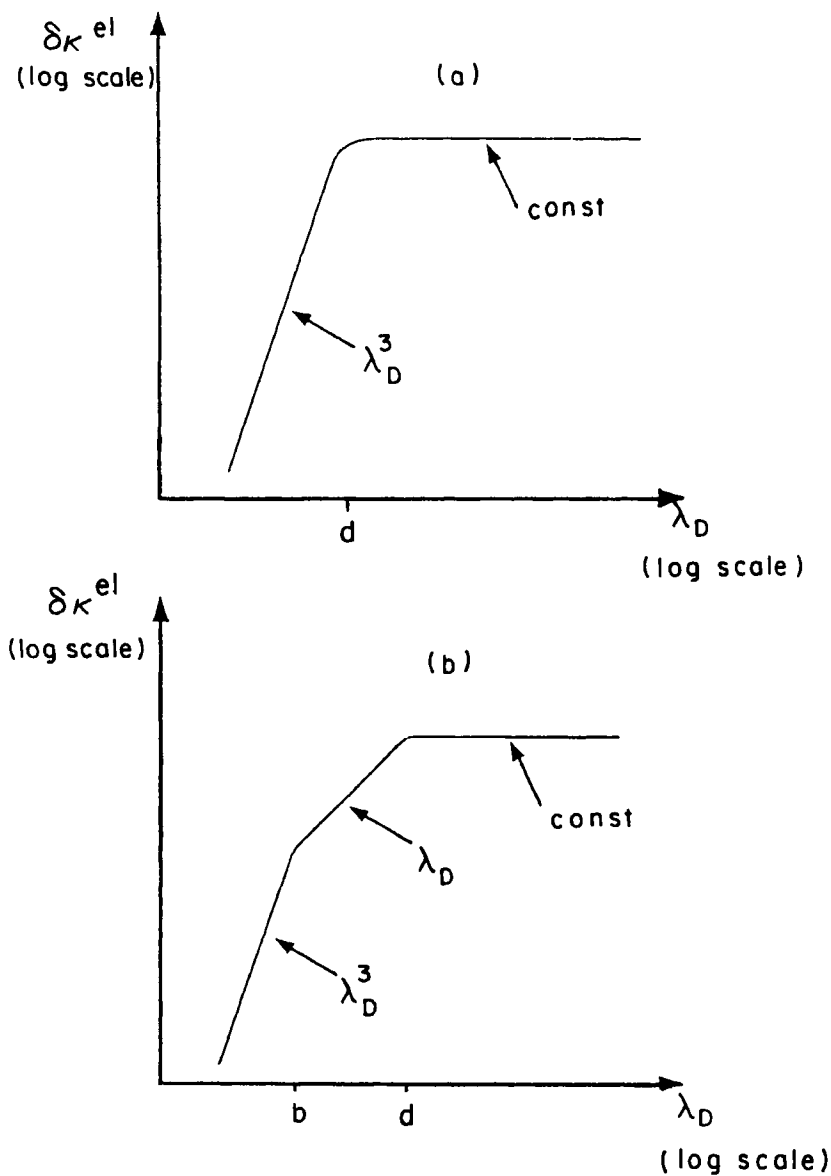


Fig. 10. Sketch of electrostatic contribution to the membrane bending modulus $\delta\kappa^{el}$ as a function of the Debye-Hückel screening length λ_D at fixed d and b . In (a), we show the case of weakly charged membranes, $b < d$. With increasing λ_D , $\delta\kappa^{el}$, first scales as λ_D^3 and then crosses over to a constant value for $\lambda_D > d$. In (b) we show the analogous plot for strongly charged membranes. In this case after an initial regime of $\delta\kappa^{el} \sim \lambda_D^3$, $\delta\kappa^{el}$ first crosses over to a linear regime, $\delta\kappa^{el} \sim \lambda_D$ at $\lambda_D > b$ followed by a second crossover to a constant value for $\lambda_D > d$. Adapted from ref. [67].

expanding it to second order in the mode amplitude u , we can identify $\delta\kappa^{\text{el}}$ as the coefficient of the $q_{\perp}^4 u^2$ term

$$\delta\kappa^{\text{el}} = \frac{1}{30\pi} \frac{T}{b^2 l} d^3. \quad (7.18)$$

Note that this result in the small-spacing Debye–Hückel for a undulating stack agrees *exactly* with the result for $\delta\kappa^{\text{el}}$ in the ideal-gas regime. Moreover, it also agrees with a calculation of $\delta\kappa^{\text{el}}$ using two concentric charged cylinders configuration.

This ends the presentation of the electrostatic contribution to the bending rigidity in the various electrostatic regimes. In fig. 10 (a) and (b), we plotted the expected scaling of $\delta\kappa^{\text{el}}$ of a stack of membranes in a lamellar phase as function of the Debye–Hückel screening length λ_{D} in the limit of weakly and strongly charged membranes, respectively. The figure shows a crossover in the scaling of $\delta\kappa^{\text{el}}$ depending on the various electrostatic regimes. The contribution to κ is the strongest for the least screened interactions when λ_{D} becomes large. Such scans can be verified experimentally by changing the strength of the electrolyte. Other possible scans will be changing the membrane spacing d or the strength of the surface charge $\sigma \sim 1/b$ by mixing together charged and non-charged (zwitterionic) amphiphiles.

8. Conclusions and future prospects

Research on the electric double layer problem started at the beginning of the century with the pioneering works of Gouy, Chapman, Debye and Hückel. Within a continuum approach (Poisson–Boltzmann theory), the electrostatics of *rigid* bodies immersed in ionic solutions is well understood. This approach was used quite successfully to investigate stability of colloidal dispersion, charged micelles and model membranes, and even polyelectrolytes. In recent years, other theories taking into account the discreteness of the charges and correlations have been developed but mainly in the simpler planar geometry. Some of the findings that cannot be explained within the Poisson–Boltzmann theory are the behavior of divalent ions like Ca^{++} which in some cases can induce an attractive interaction between membranes, and to non-monotonous profiles of the counterions in the proximity of the charge surfaces (up to a few angstroms away). Beside these points, it has been shown in numerous studies that the Poisson–Boltzmann theory is actually quite reliable.

For flexible and *heterogeneous* structures like membranes, the interplay between electrostatics and structure is far less understood because of the complexity of the problem involved. The electrostatics degrees of freedom are coupled to the membrane shape. Hence, one has to solve the electrostatic problem with variable boundary conditions in a self-consistent way. This is a tremendous task and only first attempts in this direction have been undertaken.

By considering the membrane as a flexible (and *homogeneous*) interface, the contribution of the charges to the bending moduli has been found in various electrostatic regimes (screened, unscreened, etc.). Electrostatics tends to rigidify the membranes and also suppresses the out-of-plane fluctuations of a lamellar phase composed of

a stack of membranes. However, when the membrane is heterogeneous (e.g., composed of two components), electrostatics can induce shape instabilities in relation to a lateral segregation of the two components.

In the future more complex models will, hopefully, be studied in order to make closer contact with biological membranes. Mixtures of charged and zwitterionic phospholipids, interactions between charged lipids and membrane proteins, biopolymers or other short-chain impurities are all of great importance in biological systems. When considering membranes as multi-component systems, it will be necessary to include other interactions as Van der Waals and hydration and to understand the interplay between those interactions and the electrostatic ones. Finally, even when the membrane is not charged it is composed of phospholipids which have a polar head. Dipole-dipole interactions are also of importance as they can lead to formation of dipolar domains and influence many of the membrane properties.

All of the above represent very challenging problems for future investigations. From the fundamental point of view, they relate to the physics of charged, flexible and heterogeneous structures. In addition, they can provide a better understanding of complex biological systems.

Acknowledgments

I would like to thank I. Borukhov, H. Diamant, G. Guttman, J.F. Joanny, S. Marcelja and A. Parsegian for comments and critical reading of this chapter. A part of the theoretical results presented here have been obtained in collaboration with G. Guttman, J. Harden, J.F. Joanny, C. Marques and P. Pincus. Partial support from the Israel Academy of Sciences and Humanities and the German-Israel Binational Foundation (GIF) under grant No. I-0197 is gratefully acknowledged.

References

1. Verwey, E.J.W. and J.Th.G. Overbeek, 1948, *Theory of the Stability of Lyophobic Colloids* (Elsevier, New York).
2. Israelachvili, J.N., 1990, *Intermolecular and Surface Forces* (Academic Press, London).
3. Gouy, G., 1910, *J. Phys. (France)* **9**, 457.
Gouy, G., 1917, *Ann. Phys. (Leipzig)* **7**, 129.
4. Chapman, D. L., 1913, *Philos. Mag.* **25**, 475.
5. Debye, P. and E. Hückel, 1923, *Physik Z.* **24**, 185.
Debye, P. and E. Hückel, 1923, *Physik Z.* **25**, 97.
6. Ninham, B.W. and V.A. Parsegian, 1971, *J. Theoret. Biol.* **31**, 405.
7. Kékicheff, P., S. Marcelja, T.J. Senden and V.E. Shubin, 1993, *J. Chem. Phys.* **99**, 6098.
8. Goldstein, R.E., A.I. Pesci and V. Romero-Rochin, 1990, *Phys. Rev. A* **41**, 5504.
9. Mahatny, J. and B.W. Ninham, 1976, *Dispersion Forces* (Academic, New York).
10. Tanford, C., 1980, *The Hydrophobic Effect* (Wiley, New York).
11. Parsegian, V.A., N. Fuller and R.P. Rand, 1979, *Proc. Nat. Acad. Sci. USA* **76**, 2750.
Rand, R.P., 1981, *Annu. Rev. Biophys. Bioeng.* **10**, 277.
12. Attard, P., D.J. Mitchell and B.W. Ninham, 1988, *J. Chem. Phys.* **88**, 4987.
13. Attard, P., D.J. Mitchell and B.W. Ninham, 1988, *J. Chem. Phys.* **89**, 4358.
14. For a review see: Marcelja, S., 1990, in: *Liquids at Interfaces*, eds J. Charvolin, J.F. Joanny and J. Zinn-Justin (North-Holland, Amsterdam).
15. Kjellander, R. and S. Marcelja, 1985, *J. Chem. Phys.* **82**, 2122.

16. Kjellander, R., T. Akersson, B. Jönsson and S. Marcelja, 1992, *J. Chem. Phys.* **97**, 1424.
17. Marcelja, S., 1992, *Biophys. J.* **61**, 1117.
18. Shubin, V.E. and P. Kékicheff, 1993, *J. Colloid Interface Sci.* **155**, 108.
19. McLaughlin, S.G.L., 1989, *Ann. Rev. Biophys. Biophys. Chem.* **18**, 113.
20. Hiemenz, P.C., 1977, *Principles of Colloid and Surface Chemistry* (Dekker, New York).
21. Stern, O., 1924, *Z. Elektrochem.* **30**, 508.
22. Kiometzis, M. and H. Kleinert, 1989, *Phys. Lett. A* **140**, 520.
23. Winterhalter, M. and W. Helfrich, 1992, *J. Phys. Chem.* **96**, 327.
24. For membranes with non-equal charges, see, e.g., Parsegian, V.A. and D. Gingell, 1972, *Biophys. J.* **12**, 1192.
25. Parsegian, V.A., 1966, *J. Chem. Soc. Faraday Trans.* **62**, 848.
26. Cowley, A.C., N.L. Fuller, R.P. Rand and V.A. Parsegian, 1978, *Biochemistry* **17**, 3163.
27. Langmuir, I., 1938, *J. Chem. Phys.* **6**, 873.
28. Guttman, G., 1992, M. Sci. Thesis, Tel Aviv University (unpublished).
29. Helfrich, W., 1973, *Z. Naturforsch.* **28c**, 693.
30. David, F., 1989, in: *Statistical Mechanics of Membranes and Surfaces*, Vol. 5, eds D. Nelson, T. Piran, S. Weinberg (World Scientific, Singapore).
31. Goldstein, R.E. and S. Leibler, 1989, *Phys. Rev. A* **40**, 1025.
32. Leibler, S. and D. Andelman, 1987, *J. Phys. (Paris)* **48**, 2013.
33. Janiak, M.J., D.M. Small and G.G. Shipley, 1979, *J. Biol. Chem.* **254**, 6068.
34. Findlay, E.J. and P.G. Barton, 1978, *Biochemistry* **17**, 2400.
35. Gebhardt, C., H. Gruler and E. Sackmann, 1977, *Z. Naturforsch.* **32c**, 581.
36. Wack, D.C. and W.W. Webb, 1988, *Phys. Rev. Lett.* **61**, 1210.
37. De Gennes, P.G., 1979, *Scaling Concepts in Polymer Physics* (Cornell University, Ithaca).
38. Odijk, T., 1977, *J. Polym. Sci. Phys. Ed.* **15**, 477.
39. Hofmann, S., A. Rauscher and H. Hoffmann, 1991, *Ber. Bunsenges. Phys. Chem.* **95**, 153.
40. Helfrich, W. and R.M. Servuss, 1984, *Il Nuovo Cimento* **3D**, 137. See also W. Helfrich, 1978, *Z. Naturforsch.* **33a**, 305.
41. Schulman, J.H. and J.B. Montagne, 1961, *Ann. NY Acad. Sci.* **92**, 366.
42. de Gennes, P.G. and C. Taupin, 1982, *J. Phys. Chem.* **86**, 2294.
43. Duplantier, B., R.E. Goldstein, A.I. Pesci and V. Romero-Rochin, 1990, *Phys. Rev. Lett.* **65**, 508. Duplantier B., 1990, *Physica A* **168**, 179.
44. Bensimon, D., F. David, S. Leibler and A. Pumir, 1990, *J. Phys. (France)* **51**, 689.
45. Fogden, A. and B.W. Ninham, 1991, *Langmuir* **7**, 590.
46. Winterhalter, M. and W. Helfrich, 1988, *J. Phys. Chem.* **92**, 6865.
47. Lekkerkerker, H.N.W., 1989, *Physica A* **159**, 319.
48. Mitchell, D.J. and B.W. Ninham, 1989, *Langmuir* **5**, 1121.
49. Roux, D. and C.R. Safinya, 1988, *J. Phys. (France)* **49**, 307.
50. Meunier, J., D. Langevin and N. Boccarda (eds), 1987, *Physics of Amphiphilic Layers* (Springer-Verlag, Berlin).
51. Fogden, A., D.J. Mitchell and B.W. Ninham, 1990, *Langmuir* **6**, 159.
52. Swanson, J.E. and G.W. Feigenson, 1990, *Biochemistry* **29**, 82.
53. Feigenson, G.W., 1989, *Biochemistry* **28**, 1270.
54. Guttman, G. and D. Andelman, 1993, *J. Phys. II (France)* **3**, 1411.
55. Safinya, C.R., S.A. Safran and P.A. Pincus (eds), 1990, *Macromolecular Liquids*, *Mat. Res. Soc. Pub.* **177**.
56. Sirota, E.B., D. Weitz, T. Witten and J.N. Israelachvili (eds), 1992, *Complex Fluids*, *Mat. Res. Soc. Pub.* **248**.
57. Safinya, C.R., 1990, in: *Phase Transitions in Soft Condensed Matter*, eds T. Riste and D. Sherrington (Plenum, New York).
58. Larché, F., J. Appell, G. Porte, P. Bassereau and J. Marignan, 1986, *Phys. Rev. Lett.* **56**, 1700.
59. Nallet, F., D. Roux and J. Prost, 1989, *Phys. Rev. Lett.* **62**, 276. Nallet F., D. Roux and J. Prost, 1989, *J. Phys. (France)* **50**, 3147.
60. Pincus, P., J.-F. Joanny and D. Andelman, 1990, *Europhys. Lett.* **11**, 763.

61. Leibler, S. and R. Lipowsky, 1987, *Phys. Rev. B* **35**, 7004. See also Lipowsky, R. and S. Leibler, 1987, in: *Physics of Amphiphilic Layers*, eds J. Meunier, D. Langevin and N. Bocarra (Springer, Berlin).
62. Evans, E.A. and V.A. Parsegian, 1986, *Proc. Nat. Acad. Sci. (USA)* **83**, 7132.
63. Podgornik, R. and V.A. Parsegian, 1992, *Langmuir* **8**, 557.
64. Evans, E.A. and I. Ipsen, 1991, *Electrochim. Acta* **36**, 1735.
65. Higgs, P.G. and J.-F. Joanny, 1990, *J. Phys. (France)* **51**, 2307.
66. Fuoss, R.M., A. Katchalsky and S. Lifson, 1951, *Proc. Nat. Acad. Sci. USA* **37**, 579.
67. Harden, J.L., C. Marques, J.-F. Joanny and D. Andelman, 1992, *Langmuir* **8**, 1170.

Interaction in Membrane Assemblies

V.A. PARSEGIAN

*Division of Computer Research and Technology
and National Institute of Diabetes, Digestive and Kidney Diseases,
National Institutes of Health, Bethesda,
MD 20892, USA*

R.P. RAND

*Department of Biological Sciences,
Brock University, St Catharines,
Ontario, Canada, L2S3A1*

Contents

1. Introduction	645
2. Measuring energetics of molecular assemblies and single functioning molecules	647
2.1. Osmotic stress (OS) method	648
2.2. Surface force apparatus (SFA)	653
2.3. Pipette aspiration (PA)	654
2.4. Atomic force microscopy (AFM)	654
3. Results and observations	655
3.1. General properties of forces between bilayers	655
3.2. Osmotic stress of non-lamellar aqueous compartments in lipid assemblies	670
4. Theories	677
4.1. 'Hydration' forces measured between lipid bilayers	677
4.2. Entropic/configurational models	683
4.3. Traditional forces	685
4.4. Van der Waals attraction	686
5. Coda	686
Acknowledgements	687
References	687

1. Introduction

Charting the course of the planets, probing the power of atomic nuclei, and analyzing events at all levels of complexity in between, has always required knowing operative forces. At each level, different kinds of forces emerge to dominate the organization of matter. At each level, they must be measured. Such measurements have been made with lipids that form cell membranes. Unexpected forces have been seen. Now recognized, they should be understood and can be used in rational consideration of membrane organization.

The unexpected comes from the perspective of the macromolecule and of molecular assembly. For them their aqueous milieu becomes more than a medium through which the traditional forces, Van der Waals and electrostatic, act. Water, as it 'hydrates' the participants, becomes a part of the interacting molecular components themselves. Hydration and dehydration reactions make unexpectedly large contributions to the structure and energetics of the system. It is this new perspective that we emphasize in this chapter.

Lipids are interesting first for their morphology or, better, their polymorphism, itself driven by the properties of amphiphiles in an aqueous medium. The many configurations of lipid assemblies that populate the rest of this book have their analogue in natural biological membranes. They form the boundaries defining 'in' and 'out' not only for whole cells or many viruses but also for internal compartments that arrange and carry on the cell's business. Forces within these two-dimensional assemblies can be expected to influence the function of proteins that direct the movement of material or energy between compartments. Membrane proteins behave differently when incorporated in different lipids. Can the strains in packing that drive lipid polymorphism be felt in the proteins that work in these lipids? Only through systematic measurement of packing energetics can one expect to know.

Lipids must also participate in the massive topological rearrangement required for membranes to fuse with one another while maintaining the overall integrity of the compartments they enclose. It is expected that the study of non-bilayer configurations of lipid assemblies would teach us about the energetics of that rearrangement and for that reason we extend our consideration to some of these.

In the larger sense, the field of inquiry rapidly widens beyond lipids alone. The contribution of hydration to the overall energetics of molecular assembly has been recognized for a long time, but it has been difficult to isolate and to measure. The new use of osmotic stress (OS) to measure water's role in lipid assembly [1, 2] is remarkably simple, generally applicable (fig. 1), and is capable of determining whether even extremely weak perturbations of water molecules near surfaces are energetically significant. Forces measured between large polymers like DNA [3]

and polysaccharides [4] have also shown that tiny surface perturbations of water, of chemical potential as little different from bulk water as a fraction of a calorie/mole, can result in very large interaction energies when many such water molecules are involved. Further, the cost of removing all the perturbed water, or conversely the benefit of fully hydrating a newly exposed surface, is remarkably similar among these systems and is very high at 1.5–15 kcal/mole per square nanometer of surface area. (ATP hydrolysis yields 7.3 kcal/mole.)

The OS strategy has now been applied to individually functioning molecules. Mitochondrial voltage-dependent anion channels open (hydrate) with increased difficulty in the face of decreased water activity in their vicinity. A measure of that difficulty shows that about 1000 additional water molecules become associated with the open channel [5]. Other channels show similar dependence on water for gating [6, 7], usually to an extent related to their conductance, as if most of the newly associated water is hydrating a newly created aqueous cavity. Further the coupling of channel gating and lipids is seen in the observation that non-bilayer prone lipids modify the conductance-state probabilities of alamethicin channels [8].

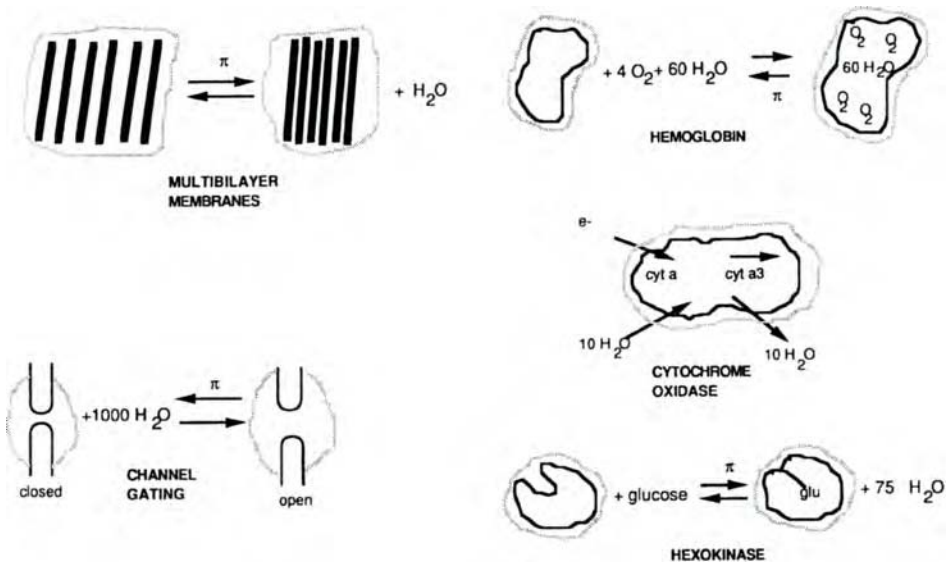


Fig. 1. In the osmotic stress (OS) strategy water activity is controlled through the concentration of a 'neutral' solute, such as a large polymer. Any aqueous compartment that is inaccessible to that solute, or is made inaccessible by a dialysis membrane, has its water activity controlled by solute concentration. Schematically, imagine the exclusion space indicated by the lightly shaded enclosing lines. In the case of single proteins, the solutes that work are those excluded from the protein's 'hydration shell', in the spirit of the extensive studies of Timasheff and his colleagues [17]. Under such osmotic pressure, π , the components of molecular assemblies get pushed together against their mutual repulsive forces. Isolated proteins undergoing reversible transitions get 'dehydrated' or, kinetically, find it more difficult to get to their more hydrated conformation. The extra, osmotic work is observed as a shift toward the dehydrated state. A measure of the sensitivity of that shift to water activity gives the difference in the number of solute-excluding water molecules associated with each conformation [10].

Individual proteins in solution, subject to osmotic stress, show clear changes in the numbers of solute-excluding molecules during the transition between conformational states. The numbers are large and their possible roles intriguing.

- Kornblatt and Hoa have measured 10 additional water molecules associated with cytochrome oxidase when cytochrome *a* binds an electron [9]. These waters are then shed as the electron is passed internally to cytochrome *a*₃. Far from being ‘futile’, the water cycle appears necessary for regulating sequential conformational change.
- Colombo, Rau and Parsegian [10] have shown that as four oxygens bind to hemoglobin, sixty additional water molecules also associate with the protein. Sixty is a surprisingly high number and appears to be related to changes in quaternary structure since O₂ binding to myoglobin seems to show no such effect. Is the hydration of 600 Å² of newly exposed surface of the oxy conformation energetically significant? If that surface is like others, its full hydration would yield more than 8 kcal/mole Hb, or 2 kcal/mole per heme group.
- Hexokinase releases at least 70 water molecules, and probably many more, in the process of closing a large cleft upon binding glucose [11]. The expulsion of so much water, a molecular mass ten times that of the substrate itself, presumably reflects the dehydration required to confine the phosphorylation to glucose and prevent the futile ‘phosphorylation’ of water [12].

These three proteins show three qualitatively different solvation reactions on substrate binding; one hydrates, one dehydrates, and one shows a hydration/dehydration cycle.

The nature of the surface perturbation of water remains an enigma. Most of these waters are unlikely to be seen either in the crystal structures of proteins or by NMR [13], since they are so weakly ‘bound’ and their residence time so short. It is now a challenge to determine their position and to assess their contribution to the overall energetics of any allosteric change as well as to the interaction and change in membrane surfaces.

Our aim in this chapter is, first, to describe how forces can actually be measured, then to survey, tabulate and illustrate the large set of force data now available for lipids. On their own, the fundamental data reviewed here allow some prediction of interactions. Whatever our limited understanding, these data provide good estimates of what it takes to bend membranes and to bring them toward ‘contact’. This is a set of facts to motivate quantitative thinking on how cell membranes, and biological macromolecules, do their work. These empirical data are a core of knowledge which still lacks satisfactory theoretical explanation. The theory section deals primarily with ideas proposed to explain bilayer hydration and hydration forces, but also mentions the traditional electrostatic, Van der Waals and steric interactions that are covered in sufficient detail elsewhere.

2. Measuring energetics of molecular assemblies and single functioning molecules

The energetics are accessible by four different complementary, techniques: osmotic stress (OS) [1, 2], pipette aspiration (PA) (see E. Evans, this book), surface force apparatus (SFA) [14, 34, 149], and atomic force microscopy (AFM) [15, 16]. Each has been amply described in other places. We sketch here the basic schemes, summarize their complementary aspects, and highlight the important facts to bear in mind when comparing respective results.

We emphasize the virtues of the osmotic stress strategy since its application can be quite general, it is largely unexploited, and its possibilities extend far beyond lipid bilayers.

2.1. Osmotic stress (OS) method

In the osmotic stress (OS) strategy [1, 2] water activity is controlled through the concentration of a solute, such as a large polymer, that is indifferent to all other system components. Any aqueous compartment that is inaccessible to that solute, or is made inaccessible by a dialysis membrane, has its water activity controlled by polymer concentration. Such solute-inaccessible compartments can be of many kinds. They are indicated in fig. 1 by the space enclosed by the dotted line, meant to represent at least the conceptual or functional equivalent of a dialysis membrane. In the case of single proteins, the solutes that work are not only polymers but also any others excluded from the protein's 'hydration shell', in the spirit of the extensive studies of Timasheff and his colleagues [17]. The size of the aqueous compartment in such cases in fact will be determined by the exclusion of the solute from the aqueous space.

Under such osmotic stress, Π_{osm} , (which we also refer to as P) the aqueous compartments will adjust to the reduced water activity of the stressing solution. In the case of molecular assemblies, such as interacting bilayers or polymers, or the lipids forming the aqueous channels of the inverted hexagonal H_{II} phase, the interacting components will get pushed together to an extent regulated by their interaction energy. Measuring distances by X-ray diffraction allows one to monitor disorder and structural transitions. Basic thermodynamics allows one to extract force as well as entropy/enthalpy [18, 19] as it varies with separation. In the case of isolated molecules undergoing reversible conformational transitions, such as membrane channels or enzymes in solution, they get 'dehydrated' or, kinetically, populate to a greater extent their 'dehydrated' conformation, observed as a shift toward the 'dehydrated state' [5–7, 9–11]. A measure of the sensitivity of that shift to water activity, or Π_{osm} , gives a measure of the difference in amount of water associated with each conformation [10, 20].

In the case of molecular arrays of lipids, equilibrium with the second phase of known water activity can also be achieved both by physically squeezing the array under a hydrostatic pressure in a chamber with a semi-permeable membrane to allow exchange with a reservoir of pure water, and by bringing the array into equilibrium with a vapor of known relative humidity (p/p_0) to create an effective osmotic pressure

$(kT/v_w) \ln(p_0/p)$, where k = Boltzmann's constant, T the absolute temperature and v_w the partial molecular volume of water [2, 21]. The chemical potential of the water with which the lipid is equilibrated, in all cases, gives the net repulsive pressure P in the aqueous compartment. The amount of water per lipid molecule removed under pressure P , ΔV_w , yields the work of dehydration, $P\Delta V_w$, which is a change in the chemical free energy of the lipids. This work is independent of any model of hydration and of any assumptions about the structure of the phospholipid phase. Given the many ways of applying osmotic stress, it is possible to bring structures to virtually complete dehydration at pressures corresponding to over 1000 atmospheres, or $\log_{10} P > 9$ when pressures are measured in dynes/cm².

X-ray diffraction and a knowledge of the composition of the equilibrated phases give the structural dimensions and their changes and ΔV_w in response to this osmotic stress. In the case of multibilayers, the repeat distance d of the lipid plus water layers is often determined to better than Angstrom accuracy.

The assignment of a measured work of dehydration to a force or energy of interaction between bilayers or to a work of rearranging the bilayers requires dissection of the measured repeat distance d into a bilayer thickness d_l and a separation d_w . It also requires recognition of the pressure P as both an intrabilayer lateral and an inter-bilayer normal stress [21]. If bilayers were incompressible, then changes in repeat spacing d would equal changes in bilayer separation d_w . A force vs. distance relation could then automatically be constructed from measured pressure P vs repeat spacing d reduced by a constant bilayer thickness d_l . But bilayers are laterally compressible, liquid-crystalline considerably more so than gel phase bilayers [21–27]. The same isotropic osmotic stress that pushes bilayers together also acts to deform them laterally. There is a decrease in cross-sectional area A and an increase in bilayer thickness d_l as the bilayers are pushed together. Consequently, estimates of these structural changes are required in order to estimate bilayer separation d_w .

Multilayers swell significantly differently in vapors near 100% relative humidity than in liquid solutions of the same water activity (see [28] for a discussion of this issue). Because this difference, regarded as a 'vapor pressure paradox', is still not properly understood and because this chapter deals with forces measured in liquid water, we omit most studies using vapor activity to infer forces.

It has been argued that DPPC multilayers, deposited by chloroform/methanol evaporation onto silicon wafers, have discrete states of hydration differing by the thickness of a water molecule. In 100% relative humidity, the multilayers swell only to 61.5 Angstroms rather than the 65 Angstroms seen in liquid water. If the discreteness of hydration steps (assumed in the procedure for fitting asymmetric diffraction peak widths) actually represents a stepwise swelling process, this might provide a useful clue to the different modes of hydration for immobilized vs. suspended bilayers [29, 38].

2.1.1. Bilayer dimensions – 'thickness' and 'separation'

To speak intelligently about the force between bilayers as a function of the distance between them, it is necessary to establish physically realistic conventions for defining the interface between lipid and water in terms of a mathematically equivalent

interface. In practice two conventions are commonly used, both of them capturing different features of bilayer interaction.

In ref. [28] we describe more fully three ways of gauging the bilayer thickness and separation from the X-ray diffraction measurements. We report here structural parameters determined either from lipid/water composition or from electron density maps, see fig. 2. The major difference in the methods is in defining the zero of separation when bilayers make molecular 'contact'. Since the structure of the polar group-water interface is diffuse, the definition of when the bilayers come into 'contact' will always be arbitrary. For identical X-ray data, the definition can make a large difference in the description of interbilayer distances, shown in fig. 3, and in estimates in contact energies. We indicate this difference in the tables of data and warn of its importance which, if ignored, can lead to unnecessary controversy when making comparisons [30]. Regardless of these differences, on the other hand, we prefer the 'composition' method since it yields the work of removing water, $P \cdot \Delta V_w$, independent of closer definition of 'contact', and explicitly takes account of the lateral compressibility of lipid layers.

The first convention, to which we refer as the 'Luzzati' or 'composition' method, is built on the thermodynamic idea of a Gibbs dividing surface. The bilayer/water interface is defined as one that divides all the water or aqueous solution from all the lipid. The multilayer repeat spacing d is the sum of a bilayer thickness d_l and water layer thickness or bilayer separation d_w where $d_l = \phi d_{\text{rep}}$ and $d_w = (1 - \phi) d_{\text{rep}}$ with ϕ the separately determined volume fraction of lipid. This Luzzati/Gibbs definition,

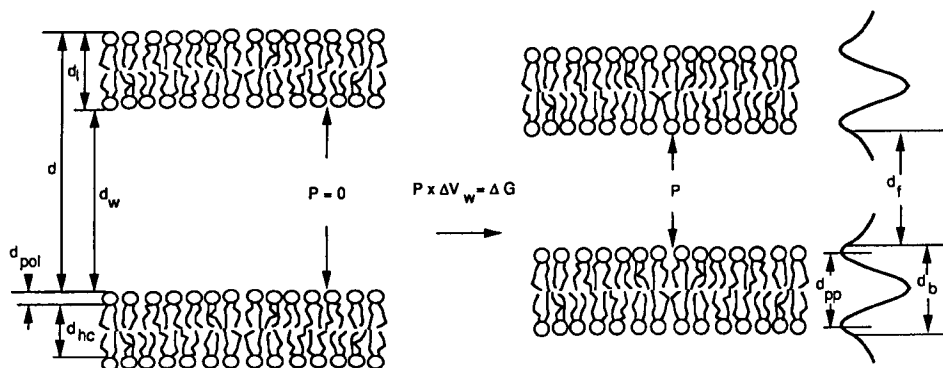


Fig. 2. Geometric parameters for describing bilayer thickness and separation as a function of applied pressure. The repeat spacing d is traditionally divided into a pure lipid layer of thickness d_l and a pure water layer thickness d_w . Polar group d_{pol} and hydrocarbon d_{hc} thicknesses can also be derived. The volume of water per lipid molecule can be written as $V_w = A d_w/2$ where A is a mean cross-sectional area projected onto the average plane of the bilayer. The work of removal of water ΔV_w under applied pressure P is a change $-P \Delta V_w = \Delta G$ in the lipid bilayer free energy. Such pressures cause a decrease in area A as well as in separation d_w . It is sometimes possible to describe the bilayer dimension by low resolution electron density distributions whose peaks correspond roughly to the location of the lipid-water interfaces. The peak-to-peak distance d_{pp} plus a constant to include the width of the polar group layer is defined to be a bilayer thickness d_b . The remaining space, $d_f (= d - d_b)$ is another measure of separation.

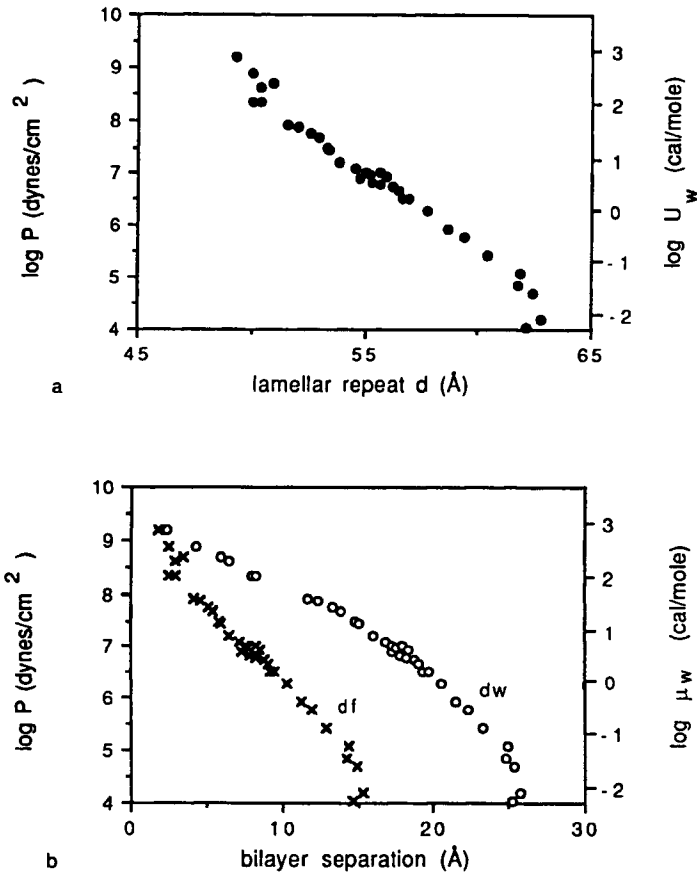


Fig. 3. Two different ways to represent forces depending on the definition of bilayer separation. (a) The empirical data gives osmotic pressure Π_{osm} ($= P$) vs. repeat spacing d for egg PC at room temperature. Data from three different laboratories essentially superimpose. [21, 46, 166]. (b) Pressure vs. bilayer separation derived two different ways. (i) separation d_w : the lipid/water interface is placed at the thermodynamically defined Gibbs dividing surface (Luzzati method) between pure-water and pure-lipid regions. (The division uses a 'phase diagram' calibration from repeat spacing vs. stoichiometrically measured weight fraction lipid, and takes into account the independently measured compressibility of bilayers.) (ii) separation d_f : the lipid/water interface is placed 5 Angstroms outside a peak in the electron density taken to represent the center of the polar region. Density maps at different water contents show little variation in the separation d_{pp} between peaks so that d_f differs from d by an additive constant. Though the two curves look very different and use different parameters, (P_0, λ, d_w) or (P_f, λ_f, d_f), they represent exactly the same work of dehydration.

based on sample composition is the natural choice for discussing the work of transfer of water to and from the lipid-water lattice, $P \cdot \Delta V_w$.

The second convention [32] uses electron density maps of the multilayer to locate peaks corresponding to the average position of the polar groups between water and

hydrocarbon regions. The bilayer thickness d_b is defined as the trans-bilayer peak-to-peak distance, d_{pp} , plus an added constant, usually ~ 10 Angstroms, to bring in all polar group material plus some associated water into the definition of 'bilayer'. So the bilayer thickness $d_b = d_{pp} + 10$ Angstroms, and one defines a 'fluid' separation between bilayers, $d_f = d - d_b$. Especially when electron density maps can be accurately ascertained, this method gives a good geometrical idea of the distances between different parts of the bilayer. Because 'bilayer' here includes water, in some cases the fluid separation d_f can take on negative values. Electron density maps, to the accuracy currently available, suggest that d_{pp} is approximately constant with water content, and fluid separation d_f is usually taken to differ from d by a subtractive constant.

Each of the above approaches suffers from allowing only an insensitive measure of bilayer compressibility, i.e. a measure of the changes in bilayer thickness or molecular area with changes in hydration. For reasons not yet properly understood, bilayer thickness d_l determined by the Luzzati method is, unlike d_b , usually not constant but reflects the change in molecular area. To take account more explicitly of compressibility, the independent and sensitive measurements of bilayer compressibility itself [28, 33] can be applied to the measurements. One begins by using either the gravimetric estimates of d_l and d_w at low enough hydration to be quite accurate, or one takes the estimates from electron densities. Then, applying measured lateral compressibilities it is possible to compute bilayer deformation and changes in d_l and d_w over a range of deformation for which compressibility is known. We now consider this procedure to be the best way now available to determine the variation of bilayer thickness with separation and hydration. The empirical P vs. d_w (but not d_f) fits given in the Tables use this procedure. This 'compressibility' approach neatly reconciles data originally interpreted either by the 'composition' or 'electron density' analyses, giving identical dehydration energies and pressure decay rates as functions of bilayer separation. (Details in ref. [28].)

2.1.2. Extracting hydration pressure, P_h , from P

As 'osmotic stress' implies, the language of forces is thermodynamic. There is an equivalence between the physical picture of pushing two bodies together and the picture of a chemical potential for making them come together by transferring material, water, from between the two bodies out to some reference solution. But purists will know immediately the risks in using 'force' or pressure to speak of the multiple events that occur when one brings together molecular aggregates in a solution. The many microscopic states that go with statements of position compel us to recognize explicitly that we are dealing with a thermodynamic quantity, a derivative of a free energy or potential of mean force, with respect to average separation.

So dissection of the measured net pressure P into its physically distinct components is a problem almost as difficult as the theoretical explanation of those components themselves. For convenience, we imagine that in the case of interacting bilayers the net force per unit area is made up of three kinds of interactions: P_h due to surface hydration, P_{vdw} from (attractive) Van der Waals or dispersion forces, and steric interactions either from the structural fluctuations of the thermally excited bilayers,

P_{fl} , or from direct interaction between polar groups before complete dehydration. Since a proper theoretical formulation of any of these components poses severe problems at the observed distances of bilayer interaction and which are considered later, we emphasize here an empirical description of P vs. d_w rather than force the data to fit into an arbitrary formalism. Still, some assumptions must be made.

Except near the limit of swelling in unlimited amounts of water, the nature of the repulsive force between neutral bilayers is essentially exponential with decay distance λ of ~ 1 to 3 Angstroms. We therefore describe this force in the form

$$P = P_0 \times \exp(-d_w/\lambda) \quad (1)$$

by fitting to points that are well away from the region where additional attractive forces create a deviation from exponentiality.

2.2. Surface force apparatus (SFA)

A second, mechanical, method of force measurement, also applied to phospholipid bilayer interactions, is by means of a 'surface force apparatus' (SFA) [14, 34]. Here one coats lipids, either by adsorption from suspension [35] or by passage through monolayers [36] onto mica sheets glued down onto cylindrical surfaces. The distance between the crossed cylinders is measured by means of interference fringes that are set up between the silvered backs of the mica sheets. Forces are read from the deflection of a cantilever spring system of variable tension that can be moved to bring the surfaces to a given separation. Repulsive forces are seen as a continuous deflection away from contact and are limited by the onset of deformation of the mica surface. Attractive forces are seen either from the position of a jump into 'contact' as surfaces are brought together with springs of different thickness, or from the position of a jump away from a spontaneously assumed minimum energy position. Relative changes in position can be measured to an accuracy of 1 Angstrom. The 'zero' of separation is computed by subtracting from the measured distance of contact between half-bilayers in air the thickness of a bilayer based on estimated phospholipid volume and the lipid cross-sectional area of the source monolayer.

A number of differences between this method and OS on spontaneously forming multilayers are of significance:

- (1) the immobilization of bilayers that comes from their attachment to the mica surface presumably removes any spontaneous fluctuations of free bilayers
- (2) the geometry of crossed cylindrical surfaces of opposite curvature requires a transformation of the measured data in order to compare it with parallel flat surfaces. To do so one routinely assumes the validity of a transformation, due to Derjaguin [37], that the force between crossed cylinders of equal radius R is the same as the force F_{sp} between a sphere of radius R and a plane flat surface. Further, this force F_{sp} is equivalent to the energy E_{pp} between plane parallel surfaces of the same material [28]. Consequently, the position of a spontaneously assumed minimum energy (zero force) position between bilayers in the multilayer system will occur at a greater separation than that seen as a point of force balance in the mica cylinder system. So, to compare

forces measured on multilayers with those between crossed cylinders it is necessary either to differentiate the cylinder-cylinder forces or to integrate multilayer forces from a hypothetical infinity. For this reason the SFA method emphasizes longer range interactions which limits its detection of shorter range forces like the hydration force [35, 36, 38].

- (3) The observation [39] that mica/glue/glass surfaces themselves deform at $F_{sp}/R \approx 10$ dyne/cm gives an upper force limit to which the SFA method can be used. For exponential forces with $\lambda = 2 \text{ \AA}$ this is equal to a maximum pressure of $P \approx 10^8$ dynes/cm² between parallel surfaces [28].
- (4) One major limitation, that also applies to the atomic force microscope, is the need for good knowledge of the condition of the lipid on the mica surfaces. Inspection of the coated mica surface with the AFM suggests that the mica surface dictates the lateral packing of at least the first monolayer of attached lipid [40]. Whether the act of forcing strong interactions between these surfaces rearranges the adsorbed layers remains largely unresolved.
- (5) The advantages of the SFA are that it is excellent for electrostatic double layer forces measured at long distances and for materials inaccessible to X-ray diffraction. Further, it is possible to measure forces between unlike surfaces.

Taking into account all these differences in technique there is sometimes good agreement between estimates of forces or energies [38]. But, given their differences and respective limitations, OS and SFA should be seen and used as complementary methods.

2.3. Pipette aspiration (PA)

Originally developed to measure the 'deformability' of whole cells and the mechanical properties of erythrocyte membranes [41–43], Evans and his colleagues [33, 44, 45] have turned pipette aspiration (PA) into a sophisticated tool for looking at bilayer mechanics and the attractive energies between bilayers (E. Evans, this book.) It is PA that provides the bilayer compressibility moduli referred to above. These estimated interaction energies can be compared with energies derived from the integrated force curves from the OS and SFA techniques. One major virtue of this method is its capability of controlling and measuring the extremely weak undulation forces originating from the thermal fluctuations of the bilayers. A combination of OS and PA on identical systems probes both the attractive and repulsive sides of the equilibrium position, and also spans a structural scale from the assembly of attracting micrometer-size vesicles into their equilibrium position, at nanometer bilayer separation.

2.4. Atomic force microscopy (AFM)

In this newest entry into the field, the force against an atomic [16] or colloidal-size [15] probe is measured as a surface moves up or down toward the probe. Still being developed, one must yet devise criteria for defining the 'zero' of probe-surface separation, and determine the composition and geometry of the interacting surfaces as they are brought together. Attempts have been made to use this technique to measure

forces between lipid-coated surfaces [167] and even to suggest some correlation between forces and surface structure [169].

3. Results and observations

It is especially important to choose carefully the form of the equations and parameters with which forces are to be tabulated and codified. Particularly when forces are unexpected, even the words used to describe them can endanger clear thinking about their physical basis. We have decided to construct several overlapping tables here listing structural and force parameters. Each table allows comparison of data subsets for related lipids. They show the degree of hydration of neutral lipids in excess water, the area per molecule A , bilayer separation d_w or d_f , volume of water V_w , adhesion energy G_{\min} between vesicles measured by pipette aspiration, and hydration force parameters where they have been measured.

From the many materials, conditions and parameters given in the tables, we have drawn comparisons to illustrate the most obvious and instructive features of bilayer-bilayer forces.

3.1. General properties of forces between bilayers

The main points stand out clearly. Even from the simple observation of applied osmotic stress vs. bilayer repeat spacing for electrically neutral egg PC in distilled water [1] (fig. 3a), it is clear that the pressure vs. spacing varies exponentially over the whole experimental range except close to the equilibrium separation (where attraction equals repulsion) and possibly at the very highest pressures. The data for P vs. d go to pressures greater than 10^9 dyn/cm or 1000 atmospheres. Treated to the different definitions of bilayer thickness, the P vs. d curve translates into very different plots of pressure vs. bilayer separation (fig. 3b) though both plots still preserve exponentiality.

We have tabulated the repulsive forces in terms of the parameters P_0 , λ with

$$P = P_0 \exp(-d_w/\lambda) \quad (2)$$

using the composition definition of bilayer thickness, and parameters P_f , λ_f with

$$P = P_f \exp(-d_f/\lambda_f) \quad (3)$$

using the electron density method for definition of thickness.

'Separation' of bilayers at close distances (fig. 3) is least well defined. According to the electron-density construction, the force shows an upward break at high osmotic pressures [46], which is largely eliminated when bilayer compressibility is taken into account [28]. This break has been interpreted as a transition from hydration to steric repulsion of the polar groups themselves.

One fundamental property that emerges from the application of osmotic stress in all systems, is that although the perturbation of water at some distance from

immersed surfaces becomes vanishingly small, the hydration energy can be very large [2, 21, 28, 47]. Figure 3 shows the difference in chemical potential of water μ_w in multilayers as a function of bilayer separation. Not until near contact is the chemical potential of applied stress similar to the many kcal/mole hydration energies of ions. Well before that distance, where the chemical potential is only \sim cal/mole, interbilayer forces reach enormous magnitudes. The reason is that even though the chemical potential energy per water molecule is little different from that of bulk water, when summed over the large numbers of molecules that must be removed, the total energy and the derivative force per area of lipid is large.

The energy to remove water from between bilayers can be derived by integrating the force curves. Forces and energies can be expressed a number of ways in order to understand their magnitude. It is useful to translate them into the spherical geometry of phospholipid vesicles, both rigid and deformable [28], and into a way that informs one about the energetics of exposing or removing hydrophilic surface from the aqueous medium.

Figure 4 has used typical hydration force and Van der Waals measured parameters to estimate the energy and force between two phospholipid vesicles of 400 Å diameter (near the smallest limiting size of such vesicles) [28].

- 1) The position of zero force between parallel bilayers, indicated by the vertical arrow, is shifted inward by about 5 Å simply by virtue of having the surfaces curve away from each other. The magnitude of this shift, surprisingly, is independent of the radius of the vesicle.
- 2) The energy of interaction indicates that spheres with thermal energy $kT = 4 \times 10^{-14}$ ergs would be able to approach only some 5 Å closer than the minimum equilibrium position. Since the energy of interaction increases with

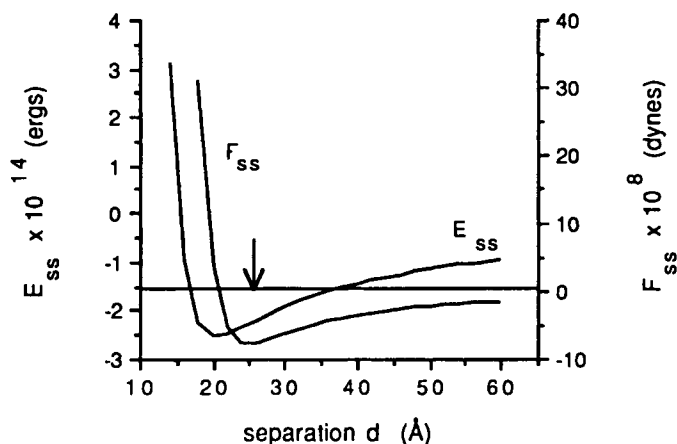


Fig. 4. Typical, measured, force distance relations for multilayers have been translated into the energy, E_{ss} , and force, F_{ss} , between spherical vesicles of 400 Å diameter. The arrow points to the equilibrium separation of parallel layers. The position of energy minimum and zero force for vesicles results simply from the geometrical change from parallel to oppositely curved bilayers, independent of the size of the latter.

vesicle radius, larger spherical vesicles will be almost entirely kept at the distance corresponding to the position of the energy minimum.

- 3) To some extent, all vesicles are deformable. The implications of vesicles flattening against each other in adhesive contact are thoroughly discussed in the chapters of Evans and of Lipowsky and mentioned in early papers on vesicle contact energies [48]. In cases where attractive forces drive deformation, vesicle interaction energies will necessarily be stronger than for purely rigid spherical vesicles. This makes the adhesive energy of deformable vesicles, such as PC and PE vesicles, very different from each other and possibly more like the interaction of parallel surfaces than of oppositely curved surfaces. It is even possible then [47] that this difference with lipid type results in a tendency for lipids in mixed vesicles to demix in the contact region.

How easy is it to remove all the water from a hydrated lipid surface and, conversely, how much free energy is available on hydrating a freshly exposed surface to water? Integrating the force curves for the lipids of table 1 gives energies that fall into two categories, approximately 1.5 and 15 kcal/mole per 100 Å² of surface [48]. This can be compared with the energy yielded by ATP hydrolysis, 7.3 kcal/mole, or energy of the hydrogen bond, 3–5 kcal/mole.

Strong hydration repulsion can be circumvented by the qualitatively different kinds of interactions that occur between acidic phospholipid bilayers exposed to divalent cation solutions. Many studies of such systems show that the attractive interactions are strong enough to break through the hydration barrier and allow very close contact. In the past much use was made of this in attempts to model membrane fusion. An example of such a remarkable change occurs in PS bilayers exposed to Ca ions. Even at micromolar Ca concentrations [49, 50], these bilayers precipitate to virtually anhydrous contact often with crystallization of hydrocarbon chains [49–51]. SFA data [39] show that the attraction induced between PG bilayers can be measured at ~20 Angstrom separations. (Whether this long-range attraction is a form of hydration force or due to ionic fluctuations [52] is not yet resolved.)

By comparing the binding constant of Ca to the outer surface of multilayers [53] with the strength of binding between bilayers [49], we estimate an energy of contact on the order of 100 ergs/cm² in these Ca-collapsed PS multilayers, quite enough to completely overcome hydration repulsion. (Method of Parsegian and Rand [48] updated with the binding constants of Feigenson [49].) The fact that this precipitate contains no detectable water argues against an attractive force based on ionic fluctuations [54, 55] and suggests rather the kind of dehydration characteristic of insoluble ionic crystals. Even so, inadequacies of using such systems to mimic cellular fusion and the rarity of finding the control characteristic of fusion in natural systems has been discussed [56–58].

It has been possible to compare experimentally measured forces between bilayers undulating within a multilayer array with those between bilayers immobilized onto rigid mica cylinders of the SFA, where undulations are presumably impossible [38]. Both data sets are for identical PCs with melted hydrocarbon chains. In the region of strong repulsion the two show similar forces with only a small horizontal shift due probably to differences in the defined 'zero' of separation. But at low pressures

Table 1
Polar groups.

lipid	d(Å)	c	A(Å ²)	d _l (Å)	d _b (Å)	d _w (Å)	d _f (Å)	V _w	V _w /PE	K	λ	λ _f	log P ₀	log P _f	G _{min}	Ref.
1																
2 DDPE	45.8	0.72	55.0	32.5		13.3		365	365							[60]
3 DAPE	57.3	0.79	58.0	47.3		10.0		290	290							[60]
4																
5 DLPE	46.1							270	270							[61]
6 POPE (30 °C)	53.2	0.79	56.6	41.8		11.4		323	323	233	0.8		12.5		0.14	[62]
7																
8 eggPE	52.9	0.64	72.1	33.8		19.1		690	690	200	1.3		12.5		0.14	[63]
9 eggPEt	52.0	0.72	65.0	37.4		14.6		474	474	200	1.1		12.3		0.20	[62]
10																
11 DLPC	59.0	0.54	64.0	31.6		27.4		877	761	145	2.0		10.6		0.01	[63]
12 DMPC (27 °C)	62.2	0.57	61.7	35.7		26.5		816	708	145	2.2		10.6		0.02	[38, 63]
13 DPPC (50 °C)	67.0	0.54	68.1	35.9		31.1		1059	919	145	2.1	1.7	11.0	8.6	0.01	[63]
14 DPPC (25 °C)	63.8	0.74	48.6	47.1		16.7		405	351	1000	1.2	1.4	12.3	9.7	0.03	[63]
15 DPPC interdigitated	49.0				40.0		9.0					1.7		8.0		
16 DOPC	64.0	0.56	72.1	35.9		28.1		1013	862	145	2.1		10.6		0.01	[63]
17 DSPC	67.3	0.71	51.6	47.7		19.6		506	431	1000	1.3		12.9		0.15	[63]
18 SOPC (30 °C)	64.6	0.63	64.3	40.6		24.0		771	667	200	2.0		10.5		0.02	[62]
19																
20 eggPC	61.9	0.60	69.5	37.0		24.9		866	749	145	2.1		10.6		0.03	[62]
21																
22 PC 16–22	63.5	0.60	69.3	38.3		25.2		873	758	145	2.1		10.1		0.01	
23 PC 18–10 22 °C	68.4		54.9		41.0		27.4									[66]
24 PC 18–10 13 °C	59.3		59.5		35.4		23.9									[66]

Table 1
(Continued)

lipid	d(Å)	c	A(Å ²)	d ₁ (Å)	d _b (Å)	d _w (Å)	d _f (Å)	V _w	V _w /PE	K	λ	λ _f	log P ₀	log P _f	G _{min}	Ref.
25 PC 22-22	73.1										1.3		10.0			[65]
26																
27 DGDG	53.2	0.73	79.8	38.8		14.4		574	328	200	1.7		10.3		0.24	[64]
28																
29 DOPS(.8M NaCl)	53.5	0.74	70.0	39.6	13.9		485	361								[64]
30																
31 DHDAА-frozen			80.0	25.0							2.9					[67]
32 DHDAА-melt			72.0	28.0							2.6		9.3			[68]
33																
34 Sphingomyelin	76.0						15.0				2.0			8.2	2.00	[69]
35																
36 Monocaprylin	44.0	0.50	30.0		21.0		23.0	690			1.3			9.2		[70]
37 Monoelaidin	64.0	0.82	20.3		52.0		12.0	244			1.3			9.7		[70]
38																
39 DPPG(pH3)	69.7				55.7		14.0				1.6			9.5		[71]

there is a distinct divergence between the two data sets; the limiting spacing of the multilayers is considerably greater than that between adsorbed bilayers. If, though, one subtracts undulatory entropic contributions from these data using the theory of Evans and Parsegian [59], one obtains good agreement [38].

This comparison of results from two such different methods actually teaches us at least two things. First, undulations act to enhance the hydration force giving it a greater apparent range. Second, at higher pressures undulations are effectively suppressed, suggesting that one can use measurements in this range to estimate the underlying hydration force.

3.1.1. Lipids with different polar groups

Figure 5, taken from table 1, compares the net interbilayer repulsive pressure and interbilayer distance for lipids of different polar groups: DGDG, POPE, DHDAA and SOPC. Lipids with no net charge swell only to a limited extent, thought to be determined by the balance of hydration repulsion and Van der Waals or polar charge correlation attraction [63, 73]. There is a clear difference between PE's or DG and the family of PC's, as the latter are able to swell almost twice as much as the former.

Even rather small surface charge densities overcome attractive forces [74]. For charged lipids, e.g., top curve fig. 5, swelling continues to an indefinite extent with

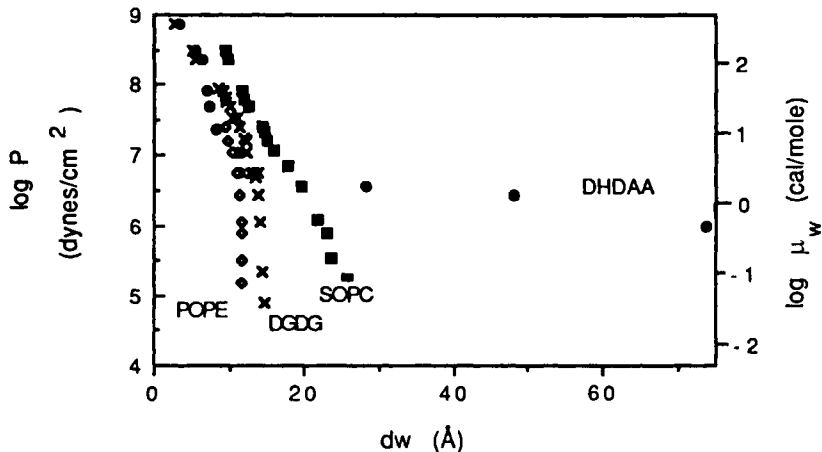


Fig. 5. Typical force vs. separation curves for four different kinds of double-chain lipids. DGDG, digalactosyl DG; POPE, palmitoyloleoyl PE; SOPC, stearyloleoyl PC; DHDAA, dihexadecyldimethylammonium acetate in 10 mM Na acetate. POPE and DGDG show weaker repulsion than SOPC (all in distilled water or weak buffer). These neutral species swell to a finite separation where repulsion is balanced by attractive forces. The charged DHDAA repels like SOPC at separations less than ~ 10 Angstroms, but shows electrostatic double layer repulsion at larger separations [67]. Pressure expressed as P , the force per unit area of bilayer, or Π_{osm} , the osmotic stress exerted on the multilayer lattice. Alternately, one may think of the work of bringing bilayers together as the work of transferring inter-bilayer water to a pure-water phase, a work involving a chemical potential difference $\Delta\mu = \mu_{bulk} - \mu_{bilayer} = v_w \Pi_{osm}$, where v_w is the molar volume of water. Note particularly how very small differences in chemical potential translate into physically large forces. The near-in 'hydration' repulsion is codified in the form $P_0 e^{(-dw/\lambda)}$ with P_0 and λ given in the tables

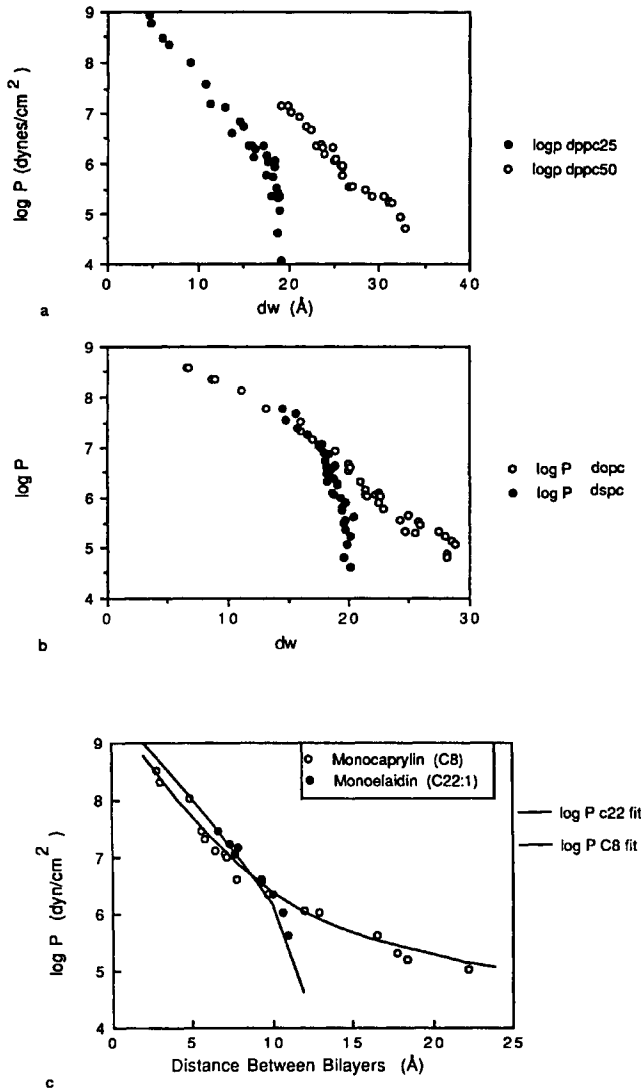


Fig. 6. Difference in hydration by bilayers with frozen and melted hydrocarbon chain bilayers. a) DPPC, dipalmitoylPC at 25 and 50 °C. b) DSPC (frozen) and DOPC (melted). In both cases, forces vary exponentially, but more water is imbibed by the melted-chain samples. At applied osmotic pressures above 10^7 dyn/cm², DPPC chains freeze. (DPPC in excess water freezes at approximately 42°C.) The difference in forces between frozen- vs. melted-chain bilayers may be primarily from melted-chain undulation forces (168). However, construction of bilayer separation by electron density maps, when the bilayer/water interface is placed outside the polar group region, give F_f , d_f values that suggest weaker repulsion between melted-chain lipids (Table 1). c) Diglycerides MC, monocaprylin, and ME, monooleidin at room temperature. Note the extra, undulatory repulsion of the melted-chain MC. Figure kindly supplied by Dr. T. McIntosh, data from [70]. Analysis of the coupling between undulation and direct interaction is given in the chapter by E. Evans.

decay constants largely consistent with electrostatic double layer theory [75–77], sometimes modified for the action of membrane undulation [59].

Comparisons between SFA and OS have been most carefully done for charged lipids. The clearest example of good agreement is for DHDAA where electrostatic double layer forces measured by the two techniques are identical [67, 68]. Several SFA measurements with charged phospholipids [36, 39, 78, 79] also show excellent agreement with double layer theory.

However, for charged and uncharged lipids alike, net repulsion from near ‘contact’ to ~ 20 Å separation can be described by an exponential with the coefficients and decay lengths given in the tables. At these distances all interbilayer forces appear to be dominated by the work needed to remove water from between bilayers.

3.1.2. Surface methylation

Table 2 and fig. 7 illustrate the effect of methyl groups on the polar group surface. Methylation appears to be a major factor in increasing hydration repulsion and the degree of maximum hydration. Methyl group density is varied either by mixing different lipid species or by looking at single lipid species with different degrees of polar group methylation. Figure 7a shows the effect of mixing pope and socp on maximum hydration. Figure 7b shows the effect on bilayer repulsion of methylating egg PE. The disproportionate effect of methyl groups on maximum swelling is probably related to the reduced ability of methylated quaternary nitrogens to form intermolecular hydrogen bonds with neighbouring lipids. In the theory section, we describe a connection between interbilayer force and structure at the bilayer interface.

3.1.3. Bilayers with mixed lipid composition

The effects of mixing lipids on maximum hydration and adhesion energies are shown in table 3 and figs 8 and 9. As with the PE's, the surprisingly low maximum hydration of DGDG itself likely reflects hydrogen bonding between polar groups.

The three combinations of lipid show quite different additive properties. The disproportion referred to above is not seen on adding SOPC to DGDG, in that the maximum hydration varies approximately linearly with mole fraction of the components. The two self-hydrogen-bonding lipids never do hydrate to a great extent although their 1/1 mixture hydrates significantly more than do the pure species.

The adhesion energies of these lipid combinations show disproportionate contributions from the components. DGDG dominates adhesion energy in its mixtures but SOPC dominates when mixed with POPE. These different properties of the various lipid mixtures may again reflect different correlations, resultant forces and hydration which are discussed in detail in the theoretical section. They may also reflect different contributions of the polar groups alone to the Van der Waals interactions.

3.1.4. Bilayers with different hydrocarbon chain conformation

Phospholipids generally take up less water when hydrocarbon chains are frozen rather than melted. Figure 6, taken from data in table 1, shows three systems, DPPC at 25 °C and 50 °C, DSPC and DOPC, and monoglycerides. Besides a lateral uncoupling of polar groups that spread on melting (see also fig. 10 for DOPC/DOG

Table 2
Methylation.

lipid	methyls/100Å ²	d(Å)	c	A(Å ²)	d _l (Å)	d _w (Å)	V _w (Å ³)	V _w /PE (Å ³)	K	λ	λ _f	log P ₀	log P _f	Ref.
1														
2 POPE	0	53.2	0.79	56.6	41.8	11.4	323	323	233	0.08		12.5		[62]
3 POPE/SOPC 19/1	2.6	54.5												[62]
4 POPE/SOPC 9/1	5.2	56.4	0.74	57.3	41.7	14.7	421	415	233	1.3		11.2		[62]
5 POPE/SOPC 4/1	1.03	59.9												[62]
6 POPE/SOPC 2/1	1.70	61.2	0.68	58.5	41.5	19.7	576	559	222	2.1		10.0		[62]
7 POPE/SOPC 3/2	2.00	63.3												[62]
8 POPE/SOPC 1/1	2.46	63.8												[62]
9 SOPC	4.66	64.6	0.63	64.3	40.6	24	771	667	200	2.0		10.5		[62]
10														
11														
12 eggPEt	0.00	52	0.72	65	37.4	14.6	474	474	200	1.1		12.3		[62]
13 eggPEt-Me	1.64	61.8	0.66	60.7	40.8	21	637	605	200	1.8		10.3		[62]
14 eggPEt-(Me) ₂	3.19	63.1	0.64	62.6	40.4	22.7	713	646	200	1.8		10.4		[62]
15 eggPC	4.31	61.9	0.60	69.5	37	24.9	866	749	145	2.1		10.6		[62]
16														
17 eggPEt-Me ₂		64.6									1.3		9.6	[80]

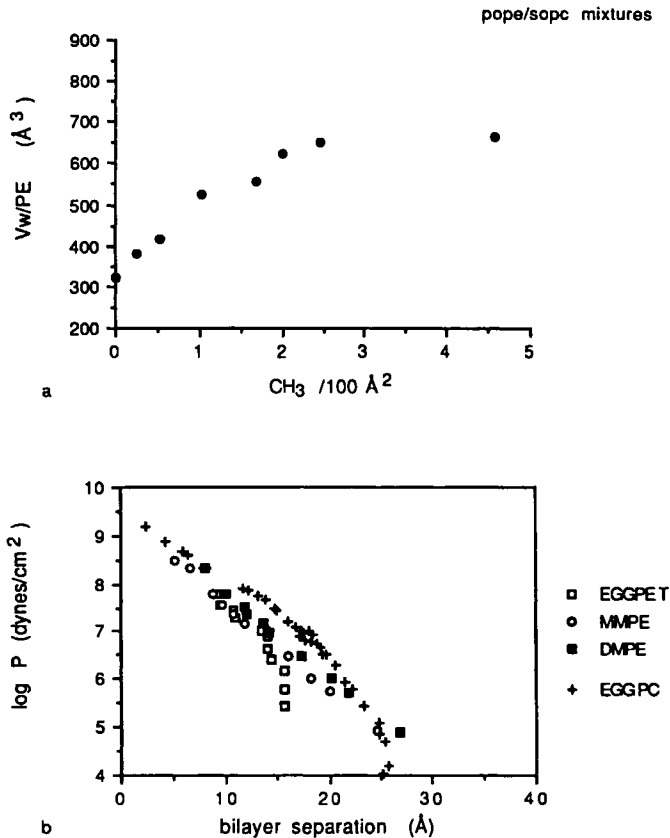


Fig. 7. (a) Disproportionate sorption of water by mixed bilayers with different levels of methylation. Volume of water taken up by POPE/SOPC mixtures in contact with pure water reservoirs without applied osmotic stress. To compensate for the different molecular weights of PE and PC polar groups, volumes are normalized to be per mass PE headgroup. By the time there is a 1/1 SOPC/POPE molar ratio, 2.5 CH₃/100 Å², the mixed bilayers have reached the same swelling as 100% SOPC. This kind of disproportionation seems not to depend on whether methyl groups are introduced by mixing or by successively methylating PE to PE-Me, PE-Me₂, and finally PC (see [28] and fig. 5). (b) Sudden increase in bilayer repulsion with first methylation of PE. Bilayers of trans-esterified eggPE-t, made from egg PC, swell noticeably less at low osmotic pressures [□] than does the mono-methylated MMPE derivative [○]. Successive addition of methyl groups, the di-methylated derivative DMPE [■] and the parent egg PC [+], makes far less difference to measured forces than does the first methylation. Data from [62].

mixtures), melted-chain bilayers are more flexible so that membrane undulation enhances direct hydration or electrostatic repulsion. This is seen in the 'unbinding' of the melted-chain monoglyceride monocaprylin compared to the limited swelling of the frozen longer chain monoglyceride monoelaidin (fig. 6c) [70].

There are cases where fluctuations probably always dominate the repulsion of weakly hydrating bilayers such as the case of the non-ionic alkylpoly(oxyethylene)

Table 3
Lipid mixtures.

lipid mix	$d_0(\text{\AA})$	c	$A(\text{\AA}^2)$	$d_l(\text{\AA})$	d_w	$V_w(\text{\AA}^3)$	V_w/PE	K	λ	$\log P_0$	G_{\min}	Ref.
1												
2												
3 3DGDG	53.2	0.73	79.8	38.8	14.4	574	328	200	1.7	10.3	0.24	[64]
4 DGDG/SOPC 45/55	57.2	0.68	72.8	38.9	18.3	666	467	200	1.8	10.6	0.18	[64]
5 SOPC (30 °C)	64.6	0.63	64.3	40.6	24.0	771	667	200	2.0	10.5	0.02	[62]
6 POPE/SOPC 2/1	61.2	0.68	58.5	41.5	19.7	576	559	222	2.1	10.0		[64]
7 POPE/SOPC 1/1											0.04	[64]
8 POPE (30 °C)	53.2	0.79	56.6	41.8	11.4	323	323	233	0.8	12.5	0.14	[62]
9 DGDG/POPE 1/1	54.0	0.72	70.2	38.9	15.1	530	385	216	1.7	10.3	0.23	[64]
10 DGDG	53.2	0.73	79.8	38.8	14.4	574	328	200	1.7	10.3	0.24	[64]
11												
12												
13 DOPE/DOPC 3/1	58.0	0.67	63.8	38.6	19.4	619	597	200	1.8	10.2	0.03	[102]
14 DOPC	64.0	0.56	72.1	35.9	28.1	1013	862	145	2.1	10.6	0.01	[63]

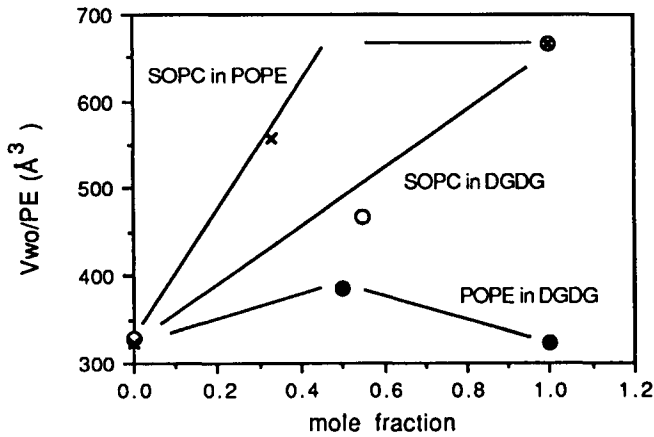


Fig. 8. Different patterns of water sorption by mixed-lipid bilayers. DGDG/POPE, [●] The 1/1 mole ratio mixture swells more than either of the pure components. POPE/SOPC, [×]. The PC added to PE brings in water out of proportion to mole ratio and a degree of swelling at the 1/1 mole ratio essentially equal to that for pure SOPC, as above. DGDG/SOPC, [o]. Continuous increase in water uptake with added SOPC. All volumes normalized per mass of PE polar group.

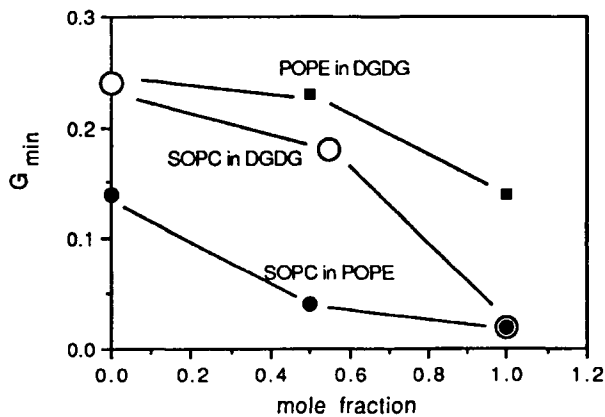


Fig. 9. Energy of adhesion G_{min} between electrically neutral bilayers in vesicles, directly measured by pipette aspiration. Mole fraction is of the first lipid in the indicated lipid mixtures. Pure DGDG bilayers show the strongest attraction ($G_{min} = 0.24$ erg/cm²), only slightly reduced by mixing with POPE [■] but more sensitive to mixing with the weakly adherent SOPC ($G_{min} = 0.02$ erg/cm²). In each case there is a disproportionate influence of the more strongly adherent species. G_{min} estimates inferred from osmotic stress measurements on multilayers are in excellent agreement with pipette aspiration values; bilayer-bilayer adhesion inferred from surface force apparatus observations on lipid-coated mica are consistently higher than those from the other two methods [28]. The difference may be due in part to suppression of undulations by immobilized bilayers and in part to additional Van der Waals attraction by the mica substrate across the thin lipid coating. Further details can be found in the chapter by E. Evans.

'PEO' surfactants whose polyethylene oxide chain polar groups are extended and might hydrate with only one layer of water. Melted bilayers separate to greater extents than when they are frozen, and there is good reason then to think that these longer spacings occur from undulatory fluctuations confined by collision between the hydrated polar regions of facing bilayers [82, 83].

3.1.5. *Bilayer additives*

Table 4 and figs 10 and 11 show the effects of adding non-amphiphilic membrane components to bilayers, such as cholesterol and diacylglycerols, which themselves appear to have no interaction with water. Their position in the bilayer is known and, grosso modo, they act as spacers whose effect is to spread lipid polar groups.

Particularly interesting is the addition of DOG to DOPC bilayers, figs 10a and b. The surprising effect is the additional swelling of a lipid that is already one of the most hydrated [87]. This and earlier observations [84] is interpreted as strong evidence that some attractive forces occur between polar groups, even for PC's, and that DOG reduces the correlations that create them.

Among its many effects on bilayers, cholesterol causes slight swelling of melted chain PC's while its addition at low concentration to bilayers with crystalline chains induces a dramatic increase in bilayer separation [63]. It has been shown by electron microscopy that this swelling goes with the induction of a ripple phase [88].

At very small separations, cholesterol eliminates that upward break attributed to the polar group steric interactions by allowing the diluted polar groups to interpenetrate [85] (fig. 11).

Ketocholestanol, a molecule similar to cholesterol but with a large dipole moment, when added to egg PC bilayers, produces hydration forces of similar decay length but of larger magnitude, consistent with the correlation between surface potential and P_f [89].

3.1.6. *Bilayers in other solvents*

Table 5 and fig. 12 shows that the phenomenon of bilayer repulsion is seen in other hydrogen-bonding solvents where the lipids self assemble into similar structures [90]. The exponential force relationship is maintained and the measured decay distances have been correlated with the size of the solvent. The coefficient of the force has been correlated with the surface potential produced by PC in these different solvents (fig. 12) [91].

3.1.7. *Long-range hydrophobic forces?*

There have been several reports, especially from SFA measurements, of remarkably long-range attractions between hydrophobized mica surfaces, e.g., [92, 93, 95, 97, 169]. The longest ranged of these mica measurements has been an exponentially varying force reaching 3000 Angstrom separation and varying with 400- or 600-Angstrom characteristic lengths. Though discussed in the language of solvent-perturbed 'hydrophobic forces' there is not yet clear evidence of a such a mechanism. A dependence on salt concentration has been reported [95, 169], and suggestions

Table 4
Lipid additives.

lipid	d(Å)	c	A(Å ²)	d _l (Å)	d _b	d _w	d _f	V _w (Å ³)	V _w /P	K	λ	λ _f	log P ₀	log P _f	Ref.
1															
2 eggPC/CHOL 1/1	65.5	0.64	95.6		42.0		23.5	1126	929	1000	1.1		13.8		[63]
3 eggPC/CHOL 1/1												2.1		9.1	[85]
4 eggPC/CHOL 2/1												1.4		9.2	[85]
5 eggPC/CHOL 4/1												1.6		8.5	[85]
6															
7 eggPC/6-ketocholestanol L 1/1	65				47.8		17.2					1.7		9.2	[69]
8															
9 DPPC/CHOL 1/1	66	0.65	87.9	43.1		22.9		1105	872	600	1.5		11.5		[63]
10 DPPC/CHOL 8/1	80	0.64	47.5	50.8		29.2		694	602	1000	2.0		10.7		[63]
11															
12 eggPC/DAG-12.5	63	0.58	81.2	36.6		26.4		1070	829	145	2.4		10.4		[84]
13															
14 dog/dopc 1/4	67														[87]
15 bov sphingo/chol	65				55.0		10.0					1.2		8.8	[69]
16 dag/chol/pe/pc				55		10									[86]

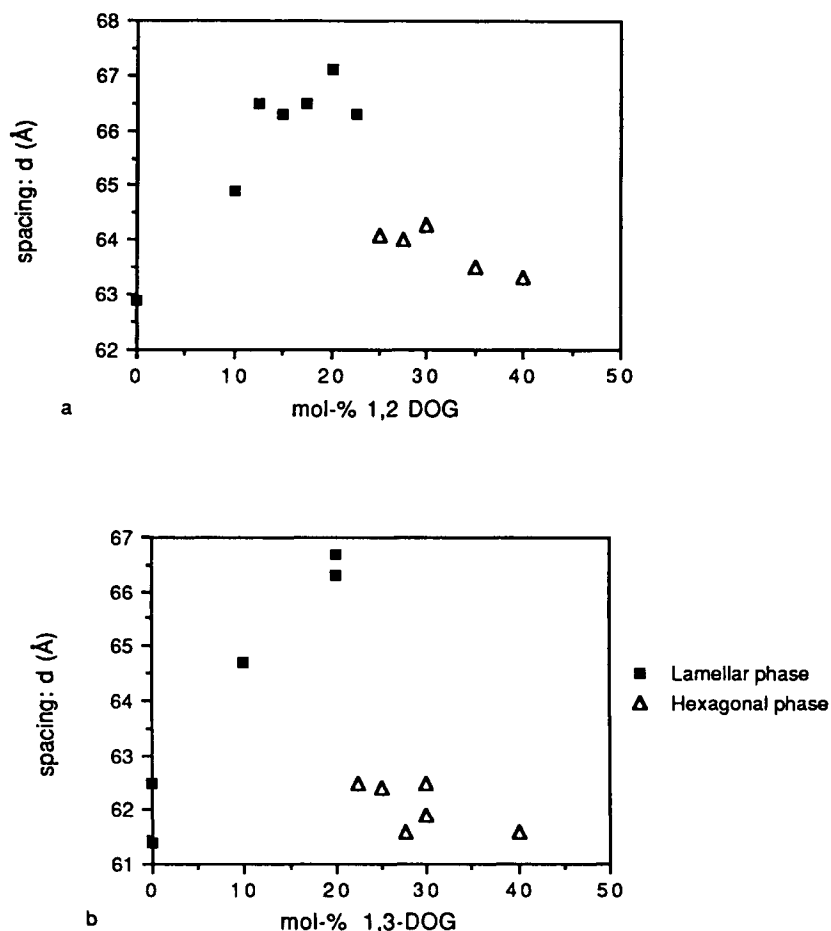


Fig. 10. Loosening of DOPC bilayers (■) and induction of the $H_{||}$ phase (△) by added dioleilglycerol (DOG). The repeat spacing of DOPC multilayers in excess water increases monotonically with either (a) 1,2- or (b) 1,3-DOG for up to 20 mole per cent added diglyceride. Higher DOG concentrations induce the $H_{||}$ phase. The 1,2-DOG mixtures here are equivalent to removal of the phosphorylcholine polar groups without any other change in the molecular structure. Quantitatively similar results have been seen with eggPC and natural diacylglycerols [84]. The increase in multilayer swelling upon removal of water-soluble polar groups suggests that there is an attractive component to DOPC bilayer interactions [115, 116] or some change in mechanical properties to increase undulatory forces ([109] and Evans and Helfrich chapters this book). The induction of the $H_{||}$ phase might also suggest relaxation of a tension in non-lamellar packing even in the liquid-crystalline L_{α} multilayer.

have been made that the phenomenon involves ionic fluctuations and surface adsorption/desorption [94]. There is not yet good evidence of its action between bilayers. For this reason, we leave these much-discussed ([95–97, 169] and references therein) interactions aside as being outside the purview of this chapter.

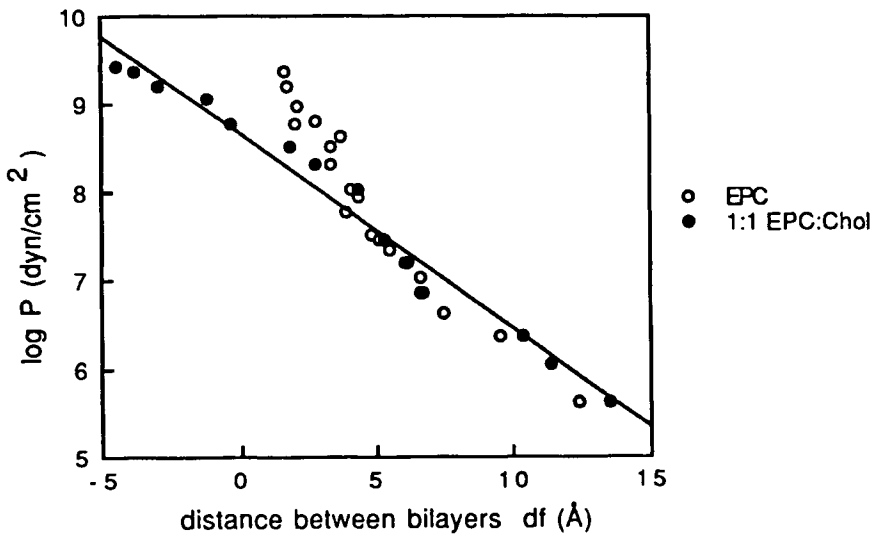


Fig. 11. Repulsion between egg PC bilayers with and without added cholesterol with separations defined from electron density maps. An upward break near $d_f = 3$ Angstroms disappears with the addition of enough cholesterol. The break is thought to come from interference of PC polar groups, an interference that is removed when PC is laterally diluted to allow the polar groups to interpenetrate (at negative d_f). In that case, the exponential 'hydration' force is realized over the full range of separations. (○) – pure PC; (●) – 1:1 Chol:PC. Figure kindly supplied by Dr. T. McIntosh, data from fig. 5 in [85].

Table 5
Different solvents.

lipid/solvent	$d(\text{\AA})$	c	$A(\text{\AA}^2)$	$d_b(\text{\AA})$	$d_f(\text{\AA})$	Ref.
1						
2 egg PC/water		64.1	39.9	1.7	8.6	[90]
3 /formamide	indef	70.1	36.5	2.4	8.26	[90]
4 /1,3propanediol	indef	75.7	33.8	2.6	8.04	[90]
5 /glycerol		68.2				[90]
6						
7 egg PC/chol 1/1/water				2.1	8.50	[90]
8 /formamide				2.9	8.50	[90]
9 /1,3propanediol				3.1	7.77	[90]

3.2. Osmotic stress of non-lamellar aqueous compartments in lipid assemblies

OS of phospholipid assemblies other than lamellar phases illustrates both the general applicability of the method and teaches some unique lessons about the energetics of the lipid monolayers. Monolayers form the structures of all phospholipid assemblies [a polymorphism considered by Seddon in this volume]. We will restrict ourselves to questions regarding the H_{\parallel} phase, shown in fig. 13, its dimensions as hydration changes, and the energetics of its structure. From the perspective of bilayers and

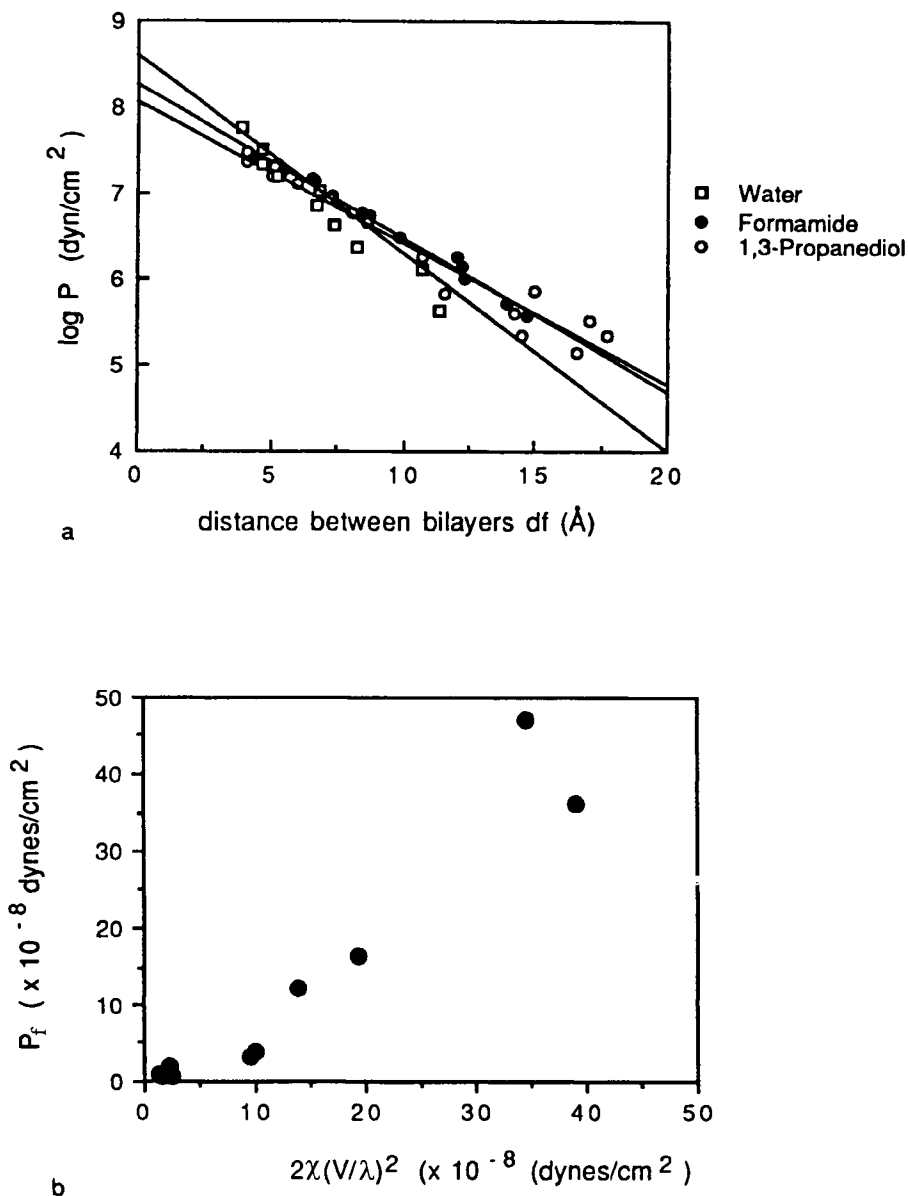


Fig. 12. (a) Repulsion between Egg PC bilayers in three different Hydrogen-bonded solvents, water (\square), formamide (\bullet), and 1,3-propanediol (\circ). In all cases, forces vary exponentially but with different slopes, thought to correlate with the mean distance between solvent molecules (taken from inverse cube root of the solvent density). (b) Plot of the measured coefficient of the hydration force, P_f , against that theoretically predicted from measured dipole potentials, V , of various lipid systems and solvents. χ is the susceptibility of the interlamellar space and λ the force decay distance. Figures kindly supplied by Dr. T. McIntosh, data from figs 5 in [85] and [80].

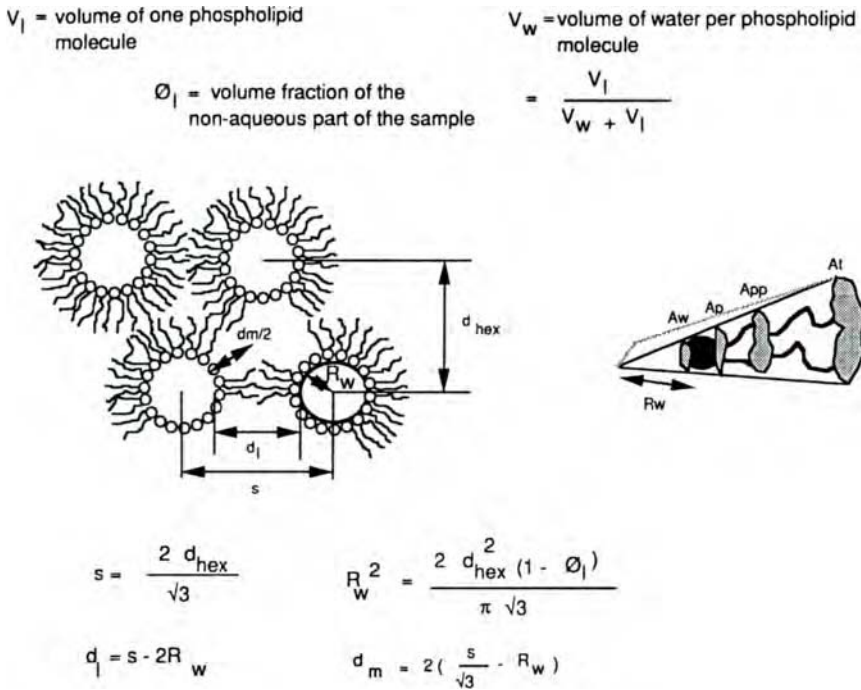


Fig. 13. Structure of the reverse hexagonal phase formed by many phospholipids, and the derivation of structural dimensions from X-ray diffraction and sample composition. d_m and d_l are molecular lengths projected onto the plane of the hexagonal lattice. A_w , A_p , A_{pp} , and A_t are the molecular areas available per molecule at the lipid/water interface, at the polar/hydrocarbon interface, at a position of constant area, and at the terminal ends of the hydrocarbon chains.

membranes $H_{||}$ is worth studying, not because of its structure per se but, because the conditions that cause bilayer-forming lipids to rearrange into the $H_{||}$ phase likely reflect stresses within bilayers that are important to their properties. The idea of a 'spontaneous' or 'intrinsic' curvature of monolayers has received much attention recently, and OS has been particularly illuminating in its definition and study.

The $L-H_{||}$ transition involves large geometrical changes that have been understood in terms of 'molecular shape', originally introduced by Luzzati (see [31] for example). When interpreted beyond the narrow context of the steric shape of a rigid molecule, to include dynamic polar group interactions and a distribution of chain conformations, such a shape concept has successfully 'predicted' phase transitions.

More recently, the global arrangement in lipid assemblies has been considered in terms of the curvature of the constituent monolayers. Gruner [98, 99] and his colleagues introduced the concept of a spontaneous or intrinsic curvature, with curvature energy to be included with other competing free energies of the system. One of the latter is the chain packing stress required to populate the different molecular lengths around the axes of the aqueous cylinder. Particularly, when the cost for

the lipid molecules to stretch the maximal interstitial distance in the H_{\parallel} phase is too high (see fig. 13) they remain assembled in the lamellar phase. For example, DOPE/DOPC mixtures form H_{\parallel} phases of large dimension and radii of monolayer curvature only with added hydrocarbon, such as tetradecane [100]. To relax to these large spontaneous radii of curvature, tetradecane is understood to be required to fill the interstice, and was shown to do so [101], which otherwise is inaccessible to the short lipid chains. Only in excess water and tetradecane, to remove all hydration and hydrocarbon chain packing stresses, is it taken that the monolayers form a stress-free spontaneous curvature which can be measured using osmotic stress [102, 103].

In spite of the success of these approaches, which are dealt with comprehensively in the chapter by Seddon, it has been surprising and particularly instructive to find examples that so obviously contradict prediction. For that reason we outline work that highlights new problems of the energetics of lipid assemblies.

Figure 13 shows the hexagonal phase and the structural parameters that can be measured by X-ray diffraction. We will use as an example pure DOPE which undergoes surprising reentrant hexagonal-lamellar transitions on dehydration [104], shown in the phase diagram in fig. 14.

Osmotic stress of the H_{\parallel} phase gives a measure of the work needed to decrease the size of the aqueous dimensions [102, 103]. DOPE's reentrant H-L-H phase transition sequence provides, as well, a unique system directly to compare the structural

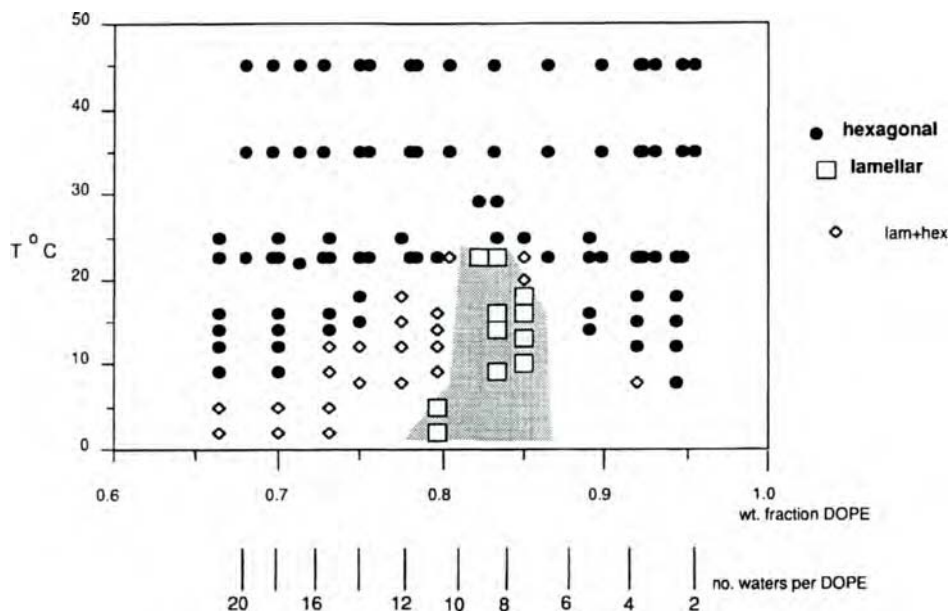


Fig. 14. Phase diagram of DOPE as a function of temperature and water concentration as determined by X-ray diffraction. At lower temperatures, there is a remarkable re-entrant hexagonal-lamellar-hexagonal phase transition sequence on removing water, either gravimetrically or by osmotic stress. This provides an opportunity to measure both the osmotic work of the transition the resultant structural changes that occur in lipid layers [104].

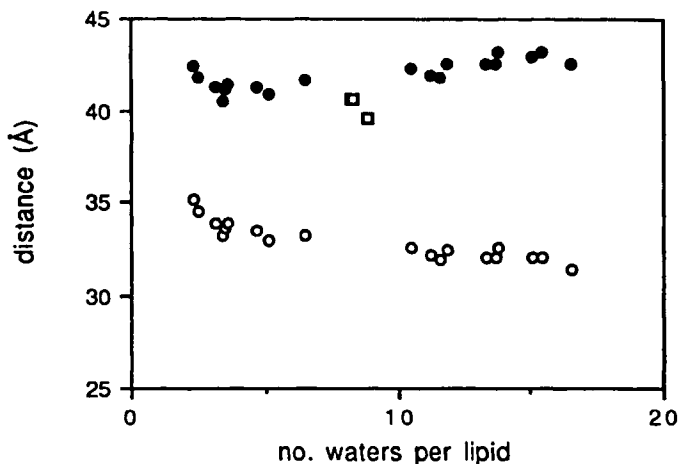


Fig. 15. Average projected lengths of two DOPE molecules in the lamellar phase (\square) and in the interaxial, d_l , (\circ) and interstitial, d_m , (\bullet) directions of the hexagonal phase, as described in fig. 13. The transition to the hexagonal phase is accompanied by a decrease in molecular length in the interaxial direction with little change in the interstitial direction. Ref. [104].

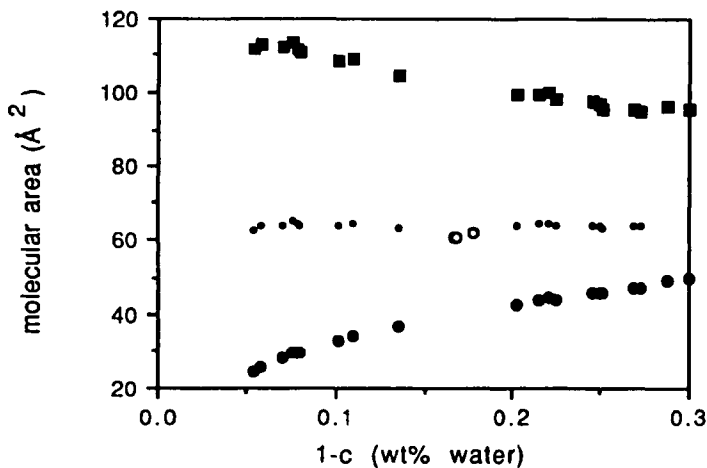


Fig. 16. Area available per DOPE lipid molecule at 22.5 °C as the water content of the phases changes. For the hexagonal phase, as water is removed the area, A_w , at the polar group-water interface (\bullet) decreases while at the terminal methyl ends of the hydrocarbon chains (\blacksquare) A_t increases. At a neutral or pivotal position the area, A_{pp} changes little with water content (\cdot). The molecular area in the intervening lamellar phase (\circ) is close to that of the neutral plane of the hexagonal phase. At the H_{\parallel} to L transition the polar group area abruptly increases and the hydrocarbon area abruptly decreases.

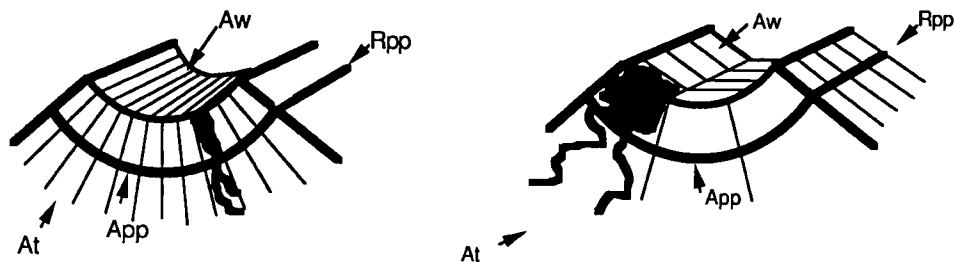


Fig. 17. The changes in sector dimensions illustrate that when the monolayer is bent, the areas of the polar and hydrocarbon ends of the molecule change in opposite directions as the molecule pivots around its position of constant area, R_{pp} . That position, the neutral plane of the monolayer, is indicated by the solid line and is close to the hydrocarbon chain/polar group interface (A_p in fig. 16). In spite of rather precise knowledge of the magnitude of these time-average molecular areas, and their changes, there is no information regarding their 'shapes', dispersity or dynamics. While it is usually assumed that the whole molecule is radially symmetric around its long axis, such symmetry cannot be the case, at least for all time scales, for the $H_{||}$ structure where some form of radial anisotropy results in the large disparity in the two principle radii of curvature, along (microns) and around (\AA) the $H_{||}$ axis. In the hexagonal phase the number of molecules around the circumference of the aqueous cylinder is unknown. This figure shows only two examples of how twelve lipid molecules, which could have radial asymmetry based on two-state rotational diffusion for example, can fill an equivalent volume of the $H_{||}$ structure. Therefore measured decreases in molecular area do not necessarily mean 'compaction' around the cylinder, since the number of molecules around the circumference and along the cylinder axis can change independently, i.e. increases in the length of the cylinder could come at the expense of a decreased circumference.

dimensional changes that occur in that transition. In several figures we show the empirical data relating the osmotic pressure and structural changes for this system. Several noteworthy facts emerge.

- (1) Figure 15 shows that the transition from the lamellar to hexagonal phase for DOPE is accompanied by an overall DECREASE in projected molecular length. The maximum molecular length, in the direction of the interstice, d_m , is equal to its length in the bilayer. The lipid dimension in the interaxial distance is 30% less. The energetics of chain stress should recognize the direction of this change.
- (2) Figure 16 shows that as the DOPE hexagonal phases are osmotically dehydrated and their monolayers curl, the molecular area in the polar group region decreases and that in the hydrocarbon chain region increases. As shown schematically in fig. 17, a fulcrum, or pivotal point or neutral plane, where little change in area occurs, is found near the polar/hydrocarbon interface within the monolayer. This raises the likelihood of non-uniform lateral interactions within the monolayer and makes it difficult to avoid the possibility that lateral stresses will vary, perhaps even in sign, along the length of the molecule.
- (3) In defining monolayer curvature at the pivotal position, the osmotic work of bending the monolayer can be fit to a simple bending energy, given by the quadratic of the deviation in curvature from the intrinsic curvature [103]. This yields bending moduli consistent with those derived from bilayer studies. It

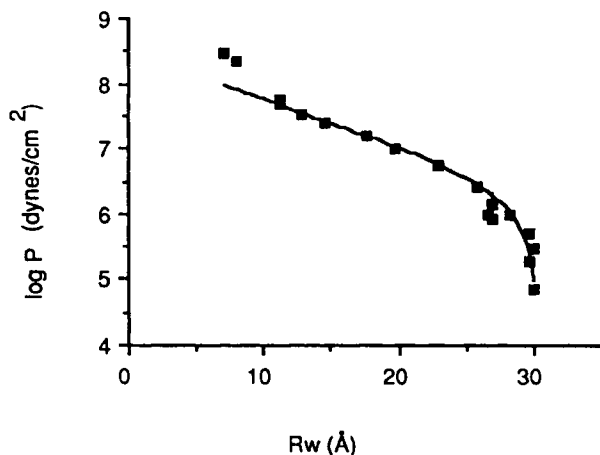


Fig. 18. Variation in the radius of the water cylinder with osmotic stress for the hexagonal phases of DOPE. Comparison of experimentally measured values (filled squares) with those expected (continuous line) by fitting a quadratic form of the monolayer bending energy. The highest two osmotic pressure points deviate from the trend and were excluded from the fit. Best-fit linear plots yield a bilayer bending modulus $K_c = 1.7 \times 10^{-12}$ ergs ($42.9kT$) and an intrinsic radius of curvature $R_0 = 30.9$ Å for DOPE.

is important to recognize that these data can also be fit with a number of other functions. So the agreement with bending alone does not preclude any of a number of other significant contributions to the energetics of the phase. A particularly insightful alternative is the recognition of both bending and compressional energy contributions to the free energy [105, 106]. While minimization of the cross coefficients of these two contributions leads to a slightly different neutral plane, the importance of the concept is the inclusion of both energies.

- (4) One especially surprising observation is the re-entrant phase transition sequence, hexagonal-lamellar-hexagonal, that occurs with pure DOPE in the course of changing hydration [104]. It is this which runs counter to previous rationalizations and predictions of phospholipid phases, based on molecular shape or curvature alone. Further, the osmotic work required to effect the transition is an order of magnitude less than that estimated to unbend the monolayers on the basis of measured bending moduli, as described above. This showed that there are contributions to free energies that have only recently been accounted for [139].

These observations have made it difficult to simplify the energetics of lipid layers. For example the concept of intrinsic or spontaneous curvature now would seem to be clearly defined only when the other contributions to the free energy become defined. We should not be surprised to find that global bilayer compressibility reflects considerable variation in local interactions along the molecular length.

But how to measure such local variations? Perhaps proteins, hosted in such a layer will emerge to be one of the most sensitive informers about these inhomogeneities.

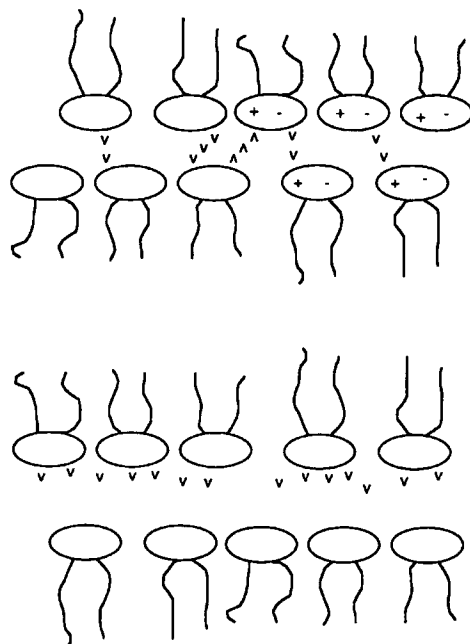


Fig. 19. Schematic illustration of the repulsive and attractive configurations thought to result in hydration forces. Reduction of one of the complementary groups to polarize or hydrogen bond with water reduces the element of correlation between polarizing groups and reduces any attractive element in the net interaction.

Interestingly, alamethicin changes its probability of occupying one of its conduction states with a change in the concentration of non-bilayer lipids into which it is incorporated [8].

4. Theories

4.1. 'Hydration' forces measured between lipid bilayers

Originally no more than the observation that it takes exponentially increasing amounts of work to remove distilled water from between electrically neutral bilayers, 'hydration force' has been interpreted in qualitatively different ways. Hobbled by difficulties intrinsic to the study of liquids, there has been a dichotomy in theories.

First, largely due to the initial insight of Marcelja and coworkers [107, 108], there is the idea that water is perturbed by the polar surface and that the exponential decay of the force is from progressively weakening perturbation of the solvent as a function of distance from the surface. (For charged lipids there is also the perturbation of ion re-distribution to create electrostatic double layer repulsion.)

Second, through the perception of Helfrich [109], flexible layers are known to repel through the loss of motional freedom that comes from collision. Besides whole-bilayer undulation, there can be flexing of zwitterionic polar groups or even the bobbing of lipid molecules for other modes of steric repulsion.

Though both themes have been elaborated and generalized, the two classes of models – solvent perturbation by surfaces vs. mechanical fluctuations of surfaces – needlessly conflict in most thinking. Through systematic measurement, it is becoming clear that both ideas appear to contain complementary and essential truths: the work to bring together membranes or macromolecules is a combination of work done against forces acting directly between membranes (as if they were stiff bodies) and of work against the configurational freedom of flexible bodies in unencumbered space. The ‘collisions’ that confine configuration are actually soft encounters [59, 128, 131, 132, 168] through direct long range forces rather than the hard steric clashes of non-interacting bodies. Figure 20 is meant to illustrate this schematically.

The mutually enhancing interplay between these different kinds of energies is described in the chapter of Evan Evans. Configurational/entropic forces are elaborated in the chapters of Wolfgang Helfrich and R. Lipowsky.

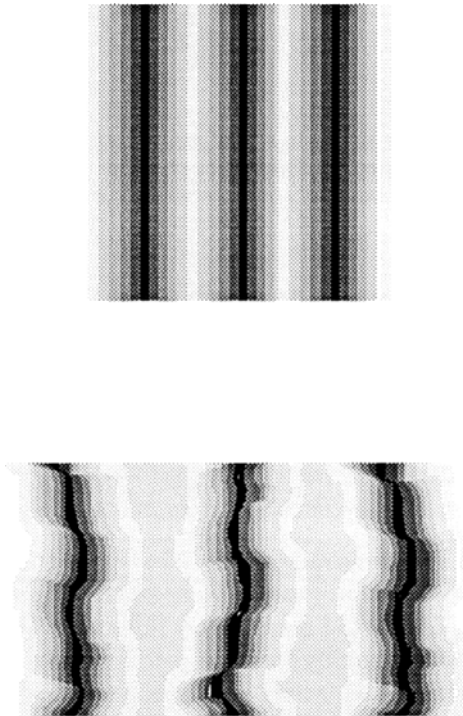


Fig. 20. Schematic illustration of the impact of fluctuations on the direct interactions between bilayers. The shading is meant to illustrate the exponential decay of direct bilayer repulsion and the increased spacing the result of the renormalization of these direct interactions when thermal fluctuations are introduced to these bilayers.

Any satisfactory theory must recognize closely related results from forces measured between DNA double helices, between stiff polysaccharides [4] and between protein fibres [161]. While these materials are outside the purview of this chapter, they provide better opportunity to connect force with molecular structure and allow a much wider range of experimental tests than are possible with phospholipids alone. In comparing repulsion measured between eggPC bilayers with that between DNA double helices in a tetramethylammonium (TMA) salt and a polysaccharide Xanthan in NaCl, one is struck by the similarity of force decay constants. If one uses the Derjaguin approximation to transform the force between cylindrical DNA molecules to what would occur between planar surfaces of the same material, one derives a curve close to that of eggPC whose defining phosphorylcholine polar group is close to that of the DNA phosphate with the tetramethylammonium counterion. The force does not seem to depend critically on whether or not phosphate and counterion are connected as in eggPC or are not bonded as in TMA-DNA! (See [161].) For separations between 5 and 15 Angstroms, xanthan and schizophyllan polysaccharide [4] interactions are essentially independent of salt concentration, strong evidence against double layer interactions.

4.1.1. Solvent perturbation models

The intrusion of a membrane or macromolecular surface into a liquid can be expected to disturb the arrangement of small molecules. One can also expect this disturbance to be progressively relieved further away from the surface. Solvent perturbation models are phrased in the grammar of ‘order parameters’, quantities known or postulated to describe the local condition or free energy density of the liquid as it deviates from its undisturbed state.

As in many order-parameter formalisms, the physical nature of the perturbation is left undefined. ‘Electrostatic’ models of water solvent have considered the polarization of water normal to the bilayer surface, the density of hydrogen bonds, the density of water molecules themselves, but might come to include non-scalar parameters, vectors or even tensors to describe hydrogen bond configuration.

In its simplest application, the method assumes that the local free energy density $g(\eta)$ of the solvent goes as the square of the (scalar) order parameter and the square of the gradient as the beginning of a power series expansion in η and its derivatives [107, 159]

$$g(\eta) = a\eta^2 + b(\text{grad } \eta)^2 \quad (4)$$

where $g(\eta)$ varies in the solvent space between membranes because $\eta = \eta(x, y, z)$. The ratio b/a is the square of a length λ a characteristic distance over which the solvent can relax from the presence of the intruding surface. To convert local free energies to interaction between surfaces, one integrates $g(\eta)$ over the inter-bilayer space to get a total free energy G , solves for the function $g(\eta(x, y, z))$ that minimizes G , then derives a force per unit area or pressure from the rate of change of total free energy with separation d_w [107, 108, 110–112]

$$P = \Delta G / \Delta d_w. \quad (5)$$

The interaction of two like surfaces is a repulsion of the form

$$P = R / \sinh^2 (d_w / (2\lambda)) \quad (6)$$

which goes to

$$P \rightarrow R e^{(-d_w / \lambda)} \quad (7)$$

at separations d_w much greater than λ .

For anti-symmetrically unlike surfaces, there is attraction of the form [62, 109]

$$P = -A / \cosh^2 (d_w / (2\lambda)) \rightarrow -A e^{(-d_w / \lambda)} \quad (8)$$

(with coefficients A , R taken to be positive).

The connection between measured exponential forces and their expression in terms of the solvent-perturbation formalism is straightforward but perhaps no more than tautological. However, with the ability to relate measured forces with known structural features of the interacting surfaces, the formalism earns higher regard. It is already clear from the primitive equations given above that a net repulsive force can be a combination of hydration attraction and repulsion whose individual contributions might be identified through closer examination of the change in forces, particularly empirically determined decay lengths, with changes in the structure of the interacting surfaces.

For better intuition about the order-parameter equations, it is instructive to see that the Debye-Huckel theory applied to the interaction of charged bodies in salt solutions is mathematically equivalent to the present equations. In ionic solutions, the perturbation is the re-distribution of ions near the charged surface; the decay distance λ is simply the Debye length λ_D of the salt solution. As presented here, the order-parameter formalism is analogous to electrostatic double layer theory with surfaces maintained at constant charge; a derivation equivalent to a constant-surface-potential boundary condition has been developed [112]. One may note too an alternate electrostatic formalism built on non-local dielectric response [108, 113–115].

4.1.2. Influence of surface structure

Since one cannot specify the precise nature of the order parameter, one can speak only formally of the features that set the values of $\eta = \eta(x, y, z)$ on the face of the bilayer. In analogy to what is done in X-ray or neutron diffraction where molecular structure is expressed as a sum of waves of matter, one can express the boundary conditions on the interacting surfaces in terms of a surface function $S(Q)$ for wave vectors Q in the (x, y) plane. $S(Q)$ can be considered a Fourier transform of the order parameter $\eta = \eta(x, y)$. For example, in the particular case of two unlike surfaces whose order parameter η on the surface is zero when averaged over the (x, y, z) plane (as might be the case for some zwitterionic lipids), the interaction is [115, 170]

$$P(d_w) \cong \frac{\alpha}{2\pi^2} \int dQ \left\{ S_1(Q) + S_2(Q) - 2\alpha \frac{S_1(Q)S_2(Q)}{k_B T} \right. \\ \left. \times (Q^2 + \lambda_w^{-2})^{-1/2} \right\} \exp(-2d_w \sqrt{(Q^2 + \lambda^{-2})}). \quad (9)$$

For like surfaces, $S_1(Q) = S_2(Q) = S(Q)$, this becomes

$$P(d_w) \cong \frac{\alpha}{\pi^2} \int dQ \left\{ S(Q) - \alpha \frac{S(Q)^2}{k_B T} (Q^2 + \lambda_w^{-2})^{-1/2} \right\} \times \exp(-2d_w \sqrt{(Q^2 + \lambda_w^{-2})}). \quad (10)$$

The parameter α is a constant determining the strength of water ordering by a polar group ($\alpha = 4\pi\epsilon_w^{-1}$ in an electrostatic analogy), λ_w^{-1} is a characteristic length of water ordering or Debye length in the electrostatic mechanism, k_B is the Boltzmann constant, and T is absolute temperature.

The first term under the integral is a kind of residual repulsive pressure from the interaction of water-organizing groups whose perturbation of solvent is interrupted by the opposing surface. The second term, relying on the similarity of surfaces, predicts attraction. The empirical decay length is a mix of the characteristic decay length, λ_w , of the solvent and the structural lengths represented by the wave vector Q . For each periodicity Q in the surface structure, the contribution to the exponential variation of P has an effective decay rate

$$\lambda_{\text{eff}} = \frac{1}{2\sqrt{Q^2 + \lambda_w^{-2}}}. \quad (11)$$

From these relations, one begins to see how less repulsive bilayers such as PE have shorter empirical λ 's that reflect attraction/repulsion competition [62]. Indeed for cases where $S(Q)$ has important values near $Q = 0$, there can be an effective halving of the exponential force decay rate compared to λ_w . Cases of strong order with short surface-wave lengths, i.e. contributions from large Q , create even shorter effective λ 's.

Given the variety of forces possible with different $S(Q)$, it is quite possible that the observed decay distances, even for the simplest phospholipids, are not those of water solvent itself. There is some experimental evidence that even PC bilayers have attractive and repulsive hydration components. For example, lateral dilution of dioleoylPC with added dioleoylglycerol (DOG) makes bilayers swell (fig. 10). The two species differ only in the absence of some zwitterionic phosphorylcholine polar groups. Is some correlation of the PC zwitterions being broken when a few of them are 'removed'. Unattached phosphorylcholine molecules on their own precipitate from solution and crystallize at concentrations far lower than the effective molar concentrations they have in multilayers [117]. Does their attachment to the bilayer surface frustrate attraction that they would otherwise express?

Polar groups, and consequently well-defined peaks in $S(Q)$, are probably also disrupted by heterogeneity of hydrocarbon chains. This loss of surface order could explain the greater repulsion between natural eggPC bilayers compared with the synthetic SOPC.

It is possible that the distribution of water-ordering centers in the z -direction, perpendicular to the plane of the bilayer, can also modify the straight-exponential

decay of forces. If one thinks of a polar region of finite thickness over which there is an accumulated modification of the solvent, the integrated effect of this region will create a force whose rate of decay reflects both the intrinsic relaxation distance of water and the distribution of organizing charges through the polar layer [118].

4.1.3. Attempts to identify order parameters

The discomfiting agnosticism of the order parameter language has motivated several attempts for more specific identification. The most popular candidate has been the polarization of water [108, 118–120]. However, such polarization should couple with electrostatic double layer forces so as to change the apparent electrostatic double layer decay lengths. This seems not to occur, e.g., [39, 67, 68, 75, 76, 79]. Rather, hydration and electrostatic forces seen between charged bilayers each vary as expected from double layer theory and from measurements on neutral bilayer systems.

Computer simulation has been challenging. Difficulties arise from the large number of water molecules that must be included, the weakness (\sim calories/mole, fig. 3) of the perturbation per water molecule (compared with the \sim kcal/mole energies of normal hydrogen bonding), the long times required to equilibrate waters near surfaces. Nevertheless, progress has been made [121, 122]. The first simulations, with rigid bilayers, showed strong periodicities in polarization incompatible with a monotonically varying forces. Rather than polarization, changes in the arrangement or density of hydrogen bonds have been suggested as better parameters [121, 123–126]. It has recently been found possible to simulate the small thermal fluctuations intrinsic to a liquid-liquid interface [126]. These polar group fluctuations in both gel and liquid-crystal phases suffice to break up the solid-lattice regime of water that appeared in early simulations. Polarization profiles in these most recent simulations vary monotonically, without oscillation, as one would expect for a monotonically varying solvation force.

Experimentally, the coefficients of hydration force measurements on lipids as different as monoglycerides, sphingomyelins, phosphatidylcholines and phosphatidylethanolamines can be shown to correlate with the square of the measured surface potential for monolayers of those lipids in contact with bilayers [80, 91] and (fig. 12b). To effect this correlation it was necessary to define the bilayer water interface outside the polar region in such a way as to include all water molecules mixed in with the polar groups (fig. 2). This definition allows one automatically to include perpendicular components of the oriented dipoles not only from the lipid but also from the water molecules in the headgroup region, a definition that matches with electrode placement above and below the complete monolayer. The good correlation suggests some connection between forces and electrostatic potential.

But, is the dipole potential the cause of water perturbation with the hydration force its effect? Or is the dipole potential an effect of the same reorganization of water that is seen also as the hydration force? When one measures the ‘dipole’ potential within bilayers, by the rejection or attraction of positive or negative ions there is not the same clear correlation with bilayer repulsion [127]. It seems more likely then that the correlation of force and dipole potential is good evidence of a fundamental

connection between hydration forces and the perturbation of water but that the dipole potential need not be regarded as the cause of hydration.

4.2. Entropic/configurational models

4.2.1. Undulatory forces

Left free in unlimited solvent, flexible bilayers will bend to occupy space far greater than their actual, relatively negligible, volume. The structures accessed through bilayer or vesicle flexibility are well-described in other chapters of this book (Sackmann, Andelman, Lipowsky, Evans, Helfrich). The free energetic consequence of confinement into multilayers that is felt as a repulsive force.

If there were no direct interaction between flexible bilayers except that no two bilayers could occupy the same place, then confinement would take the form of an infinitely hard wall preventing each membrane from billowing past its neighbors. By expressing this restraint in the language of a mutual molecular field of neighbors, Helfrich [109] treated the bending of bilayers as an ensemble of periodic waves whose sum at any place on the membrane could not exceed a fixed maximum proportional to the average water space d_w between neighbors.

For the 'hard wall' case, one early result of Helfrich suggested that bilayer undulations produce a free energy of interaction per unit area that goes as the inverse square of d_w ,

$$F/A = (3\pi^2(kT)^2/128) \times (1/\kappa d_w^2) \quad (12)$$

where κ is the bending modulus (eq. (31), ref. [109]). The power-law variation is qualitatively different from what is seen between phospholipid bilayers interacting across water, but the predicted motion corresponding to this kind of interaction has been verified by X-ray scattering by multilayers of hydrocarbon, surfactant and brine [129, 130]. (In that case, there is a thick hydrocarbon layer, and fluctuations are in the thickness of that layer rather than in the thickness of the salt solution between surfactant monolayers.) These power-law steric interactions are discussed at length elsewhere in this volume. The reader should be aware that there are several alternate versions of the inverse-square steric free energy, even in the original paper [109] and that the various coefficients are still a matter of active study.

This result is qualitatively modified when neighboring bilayers are repelled by an exponential direct force

$$P = P_0 \exp(-d/\lambda) \quad (13)$$

between layers to give [59, 127] a limiting result

$$P_H(d) = (\pi kT/32) \times (P_0^{1/2}/(\kappa\lambda^3))^{1/2} \times (e^{-d/2\lambda}). \quad (14)$$

The expected contribution of undulatory fluctuations is exponential with a decay rate half that of the underlying force! One might think of this as fluctuation-enhanced hydration (or electrostatic double layer) repulsion or as hydration-enhanced undulatory repulsion [59, 128].

When the direct pressure $P = P_0 e^{(-d/\lambda)}$ grows sufficiently strong, undulations are suppressed. The direct term dominates. Coupling of direct forces with motion has been measured in DNA lattices where it is possible to measure both the intermolecular free energy and the extent of molecular motion [131, 132]. A more ample treatment of interlamellar forces, bilayer fluctuations and interaction energy, as well as the added suppression of undulation by lateral attention applied to vesicular bilayers is to be found in the chapters by W. Helfrich, R. Lipowsky, D. Andelman and E. Evans.

4.2.2. Entropic mechanisms as alternatives to 'hydration'

There have been several attempts to describe bilayer repulsion in terms of disorder and fluctuations in the polar groups, whole molecules or even patches of bilayers. In no case have these models adequately addressed the large range of the observed forces (four to five decades of pressure) or the sensitivity of forces to molecular structure or packing.

The first of these models for forces assumed that repulsion was due to disorder of the phospholipid polar groups [133]. To achieve an upper-bound estimate of this disorder, the model cut the bond connecting the negative phosphate to the positive choline group of the PC zwitterion to create a counterion-only electrostatic double layer repulsion between facing bilayers. Even this upper-bound estimate of repulsion turned out to predict much too small forces when they were directly measured six years later [1].

Since then there have been several other models of phospholipid head group configuration and electrostatic (Coulombic or image charge) interaction which have required many adjustable parameters, have been confined to relatively small ranges of forces, have used definitions of separation different from those in the actual experiment, and which predict attractive as well as repulsive forces [134–138].

If polar group configuration does create steric repulsion between bilayers, it is probably occurring at distances shorter than the domain of exponentially varying 'hydration' forces. For several phosphatidylcholines and for their near-relative sphingomyelin, it is sometimes possible to see a clear upward break at separations where electron density maps say that polar groups should be colliding (fig. 11). These steric interactions disappear when polar groups are laterally diluted by adding cholesterol (fig. 11) [46, 85]. A spring model of polar group repulsion [138] might be nicely adapted to fit these steric forces if one shifts the bilayer separations used in the original theory to coincide with the definition of fluid spacing d_f built on electron density maps (T.J. McIntosh, personal communication).

A molecular protrusion model, imagines individual phospholipid molecules independently emerging from bilayers to create a pressure on the opposing surface as far as 15-to-20 Angstroms away [140, 141]. The work of emergence is taken to be a kind of water/carbon interfacial energy of a cylindrical hydrocarbon chain, an energy linear in the extent of protrusion with a consequent probability that decreases exponentially with protrusion length. Though the model does give exponential repulsion, it has been critically examined on several grounds [142, 143].

- If phospholipids protrude so easily (only $1 kT$ cost for each $\lambda = 2$ Angstroms emergence), their solubility would be 10^2 to 10^6 times that measured.

- Measured forces are exquisitely sensitive to methylation (fig. 7) of the terminal amine, a variation that should have no effect on the work or probability of chain protrusion.
- Hydration repulsion is virtually the same for frozen-chain sphingomyelin and melted-chain eggPC which have the same polar-group and molecular area.
- Hydration repulsion decay lengths are the same for double-chain zwitterionic PC and for bilayers made of equal amounts of positive and negative species.
- The force coefficient P_f correlates with the monolayer surface potential [88], a parameter that should have little relation to molecular protrusion.

The forces considered in a 'blister' model are explicitly restricted to bilayers loosely stuck to solid surfaces. The idea is that patches or blisters of bilayers, not monolayers, can lift off from the solid substrate and push against the bilayer on the opposite surface. With selected parameters, one can predict forces that go as $e^{(-d/\lambda)}$ (among many possible contributions to the total interaction) [144, 145].

4.3. Traditional forces

Electrostatic interactions are specifically treated in the chapter by David Andelman. Superficially, except for their modification by bilayer undulation, electrostatic double layer forces between charged membranes appear to behave according to classical theory [146–152]. One may now cite data for stiff frozen bilayers [71, 139], and for highly charged bilayers in weakly screening low-salt solutions [68, 75] or for bilayers immobilized onto mica surfaces [39, 79]. The apparent accuracy of theory in those cases allows one to identify the conditions where electrostatic double layer interaction no longer describes bilayer repulsion, and allows one then to recognize the clear upward breaks at 8-to-15 Angstrom separation that declare the onset of hydration forces.

However, appearances can be deceptive. The remarkable apparent success of classical theory (at least for 1 : 1 electrolytes) at unexpectedly high potentials and salt concentrations seems to result from a cancellation or compensation of ionic size effects, specific binding of discrete ions, non-linearities in double layer equations, or many-body ion-ion correlations that create an effective surface charge and an effective locus of the charge [151, 159]. Strong binding of ions to membranes can kill double layer repulsion and even create attraction and membrane adhesion [52]. Similarly, ionic fluctuation, especially of divalent ions, can create attractive forces, an ionic-monopole version of Van der Waals forces.

Predicted fluctuations in ionic double layers or on charged surfaces can create attractive forces [153–157]. Correlated configurations of zwitterions on neutral bilayers are expected to produce attractive forces [157], but it is not clear whether their interaction should be formulated in terms of straight electrostatics with dielectric boundaries and image forces or by the kind of order parameter formalism that describes hydration forces.

But liquid crystalline bilayers can flex. The thermal fluctuations allowed by this flexibility, when restricted by electrostatic double layer interactions, creates interactions of longer range and slower decay than seen in rigid systems [59, 128]. Theories

of fluctuation-enhanced double layer repulsion have been developed and tested not only for charged bilayers but also for flexible linear polyelectrolytes [131, 132]. The nature of enhancement is equivalent to that seen with expansion of hydration interactions.

4.4. *Van der Waals attraction*

Except for the phosphatidylethanolamines (PE's) that show unexpectedly strong attraction, there seems little reason to question the role of Van der Waals charge fluctuation interactions [149, 153, 160] between lipid bilayers. Evidence from direct measurement of attractive contact energies (Evans chapter this volume and references therein) as well as from force measurements suggests that Van der Waals forces are adequate to provide the attraction between bilayers for them to form multilayer lattices. (Measurement of attraction between bilayers on mica surfaces must include consideration of mica contributions as well [180]. This mica-mica attraction might explain the stronger attractions inferred between PC bilayers coatings vs. those directly measured between bilayer vesicles [45, 79, 38].)

Given the number of unknown structural features and the number of adjustable parameters in competing models, it will probably be a while until there is a full and reliable theory of bilayer interactions. It may even be that, as in the theory of ionic solutions where one must be satisfied with the empirical 'dielectric constant' as a trick to adapt Coulomb's Law, one must learn to be satisfied with practical expressions that allow measured forces to be used with reasonable reliability before they are properly understood.

5. Coda

Beginning with observations that lipid bilayers resist dehydration, then making a systematic inquiry into forces between (and within) lipid assemblies, has led to new ways to speak of these interactions.

One can now re-view membrane lipid organization in natural systems and in practical applications.

Lipid phase transitions, already known to change with water content, come to be seen in terms of dehydration energies.

Membrane fusion, ubiquitous in cell biology and of practical concern in drug delivery, by its very nature depends on the forces encountered bringing together previously stable membranes.

Now one can see an exquisite sensitivity of forces to lipid chemistry – methylation of surfaces, mixing of lipid type, even composition of hydrocarbon chains far from the membrane exterior – and can recognize the large work needed to bring together lipid surfaces. But it is still difficult to explain these forces either in terms of traditional colloid theories or with new models of solvent perturbation or of molecular configuration.

The same techniques that enable force measurement among lipids also reveal strikingly similar forces between other kinds of materials – proteins, nucleic acids,

polysaccharides. One can even go on to think of forces within large biomolecules as they change conformation.

Probably most important, the concept of force measurement at nanometer separations, and the methods developed to evaluate them, provide a quantitative logic to think about the novel ways in which matter behaves on the nanometer scale.

Acknowledgements

RPR is a Research Fellow of the Canada Council's Killam Program and acknowledges the financial support of The Natural Sciences and Engineering Research Council of Canada and the invaluable help of Mrs. Nola Fuller. VAP thanks the Office of Naval Research (U.S.A.) for a supplementary grant.

References

1. Le Neveu, D.M., R.P. Rand and V.A. Parsegian, 1976, *Nature* **259**, 601; Le Neveu, D.M., R.P. Rand, V.A. Parsegian and D. Gingell, 1977, *Biophys. J.* **18**, 209.
2. Parsegian, V.A., R.P. Rand, N.L. Fuller and D.C. Rau, 1986, in: *Methods in Enzymology*, Vol. 127, ed. L. Packer (Academic Press, New York) p. 400.
3. Rau, D.C., B.K. Lee and V.A. Parsegian, 1984, *Proc. Nat. Acad. Sci. USA* **81**, 2621.
4. Rau, D.C. and V.A. Parsegian, 1990, *Science* **249**, 1278.
5. Zimmerberg, J. and V.A. Parsegian, 1986, *Nature* **323**, 36.
6. Rayner, M.D., J.G. Starkus, P.C. Ruben and D.A. Alicata, 1992, *Biophys. J.* **61**, 96.
7. Zimmerberg, J., F. Bezanilla and V.A. Parsegian, 1990, *Biophys. J.* **57**, 1049.
8. Keller, S.L., S.M. Bezrukov, S.M. Gruner, I. Vodyanoy and V.A. Parsegian, 1992, *Biophys. J.* **61**, A115.
9. Kornblatt, J.A. and G. Hui Bon Hoa, 1990, *Biochemistry* **29**, 9370.
10. Colombo, M.F., D.C. Rau and V.A. Parsegian, 1992, *Science* **256**, 655.
11. Rand, R.P., N.L. Fuller, P. Butko, G. Francis and P. Nicholls, 1993, *Biochemistry* **32**, 5925.
12. Steitz, T.A., M. Shoham and W.S. Bennett, 1981, *Phil. Trans. R. Soc. London B* **293**, 43.
13. Otting, G., E. Liepinsh and K. Wuthrich, 1991, *Science* **254**, 974.
14. Israelachvili, J.N. and G.E. Adams, 1978, *J. Chem. Soc. Faraday Trans. I* **74**, 975.
15. Ducker, W.A., T.J. Senden and R.M. Pashley, 1991, *Nature* **353**, 239.
16. Butt, H.-J., 1991, *Biophys. J.* **60**, 1438.
17. Arakawa, T. and S.N. Timasheff, *Biochemistry* **24**, 6536 and 6545.
18. Leikin, S., D.C. Rau and V.A. Parsegian, 1991, *Phys. Rev. A* **44**, 5272.
19. Prouty, M.S., A.N. Schechter and V.A. Parsegian, 1985, *J. Mol. Biol.* **184**, 517.
20. Parsegian, V.A., R.P. Rand, M. Colombo and D.C. Rau, 1994, *Membrane Electrochemistry*, in: *Advances in Chemistry Series*, Vol. 235, ed. M. Blank and I. Vodyanoy (Am. Chem. Soc.) p. 177.
21. Parsegian, V.A., N.L. Fuller and R.P. Rand, 1979, *Proc. Nat. Acad. Sci. USA* **76**, 2750.
22. Kwok, R. and E. Evans, 1981, *Biophys. J.* **35**, 637.
23. Evans, E.A. and D. Needham, 1987, in: *Physics of Amphiphiles*, eds J. Mennier and D. Langevin (Springer, Berlin).
24. Evans, E. and R. Kwok, 1982, *Biochemistry* **21**, 4874.
25. Evans, E. and D. Needham, 1986, *Faraday Discuss. Chem. Soc.* **81**, 267.
26. Luzzati, V., 1968, in: *Biological Membranes*, ed. D. Chapman (Academic Press, New York) p. 71.
27. Evans, E.A., R. Skalak, 1980, in: *Mechanics and Thermodynamics of Biomembranes* (CRC Press, Boca Raton, FL).
28. Rand, R.P. and V.A. Parsegian, 1989, *Biochim. Biophys. Acta* **988**, 351.
29. Seul, M., 1988, *Phys. Rev. Lett.* **60**, 1150.
30. Israelachvili, J.I. and H. Wennerström, 1992, *J. Phys. Chem.* **96**, 520.
31. Luzzati, V. and F. Husson, 1962, *J. Cell Biol.* **12**, 207.

32. McIntosh, T.J. and S.A. Simon, 1986, *Biochemistry* **25**, 4058.
33. Evans, E. and D. Needham, 1987, *J. Phys. Chem.* **91**, 4219.
34. Israelachvili, J. and J. Marra, 1986, *Methods Enzymol.* **127**, 353.
35. Horn, R., 1984, *Biochim. Biophys. Acta* **778**, 224.
36. Marra, J., 1985, *J. Colloid Interface Sci.* **107**, 446.
37. Derjaguin, B.V., 1934, *Kolloid Z.* **69**, 155.
38. Horn, R.G., J.N. Israelachvili, J. Marra, V.A. Parsegian and R.P. Rand, 1988, *Biophys. J.* **54**, 1185.
39. Marra, J., 1986, *Biophys. J.* **50**, 815.
40. Tsao, Y.-H., S.X. Yang and D.F. Evans, 1992, *Langmuir* **8**, 1188.
41. Mitchison, J.M. and M.M. Swann, 1954, *J. Exp. Biol.* **31**, 443.
42. Rand, R.P. and A.C. Burton, 1964, *Biophys. J.* **4**, 115.
43. Rand, R.P., 1964, *Biophys. J.* **4**, 303.
44. Evans, E.A., 1980, *Biophys. J.* **31**, 425.
45. Evans, E. and M. Metcalfe, 1984, *Biophys. J.* **46**, 423.
46. McIntosh, T.J., A.D. Magid and S.A. Simon, 1987, *Biochemistry* **26**, 7325.
47. Rand, R.P., 1981, *Annu. Rev. Biophys. Bioeng.* **10**, 277.
48. Parsegian, V.A. and R.P. Rand, 1983, *Ann. NY Acad. Sci.* **416**, 1; Evans, E.A. and V.A. Parsegian, *ibid.* **416**, 13.
49. Feigenson, G.W., 1986, *Biochemistry* **25**, 5819.
50. Florine, K.I. and G.W. Feigenson, 1987, *Biochemistry* **26**, 1757.
51. Portis, A., C. Newton, W. Pangborn, D. Papahadjopoulos, 1979, *Biochemistry* **18**, 780.
52. Marcelja, S. 1992, *Biophys. J.* **61**, 1117.
53. Eisenberg, M., T. Gresalfi, T. Riccio and S. McLaughlin, 1979, *Biochemistry* **18**, 5213.
54. Guldbrand, L., B. Jonsson, H. Wennerström and P. Linse, 1984, *J. Chem. Phys.* **80**, 2221.
55. Kjellander, R. and S. Marcelja, 1985, *Chem. Scr.* **25**, 112.
56. Rand, R.P., B. Kachar and T.S. Reese, 1985, *Biophys. J.* **47**, 483.
57. Kachar, B., N. Fuller and R.P. Rand, 1986, *Biophys. J.* **50**, 779.
58. Rand, R.P. and V.A. Parsegian, 1986, *Annu. Rev. Physiol.* **48**, 201.
59. Evans, E. and V.A. Parsegian, 1986, *Proc. Nat. Acad. Sci. USA* **83**, 7132.
60. Seddon, J.M., G. Cevc, R.D. Kaye and D. Marsh, 1984, *Biochemistry* **23**, 2634.
61. Seddon, J.M., K. Harlos and D. Marsh, 1983, *J. Biol. Chem.* **258**, 3850.
62. Rand, R.P., N.L. Fuller, V.A. Parsegian and D.C. Rau, 1988, *Biochemistry* **27**, 7711.
63. Lis, L.J., M. McAlister, N.L. Fuller, R.P. Rand and V.A. Parsegian, 1982, *Biophys. J.* **37**, 657.
64. Rand, R.P., Unpublished.
65. Simon, S.A., J. McIntosh and A.D. Magid, 1988, *J. Colloid Interface Sci.* **126**, 74.
66. McIntosh, T.J., S.A. Simon, J.C. Ellington Jr. and N.A. Porter, 1984, *Biochemistry* **23**, 4038.
67. Parsegian, V.A., R.P. Rand and N.L. Fuller, 1991, *J. Phys. Chem.* **95**, 4777.
68. Tsao, Y.-H., D.F. Evans, R.P. Rand and V.A. Parsegian, 1993, *Langmuir* **9**, 233.
69. McIntosh, T.J., S.A. Simon, D. Needham and C.-H. Huang, 1992, *Biochemistry* **31**, 2012 and 2020.
70. McIntosh, T.J., A.D. Magid and S.A. Simon, 1989, *Biophys. J.* **55**, 897.
71. McIntosh, T.J., A.D. Magid and S.A. Simon, 1990, *Biophys. J.* **57**, 1187.
72. Simon, S.A., T.J. McIntosh and A.D. Magid, 1988, *J. Colloid Interface Sci.* **126**, 74.
73. LeNeveu, D.M., R.P. Rand, V.A. Parsegian and D. Gingell, 1977, *Biophys. J.* **18**, 209.
74. Gulik-Krzywicki, T., A. Tardieu and V. Luzzati, 1969, *Mol. Cryst. Liq. Cryst.* **8**, 285.
75. Cowley, A.C., N.L. Fuller, R.P. Rand and V.A. Parsegian, 1978, *Biochemistry* **17**, 3163.
76. Loosley-Millman, M.E., R.P. Rand and V.A. Parsegian, 1982, *Biophys. J.* **40**, 221.
77. Dubois, M. and Th. Zemb, 1991, *Langmuir* **7**, 1352.
78. Marra, J., 1988, *J. Colloid Interface Sci.* **109**, 11.
79. Marra, J., J.N. Israelachvili, 1985, *Biochemistry* **24**, 4608.
80. Simon, S.A., C.A. Fink, A.K. Kenworthy and T.J. McIntosh, 1991, *Biophys. J.* **59**, 538.
81. Rand, R.P., D. Needham and E. Evans, In preparation.
82. Carvell, M., D.G. Hall, I.G. Lyle and G.J. Tiddy, 1986, *Faraday Discuss. Chem. Soc.* **81**, 223.
83. Adam, C.G., J.A. Durrant, M.R. Lowry and G.J. Tiddy, 1984, *J. Chem. Soc. Faraday Trans. I* **80**, 789.

84. Das, S. and R.P. Rand, 1986, *Biochemistry* **25**, 2882.
85. McIntosh, T.J., A.D. Magid and S.A. Simon, 1989, *Biochemistry* **28**, 17.
86. Coorsen, J.R. and R.P. Rand, 1989, *Biochem. Cell Biol.* **68**, 65.
87. Bech, J. and R.P. Rand, 1992, In preparation.
88. Simon, S.A. and T.J. McIntosh, 1991, *BBA* **1064**, 69.
89. Simon, S.A., T.J. McIntosh, A.D. Magid and D. Needham, 1992, *Biophys. J.* **61**, 786.
90. McIntosh, T.J., A.D. Magid and S.A. Simon, 1989, *Biochemistry* **28**, 7904.
91. Simon, S.A. and T.J. McIntosh, 1989, *Proc. Nat. Acad. Sci. USA* **86**, 9263.
92. Israelachvili, J.N. and R.M. Pashley, 1982, *Nature* **300**, 341.
93. Pashley, R.M., P.M. McGuiggan, B.W. Ninham and D.F. Evans, 1985, *Science* **229**, 1088.
94. Podgornik, R., 1989, *J. Chem. Phys.* **91**, 5840.
95. Claesson, P.M. and H.K. Christenson, 1988, *J. Phys. Chem.* **92**, 1650.
96. Attard, P., 1989, *J. Phys. Chem.* **91**, 5840.
97. Christenson, H.K. and P.M. Claesson, 1988, *Science* **239**, 390.
98. Kirk, G.L., S.M. Gruner and D.L. Stein, 1984, *Biochemistry* **23**, 1093.
99. Gruner, S.M., 1989, *J. Phys. Chem.* **93**, 7562.
100. Kirk, G.L. and S.M. Gruner, 1985, *J. Physique* **46**, 761.
101. Turner, D.C., S.M. Gruner and J.S. Huang, 1992, *Biochemistry* **31**, 1340 and 1356.
102. Gruner, S.M., V.A. Parsegian and R.P. Rand, 1986, *Faraday Discuss. Chem. Soc.* **81**, 29.
103. Rand, R.P., N.L. Fuller, S.M. Gruner and V.A. Parsegian, 1990, *Biochemistry* **29**, 76.
104. Gawrisch, K., V.A. Parsegian, D.A. Hajduk, M.W. Tate, S.M. Gruner, N.L. Fuller and R.P. Rand, 1992, *Biochemistry* **31**, 2856.
105. Kozlov, M. and M. Winterhalter, 1991, *J. Phys. II France* **1**, 1077.
106. Kozlov, M. and M. Winterhalter, 1991, *J. Phys. II France* **1**, 1085.
107. Marcelja, S. and N. Radic, 1976, *Chem. Phys. Lett.* **42**, 129.
108. Gruen, D.W.R. and S. Marcelja, 1983, *J. Chem. Soc. Faraday Trans. 2*, **79**, 225.
109. Helfrich, W., 1978, *Z. Naturforsch.* **33a**, 305.
110. Kornyshev, A.A. and S.L. Leikin, 1989, *Phys. Rev. A* **40**, 6431.
111. Leikin, S., 1991, *J. Chem. Phys.* **95**, 5224.
112. Cevc, G., R. Podgornik and B. Zeks, 1982, *Chem. Phys. Lett.* **91**, 193.
113. Dzhavakhidze, P.G., A.A. Kornyshev and V.G. Levadny, 1986, *Phys. Lett. A* **118**, 203.
114. Dzhavakhidze, P.G., A.A. Kornyshev and V.G. Levadny, 1988, *Nuovo Cimento* **D10**, 627.
115. Leikin, S. and A.A. Kornyshev, 1990, *J. Chem. Phys.* **92**, 6890.
116. Kornyshev, A.A. and S.L. Leikin, 1989, *Phys. Rev. A* **40**, 6431.
117. Schumaker, G. and H. Sandermann, 1976, *Biochim. Biophys. Acta* **448**, 642.
118. Cevc, G., 1990, *J. Chem. Soc. Faraday II* **87**, 2733.
119. Schiby, D. and E. Ruckenstein, 1983, *Chem. Phys. Lett.* **95**, 435.
120. Cevc, G. and D. Marsh, 1985, *Biophys. J.* **47**, 21.
121. Kjellander, R. and S. Marcelja, 1985, *Chem. Phys. Lett.* **120**, 393.
122. Kjellander, R. and S. Marcelja, 1885, *Chem. Scr.* **25**, 73.
123. Attard, P. and M.T. Batchelor, 1988, *Chem. Phys. Lett.* **149**, 206.
124. Berkowitz, M.L. and K. Raghavan, 1991, *Langmuir* **7**, 1042.
125. Raghavan, K., M.R. Reddi and M.L. Berkowitz, 1992, *Langmuir* **8**, 233.
126. Marrink, S.-J., M. Berkowitz and H.J.C. Berendsen, 1993, *Langmuir* **9**, 3122.
127. Gawrisch, K., D. Ruston, J. Zimmerberg, V.A. Parsegian, R.P. Rand and N. Fuller, 1992, *Biophys. J.* **61**, 1213.
128. Podgornik, R. and V.A. Parsegian, 1992, *Langmuir* **8**, 557.
129. Safinya, C.R., D. Roux, G.S. Smith, S.K. Sinha, P. Dimon, N.A. Clark and A.M. Bellocq, 1986, *Phys. Rev. Lett.* **57**, 2718.
130. Roux, D. and C.R. Safinya, 1988, *J. Phys. France* **49**, 307.
131. Podgornik, R., D.C. Rau and V.A. Parsegian, 1989, *Macromolecules* **22**, 1780.
132. Podgornik, R. and V.A. Parsegian, 1990, *Macromolecules* **23**, 2265.
133. Parsegian, V.A., 1967, *Science* **156**, 939.
134. Jonsson, B. and H. Wennerström, 1983, *Chem. Scr.* **22**, 221.

135. Jonsson, B. and H. Wennerström, 1983, *J. Chem. Soc. Faraday Trans.* 2 **79**, 19.
136. Kjellander, R., 1984, *J. Chem. Soc.* **80**, 1323.
137. Granfeldt, M.K., B. Jonsson and H. Wennerström, *Mol. Phys.* **64**, 129.
138. Granfeldt, M.K. and S.J. Miklavic, 1991, *J. Phys. Chem.* **95**, 6351.
139. Kozlov, M.M., S. Leikin and R.P. Rand, 1994, *Biophys. J.* **67**, 1603.
140. Israelachvili, J.N. and H. Wennerström, 1990, *Langmuir* **6**, 873.
141. Israelachvili, J.N. and H. Wennerström, 1992, *J. Phys. Chem.* **96**, 520.
142. Parsegian, V.A. and R.P. Rand, 1991, *Langmuir* **7**, 1299.
143. Parsegian, V.A. and R. P. Rand, 1992, *Langmuir* **8**, 1502.
144. de Gennes, P.-G. and P. Pincus, 1990, *C.R. Acad. Sci.* **310**, 697.
145. de Gennes, P.-G., in: NATO ASI series, ed. Th.K. Karalis (Springer, Berlin) p. 595.
146. Verwey, E.J.W. and J.Th.G. Overbeek, 1948, *Theory of the Stability of Lyophobic Colloids* (Elsevier, Amsterdam).
147. Derjaguin, B.V., N.V. Churaev and V.M. Miller, 1987, *Surface Forces* (Consultants Bureau, New York).
148. Cevc, G. and D. Marsh, 1987, *Phospholipid Bilayers* (Wiley-Interscience, New York).
149. Israelachvili, J.N., 1984, *Intermolecular Forces* (Academic Press, New York).
150. Carnie, S.L. and G.M. Torrie, 1984, *Adv. Chem. Phys.* **56**, 141.
151. Langner, M., D. Cafiso, S. Marcelja and S.G.L. McLaughlin, 1990, *Biophys. J.* **57**, 335.
152. McLaughlin, S.G.L., 1989, *Annu. Rev. Biophys. Biophys. Chem.* **18**, 113.
153. Mahanty, J. and B.W. Ninham, 1976, in: *Dispersion Forces* (Academic Press, London).
154. Kjellander, R. and S. Marcelja, 1988, *J. Physique* **49**, 1009.
155. Kjellander, R., T. Akesson, B. Jonsson and S. Marcelja, 1992, *J. Chem. Phys.* **97**, 1424.
156. Podgornik, R., 1989, *J. Chem. Phys.* **91**, 5840.
157. Attard, P., R. Kjellander, D.J. Mitchell and B. Jonsson, 1988, *J. Chem. Phys.* **89**, 1664.
158. Attard, P., D.J. Mitchell and B.W. Ninham, 1988, *Biophys. J.* **53**, 457.
159. Kjellander, R. and S. Marcelja, 1986, *Chem. Phys. Lett.* **127**, 402.
160. Parsegian, V.A., 1975, in: *Physical Chemistry: Enriching Topics from Colloid and Interface Science*, eds H. van Olphen and K.J. Mysels (Theorex, LaJolla).
161. Leikin, S., V.A. Parsegian, D.C. Ran and R.P. Rand, 1993, *Annu. Rev. Phys. Chem.* **44**, 369.
162. Guldbbrand L., B. Jonsson and H. Wennerström, 1982, *J. Colloid Interface Sci.* **89**, 532.
163. Goldstein, R.E. and S. Leibler, 1989, *Phys. Rev. A* **40**, 1025.
164. Leikin, S. and A.A. Kornyshev, 1991, *Phys. Rev. A* **44**, 1156.
165. Cevc, G., 1989, *J. Physique* **50**, 1117.
166. Torbet, J. and M.H.F. Wilkins, 1976, *J. Theoret. Biol.* **62**, 447.
167. Radmacher, M., R.M. Zimmerman and H.E. Gaub, 1992, in: *The Structure and Conformation of Amphiphilic Membranes*, eds R. Lipowsky, D. Richter and K. Kremer (Springer, Berlin).
168. Evans, E.A. and W. Rawicz, 1990, *Phys. Rev. Lett.* **64**, 2094.
169. Tsao, Y.-H., D.F. Evans and H. Wennerström, 1993, *Science* **262**, 547.
170. Leikin, S. and V.A. Parsegian, 1994, *Proteins: Structure, Functions and Genetics* **19**, 73.

Tension-Induced Mutual Adhesion and a Conjectured Superstructure of Lipid Membranes

W. HELFRICH

*Fachbereich Physik, Freie Universität Berlin,
Arnimallee 14, 14195 Berlin, Germany*

Contents

1. Introduction	693
2. Mutual adhesion of lipid membranes induced by lateral tension: experiments	695
3. Tentative theory of induced adhesion	705
4. The contradictions of induced adhesion	709
5. Other indications of lipid membrane complexity and superstructure	713
6. Conclusion	717
Acknowledgements	718
References	718

1. Introduction

Parallel fluid membranes in water repel or attract each other and the dependence of the forces on spacing can result in an equilibrium state of mutual adhesion. Attraction and adhesion are either spontaneous or induced by lateral tension. In induced adhesion, the tension acts by suppressing out-of-plane fluctuations, thus enabling Van der Waals attraction to prevail over repulsion by fluctuations and other repulsive interactions.

It is not clear whether the most common electrically neutral lipid membranes such as the bilayers of phosphatidylcholine (PC), phosphatidylethanolamine (PE) and digalactosylacylglycerol (DGDG) display spontaneous mutual adhesion. Some researchers inferred this from finding by X-ray diffraction a stationary maximum period of multilayer systems in excess water [1]. Studying giant vesicles, E. Evans and coworkers measured the mutual adhesion energies of PC, PE and DGDG membranes to be $(0.01 - 0.015) \text{ mJ/m}^2$, $(0.12 - 0.15) \text{ mJ/m}^2$ and 0.22 mJ/m^2 , respectively [2, 3]. Our own experiments on lipid/water systems did not yield any evidence for mutual spontaneous adhesion of PC and PE bilayers. There appears to be a conflict between our results and those of Evans which needs to be resolved. It may be related to the fact that we did not mechanically disturb the membranes but only watched them under the microscope, while in Evans' studies giant vesicles were manipulated with micropipettes. However, we and Evans and many others utilized the spontaneous swelling of these lipids in water to obtain single membranes and vesicles.

A large amount of theoretical work has been devoted in recent years to the 'unbinding transition' of fluid membranes, i.e. the transition from mutual spontaneous adhesion to the unbound state, as some parameter is varied. These studies started with the renormalization group treatment by Lipowsky and Leibler [4] and were continued mostly by Lipowsky and his group [5], with a few contributions from others [6–9]. Lateral tension, which by definition is not required for spontaneous adhesion, was taken to be zero in these calculations. The renormalization group flow equations of fluid membranes with a bending stiffness in three dimensions are identical to those of stretched polymers in two dimensions [10]. Although the identity holds only to a first approximation [6, 8], it is often invoked since the polymer problem can be expressed exactly by a Schrödinger-type equation, thus allowing analytical solutions. Numerical studies and other theoretical methods all showed the equilibrium mean spacing $\langle z \rangle_{\text{eq}}$ of parallel undulating membranes to obey

$$\langle z \rangle_{\text{eq}} \sim (A_c - A)^{-\psi} \quad (1)$$

as the control parameter A approaches from below its critical value A_c where the membranes cease to adhere. The control parameter may be the strength of an attractive interaction potential ($A < 0$) or temperature ($A > 0$). The critical exponent

of unbinding is generally predicted to be $\psi = 1$ for a pair of adhering membranes. Recent numerical results suggest $\psi < 1$ for three and more equal membranes in mutual spontaneous adhesion [11], which is contested on analytical grounds in the case of stretched polymers [9].

On the experimental side, there is to date only one known example of an unbinding transition [12]. DGDG in 100 mM NaCl solution was found to swell indefinitely at elevated temperatures. Adjacent membranes went into spontaneous adhesion when subsequently the temperature was lowered. The reversible transition appeared to be continuous, but it was not possible to check the scaling law (1). The transition temperature varied wildly among seemingly equal samples and decreased slowly in the course of days. Spontaneous adhesion was never seen when no salt was present.

Adhesion induced by lateral tension occurs with PC, PE and DGDG bilayers [13–17]. Its accidental occurrence in highly swollen lipid samples is a rare phenomenon which we overlooked for years. Induced adhesion, unlike spontaneous adhesion, is characterized by contact angles of the adhering single membrane that are practically independent of lateral tension. In general, the tensions are below 10^{-3} mN/m so that they can be read from the contact rounding, i.e. a rounding of the membrane next to the area of adhesive contact. Contact angles are always less than 90° , as is necessary since the component of the tension parallel to the contact area has to be positive in the case of induced adhesion.

The experiments with DGDG in salt solution, showing both kinds of adhesion, confirmed that we had seen induced adhesion with PE and PC. Moreover, induced adhesion could be brought about willfully by two reversible procedures which were investigated with egg yolk PC (EYPC). One of them is osmotically controlled, the tension being generated by osmotic inflation of vesicles [14, 15]. The other is temperature controlled and operates in multilayer systems, the lateral tension resulting from membrane area contraction due to cooling. In both cases there was little or no dependence on salt concentration or initial temperature, which is direct evidence against spontaneous adhesion.

The theoretical treatment of mutual adhesion induced by lateral tension is difficult because of the simultaneous action of bending rigidity and lateral tension. We have tried to explain the experimental data in terms of undulatory repulsion, partially suppressed by tension, and attraction through a $1/z^2$ Van der Waals potential [14–16]. This approach leads to the scaling laws

$$\langle z \rangle_{\text{eq}}^2 \sim 1/\sigma \quad (2)$$

and

$$g_{\text{ad}} \sim \sigma, \quad (3)$$

where σ is the lateral tension and g_{ad} the adhesion energy between membranes per unit area of adhesive contact. A derivation of the same scaling laws, but for a different regime near the critical point of unbinding where the spacings are large, has been given by Lipowsky and Seifert [18]. Both (2) and (3) agree with the experimental

data, a coincidence regarded at first [14] as proof that the membranes are driven apart by the usual thermal undulations. However, a comparison of the values of the adhesion energy obtained from two different formulas, the Young equation and another energy balance, revealed discrepancies of two orders of magnitude. They forced us to postulate that at very low tensions (ca. 10^{-5} mN/m) the membranes store several times the excess area that is expected to reside in the undulations. This anomalous membrane roughness, in turn, requires for its support a membrane superstructure. In the meantime we have searched with more direct experimental methods for both superstructure and roughness.

The following is a review of our experiments on induced adhesion and their theoretical interpretation. There seems to be no similar work by other authors in the literature. At the end of the article we will compile additional evidence, direct or circumstantial, for a superstructure, an anomalous roughness or, generally, anomalous behavior of the lipid membranes investigated.

2. Mutual adhesion of lipid membranes induced by lateral tension: experiments

Accidental and osmotically controlled induced adhesion were studied in very dilute samples containing less than 1 wt% of lipid. To prepare a sample cell some μg of the material were put on an object slide and covered in general with twice distilled water. The samples had an area of a few cm^2 and a thickness of $100\ \mu\text{m}$ to $2\ \text{mm}$, depending on the experiment. After mounting the cover slip the cell was sealed with a glue or silicone grease to prevent evaporation. Giant vesicles and other extended membranes developed within hours or days. Their contours were studied by means of phase contrast light microscopy.

We first reported on accidental induced adhesion of EYPC bilayers at a meeting in Italy in 1982 [13]. The phenomenon was demonstrated by a picture of a fluctuating tubular vesicle adhering to a tight convex membrane. We inferred from it that stretching one of two membranes may be enough to induce adhesion between them. In this singular case of a free vesicle sticking to a stretched membrane, adhesion may have been promoted by the tubular geometry which restricts membrane undulations [19]. The lateral tension of the fluctuating membrane was estimated from contact rounding by use of the relationship

$$\xi_d^2 = \frac{\kappa}{\sigma} \quad (4)$$

which gives the deflection (or rounding) length ξ_d as a function of bending rigidity κ and lateral tension σ . Employing $\kappa = 2 \times 10^{-19}$ J, we computed $\sigma = 10^{-4}$ mN/m. A Young equation,

$$g_{ad} = (1 - \cos \psi)\sigma, \quad (5)$$

was used to obtain the adhesion energy g_{ad} per unit area from the contact angle ψ and the lateral tension of the fluctuating membrane.

Next, we tried to bring about induced adhesion by osmotic inflation of EYPC vesicles. For this purpose we exchanged the external aqueous medium to decrease the molarity of the NaCl or glucose solution (which at the beginning of the experiment was the same inside and outside the vesicles). Since the exchange swept away free vesicles, only those could be studied that were attached to the glass for unrecognizable reasons. Lowering the concentration by somewhere between 0.2 and 20% (larger changes led to membrane rupture), we were able to achieve induced adhesion between spherical vesicles. The areas of membrane adhesion originated from initial points of contact. An example is shown in fig. 1. Adhesion could sometimes be turned on and off several times by alternating the molarities. Also, it tended to disappear spontaneously within minutes or hours, but could be brought back by further reducing the molarity. The maximum contact angle of symmetric pair adhesion (see below) was 45° . Despite great efforts, no other information could be extracted from these poorly reproducible experiments. Failing to publish the results in *Nature*, we finally presented fig. 1 at a conference in the USA in 1985 and had it published in the proceedings [14].

We then engaged in an extensive study of accidental induced adhesion in very dilute PC samples, using mostly EYPC which was purchased from various sources. A comprehensive description of this work, including osmotically controlled adhesion, has been given in a journal article [15]. Examples of accidental induced adhesion are shown in figs 2–4. The most remarkable property of induced adhesion is the constancy of the contact angles. It could be verified over two orders of magnitude of the lateral tension for symmetric pair adhesion, i.e. two bilayers of equal ψ and σ forming a plane area of adhesive contact. The data are collected in fig. 5 where the adhesion energy is plotted versus the lateral tension. The latter was obtained from eq. (4) by inserting the rounding length and $\kappa = 2 \times 10^{-19}$ J. For the details of finding ξ_d we refer to the original paper. The adhesion energy was computed from the tension by use of the Young equation for symmetric pair adhesion

$$g_{ad} = 2(1 - \cos \psi)\sigma \quad (6)$$

which differs from (5) by the factor 2. Apart from some scatter, the points very nearly follow a slope of unity in the doubly logarithmic plot. This slope reflects the constancy of the contact angle which on average was 40° (ψ never exceeded 45° and rarely was below 30°). A constant angle ψ in (6) entails the scaling law (3).

Besides symmetric pair adhesion we concentrated on the adhesion of a single membrane to a bundle of n other membranes in the limit of large n . The contact angle of the single membrane increases with n to reach its maximum of 70° practically at $n = 6$, while the contact angle of the bundle goes to zero at the same time. Evidently, for $n \geq 6$, the system is like a single membrane adhering to a rigid wall so that the relevant Young equation is (5) instead of (6).

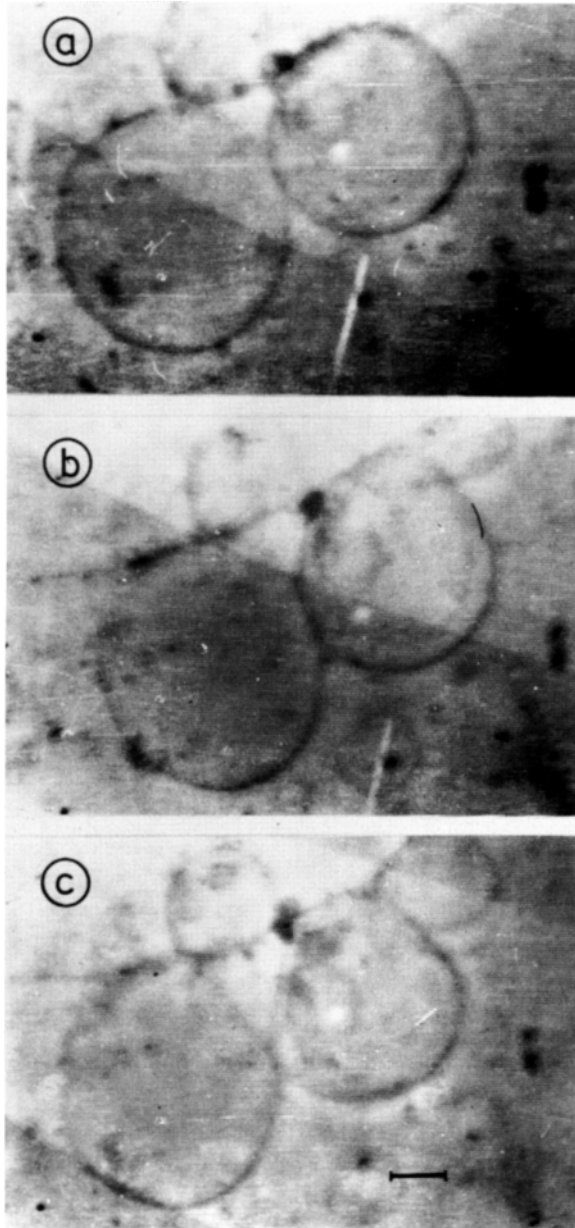


Fig. 1. Osmotically controlled induced adhesion of EYPC vesicles attached to glass slide. The same vesicles (a) in 156 mOsm NaCl solution prior to osmotic inflation, (b) in 131 mOsm after first inflation, and (c) in 131 mOsm after third inflation and spontaneous ceasing of adhesion. (Before the last picture, adhesion was turned on and off 3 and 2 times, respectively, by alternating between 156 and 131 mOsm.) The bar represents 10 μm .

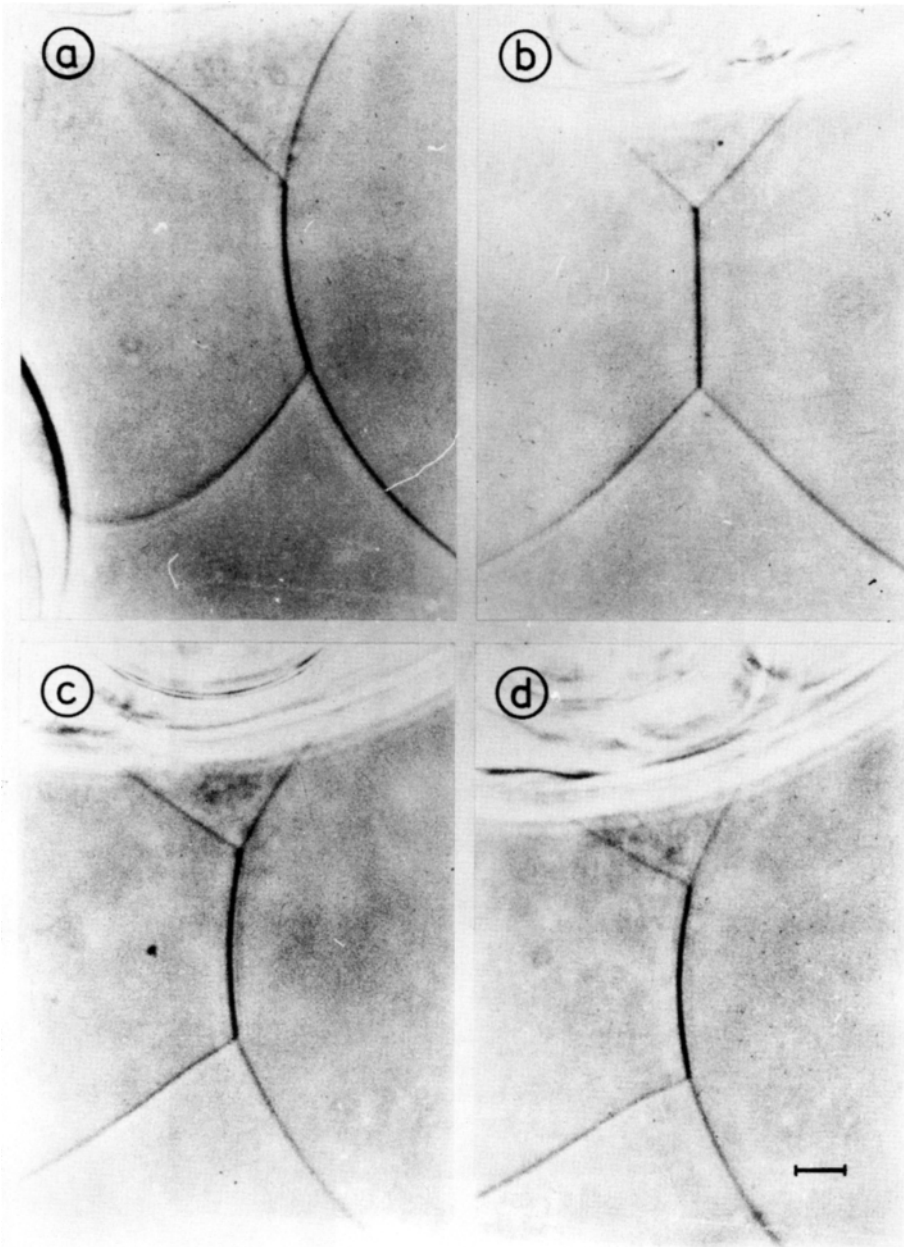


Fig. 2. Accidental induced adhesion of dimyristoyl phosphatidylcholin (DMPC) membranes. Evolution with time of an adhesive contact of two membranes. The left membrane displays contact rounding in (a), (c) and (d). Symmetric adhesion without visible contact rounding is seen in (b). The bar represents 10 μm .

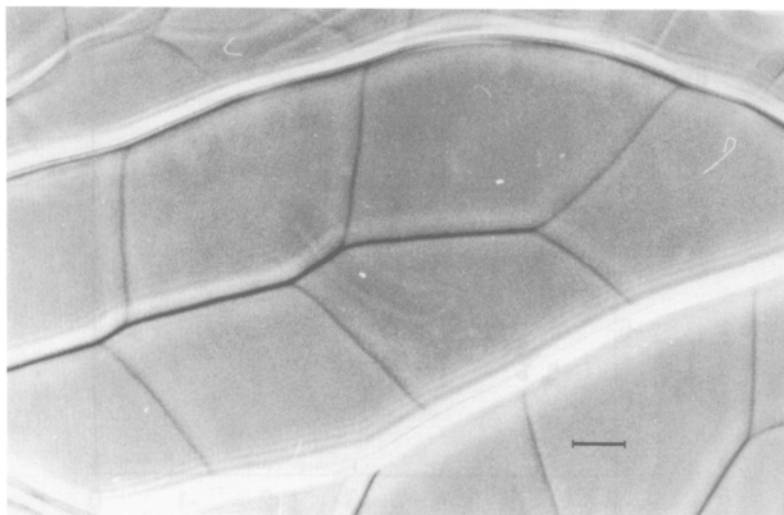


Fig. 3. A 'branched' structure of EYPC membranes displaying induced adhesion. There is symmetric pair adhesion and the adhesion of single membranes to bundles. Contact roundings are well visible. The bar represents 10 μm .

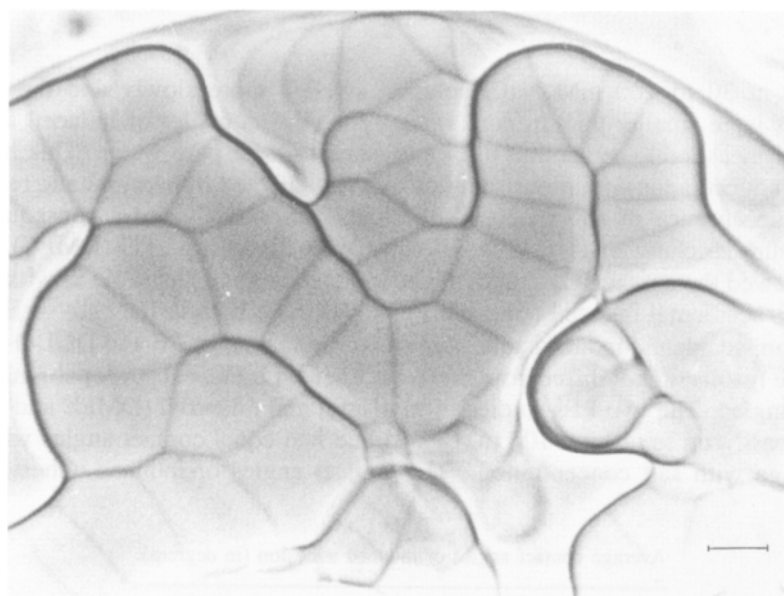


Fig. 4. Induced adhesion of dimyristoyl phosphatidylethanolamine (DMPE) membranes. One sees the same phenomena as in fig. 3. Some of the contact angles are on the low side for PE. The bar represents 10 μm .

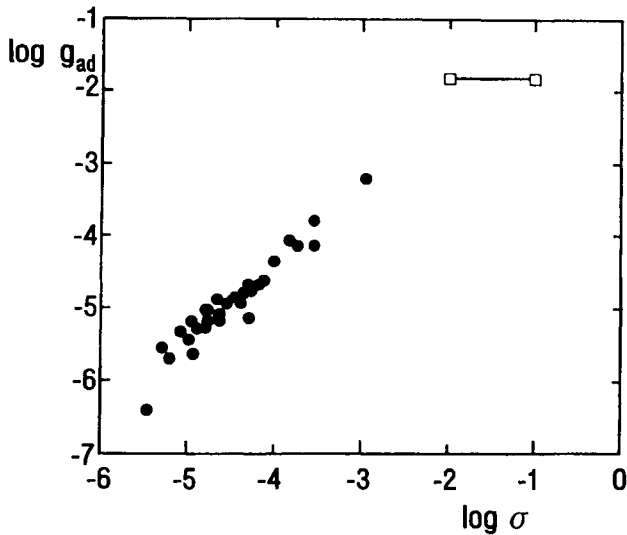


Fig. 5. Adhesion energy g_{ad} of symmetric pair adhesion induced by lateral tension plotted vs. lateral tension σ . The units are mJ/m^2 and mN/m , respectively. The point at $\sigma = 10^{-3}$ mN/m represents DMPC, all others EYPC. See text for explanations. The open boxes indicate the results of Evans and Metcalfe for EYPC which were measured with the tension of the more flaccid membrane being between 10^{-2} and 10^{-1} mN/m .

EYPC in 30 to 100 mM NaCl solution swelled more slowly and the swollen structures were smaller than in pure water. The contact angles of induced adhesion were still measurable and found to be the same as with pure water. This indicates that the induced adhesion in our samples was not affected by electrostatic repulsion, so that the absence of spontaneous adhesion is most likely not a consequence of electric surface charges. A few experiments with dimyristoyl PC (DMPC) in pure water showed the contact angle of symmetric adhesion to be the same as with EYPC. However, accidental induced adhesion was much rarer than in the case of EYPC.

Later on, accidental induced adhesion was investigated for PE and DGDG bilayers [17]. The results do not differ from those obtained with PC, except for slightly larger contact angles. The two PEs studied, dimyristoyl and dilauroyl (DMPE and DLPE), swelled easily up to at least 100 mM NaCl and had equal contact angles which did not change with salt concentration. The contact angles of induced adhesion were

Table 1
Average contact angles of induced adhesion (in degrees).

	PC	PE	DGDG
symmetric pair	40	45	55
single membrane to stack	70	80	85

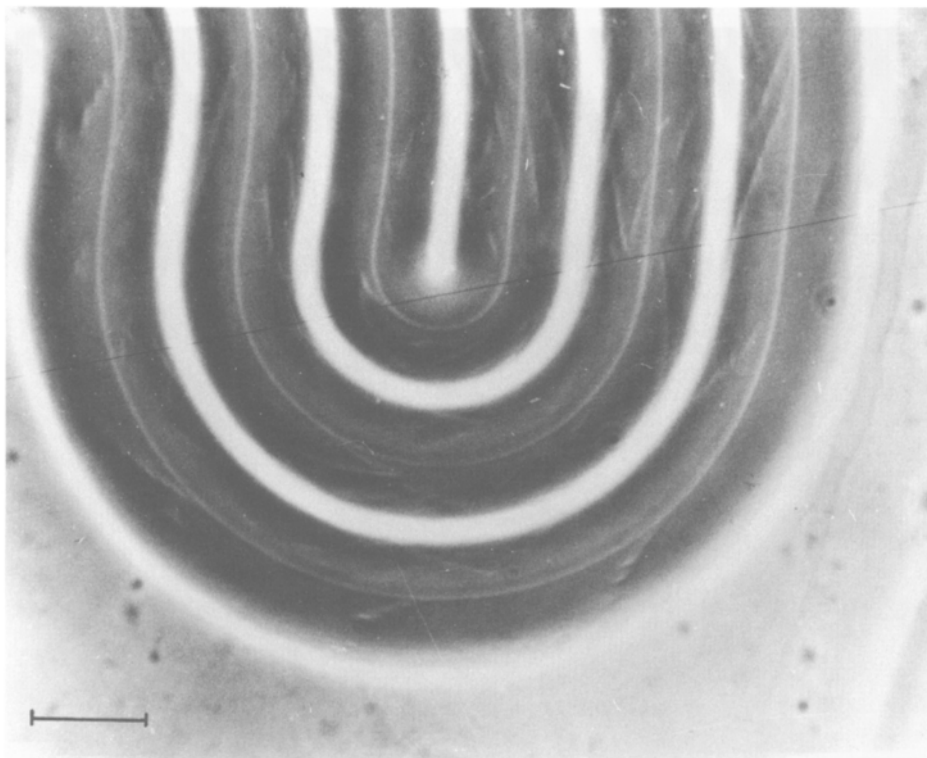


Fig. 6. Induced adhesion brought about by cooling. The picture shows EYPC myelin cylinders in a sample being cooled after swelling at 55 °C. The three curved cylinders span the 20 μm thick sample cell; the white center lines are their water cores. Actually, one sees three sections of the same folded cylinder which is attached to a planar multilayer system. The PC density in the planar system is ca. 45 vol.%. The bar represents 20 μm . The instantaneous temperature is 51°C. Note the oblique white lines, the first sign of induced adhesion.

registered for both symmetric pair adhesion and adhesion of a single membrane to a stack of adhering membranes. The average contact angles of PC, PE and DGDG bilayers are compiled in table 1.

In all the studies of accidental induced adhesion we changed between at least two different glues or a glue and a silicon grease without noticing an effect on the contact angles.

Induced adhesion of EYPC bilayers may have been seen also by Israelachvili, Zasadzinski and coworkers [20]. They studied small vesicles of diameters near 100 nm, osmotically inflated or not, in freeze fracture electron microscopy and found adhesive contacts between them. The contact angles of symmetric pair adhesion were similar to those of our experiments. The results were explained in terms of an attractive hydrophobic interaction between stretched membranes which is proportional to lateral

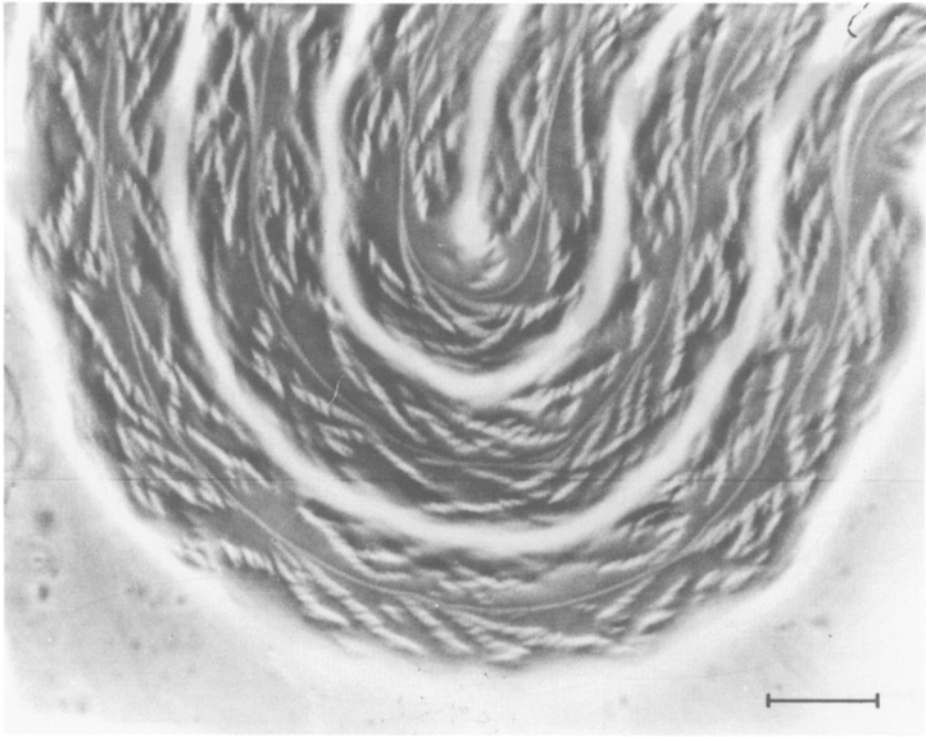


Fig. 7. Same as in fig. 6, but the instantaneous temperature is 45 °C. Note the compartments (white) separated by membrane bundles (dark).

tension [21]. The proportionality agrees with (3), but the interaction is 'direct', i.e. relating to flat membranes without any undulations. Ignoring undulations and other roughness seems dangerous as it would imply a collapse of unstressed membranes into a bound state of (slightly) increased membrane area.

In addition to the osmotic inflation of vesicles there is another kind of controlled induced adhesion which was observed in swollen multilayer systems. It is brought about by cooling and was studied only with EYPC in pure water [16]. To achieve fairly uniform alignment of the membranes parallel to the glass, the samples were prepared by squeezing the slightly hydrated lipid between the slides to a thickness of about 20 μm . The remaining 90% of the cell volume were filled with twice distilled water. Mechanical sealing obviated the use of a glue. The local lipid density and thus the mean membrane spacing could be monitored during the swelling process by measuring the intensity of EYPC fluorescence.

The adhesion caused by cooling has been described in the second of a series of light-microscopic studies of swollen EYPC multilayer systems. The first deals with the swelling process and, in particular, with the generation of myelin cylinders

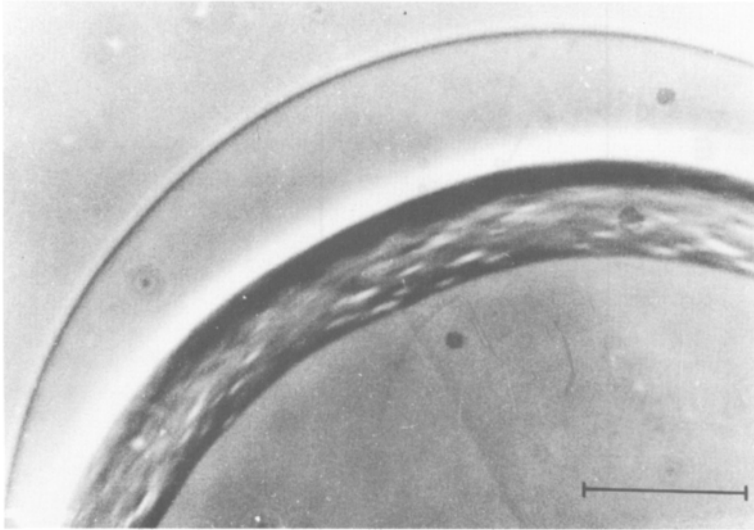


Fig. 8. Induced adhesion brought about by cooling. The picture shows the semicylindrical border of an EYPC planar multilayer system. There is a stray membrane on the side of free water. The 18 μm thick sample is being cooled after swelling at 65°C. The PC density in the planar system is ca. 40 vol.%. The instantaneous temperature is ca. 55°C. Note the white islands in the border, the first sign of induced adhesion.

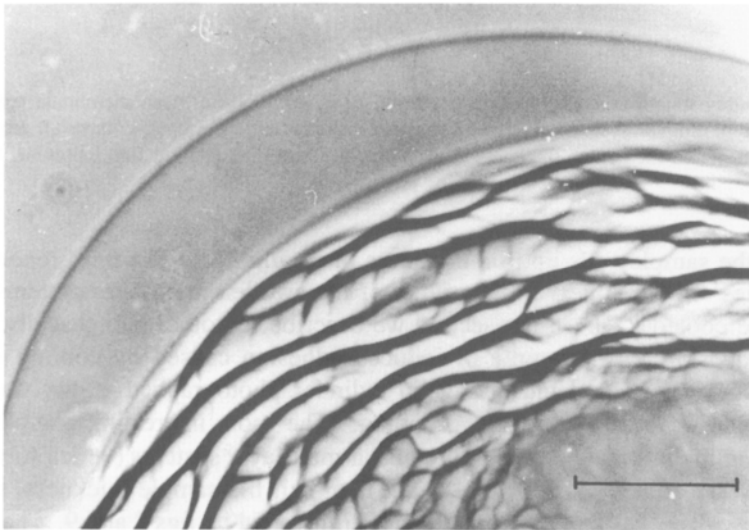


Fig. 9. Same as in fig. 8, but the instantaneous temperature is 25°C. Note the increased width of the border and the numerous branchings. Some of the thinnest dark lines are single membranes.

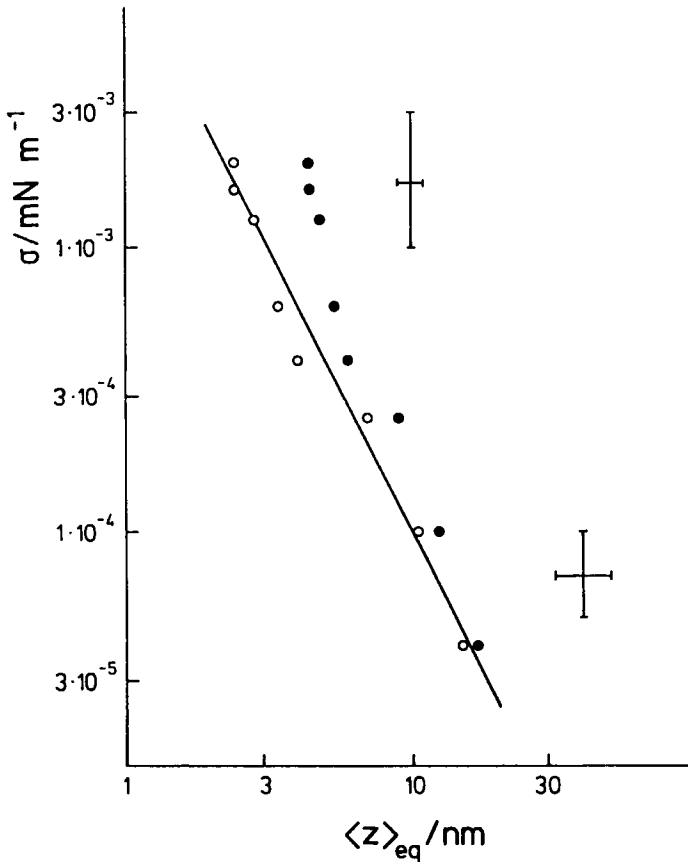


Fig. 10. Doubly logarithmic plot of lateral tension σ vs. equilibrium mean membrane spacing $\langle z \rangle_{eq}$ in the planar multilayer system. The solid dots are the raw data, the open dots result from an arbitrary increase of the membrane thickness from 3.8 to 5.8 nm. The straight line represents the scaling law (2).

spanning the sample cells up to a thickness of $40 \mu\text{m}$ [22]. The third reports on the 'dark bodies' which appear in about half of the swollen multilayer systems as soon as they are cooled [23]. In the second we describe the other half that display only induced adhesion. An example of induced adhesion caused by cooling is shown in figs 6 and 7 which depict a myelin cylinder photographed at two subsequent moments as the temperature was dropping. The most interesting sample regions were the semicylindrical borders of the planar multilayer systems (which form myelin cylinders when folded). They were wider than half the sample thickness, the width increasing with decreasing temperature, as is illustrated by figs 8 and 9. The widened semicylinders permitted us to discern single membranes, read their contact angles and rounding lengths, and measure the thickness of stacks, i.e. thick bundles of many

mutually adhering membranes. The average contact angle of a single membrane adhering to a stack was found to be 70° , thus equaling the contact angle of accidental adhesion to a bundle of six or more membranes. Temperature controlled induced adhesion is reversible, leaving no visible traces when the temperature differences are small enough.

The lateral tension inducing adhesion in swollen multilayer systems results from the membrane area contraction which accompanies cooling. Decreasing the temperature by a few K was usually sufficient to produce first signs of adhesion in the semicylindrical border. Even when several times larger, the decreases did not result in tensions strong enough to induce adhesion in the planar regions of the multilayer system. This can be explained by a complicated theoretical model predicting the tension to be self-limiting [16]. An important parameter of the model is the thermal area expansivity of the bilayer which was measured by Evans to be $2.4 \times 10^{-3} \text{ K}^{-1}$ for EYPC [24]. In its asymptotic limit the tension is just strong enough to neutralize membrane interaction in the planar multilayer system, thus facilitating the necessary restructuring. A check of the model consists in adding up the widths of the separate stacks in the semicylindrical border. When this could be done the total width equaled half the sample thickness, in agreement with the model. Identifying $\langle z \rangle_{\text{eq}}$ with the mean membrane spacing in the planar multilayer system and estimating σ from the contact rounding, we were able to obtain the lateral tension as a function of the equilibrium spacing produced by it.

Data obtained from different samples are collected in fig. 10. The tensions were calculated from (4), this time with $\kappa = 1 \times 10^{-19} \text{ J}$. The scaling law (2) was reproduced when an impenetrable layer of 2 nm was added to the assumed membrane thickness of 3.6 nm, which is a primitive way of dealing with hydration forces (see below). Although the proof of the scaling law may be doubted because of the large experimental errors, the orders of magnitude, $\langle z_{\text{eq}} \rangle = 10 \text{ nm}$ at $\sigma = 10^{-4} \text{ mN/m}$, seem reliable, apart from the uncertainty of κ that is reflected in an equal uncertainty of σ .

3. Tentative theory of induced adhesion

There is little theoretical work on adhesion induced by lateral tension. In all of it, standard thermal undulations are the only membrane roughness taken into account. We tried to explain induced adhesion in terms of the interplay of Van der Waals attraction and undulatory repulsion. The Van der Waals interaction energy per unit area between two flat membranes in the half-space approximation is

$$g_{\text{vdw}} = - \frac{H}{12\pi z^2} \quad (7)$$

where H is the Hamaker constant. This approximation is thought to be good up to rather large spacings, the true value falling below 50% of (7) only at $z \approx 20 \text{ nm}$ [25]. The wide range of applicability of (7), due to the enormous difference in dielectric constant between water and hydrocarbon, presupposes an unscreened zero frequency

contribution. The finite membrane thickness makes Van der Waals attraction drop with $1/z^4$ at larger spacings. Repulsive short-range forces, called hydration forces, dominate at spacings below ca. 3 nm [26]. The undulations produce a repulsive interaction which was calculated by various methods for multilayer systems in the ideal case of purely steric interaction. In the earliest calculation, which integrates over fluctuation modes and uses a self-consistency relation, the energy of undulatory interaction per unit area was found to be

$$g_{\text{und}} = \frac{3\pi^2}{128} \frac{(kT)^2}{\kappa \langle z \rangle^2}, \quad (8)$$

$\langle z \rangle$ being the mean spacing imposed by an external constraint [27]. The formula, in particular the numerical factor, was experimentally confirmed within 20% for very flexible nonlipid bilayers [28, 29]. However, the theoretical strength of undulatory interaction came out smaller in other treatments [30]. It is about 2/3 as large if a sum over the membranes is taken instead of an integral in z direction [31] and about 1/2 as large as (8) in Monte Carlo simulation [32] and renormalization group calculations [33]. Note that both interaction energies, (7) and (8), vary as the inverse square of spacing, z being fixed in one case and averaged in the other.

A formula like (8), but with a poor numerical factor, can be obtained from an ‘independent membrane piece’ approximation [13, 16]. For simplicity, one considers here a single membrane between parallel rigid walls of distance $2d$. The idea of the approximation is to cut the membrane into equal pieces, e.g., squares, so that the thermal undulations of each piece fill a certain fraction of the interval between the walls. Assuming the pieces to act as the particles of a one-dimensional ideal gas, one arrives at the pressure exerted on the wall by the undulating membrane.

It is an advantage of the independent membrane piece approximation that lateral tension can be taken into account in calculating the mean square fluctuation amplitude $\langle u^2 \rangle$ of the quadratic piece [13, 16]. Assuming a square of area S with periodic boundary conditions, one has for a single undulation mode of wave vector \vec{q} the mean square amplitude

$$\langle |u_{\vec{q}}|^2 \rangle = \frac{kT}{(\sigma q^2 + \kappa q^4)S}. \quad (9)$$

Integration over the \vec{q} plane leads to

$$\langle u^2 \rangle = \frac{kT}{4\pi\sigma} \ln \left(1 + \frac{\sigma}{\kappa q_{\text{min}}^2} \right) \quad (10)$$

where the lower wave vector cutoff is, to a good approximation, given by

$$q_{\text{min}}^2 = \frac{\pi^2}{S}, \quad (11)$$

and the upper wave vector cutoff need in general not be considered. Taking the limit of (10) for $\sigma \rightarrow 0$ gives the correct result for $\sigma = 0$. The area S as a function of σ may be obtained by assuming

$$\langle u^2 \rangle = \frac{d^2}{6}, \quad (12)$$

where $d^2/6$ is the geometric mean of the mean square fluctuation amplitudes of a simple sine wave ($\sin qx$) and a product wave ($\sin qx \sin qy$), both restricted to the interval $2d$ [13–15]. Eliminating $\langle u^2 \rangle$ between (10) and (12), one finds

$$S(\sigma) = \frac{\pi^2 \kappa}{\sigma} \left[\exp \left(\frac{2\pi\sigma d^2}{3kT} \right) - 1 \right] \quad (13)$$

which has to be inserted in

$$P_{\text{und}} = \frac{kT}{S(\sigma)2d} \quad (14)$$

to obtain the undulation pressure P_{und} on the walls. The effect of σ on S and, thus, P_{und} becomes significant when the exponent in (13) approaches unity. In the limit $\sigma \rightarrow 0$ a first order expansion of the exponential function leads to $S(0) \sim \langle z \rangle^2$ as expected. The ratio $S(0)/S(\sigma)$ may be regarded as the reduction factor of the undulation pressure in the presence of tension.

Since we are interested in a multilayer system rather than a membrane between rigid walls we apply this reduction factor to the undulation pressure derived from (8), writing

$$P_{\text{und}}(\sigma) = - \frac{\partial g_{\text{und}}}{\partial \langle z \rangle} \frac{S(0)}{S(\sigma)}. \quad (15)$$

Let us now superimpose P_{und} and the Van der Waals pressure P_{vdw} derived from (6),

$$P_{\text{vdw}} = - \frac{\partial g_{\text{vdw}}}{\partial z} = - \frac{H}{6\pi z^3} \quad (16)$$

and calculate the equilibrium spacing $\langle z \rangle_{\text{eq}}$ from

$$P_{\text{vdw}} + P_{\text{und}} = 0. \quad (17)$$

If one puts $z = \langle z \rangle_{\text{eq}}$, the result is

$$\frac{S(\sigma)}{S(0)} = \frac{9\pi^3(kT)^2}{32H\kappa}. \quad (18)$$

Replacing d by $\langle z \rangle_{\text{eq}}$ and expanding the exponential up to second order, one obtains from (13)

$$\frac{S(0)}{S(\sigma)} = 1 - \frac{\pi\sigma}{3kT} \langle z \rangle_{\text{eq}}^2 \quad (19)$$

to first order in $\sigma \langle z \rangle^2$. Combination of the last two equations results in

$$\langle z \rangle_{\text{eq}}^2 = \frac{H_c - H}{H} \frac{3kT}{\pi\sigma} \quad (20)$$

if use is made of the ‘critical’ Hamaker constant $H_c = (9\pi^3/32)(kT)^2/\kappa$ for which (17) holds with $\sigma = 0$. The ensuing scaling law

$$\langle z \rangle_{\text{eq}}^2 \sim 1/\sigma \quad (21)$$

is not only a consequence of the expansion but follows generally from $S(0)/S(\sigma)$ as given by (13). It also seems to follow from Sornette’s renormalization group treatment of undulatory membrane repulsion in the presence of lateral tension [34]. Insertion of (21) into the half-space potential (7) results in the scaling law relating adhesion energy to lateral tension,

$$g_{\text{ad}} \sim \sigma. \quad (22)$$

We refrain from writing down an explicit formula for g_{ad} . Any differences between pairs, bundles and multilayer systems of membranes should not affect the scaling laws. Note that (21) and (22) are identical to (2) and (3), respectively.

A completely independent argument confirms the scaling laws (21) and (22) [15]. It is based on the observation that the undulations of a single membrane bound by an attractive $1/z^2$ potential are characterized by two lengths. These are the deflection length defined by (1) and the lateral correlation length ξ which apart from a numerical factor near unity satisfies

$$\xi^2 = \frac{\kappa}{kT} \langle z \rangle_{\text{eq}}^2. \quad (23)$$

The ratio of the two lengths should depend only on the ratio H/H_c , so that

$$\xi^2/\xi_d^2 = \frac{\sigma}{kT} \langle z \rangle_{\text{eq}}^2 = f(H/H_c), \quad (24)$$

which immediately entails (21) and (22). A detailed way of proving the two identities of (24) is to consider a deformed membrane pieces, multiply their lengths either including or excluding z by the same factor, and require the energies of bending, pulling in area, and of the Van der Waals interaction (7) to be invariant. Note that the bending rigidity enters neither the exponent in (13) nor the length ratio in (24).

The confirmation of the scaling laws (21) and (22) by the direct argument of the last paragraph is welcome since the superposition of potential and undulatory energies is not necessarily correct, neither quantitatively nor qualitatively [4]. In the explicit equations, however, the errors of the numerical factors and the critical Hamaker constant are probably large. Uncertainties concerning the validity of the bare scaling laws arise from the use of the half-space law (7) which is only an approximation of the real Van der Waals interaction.

It has been shown above that the experimental data about induced adhesion agree very well with the scaling law (21) or (2) and are compatible with the scaling law (22) or (3). The twofold conformity seems to prove that induced adhesion can be fully understood in terms of standard thermal undulations besides Van der Waals attraction. However, this early conclusion [14] had to be dropped later on in view of conflicting numbers obtained from two different formulas for the adhesion energy [15]. Also, the measured equilibrium spacings seem too small, at the estimated tensions, to be compatible with undulation theory [16]. These discrepancies are to be examined next.

4. The contradictions of induced adhesion

In discussing the contradictory formulas for the adhesion energy we at first assume, as is common in the theory of elasticity, that the changes in membrane area can be neglected in calculating elastic energy densities. To this approximation, the adhesion energy per unit area of a single membrane adhering to a stack of membranes satisfies the energy balance

$$g_{ad} = g_f - g_b \quad (25)$$

besides the Young equation (5). Here g_f and g_b are the energies of the free and bound states, respectively, per unit area of membrane. For symmetric pair adhesion, the right sides of (5) and (25) have to be multiplied by 2 and g_{ad} and g_b may change somewhat (which we do not express by different symbols). With induced adhesion all three energy densities depend on lateral tension. If one wants to be precise, one has to distinguish between the tensions σ_b and σ of the membrane where it is bound and free, respectively. They are related by

$$\sigma_b = \sigma \cos \psi. \quad (26)$$

We do not make here this distinction, using σ indiscriminately.

The part of g_f that is due to the suppression of undulations by tension can be calculated from the relative contraction of base area, $\Delta A/A_0 < 0$, due to the undulations [13]. Here and in the following, A_0 is the real membrane area in the absence of lateral tension, while ΔA is the difference between the projected area A and A_0 . Considering a square piece of membrane, we have for a single mode the relative change

$$\left(\frac{\Delta A}{A_0} \right)_{\vec{q}} = -\frac{1}{2} q^2 \langle |u_{\vec{q}}|^2 \rangle. \quad (27)$$

Integration over the \vec{q} plane yields, because of (9),

$$\frac{\Delta A}{A_0} = -\frac{kT}{8\pi\kappa} \ln \frac{\pi^2/a^2 + \sigma/\kappa}{\pi^2/A_0 + \sigma/\kappa} \quad (28)$$

where the molecular length a controls the upper cutoff wave vector π/a . For a wide range of tensions, $\kappa\pi^2/A_0 < \sigma < \kappa\pi^2/a^2$, eq. (28) simplifies to

$$\frac{\Delta A}{A_0} = -\frac{kT}{8\pi\kappa} \ln \frac{\kappa\pi^2}{\sigma a^2} \quad (29)$$

which no longer depends on A_0 . Obviously, $\Delta A/A_0$ increases towards zero as the tension goes up. Stretching of undulations has to be complemented by Hookean stretching, $\Delta A/A_0 = \sigma/\lambda \geq 0$, where λ is the stretching modulus of the bilayer. Inserting both contributions into the differential energy balance

$$dg_f = \sigma \frac{d(\Delta A/A_0)}{d\sigma} d\sigma \quad (30)$$

we obtain

$$g_f = \frac{kT}{8\pi\kappa} \sigma + \frac{1}{2\lambda} \sigma^2. \quad (31)$$

The Hookean term can be neglected for the tensions of interest, $10^{-6} \text{ mN/m} < \sigma < 10^{-3} \text{ mN/m}$, as λ was measured to be about 200 mN/m for the lipid membranes of our studies [24]. (These tensions are also far below $\kappa\pi^2/a^2$, the upper limit of validity of (29).) We do not try to calculate the energy of the bound state, g_b . However, it is easy to realize that g_b must be positive because otherwise the membrane would adhere spontaneously. This and the omission of the Hookean term permit us to deduce from eq. (25) the inequality

$$g_{ad} < \frac{kT}{8\pi\kappa} \sigma. \quad (32)$$

For a numerical comparison of the two relationships for the adhesion energy, (5) and (32), we focus on EYPC bilayers. The bending rigidity of no other fluid membrane has been measured more often, by more experimental methods, and with the results varying more widely. The mean values of different studies are spread over a power of ten, namely $\kappa = (0.24 - 2.3) \times 10^{-19} \text{ J}$ [35–37] (see also below). Using these numbers and, in addition, the contact angle of the single PC membrane adhering to a bundle, $\psi = 70^\circ$, and the room temperature value $kT = 4 \times 10^{-21} \text{ J}$, we obtain from the Young equation (5)

$$g_{ad} = 0.66\sigma \quad (33)$$

and from the inequality (32)

$$g_{ad} < (0.66 - 6.6) \times 10^{-3} \sigma. \quad (34)$$

Evidently, there is a glaring discrepancy of two or three orders of magnitude between the two formulas. It is reduced only by a factor of three for symmetric adhesion with $\psi = 40^\circ$. Similar contradictions are found for PE and DGDG membranes.

The conflict is mitigated but not removed if the changes in membrane area are taken into account. With $\alpha = A/A_0$ denoting the ratio of projected area at arbitrary σ to real area at $\sigma = 0$, one easily finds the corrected Young equation

$$\alpha_b g_{ad} = (\alpha_f - \alpha_b \cos \psi) \sigma \quad (35)$$

and the corrected other energy balance

$$\alpha_b g_{ad} = (\alpha_f g_f - \alpha_b g_b) \quad (36)$$

for adhesion of the single membrane to the stack. The energies g refer to unit projected area, while their products with the respective α refer to unit real area at $\sigma = 0$. Let us rewrite (35) as

$$g_{ad} = \left(\frac{\alpha_f}{\alpha_b} - \cos \psi \right) \sigma \quad (37)$$

and keep of (36) the only inequality

$$g_{ad} < \frac{\alpha_f}{\alpha_b} g_f \quad (38)$$

where again use is made of $g_b > 0$. The last two relationships replace (5) and (32). Neglecting Hookean elasticity, i.e. taking the real area to be fixed, and using (29), one has

$$\alpha_f = \left(1 + \frac{\Delta A}{A_0} \right) = 1 - \frac{kT}{8\pi\kappa} \ln \frac{\kappa\pi^2}{\sigma a^2} < 1. \quad (39)$$

A new, improved calculation starting from the product of the correction factors for all the modes,

$$\frac{\Delta A}{A_0} = \Pi_{\vec{q}} \left[1 - \left(\frac{\Delta A}{A_0} \right)_{\vec{q}} \right], \quad (40)$$

gives

$$\alpha_f = \frac{1}{1 + \frac{kT}{8\pi\kappa} \ln \frac{\kappa\pi^2}{\sigma a^2}} \quad (41)$$

which becomes (39) again for $\alpha_f \rightarrow 1$. With $\kappa = 0.24 \times 10^{-19}$ (the lowest experimental value), $a = 1$ nm, $\sigma = 1 \times 10^{-5}$ mN/m and room temperature, we find from (41) $\alpha_f = 0.90$ which may be regarded as a lower limit to α_f for EYPC.

Finally, we write down a differential equation for the energy of undulation stretching per unit real area of free membrane which follows from (41) and replaces (30)

$$d(\alpha_f g_f) = \sigma \frac{d\alpha_f}{d\sigma} d\sigma = \frac{\frac{kT}{8\pi\kappa}}{\left(1 + \frac{kT}{8\pi\kappa} \ln \frac{\kappa\pi^2}{\sigma a^2}\right)^2} d\sigma. \quad (42)$$

From (41) and (42) one obtains the inequality

$$\alpha_f g_f < \alpha_f^2 \frac{kT}{8\pi\kappa} \sigma \quad (43)$$

and, in combination with (38),

$$g_{ad} < \frac{\alpha_f^2}{\alpha_b} \frac{kT}{8\pi\kappa} \sigma. \quad (44)$$

For a conservative comparison of (37) and (44) we assume the most favorable case, $\alpha_b = 1$, in (37) and replace α_f^2/α_b by unity in (44). Inspection for EYPC shows that this reduces the discrepancy between the Young equation and the other energy balance only marginally for the single membrane adhering to a stack of other membranes. The situation is similar for symmetric pair adhesion of EYPC membranes and for both kinds of adhesion of PE and DGDG bilayers.

In order to bridge the gap between the Young equation and the other energy balance, we postulated an anomalous roughness of the investigated lipid membranes which stores much more membrane area than do the thermal undulations. A natural way of dealing with such an extra roughness, suggested by the agreement of experimental and theoretical scaling laws, is to use the same formulas as above but adopt a hypothetical κ much smaller than the measured values. A dramatic reduction of the hypothetical bending rigidity down to about 3×10^{-21} J, for EYPC would be required to make inequality (44) compatible with (38). This would imply $\alpha_f \approx 0.4$ or, in other words, a stored area 1.5 times the base area. Less storage but an even smaller hypothetical κ may be inferred from the argument that the superstructure could have a larger cutoff length in (41) than the molecular length a . In any event, the stored area has to be several times the 10% of the base area ($\alpha_f = 0.90$) which we maximally estimated for the undulations of EYPC bilayers.

From the experiments with EYPC multilayer systems we obtained $\langle z \rangle_{eq} = 10$ nm at a tension which initially was estimated at 10^{-4} mN/m. With $\kappa = 2.4 \times 10^{-20}$ J, instead of the 1×10^{-19} J used originally, the tension decreases proportionally. Insertion of these tensions, besides $\langle z \rangle_{eq}$, into (20) leads to Hamaker constants less than 4 or 1% below its critical value. This is another result that is difficult to reconcile with undulation theory as it means that very small parameter changes would have been

sufficient to cause spontaneous adhesion which we never saw. (A further argument to this effect [6], assuming a collapse rather than a gradual decrease of the net repulsion with increasing H , is incorrect.) We may conclude from the estimate that the anomalous roughness is much more sensitive to lateral tension than would be standard undulations producing the same equilibrium mean spacing.

5. Other indications of lipid membrane complexity and superstructure

In our light microscopic studies of induced adhesion we did not see any superstructure or anomalous roughness and, for a long time, suspected none. However, there are some observations pointing to complexities of lipid membranes which are older than the contradictions of induced adhesion. The first serious indication of anomalous mechanical properties of PC membranes emerged in measurements of the bending rigidity [36]. Registering the fluctuations of the angle made by the ends of tubular PC vesicles, we noticed in addition intermittent rapid wiggle-like fluctuations of the tubes which were stronger with distearoyl PC (DSPC) than with shorter-chain saturated PC's and EYPC. The wiggles disappeared within a second and after a few seconds reappeared usually in another section of the tube; they rarely covered the whole length of it. Sometimes we also saw a knee which lasted up to 4 s and could migrate along the tube. Estimating the bending energies of wiggles and knees on the basis of the bending rigidity derived from the mean square fluctuation angle, $\kappa \approx 2 \times 10^{-19}$ J, we found these energies much too high for thermal excitation. The lower bending rigidities measured in the meantime with other methods may reduce the energies to acceptable levels, but the intermittency of the wiggles can still not be explained in terms of undulations and their relaxation.

Another strange property of EYPC bilayers is the existence of a dispersive phase [23]. It forms in the highly swollen multilayer systems displaying induced adhesion upon cooling. When these samples are annealed for several hours at less than 15 °C, the planar multilayer system breaks up into water chambers separated by one or more membranes. Subsequently raising the temperature beyond 15 °C results in the precipitation of many flakes in each chamber which display Brownian motion and rapidly fuse to form one 'dark body' per chamber. These spherelike bodies are probably made of a single multiply self-connected membrane. When the temperature is decreased below 15 °C again, the dark bodies fade and the dispersive phase is reestablished. The nature of the dispersive phase is still unknown, but its existence and its reversible transformation are evidence for an amazing complexity of EYPC membranes. A dispersion contrasts sharply with the fact that, when stressed, the EYPC membranes rupture only at tensions of (3–4) mN/m [23].

There is a third phenomenon, well-known and discovered early on by Evans [38], which possibly hints at anomalous membrane properties. Micromanipulation reveals that vesicles tend to be connected by microscopically invisible tethers. Their presence becomes apparent only when a vesicle is aspirated by the micropipette and pulled away. Tethers are thought to be thin tubes formed by the highly curved membrane. If the energy of tube formation equals the regular bending energy of a cylinder, the

tube has to be stabilized (in the absence of spontaneous curvature) by a pull of the force $2\pi\kappa/r$, r being the radius [39]. Since it is difficult to understand the origin of these forces one may wonder whether the tethers are possibly stabilized by some unknown property of the membrane. Another reason to suspect such a stabilization is the occurrence of huge batteries of tubes, at first too thin to be optically resolved, in dilute EYPC samples during the swelling process [40].

The contradictions that arose in the quantitative analysis of induced adhesion carry more weight than those precursory observations. They were obtained with the bilayers of many different lipids and they are based on experiments which are in part controllable and yield physical quantities such as contact angles, lateral tensions and mean spacings. We see no possibility of removing the conflict other than to postulate an anomalous roughness of the membranes which, in turn, has to be supported by a membrane superstructure. The most direct method to search for these two membrane features is cryo-transmission electron microscopy. Fortunately, E. Zeitler permitted us to do such studies at the Fritz-Haber-Institut. In early 1988 we obtained the first electron micrograph showing EYPC vesicles with grainy membranes. The typical 'period' of the irregular black and white pattern is about 5 nm. Encouraged by the pictures, we proposed also in 1988 a tentative model for the superstructure [41]. Its basic element is a local saddle deformation about as large as the membrane thickness of ca. 4 nm. The saddle is stabilized by higher order bending elasticity so that an energy barrier has to be overcome to create or destroy it. Each saddle in an otherwise flat membrane is surrounded by two highs and two lows which the saddles should tend to share in order to save regular bending energy. The resulting cooperativity of the saddles may be expected to give rise to membrane deformations on a scale larger than a saddle, thus creating most of the anomalous roughness. Lateral tension above a certain threshold should lead to the destruction of the superstructure, leaving a rather smooth membrane which still performs thermal undulations. When the tension is turned off, the superstructure will reappear in the course of time. In such a model, the anomalous roughness depends on the history of the membrane and is sensitive to lateral tension and, perhaps, other factors.

The first electron micrograph showing an EYPC vesicle with a grainy membrane was presented at a conference in 1989 [42]. While the vesicles displaying grainy membranes were nearly spherical, we obtained in early 1990 angular EYPC vesicles [43, 44]. Their shapes differ markedly from those seen in light microscopy despite the theoretical scale invariance of vesicle shapes. We think that the angularity is an example of the anomalous roughness for which we were looking. The lack of graininess in these membranes, and the general rarity of grainy membranes, is attributed to the leveling action of the high lateral tensions that arise during the rapid freezing of the samples. The tensions, a consequence of the large thermal expansivity of lipid membranes [24], are manifested by a number of artefacts. A comprehensive description of the results obtained so far with cryo-transmission electron microscopy has just been published [45].

Other authors made some similar observations with cryo-transmission electron microscopy. The graininess has recently been found by Lücken and Jäger in vesicular membranes of EYPC, soya PC, and DMPC, each containing some cholesterol [46].

Small (100 nm long) elongated vesicles with a sharp notch on one side, resembling hearts apart from the missing tip, have been seen in the Sackmann group in samples of pure DMPC [47], while we found an EYPC vesicle with such a shape [45]. The notches appear to be very pronounced, highly localized saddles.

In another attempt to prove the existence of an anomalous roughness in a direct manner we measured the apparent membrane area as a function of lateral tension by deforming fluctuating spherical vesicles into prolate ellipsoids with electric fields (which simultaneously lifted them from the object slide) [37]. This is a very gentle method as there is no lower limit to the lateral tension produced by the Maxwell stresses and its upper limit is about 10^{-3} mN/m. Plotting area versus the logarithm of tension usually resulted in straight lines as predicted by (29). The bending rigidities computed from the slopes were the lowest ever recorded for the six lipids studied, ranging from 3.4×10^{-20} J for dilauroyl PC to 1.1×10^{-20} J for DGDG, with EYPC and three other PC's including stearyloleoyl PC (SOPC) in between [37]. Interestingly, some of the palmitoyloleoyl PC and EYPC vesicles could be stretched, reversible and without hysteresis, by up to 17% instead of the typical 2 to 5%. The large increase in area suggests the presence of a substantial anomalous roughness. Plotting these areas as usual versus the logarithm of tension resulted in S-shaped curves, but plotting them versus the logarithm of the squared field strength gave straight lines again (except at the lowest fields) the slopes of which suggest a bending rigidity of ca. $(1/3)kT$. The very low value is of the order of our estimate of the effective bending rigidity which would be needed to remove one of the contradictions of induced adhesion.

The difficulties of measuring the bending rigidities of lipid bilayers may also point to complex behavior. The mean values of κ obtained in different studies seem to depend on the experimental method. The largest values were derived from the bending fluctuations (uniform bending mode) of tubular vesicles [35, 36] while the smallest were computed from the electric deformation of spherical vesicles [37]. Intermediate values resulted from the fluctuation mode analysis of spherical vesicles [48]. The largest and smallest mean values were seen to differ by a factor of ten in the case of EYPC, the only lipid bilayer whose bending rigidity was measured with both fluctuating tubes and electrically deformed spheres. It is not only the disagreement between the mean values found by different methods that poses a problem. In addition, it appears to be typical of most methods that in a series of equal experiments the scatter of κ as measured with different vesicles is larger than the error of κ as obtained from a single vesicle.

If there is a bilayer superstructure, it could provide an explanation for the uncertainties of the bending rigidity. A dependence of the superstructure on membrane geometry could manifest itself in a disagreement of the results obtained with different methods and a dependence on the vesicle's history would produce scatter. Moreover, the superstructure could make the bending rigidity depend on fluctuation wavelength. Obviously, a disordered superstructure offers a bewildering multitude of theoretical possibilities. Specific assignments seem premature as long as we know almost nothing about the effects of impurities and temperature on the bending rigidity. The membrane may be contaminated by glues, perhaps even silicone greases,

and by chemical degradation. Angelova et al. reported a decrease of the bending rigidity of EYPC from 0.7 to 0.5×10^{-19} J in the course of two weeks [49]. In recent comparative measurements we found a systematic difference between the bending rigidities obtained with two different methods from the same spherical vesicles [50]. We also noted in these studies that the very low values of κ extracted from the electric deformation of spheres rose by a factor of two when the glue was separated from the sample by a barrier of silicone grease.

A dramatic change of the intrinsic bending rigidity by impurities dissolved in the bilayer seems unlikely. However, impurities inducing a local spontaneous bilayer curvature can reduce its bending rigidity to very low values [51, 52]. In a microscopic picture, each such impurity molecule produces a mobile hat in the membrane [41, 53]. In contrast, the superstructure is thought to be built from local saddles. One of the reasons for this assumption is that the superstructure does not appear to have a dramatic effect on the bending rigidity. Both a decrease and an increase of the bending rigidity are conceivable consequences, depending on whether the superstructure mainly rigidifies or roughens the bilayer. A superstructure may also be very sensitive to impurities.

Rather well reproducible values of κ seem to have been measured when the vesicles were aspirated with a micropipette. In one of two such studies, κ was computed, by use of (29), from the apparent membrane stretching as a function of lateral tension [54]. In another experiment, a tether was pulled from a vesicle held by a micropipette and κ was calculated from the tether radius and the pulling force [39]. The results of the two methods can be compared for stearylloleoyl phosphatidylcholine (SOPC), a lipid similar to EYPC, κ being $(0.90 \pm 0.06) \times 10^{-19}$ J and $(1.20 \pm 0.17) \times 10^{-19}$ J, respectively. One may speculate that the small errors and the good agreement of these results are due to the high lateral tensions occurring in these experiments. They could easily be sufficient to destroy anomalous roughness and superstructure, which leaves membranes that are roughened only by the thermal undulations controlled by bending rigidity and lateral tension. The electric deformation [37] and the fluctuation mode analysis [55] of spherical vesicles yielded 0.26×10^{-19} J $\pm 20\%$ and 1.4×10^{-19} J $\pm 20\%$, respectively.

High lateral tension produced by vesicle aspiration (and perhaps by other steps in the preparation of samples for micromanipulation) may also explain why Evans appears to find spontaneous adhesion while we do not, the conflict noted in the Introduction. We suspect that Evans' membranes lost the superstructure before or during the measurements, while ours kept it as they were not manipulated. The smoother the membranes, the more likely they are to spontaneously adhere to each other. Therefore, it is tempting to conclude that the postulated superstructure, regardless of how much anomalous roughness it generates, is a precondition for membrane separation. Such an interpretation is supported by the finding that the X-ray signal indicating the period of a multilayer system does not shift or broaden after the initial absorption of water, but vanishes gradually in those cases where the swelling continues [56]. We suspect that the multilayer system stops water uptake upon reaching the so-called equilibrium spacing, with the outermost membranes tending to peel off when the absence of constraints permits them to assume the superstructure.

According to this model the adhesion observed by Evans is, in a strict sense, not spontaneous but induced by high lateral tension applied previously (or simultaneously). Therefore, the energy of adhesion should be lower than the energy of stretching the adhering pieces of membrane prior to their mutual adhesion. A substantial fraction of the stretching energy would be used in this case to level the superstructure, because the real (Hookean) stretching of the tight membrane at $\sigma = 1$ mN/m does not bind enough energy. In other words, it seems impossible to explain the adhesion energies measured by Evans in terms of asymmetric induced adhesion without invoking the superstructure.

Finally, circumstantial evidence for membrane complexity is possibly provided by vesicle budding. The formation of a mother-daughter pair, i.e. two spheres of different size connected by a narrow constriction, usually starts from an ellipsoidal shape. In the experiments of Käs et al. budding was driven by a rising temperature and typically proceeded through asymmetric shapes such as eggs and pears [57, 58]. A continuous transition through these shapes is predicted by the so-called bilayer-couple model [57, 59, 60]. According to the model, a shape independent difference in area between the monolayers forming the bilayer is the control parameter of the transition and determines the equilibrium shapes at a given stage. An alternative model, in which a shape independent spontaneous curvature of the bilayer assumes the role of the control parameter, predicts an abrupt transition from the ellipsoid to the mother-daughter pair [59–61]. There is also a complete model that takes monolayer stretching and its energy into account and comprises the two other models as limiting cases [62–64]. Starting from the complete model and the bilayer stretching moduli as measured by Evans [3, 24, 54], we showed that budding should closely follow the spontaneous curvature model, in contrast with the prevailing experimental process [65]. Käs and Sackmann took care that they had equilibrium shapes by increasing the temperature only very slowly, sometimes in steps of 0.1 K at intervals of 15 minutes [58]. Barring the possibility that the eggs and pears were fluctuations taking the vesicle up to and over an energy barrier [66], their observation appears to be another sign of complex mechanical properties which are not part of our usual picture of these membranes. The impression of complexity is reinforced by other irregularities of budding reported by Käs et al. [58] and by us [65]. Moreover, E. Evans found that upon increasing the membrane area by raising the temperature vesicles can erupt to form fully connected highly irregular structures, among them outward and inward buds on the same membrane [38, 54].

6. Conclusion

The present article has been written with great hesitation. On the one hand, it seems useful to discuss the puzzles of vesicular lipid membranes. This may speed up their resolution by new experiments and theories. On the other hand, the concepts put forward to solve the problems raise many questions which should be addressed first in order to avoid serious mistakes. We have not yet seen grainy membranes and angular vesicles of a one-component lipid, and we would like to know the time

taken by the unstressed single membrane to develop the conjectured superstructure. Clearly, it is much too early for an authoritative review. To convince (or persuade) the reader of superstructure and anomalous roughness, adhesion induced by lateral tension, on which there is a large body of data, has been elaborated with estimates. However, the result of these estimates, a stored excess area about as large as the projected area or larger, is disquieting in view of the scanty evidence provided by angular vesicles and very stretchable membranes. The last part of this article is a list of intriguing observations which seem to suggest a membrane superstructure or, at least, membrane complexity.

It is an interesting question if nature makes use of induced adhesion in cell biology. The large and tension independent contact angles of induced adhesion would permit extended and rather stable contact of plasma membranes. Induced adhesion has the advantage over spontaneous adhesion that it is terminated when the tension becomes zero. From a general point of view, complex behavior could enable lipid membranes to perform many different and even seemingly contradictory functions. Were the lipids which we investigated, i.e. PC, PE and DGDG, selected by nature for engineering purposes? If so, are their special properties still needed in the presence of highly evolved proteins which control most membrane functions? We do not know the answers, but think that the bilayers of typical biological lipids, being the matrix for these proteins, deserve very careful examination.

Acknowledgements

My thanks go to my students and coworkers who were willing to do so many explorations into the field of lipid membranes. It was their discoveries which allowed me to play with theoretical models for these mysterious systems. I am particularly grateful to W. Harbich and R.M. Servuss who were the pioneers and spent very many years in my group. More recently, M. Mutz and M. Kummrow continued the explorative work. The search for superstructure and anomalous roughness by cryo-transmission electron microscopy is being carried out by B. Klösgen who joined the group as a postdoc. The work was supported in a large measure by the Deutsche Forschungsgemeinschaft through personal research grants and Sonderforschungsbereich 312.

References

1. LeNeveu, D.M., R.P. Rand, V.A. Parsegian and R.P. Gingell, 1977, Measurement and modification of forces between lecithin bilayers, *Biophys. J.* **18**, 209–230.
2. Evans, E. and M. Metcalfe, 1984, Free energy potential for aggregation of giant, neutral lipid bilayer vesicles by van der Waals attraction, *Biophys. J.* **46**, 423–426.
3. Evans, E. and D. Needham, 1987, Physical properties of surfactant bilayer membranes: Thermal transitions, elasticity, rigidity, cohesion, and colloidal interactions, *J. Phys. Chem.* **91**, 4219–4228.
4. Lipowsky, R. and S. Leibler, 1986, Unbinding transitions of interacting membranes, *Phys. Rev. Lett.* **56**, 2541–2544.
5. Lipowsky, R. and S. Leibler, 1987, Erratum, *Phys. Rev. Lett.* **59**, 1983.
6. For a review, see R. Lipowsky, *Statistical physics of flexible membranes*, 1993, *Physica A* **194**, 114–127.
6. Helfrich, W., 1989, Spontaneous and induced adhesion of fluid membranes, in: *Phase Transitions of Soft Matter*, eds T. Riste and D. Sherrington (Plenum, New York) pp. 271–281.

7. Milner, S.T. and D. Roux, 1992, Flory theory of the unbinding transition, *J. Phys. I France* **2**, 1741–1754.
8. Helfrich, W., 1993, Mean-field theory of n-layer unbinding, *J. Phys. II France* **3**, 385–393.
9. Burkhardt, T.W. and P. Schlottmann, 1993, Unbinding transition in a many-string system, *J. Phys. A* **26**, L 501.
10. Lipowsky, R., 1988, Lines of renormalization group fixed points for fluid crystalline membranes, *Europhys. Lett.* **7**, 255–261.
11. Cook-Röder, J. and R. Lipowsky, 1992, Adhesion and unbinding of bunches of fluid membranes, *Europhys. Lett.* **18**, 433–438.
11. Netz, R.R. and R. Lipowsky, Critical behavior of three interacting strings, 1993, *Phys. Rev. E* **47**, 3039.
11. Netz, R.R. and R. Lipowsky, Three interacting strings in two dimensions: Nonuniversal and multiple unbinding transitions, *J. Phys. I (France)*, submitted.
11. Netz, R.R. and R. Lipowsky, 1993, The unbinding of symmetric and asymmetric stacks of membranes, *Phys. Rev. Lett.* **21**, 3596–3599.
12. Mutz, M. and W. Helfrich, 1989, Unbinding transition of a biological model membrane, *Phys. Rev. Lett.* **62**, 2881–2884.
13. Helfrich, W. and R.M. Servuss, 1984, Undulations, steric interaction and cohesion of fluid membranes, *Il Nuovo Cimento D* **3**, 137–151.
14. Servuss, R.M. and W. Helfrich, 1987, Undulation forces and the cohesion energy of egg lecithin membranes, in: *Physics of Complex and Supermolecular Fluids*, eds S.A. Safran and N.A. Clark, (Wiley, New York) pp. 85–100.
15. Servuss, R.M. and W. Helfrich, 1989, Mutual adhesion of lecithin membranes at ultralow tensions, *J. Phys. France* **50**, 809–827.
16. Harbich, W. and W. Helfrich, 1990, Adhesion of egg lecithin multilayer systems produced by cooling, *J. Phys. France* **51**, 1027–1048.
17. Mutz, M., R.M. Servuss and W. Helfrich, 1990, Giant membranes of swollen phosphatidylethanolamines and glycolipids, *J. Phys. France* **51**, 2557–2570.
18. Lipowsky, R. and U. Seifert, 1991, Adhesion of membranes: A theoretical perspective, *Langmuir* **7**, 1867–1873.
19. Helfrich, W. and W. Harbich, 1985, Adhesion and cohesion of tubular vesicles, *Chem. Scr.* **25**, 32–36.
20. Bailey, S.M., S. Chiruvolu, J.N. Israelachvili and J.A. Zasadzinski, 1990, Measurements of forces involved in vesicle adhesion using freeze-fracture electron microscopy, *Langmuir* **6**, 1326–1329.
21. Helm, C., J.N. Israelachvili, P.M. McGuiggan, 1992, Role of hydrophobic forces in bilayer adhesion and fusion, *Biochemistry* **31**, 1794–1805.
22. Harbich, W. and W. Helfrich, 1984, The swelling of egg lecithin in water, *Chem. Phys. Lipids* **36**, 39–63.
23. Harbich, W. and W. Helfrich, 1990, Phases of egg phosphatidylcholine in an abundance of water, *Chem. Phys. Lipids* **55**, 191–205.
24. Kwok, R. and E. Evans, 1981, Thermoelasticity of large lecithin bilayer vesicles, *Biophys. J.* **35**, 637–652.
25. See, e.g., Mahanta J. and B.W. Ninham, 1976, *Dispersion Forces* (Academic Press).
26. See, e.g., Rand R.P. and A. Parsegian, 1989, Hydration forces between phospholipid bilayers, *Biochim. Biophys. Acta* **988**, 351–376.
27. Helfrich, W., 1978, Steric interaction of fluid membranes in multilayer systems, *Z. Naturforsch.* **33a**, 305–315.
28. Safinya, C.R., D. Roux, G.S. Smith, S.K. Sinha, P. Dimon, N.A. Clark and A.M. Bellocq, 1986, Steric interaction in a model multimembrane system: A synchrotron X-ray study, *Phys. Rev. Lett.* **57**, 2518–2521.
29. Bassereau, P., J. Marignan and G. Porte, 1987, An X-ray study of brine swollen lyotropic lamellar phases, *J. Physique* **48**, 673–678.
29. Porte, J., 1992, Lamellar phases and disordered phases of fluid bilayer membranes, *J. Phys.: Cond. Matter* **4**, 8649–8670 (review).

30. Janke, W., 1990, Entropic repulsion between fluctuating surfaces, *Int. J. Modern Phys.* **B4**, 1763–1808 (review).
31. Kleinert, H. and W. Janke, 1987, Fluctuation pressure of a stack of membranes, *Phys. Rev. Lett.* **58**, 144–147.
32. Gompper, G. and D.M. Kroll, 1989, Steric interactions in multilamellar systems: A Monte Carlo study, *Europhys. Lett.* **9**, 59–64.
33. David, F., 1990, Renormalization group treatment of entropic interactions in lamellar phases, *Colloque de Physique C7*, 115–129 (supplement to *J. Phys. France* **51**).
34. Sornette, D., 1986, Steric Interaction between wandering walls: study of the strong deviation from mean-field theory, *Europhys. Lett.* **2**, 715–724.
35. Servuss, R.M., W. Harbich and W. Helfrich, 1976, Measurement of the curvature-elastic modulus of egg lecithin bilayers, *Biochim. Biophys. Acta* **436**, 900–903.
36. Beblík, G., R.M. Servuss and W. Helfrich, 1985, Bilayer bending rigidity of some synthetic lecithins, *J. Physique* **46**, 1773–1778.
37. Kummrow, M. and W. Helfrich, 1991, Deformation of giant lipid vesicles by electric fields, *Phys. Rev. A* **44**, 8356–8360.
Kummrow, M., 1992, Lichtmikroskopische Untersuchungen zur Deformation biologischer Modellmembranen im elektrischen Feld. Dissertation, Fachbereich Physik, Freie Universität Berlin.
38. E. Evans, Private communication.
39. Waugh, R.E., J. Song, S. Svetina and B. Žekš, 1992, Local and nonlocal curvature elasticity in bilayer membranes by tether formation from lecithin vesicles, *Biophys. J.* **61**, 974–982.
40. Servuss, R.M., 1989, Local and nonlocal curvature elasticity in bilayer membranes by tether formation from lecithin vesicles, Color scatterers in egg lecithin water systems, *Chem. Phys. Lipids* **50**, 87–97.
41. Helfrich, W., 1989, Hats and saddles in lipid membranes, *Liq. Cryst.* **5**, 1647–1658.
42. Helfrich, W. and B. Klösgen, 1990, Adhesion and roughness of biological model membranes, in: *Dynamics and Patterns in Complex Fluids*, eds A. Onuki and K. Kawasaki, Springer Proc. Phys. **52**, 2–18.
43. Helfrich, W. and B. Klösgen, 1993, Some complexities of simple lipid membranes, in: *Proceedings of the Workshop on Dynamical Phenomena at Surfaces, Interfaces and Membranes*, Les Houches 1991, eds D. Beysens, N. Boccara and G. Forgacs (Nova Science Publishers, Commack, NY) pp. 211–220.
44. Klösgen, B. and W. Helfrich, 1992, Electron microscopy of biological model membranes, in: *The Structure and Conformation of Amphiphilic Membranes*, eds R. Lipowsky, D. Richter and K. Kremer, Springer Proc. Phys. **66**, 105–112.
45. Klösgen, B. and W. Helfrich, 1993, Special features of phosphatidylcholine vesicles as seen in cryo-transmission electron microscopy, *Eur. Biophys. J.* **22**, 329–340.
46. Lücken, U. and J. Jäger, 1992, The structure of membranes and membrane proteins embedded in amorphous ice, in: *Proc. 50th Annual Meeting of the Electron Microscopy Society of America*, eds G.W. Bailey, J. Bentley and J.A. Small (San Francisco Press, San Francisco) pp. 432–433, and private communication.
47. Weiss, A., 1989, Kryo-Elektronenmikroskopie an Phospholipidvesikeln. Diplomarbeit, Fakultät für Physik, Technische Universität München.
48. Faucon, J.F., M.D. Mitov, P. Méléard, I. Bivas and P. Bothorel, 1989, Bending elasticity and thermal fluctuations of lipid membranes: Theoretical and experimental requirements, *J. Phys. France* **50**, 2389–2397.
49. Angelova, M.I., S. Soléau, Ph. Méléard, J.F. Faucon and P. Bothorel, 1992, Preparation of giant vesicles by external AC fields: Kinetics and application, *Colloid Polym. Sci.* **89**, 127.
50. Niggemann, G., M. Kummrow and W. Helfrich, to be published.
51. Safran, S.A., P. Pincus and D. Andelman, 1990, Theory of spontaneous vesicle formation in surfactant mixtures, *Science* **248**, 345–356.
52. Kozlov, M.M. and W. Helfrich, 1992, Effects of a cosurfactant on the stretching and bending elasticities of a surfactant monolayer, *Langmuir* **8**, 2792–2797.

53. Helfrich, W. and M.M. Kozlov, 1994, Flexibility and roughness of mixed and partially polymerized bilayers in terms of the hat model and local bending frustration, *J. Phys. France II*, **4**, 1427.
54. Evans, E. and B. Rawicz, 1990, Entropy-driven tension and bending elasticity in condensed-fluid membranes, *Phys. Rev. Lett.* **64**, 2094–2097.
55. Häckl, W., 1994, Anwendung der computergestützten Mikroskopie zur Messung von elastischen Eigenschaften von Membranen. Diplomarbeit, Fakultät für Physik, Technische Universität München. **49**, 77.
56. Hartung, J., W. Helfrich and B. Klösgen, 1994, Transformation of phosphatidylcholine multilayer systems in excess water, *Biophys. Chem.* **49**, 77.
57. Berndt, K., J. Käs, R. Lipowsky, E. Sackmann and U. Seifert, 1990, Shape transformations of giant vesicles: extreme sensitivity to bilayer asymmetry, *Europhys. Lett.* **13**, 659–664.
58. Käs, J. and E. Sackmann, 1991, Shape transitions and shape stability of giant phospholipid vesicles in pure water induced by area-to-volume changes, *Biophys. J.* **60**, 825–844.
59. Seifert, U., K. Berndt and R. Lipowsky, 1991, Shape transformations of vesicles: phase diagram for spontaneous-curvature and bilayer-coupling model, *Phys. Rev. A* **44**, 1182–1202.
60. Miao, L., B. Fourcade, M. Rao, M. Wortis and R.K.P. Zia, 1991, Equilibrium budding and vesiculation in the curvature model of fluid membranes, *Phys. Rev. A* **43**, 6843–6856.
61. Wiese, W. and W. Helfrich, 1990, Theory of vesicle budding, *J. Phys.: Cond. Matter* **2**, SA329–SA332.
62. Helfrich, W., 1974, Blocked lipid exchange in bilayers and its possible influence on the shape of vesicles, *Z. Naturforsch.* **29c**, 510–515.
63. Evans, E., 1974, Bending resistance and chemically induced moments in membrane bilayers, *Biophys. J.* **14**, 923–931.
64. Svetina, S., M. Brumen and B. Žekš, 1985, Lipid bilayer elasticity and the bilayer couple interpretation of red cell shape transformations and lysis, *Stud. Biophys.* **110**, 177–184.
65. Wiese, W., W. Harbich and W. Helfrich, 1992, Budding of lipid bilayer vesicles and flat membranes, *J. Phys.: Condens. Matter* **4**, 1647–1657.
66. Miao, L., U. Seifert, M. Wortis and H.G. Döbereiner, 1994, Budding transitions of fluid bilayer vesicles: the effect of area difference elasticity, *Phys. Rev. E* **49**, 5389.

This Page Intentionally Left Blank

Physical Actions in Biological Adhesion

E. EVANS

*Departments of Pathology and Physics,
University of British Columbia,
Vancouver, B.C., Canada V6T 2B5*

Contents

1. Preface: Biological view of adhesion	725
2. Introduction: Physical view of adhesion	726
3. Mechanics of adhesion: Macroscopic view	728
4. Membranes: Macrocolloids	734
4.1. Van der Waals attraction	735
4.2. Electric double layer repulsion	736
4.3. Entropy-driven repulsion between flexible membranes	736
4.4. Depletion driven attraction	737
5. Biological adhesion: Contact formation	740
5.1. Spreading by cytoskeletal contraction	740
6. Biological adhesion: Focal bonding	742
6.1. Strength of attachment	742
6.2. Microscopic dynamics of rupture	745
7. Biological adhesion: Macroscopic contacts	746
7.1. Contour roughness, mechanical stiffness and impingement	746
7.2. Mesoscale mechanics of fracture	750
8. Summary comment	752
Acknowledgement	752
References	752

1. Preface: Biological view of adhesion

Tissue assembly (development) and other biological functions (like identification and removal of alien organisms in immune defense) involve complex adhesive interactions. Biologists have identified and isolated many molecular 'adhesins' responsible for cellular adhesion processes [1]. Classification of receptors and ligands in cell adhesion has become a major enterprise in mammalian biology. The list is long and some of the evidence is circumstantial (e.g., 'cell sticking versus nonsticking' in relation to competitive binding of ligands to putative sites of adhesive activity). Unfortunately, little is known about the microscopic bonding actions (physical-chemical) between cell adhesion molecules. In any case, the present view of cell adhesion in biology is *briefly* outlined here to provide a comparative perspective for the discussion of physical actions that will follow.

The collective dogma (for mammalian cells) is that cell adhesion molecules fall into four *groups*.¹

- (i) *Integrins*: a family of membrane glycoproteins composed of α and β subunits. The ligand binding site is formed by both subunits; the cytoplasmic domains are thought to be connected to the cell cytoskeleton. Integrins are receptors for extracellular matrix proteins. In many instances, a specific amino acid sequence (Arg-Gly-Asp = RGD) is believed to participate in recognition [2]. Subfamilies of integrins are distinguished by their β subunits: $\beta 1$ (CD29) – VLA proteins; $\beta 2$ (CD18) – leukocyte integrins; and $\beta 3$ (CD61) – cytoadhesins. The $\beta 1$ subfamily binds to extracellular matrix proteins fibronectin, collagen, and laminin. The $\beta 2$ subfamily is unique to leukocytes [3] and is thought to be important in converting circulating leukocytes to adherent tissue cells. The best characterized molecule of the $\beta 3$ subfamily is glycoprotein IIb/IIIa (α IIb β 3) (CD41/CD61), found exclusively on platelets and megakaryocytes. Glycoprotein IIb/IIIa plays a central role in platelet aggregation and clotting.
- (ii) *Selectins*: another family of calcium-dependent membrane glycoproteins. To date, selectins have been found only on circulating cells and endothelium. LAM-1 (LECAM-1), expressed on neutrophils, monocytes and most lymphocytes, facilitates binding to endothelium during lymphocyte recirculation and neutrophil emigration at inflammatory sites. ELAM-1 expressed on activated endothelial cells promotes the adhesion of leukocytes. 'Rolling' attachment of

¹ The author is grateful to his colleague and collaborator Dr. Susan Tha for providing the summary paraphrased in this paragraph.

leukocytes to endothelium seems to be mediated by selectins whereas ‘spreading’ adhesion appears to require $\beta 2$ integrins LFA-1 and Mac-1 via ICAM-1 [4].

- (iii) *Ig superfamily*: a diverse group of molecules whose structure resembles a sandwich of β -pleated sheets with disulfide bonds. The prototypical molecule is immunoglobulin. N-CAM is also a member of this superfamily [15]. Other Ig superfamily molecules function in immune response [6]. Lastly,
- (iv) *Cadherins*: a separate family of cell adhesion molecules without structural homology to other adhesion molecules [7]. Cells in solid tissues express at least some member of the cadherin family all of which exhibit calcium-dependent homophilic binding. Even though the size of the cytoplasmic domains vary greatly between these groups of cell adhesion molecules, all possess massive extracellular domains that extend prominently from the bilayer core of the membrane.

Other than for surface recognition, it is not clear why cells require a plethora of ‘sticky’ molecules (many types reside on the same cell) *or* what differences exist in physical strength of attachment amongst these ‘adhesins’? One characteristic is common to all specific adhesion sites on cells: i.e. the surface density is relatively low. On the average, tens of nanometers separate adhesion sites ($\sim 10^4$ lipids per site). As will be discussed, the paucity of potential attachments leads to complex mechanics of adhesion and often to catastrophic effects when adherent cells are separated.

2. Introduction: Physical view of adhesion

Exposure of the underlying physics in biological adhesion is difficult because of strong ‘coupling’ between cellular biochemistry, structure, and microscopic action. Idealized concepts only provide a phenomenological characterization of adhesion embodied in an ‘adhesion energy’ w_a (energy/unit area of contact). The view is predicated on the assumption that interfaces are smooth and adhere by intimate-uniform contact. Furthermore, the incremental energy w_a gained in contact formation is assumed to equal the mechanical energy w_f required to separate (‘fracture’) the contact: i.e. the process is energetically reversible ($w_a \equiv w_f$). Ideal adhesion of smooth contacts is the physical metaphor for ‘wetting-like’ adhesion originally developed in the 19th century [8] to describe spreading and contact angle behavior of liquid drops on solid substrates (or shapes of immiscible liquid interfaces). To some extent, the classical concept can be useful to model adhesion of liquid-like membranes that possess microscopically smooth surfaces. For instance, adhesion of lipid bilayer vesicles driven by colloidal-type attractions can be represented by a reversible adhesion energy related to microscopic physical forces between the surfaces. (*But* even for ‘smooth’ vesicle adhesion, the connection between macroscopic adhesion energy and microscopic interactions is obscured by hidden thermal excitations.) Situations of ‘ideal adhesion’ are easy to recognize since contacts spread spontaneously without mechanical impingement (‘push’) and the spreading actions

(‘wetting’) create membrane tensions. However, the nonspecific attractions that produce ideal adhesion between lipid bilayer vesicles do not drive cell adhesion in biology!

The fluid-like property of cell interfaces has stimulated several kinetic and thermodynamic models for cell adhesion [9]. These elegant developments have been extensively parameterized to represent a wide range of chemical features which leads to a rich spectrum of predictions. As with the classical adhesion energy approach, the models are based on a smooth surface abstraction for contact; and the kinetics are essentially near equilibrium processes. Consequently, the models must be regarded as primarily phenomenological. An important conclusion from thermodynamic models is that the spreading energy at full equilibrium is scaled by the effective surface pressure of adhesion sites: i.e. $w_a \sim \tilde{n}_B kT$ where \tilde{n}_B is the surface density (number/area) of adherent receptors [10]. The free energy of binding determines the fraction of bound adhesion sites at equilibrium; but the energy increment gained as bonds form balances the energy increment lost as bonds dissociate. Only entropy confinement is left to expand the contact. However, far from equilibrium, the mechanical work to separate the contact w_f approaches a limit characterized by the binding energy [10]. The caveat for biological cell adhesion is that receptor densities are usually very low ($< 10^{11}/\text{cm}^2$). Thus, the equilibrium energy scale for spreading is weak ($< 4 \times 10^{-3} \text{ erg}/\text{cm}^2$) in comparison to mechanical energies for deformation of the cell cortex.

Biological cells adhere to other cells or material substrates by completely *nonideal* processes. Attraction appears to be short range and localized to molecular-focal attachments (e.g., created by molecular bridges with agglutinins or direct bonds with intrinsic cell adhesion molecules). Interfacial forces of attraction between cells are not sufficient to pull the surfaces together. Clear evidence of this feature is that cells normally do not spread spontaneously on a substrate unless pushed into contact by external forces (mechanical impingement). Left alone, cells increase contact area either slowly through structural relaxation *or* rapidly by active motility. The behavior is simple: cells stick where they ‘crawl, flow, or are pushed’!

Most receptors and molecular adhesion sites on cell surfaces are relatively mobile; thus, it is expected that (given time) the focal character of intersurface bonding should be dispersed by lateral diffusion. Eventually, equilibrium should be reached where regions of contact are uniformly bonded. Based on measurements [11] of receptor diffusivity ($> 10^{-11} \text{ cm}^2/\text{sec}$) and characteristic lengths of 10^{-4} cm , only a few minutes should be required to reach this fully-bound state. In fact, receptor diffusion does appear to promote large regions of adherent contact for fluid-like interfaces with high densities of adhesive ligands (e.g., agglutination of lymphocytes by lectins – see Bongrand chapter and ref. [12]). On the other hand, unstimulated cells often take many hours to spread on surfaces even though the cells adhere immediately at a few points *or* can be made to adhere strongly by mechanical impingement of the cell against the substrate. Hence, biological cell adhesion seems to be ‘kinetically trapped’ to a great extent, much more than can be accounted for by diffusive limitations. Kinetic restrictions and strong focal bonding between cell membranes show-up in physical studies of cellular adhesion as irreversible behavior: i.e. little

(if any) detectable tendency (affinity) to spontaneously spread *but* strong force is needed to subsequently detach an adherent cell ($w_a \ll w_f$). Indeed, the strength of attachment after contact can be enormous – greater than the structural integrity of the cell material; and separation often leads to material rupture of the interface [13].

This phenomenological scenario indicates that physical actions in cell adhesion can be conceptually partitioned into mechanisms that lead to ‘ideal’ and ‘nonideal’ behavior. However, significant aspects of adhesion in biology are peculiar to cellular biochemistry and specific types of substrates. These particular features will be ignored here in order to focus on the general mechanisms involved in all biological adhesion processes. Macroscopic energy densities for contact formation *vis a vis* separation provide the physical diagnostics of adhesion; thus, a brief review of the macroscopic mechanics of adhesion will be given first accompanied by examples of adhesion experiments.

3. Mechanics of adhesion: Macroscopic view

Cell structure is heterogeneous and anatomically complex, but the interior is often a soft liquid-like environment. Thus, mechanical stresses become distributed almost uniformly as hydrostatic pressure. The major stress variation occurs within a layer near the cell surface, i.e. the cell cortex, which can be as thin as a lipid bilayer ($\sim 40 \text{ \AA}$) or as thick as an actin meshwork ($> 10^3 \text{ \AA}$). Even so, the cortex thickness is usually much smaller than the radii of curvature that characterize the macroscopic cell shape. Because of this, stresses can be integrated through the cortex to create macroscopic force cumulants or resultants called ‘tension’ (force/length) that balance external forces to first order *plus* ‘moments of stress’ that contribute higher order bending corrections [14]. These resultants embody the mechanical opposition to deformation when cells adhere to surfaces or are forced to separate from contact. In the mechanical sense, the cell cortex is reduced to a thin shell, labeled as a ‘membrane’ by mechanicians [14]. However, the mechanical membrane includes the lipid bilayer, extrafacial glycocalyx, and subsurface cytoskeleton scaffolding – i.e. *everything* (including microscopic ‘roughness’) from the liquid-like cytoplasm to the external aqueous medium. Even though this region can exceed $10^2 \times$ the thickness of the lipid bilayer, it still behaves mechanically like a ‘membrane’ provided that the principal radii of curvature (R_1, R_2) for the cell shape exceed the thickness by an order of magnitude or more. Certainly, the mechanical membrane abstraction oversimplifies the stress distribution in some cells; but the approach provides an easily understood way to connect the macroscopic mechanics of cell deformation to microscopic physics of adhesion.

At mechanical equilibrium (where a cell is stationary or moving very slowly), adhesion is characterized macroscopically by the differential balance between mechanical work expended to deform the cell capsule *vis a vis* energy gained with interfacial contact. In situations of *strong* adhesion (where high tensions are involved), mechanical equilibrium of an adherent capsule is deceptively simple: i.e. the energy either gained (w_a) per unit area of contact formation or expended (w_f)

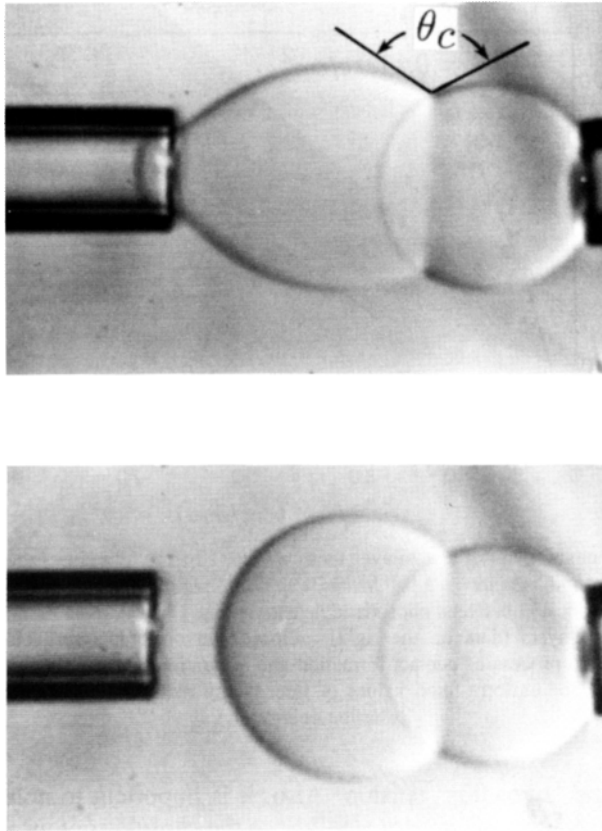


Fig. 1. *Strong* adhesion (adhesion energies $w_a > 10^{-3}$ erg/cm²) and spreading of a neutral lipid bilayer vesicle onto a stiff pressurized vesicle (diameters $\sim 20 \mu\text{m}$). The adhesion process is ‘ideal’ as verified by the reversibility of bilayer tension versus apparent contact angle θ_c ; tension is controlled by pipet suction pressure.

to separate a unit area of contact is directly proportional to the tension τ_m in the cortical shell or membrane,

$$\left. \begin{matrix} w_a \\ w_f \end{matrix} \right\} = \tau_m(1 - \cos \theta_c) \tag{1}$$

where $(1 - \cos \theta_c)$ is a mechanical leverage factor that depends on the ‘apparent’ contact angle θ_c between the capsule contour and substrate outside the perimeter of the contact as shown in fig. 1. As indicated, the proportionality also holds for both formation and separation (fracture) of contact; but the ‘peeling’ tension may not

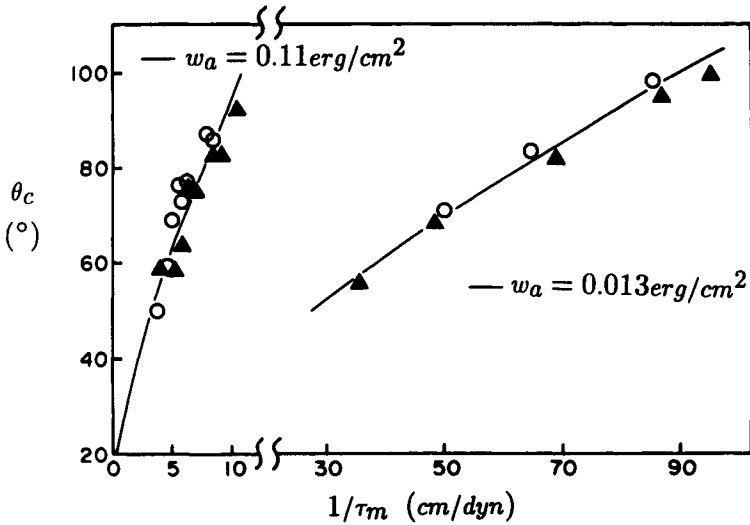


Fig. 2. Results for contact angles and bilayer tensions derived from adhesion experiments (cf. fig. 1) with neutral phospholipid vesicles in a 0.1 M NaCl solution. Attraction was driven by Van der Waals forces with stronger adhesion between phosphatidylethanolamine bilayers (data on the left) than between phosphatidylcholine bilayers (data on the right). Closed and open data symbols represent discrete equilibrium steps in the process of contact formation and separation, respectively. The solid curves are correlations predicted for uniform-fixed values of free energy reduction per unit area of contact (i.e. adhesion energy w_a).

be the same as the 'spreading' tension. Also, it is important to note that the actual contact angle at the substrate is very small since the capsule contour is nearly tangent to the surface within the contact region. The important features of adhesion for membrane capsules are illustrated by the example in fig. 1 of lipid bilayer vesicles drawn together by Van der Waals attraction. In fig. 1, the angle appears distinct because cortical bending stiffness is overwhelmed by the tension force. Clearly, if 'bigger magnification' were possible, we would see a continuous bend of the contour to microscopic-tangential contact. The mechanical balance (eq. (1)) for *strong* adhesion of fluid-like capsules (shown in fig. 1) is demonstrated in fig. 2. These data were derived from measurements [15] of tension and contact geometry for adhesion of lipid bilayer vesicles driven by colloidal attraction.² Unlike *free* liquid interfaces, both bilayer tension and angle θ_c are variable; but the adhesion energy is uniform, constant, and reversible. The reason that the tension can vary

² The method for control of the adhesion process involved manipulation of vesicles by micropipets. The vesicles were maneuvered into close proximity, allowed to adhere, and pressurized by pipet suction. The tension in each vesicle was regulated by suction pressure. One vesicle was stiffened by high tension whereas the other vesicle was allowed to spread on the stiff vesicle to an extent limited by a low bilayer tension (fig. 1a). Reversibility of adhesion was verified by measurements of tension versus contact angle for both formation and separation of the contact. When released from the pipet, the adherent vesicle spread to maximum contact limited by fixed surface area and volume as shown in fig. 1b.

is because the lipid bilayer is a tightly condensed material [16]. The tension is a stiff-elastic response to pressurization that arises when the vesicle area is required to increase as the adhesive contact spreads. Hence, the vesicle area: volume ratio is the principal determinant of the contact geometry (i.e. angle θ_c).

For microscopically 'rough' cells, the effective area of the cell cortex can be increased by smoothing roughness which enables formation of large macroscopic contacts at low stress. The expansion of the cell cortex usually requires tensions that increase slightly with area, i.e. $\tau_m = \tau_0 + K(\Delta\bar{A}/\bar{A})$ where \bar{A} represents the macroscopic-scale (apparent) area of the cortex. The elastic constant K for lipid bilayers is very large (10^2 – 10^3 dyn/cm) and the 'natural' (reference) tension τ_0 is zero. Thus, the area of lipid bilayer vesicles remains essentially constant throughout the adhesion process. By comparison, the elastic constant for expansion of the cell cortex is usually much smaller ($< 10^{-2}$ – 10^{-2} dyn/cm for cells like blood phagocytes). Thus, by unwrinkling the superficial bilayer, the cortex area can easily be enlarged to allow adhesive contact. In living cells, these properties appear to be regulated by contractile processes in the cortex. The relationship between adhesion energy, cortical tension, and apparent contact angle θ_c is modeled in fig. 3 for adhesion of

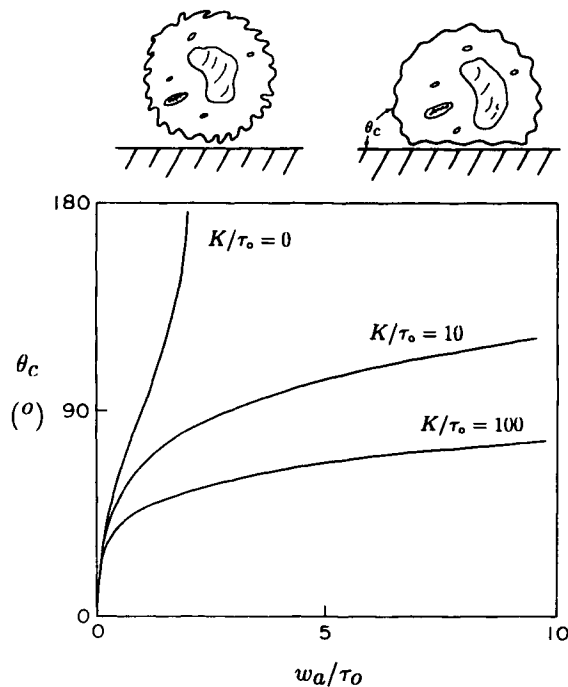


Fig. 3. Predictions of contact angle θ_c in relation to adhesion energy w_a for adhesion of a macroscopically spherical cell to a flat substrate. The cortex of the cell is assumed to possess an initial cortical tension τ_0 with an elastic expansion modulus K so that the tension in the cortex is given by $\tau_m = \tau_0 + K(\Delta\bar{A}/\bar{A})$. For biological cells, the increase $\Delta\bar{A}$ in macroscopic area is provided by smoothing of bilayer wrinkles as illustrated in the sketches.

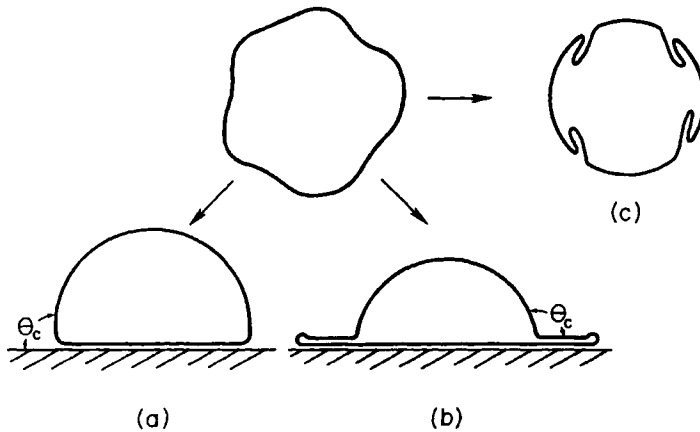


Fig. 4. Illustration of the competition between substrate adhesion and 'self' adhesion for a flexible membrane capsule with excess surface area. (a) Equilibrium shape of the capsule in the regime dominated by substrate attraction. (b) Equilibrium shape when membrane 'self' adhesion energy w_m is comparable to substrate adhesion energy w_a . (c) Equilibrium shape driven by 'self' adhesion without contact to the substrate.

a macroscopically spherical cell to a flat substrate. This relation shows why smooth lipid bilayer spheres ($K \gg w_a$) only adhere with small contact areas ($\theta_c < 30^\circ$).

For simple membrane capsules with excess surface area, a subtle feature of *strong* adhesion is that the membrane may 'self adhere' as well as spread on another substrate. This situation is shown schematically in fig. 4. For strong adhesion (where bending rigidity is negligible), there is a critical angle θ_c^* beyond which the membrane can 'lap onto itself' driven by a self attraction energy w_m . Simple energetics for fluid membranes predict that the transition illustrated in fig. 4a→b should occur when,

$$\cos \theta_c \leq (w_m/w_a - 1)/(w_m/w_a + 1) \quad (2)$$

governed by the ratio w_m/w_a of self attraction to substrate attraction energies. An obvious corollary to the situation depicted in fig. 4b is self adhesion without contact to a substrate (fig. 4c). Clearly, this type of behavior is possible when the membrane tension (determined by pressurization of the capsule) falls to the level of the self attraction energy (i.e. $\tau_m \simeq w_m$). There are many geometric variations on this self adhesion theme. Because biological membranes are optically invisible, self adhesion is most easily recognized when a capsule appears to stop spreading on a substrate even though additional contact area is made available by reduction in volume. Self adhesion behavior is frequently observed in experiments with lipid bilayer vesicles. For example, it is difficult to achieve adhesion between weakly attracting vesicles of different compositions when self attraction of each membrane is stronger. Self adhesion requires that elastic energies of deformation be small compared with the

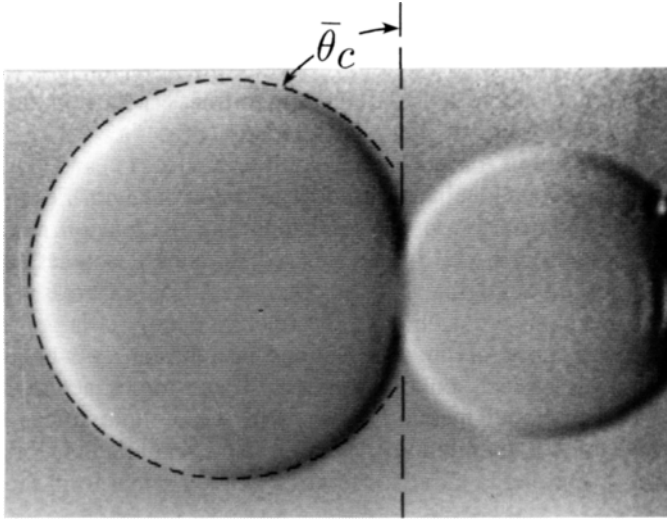


Fig. 5. *Weak* adhesion (adhesion energies $w_a \ll 10^{-3}$ erg/cm²) of a lipid bilayer vesicle to a stiff pressurized vesicle (diameters ~ 20 μ m) in 0.1 M NaCl. (Here, the neutral lipid bilayers were doped with a small percentage ($\sim 5\%$) of negatively charged lipid to reduce attraction.) The continuous bend of membrane to the contact zone demonstrates the bilayer bending rigidity and exposes the parallel contact between the membrane surfaces.

attraction energies. As such, fluid membrane interfaces with weak bending rigidities are most susceptible to self adhesion – especially when membrane attractions are *strong*.

As membrane attraction weakens, bending rigidity as well as other ‘stiffnesses’ in the capsule shell lead to significant deviation from the classical energetics for a ‘fluid interface’ represented by the Young–Dupre relation (eq. (1)). When adhesion is *weak*, the small region of membrane bending can reach macroscopic dimensions. The weak regime of adhesion is demonstrated in fig. 5. Here, bending rigidity (higher order ‘moments’ of stress in the membrane or cell cortex) becomes comparable to the mechanical action of the tension force. Precise mechanical analysis of this situation is not trivial; major numerical computations are required to calculate the capsule geometry and energetic balance [17, 18]. However, a good first-order approximation [15] to the analysis is given by,

$$w_a - (w_a \cdot e_0)^{1/2} \simeq \tau_m(1 - \cos \bar{\theta}_c) \quad (3)$$

where $\bar{\theta}_c$ is the effective contact angle indicated by the flattened capsule shape (cf. fig. 5). The constant e_0 is the elastic bending energy threshold that must be overcome to initiate contact, i.e. $e_0 = k_c/2R^2$ with R as the characteristic capsule radius, k_c is the elastic modulus for bending. For smooth cell-size capsules, the threshold is extremely small when the rigidity is dominated only by the lipid bilayer

$k_c \sim 10^{-12}$ erg [16] and $R > 10^{-4}$ cm ($e_0 \ll 10^{-4}$ erg/cm²); but the effect of bending stiffness remains important even when $w_a/e_0 \sim 10$ (as indicated by the ‘geometric mean’ of adhesion energy and bending energy threshold). (Note: the size of the bending-dominated contour follows from the mechanical boundary condition at the perimeter of the contact where tension, bending stiffness, adhesion, and membrane curvature are related by $1/R_c = \sqrt{2w_a/k_c}$, refs [17–18].)

The macroscopic relations for mechanical equilibrium, eqs (1) and (3), demonstrate that discrimination between ideal and nonideal adhesion behavior lies in observation of both the tension induced by contact spreading *and* the tension required to peel the contact apart. Thus, if a cell is not stressed by natural contact spreading, the adhesion energy must be negligible. On the other hand, if large stresses are produced in the cell under mechanical detachment, the fracture energy is large. Turning now to the microscopic features of physical actions in adhesion, we begin with ideal processes driven by classical ‘colloid forces’. These forces act ubiquitously on particles suspended in liquid media. As we will see, colloid forces only govern adhesion for the simplest membrane structures (e.g., smooth lipid bilayers) *or* in unusual situations where large attractions persist at long range from the surfaces.

4. Membranes: Macrocolloids

Membranes are supermolecular assemblies of organic molecules localized to a thin interfacial layer – from 30 Å to > 500 Å in thickness. Thus, membranes are macrocolloids that act on each other *nonspecifically* through the classical interactions well-established from the study of particle suspensions (e.g., ink, milk, clays, etc.). The prominent attribute of colloid interactions is that they essentially superpose (neglecting subtle effects). The net interaction can be expressed by a force σ_n per unit surface area that depends only on separation ‘ z ’ between surfaces. Thus, adhesion is driven by a physical potential that cumulates the action of all the forces from macroscopic separations to microscopic contact. The reversible potential (adhesion energy w_a) represents the energetic balance between attractive and repulsive interactions, i.e.

$$w_a = - \int_{\infty}^{z_c} \sigma_n dz. \quad (4)$$

Colloid interactions are commonly classified according to their range of action: *Long range* forces include electrostatic forces that decay exponentially ($\sigma_{es} \sim -P_{es} \times e^{-z/\lambda_{es}}$) in electrolyte solutions (e.g., the decay length $\lambda_{es} \sim 10$ Å and 0.1 M NaCl) and an inverse power-law (Van der Waals) attraction ($\sigma_{vdw} \sim A_H/z^2$) that extends effectively to macroscopic distances [19–21]. Van der Waals forces emanate mainly from the hydrocarbon core of the lipid bilayer [20]. In addition, steric exclusion of macromolecules from interfacial regions leads to long range ‘depletion’ attraction ($\sigma_M \sim \Pi_M e^{-z/\xi}$) that also decays exponentially with distance [22]. The decay length ξ is established by the correlation length for the macromolecular concentration field (typically the ‘size’ of the molecule, e.g., ~ 10 – 100 Å). Of the long range forces, Van der Waals attraction should dominate at large separations to draw membranes

into adherent contact. For 'atomically-smooth' surfaces, the attraction creates large adhesion energies characteristic of liquid interfacial energies, e.g., ~ 50 ergs/cm² or more. However, as shown by the results in fig. 2, adhesion of 'smooth', neutral bilayers yields adhesion energies [23] that are orders of magnitude smaller (~ 0.01 – 0.1 erg/cm²).

Weak adhesion of neutral bilayers exposes the existence of a strong *short range* repulsion that prevents direct atomic contact. The short range force is often referred to as a 'hydration' force because it opposes condensation of all 'hydrated' molecular interfaces, e.g., DNA, proteins, and surfactant lipid molecules (ref. [24]; see Rand and Parsegian chapter for elaboration). At small separations, repulsion between lipid bilayers becomes enormous! Several hundred atmospheres of pressure are required to push bilayer surfaces to < 10 Å; but the repulsion decays rapidly with exponential-like character ($\sigma_h \sim -P_h e^{-x/\lambda_h}$; decay length $\lambda_h \sim 2$ – 3 Å). The major consequence of the 'hydration' force is to stabilize neutral bilayer adhesion at separations between 10–30 Å. Since Van der Waals forces decrease as $\sim 1/\text{distance}^2$, increasing separation from 'atomic' (1 Å) distances to 10–30 Å diminishes the potential for adhesion by 1/100–1/1000! Clearly, the 'hydration' force is essential for biological existence! Without it, bilayers (DNA and many proteins in solution as well) would collapse to condensed (dehydrated) states – destroying membrane structure and prohibiting biological function. Surprisingly, the physical origin of this force remains obscure at present. Several actions probably contribute to repulsion at short range: steric forces, solvent structure forces, electrostatic forces, etc., all of which are supported to some degree by experimental evidence. General study of colloid forces at *short* and *long* range is a major scientific activity which need not be reviewed here. The important question is: what roles do these ever-present actions play in biological adhesion processes?

4.1. Van der Waals attraction

The impact of colloid attraction depends strongly on the structure of the interface, principally topographical 'roughness' and electrical charge distribution. For example, smooth bilayer vesicles composed of electrically-neutral species (e.g., phosphatidylcholine PC and phosphatidylethalamine PE) adhere spontaneously in salt buffer ($> 10^{-3}$ M NaCl) as shown in fig. 1. However, the values of adhesion energy differ by an order of magnitude for the two lipids (PC ~ 0.01 erg/cm² and PE ~ 0.1 erg/cm²). The reason is that the 'hydration' force is larger in PC bilayers; the bilayer separation is increased from ~ 12 Å for PE to ~ 27 Å for PC (as measured by X-ray diffraction methods – see Rand and Parsegian chapter). In contrast to lipid bilayers, biological membranes (even macroscopically smooth red blood cells) show *no* tendency to spontaneously spread on one another in 0.1 M NaCl! The diminished attraction is not surprising since large extrafacial peptidoglycan moieties limit bilayer separations to > 100 Å. Hence, the adhesion potential due to Van der Waals forces should be extremely small (below 10^{-3} erg/cm² since the attraction diminishes as $1/\text{distance}^4$ at large separations). Therefore, macromolecular and other steric 'roughness' essentially quench Van der Waals forces so that they can usually be neglected in biological adhesion. However, this colloid action persists as a background attraction.

4.2. Electric double layer repulsion

Even though Van der Waals attraction can be neglected, electrostatic forces (mainly repulsive between cell surfaces because of the preponderance of negative charge) can play an important regulatory role in biological cell adhesion. Electrostatic repulsion in electrolyte solutions originates from osmotic pressure between surfaces created by an excess of counterions drawn into the gap to neutralize the electric field created by surface charges. In 0.1 M monovalent salt solutions, the repulsion decreases rapidly with separation; the exponential decay length λ_{es} is about 10 Å. Because of the limited range, the principal effect of surface electrical charge is to reduce the adhesion potential near contact. This consequence is clearly shown by adhesion of lipid bilayer vesicles that contain small admixtures of negatively charged lipids (e.g., phosphatidylserine PS). Although weakened, the adhesion process remains 'ideal' – consistent with the direct dependence of electrostatic interaction on distance. Adhesion energies diminish rapidly with small increases in bilayer charge content [28] as shown in fig. 6 (e.g., a ratio of PC:PS of only 20 : 1 reduces the potential for adhesion by an order of magnitude from 10^{-2} to 10^{-3} erg/cm²). Biological cell surfaces possess much higher charge densities; but the charges are distributed over a thick glycocalyx outside the bilayer core. Because of 'screening' by ions in the electrolyte environment, repulsion acts primarily at short distances within about a decay length λ_{es} from the outer end of the glycocalyx and only charges that lie within a decay length from the end of the glycocalyx will contribute to the repulsion. Given a volumetric charge density $\bar{\rho}$ (i.e. charge/volume) in the glycocalyx, repulsion can be approximated by an interaction between surface charge densities of $\bar{\rho}\lambda_{es}$ 'pinned' to the periphery of each glycocalyx. (The magnitude of the prefactor P_{es} for repulsion ranges between 1–10 Atm (10^6 – 10^7 dyn/cm²) for surface charge densities in the range of 10^{12} – 10^{13} /cm² characteristic of cell interfaces.)

4.3. Entropy-driven repulsion between flexible membranes

A subtle feature of highly flexible membrane structures (e.g., lipid bilayers and red blood cell membranes) is that repulsion is greatly extended by confinement of thermal fluctuations [25–27]. Random microscopic variations in surface contour establish a significant configurational entropy for the membrane. The thermal-bending excitations are collective modes with a continuous spectrum of wavelengths from microscopic to macroscopic dimensions visible to an observer. For instance, red blood cell 'flicker' is the long wavelength manifestation of this 'Brownian' behavior. When membranes are forced into close proximity by attractive fields or mechanical impingement, entropy is confined (i.e. 'heat' is forced out) which requires mechanical work. For unstructured and noninteracting surfaces, the entropy reduction leads to a simple inverse-square law of steric repulsion (predicted many years ago by Helfrich – ref. [25]). However, of even greater consequence for *interacting* surfaces, the superposed action of *all* fields is altered to extend repulsion and diminish attraction [28–29]. The nonclassical effect is clearly evident in the precipitous quench of attraction between weakly charged vesicles (cf. fig. 6). In general, nontrivial calculations are required to predict steric effects when fields are presented; but qualitatively, there

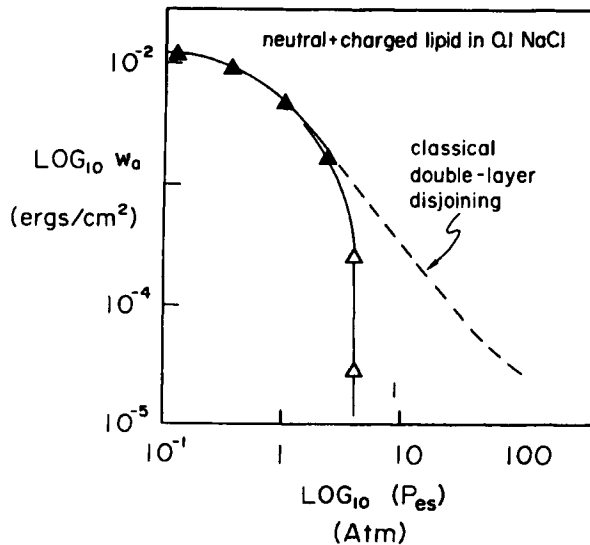


Fig. 6. Free energy potentials (adhesion energies) for adhesion of neutral lipid vesicles with small admixtures (0–6%) of electrically charged lipids in 0.1 M NaCl plotted as a function of the prefactor P_{es} for electric double layer repulsion. Solid triangles represent the strong adhesion regime where behavior is consistent with classical double layer predictions (dotted curve). Open triangles demonstrate the precipitous departure from classical disjoining that results from confinement of thermally excited fluctuations in membrane conformation. No attraction is observed between lipid bilayers that contain more than 1 charged lipid per 15–20 neutral lipids.

is a threshold-like behavior for flexible membrane capsules where the potential for adhesion is cut-off at a low level (e.g. $\sim 10^{-4}$ erg/cm²). Thermal fluctuations moderate adhesion of synthetic surfactant membranes and even highly flexible surfaces of mammalian red blood cells. However, in most cases, the effect can be neglected in the adhesion of cellular organisms. The cell cortex and cytostructure are too rigid to be displaced significantly by thermal excitations.

4.4. Depletion driven attraction

One type of colloid attraction can be significant in biological adhesion: i.e. macromolecular 'depletion' forces. The attraction is similar in origin and functional form – but opposite in sign – to electric double layer repulsion. Depletion forces are driven by *reductions* in osmotic pressure at the midpoint between surfaces which accompany steric exclusion of macromolecular solutes from nonadsorbant interfaces [22]. Because of random molecular motion, the exclusion fields interact at long range to attenuate the concentration in the gap even when separations exceed molecular dimensions. The correlation length ξ of the concentration field establishes the decay length for the depletion force and the osmotic pressure Π_M contributed by the macromolecular constituents sets the magnitude of the interaction. (Note: for

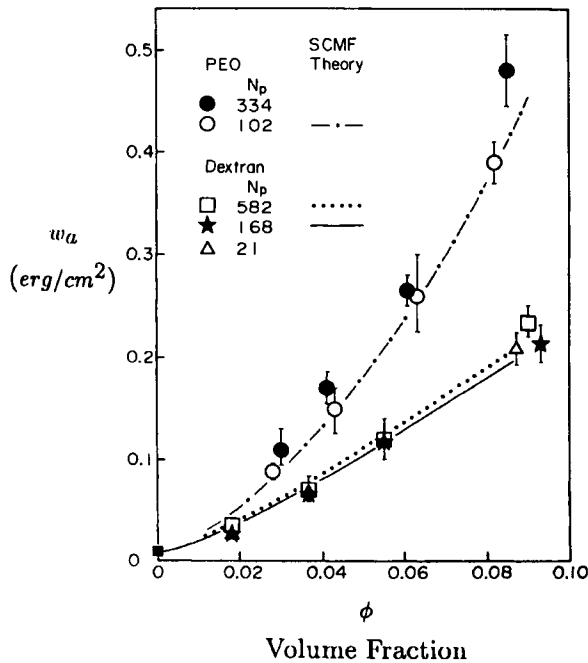


Fig. 7. Free energy potentials (adhesion energies) for adhesion of neutral lipid bilayer vesicles in concentrated solutions of nonadsorbing polymers (dextran and polyethylene oxide PEO). Curves are predictions for the 'depletion' interaction derived from Self Consistent Mean-Field SCMF theory [22]. The intercept at zero volume fraction is the level of adhesion energy produced by Van der Waals forces between the neutral vesicle surfaces. Note: there is no dependence on the size N_p (number of monomer segments) of the soluble polymer as expected for this 'semi-dilute' regime in good solvent conditions.

nonpolymeric macromolecules, molecular size essentially determines the correlation length ξ . However, for large flexible polymers in solution, the decay length is established by volume fraction and 'quality' of the solvent – refs [22] and [30].) Because of the exponential dependence on separation, the potential contributed by depletion forces scales as $\Pi_M \xi$. Hence, concentrated solutions of large polymers can produce strong aggregation of membrane capsules and cells. For example, adhesion of lipid bilayer vesicles in concentrated solutions of dextran and polyethylene oxide polymers demonstrates an enormous increase in potential for aggregation with smooth surfaces (fig. 7). Although much weaker than polymer-driven adhesion, the potential for lipid bilayer vesicle adhesion in plasma proteins (albumin and fibrinogen) also increases in direct proportion to osmotic pressure of the protein solution and protein dimension [22].

In contrast with smooth lipid bilayers, aggregation of red blood cells in concentrated polymer and fibrinogen solutions is characterized by much lower adhesion energies ($\sim 10^{-3}$ – 10^{-2} erg/cm^2); no aggregation is seen in monomeric albumin solutions. Clearly, the important factor is interfacial structure. For cell surfaces, small

molecules like albumin easily penetrate into the glycocalyx to greatly diminish depletion whereas larger species like fibrinogen are excluded from the glycocalyx to extend depletion. This explains why aggregation occurs when polymers of albumin are present. For cell surfaces, the potential for adhesion is reduced both by penetration of the solute into the glycocalyx and electrostatic repulsion between superficial charges. In relation to biology, the important feature is that environments of concentrated proteins in sera and connective tissue gels can contribute 'pressures' to

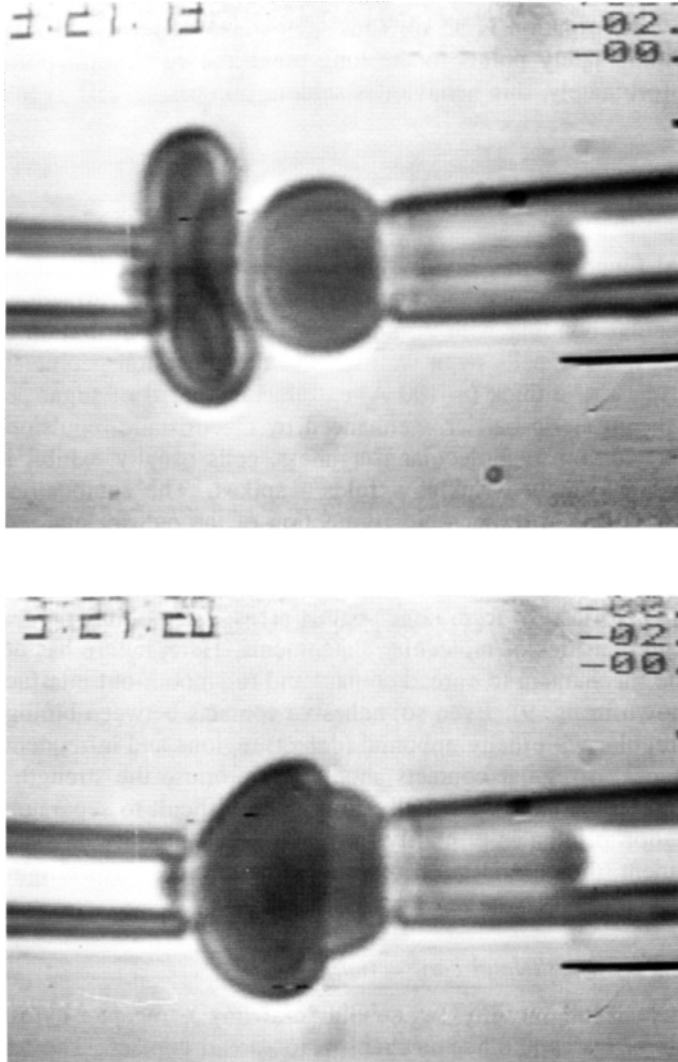


Fig. 8. Spontaneous adhesion and spreading of a red blood cell onto a spherulated red cell surface in a concentrated solution of high molecular weight dextran polymer. Note: the 'ideal' character of the adhesion process is demonstrated by the elastic deformation of the cell where the membrane 'spreading' tension is on the order of the adhesion energy (10^{-3} – 10^{-2} erg/cm²).

draw surfaces closer together when protein solutes are excluded from contact zones. For example, agglutination of cells by antibodies is strongly enhanced in concentrated solutions of nonadsorbing polymers [31]. Similarly, ineffective agglutinins and viruses are often 'potentiated' by polymer solutions [32].

A universal feature of depletion forces is that they lead to ideal adhesion where adhesion energy matches separation (fracture) energy. For example, red cells are elastically deformed by contact spreading in polymer solutions (fig. 8); tension builds-up in the membrane to oppose the adhesion potential. Spontaneity of spreading and cell body deformation is an obvious 'signature' of ideal adhesion which – if observed – immediately points to the long range nature of attraction between the surfaces. Unfortunately, this behavior is seldom (almost never!) seen in biological cell adhesion.

5. Biological adhesion: Contact formation

For biological functions that involve interactions between cells, nature has chosen to suppress the labile-spontaneous action of colloid forces. Attraction is restricted to focal-molecular bonding with no apparent long range contribution from Van der Waals forces. As such, cells seem well stabilized against nonspecific adhesion. The universal presence of a thick (~ 100 Å) extrafacial 'forest' of sugar peptides establishes a significant steric barrier – enhanced by electrostatic repulsion local to the periphery. In addition to molecular roughness, cells usually exhibit large contour roughness in the form of wrinkles – folds – spikes. The contour or 'topographical' roughness is driven by tectonic contraction of the cytoskeletal structure in the cell cortex. The strong steric impedance to adhesion is augmented by mechanical rigidity of the cortex which enables cells to easily avoid adhesion except at very localized promontories. To form large contact areas, a smoothing process is required to achieve high densities of molecular attachments. Here, nature has developed cell motility as the mechanism to spread contact and to smooth-out interfacial asperities (examples shown in fig. 9). Even so, adhesive contacts between biological cells often appear irregular with many unbound (defect) regions and infrequent attachments between surfaces. Irregular contacts should compromise the strength of adhesion. However, cell-cell contacts are usually strong and difficult to separate. Since initial contact formation originates primarily from active cell motility *or* external mechanical impingement, the central question is what determines the strength of adhesion in biology?

5.1. Spreading by cytoskeletal contraction

More subtle than cell motility (amoeboid 'crawling'), receptor-cytoskeletal 'coupling' in cells provides another mechanism to spread contact. The action requires that contractile stresses (tensions) in the subsurface cortical network be transmitted to the intersurface attachments through receptor linkages and that cortical contraction outside of the contact region be much stronger than inside the contact. This differential contraction in the cortex creates a *mechanical* spreading energy given by

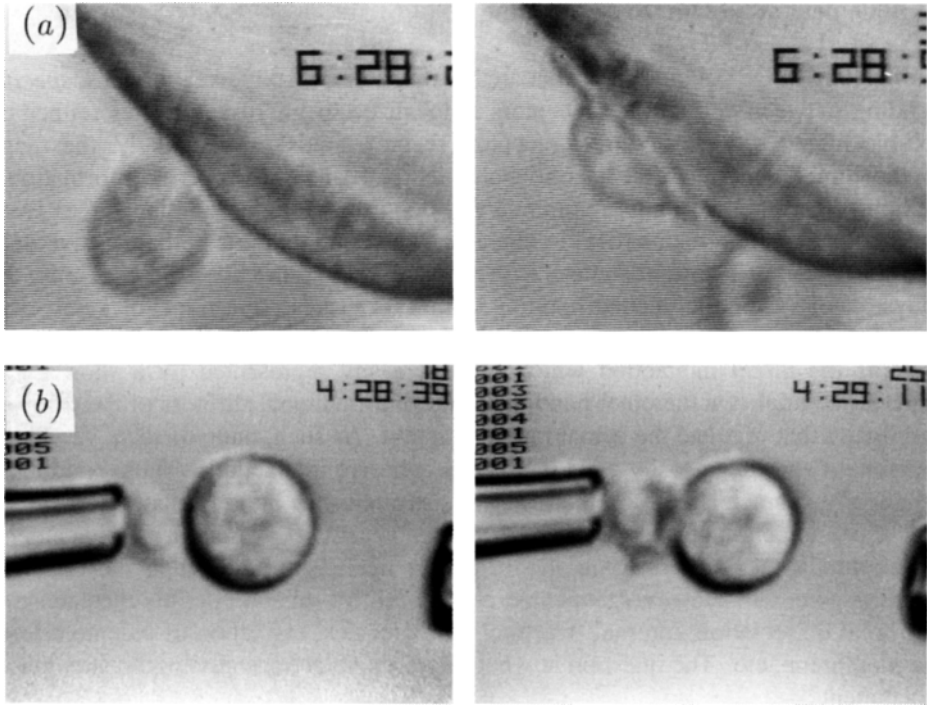


Fig. 9. Examples of the ‘universal’ mechanism that drives biological cell contact formation: video micrographs of a blood granulocyte actively (a) spreading on an endothelial cell surface and (b) engulfing a yeast pathogen.

excess contractile tension $\Delta\tau_N$ in the network. As such, mechanical equilibrium is again approximated by a ‘Young–Dupre’ relation,

$$\Delta\tau_N = (\tau_{Bl} + \tau_N)(1 - \cos\theta_c) \quad (5)$$

where $\tau_m = \tau_{Bl} + \tau_N$ is the total tension contributed by bilayer and network forces, respectively. In this way, binding of cell surface receptors can signal a mechanical transduction to spread contact and stress the adherent cell. To a casual observer, the response would seem like ideal ‘wetting’ (as if driven by a true adhesion energy); but actually the process is driven by cytoskeletal action. An amplifying feature is that surface roughness is diminished to simultaneously promote recruitment of new adhesive attachments and strengthen adhesive contact. Differential contraction in membrane cytoskeletal structures may be an essential mechanism for separation of different cell types in tissue development. Such a mechanism could account for the ‘apparent’ surface energy driven organization of mixed-cell aggregates that was observed many years ago [36]. A major ‘clue’ is that the ‘apparent’ surface energies deduced from measurements of interfacial tension [36] were quite large $\sim 1 \text{ erg/cm}^2$, too large (by at least 10^2 !) to have been created by equilibrium attachments between cell surface receptors. On the other hand, differential contraction in the cytoskeletal structure of cells *can* easily produce mechanical energies of $\sim 1 \text{ erg/cm}^2$.

6. Biological adhesion: Focal bonding

Unlike long range colloid forces that are distributed uniformly over surfaces, *specific* bonding between cell surface receptors is localized to microscopic sites (either by soluble ligand bridges or direct receptor-receptor bonds). Most likely, the range of the direct bonding force is only 'atomic' in scale. However, conformational flexibility and thermal motion combine to extend the range of bonding force. Even so, the attachment remains focal in character where attraction is perhaps active only over distances of a few nanometers. Again different from colloid interactions, the 'physics' of specific molecular bonding cannot be expressed in terms of a universal potential of mean force. Conceptually, local atomic structure of the binding domain governs the direct interaction which is most easily represented by a short range contact potential. On the other hand, it is the conformational stiffness of the receptor and ligand that regulate the actual range of action. As such, unpredictable variations in strength and range easily arise in specific adhesive interactions. Thus, bonding is principally characterized by a thermodynamic affinity for bond formation at contact and a phenomenological rupture force that represents the strength of attachment. Conceptually, the rupture force should be the maximum gradient in the effective bonding potential. However, attachments may fail by several possible mechanisms: i.e. bond dissociation, internal 'fracture' of molecules, extraction of receptors from the membrane, etc. The question is what microscopic actions govern the strength of attachment?

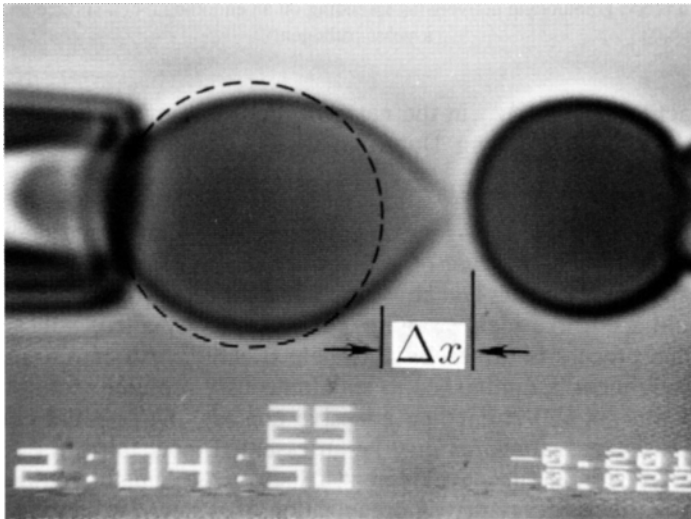


Fig. 10. Video micrograph of a micromechanical measurement of rupture strength for a molecular-point attachment between red blood cell surfaces (formed by an agglutinin cross bridge). Displacement Δx of the pressurized cell on the left provides a direct measure of the force applied to the focal attachment site. Note: the force at detachment was order 10^{-6} dyn (10^{-11} N) and was determined from the membrane tension τ_m plus the displacement Δx (i.e. $f \sim \tau_m \Delta x$).

6.1. Strength of attachment

A significant 'clue' to microscopic determinants of adhesive strength has come from measurements [13] of discrete forces required to rupture focal attachments between red blood cells as demonstrated in fig. 10.³ As shown in fig. 11, the rupture forces grouped around a common value of $1-2 \times 10^{-6}$ dyn (10^{-6} dyn = 10^{-11} N) for several agglutinins (lectin, monoclonal antibody, polyclonal sera) with no obvious dependence on bond chemistry. Surprisingly, this magnitude of rupture force ($\sim \mu$ dyn) is an order of magnitude below values expected for weak hydrogen bonds and well below stronger types of chemical forces! What type of failure process could be so weak and nonspecific in character? The evidence strongly indicated that single molecular attachments (receptors) were extracted from the lipid bilayer core of the membrane. To examine this hypothesis, a comparative fluorescence assay was devised in which either the agglutinin was prepared in advance with a fluorescent label *or* the proteins in a native cell membrane were chemically conjugated with a fluorescent label. Then with each type of label preparation, large contact areas were produced by mechanical impingement of the native red cell against a chemically-rigidified test cell studded with agglutinin. The contacts were separated and the fluorescent 'footprints' left by the labelled constituents were examined to determine the locus of 'fracture'. The results clearly demonstrated that the agglutinin remained bound to receptors and that receptors were extracted from the native cell membrane [13, 31]. In engineering language, fracture of the adherent contact was obviously cohesive material failure not adhesive failure! Interestingly, the appropriate magnitude for the force (to pull a receptor out of a lipid bilayer) was predicted many years ago from simple considerations [33]. Based on theoretical concepts, the force should scale with the perimeter of the attachment (the square root of the number of hydrophobic membrane spanning sequences that form the attachment site) which is relatively insensitive to receptor structure. The lipid bilayer anchoring force establishes a universal threshold for rupture of the focal attachments between cell membranes *unless* adhesive bonds are

³ To isolate microscopic attachments, a pressurized-spherical red cell was 'touched' to a chemically-fixed test cell surface prebound with agglutinin. By significantly reducing the level of agglutinin bound to the test cell, touching at a point only resulted in adhesion in about half of the attempts. This statistic implied that focal adhesion involved only 1 or 2 microscopic agglutinin bridges. When the pressurized cell was retracted by the pipet (fig. 10), the small attachment force deformed the cell until rupture occurred. The observed displacement Δx at the time of rupture provided a direct measure of the peak force for the microscopic contact as readily determined from a simple mechanical proportionality,

$$f_n = k_{\text{RBC}} \Delta x.$$

The elastic 'spring constant' k_{RBC} for red cell extension is approximated by,

$$k_{\text{RBC}} \simeq 2\pi \cdot \tau_m / \{ \ln(2R_0/R_p) + \ln(R_0 \sqrt{\tau_m/k_c}) \},$$

$$\tau_m = \Delta P \cdot R_p / 2[1 - R_p/R_0],$$

where P is the pipet suction applied to pressurize the deformable cell; R_p , R_0 are radii of the pipet lumen and outer spherical portion of the cell, respectively.

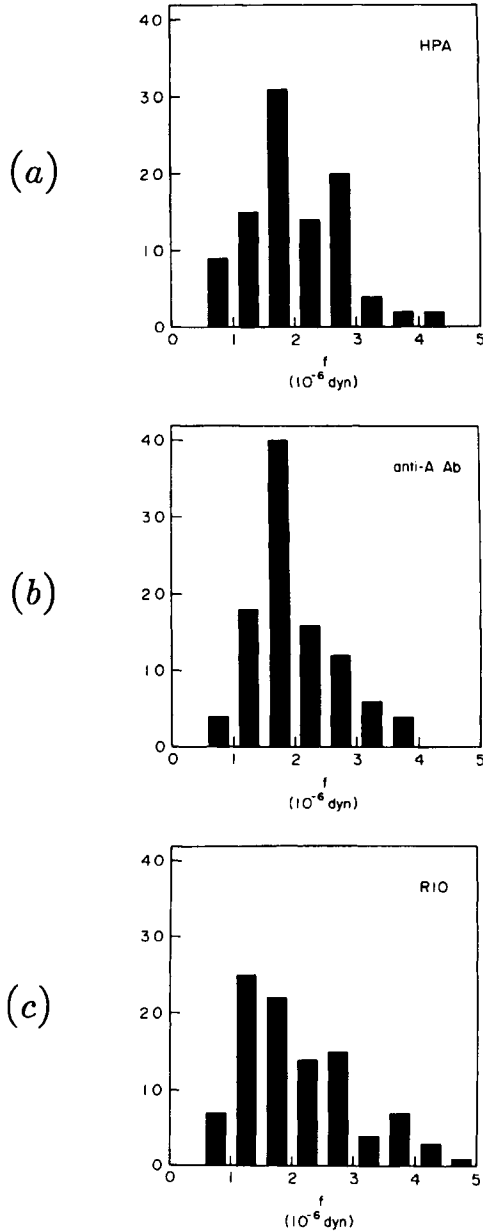


Fig. 11. Summary of forces measured for rapid detachment ($< 1-5$ sec) of red blood cells bonded at microscopic points by three different agglutinins. The cells were retracted at a steady rate of $0.4 \mu\text{m}/\text{sec}$. The histograms cumulate results from tests with cells attached by the following agglutinins: (a) the snail lectin HPA and (b) anti-A serum both of which bind to blood type A antigens (thought to be mostly glycolipids); (c) R10 monoclonal antibody to red cell glycoprotein A (a membrane integral protein).

extremely weak. Most likely, the major determinant of attachment strength is the presence *or* absence of linkage to the cortical cytoskeleton underneath the membrane. Because of the low value of the lipid bilayer anchoring force, it is likely that transient encounters between cells of the immune system and other cells may involve transfer of microscopic components from the weakest cell interface to the strongest. This could be a direct mechanism for cellular communication and perhaps important in ‘recognition’.

6.2. Microscopic dynamics of rupture

Dynamics enters into the mechanics of contact fracture in two ways: First, forces that separate cell contacts act through the viscous materials of cell structure. Second, the microscopic failure of focal attachments involves time-dependent random processes. Cell materials often dominate the time response when adherent cells are separated. In many situations, cell compliance and dissipation compromise mechanical analysis of cell adhesion experiments and lead to unfounded conclusions. However, cell material response is peculiar to cell structure and method of mechanical loading. Thus, these particular features will not be addressed here in order to focus on the more general impact of microscopic processes on dynamic behavior.

When considering microscopic actions, we must keep in mind that biological membranes are ‘soft’ – almost liquid like interfaces – where thermal excitations play a major role in all events. Consequently, the forces observed to rupture focal contacts represent the macroscopic outcome of stochastic events (evident from the spread of forces in fig. 11). A random process for failure of focal attachments is expected to depend on the number of molecular connections within the attachment, magnitude and duration of the externally-applied force, etc. Even for three variables (number of molecular connections, magnitude of the applied force, and time), theoretical description of the random process may not be trivial. However, a simple abstraction provides a rich venue for demonstrating major features of failure. In the simple model, failure is represented by a frequency ν or rate of failure (number of events/time) which is an average over a large ensemble of times to reach failure for single attachments exposed to a specific level of force f [13]. Conceptually, the frequency should increase as the applied force increases; but the dependence on force may be very complicated. Phenomenologically, ‘weak’ versus ‘strong’ dependence on force can be approximated by a power law [13],

$$\nu \approx \nu_0(f/f_0)^a \quad (6)$$

which involves three parameters: intrinsic rate ν_0 and force f_0 for failure, and an exponent ‘a’. For a stationary random process, the probability density for failure (the fraction of molecular attachments that fail within a small increment of time) should decay exponentially with time, i.e.

$$p(t, f) \approx \nu \cdot e^{-\nu t} = \nu_0 \left(\frac{f}{f_0} \right)^a e^{-\nu_0(f/f_0)^a t} \quad (7)$$

following an instantaneous application of force. However, the force can never be applied instantly so this is not the appropriate statistical density to predict experimental observations. In experiments, the force always builds-up at a finite rate, $f = \dot{f} \cdot t$, which implies that the probability density for failure of single molecular attachments will be peaked, i.e.

$$p(t, f) \approx \nu_0 b (\nu_0 t)^\alpha e^{-b(\nu_0 t)^{\alpha+1}/\alpha+1}, \quad (8)$$

$$b \equiv a(\dot{f}/\nu_0 f_0)^\alpha.$$

The likelihood of failure increases initially with time and then decays exponentially. For constant rate of force increase, the forces at rupture in experiments should group around a ‘most frequent’ force \hat{f} that is derived from the time t' where the probability density is maximal (i.e. $\hat{f} = \dot{f} \cdot t'$),

$$\hat{f} \approx f_0(\dot{f}/a\nu_0 f_0)^{1/\alpha+1}. \quad (9)$$

The ‘most frequent’ force is scaled by the intrinsic microscopic force f_0 that underlies the failure process; but the dynamics shows up in the statistics of failure. If the force gradient is steep near failure ($a \gg 1$), the rupture force will depend weakly on the rate of loading \dot{f} . As will be discussed, predictions of the simple microscopic rupture process are qualitatively consistent with the macroscopic dynamics of separation for large agglutinin-bonded regions between red blood cells.

7. Biological adhesion: Macroscopic contacts

As already noted, formation of large contact regions in biological adhesion is driven mainly by external processes (either cell motility or mechanical impingement). The localized action of bonding is obscured by the macroscopic dynamics of cell deformation as contact spreads. The principal resultant of bonding affinity is to establish the surface density \tilde{n}_B (number/area) of binding sites for intersurface attachments. However, the actual density \tilde{n}_a of attachments depends on several mesoscopic factors:

- (i) contour roughness and local mechanical stiffness of the membrane cortex;
- (ii) receptor diffusion and convective transport;
- (iii) receptor-cytoskeletal linkage and cytochemical ‘induction’ (e.g., active insertion and deletion of membrane receptors);
- (iv) steric hindrance by large surface moieties; etc!

Any of these factors can significantly alter the density of attachments. However, one physical factor will be emphasized because it clearly regulates the patency and strength of all cell adhesive contacts: mesoscale roughness and mechanical stiffness.

7.1. Contour roughness, mechanical stiffness and impingement

Topographical roughness is a prominent characteristic of all cell surfaces (even the seemingly-smooth red blood cell) since wrinkles and other irregularities are produced in the plasma bilayer as a consequence of cortical contraction and structure.

These mesoscale contour variations lead to geometric frustration of intersurface attachments. The frustration is compounded by local mechanical rigidity which can prevent the surface from being smoothed by adhesion at promontories. Ideally, the surface pressure of bound receptors should promote contact spreading. For typical values of receptor density on the order of $< 10^{11}/\text{cm}^2$, the maximum spreading pressure is of order $< 4 \times 10^{-3} \text{ erg}/\text{cm}^2$. The spreading action must exceed the local mechanical opposition to deformation in order to smooth the surface. Even in the absence of stiffness from the cytoskeletal cortex, the mechanical energy threshold will be at least the order of membrane bending energy, i.e. k_c/R_c^2 , where $1/R_c$ is the characteristic curvature for a small promontory ($> 10^5 \text{ cm}^{-1}$). Given that $k_c > 10^{-12} \text{ erg}$, the bending energy $k_c/R_c^2 \sim 10^{-2} \text{ erg}/\text{cm}^2$ will exceed the equilibrium potential for contact spreading. (Similarly, fluctuations in local curvature driven by thermal bending excitations can only advance contact when $\tilde{n}_B kT > k_c/R_c^2$.) Hence, roughness becomes trapped by mechanical stiffness – not restricted by lateral mobility of receptors – and is frozen by bonding at the promontories.

Mesoscale roughness and mechanical stiffness clearly impede contact formation and moderate strength of adhesion when red cells are agglutinated by multivalent (bridging) antibodies and lectins [31]. These features are demonstrated in the video microscope images shown in fig. 12. Here, driven by mechanical impingement, large contact regions were agglutinated between red blood cells by monoclonal antibodies and then separated.⁴ As the cells were separated, the peeling tension had to be increased progressively to reduce the contact dimension as shown in fig. 13. Because the detachment angle θ_c remained close to 90° , the peeling tension at the perimeter provided a direct measure of the fracture energy w_f . Consistent with the absence of spontaneous spreading, the initial level of tension was very low ($< 10^{-2} \text{ dyn}/\text{cm}$); but tensions of $\sim 1 \text{ dyn}/\text{cm}$ were necessary to fully detach the cell. The first surprise was that over the thirty-fold range of separation rates accessible to experiment (detachment from seconds to minutes), there was no detectable change in fracture energy! The other surprise was the absence of specific dependence on the type of agglutinin! Progressive strengthening of adhesion with separation appeared to be nonspecific (governed only by the amount of agglutinin prebound to the test cell and magnitude of impingement pressure) and insensitive to peeling rate. There was a clear phenomenological message: an important physical mechanism amplifies adhesive strength as biological cell contacts are separated!

Discussed earlier, the microscopic origin of strength for these agglutinin attachments appeared to be lipid bilayer ‘anchoring’ with a common magnitude for rupture

⁴ In these tests, a chemically rigidified red blood cell (preswollen to form a sphere) was used as an adhesive substrate for attachment of a normal red blood cell. To maximize the availability of attachment sites, monoclonal antibodies or lectins were bound at saturation only to the test particle surface in advance of the experiment. The normal red cell was not exposed to the agglutinin until surface contact. The normal red cell was maneuvered by micropipet to touch the agglutinin studded cell, but the cell only adhered to the test cell at a focal site without spreading. To produce large regions of contact, mechanical impingement was required as shown in fig. 12a. Finally, the flaccid cell was separated from the test cell by mechanical suction into the pipet (fig. 12b). The peeling tension at the perimeter of contact was derived from the suction pressure by straightforward mechanical analysis [34].

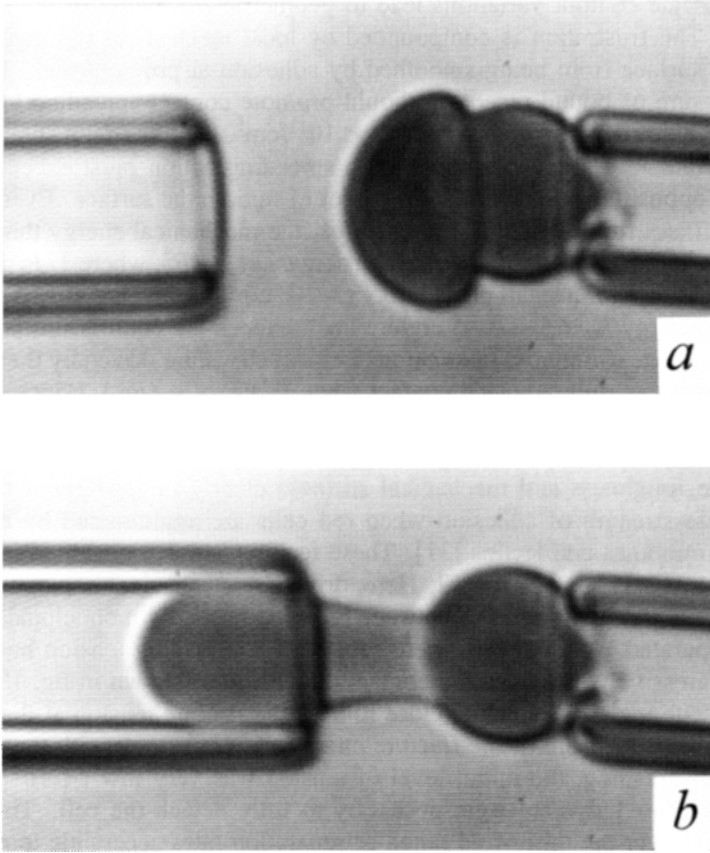


Fig. 12. Video micrographs of micromechanical assembly and detachment of a normal red blood cell to/from a chemically-rigidified red cell prebound with agglutinin molecules (monoclonal antibodies or lectins). The cells were maneuvered to touch and adhered focally but did not spread spontaneously. Subsequent to mechanical impingement (a), the flaccid red cell was detached (b) from the rigid cell by pipet suction. Note the tenacious attachment as evidenced by extreme deformation of the flaccid cell.

force. Taking the rupture force for a single attachment site as constant and of order $\sim 1\text{--}2 \mu\text{dyn}$, it was deduced that the maximum level of peeling tension ($\sim 1 \text{ dyn/cm}$) corresponded to complete bonding of all agglutinin sites local to the contact perimeter. This follows from the maximum number of agglutinin receptors per length of contact given by the square root of surface density; the surface density $\tilde{n}_B \sim 10^6/\text{red}$ blood cell implies the maximum number per length of $10^2/\mu\text{m}$. By comparison, the number of attachments per length of perimeter consistent with the low values of tension at the beginning of contact separation ($\sim 0.01 \text{ dyn/cm}$) would be only a few attachments (< 10) per μm ! The comparison shows that amplification of fracture strength arises from major recruitment of microscopic attachments. What immediately comes to mind is accumulation of receptors driven by lateral forces tangent

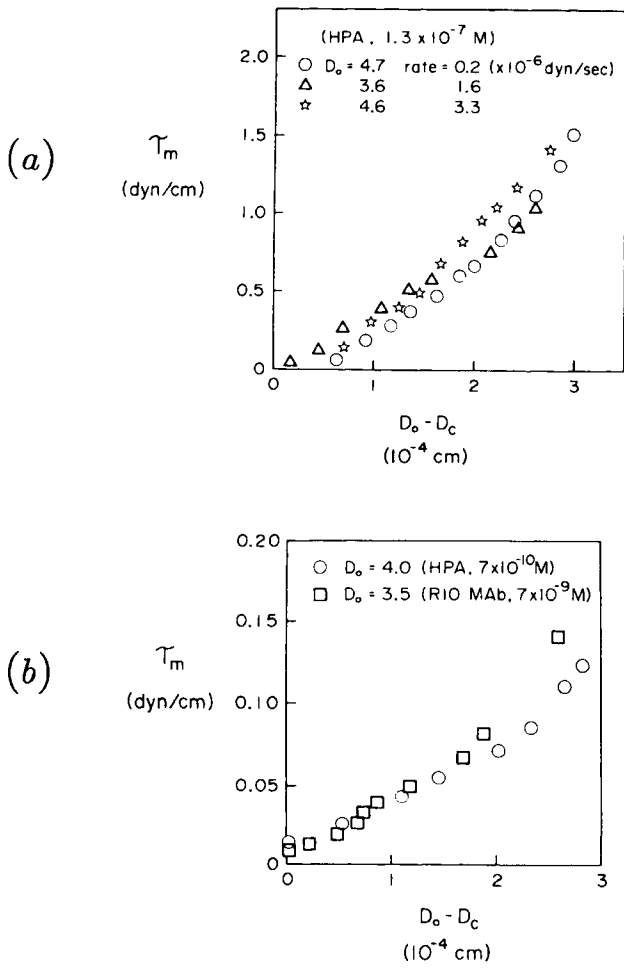


Fig. 13. Fracture energies (given by peeling tension τ_m) plotted versus separation (reduction in contact dimension) for red cell pairs agglutinated by monoclonal antibodies (R10) and snail lectin (HPA) which bind to different membrane receptors. The agglutinin concentrations used to precoat each test cell are given for both sets of experiments. (a) The fracture process appears to be insensitive to the rate of cell detachment. (b) The fracture process appears to be 'nonspecific' with no recognizable dependence on the chemically different agglutinins.

to the membrane (i.e. drag of receptors into the contact zone). Indeed, this often happens when adherent cells are separated [35]. However, for the tests illustrated in fig. 12 (and the results in fig. 13), proteins in the substrate cell had been chemically cross-linked [31]. Thus, the amplification of adhesive strength resulted from a different mechanism. Most likely, attachments were recruited by smoothing interfacial roughness interior to the contact as the cells were separated. Compelling evidence for this hypothesis is the frequent macroscopic observation that large-trapped fluid

pockets ('blisters') disappear from a contact zone during separation. Similarly, numerous mesoscopic defects (irregular attachment) have been seen along adhesive contacts in electron micrographic sections of agglutinated cells [37]. Consistently, mechanical analysis (to be described next) shows that a local mechanical pressure exists to push the surfaces together inside the contact region. Furthermore, the local compression of the contact is accompanied by lateral shear of the membrane relative to the substrate. Clearly, local impingement and tangential smoothing of interfacial roughness will lead to new attachments. The important lesson is that mechanical impingement and interfacial smoothing are *inherent* to the mechanical process of separation for flexible membranes.

7.2. Mesoscale mechanics of fracture

The mechanics of fracture couples macroscopic peeling tension to microscopic attachment forces. The macroscopic consequence of focal bonding is that mechanical stresses (tension and stresses normal to the surface) appear to be discontinuous at the perimeter of the contact region [10]. However, in a conceptually magnified view (as illustrated in fig. 14), membrane tension remains continuous along the contour; the detachment force f is produced by local bending stress derived from gradients (dc_m/ds) of membrane curvature, i.e.

$$Q_m \approx k_c \frac{\partial c_m}{\partial s} \approx f \sqrt{\tilde{n}_a}. \quad (10)$$

The attachment force per length of perimeter is $\sqrt{\tilde{n}_a} \cdot f$ given the surface attachment density \tilde{n}_a . In turn, local bending stresses are coupled to the macroscopic peeling tension τ_m through a leverage factor $\sin \theta_c$; again θ_c is the 'apparent' contact angle observed macroscopically. As such, the peeling tension becomes proportional to the average bond force along the perimeter, i.e.

$$\tau_m \sin \theta_c \approx f \sqrt{\tilde{n}_a}. \quad (11)$$

Two mechanical corollaries accompany the relation between tension and attachment force. First of all, the peeling tension creates small lateral forces f_t on attachments (as well as direct extensional forces f). The lateral force is produced by a small deviation of the detachment force from the local membrane normal (i.e. the surfaces are not exactly parallel at the perimeter of the contact). From mechanical analysis [10], the deviation angle θ^* and the lateral force $f_t \sim f \cdot \theta^*$ are predicted to depend on membrane bending stiffness and the effective range l_B for action of single attachments. The result is that the deviation angle is a very weak function of peeling tension,

$$\theta^* \sim l_B^{1/2} (\tau_m / k_c)^{1/4}.$$

Hence, the lateral force is essentially proportional to peeling tension but small in magnitude. In the absence of cytoskeletal restrictions, these lateral forces drive receptors to accumulate at the contact perimeter.

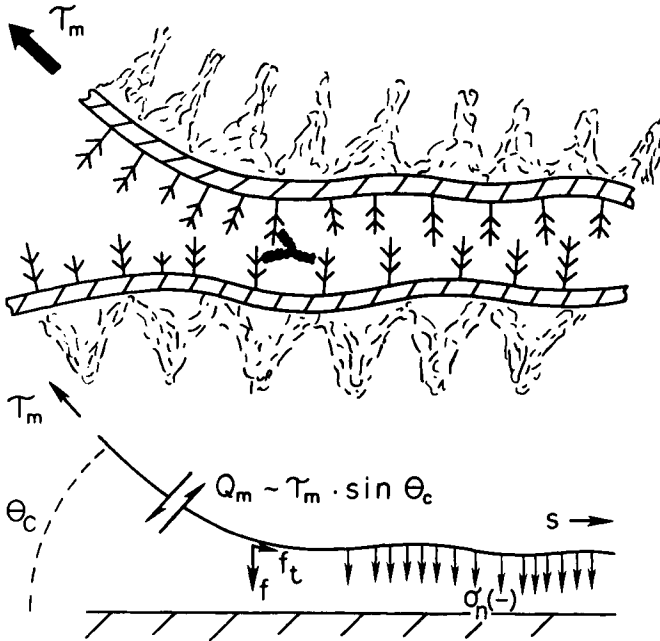


Fig. 14. Schematic of ‘mesoscale’ fracture for membranes bonded by focal-molecular attachments (symbolized by ‘Y’ in the upper sketch). Membrane bending stress Q_m at the perimeter of the contact creates the force f to detach the focal bond and a tangential force f_t acts to drag the attachments into the contact. Bending about the focal bond leads to a normal-compressive stress σ_n (pressure) that pushes the surfaces together.

Second, peeling produces a normal-compressive pressure on the membrane interior to the contact. Attachments along the perimeter form a ‘fulcrum’ around which membrane bending forces create an impingement pressure inside the contact. This pressure pushes the membrane surface towards the substrate surface over a narrow region d_c (governed by the bond extension l_B and local radius of curvature $-R_c$) with a magnitude σ_n that scales as,

$$d_c \sim l_B^{1/2} (k_c / \tau_m)^{1/4},$$

$$\sigma_n \sim -Q_m / d_c \sim -\tau_m (\tau_m / k_c l_B^2)^{1/4}.$$

The impingement pressure easily reaches the level of 1 Atm (10^6 dyn/cm²) when tensions are large (~ 1 dyn/cm). Importantly, impingement locally smoothes the irregular membrane contour and promotes recruitment of new attachments inside the contact zone.

The mesoscale mechanics predicts that peeling tensions should lie between specific bounds: i.e. a minimum level of tension below which the membrane contact can spread by local bonding *and* a maximum level of tension above which the membrane

is detached from the substrate. The ‘adiabatic’ (kinetically-trapped) mechanical limits expose the *nonideal* character of the adhesion process and are expressed by the following inequality (neglecting trigonometric factors of contact angle):

$$k_c l_B^2 \tilde{n}_B^2 < \tau_m < \hat{f} \sqrt{\tilde{n}_a}.$$

Therefore, the membrane tension ranges between a lower value governed by the paucity of attachments and an upper value established by the peak force \hat{f} required to rupture attachments. The lower bound is dictated simply by the requirement that the curvature of the membrane contour proximal to the contact perimeter must be ‘flattened’ sufficiently to allow formation of new attachments at a distance of $(1/\tilde{n}_a)^{1/2}$ beyond the perimeter *and* within the range l_B of bonding action. When practical values are introduced for these parameters, the level of tension compatible with contact spreading is less than 10^{-3} dyn/cm. By comparison, the level of tension necessary to peel the contact apart can easily reach 1 dyn/cm when microscopic rupture forces are on the order of 10^{-6} dyn or more. Phenomenologically, the *strength* of adhesion is determined by both the rupture force \hat{f} and the density \tilde{n}_a of attachment sites. If the attachment strength remains constant throughout contact separation, the level of tension required to separate an adhesive contact will be governed primarily by the local density of attachments. As already emphasized, the subtle aspect is that the rupture force \hat{f} may be unrelated to the chemistry of the bond that initiated attachment. The rupture force measures the failure of the weakest component in the adhesion complex!

8. Summary comment

As described in the text, biological cell adhesion is a complex situation which (except in rare cases) cannot be treated as an ideal ‘wetting-like’ process. Consequently, it is not possible to write down a set of universal ‘laws’ that explicitly cover all cell adhesion phenomena. The objective here has been to expose unconventional features of biological cell adhesion and to relate microscopic actions to macroscopic behavior. Although important aspects have been overlooked, major physical determinants have been identified which are expected to be involved in every cell adhesion process.

Acknowledgement

The author gratefully acknowledges the support of the US National Institutes of Health through grants HL45099, HL31579, and the Canadian Medical Research Council through grant MT7477. The author is an Associate in the ‘Science of Soft Surface and Interfaces’ Program sponsored by the Canadian Institute for Advanced Research.

References

1. Springer, T.A., 1990, *Nature* **346**, 425.
2. Ruoslahti, E. and M.D. Pierschbacher, 1987, *Science* **238**, 491.

3. Kishimoto, T.K., R.S. Larson, A.L. Gorbi, M.L. Dustin, D.E. Staunton and T.A. Springer, 1990, in: *Leukocyte Adhesion Molecules*, eds T.A. Springer et al. (Springer, New York) p. 7.
4. Lawrence, M.D. and T.A. Springer, 1991, *Cell* **65**, 859.
5. Cunningham, B.A., J.J. Hemperly, B. Murray, E.A. Prediger, A. Brackenbury and G.M. Edelman, 1987, *Science* **236**, 799.
6. Dustin, M.L. and T.A. Springer, 1991, *Annu. Rev. Immunol.* **9**, 27.
7. Takeichi, M., 1991, *Science* **251**, 1451.
Magee, A.I. and R.S. Buxton, 1991, *Curr. Opin. Cell Biol.* **3**, 854.
8. Adamson, A.W., 1982, *Physical Chemistry of Surfaces* (Wiley, New York).
9. Bell, G.I., M. Dembo and P. Bongrand, 1984, *Biophys. J.* **45**, 1051.
Hammer, D.A. and D.A. Lauffenburger, 1987, *Biophys. J.* **52**, 475.
Cozens-Roberts, C., D.A. Lauffenburger and J.A. Quinn, 1990, *Biophys. J.* **58**, 841.
10. Evans, E.A., 1985, *Biophys. J.* **48**, 175.
Dembo, M., D.C. Torney, K. Saxman and D.A. Hammer, 1988, *Proc. R. Soc. London Ser. B* **234**, 55.
11. Jacobson, K., A. Ishihara and R. Inman, 1987, *Annu. Rev. Physiol.* **49**, 163.
Vaz, W.L., Z.I. Derzko and K.A. Jacobson, 1982, *Cell Surf. Rev.* **8**, 83.
12. Capo, C., F. Garrouste, A.-M. Benoliel, P. Bongrand, A. Ryter and G.I. Bell, 1982, *J. Cell Sci.* **56**, 21.
13. Evans, E.A., A. Leung and D. Berk, 1991, *Biophys. J.* **59**, 838.
14. Evans, E. and R. Skalak, 1980, *Mechanics and Thermodynamics of Biomembranes* (CRC Press, Boca Raton, FL).
Flügge, W., 1966, *Stresses in Shells* (Springer, New York).
15. Evans, E., 1990, **43**, 327.
16. Bloom, M., E. Evans and O.G. Mouritsen, 1991, **24**, 293.
17. Evans, E.A., 1980, *Biophys. J.* **30**, 265.
Skalak, R., P.R. Zarda, K.-M. Jan and S. Chien, 1981, *Biophys. J.* **35**, 771.
18. Seifert, U. and R. Lipowsky, 1990, *Phys. Rev. A* **42**, 4768.
19. Verwey, E.J.W. and J.Th.G. Overbeek, 1948, *Theory of the Stability of Lyophobic Colloids* (Elsevier, Amsterdam).
20. Parsegian, V.A., 1975, in: *Physical Chemistry: Enriching Topics from Colloid and Surface Chemistry*, eds J. van Olphen and K.J. Mysels (Theorex, La Jolla, CA) p. 27.
Mahanty, J. and B.W. Ninham, 1976, *Dispersion Forces* (Academic Press, London).
21. Israelachvili, J., 1985, *Intermolecular and Surface Forces* (Academic Press, San Diego, CA).
22. Evans, E. and D. Needham, 1988, *Macromolecules* **21**, 1822.
Evans, E., 1989, *Macromolecules* **22**, 2277.
Evans, E., D. Needham and J. Janzen, 1987, in: *Proteins at Interfaces*, eds J.L. Brash and T.A. Horbett, *ACS Symposium Series* **343**, 88.
23. Evans, E. and D. Needham, 1987, *J. Phys. Chem.* **91**, 4219.
24. LeNeveu, D.M., R.P. Rand, V.A. Parsegian and D. Gingell, 1977, *Biophys. J.* **18**, 209.
Parsegian, V.A., N.L. Fuller and R.P. Rand, 1979, *Proc. Nat. Acad. Sci. USA* **76**, 2750.
25. Helfrich, W., 1978, *Z. Naturforsch.* **33A**, 305.
26. Lipowsky, R. and S. Leibler, 1986, *Phys. Rev. Lett.* **56**, 2541.
27. Evans, E. and V.A. Parsegian, 1986, *Proc. Nat. Acad. Sci. USA* **83**, 7132.
28. Evans, E., 1991, *Langmuir* **7**, 1900.
29. Lipowsky, R. and U. Seifert, 1991, *Langmuir* **7**, 1867.
30. Joanny, J.F., L. Leibler and P.G. de Gennes, 1979, *J. Polym. Sci. Polym. Phys. Ed.* **17**, 1073.
31. Evans, E., D. Berk, A. Leung and N. Mohandas, 1991, *Biophys. J.* **59**, 849.
32. Jandl, J.H. and W.B. Castle, 1956, *J. Lab. Clin. Med.* **47**, 669.
Haywood, A.M. and B.P. Boyer, 1986, *Biochemistry* **25**, 3925.
33. Bell, G.I., 1978, *Science* **200**, 618.
34. Berk, D. and E. Evans, 1991, *Biophys. J.* **59**, 861.
35. Evans, E. and A. Leung, 1984, *J. Cell Biol.* **98**, 1201.
Tozeren, A., K.-P. Sung and S. Chien, 1989, *Biophys. J.* **55**, 479.

36. Steinberg, M.S., 1970, *J. Exp. Zool.* **173**, 395.
Steinberg, M.S. and D.R. Garrod, 1975, *J. Cell Sci.* **18**, 385.
37. Coakley, W.T., L.A. Hewison and D. Tilley, 1985, *Eur. Biophys. J.* **13**, 123.

Adhesion of Cells

P. BONGRAND

*Laboratoire d'Immunologie,
Hôpital de Sainte-Marguerite,
BP29, 13277 Marseille Cedex 09, France*

Contents

1. Introduction	757
2. Representative models of cell adhesion	758
2.1. Interaction between cytotoxic T lymphocytes and target cells	758
2.2. Neutrophil adhesion to endothelium	761
2.3. Interactions between cells and artificial surfaces	764
3. Biophysical characterization of cells	769
3.1. Cell shape control	770
3.2. Cell surface roughness: the submicrometer scale	773
3.3. Relevance of the concept of surface tension to biological membranes	776
3.4. Molecular structure of the cell surface	777
4. Models for the sequential steps of cell adhesion	783
4.1. Cell-cell approach	783
4.2. Initiation of adhesion	790
4.3. Analysis of the 'equilibrium' shape of cell-cell contacts	794
4.4. Cell-cell separation	795
Conclusion	796
References	796

1. Introduction

Cell adhesion is a fascinating process. First, it plays a key role in many situations of biological and medical interest. Secondly, it is probably the best cell function to be considered for biophysical modeling from the micrometer to the molecular level. Thirdly, studying the biophysical aspects of cell adhesion leads to face many important problems of physics and physical chemistry as well as cell physiology.

There are at least two ways of approaching the problem of cell adhesion. A first strategy would be to perform a thorough study of a simplified model likely to share some fundamental properties with biological systems. Far reaching results were obtained along this line by studying adherence-induced deformations of individual conjugates made between lipid vesicles and/or red cells of known mechanical properties [28, 66]. As another example, detailed studies of the motion of antibody-coated red blood cells in controlled hydrodynamic flow yielded important information on the formation and rupture of intercellular bonds [169].

The aforementioned approaches yielded very useful data, and improved both biological and physical knowledge. However, several parameters likely to influence the adhesive properties of nucleated cells cannot be explored with model vesicles or even erythrocytes. Thus, the lateral displacements of adhesion molecules depend on cytoskeletal constraints [168] and active cell processes [176] that are clearly quite different in blood leukocytes and red cells. Further, whereas erythrocytes are fairly smooth at the submicrometer level, nucleated cells are studded with a variety of protrusions, blebs, ruffles, microvilli or lamellipodia with complex mechanical behavior and an obvious influence on adhesive interactions [129]. It seems therefore warranted to study biologically relevant models with available experimental and theoretical tools, even if data interpretation is less clearcut than with simpler systems. Indeed, understanding cell adhesion first requires that we identify the key parameters influencing this process and obtain reliable order-of-magnitude estimates for them.

The aim of the present review is to gather biological and biophysical data that are widely scattered in the literature, in order to allow biophysicists with a general knowledge of cell biology to assess the relevance of current physical concepts to cell adhesion. Hopefully, this might be useful to anyone willing to start research in this field. Therefore, we refer the reader to other reviews for a basic description of intermolecular forces [98] and their relevance to biological systems [22–24] as well as methods for studying cell adhesion [42].

First, we shall discuss some biological models of cell adhesion (with a bias related to the author's field of interest) in order to convey a quantitative feeling for the phenomena we are willing to study.

Secondly, we shall review some experimental data that may help build a working model of the basic 'adhering cell'.

Thirdly, we shall discuss the sequential steps of cell adhesion and current physical theories that are relevant to the involved mechanisms.

2. Representative models of cell adhesion

It is difficult to describe cell adhesion in some detail without referring to well defined biological models. Indeed, quite different parameters are expected to play a critical role in diverse situations. For example, the rapid adhesion of leukocytes to endothelial cells in flowing blood should not be modeled in the same way as the slow spreading of fibroblasts on culture dishes.

We shall describe three models of potential interest for biophysicists with some basic references allowing easier access to recent literature. Completeness was deliberately sacrificed for the sake of clarity.

2.1. Interaction between cytotoxic T lymphocytes and target cells

Cytotoxic T lymphocytes (CTLs) are able to recognize specific targets with exquisite specificity. Thus, they can detect infected cells expressing minute amounts of viral components on their membrane. The cytotoxic process involves sequential steps that were described in several excellent reviews [18, 93]. First, the CTL binds to the target, forming a 'conjugate' (fig. 1). Then, during the following 10–15 minutes, it inflicts on the target an irreversible damage, called the 'lethal hit': this probably includes a combination of events such as secretion of lytic molecules (e.g., perforin), fas-based signalling, possibly mechanical damage [86, 93]. The lethal hit does not provoke immediate morphological transformation of the target [93, 181]. However, a few tens of minutes after the recognition stage, the CTL spontaneously separates from its prey [148] which will disintegrate during the following 2–3 hours.

Many studies were devoted to the binding stage of T cell-mediated cytotoxicity. Adhesion may occur within a few seconds after intercellular contact, and electron microscopy revealed tight interactions between membranes in contact areas [103]. In a quantitative kinetic study, CTLs and target cells were centrifuged and different samples were processed at regular intervals for optical and electron microscopical study [76]. Numerous conjugates were found as soon as 60 seconds after contact formation, with a maximum 30 minutes later. Maximum membrane apposition was achieved within one minute, with apparent contact areas of the order of 10–20 μm^2 . (These areas were defined as the regions where CTL and target membranes were separated by a gap thinner than 250 nm on electron micrographs.)

In other series of experiments, the mechanical strength of adhesion was estimated by subjecting conjugates to calibrated laminar flows of increasing velocity. The shear rate required to disrupt 50% of conjugates was about 100,000 s^{-1} [26, 27], corresponding to a maximum separating force of [22]:

$$F = 19.2\mu a^2 G = 3 \times 10^{-8} \text{ newton} \quad (1)$$

where μ is the medium viscosity, a is the cell radius and G is the shear rate. This represents an upper limit for the actual separating force since cell doublets were

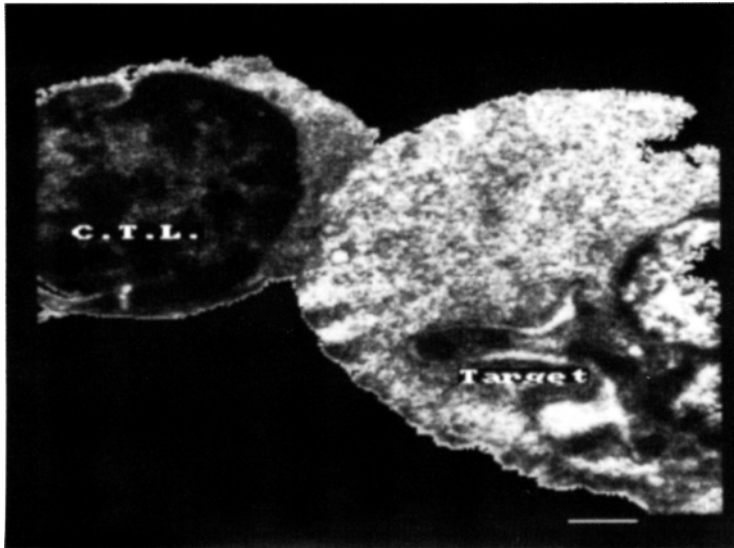


Fig. 1. Interaction between a cytotoxic *T* lymphocyte and target cell. A typical conjugate made between a murine cytotoxic *T* lymphocyte (CTL) of C57BL/6 origin and a specific target cell (S194 myeloma cell) was processed for electron microscopy as described in ref. [76]. Extensive membrane apposition is apparent in the contact area. Bar is 1 μm .

probably oriented at random with respect to the velocity gradient, and this gradient was not spatially uniform. It was shown that this force was close to the cell membrane resistance, and conjugate disruption was often associated to target rupture [26].

In other studies [165, 172], conjugates were formed between individual CTLs and targets maintained on the tip of glass micropipettes by moderate aspiration. After 10 minute contact, the pipette holding the CTL was pulled away by micromanipulation, with increasing pressure. The minimal aspiration pressure required to break the conjugate was recorded. The maximal axial pipette force was about 4×10^{-9} N. This is not inconsistent with hydrodynamic data since

- i) marked differences are found between diverse populations of CTLs and target cells, and
- ii) the hydrodynamic force was exerted on the conjugates during a very brief time, and an inverse relationship was found between the minimum intensity and duration of application of the force required to rupture cell-substrate bonds [128].

In addition to the availability of quantitative data, the CTL model is of particular interest since extensive studies were devoted to the identification of adhesion molecules involved in conjugate formation. Adhesion is indeed achieved by combination of several binding mechanisms. See table 1 for more information on some important adhesion molecules.

Table 1
Properties of some molecules involved in leukocyte adhesion.

Name	Distribution	Ligand(s)	Length (nanometer)	Structure	Functional properties	Reference
Intercellular adhesion molecule 1 (ICAM-1)	Leukocyte, endothelium	LFA-1	18.7	single chain 90–110 kd		[160, 161]
Lymphocyte, function associated 1 (LFA-1, CD11a/CD18)	Leukocytes	ICAM-1, 2, 3	20	α chain 180 kd β 2 chain 95 kd	regulated by cell activation transduces costimulatory signal	[97, 160]
E-selectin (ELAM-1)	Endothelial cells	sialyl lewis X	28	protein 115 kd		[19, 160]
T cell receptor	T lymphocytes	peptide+ histocompatibility molecule	8	multichain, recognition by heterodimer 2 \times 30 kd	several activation pathways	[182]
CD8 (Lyt2/Lyt3)	T lymphocyte subpopulation	class I histocompatibility	\approx 20	homomultimer 34 kd	adhesion+signal transduction	[20, 160]
Major histocompatibility class I molecules (HLA-A, B, C)	ubiquitous	peptide and CD8	< 10	β 2-microglobulin + α chain 45 kd	Signal ?	[21]

We list some properties of adhesion molecules referred to in text. ICAM-1 belongs to the immunoglobulin superfamily. LFA-1 is a β 2 integrin found on leukocytes together with MAC-1 (Mo1, CR3, CD11b/CD18) and p150/95 (CD11c/CD18). The recently defined selectin family includes E-selectin, P-selectin (CD62, PADGEM, GMP140), transiently expressed by activated platelets and endothelial cells, and L-selectin (LAM-1, MEL-14) expressed on leukocytes.

L-selectin is the major ligand of E-selectin on neutrophils.

First, specific recognition results from the association between T-cell receptors on the CTL and antigenic structures on the target. In physiological situations, these structures are usually complexes made between class I major histocompatibility complex (MHC) molecules and oligopeptides resulting from partial degradation of foreign material. In this case, only a minor fraction of the hundreds of thousands of MHC molecules [112] on the target membrane may be associated to a polypeptide antigen. Indeed, as few as 200 such complexes may suffice to allow recognition [35]. However, for practical reasons, many experiments were done with CTLs specific for allogeneic cells. In this case, a different proportion of target MHC class I molecules may serve as binding sites (this was the case in aforementioned determinations of binding strength).

The exquisite sensitivity of CTL recognition is due to the frequent involvement of accessory ligand molecules. Thus, CD8 molecules on the CTL will bind MHC class I molecules on the target. It was indeed shown that the overexpression of CD8 on transfected cell lines was sufficient to induce conjugate formation [139]. The accessory role of CD8/MHC interaction in CTL-target binding is supported by experimental data suggesting that CTLs with high affinity antigen receptor were less dependent on CD8 than CTLs with lower affinity [110].

In addition, CTLs are endowed with several accessory antigen-independent adhesion pathways [158]. LFA-1 molecules expressed on the CTL membrane will bind to ICAM molecules that are present on many target cells (table 1). A peculiarity of this adhesion system is that LFA-1 molecules must be activated before they can bind their ligand. Many activation pathways were described, including T-cell receptor (TCR) engagement after ligand recognition [140]. Other adhesive couples, such as CD2 (on the CTL) versus LFA3 (on the target) were described [158]. However, a more complete description of CTL adhesion would not fall within the scope of the present review.

A final point of interest in this model is the demonstration that conjugate formation usually results in marked redistribution of adhesion-involved and adhesion-independent molecules in cell-cell contact area. This redistribution was expected as a thermodynamic consequence of binding affinity and lateral mobility of membrane molecules [16]. Further, micromanipulation experiments showed that the affinity between CTL and target membranes increased when the contact area decreased, during contact disruption [172], which might be viewed as a consequence of the increase of bond density in the shrinking contact area. Finally, qualitative [109] and quantitative [6] immunofluorescence studies demonstrated about twofold increase of adhesion molecules in contact areas between target cells and CTLs.

2.2. Neutrophil adhesion to endothelium

The adhesion of blood granulocytes (fig. 2) is of high interest for several reasons. First, this is a key event in acute inflammation. Secondly, our knowledge of the adhesion molecules involved in this model exhibited a dramatic progress during the last few years [191]. Thirdly, many biophysical studies were done on the mechanical properties of blood granulocytes [134], thus allowing easier elaboration of quantitative models for adhesion. Fourthly, the physiological conditions of granulocyte

adhesion are relatively well known. Indeed, many remarkable studies were done on blood flow in capillary vessels, using intravital microscopy [11, 123, 154, 166]. This point is of importance, since it is now widely accepted that different binding molecules can be involved in adhesion at rest and under dynamic conditions [14]. Here are some points of interest.

In normal blood, about 50% of granulocytes are adhering to the vessel surface (this is the so-called margined pool), and half are flowing. Local adhesion may be rapidly induced by a complex modulation of the expression of adhesive molecules on the surfaces of granulocytes and endothelial cells.

There are two main groups of adhesive interactions [191]: first, leukocyte β 2-integrins (i.e. LFA1 also called CD11a/CD18, Mac-1 or CD11b/CD18, and p150-95 or CD11c/CD18) will bind ICAMs that are constitutively expressed on endothelial cells (table 1). As mentioned above, some kind of leukocyte activation is required for this binding. Secondly, lectin-sugar interactions may occur. Lectin molecules are inducible P-selectin (GMP140, CD62, PADGEM) and E-selectin (ELAM-1) on endothelial cells and L-selectin (LAM-1) constitutively expressed by neutrophils (see [160] for an illuminating review on these adhesion molecules). All these selectins were recently reported to recognize a common carbohydrate epitope that may be expressed by different molecules on cell membranes [77].

Now, leukocyte-endothelium adhesion is expected to be easiest in postcapillary venules where the shear rate G is minimal (see fig. 3 for definitions). Reported values of the wall shear rate G_w in these venules range between 100 and 1000 s^{-1} [11, 123, 154, 166]. According to the definition of G_w , the fluid velocity at distance d from the vessel wall is the product $G_w d$. As will be explained below, the velocity of a cell of radius a close to the vessel surface is expected to be in the order of



Fig. 2. Granulocyte-endothelium interaction in a laminar chamber flow. Human granulocytes (arrow) were subjected to a laminar shear flow (shear rate $4 s^{-1}$) in a previously described chamber [170]. The chamber floor is coated with human umbilical endothelial cells [193]. Bar is 10 μm .

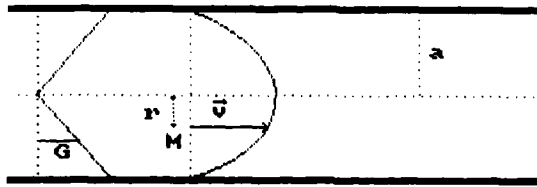


Fig. 3. Laminar flow through a cylindrical pipe. The velocity \vec{v} is everywhere parallel to the duct axis. At any point M separated from this axis by a distance r , one has $v(r) = 2Q(a^2 - r^2)/\pi a^4$, where Q is the flow rate (in m^3/s) and a the duct radius. The velocity is thus zero at the wall and attains its maximum on the axis. The shear rate $G = |dv/dr|$ is linearly dependent on r , with its maximum value at the wall and zero value on the axis.

$G_w a$ if there is no tight apposition between the cell and the endothelium. Hence, the velocity of a typical flowing granulocyte of radius $4 \mu\text{m}$ is expected to be higher than several hundreds of $\mu\text{m}/\text{s}$. Also, the viscous force exerted on a bound spherical cell of radius a is [22]

$$F = 32\mu a^2 G_w \quad (2)$$

where μ is the medium viscosity, a the cell radius and G the shear rate. This yields a dragging force ranging between 5×10^{-8} and 5×10^{-7} N.

Now, a remarkable observation made in *in vivo* studies [123, 166] was that a notable proportion of granulocytes 'rolled' with a translation velocity ranging between 10 and about $50 \mu\text{m}/\text{s}$, i.e. about ten times lower than expected. This rolling phenomenon was inhibited by infusion of polyelectrolytes such as protamin and sulfated polysaccharides [166].

Recently, much information was obtained on this phenomenon by Lawrence and Springer who studied the movement of neutrophils subjected to a laminar shear flow along a surface coated with various amounts of purified ICAM and P-selectin molecules, acting respectively as ligands for the leukocyte $\beta 2$ -integrins and LAM-1. This was done in a flow chamber allowing continuous monitoring of cell movement [111]. The translation velocity U of many leukocytes moving close to the wall was about $500 \mu\text{m}/\text{s}$ when the wall shear rate was about 250 s^{-1} , corresponding to a ratio $U/G_w a$ of about 0.5 (where a is the cell radius). This result may be compared to theoretical estimates obtained by Goldman et al. [78] who studied the movement of a neutrally buoyant sphere subjected to a laminar shear flow near a plane surface (fig. 4). The estimated value of $U/G_w a$ varied between 0.68 and 0.45 when the ratio δ/a between the cell-to-surface gap and the cell radius varied between 0.045 and 0.003 (i.e. $0.18 \mu\text{m}$ and 12 nm for a cell of $4 \mu\text{m}$ radius). Although the relevance of Goldman's results to the movement of actual cells may be questioned (see [170] for an experimental check of the theory), it may be concluded that the aforementioned velocity is indicative of a rather unconstrained motion.

Further, when the surface was coated with P-selectin, a proportion of cells exhibited much lower translational velocities of a few $\mu\text{m}/\text{s}$, with visible rolling. However, the

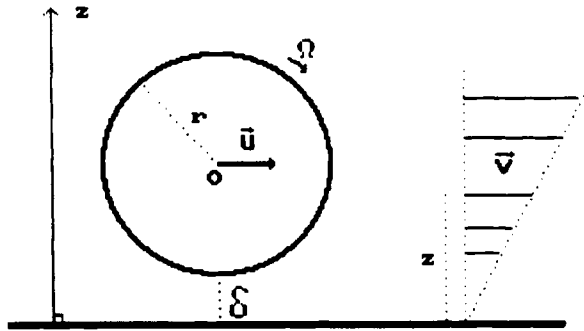


Fig. 4. Motion of a sphere subjected to a laminar shear flow near a plane surface. The motion of a neutrally buoyant sphere subjected to a laminar shear flow near a plane surface was determined by Goldman et al. [82]. The displacement is a combination of a translation with velocity U parallel to the wall and angular velocity Ω . When the distance δ between the sphere and the wall becomes small, the dimensionless ratios U/Gr and Ω/G decrease very slowly, as $1/\ln \delta$.

P-selectin could not induce strong adhesion: if the flow was stopped and resumed several minutes later, cells started to roll again.

In contrast with the above data, when activated leukocytes were driven along an ICAM-1-coated surface with substantial flow rate, no rolling nor attachment was observed. However, if cells were deposited on the same surface under static conditions, they readily spread within 5 minutes, and they remained bound when the flow was resumed. Finally, attachment under flow conditions could occur when the surface was coated with both ICAM-1 and P-selectin. Hence, selectins can induce rapid but transient adhesion, whereas integrins can form strong adhesions provided the interaction time is fairly long. Possible explanations for the different behavior of these molecular species will be discussed in section 4.

2.3. Interactions between cells and artificial surfaces

The increasing practice of cell culture was a strong incentive to study the mechanism of interaction between different cell populations and culture dishes (fig. 5). Also, the use of artificial polymers for medical purpose (e.g., as implants in dentistry or surgery, as contact lenses in ophthalmology, as dialysis membranes in nephrology) triggered strong interest for the relationship between the surface properties of polymers, cell adhesion and spreading. In the present section, we shall describe some basic data. Biophysical approaches relevant to these problems will be reviewed in section 4.

2.3.1. Surface energy

Much experimental evidence suggests that nonspecific physical properties related to surface energy play an important role in the interactions between cells and polymer surfaces in a protein-free environment. We shall first recall some basic definitions [4, 24].

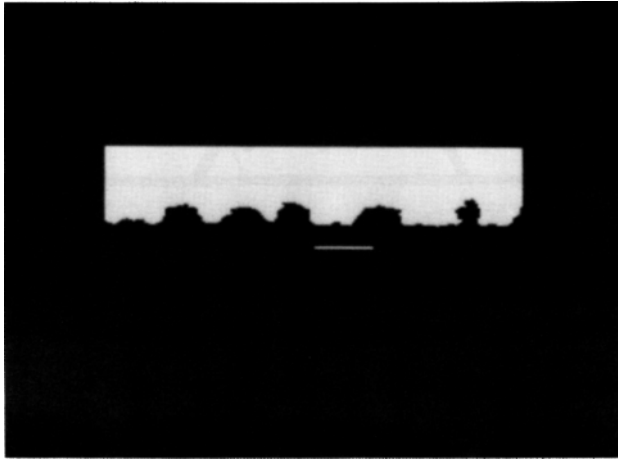


Fig. 5. Cell adhesion to flat surface. Cells from the P388D1 murine macrophage-like cell line were deposited on a glass coverslip. A fluid phase fluorescent marker (fluoresceinated dextran) was added in the bulk medium and cells were examined with a confocal laser scanning microscope, thus allowing direct visualization of sections perpendicular to the coverslips. Bar is 18 μm .

The surface energy γ of a homogeneous substance is simply the free energy increase associated to the formation of a free surface of unit area in vacuum. The interfacial energy γ_{12} between two media (1) and (2) is the free energy required to create an interface of unit area between both media. The work of adhesion between media (1) and (2) is the work done by the system when two free surfaces of media (1) and (2) are brought into contact. Clearly,

$$W_{12} = \gamma_1 + \gamma_2 - \gamma_{12}. \quad (3)$$

Now, in situations of biological interest, adhesion is performed in aqueous solution (this is medium 3). The work of adhesion between two media (1) and (2) embedded in a third medium (3) is given by

$$W_{12}^3 = \gamma_{13} + \gamma_{23} - \gamma_{12}. \quad (4)$$

The surface energies of liquids and the free energies of liquid/liquid interfaces can be measured directly. However, direct experimental determination of the surface energies of solids is much more difficult to achieve. The most widely used procedure consists of measuring the contact angle of liquid droplets on solid surfaces (fig. 6) and using the Young–Dupré equations

$$\gamma_{LV} \cos \theta + \gamma_{LV} - \gamma_{SV} = 0. \quad (5)$$

Hence, only the difference $(\gamma_{S1} - \gamma_{SV})$ can be measured. Much work was devoted to the derivation of ‘combining rules’ allowing determination of all parameters. Unfortunately, whereas this approach met with some success when polymers and simple

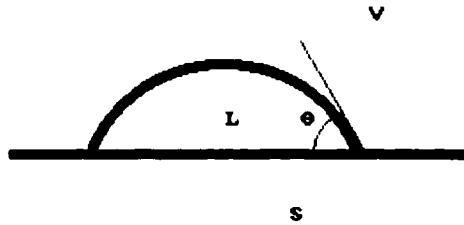


Fig. 6. Definition of contact angles. A droplet of a liquid L is deposited on a plane solid surface S. The third phase may be a vapor (V) or a liquid immiscible with L. Experimental determination of the contact angle θ between the solid surface and a plane tangent to the upper droplet surface on the three-phase-line provides a relationship between the three interfacial energies (SL, SV and LV).

organic liquids were considered, its relevance to biological systems is questionable due to the multiplicity of specific interactions that cannot be accounted for by these formulae (see section 4 for more details).

The simplest combination rule, that apply to series of apolar media, may be written as

$$\gamma_{12} = (\sqrt{\gamma_1} - \sqrt{\gamma_2})^2. \quad (6)$$

This formula is a consequence of the assumption that the work of adhesion between substances (1) and (2) is a product of material parameters characteristic of (1) and (2). See section 4.2.1.

Combining equations (6) and (3) yields the work of adhesion between two materials (1) and (2) embedded in medium (3):

$$W_{12}^3 = 2(\sqrt{\gamma_3} - \sqrt{\gamma_1})(\sqrt{\gamma_3} - \sqrt{\gamma_2}). \quad (7)$$

Thus, the work of adhesion will be positive (i.e. the media will stick together) unless $\gamma_1 < \gamma_3 < \gamma_2$ or $\gamma_2 < \gamma_3 < \gamma_1$. If the surface energy γ_3 of the bulk medium is equal to the surface energy of one of these substances (say 1), the work of adhesion will be zero, and thus will not depend on the surface tension of the other material.

Now, we shall review some experimental data: a very interesting series of experiments were performed by Van Oss and coworkers [138] who studied the adhesion of blood neutrophils and platelets to a series of polymer surfaces (the contact angle of water on these surfaces varied between 110 and 24 degrees). The medium was a saline solution supplemented with various amounts of dimethyl sulfoxide with a surface free energy ranging between 63.2 and 72.8 mJ/m² (15% and 0% dimethyl sulfoxide respectively). In accordance with simple theoretical predictions, adhesion was respectively increasing, constant or decreasing when the substrate surface energy was increased if the medium surface energy was respectively lower than, equal to or higher than the estimated free energy of the cell surface. Similar results were obtained when glutaraldehyde-treated erythrocytes were used as test particles [3].

The influence of the substrate free energy on the adhesion and spreading of different cell lines was later confirmed by other authors [151].

However, the above studies revealed that cell adhesion occurred when the estimated work of adhesion was zero, which suggested that other unaccounted interactions might play a role in cell-substrate binding [3].

2.3.2. Surface charge

It has long been shown with electrophoretic measurements that mammalian cells bear a net negative charge [133]. Electrostatic repulsion may thus in principle inhibit adhesion between cells and negative surfaces. For the sake of clarity, quantitative calculations will be described in section 4, and we shall now review some notable experimental results.

First, it was unambiguously demonstrated that cell-cell or cell-surface adhesion could be efficiently inhibited by electrostatic repulsion in solutions of low ionic strength (say 1 mM NaCl or less). This was shown in very elegant experiments by Gingell and Todd who studied the equilibrium position of glutaraldehyde-treated erythrocytes sedimenting on a charged oil-saline interface [81]: at low ionic strength, red cells remained about 100 nm above the interface, which would have efficiently prevented the formation of specific bonds.

However, in physiological media (i.e. about 150 mM NaCl and a few mM divalent cations), electrostatic repulsion between charged surfaces is screened by counterions with an exponential decay of characteristic length close to 0.8 nm (this is the Debye-Hückel length). It is therefore of interest to consider experiments performed at physiological ionic concentration. Sugimoto [163] studied the behavior of fibroblasts deposited on two different surfaces: glutaraldehyde-polymerized bovine albumine had a high negative charge. When polylysine was added to the polymerizing mixture, the surface charge was decreased by more than 50% as assessed by electrophoretic mobility determinations. When cells were deposited on the less negative substrate, they flattened and became immobile. Electron microscopical studies revealed much tighter apposition between cell and substrate surfaces when polylysine was added.

Similar results were obtained in a study made on the interaction between rat macrophages and sheep erythrocytes that had been made hydrophobic by glutaraldehyde treatment: the negative charge of these erythrocytes was decreased either by coating them with positively charged polylysine molecules or by removing negative sialic acid groups by neuraminidase treatment. In both cases, the efficiency of macrophage-particle adhesion was dramatically increased [30], and electron microscopy revealed tighter apposition between macrophage and erythrocyte surfaces when the negative charge was decreased [29, 129]. Concordant conclusions were obtained by Rutishauser and colleagues who studied the tightness of apposition between neural cells bound by intact or desialylated Neural Cell Adhesion Molecules [149].

Electrostatic repulsion may thus modulate the tightness of cell-cell or cell-substrate adhesion.

2.3.3. Other cell surface properties

Margolis and colleagues studied the adhesion of mouse fibroblasts to lipid films adsorbed on glass surfaces [120, 121]: Adherence was better with gel-crystalline than

with fluid phases. In other experiments performed by Springer and colleagues, lymphocytes were deposited on solid surfaces coated with adhesion molecules (LFA-3 or ICAM) that were either immobile or free to diffuse: similar spreading was obtained in both cases [32].

2.3.4. *Macromolecule adsorption*

An important point concerning the interpretation of experimental data is that solid surfaces exposed to serum-containing media will rapidly become coated by a layer of adsorbed molecules [13]. This possibility cannot be ruled out when experiments are conducted in protein-free solution, since most cells constitutively release diverse macromolecules that can serve as intermediates for substrate adhesion. As an example, fibroblasts secrete fibronectin, a protein made of two subunits of 250,000 molecular weight that possesses multiple binding sites and readily adheres to polymer surfaces [87] as well as specialized membrane receptors on the fibroblast (see [40] for more details on these molecules). Similarly, glycosaminoglycans such as hyaluronic acid or chondroitin sulphate may mediate cell adhesion [155] by adhering to both cell membranes and culture surfaces.

Clearly, the physiological importance of the intrinsic physico-chemical properties of substrates might be questioned if they are coated with a layer of biological macromolecules in all physiologically relevant conditions. However, two points must be noticed. First, the properties of tested surfaces may influence the nature of adsorbed molecules by influencing the competition between solute substances [2, 41]. Secondly, adsorbed proteins may exhibit conformational changes that may depend on the substrate properties [159]. Indeed, several authors suggested that the surface structure of adsorbed molecules might reflect the nature of the underlying substrate [2, 151].

2.3.5. *Mechanical properties of cell-substrate adhesion*

Many authors attempted to measure the mechanical strength of cell-substrate adhesion. We shall present some representative results.

The micromanipulation approach consisted of detaching adherent cells with a flexible micropipette. Suitable calibration allowed quantitative derivation of the applied force from the pipette curvature as measured immediately before detachment. This procedure was recently used by Gingell and colleagues [78] who measured at the same time the strength of adhesion and the area of tight apposition between cells and substrate (they made use of interference reflection microscopy). The strength of adhesion between *Dictyostelium discoideum* and an hydrophobic substrate (silanized glass) was of the order of 10 nanonewton, with a close contact area of 1–4 μm^2 . In other experiments, McKeever used the same approach to measure the strength of adhesion between macrophages and glass surfaces: the reported value was about 100 nanonewton [125].

Following another approach, Bongrand and colleagues deposited adherent cells in glass capillary tubes. After a suitable adhesion time, cells were subjected to hydrodynamic flows of increasing strength. In some cases, viscous dextran solution

had to be used in order to ensure that the flow be laminar. The main conclusions were as follows:

- i) the minimal flow rate required to detach cells was dependent on the duration of force application.
- ii) A tangential force on the order of 50 nanonewton per cell was required to separate macrophage-like P388D1 cells from glass surfaces [128], similar values were obtained when blood granulocytes were separated from glass surfaces coated with various molecular species such as albumin, fibronectin, concanavalin A or polylysine [127] and human melanoma cells were detached from fibronectin-coated glass surfaces [8].

A third approach consisted of subjecting adherent cells to a centrifugal force. Easty and colleagues could separate murine tumor cells from glass substrates with a centrifugal acceleration in the order of $1,000\times g$ parallel to the substrate plane. The corresponding force was thus about 0.1 nN [57]. Corri and Defendi centrifuged glass surfaces bearing adherent macrophages or red cells. The minimal force required to break cell substrate adhesion was 56 nanonewton for macrophages and less than 0.1 nanonewton for erythrocytes [37]. Interestingly, the authors noted that the minimal separating force was decreasing when the duration of application was increased. Using a similar experimental setup, McClay and colleagues [124] found that adhesions between chick embryo cells could be ruptured by a force of about 0.1 nN. However, when these cells were deposited on polylysine-coated surfaces, they resisted a centrifugal acceleration of $3,000\times g$, corresponding to a force higher than 3 nN.

In conclusion, we described three general models of cell adhesion in order to help the reader evaluate the significance of the problems discussed below. These examples showed that biological adhesion is mediated by an impressive number of ligand molecules and that binding may be modulated by nonspecific physical interactions.

3. Biophysical characterization of cells

The first step to a biophysical modeling of cell adhesion is to build a quantitative description of the cell features likely to play a role in this process. This goal is made difficult by the diversity of living cells: If we consider only a single cell type, the interest of our description will be restricted by the difficulty of assessing its relevance to other models. On the other hand, gathering conclusions from studies performed with widely different cell species is not warranted. Therefore, we shall try to keep an intermediate way: we shall essentially refer to leukocytes (i.e. lymphocytes, monocytes and granulocytes) that are ideally suited to studies done at the individual cell level. Occasional data concerning other cell populations will also be provided for comparison.

We shall sequentially consider three different scales: first, the micrometer scale, i.e. general cell shape control as studied with conventional optical microscopy. Secondly, the submicrometer scale, as observed with electron microscopy, since an important step of cell adhesion is the tight apposition of binding surfaces in order to allow

molecular bonding. Finally, we shall describe the molecular organization of the cell surface, with an attempt to describe general physical properties without delving into a description of individual molecular species. Clearly, present knowledge does not allow the derivation of quantitative relationships between the three organization levels we mentioned.

3.1. Cell shape control

Many cell types are fairly spherical when they are maintained in suspension under resting conditions (however, some cell populations may display micrometer-sized protuberances that cannot be neglected, see, e.g., [170]). Spontaneous deformations can be induced by biochemical stimuli in absence of any adhesive interaction. Thus, exposing suspended neutrophils to chemotactic factors such as formyl methionyl peptides will induce spectacular cell polarization within a few minutes (fig. 7).

Now, if a rounded cell is deposited on a substrate, it will exhibit some kind of flattening (fig. 5). This deformation may involve several mechanisms. First, the cell may flatten under the mere influence of gravity. Secondly, adhesive cell-substrate interactions may act as a tensile force triggering cell spreading with strong analogy to the spreading of a liquid droplet on a solid surface as a consequence of the balance between interfacial forces. Thirdly, the cell may send active lamellipodia that will be secondarily bound by the substrate. Since adhesive interactions may deliver activating signals, it is very difficult to discriminate between these mechanisms [43]. However, it may be useful to estimate the minimal force required to deform a cell in absence of known activation, since such deformation may be a prerequisite to adhesion in some circumstances.

Many procedures were used to study bulk cell deformability, including centrifugation on a surface with measurement of induced deformation [94, 131], determination of the resistance to indentation with a moving stylus [141, 142] or aspiration into a glass micropipette. The latter method was probably the most widely used during the last ten years and provided a wealth of information of granulocyte deformability. The main conclusions are as follows. When a typical granulocyte of about $4\ \mu\text{m}$ diameter is sucked into a pipette of, e.g., $2\text{--}3\ \mu\text{m}$ diameter with a pressure higher than some threshold value [67], it forms a protrusion that will enter the pipette and grow with a velocity depending of the pressure and pipette size. If the pipette is large enough (e.g., $4\ \mu\text{m}$ diameter), the cell will readily acquire a sausage-shape and flow into the pipette. If the pipette diameter is smaller, the deformation will be limited by a maximum extension of the apparent membrane area that may increase by a factor of about two [72]. If the pressure is reversed, the cell will be expelled and it will resume its spherical shape within several tens of seconds ([164], see fig. 8). All authors observed both viscous and elastic behavior, and several quantitative models were elaborated to account for measured deformations. In a remarkable work, Schmid-Schönbein and colleagues [154] studied the small deformations induced within a few seconds by moderate aspiration. They modeled cells as homogeneous standard viscoelastic solids (fig. 9) and readily solved the equations of deformations. They were thus able to derive three material constants: the elastic stiffness coefficients $k_1 = 275\ \text{dyn/cm}^2$, $k_2 = 737\ \text{dyn/cm}^2$ and a viscosity coefficient $\mu = 130\ \text{dyn}\cdot\text{s/cm}^2$.

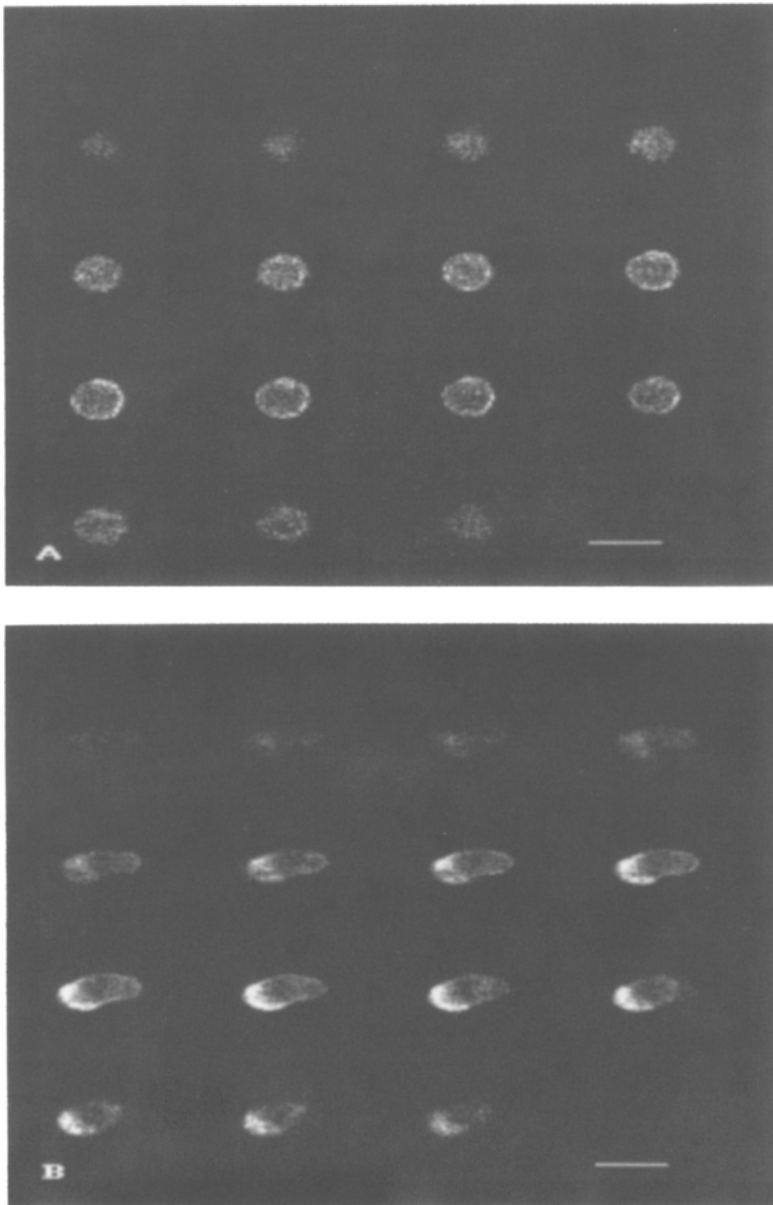


Fig. 7. Cell shape control. Human granulocytes were fixed and labelled with a fluorescent phalloidin derivative to reveal actin microfilaments. They were then studied with confocal laser scanning microscopy and series of 16 sections separated by a distance of $1 \mu\text{m}$ are shown. A: resting cell maintained in suspension. It is spherical. B: cell pretreated with a chemoattractant for 15 minutes. It exhibits marked polarization with a microfilament concentration at the cell leading edge. Bar is $18 \mu\text{m}$.

In another series of experiments, Evans studied large granulocytes deformations [67] and results were consistent with the model of a tensile surface (about 0.01 dyn/cm tension) surrounding a highly viscous fluid (a later figure for the viscosity was about 1,000 dyn-s/cm² [72]). Later reports led the authors to propose more sophisticated models, with a combination of a stressed surface and visco-elastic interior, in order to account for mechanical cell behavior during aspiration and shape recovery [56, 164, 173].

Since a more complete discussion of cell shape control would not fall into the scope of the present review, we shall add only a few points.

Whereas proposed models may satisfactorily account for cell deformations caused by a restricted range of applied force intensity and duration, it may be dangerous to use material parameters to predict cell behavior under conditions widely different from those used to derive these parameters.

It was often stressed that individual cells might display quite diverse behavior. Indeed, studying single cells makes apparent the danger of considering only mean values determined on cell populations.

Many different cell species were studied with the micropipette aspiration technique. In the author's laboratory, rat macrophages [129], macrophage-like [131] or lymphoid [76, 131] and basophilic [96] cell lines and human melanoma cells [8] were studied with this technique. An important conclusion is that very marked differences may be found between cells in an apparently homogeneous cell population.

Interestingly, the spontaneous traction exerted on their substrate by epithelial cells was quantified: fibroblasts deposited on an elastic surface exerted a constant traction on the order of 0.001 dyne/cm along the advancing margin [89]. More recently, the

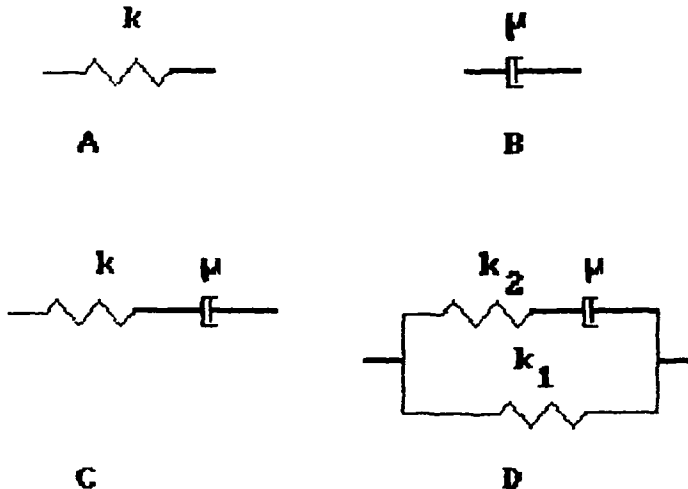


Fig. 8. Simple models to represent cell mechanical properties. The following mechanical model may be considered to represent the properties of a volume element of a solid body. (A) elastic medium with spring constant k . The force F is proportional to displacement $(x - x_0)$, where x_0 is the unperturbed length. (B) viscous medium, the force is proportional to the rate of deformation dx/dt . (C) Maxwell solid. (D) Standard viscoelastic medium.

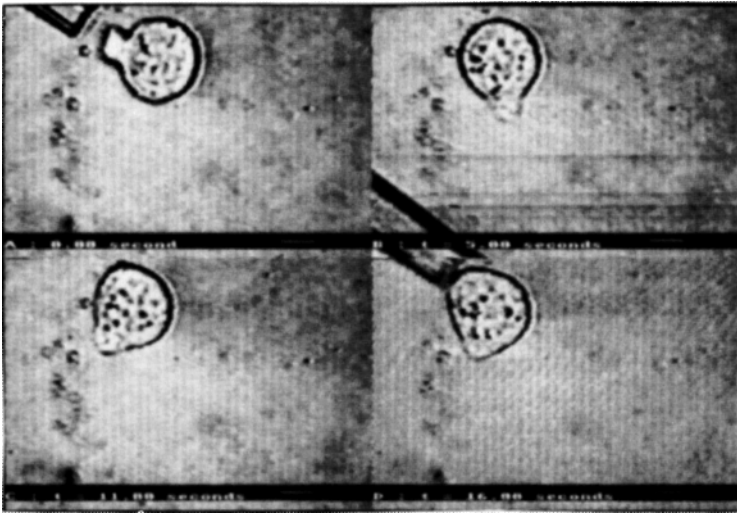


Fig. 9. Cell shape recovery after micropipette aspiration. A murine macrophage-like P388D1 cell was sucked into a micropipette, then expelled and observed while it recovered its spherical shape. It is shown 0 s (A), 5 s (B), 11 s (C) and 16 s (D) after expulsion. Bar is 4 μm .

contractile force of fibroblasts and endothelial cells was estimated at 4.5×10^4 and 6×10^4 dyne/cm² respectively (i.e. on the order of 0.045–0.06 dyne/cm on the cell margin, assuming a cell thickness on the order of 1 μm [106]. These estimates are fairly close to the values reported for neutrophils, and may represent a minimum order of magnitude for the adhesive energy required to induce the formation of a substantial contact area between a cell and an adhesive substrate in absence of active deformation.

A final point of interest is the mechanical strength of cell membranes. Although marked differences are found between tested cell populations, following our experience, membrane rupture is not an uncommon event when cells of 4–7 μm diameter are subjected to a sucking pressure of 25 cm H₂O with a pipette of 2–3 μm inside diameter (see, e.g., [8]). The corresponding tension is about 2 dyne/cm. Obviously, the membrane resistance sets a limit to the strength of cell-cell and cell-surface adhesion.

3.2. Cell surface roughness: the submicrometer scale

The interpretation of quantitative data on cell contact formation and binding strength is crucially dependent on the actual area of membrane regions involved in adhesion [88]. Further, the electron microscopic study of cell surfaces reveals the presence of numerous protrusions of variable size that are often inapparent when cells are observed with conventional microscopy. Finally, when contact areas between adherent cells are studied with electron microscopy [76, 129] it often appears that the distance

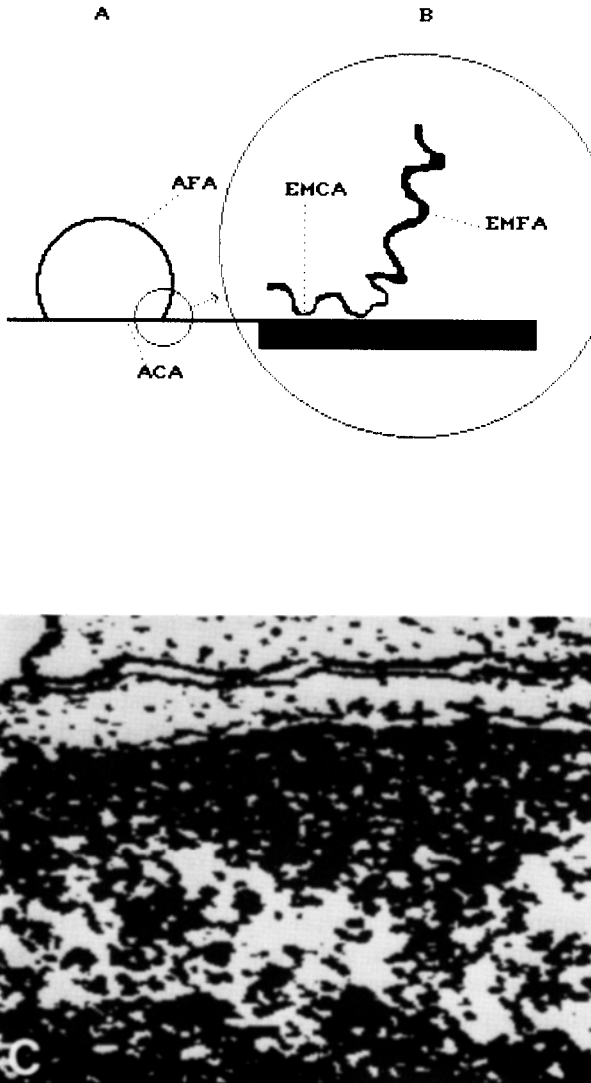


Fig. 10. Apparent and actual adhesion areas. Figure A represents a typical substrate-bound cell depicted with the resolution of conventional optical microscopy. The apparent free area (AFA) is the area of a portion of a sphere and the apparent contact area (ACA) is a disc. Figure B represents a portion of the figure depicted with the resolution of electron microscopy. The electron microscopic free area (EMFA) is larger than the apparent free area due to the presence of numerous cell surface asperities. In the apparent contact area, only a fraction of the cell membrane is separated from the surface by a gap compatible with molecular bonding. This defines the electron microscopic contact area (EMCA). It is not easy to determine whether the whole EMCA is involved in binding. Figure C represents a binarized image of an electron micrograph representing a portion of the interaction area between concanavalin-A-agglutinated rat thymocytes [31]. Bar is $0.1 \mu\text{m}$.

between the phospholipid bilayers of the plasma membranes is very irregular, with a combination of zones of apparent molecular contact (the distance between bilayers is in the order of 20–40 nm) and regions where membranes are separated by a gap of several hundreds of nanometers that is obviously incompatible with adhesion between membrane intrinsic receptors (see next section).

In order to clarify this point, it is important to give a precise definition of the parameters we are studying (fig. 10): First, the *apparent cell area* may be defined as the area of a smoothed cell where only details visible with optical microscopy are retained. This area is simply $4\pi R^2$ for a spherical cell of radius R . Second, the *actual membrane area* is the bilayer area. This may be derived from quantitative processing of electron microscopical images, using basic formulae of stereology [61]. Similarly, the *apparent binding area* is the area of the region where cells appear bound when studied with optical microscopy. The *electron microscopic binding area* is the area of the region where the intermembrane distance is compatible with molecular adhesion. This last definition requires several points of caution. First, it is not proven that there are actual molecular bonds in a region where the intermembrane distance is consistent with bonding. Secondly, since the relative orientation of a microscopic section plane and interacting membranes is random, the apparent intermembrane distance as estimated on micrographs is expected to be higher than the actual distance (it may be shown that the mean apparent distance is about twice the actual distance [76]). Thirdly, it is difficult to assess the influence of sample processing for electron microscopy on intermembrane distance.

We shall now describe some experimental data relevant to the control of cell roughness.

An important result emerging from numerous observations made on living cells is that they deform with constant volume, variable *apparent area* and constant *actual membrane area*. Indeed, it has long been demonstrated that erythrocytes deformed with essentially constant area, since membrane rupture occurred after a few percent relative area increase [71]. Further, the observation of the deformation of mesenchyme cells suggested that the formation of a protrusion inhibited the appearance of other protrusions, due to a mechanical resistance of the membrane [184]. Also, electron microscopic studies confirmed that microvilli and blebs acted as reserve surface membrane [63]. It was estimated that the actual membrane area of mastocytoma cells was between 50% and 100% higher than the apparent area [105]. The excess area of blood cells compared to spheres of equal volume was reported to range between 44% and 130% [34]. These estimates were fairly consistent with the report that the maximal apparent area increase of blood granulocytes sucked into micropipettes was in the order 110–120%, supposedly corresponding to full membrane extension [72].

The size of cell surface asperities may be readily estimated from electron micrographs: the length of protrusions was 0.4–0.5 μm in mastocytoma cells [105] and kidney fibroblasts [63]. Values as high as 2 μm were found on a T-cell hybridoma with particularly large protrusions that appeared in optical microscopy [170]. This must be considered as a maximum value. The thickness of protrusions was about

0.1 μm in aforementioned studies. These values seem representative of images found on many cell types.

An important point is that cell surface protrusions may resemble sheets or cylinders, depending on cell type, with similar appearance on transmission micrographs. Scanning electron microscopy may be useful to derive the three-dimensional cell shape.

An important problem is to determine the mechanical properties of cell surface asperities: micropipette aspiration studies cannot tell us whether the cell membrane must be viewed as a flaccid surface subtended by the subplasmalemmal cytoskeletal network, or whether each asperity is endowed with mechanical resistance and individually resists smoothing (as was assumed in [129]). Indirect evidence is provided by immunofluorescence studies: cell protrusions were demonstrated to contain actin as well as cytoskeletal and membrane binding structures such as vinculin, talin, α -actinin and filamin [45]. Hence it seems reasonable to ascribe these asperities material parameters similar to those derived for bulk cells. However, more precise studies are needed to understand the behavior of these asperities during the first steps of contact formation.

3.3. *Relevance of the concept of surface tension to biological membranes*

The concept of surface tension proved very useful to relate the adhesion-induced deformations of liquid droplets or lipid vesicles to interaction energies [4, 69]. It is thus warranted to ask whether this can be applied to nucleated cells such as leukocytes.

An important difficulty is that there is no rigorous experimental means of discriminating between the membrane and cytoplasm resistance to deformation. Therefore, the derivation of a surface tension from deformation measurements requires some assumptions concerning the mechanical properties of the cell interior. The experimental observation that many cells

- i) are spherical in suspension, and
- ii) recover to the spherical shape after deformation (figs 7, 8) strongly supports the proposal by Evans [67] that the mechanical properties of blood granulocytes might be accounted for by the model of a highly viscous liquid surrounded by a tensile membrane.

According to this concept, the relationship between the *effective membrane tension* and apparent cell area increase might be derived from the *equilibrium value* of the length of protrusions obtained by sucking cells into micropipettes with varying pressure. The finding by Evans that granulocytes entirely penetrated through a pipette when the suction pressure was higher than a threshold level inversely related to the pipette diameter and required to obtain the formation of a spherical protrusion strongly suggested that the tension was fairly constant (provided the membrane was not fully extended). This tension ranged between 0.01 and 0.035 dyne/cm. However, when macrophages, activated lymphocytes or melanoma cells were subjected to micropipette aspiration, the growth of the cell protrusion often stopped before complete cell entry into the pipette. It is not clear whether this arrest was due to

an actual increase of membrane tension concomitant with apparent area increase, or a blockade when the cell nucleus or some other cytoplasmic structure entered the pipette tip (this point is emphasized in ref. [8] see also fig. 12). This may impair the significance of empirical relationships obtained between apparent surface tension and apparent membrane area increase [76, 129].

Further, the concept of membrane tension is useless at the electron microscopical level. If we assume that the plasma membrane is a folded sheet of low mechanical resistance deposited on an underlying 'contractile carpet' [67], the thermodynamic cost of creating a *small* contact region with a smooth surface will be zero for a leukocyte, in contrast to an erythrocyte that exhibits an intrinsic biconcave shape. This difference may account for the well known difficulty to make erythrocytes stick to rigid surfaces as compared to other cell types.

Another possibility would be that the polymorphism of membrane lipids in leukocytes might favor the occurrence of a variety of microdomains with different curvatures, allowing each lipid molecule to find an ideally suited environment. In this case, a folded appearance would be favored. Clearly, more work is required before we understand the mechanisms responsible for cell surface roughness at the micrometer and submicrometer level.

3.4. Molecular structure of the cell surface

We shall only review some peculiar properties with an obvious relevance to cell adhesion. The point we wish to address may be summarized as follows: suppose the distance between two cells is gradually decreased. It is probable that they will first exert some mutual repulsion (otherwise, spontaneous agglutination would occur in absence of any specific bonding). The force/distance law characterizing this repulsion must depend on many parameters, including the density of charges and membrane-bound stabilizing polymers, and the mobility of these molecules. Indeed, if contact is made slow enough, repulsive molecules are expected to depart from the contact region or gather into restricted areas, as predicted in view of theoretical considerations [16] and suggested by electron microscopical evidence [149].

The following data may be of interest in this respect.

3.4.1. Bulk composition of plasma membranes

Estimates for mean membrane composition were suggested in previous reviews [7, 23, 24]. More details can be found in standard textbooks on cell membranes [80]. The basic structure of the plasma membrane is a phospholipid bilayer where intrinsic glycoproteins and glycolipids are embedded. A reasonable order of magnitude for the composition is 45% protein / 45% lipid / 10% carbohydrate. Assuming a mean phospholipid/cholesterol ratio of 0.72, the mean area for (1 phospholipid + 0.72 cholesterol) is 0.77 nm^2 [114], corresponding to a molecular weight of about 1,000. Modeling proteins as globular units of 4 nm diameter and 50,000 molecular weight, the occupied area is about $2.75 \times 10^9 \text{ cm}^2$ per gram (i.e. 0.45 g protein and 0.45 g lipid), with 25% of the total area occupied by proteins.

Another estimate may be useful: assuming that water represents about 70% of the mass of a standard cell [113], the dry mass of a typical leucocyte of 4 μm radius and

1.077 g/cm³ density is about 8.7×10^{-11} g, with a corresponding membrane area of 400 μm^2 (i.e. twice the apparent area). The plasma membrane therefore represents 1–2/100,000 of the total cell dry weight.

3.4.2. *Intrinsic membrane glycoproteins*

Since many adhesion receptors are intrinsic membrane proteins, it is important to have a general feeling of their shape and flexibility. Members of the immunoglobulin superfamily are an important example of such proteins. They are made of one or several domains of about $2.5 \times 2.5 \times 4$ nm, with fairly high rigidity and bound by structures of variable flexibility. Thus, surface immunoglobulin G found on B lymphocytes may protrude by about 10 nm above the bilayer, with easy rotation of the external antigen binding sites [175]. Class I major histocompatibility complex molecules that are found on nearly all cell species have a similar size (with a 3-domain chain associated to $\beta 2$ -microglobulin). ICAM-1 molecules, that have an obvious adhesive function, are made of two seemingly rigid rods of 11.8 and 6.9 nm length separated by a fairly flexible region [161]. Human fibronectin receptors were described as intrinsic membrane proteins with an extracellular region of 12–14 nm length. Hence, intrinsic membrane proteins may be viewed as structures of 10–20 nm length with limited flexibility.

3.4.3. *The glycocalyx*

Electron microscopic studies have long revealed that in nearly all tested cells the phospholipid bilayer of the plasma membrane was coated with a low density region of varying depth [178], ranging between a few tens and several hundreds of nanometers [122, 178, 187]. This 'fuzzy coat', or 'glycocalyx' was first revealed by the occurrence of a gap between plasma membranes in contact regions between adherent cells [122]. This was later reported to be stained with various procedures such as periodic acid Schiff (PAS), phosphotungstic acid (PTA), Colloidal iron or thorium, ruthenium red, alcian blue, and it was suggested that this region had relatively high polysaccharide content. Other biochemical studies showed that most membrane carbohydrates were oligosaccharidic chains bound to glycoproteins or glycolipids. They are made of less than eight [36] to 20 [178] monosaccharide units, corresponding to an extended length lower than 5–10 nm.

Thus, the structure extending outside the 20 nm region next to the phospholipid bilayer represents a minimal fraction per weight of the membrane. It includes glycosaminoglycans that are made of repetitive monosaccharide units: hyaluronic acid is made of several thousands repeats of a characteristic disaccharide sequence (N-acetyl glucosamine $\beta 1$ –4 glucuronic acid) $\beta 1$ –3. Similarly, chondroitin sulfate is made of hundreds of units [108]. These chains are relatively unbranched [10]. Since their conformation may play an essential role in adhesion, we give some basic results and refer the reader to more complete references for additional details [10].

The conformation of long flexible polymer chains received much attention, and basic ideas are described in the classical book by Flory [75]. This conformation is essentially dependent on the interaction between the solvent and repeating units. If there is no free energy variation associated to the transfer of monomers into

solvent (this is the case for so-called θ solvent conditions), the chain conformation is well approximated by classical random walk models, and the end-to-end distance is proportional to the square root of the number N of monomer units. Now, if the transfer of monomer units into solvent results in a net free energy decrease, the net repulsion between the monomers will provoke a relative expansion of the chain, and the molecular size will increase as a power of N that will be higher than 0.5. This property can be used to study polymer conformation by measuring the viscosity of dilute polymer solutions. The starting point is Einstein's formula that states that the viscosity μ of a suspension of rigid spheres is

$$\mu = \mu_0(1 + 2.5\Phi) \quad (8)$$

where μ_0 is the viscosity of the pure solvent and Φ is the fraction of the total volume occupied by the spheres [60]. It may be shown that individual polymer molecules behave like hard spheres. Thus, defining the intrinsic viscosity as

$$\mu_{sp} = \lim_{c \rightarrow 0} (\mu - \mu_0) / \mu_0 c \quad (9)$$

where μ and μ_0 are the viscosities of the polymer solution (of concentration c expressed in g/dl) and pure solvent respectively, it is found that this parameter is related to the molecular size of polymers following the empirical Mark-Houwink formula

$$\mu_{sp} = KM^\alpha \quad (10)$$

where M is the polymer molecular weight, and α is an empirical coefficient that is close to 0.5 in a θ solvent and is expected to be higher than 0.8 if the polymer is rigid and rod-like rather than coiled.

The Mark-Houwink coefficient was about 0.8 for hyaluronate and was sometimes higher than 1 for chondroitin sulfate [10]. It is concluded that water is probably a good solvent for polysaccharides constituting the cell coat. This point is of importance if we wish to predict intercellular forces during cell-to-cell approach.

Another point of interest is the mode of attachment of glycosaminoglycans to the cell surface. They may be bound to core proteins, forming proteoglycans [189]. These proteins may be inserted in the membrane with a transmembrane and intracellular regions, or covalently bound to a phosphatidyl inositol group. Also, glycosaminoglycans can interact with other elements of the pericellular matrix [91, 189]. Thus, fibronectin binds to heparin [136]. Also, the CD44 membrane protein has an affinity for hyaluronic acid [90]. Interactions between glycosaminoglycans were also described [10]. In conclusion, glycosaminoglycans may be viewed as long unbranched chains firmly anchored to plasma membranes with multiple low affinity binding sites to this membranes. Functional interactions were also reported between proteoglycans and submembranar cytoskeletal elements [188].

An important point is the concentration of these sugars in the pericellular matrix: this is difficult to quantify since the cell coat may be partially removed by rather mild

Table 2
Some physical properties of a standard cell.

Parameter	Order of magnitude
Radius (sphere)	4 μm
Density	1.077
Apparent membrane area	200 μm^2
Actual membrane area	400 μm^2
Length of microvilli	0.5–2 μm
Thickness of microvilli	0.1 μm
Electric charge	-0.024 Coulomb/ m^2
Membrane tension (at rest – ref. [67])	≤ 0.02 mN/m
Membrane tension (10–20% apparent area increase – ref. [129])	1 mN/m
Glycocalyx thickness	50 nm
monosaccharide density in external glycocalyx zone	0.5 residue/ nm^2

Some parameters relevant to cell-cell adhesion were evaluated to allow a quantitative assessment of different forces likely to influence initial contact. Note that the estimates for surface tension are heavily dependent on the choice of a mechanical model to interpret experimental data (see 3.3).

procedures such as washing in denaturing medium [44] or possibly in physiological solutions [33]. Taniguchi and colleagues assayed leukocyte associated glycosaminoglycans [167]: they found 36 μg uronic acid per 100 ml blood. Estimating blood leukocyte concentration at $6 \times 10^8/\text{ml}$ with 400 μm^2 actual membrane area per cell, the uronic acid concentration would be about 0.5 monomer/ nm^2 . In another study, the concentration of uronic acids and hexosamines were 23.5 and 20.4 nmole per 10 mg dry weight of SV40-transformed green monkey kidney cells [119]. Using a tentative estimate of 2×10^{-13} g per μm^2 membrane area, we obtain about 0.5 monomer per nm^2 , in accordance with the aforementioned estimate. We assumed that essentially all assayed molecules were localized on the cell surface, which is supported by the finding that most cell sulfated proteoglycans may be removed by proteolytic treatment [147].

Other components of the cell coat are proteins such as fibronectin or laminin. The fibronectin molecules is made of two strands of 61 nm length, bound at their ends with a fixed angles. They display limited flexibility with three preferential bending sites [62]. More than 100,000 fibronectin molecules were reported to be bound by fibroblasts with an affinity constant of 3.6×10^{-8} M [126]. The binding of such molecules to the cell surface may involve multiple low affinity binding sites since this was competitively inhibited with the Arg-Gly-Asp-Ser (RGDS) tetrapeptide that displayed an apparent affinity constant of 6×10^{-4} M for their binding site [144]. These figures may be useful since the RGDS sequence is involved in many adhesive interactions.

Laminin is also a component of the extracellular matrix that may bind to the cell surface. It appears as made of three short rods (36 nm length) and one long arm (77 nm) of limited flexibility bound on one end [62]. The above estimates are summarized in table 2.

3.4.4. Static distribution and mobility of membrane molecules

Cell cell adhesion is expected to depend i) on the nature of cell surface molecules that will first meet when two cells collide each other, and ii) the possibility that adhesive molecules get matched and concentrated in contact areas.

We shall first consider the static distribution of membrane molecules. We shall not describe the polarization of some cell populations that grow in an anisotropic environment (e.g., thyroid cells with apical and basal sides). Although the membrane molecules of suspended leucocytes are often considered as randomly distributed, some reports suggest that it may not be the case. Thus, Abbas and colleagues [1] analyzed the distribution of surface immunoglobulins on murine B lymphocytes and found that it was non-random to a high degree of statistical significance, with small clusters and patterns of interconnecting networks. Many authors compared the density of potentially adhesive molecules on microvilli and flat membrane areas. Concanavalin A, a lectin with a specificity for α -methyl mannose, was uniformly distributed on rat lymphocytes [183]. Similarly, membrane immunoglobulins were uniformly distributed on murine lymphocytes [115] but they were concentrated on the microvilli of ATP-depleted murine spleen cells [50]. More recently, the L-selectin adhesion molecule was found to be concentrated on the tip of neutrophil microvilli [143]. Interestingly, the activation of human neutrophils with phorbol esters concomitantly induced spontaneous clustering and functional activation of complement receptors [52]. Finally, a point that may be of interest is that a local concentration increase of acetylcholine receptors induced their aggregation on muscle cells [162]. These data strongly support the view that at least some membrane molecules are non-randomly distributed, and that this may influence adhesion.

The mobility of membrane molecules received much attention. The most popular method of studying molecular movements is probably based of fluorescence recovery after photobleaching (FRAP; [152]). Briefly, a population of membrane molecules are tagged with fluorescent groups and the beam of a laser matching the excitation wavelength of the fluorophore is focused on a limited area (in the order of $1 \mu\text{m}^2$) of the cell surface. The laser power is transiently increased in order to bleach fluorescent groups. The same area is then illuminated with lower intensity, and the variations of fluorescence are recorded. It is thus possible to derive the diffusion coefficient of fluorescent groups, and the fraction of mobile molecules in this population. The diffusion coefficient of several membrane molecules on lymphocytes (surface immunoglobulin or Thy1 molecule) was in the order of $3 \times 10^{-10} \text{ cm}^2/\text{s}$ with a proportion of mobile molecules ranging between 50% and 90%. This value, which is representative of experimental data obtained on many proteins, was claimed to be about tenfold lower than the hydrodynamic limit [168], and the diffusion coefficient of membrane molecules was increased in 'blebs' induced on the membrane of muscle cells or on spectrin-depleted erythrocytes [107], thus strongly suggesting that the mobility of cell surface molecules was essentially limited by lateral constraints and interactions with submembranar cytoskeletal elements. This hypothesis was later tested by comparing the diffusion coefficient of wild-type molecules and engineered molecules with substantial deletions of intracytoplasmic domains: surprisingly, similar diffusion coefficients were obtained for normal and deleted class I

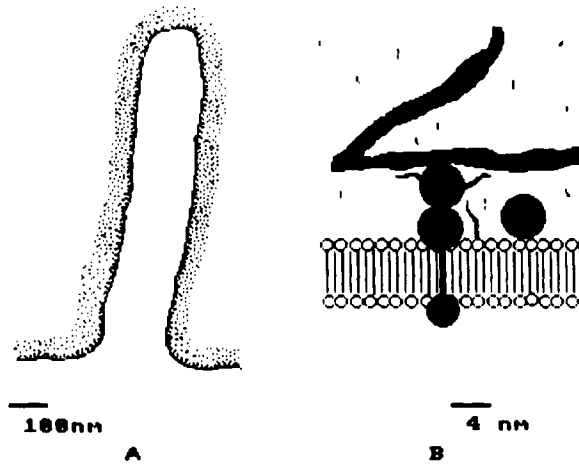


Fig. 11. The cell surface. The cell surface is represented on the left (A) with submicrometer resolution. A typical microvillus of $0.1 \mu\text{m}$ thickness is studded with intrinsic membrane proteins. The monosaccharides of the cell glycocalyx are represented as individual points with realistic density. However, these points are much larger than individual hexasaccharides: otherwise, they would not be visible. Figure B represents a region of the cell surface with molecular resolution. The large V-shaped extracellular structure might represent a part of a fibronectin molecule (no fibronectin receptor is shown). Glycocalyx structures are represented with fairly realistic size and density. They are parts of long chains that intersect the plane of the drawing.

histocompatibility molecules [58], viral proteins [157] or epidermal growth factor receptor [117]. However, the mobility of class II major histocompatibility antigen was substantially increased after removal of cytoplasmic domains [180]. The apparent discrepancies between aforementioned results can be resolved if it is suggested that the mobility of membrane molecules is limited by i) extensive interactions between the extracellular domains of most molecules and ii) interactions between the intracytoplasmic domains of some molecular species and cytoskeletal elements. This concept is supported by recent experimental data. The diffusion constant of class I major histocompatibility molecules (L^d) that were either native or deprived of 1, 2 or 3 glycosylation sites was determined [185]: D increased from 6×10^{-10} to $17 \times 10^{-10} \text{ cm}^2/\text{s}$. In other experiments, chimeric molecules with transmembrane or glycoposphatidylinositol linkage and extracellular domains from Thy-1 molecule, placental alkaline phosphatase or vesicular stomatitis virus G proteins were studied. It was concluded that ectodomains accounted for the major part of resistance to displacement [190]. Further, lymphocytes were transfected with genes coding for wild-type CD8 molecules or CD8 molecules with extensive deletion of intracellular and transmembrane domains. They were exposed to anti-CD8 antibodies in order to induce capping [174]: similar redistribution of cytoskeletal elements was found, suggesting that interactions between Cd8 molecules and microfilaments were mostly mediated by interactions between extracellular domains of membrane molecules [9]. Finally, a recent study made on the movements of cell surface histocompatibility

molecules labeled with colloidal gold [58] revealed that the long-distance displacements were limited by a dynamic (temperature dependent) barrier, restricting the amplitude of most movements to less than $1 \mu\text{m}$. In conclusion, cell surface glycoproteins comprise a substantial fraction of immobile elements (diffusion constant less than $10^{-12} \text{ cm}^2/\text{s}$) and a fraction of similar importance with a diffusion constant ranging between 10^{-10} and about $3 \times 10^{-9} \text{ cm}^2/\text{s}$. Movements are essentially restrained by extensive interactions between extracellular domains of membrane molecules and occasional interaction between some intracellular domains and cytoskeletal elements. Finally, it must be recalled that cross-linking membrane molecules may result in enhancing their interactions with microfilaments [74] and large scale redistribution (as exemplified by the capping phenomenon [174]).

Conclusion. We have now reviewed some biophysical properties of living cells, with a particular emphasis on leucocytes. The quantitative estimates of different cell parameters will be used to discuss the relevance of different theoretical models to the adhesive behavior of these cells. A tentative sketch of the cell surface is shown on fig. 11.

4. Models for the sequential steps of cell adhesion

We shall now discuss the relevance of different theoretical models to the adhesion of nucleated cells. As emphasized in the first section of this review, our point is not to describe basic concepts and results obtained by physicists and physical chemists, but to make use of available data to select the theories that seem most relevant to cell biology. We shall consider sequentially the following steps of the adhesive process:

- Cell-cell or cell-substrate approach.
- Initial bond formation.
- Cell membrane reorganization in contact areas.
- Cell-substrate detachment.

4.1. Cell-cell approach

The probability of bond formation between two cells or a cell and a solid surface bearing complementary molecules is obviously dependent on the mutual force exerted by approaching structures. The complexity of cell membranes would make hopeless any rigorous attempt at achieving an *ab initio* derivation of these forces. Indeed, we may quote the introductory sentence of the celebrated book by Eyring and colleagues [73] “In so far as quantum mechanics is correct, chemical questions are problems in applied mathematics. In spite of this, chemistry, because of its complexity, will not cease to be in large measure an experimental science ...”.

The complexity of cellular and colloidal systems led many authors to focus on particular noncovalent interactions that may not be independent. Thus, in a recent paper [176], Van Oss reviewed 17 interactions that might be reduced to a lesser number of more ‘fundamental’ forces. We shall only mention a few approaches to cell interactions.

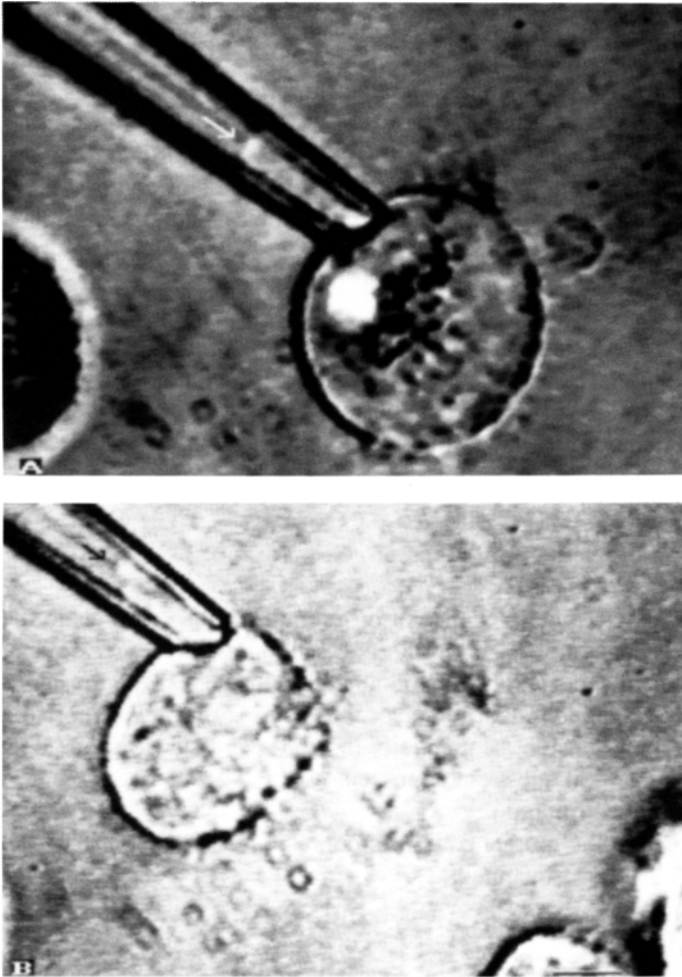


Fig. 12. Solid-like behavior of a cell. Human melanoma cells were sucked into micropipettes [8]. The tip of protrusions (arrows) is not spherical, indicating that the cell did not behave as a liquid. Bar is $8 \mu\text{m}$.

4.1.1. Conditions of contact formation

In order to estimate quantitatively the relevance of a given interaction to cell adhesion, we need some guidelines for performing rough calculations. In view of aforementioned data, the initial contact should involve the tip of microvilli. This is indeed supported by morphological studies made on the initial step of platelet aggregation [79], mutual adhesion of embryonic neural retina cells [17] or concanavalin A-induced fibroblast agglutination [186]. The initial contact area should thus be in the order of $0.01 \mu\text{m}^2$ (or 10^{-14} m^2).

The minimal binding energy required to influence cell adhesion is in the order of kT (where k is Boltzmann's constant and T is the absolute temperature), since bond formation cannot occur if cells are not maintained against thermal agitation. The corresponding value is about 4×10^{-21} J.

Further, a repulsive force cannot influence adhesion if it is weaker than the sedimentation force (during *in vitro* experiments), i.e. about 10^{-13} N. Also, it is likely that under *in vivo* conditions where cells are often bound to matrix components, the minimal force required to influence the formation of new adhesions is the protrusive force of cell microvilli. Although this is not well known, a reasonable order of magnitude is about 10^{-11} N, corresponding to the force required in order that a cylindrical microvillus of $0.1 \mu\text{m}$ diameter progress against the basal tension of a resting neutrophil [72]. This force is similar to the sedimentation force under mild centrifugation.

Finally, it must be noted that a reasonable value for the interbilayer distance during the association of membrane intrinsic receptors is twice the size of extracellular domains, i.e. between 10 and 20 nanometers.

The above estimates will be used to test the relevance of several interactions to cell adhesion.

The experimental success met by the DLVO theory of the stability of lyophobic colloids (independently elaborated by Derjaguin and Landau, and Verwey and Overbeek) prompted its application to biological systems [39]. The basic idea was to consider the balance between Van der Waals attraction and electrostatic repulsion (see, e.g., [24] for a review with reference to biological cells).

4.1.2. Electrodynamic attraction

The unretarded force F between two parallel lipid bilayers with thickness a and distance d is attractive, with intensity (per unit area)

$$F = (A/6\pi)(1/d^3 - 2/(d+a)^3 + 1/(d+2a)^3) \quad (11)$$

where A is called the Hamaker constant. Its value is of the order of 5×10^{-21} J in aqueous medium [98]. The corresponding energy W is given by

$$W = -(A/12\pi)(1/d^2 + 1/(d+2a)^2 - 2/(d+a)^2). \quad (12)$$

Considering two lipid bilayers of width 0.45 nm and area $0.01 \mu\text{m}^2$ separated by a gap of 10 nm width, the attractive force and energy are respectively 1.3 piconewton and $1.1 kT$ respectively (table 3). These values are negligible under standard experimental conditions.

4.1.3. Electrostatic repulsion

Since cells bear a net negative charge, they are expected to exert a mutual repulsion. In biological media, this repulsion is much lower than it would be in vacuum, since it is screened by water (with a relative dielectric constant of about 80) and electrolytes. In dilute solutions, it may be shown that the presence of free ions results in dividing

the interaction potential between two charges at distance r by a factor of $\exp(Kr)$, where $1/K$ is the 'Debye-Hückel length' (see, e.g., [24] for a brief review). This parameter can be calculated with the formula

$$K = \left(\sum_i c_i q_i^2 / \epsilon kT \right)^{1/2} \quad (13)$$

where the summation is over all ion species of concentration c_i (molecules/m³) and electric charge q_i , k is Boltzmann's constant, ϵ is the dielectric constant of water and T is the absolute temperature. In 150 mM NaCl solutions, the limit of validity of the simple theory is reached, but this can be used when electric fields are low. The Debye-Hückel length is about 0.8 nm and the interaction force and energy per unit area between two parallel plates with surface charge and separation d is [24, 98]

$$F \approx (2\sigma^2/\epsilon) \exp(-Kd), \quad (14)$$

$$W \approx 2(\sigma^2/\epsilon K) \exp(-Kd). \quad (15)$$

Considering two plates with surface charge equal to 0.02 C/m² and distance 10 nm, and 0.01 μm^2 area, F and W are respectively 4.2×10^{-14} N and 0.008 kT . These values are too low to influence bond formation.

However, the above calculation is based on the unwarranted assumption that the negative electric charge of cell membranes is concentrated near the phospholipid bilayer. If this charge is considered as scattered over the whole glycocalyx, another treatment is required. The simplest procedure is to consider these charges as uniformly distributed in a layer of thickness L . Since the charge density is low, we may use the simplest form of Debye-Hückel theory, and write the interaction energy between two charges q and q' separated by a distance r as

$$W = (qq'/4\pi\epsilon r) \exp(-Kr). \quad (16)$$

Table 3
Order of magnitude of several intercellular forces (for a contact area of 10^{-14} m² and interbilayer distance of 10 nm).

Interaction	Force (piconewton)	Energy (kT units)
Electrostatic: – charges on lipid polar groups	0.04	0.008
Electrostatic: – uniform volume distribution	72	125
Van der Waals attraction	1	1
Compression of surface anchored chains	9	50
Single molecular bond	5	10–20

The magnitude of several interactions was evaluated as described. It is concluded that cell-bound polyelectrolytes may prevent bond formation in usual conditions of encounter.

The electrostatic energy of the cell coat is then readily calculated as

$$W = \sigma^2 / 2\epsilon K^2 L \quad (17)$$

where σ is the equivalent surface charge density (i.e. volume density multiplied by cell coat thickness L). If we assume that cell coats are uniformly compressed when the cell surfaces are separated by a distance d lower than L , the interaction energy may be readily calculated as

$$W = \sigma^2(4/d - 2/L)/2\epsilon K^2. \quad (18)$$

Taking L as 20 nm and d as 10 nm, we obtain the estimates

$$F = 30 \text{ nanonewton}, \quad W = 124 \text{ } kT$$

for the repulsive force F and the energy W for an interaction area of 10^{-14} m^2 . These values are not negligible. However, we used very crude assumptions and more refined estimates might be needed. As will be discussed now, the most satisfactory approach from a theoretical point of view might be to use the framework of polymer theory and consider cell surfaces as coated with bound polyelectrolyte layers.

4.1.4. Cell-cell repulsion as an example of steric stabilization

The need to prepare stable colloid dispersions is often encountered in industrial practice. Indeed, micrometer size hydrophobic particles will spontaneously agglutinate in aqueous media unless some repulsive interaction prevents mutual approach. Hence, it may be argued that the problem of living cells may be to prevent useless adhesion as well as initiating purposeful contacts.

Electrostatic stabilization is achieved by coating colloid particles with charged groups. However, this is known to be inefficient in ionic solutions such as biological media [137] due to the screening of repulsive forces by counterions. Under these conditions, agglutination may be prevented by coating particles with adsorbed or grafted macromolecules. This is (unfortunately?) called steric stabilization. Much experimental and theoretical work was done to clarify this phenomenon. We refer the reader to recent reviews for more information on polymer physics [46], polymer at interfaces [47, 48] and especially steric stabilization [137]. We give only a brief summary of the problems encountered when applying these concepts to cellular systems.

The basic framework for describing long flexible chains is described in Flory's book [75]. A chain may be visualized as a sequence of N linear segments of length l with free rotation at the intersections. If rotation is hindered by molecular interactions, it is possible to consider an 'equivalent' chain with N' segments of length l' with free rotation ($N' < N$ and $l' > l$). The chain static conformation may be viewed as a weighted average of a large set of conformations. The probability $P(c)$ of each conformation c is given by

$$P(c) = \exp(-F(c)/kT)/Z \quad (19)$$

where the partition function Z is given by

$$Z = \sum_{\{c\}} \exp(-F(c)/kT) \quad (20)$$

where k is Boltzmann's constant, T is the absolute temperature and $F(c)$ is the free energy contribution of segment-segment, segment-solvent and solvent-solvent interactions. The partition function Z is related to the total free energy F by the standard formula

$$F = -kT \ln(Z). \quad (21)$$

Note that dynamic aspects are not considered.

If solvent and monomer groups are similar, all $F(c)$ are identical. This situation usually occurs at a well defined temperature (since $F(c)$ is usually dependent on T) which is called the θ temperature. One may also refer to a θ solvent. All configurations are then equivalent, which makes easier the determination of Z with statistical techniques (see [5] for a compact presentation as a prerequisite to dynamical studies). The 'root mean square end-to-end distance' (i.e. the square root of the mean square of end-to-end distance) is thus simply $l\sqrt{N}$. Another quantity of interest is the radius of gyration (R_g), that is defined as usual as the square root of the mean squared distance between the center of gravity of the chain and monomers.

$$R_g = l\sqrt{(N/6)}. \quad (22)$$

Now, the number of possible configurations is reduced by the constraint that only one monomer can be located at a given point. The partition function is further reduced in non- θ conditions. As indicated in section 3, water is a good solvent for polysaccharides found on the cell surface. This means that monomer-monomer interactions result in a free energy increase. This leads to a reduction of the probability of occurrence of more compact configurations, and the radius of gyration varies as $N^{0.6}$ rather than \sqrt{N} .

Consider now cell-to-cell approach. This may result in a free energy increase for several different reasons:

- i) When the intercellular distance is less than twice the extended length of surface chains, there is a reduction of possible configurations and increased weight of monomer-monomer interactions. In a good solvent, this results in a free energy increase that may be viewed as a mixing free energy.
- ii) If the extended length (Nl) of chains is higher than the interbilayer distance, some configurations are made impossible, and compact configurations, with monomer-monomer interactions, are favored. This interaction may be viewed as a chain compression effect.
- iii) The interaction is made more complex if intermolecular associations (specific or non specific, see below) occur between cell surfaces. In this case, bridges may be formed between surfaces and negative free energy variations can be

observed. Also, if surface chains are adsorbed rather than anchored, desorption or adsorption phenomena can occur. It is very difficult to account for these phenomena, however, we shall neglect them in the present section. This simplification may be valid if intermolecular associations are treated separately, and if cell-cell approach is too rapid to allow adsorption or desorption.

As emphasized by Israelachvili in his recent monograph [98], there is no universal 'ready-to-use' theory of steric stabilization. Also, the presence of charged groups on cell surface polymers makes more difficult the application of many current models. Therefore, in view of available results, we propose the following approach, while emphasizing that more work is clearly needed in this domain:

First, it was noted that several hours were required for equilibrium during the mutual approach between mica surfaces bearing polymer molecules in a good solvent [100]. Hence, it seems warranted to neglect polymer adsorption and desorption during the first steps of cell-to-cell approach and refer to interactions between surfaces with grafted, non-adsorbing polymers.

Secondly, if we model cell surface polymers as linear molecules with 1,000 units of monomers each and an mean of 0.5 monomer per nm^2 , the mean distance between chains is in the order of $1/\sqrt{(0.0005)} = 45 \text{ nm}$. This is not very different from the glycocalyx thickness, which suggests that chains may be considered as fairly independent (this is the so-called 'mushroom regime' defined by de Gennes).

If we neglect chain-chain interaction, we may estimate the compression contribution to cell-cell repulsion by making use of a theory elaborated by Dolan and Edwards who first treated the θ -solvent case [54] and later extended their calculation to a more general situation allowing monomer-monomer repulsion and excluded volume effects. The latter theory was much more complex and did not yield simple analytical formulae [55]. Since we are mainly interested in order-of-magnitude estimates, we shall use the results obtained in the first paper. The authors obtained two different formulae with complementary ranges of validity. For large separations d of the plane surfaces (greater than $l\sqrt{N}$), the free energy was found to be

$$F = -kT \ln (1 - 2 \exp(-3d^2/2Nl^2)). \quad (23)$$

For small separations (d smaller than about $1.7l\sqrt{N}$), they obtained

$$F = -kT \left(\ln (d\sqrt{(3/8\pi N)/l}) - \pi^2 l^2 N/6d^2 \right). \quad (24)$$

This result was very conveniently simplified by Israelachvili [98]. When the distance between the cell surfaces ranges between $2R_g$ and $8R_g$, where R_g is the radius of gyration, the repulsive free energy per chain is

$$W \approx 36kT \exp(-d/R_g). \quad (25)$$

Assuming a monomer density Γ of 0.5 monomer per nm^2 and a mean number of 1,000 monomers per chain, the interaction between two cells separated by a gap of 10 nm with a contact area of $0.01 \mu\text{m}^2$ is

$$F = 180kT \exp(-10/R_g) \quad (26)$$

where R_g is expressed in nanometer. A minimal estimate of R_g for standard cells would be about 8 nm, assuming a value of 0.6 nm for l (this is the length of an hexasaccharide group [102] and using equation (22). The minimal value of W would then be about $50kT$ with a corresponding force of $50kT/R_g \approx 8.8 \times 10^{-12}$ newton. It is concluded that steric stabilization may significantly impair the contact between cell microvilli. It is thus warranted to look for more precise data on these interactions. In this respect, it is worth recalling that the occurrence of fairly long-ranged repulsion between surfaces bearing adsorbed electrolytes was demonstrated experimentally with Israelachvili's surface force apparatus [118].

4.1.5. Other interactions

We refer the reader to specialized reviews for more details on diverse interactions that are not obviously relevant to nucleated cells [98]. We only mention some of these forces.

When the distance between two molecularly smooth surfaces is of the order of several diameters of solvent molecules (i.e. 0.2 nm for water), very strong forces may be generated by the ordering of these molecules in sequential planes parallel to the surfaces. Repulsive [116], attractive [99] or even oscillatory [98] forces were thus described. The intensity exhibits a fairly exponential decay with a characteristic length in the order of several tenths of nanometer. These interactions are not likely to play a role in cell-cell adhesion, since the interbilayer distance remains fairly high, and interacting surface are not molecularly smooth. However, these interactions might play a role in membrane fusion.

When the distance between two flexible surfaces is decreased, the shape fluctuations due to thermal agitation may be somewhat inhibited, which results in a repulsive force [92]. This interaction may be significant when very flexible structures such as lipid vesicles or erythrocytes are considered [70]. However, this must be much weaker when nucleated cells are considered, since their membranes are much more rigid.

Finally, the exclusion of macromolecules in the intercellular space may result in osmotic attraction. The force per unit area is simply nkT , where n is the macromolecule concentration in the bulk medium. The adhesive energy per unit area is $nkTD$, where D is the diameter of macromolecules. Considering plasma as a representative medium, the major macromolecule is albumin with a concentration in the order of 3.9×10^{23} molecules/m³ and a diameter in the order of 5 nm. The corresponding force and energy for an interaction area of $0.01 \mu\text{m}^2$ are respectively 1.6×10^{-11} newton and $20kT$. However, the exclusion of these molecules from contact area may depend on the tightness of adhesion [135]. Indeed, the possibility of performing immunofluorescence labeling in regions of contact between cytotoxic T lymphocytes and target cells suggests that molecules as large as immunoglobulin G (MW 150,000) are not always excluded from adhesion areas [6].

4.2. Initiation of adhesion

4.2.1. Surface energy approach

We shall only add some comments to the experimental results described in section 2.3.1.

A thermodynamic approach would seem in principle ideally suited to obtain general results concerning complex systems. Thus, it seems reasonable to try and derive the work of adhesion between cell surfaces from parameters measured on isolated cells. The aforementioned finding that equilibrium may not be reached before a very prolonged contact does not suffice to invalidate this approach, since many empirical procedures may be used to deal with systems that were in fact out of equilibrium (see for example discussions concerning contact angle hysteresis [4]).

The simplest approximation, first discovered by Raleigh and further emphasized by Good and colleagues [84] was to express the work of adhesion between two substances (1) and (2) as

$$W_{12} = p_1 p_2 \quad (27)$$

where p_1 and p_2 are intrinsic parameters of media (1) and (2). This formula yields

$$\gamma_{12} = \gamma_1 + \gamma_2 - 2\sqrt{\gamma_1 \gamma_2} \quad (28)$$

connecting the interfacial free energy γ_{12} of the (1–2) interface to the surface energies γ_1 and γ_2 of (1) and (2). It was soon recognized that this relationship only held between limited series of liquid media and it was suggested to split surface energies into several components. The most popular procedure was to discriminate between London ('dispersion') and polar components (see, e.g., [104]) and write

$$\gamma = \gamma^d + \gamma^p. \quad (29)$$

Thus, the surface free energy of water (73 mJ/m²) was written as a sum of a minor dispersive component (21 mJ/m²) and a major polar component (52 mJ/m²). Equation (23) is then replaced with

$$\gamma_{12} = \gamma_1 + \gamma_2 - 2\sqrt{\gamma_1^d \gamma_2^d} - 2\sqrt{\gamma_1^p \gamma_2^p}. \quad (30)$$

Other more sophisticated formulae were used (e.g., harmonic mean instead of geometric mean) without marked conceptual difference. A significant progress was the introduction of the concept of monopolar surfaces by Van Oss and colleagues [117], who emphasized the difference between molecules with a dipolar moment, and molecules with the capacity to form hydrogen bonds, either as proton donors or acceptors. They suggested that numerous biopolymers were in fact 'monopolar', by acting essentially either as electron donors or electron acceptors. Thus, they wrote the surface energy of a medium as

$$\gamma = \gamma^{LW} + \gamma^+ + \gamma^- \quad (31)$$

thus defining a Lifshitz–Van der Waals term, a proton-donating and a proton-accepting term. Finally, they suggested that the three interfacial components of a surface might be determined experimentally by contact angle determinations, using as test liquids diodomethane (an essentially apolar substance), dimethylsulfoxide (a liquid with an

essentially zero proton-donating component) and, e.g., water, where γ^+ and γ^- were set equal for the sake of convenience.

However, several problems make difficult the application of the aforementioned concepts to biological systems.

Firstly, the combination rules we mentioned can be subjected to direct experimental check only if all tested phases are liquid, thus allowing straightforward determination of all interfacial energies. However, the study of the surface properties of solids is much more difficult to achieve. This is a major difficulty, since the behavior of solid surfaces may be quite different from that of liquids [5] and cell surfaces cannot be treated as liquid structures. The impossibility to perform a direct test of theoretical formulae makes it difficult to assess the value of new ideas.

Secondly, even the incomplete measurements that can be performed on solid surfaces raise specific problem. Thus, the contact angles measured on cell monolayers depend on the conditions of preparation of these monolayers, which supports the suggestion that we are not dealing with equilibrium parameters [130]. Several authors studied the surface properties of biological cells by studying their partition between two immiscible phases [156]. This approach is quite attractive, but the derivation of quantitative parameters from experimental data is not straightforward.

Thirdly, whereas usual surface energies are in the order of several tens of mJ/m^2 , the intercellular interaction energies are much lower (see section 2). This means that there is a need for very accurate combination rules. These are not available at the present time.

Fourthly, it must be reminded that 'specific' interactions are not accounted for by the thermodynamic approach. This may be a problem with biological systems since many low-affinity interaction between complementary structural groups are probably involved in cell-cell interactions (e.g., interactions involving RGDS sequences described in section 2).

In conclusion, whereas the thermodynamic approach met with some success in describing the interaction between cells and polymer surfaces (see in this respect an interesting attempt as relating the thermodynamic approach to DLVO theory [179]), more work is needed before it may be used to assess the importance of nonspecific interactions between cells bound by specific ligands.

4.2.2. Consideration of ligand-receptor bonds

A fairly simple and powerful theoretical framework was suggested by George Bell [15] who emphasized several important ideas.

First, he obtained estimates for the kinetics of bond formation between membrane-associated molecules. The basic idea was to use the forward and reverse kinetic constants k_f and k_r for the equilibrium



The ratio k_f/k_r represents the equilibrium constant K , which was considered as independent of diffusion constants: this assumption allowed to use for K the range of values measured for association between soluble molecules. The approximation

was to neglect the difference between soluble and membrane molecules with respect to the free energy increase due to the loss of degrees of freedom as a consequence of complex formation. It was thus possible to estimate a reasonable order of magnitude for the maximum rate of bond formation as

$$dN_b/dt < 1.3 \times 10^{-2} N_1 N_2 \mu\text{m}^{-2} \quad (33)$$

where N_b , N_1 and N_2 are the numbers of complexes (1–2) and free molecules (1 or 2) on interacting cells per squared micrometer.

An other important point was the estimate of the maximum strength of a molecular bond: Bell estimated at about 10^{-11} newton the force required to uproot a receptor. This value was very close to experimental estimates later obtained by Goldsmith [169] and Evans [66].

Another concept emphasized by Bell [15] was an estimate of the effect of tension on the lifetime of a molecular bond. Using experimental data obtained on the lifetime of material samples subjected to varying loads [192], Bell suggested the following formula for the rate of bond dissociation:

$$k_r = k_{r0} \exp(\Gamma F/kTN_b) \quad (34)$$

where F is the total disruptive force, N_b is the number of bonds (the force is thus F/N_b per bond) and Γ is a constant that was taken as 0.5 nm.

The framework suggested by Bell was extended by Hammer and Lauffenburger [88] who considered the dynamic adhesion of cells to adhesive substrates in a viscous shear flow. They took care of the mobility of cell surface receptors and stress applied to molecular bonds. They were thus able to define a rate-controlled high affinity regime and a affinity-controlled low-affinity regime. In a later paper, this model was extended to a probabilistic framework accounting for the fluctuations of bond number [38]. This point was of obvious importance since adhesion can be initiated by very few bonds, and initial attachment is heavily dependent on the duration of the first bond. The authors concluded that the previous deterministic approach could underestimate the time needed for cell attachment and overestimate the time required for cell detachment.

The aforementioned approach was extended along different lines by Dembo and colleagues [49] who coupled the equations for deformation of an elastic membrane with equations for the kinetics of bond formation. They introduced the concept of 'catch bond' by noticing that the disruption of a stretched bond might be in principle slower than that of an unstressed bond. This is consistent with thermodynamic principles if the formation of stressed bonds is also much slower than the formation of unstressed ones. This concept is important since it suggests the interest of studying the effect of stress on the kinetic constants of bond formation and dissociation. This may be useful to understand the significance of different ligand-receptor couples recently demonstrated on the membranes of different cell populations. This may also be important to understand the conditions required for 'rolling' as described in section 2. However, more experimental data are required to support the validity of this interesting concept.

4.3. Analysis of the 'equilibrium' shape of cell-cell contacts

Electron microscopical studies of cell-cell contact areas demonstrated that the extension of the adhesive area [31] or the tightness of apposition between bound membranes [29] were increased when the adhesive bond density was increased [31] or nonspecific repulsive forces were decreased [29, 129]. It was thus tempting to build a model for the equilibrium shape of intercellular contact. Bell and colleagues [16] described a model of cell-cell adhesion with a balance between bond formation by mobile ligand and receptor molecules and nonspecific repulsion. Using phenomenological expressions for the repulsive force and bond elasticity, they estimated the equilibrium contact area and intermembrane distance with complete neglect of the cell mechanical behavior. Hence, this approach yielded a thermodynamic limit for the contact area. They stressed that active movements of one or another of the cells could however influence the kinetics of contact formation.

Other models of adhesion between solid surfaces described binding as a balance between adhesive surface forces and mechanical resistance of the surfaces. A basic model was described by Johnson and colleagues [101] to account for the adhesion of two solid elastic spheres with contact forces. They cleverly adapted Hertz's theory for the contact deformation of two spheres pushed against each other by a known load P . The main results of the adhesion theory may be sketched as follows. The radius a of the contact disc between a sphere of radius R and a rigid plane is

$$a = (R/K)(P + 3\Gamma R + \sqrt{-6\Gamma\pi RP + 9\Gamma^2\pi^2 R^2}) \quad (35)$$

where Γ is the work of adhesion per unit area and K is given by

$$K = (1 - \sigma^2)/(\pi E) \quad (36)$$

where σ is Poisson ratio and E is Young modulus. Another result is that the force required to separate surfaces is

$$P = -3\Gamma\pi R/2. \quad (37)$$

A difficulty with this theory is that infinite stress was predicted at the rim of the contact disc. This led Derjaguin and colleagues to introduce noncontact forces [51] (in fact, the first author of the latter paper had studied the effect of contact deformation on adhesion as soon as 1934, see [51]). These theories proved a sound basis to study the adhesion of solids, and they were subjected to experimental check [95]. Also, they were used to account for the interaction between rough surfaces by modeling asperities as protrusions with spherical tip and varying length [85]. These theories prompted later attempts at accounting for the modification of cell surface roughness in regions of contact with smooth surfaces. Rat macrophages were made to bind smoother glutaraldehyde-treated erythrocytes, and electron micrographs were used to measure the roughness of the macrophage membrane in free and contact areas. Then, assuming that the major part of the macrophage resistance to smoothing was located in microvilli, the adhesive energy was derived by considering the balance

between macrophage mechanical properties and adhesive forces [129]. However, the validity of the basic assumption was, admittedly, very difficult to check thoroughly.

A more rigorous approach was undertaken by Evans who derived the work of adhesion between the smooth surfaces of lipid vesicles or erythrocytes by measuring the encapsulation of a more rigid vesicles by a flaccid one, and considering the equilibrium between adhesive energy and mechanical resistance of interacting surfaces [69]. Also, he provided theoretical models of membrane-membrane adhesion where he incorporated the effects of membrane resistance to bending and tension as well as bond stretching. In the case of a continuum of molecular cross-bridges, the classical Young equation was found to be consistent with the model [64]. When he used a discrete distribution of cross-bridges, two interesting conclusions were reached [65]. First, the minimum tension required to separate adherent membranes might be different from the maximum tension induced in the membrane during contact formation. Secondly, he demonstrated the existence of lateral forces exerted on bonding structures, which might result in bond accumulation in contact zones during cell-cell separation. This possibility was strongly supported by the finding that increased membrane tension increased during the separation of lectin-attached red cells [68] as well as conjugated cytotoxic lymphocytes and target cells [172]. The latter experimental study prompted the elaboration of a dynamic model of conjugate formation involving a lateral diffusion of membrane molecules [171].

In conclusion, it seems now well established that the structure of cell-cell contact area is dependent on several well defined parameters such as bond energy, lateral mobility of binding molecules, bond elasticity, mechanical resistance of the cell membrane, nonspecific repulsion between interacting cells. Many models were elaborated to integrate these parameters into an unified theoretical framework. The main difficulty is that specific approximations are required to make these models tractable. This is possible only if the experimental values of numerical parameters or the behavior of empirical force/distance curves are known. However, these parameters are not known with sufficient accuracy at the present time. Also, it is likely that different biological systems behave in quite different ways, and a single workable model may not account for all situations of physiological interest. However, much progress was done during the last years and a reliable modeling of cell-cell initial adhesion no longer seems an impossible goal.

4.4. Cell-cell separation

Many aforementioned reports demonstrated that cell adhesion does not behave as a reversible process. Indeed, initial contact is rapidly followed by several active processes such as reorganization of membrane molecules, cytoskeletal concentration in adhesive regions, and possibly glycocalyx reorganization in order to minimize repulsion. It is therefore not surprising that the minimal force required to prevent bond formation may be much lower than the force required to detach bound cells (see, e.g., [128]). Indeed, cell separation may often be considered either as an active process where the cell chooses to release its 'grip' [146]. Alternatively, forced cell detachment may reflect membrane rupture rather than bond dissociation (see, e.g., [26]). Hence, the process of cell separation will not be further discussed in the present review.

Conclusion

The aim of this work was to describe present experimental and theoretical knowledge on the initial steps of cell adhesion. Since this encompasses many different fields of physics and biology, we chose to present a brief and incomplete sketch of available data, in order to make important issues more apparent. Our hope is that this will help biophysicists to enter the fascinating field of cell adhesion.

References

1. Abbas, A.K., K.A. Ault, M.J. Karnovsky and E.R. Unanue, 1975, Non random distribution of surface immunoglobulin on murine B lymphocytes, *J. Immunol.* **114**, 1197–1204.
2. Absolom, D.R., C.J. van Oss, W. Zingg and A.W. Neumann, 1982, Phagocytosis as a surface phenomenon. Opsonization by aspecific adsorption of IgG as a function of bacterial hydrophobicity, *J. Reticuloendothelial Soc.* **31**, 59–70.
3. Absolom, D.R., W. Zingg, C. Thomson, Z. Policova, C.J. van Oss and A.W. Neumann, 1985, Erythrocyte adhesion to polymer surfaces, *J. Colloid Interface Sci.* **104**, 51–59.
4. Adamson, A.W., 1982, *Physical Chemistry of Surfaces* (Wiley, New York).
5. Andrade, J.D., S.M. Ma, R.N. King and D.E. Gregonis, 1979, Contact angles at the solid-water interface, *J. Colloid Interface Sci.* **72**, 488–494.
6. André, P., A.M. Benoliel, C. Capo, C. Foa, M. Buferne, C. Boyer, A.M. Schmitt-Verhulst and P. Bongrand, 1990, Use of conjugates made between a cytolytic T cell clone and target cells to study the redistribution of membrane molecules in cell contact areas, *J. Cell Sci.* **97**, 335–347.
7. André, P. and P. Bongrand, 1990, Cell-cell contacts, in: *Biophysics of the Cell Surface*, eds R. Glaser and D. Gingell (Springer, Berlin) pp. 287–322.
8. André, P., C. Capo, A.M. Benoliel, P. Bongrand, F. Rougé and C. Aubert, 1990, Splitting cell adhesiveness into independent measurable parameters by comparing ten human melanoma cell lines, *Cell Biophys.* **17**, 163–180.
9. André, P., J. Gabert, A.M. Benoliel, C. Capo, C. Boyer, A.M. Schmitt-Verhulst, B. Malissen and P. Bongrand, 1991, Wild type and tailless CD8 display similar interaction with microfilaments during capping, *J. Cell Sci.* **100**, 329–337.
10. Arnott, S., A. Rees and E.R. Morris, 1983, *Molecular Biophysics of the Extracellular Matrix* (Humana Press, Clifton).
11. Atherton, A. and G.V.R. Born, 1972, Quantitative investigations on the adhesiveness of circulating polymorphonuclear leukocytes to blood vessel walls, *J. Physiol.* **222**, 447–474.
12. Ault, K.A. and E.R. Unanue, 1978, in: *Theoretical Immunology*, eds G.I. Bell, A.S. Perelson and G.H. Pimbley (Marcel Dekker, New York) pp. 145–169.
13. Baier, R.E. and L. Weiss, 1975, Demonstration of the involvement of adsorbed proteins in cell adhesion and cell growth on solid surfaces, *Adv. Chem. Ser.* **145**, 300–307.
14. Baumgartner, H.R., T.B. Tschopp and D. Meyer, 1980, Shear rate dependent inhibition of platelet adhesion and aggregation on collagenous surfaces by antibodies to human factor VIII/von Willebrand factor, *Br. J. Haematol.* **44**, 127–139.
15. Bell, G.I., 1978, Models for the specific adhesion of cells to cells, *Science* **200**, 618–627.
16. Bell, G.I., M. Dembo and P. Bongrand, 1984, Cell adhesion – competition between nonspecific repulsion and specific bonding, *Biophys. J.* **45**, 1051–1064.
17. Ben Shaul, Y. and A. Moscona, 1975, Scanning electron microscopy of aggregating embryonic neural retina cells, *Exp. Cell Res.* **95**, 191–204.
18. Berke, G., 1980, Interaction of cytotoxic T lymphocytes and target cells, *Prog. Allergy* **27**, 69–133.
19. Bevilacqua, M.P., S. Stengelin, M.A. Gimbrone and B. Seed, 1989, Endothelial leukocyte adhesion molecule 1: An inducible receptor for neutrophils related to complement regulatory proteins and lectins, *Science* **243**, 1160–1165.
20. Bierer, B.E., B.P. Sleckman, S.E. Ratnovsky and S.J. Burakoff, 1989, The biologic roles of CD2, CD4 and CD8 in T cell activation, *Annu. Rev. Immunol.* **7**, 579–599.

21. Bjorkman, P., M. Saper, B. Samraoui, W. Bennett, J. Strominger and D. Wiley, 1987, Structure of the human class I histocompatibility antigen HLA-A2, *Nature* **329**, 506–512.
22. Bongrand, P., 1988, *Physical Basis of Cell-Cell Adhesion* (CRC Press, Boca Raton, FL).
23. Bongrand, P. and G.I. Bell, 1984, Cell-cell adhesion: Parameters and possible mechanisms, in: *Cell Surface Dynamics: Concepts and Models*, eds A.S. Perelson, C. DeLisi and F.W. Wiegel (Marcel Dekker, New York) pp. 459–493.
24. Bongrand, P., C. Capo and R. Depieds, 1982, Physics of cell adhesion, *Prog. Surf. Sci.* **12**, 217–286.
25. Bongrand, P., C. Capo, J.L. Mège and A.M. Benoliel, 1988, Use of hydrodynamic flows to study cell adhesion, in: *Physical Basis of Cell-Cell Adhesion*, ed. P. Bongrand (CRC Press, Boca Raton, FL) pp. 125–156.
26. Bongrand, P. and P. Golstein, 1983, Reproducible dissociation of cellular aggregates with a wide range of calibrated shear forces: Application to cytolytic lymphocyte-target cell conjugates, *J. Immunol. Methods* **58**, 209–224.
27. Bongrand, P., M. Pierres and P. Golstein, 1983, T cell-mediated cytotoxicity: On the strength of effector-target cell interaction, *Eur. J. Immunol.* **13**, 424–429.
28. Buxbaum, R., E. Evans and D.E. Brook, 1982, Quantitation of surface affinities of red blood cells in dextran solutions and plasma, *Biochemistry* **21**, 3235–3239.
29. Capo, C., P. Bongrand, A.M. Benoliel, A. Ryter and R. Depieds, 1981, Particle-macrophage interaction: Role of surface charges, *Ann. Immunol. (Inst. Pasteur)* **132D**, 165–173.
30. Capo, C., F. Garrouste, A.M. Benoliel, P. Bongrand and R. Depieds, 1981, Nonspecific binding by macrophages: Evaluation of the influence of medium-range electrostatic repulsion and short-range hydrophobic interaction, *Immunol. Commun.* **10**, 35–43.
31. Capo, C., F. Garrouste, A.M. Benoliel, P. Bongrand, A. Ryter and G.I. Bell, 1982, Concanavalin A-mediated thymocyte agglutination: A model for a quantitative study of cell adhesion, *J. Cell Sci.* **56**, 21–48.
32. Carpen, O., M.L. Dustin, T.A. Springer, J.A. Swafford, L.A. Beckett and J.P. Caulfield, 1991, Mobility and ultrastructure of large granular lymphocytes on lipid bilayers reconstituted with adhesion receptors LFA-1, ICAM-1 and two isoforms of LFA-3, *J. Cell Biol.* **115**, 861–871.
33. Carr, I., G. Everson, A. Rankin and J. Rutherford, 1970, The fine structure of the cell coat of the peritoneal macrophage and its role in the recongition of foreign material, *Z. Zellforsch. Microsk. Anat.* **105**, 339–349.
34. Chien, S., G.W. Schmid-Schönbein, K.L.P. Sung, E.A. Schmalzer and R. Skalak, 1984, Viscoelastic properties of leukocytes, in: *White Cell Mechanics – Basic Science and Clinical Aspects*, eds H.J. Meiselman, M.A. Lichtman and P.L. LaCelle (Alan Liss, New York) pp. 19–51.
35. Christink, E.R., M.A. Luscher, B.H. Barber and D.B. Williams, 1991, Peptide binding to class I MHC on living cells and quantitation of complexes required for CTL lysis, *Nature* **352**, 67–70.
36. Cook, G.M.W., 1976, Techniques for the analysis of membrane carbohydrates, in: *Biochemical Analysis of Membranes*, ed. A.H. Madden (Chapman and Hall, London) pp. 283–351.
37. Corri, W.D. and V. Defendi, 1981, Centrifugal assessment of cell adhesion, *J. Biochem. Biophys. Med.* **4**, 29–38.
38. Cozens-Roberts, C., D.A. Lauffenburger and J.A. Quinn, 1990, Receptor-mediated cell attachment and detachment kinetics. I – Probabilistic model and analysis, *Biophys. J.* **58**, 841–856.
39. Curtis, A.S.G., 1967, *The Cell Surface: Its Molecular Role in Morphogenesis* (Logo Press, Academic Press, New York).
40. Curtis, A.S.G., 1988, The data on cell adhesion, in: *Physical Basis of Cell-Cell Adhesion*, ed. P. Bongrand (CRC Press, Boca Raton, FL) pp. 207–225.
41. Curtis, A.S.G. and J.V. Forrester, 1984, The competitive effect of serum proteins on cell adhesion, *J. Cell Sci.* **71**, 17–35.
42. Curtis, A.S.G. and J.M. Lackie, 1991, *Measuring Cell Adhesion* (Wiley, New York).
43. Curtis, A.S.G., M. McGrath and L. Gasmi, 1992, Localised application of an activating signal to a cell: Experimental use of fibronectin bound to beads and the implications for mechanisms of adhesion, *J. Cell Sci.* **101**, 427–436.

44. David, G., V. Lories, A. Heremans, B. van der Schuerent, J.J. Cassiman and H. van den Bergh, 1989, Membrane-associated chondroitin sulfate proteoglycans of human lung fibroblast, *J. Cell Biol.* **108**, 1165–1175.
45. de Biasio, R.L., L.L. Wang, G.W. Fisher and D.L. Taylor, 1988, The dynamic distribution of fluorescent analogues of actin and myosin in protrusions at the leading edge of migrating swiss 3T3 fibroblasts, *J. Cell Biol.* **107**, 2631–2645.
46. de Gennes, P.G., 1979, *Scaling Concepts in Polymer Physics* (Cornell University Press, Ithaca).
47. de Gennes, P.G., 1987, Polymer at interfaces: A simplified view, *Adv. Colloid Interface Sci.* **27**, 189–209.
48. de Gennes, P.G., 1988, Model polymer at interfaces, in: *Physical Basis of Cell-Cell Adhesion*, ed. P. Bongrand (CRC Press, Boca Raton, FL) pp. 39–60.
49. Dembo, M., D.C. Torney, K. Saxman and D. Hammer, 1988, The reaction-limited kinetics of membrane-to-surface adhesion and detachment, *Proc. R. Soc. London Ser. B* **234**, 55–83.
50. de Petris, S., 1978, Preferential distribution of surface immunoglobulins on microvilli, *Nature* **272**, 66–68.
51. Derjaguin, B.V., V.M. Muller and Y.D. Toporov, 1975, Effect of contact deformations on the adhesion of particles, *J. Colloid Interface Sci.* **115**, 480–492.
52. Detmers, P.A., S.D. Wright, E. Olsen, B. Kimball and Z.A. Cohn, 1987, Aggregation of complement receptors of human neutrophils in the absence of ligand, *J. Cell Biol.* **105**, 1137–1145.
53. Doi, M. and S.F. Edwards, 1988, *The Theory of Polymer Dynamics* (Clarendon Press, Oxford).
54. Dolan, A.K. and S.F. Edwards, 1974, Theory of the stabilization of colloids by adsorbed polymer, *Proc. Roy. Soc.* **A337**, 509–516.
55. Dolan, A.K. and S.F. Edwards, 1975, The effect of excluded volume on polymer dispersant action, *Proc. Roy. Soc.* **A343**, 427–442.
56. Dong, C., R. Skalak, K.L.P. Sung, G.W. Schmid-Schönbein and S. Chien, 1988, Passive deformation analysis of human leucocytes, *J. Biomech. Eng.* **110**, 27–36.
57. Easty, G.C., D.M. Easty and E.J. Ambrose, 1960, Studies of cellular adhesiveness, *Exp. Cell Res.* **19**, 539–548.
58. Edidin, M., S.C. Kuo and M.P. Sheetz, 1992, Lateral movement of membrane glycoproteins restricted by dynamic cytoplasmic barriers, *Science* **254**, 1379–1382.
59. Edidin, M. and M. Zuniga, 1984, Lateral diffusion of wild-type and mutant Ld antigens in L cells, *J. Cell Biol.* **99**, 2333–2335.
60. Einstein, A., 1956, *Investigations of the Theory of Brownian Movement* (Dover, New York).
61. Elias, H., A. Hennig and E. Schwartz, 1971, Stereology: Application to biomedical research, *Physiol. Rev.* **51**, 158–200.
62. Engel, J., E. Odermatt and A. Engel, 1981, Shapes, domain organizations and flexibility of laminin and fibronectin, two multifunctional proteins of the extracellular matrix, *J. Mol. Biol.* **150**, 97–120.
63. Erickson, C.A. and J.P. Trinkaus, 1976, Microvilli and blebs as sources of reserve surface membrane during cell spreading, *Exp. Cell Res.* **99**, 375–384.
64. Evans, E.A., 1985, Detailed mechanics of membrane-membrane adhesion and separation. I – Continuum of molecular cross-bridges, *Biophys. J.* **48**, 175–183.
65. Evans E.A., 1985, Detailed mechanics of membrane-membrane adhesion and separation. II – Discrete kinetically trapped molecular cross-bridges, *Biophys. J.* **48**, 175–183.
66. Evans, E., D. Berk and A. Leung, 1991, Detachment of agglutinin-bonded red blood cells. I – Forces to rupture molecular point attachments, *Biophys. J.* **59**, 838–848.
67. Evans, E.A. and B. Kukan, 1984, Passive material behavior of granulocytes based on large deformation and recovery after deformation test, *Blood* **64**, 1028–1035.
68. Evans, E.A. and A. Leung, 1984, Adhesivity and rigidity of red blood cell membrane in relation to WGA binding, *J. Cell Biol.* **98**, 1201–1208.
69. Evans, E.A. and M. Metcalfe, 1984, Free energy potential for aggregation of mixed PC:PS lipid vesicles in glucose polymer (dextran), *Biophys. J.* **45**, 715–720.
70. Evans, E.A. and V.A. Parsegian, 1986, Thermal-mechanical fluctuations enhance repulsion between bimolecular layers, *Proc. Nat. Acad. Sci. USA* **83**, 7132–7136.

71. Evans, E.A. and R. Skalak, 1980, *Mechanics and Thermodynamics of Biomembranes* (CRC Press, Boca Raton, FL).
72. Evans, E.A. and A. Yeung, 1989, Apparent viscosity and cortical tension of blood granulocytes determined by micropipet aspiration, *Biophys. J.* **56**, 151–160.
73. Eyring, E., J. Walter and G.E. Kimball, 1944, *Quantum Chemistry* (Wiley, New York).
74. Flanagan, I. and G.L.E. Koch, 1978, Cross-linked surface Ig attaches to actin, *Nature* **273**, 278–281.
75. Flory, P.J. 1981, *Principles of Polymer Chemistry* (Cornell University Press, Ithaca).
76. Foa, C., J.L. Mège, C. Capo, A.M. Benoliel, J.R. Galindo and P. Bongrand, 1988, T-cell mediated cytotoxicity: Analysis of killer and target deformability and deformation during conjugate formation, *J. Cell Sci.* **89**, 561–573.
77. Foxall, C., S.R. Watson, D. Dowbenko, C. Fennie, L.A. Lasky, M. Kiso, A. Hasegawa, D. Asa and B.K. Brandley, 1992, The three members of the selectin receptor family recognize a common carbohydrate epitope, the sialyl lewis oligosaccharide, *J. Cell Biol.* **117**, 895–902.
78. Francis, G.W., L.R. Fisher, R.A. Gamble and D. Gingell, 1987, Direct measurement of cell detachment on single cells, using a new electromechanical method, *J. Cell Sci.* **87**, 519–523.
79. Frojmovic, M., K. Longmire and T.G. van de Ven, 1990, Long range interactions in mammalian platelet aggregation. II – The role of platelet pseudopod number and length, *Biophys. J.* **58**, 309–318.
80. Gennis, R.B., 1989, *Biomembranes – Molecular Structure and Function* (Springer, New York).
81. Gingell, D. and I. Todd, 1980, Red blood cell adhesion. II – Interferometric examination of the interaction with hydrocarbon oil and glass, *J. Cell Sci.* **41**, 135–149.
82. Goldman, A.J., R.G. Cox and H. Brenner, 1967, Slow viscous motion of a sphere parallel to a plane wall. II – Couette flow, *Chem. Eng. Sci.* **22**, 653–660.
83. Golstein, P. and E.E. Smith, 1976, The lethal hit stage of mouse T and non T cell mediated cytotoxicity: Differences in cation requirements and characterization of an analytical ‘cation pulse’ method.
84. Good, R.J., 1977, Surface free energy of solids and liquids: Thermodynamics, molecular forces and structure, *J. Colloid Interface Sci.* **59**, 398–419.
85. Greenwood, J.A. and J.B.P. Williamson, 1966, Contact of nominally flat surfaces, *Proc. R. Soc. London Ser. A* **295**, 300–319.
86. Grimm, E., Z. Price and B. Bonavida, 1979, Studies on the induction and expression of T cell-mediated immunity. III. Effector-target junctions and target cell membrane disruption during cytotoxicity, *Cell Immunol.* **46**, 77–99.
87. Grinnell, F. and M.K. Feld, 1982, Fibronectin adsorption on hydrophilic and hydrophobic surfaces detected by antibody binding and analyzed during cell adhesion in serum-containing medium, *J. Biol. Chem.* **257**, 4888–4893.
88. Hammer, D.A. and D.A. Lauffenburger, 1987, A dynamical model for receptor-mediated adhesion to surfaces, *Biophys. J.* **52**, 475–487.
89. Harris, A.K., P. Wild and D. Stopak, 1980, Silicone rubber substrata: A new wrinkle in the study of cell locomotion, *Science* **208**, 177–179.
90. Haynes, B.F., M.J. Telen, L.P. Hale and S.M. Denning, 1989, CD44 – A molecule involved in leukocyte adherence and T cell activation, *Immunol. Today* **10**, 423–428.
91. Hedman, K., S. Johansson, T. Vartio, L. Kjellén, A. Vaheri and H. Hook, 1982, Structure of the pericellular matrix: Association of heparan and chondroitin sulfates with fibronectin-procollagen fibres, *Cell* **28**, 603–671.
92. Hellfrich, W., 1978, Steric interaction of fluid membranes in multilayer systems, *Z. Naturforsch.* **33a**, 305–315.
93. Henkart, P.A., 1985, Mechanisms of lymphocyte-mediated cytotoxicity, *Annu. Rev. Immunol.* **3**, 31–58.
94. Hiramoto, Y., 1969, Mechanical properties of the protoplasm of the sea urchin egg. I – Unfertilized egg, *Exp. Cell Res.* **56**, 201–208.
95. Horn, R.G., J.N. Israelachvili and F. Pribac, 1987, Measurement of the deformation and adhesion of solids in contact, *J. Colloid Interface Sci.* **115**, 480–492.

96. Horoyan, M., A.M. Benoliel, C. Capo and P. Bongrand, 1990, Localization of calcium and micro-filament changes in mechanically stressed cells, *Cell Biophys.* **17**, 243–256.
97. Hynes, R.O., 1992, Integrins: Versatility, *n* modulation and signaling in cell adhesion, *Cell* **69**, 11–25.
98. Israelachvili, J., 1991, *Intermolecular and Surface Forces* (Academic Press, New York).
99. Israelachvili, J. and R. Pashley, 1982, The hydrophobic interaction is long-range decaying exponentially with distance, *Nature* **300**, 341–342.
100. Israelachvili, J., R.K. Tandon and L.R. White, 1979, Measurement of forces between two mica surfaces in aqueous poly (ethyleneoxide) solutions, *Nature* **277**, 120–121.
101. Johnson, K.L., K. Kendall and A.D. Roberts, 1971, Surface energy and the contact of elastic solids, *Proc. R. Soc. London A* **324**, 301–313.
102. Kabat, E.A., 1968, *Structural Concepts in Immunology and Immunochemistry* (Holt, Rinehart and Winston, New York).
103. Kalina, M. and G. Berke, 1976, Contact regions of cytotoxic T lymphocyte-target cell conjugates, *Cell Immunol.* **25**, 41–51.
104. Kinloch, A.J., 1980, The science of adhesion – Part I: Surface and interfacial aspects, *J. Mater. Sci.* **15**, 2141–2166.
105. Knutton, S.K., M.C.B. Sumner and C.A. Pasternak, 1975, Role of microvilli in surface charge of synchronized P815Y mastocytoma cells, *J. Cell Biol.* **66**, 568–576.
106. Kolodney, M.S. and R.B. Wysolmerski, 1992, Isometric contraction by fibroblasts and endothelial cells in tissue culture: A quantitative study, *J. Cell Biol.* **177**, 73–82.
107. Koppel, D.E., M.P. Sheetz and M. Schindler, 1981, Matrix control of protein diffusion in biological membranes, *Proc. Nat. Acad. Sci. USA* **78**, 3576–3580.
108. Kraemer, P.H., 1979, Mucopolysaccharides: Cell biology and malignancy, in: *Surfaces of Normal and Malignant Cells*, ed. R.O. Hynes (Wiley, New York).
109. Kupfer, A. and S.J. Singer, 1989, Cell biology of cytotoxic and helper T cell functions, *Annu. Rev. Immunol.* **7**, 309–338.
110. Langlet, C., G.A. Neil and L.A. Sherman, 1987, The mechanism of anti-Lyt2 inhibition of antibody-directed lysis by cytotoxic T lymphocytes, *J. Immunol.* **139**, 3590–3596.
111. Lawrence, M.B. and T.A. Springer, 1991, Leukocytes roll on a selectin at physiologic flow rates: Distinction from and prerequisite for adhesion through integrins, *Cell* **65**, 859–873.
112. LeBouteiller, P.P., Z. Mishal, F.A. Lemonnier and F.M. Kourilsky, 1983, Quantification by flow cytometry of HLA class I molecules at the surface of murine cells transformed by cloned HLA gene, *J. Immunol. Methods* **61**, 301–315.
113. Lehninger, A., 1973, *Biochimie* (Flammarion, Paris).
114. Levine, Y.K., 1972, Physical studies of membrane structure, *Prog. Biophys. Mol. Biol.* **24**, 1–74.
115. Lipscomb, M.F., K.V. Holmes, E.S. Vitetta, U. Hammerling and J.W. Uhr, 1975, Cell surface immunoglobulin. XII – Localization of immunoglobulin on muring lymphocytes by scanning immunoelectron microscopy, *Eur. J. Immunol.* **5**, 255–259.
116. Lis, L.J., M. Mcalister, N. Fuller, R.D. Rand and V.A. Parsegian, 1982, Interaction between neutral phospholipid bilayer membranes, *Biophys. J.* **37**, 657–666.
117. Livnek, E., M. Benveniste, R. Prywes, S. Felder, Z. Kam and J. Schlessinger, 1986, Large deletions in the cytoplasmic kinase domain of the epidermal growth factor receptor do not affect its lateral mobility, *J. Cell Biol.* **103**, 327–331.
118. Luckham, P.F. and J. Klein, 1984, Forces between mica surfaces bearing adsorbed polyelectrolytes, *J. Chem. Soc. Faraday Trans.* **80**, 865–878.
119. Makita, A. and H. Shimojo, 1973, Polysaccharides of SV40-transformed green monkey kidney cells, *Biochim. Biophys. Acta* **304**, 571–574.
120. Margolis, L.B., E.V. Dyatovitskaya and L.D. Bergelson, 1978, Cell-lipid interaction: Cell attachment to lipid substrates, *Exp. Cell Res.* **111**, 454–457.
121. Margolis, L.B., A.N. Tikhonov and E.Y. Vasilieva, 1980, Platelet adhesion to fluid and solid phospholipid membranes, *Cell* **19**, 189–195.
122. Martinez-Palomo, A., 1970, The surface coats of animal cells, *Int. Rev. Cytol.* **29**, 29–75.

123. Mayrovitz, H.N., 1992, Leukocyte rolling. A prominent feature of venules in intact skin of anesthetized hairless mice, *Am. J. Physiol.* **262**, H157–H161.
124. McClay, D.R., G.M. Wessel and R. B. Marchase, 1981, Intercellular recognition: Quantitation of initial binding events, *Proc. Nat. Acad. Sci. USA* **78**, 4975–4979.
125. McKeever, P.E. 1974, Methods to study pulmonary alveolar macrophage adherence: Micromanipulation and quantitation, *J. Reticuloendothelial Soc.* **16**, 313–317.
126. McKeown-Longo, P.J. and D.F. Mosher, 1983, Binding of plasma fibronectin to cell layers of human skin fibroblasts, *J. Cell Biol.* **97**, 466–472.
127. Mège, J.L., C. Capo, P. André, A.M. Benoliel and P. Bongrand, 1990, Mechanisms of leukocyte adhesion, *Biorheology* **27**, 433–444.
128. Mège, J.L., C. Capo, A.M. Benoliel and P. Bongrand, 1986, Determination of binding strength and kinetics of binding initiation – a model study made on the adhesive properties of P388D1 macrophage-like cells, *Cell Biophys.* **8**, 141–160.
129. Mège, J.L., C. Capo, A.M. Benoliel and P. Bongrand, 1987, Use of contour analysis to evaluate the affinity between macrophages and glutaraldehyde-treated erythrocytes, *Biophys. J.* **52**, 177–186.
130. Mège, J.L., C. Capo, A.M. Benoliel, C. Foa and P. Bongrand, 1984, Nonspecific cell surface properties: Contact angle of water on dried cell monolayers, *Immunol. Commun.* **13**, 211–227.
131. Mège, J.L., C. Capo, A.M. Benoliel, C. Foa and P. Bongrand, 1985, Study of cell deformability by a simple method, *J. Immunol. Methods* **82**, 3–15.
132. Mège, J.L., C. Capo, A.M. Benoliel, C. Foa, J.R. Galindo and P. Bongrand, 1986, Quantification of cell surface roughness: A method for studying cell mechanical and adhesive properties, *J. Theoret. Biol.* **119**, 147–160.
133. Mehrishi, J.N., 1972, Molecular aspects of the mammalian cell surface, *Prog. Biophys. Mol. Biol.* **25**, 3–70.
134. Meiselman, H.J., M.A. Lichtman and P.L. LaCelle, 1984, *White Cell Mechanics: Basic Sciences and Clinical Aspects* (Alan Liss, New York).
135. Michl, J., M.M. Pieczonka, J.C. Unkeless, G.I. Bell and S.C. Silverstein, 1983, Fc Receptor modulation in mononuclear phagocytes maintained on immobilized immune complexes occurs by diffusion of the receptor molecule, *J. Exp. Med.* **157**, 2121–2139.
136. Mosher, D.F., F.J. Fogerty, M.A. Chernousov and E.L.R. Barry, 1991, Assembly of fibronectin into extracellular matrix, *Ann. NY Acad. Sci.* **614**, 167–180.
137. Napper, D.H., 1983, *Polymeric Stabilization of Colloid Dispersions* (Academic Press, London).
138. Neumann, A.W., D.R. Absolom, C.J. van Oss and W. Zingg, 1979, Surface thermodynamics of leukocyte and platelet adhesion to polymer surfaces, *Cell Biophys.* **1**, 79–92.
139. Norment, A.M., R.D. Salter, P. Parham, V.H. Engelhard and D.R. Littman, 1988, Cell-cell adhesion mediated by CD8 and MHC class I molecules, *Nature* **336**, 79–81.
140. Pardi, R., L. Inverardi and J.R. Bender, 1992, Regulatory mechanisms in leukocyte adhesion: Flexible receptors for sophisticated travelers, *Immunol. Today* **13**, 224–230.
141. Pasternak, C. and E.L. Elson, 1985, Lymphocyte mechanical response triggered by cross-linking surface receptors, *J. Cell Biol.* **100**, 860–872.
142. N.O. Petersen, W.B. McConnaugley and E.L. Elson, 1982, Dependence of locally measured cellular deformability on position of the cell, temperature and cytochalasin B, *Proc. Nat. Acad. Sci. USA* **79**, 5327–5331.
143. Picker, L.J., R.A. Warnock, C.K. Arburns, C.M. Doershnik, E.L. Berg and E.C. Butcher, 1991, The neutrophil selectin LECAM-1 presents carbohydrate ligands to the vascular selectin, *Cell* **66**, 921–933.
144. Piersbacher, M.D. and E. Ruoslahti, 1984, Cell attachment activity of fibronectin can be duplicated by small synthetic fragments of the molecule, *Nature* **309**, 30–33.
145. Podack, E.R. and M.G. Lichtenheld, 1991, A central role of perforin in cytotoxicity?, *Annu. Rev. Immunol.* **9**, 129–157.
146. Rees, D.A., C.W. Lloyd and D. Thom, 1977, Control of grip and stick in cell adhesion through lateral relationships of membrane glycoproteins, *Nature* **267**, 124–128.

147. Robbin, R., S.O. Albert, N.A. Gelb and P.H. Black, 1975, Cell surface changes correlated with density dependent growth inhibition. Glycosaminoglycan metabolism in 3T3, SV3T3 and conA-selected revertant cells, *Biochemistry* **14**, 347–357.
148. Rothstein, T.L., M. Mage, G. Jones and L.L. McHugh, 1978, Cytotoxic T lymphocyte sequential killing of immobilized allogeneic tumor target cells measured by time lapse microcinematography, *J. Immunol.* **121**, 1652–1656.
149. Rutishauser, U., A. Acheson, A.K. Hall, D.M. Mann and J. Sunshine, 1988, The neural cell adhesion molecule (NCAM) as a regulator of cell-cell interactions, *Science* **240**, 53–57.
150. Ryan, T.A., J. Myers, D. Holowka, B. Baird and W.W. Webb, 1988, Molecular constraint on the cell surface, *Science* **239**, 61–64.
151. Schackenraad, J.M., H.J. Busscher, C.R.H. Wildevuur and J. Arends, 1988, Thermodynamic aspects of cell spreading on solid substrata, *Cell Biophys.* **13**, 75–91.
152. Schlessinger, J., L.S. Barak, G.G. Hammer, K.M. Yamada, I. Pastan, W.W. Webb and E.L. Elson, 1977, Mobility and distribution of a cell surface glycoprotein and its interaction with other membrane components, *Proc. Nat. Acad. Sci. USA* **74**, 2909–2913.
153. Schmid-Schönbein, G.W., K.L.P. Sung, H. Tozeren, R. Skalak and S. Chien, 1981, Passive mechanical properties of human leucocytes, *Biophys. J.* **36**, 243–256.
154. Schmid-Schönbein, G.W., S. Usami, R. Skalak and S. Chien, 1980, The interaction of leukocytes and erythrocytes in capillary and post-capillary vessels, *Microvas. Res.* **19**, 45–70.
155. Schubert, D. and M. Lacorbière, 1980, A role of secreted glycosaminoglycans in cell-substratum adhesion, *J. Biol. Chem.* **255**, 11564–11569.
156. Schürch, S., D.F. Gerson and D.J.L. McIver, 1981, Determination of cell-medium interfacial tensions from contact angles in aqueous polymer systems, *Biochim. Biophys. Acta* **640**, 557–571.
157. Scullion, B.F., Y. Hou, L. Puddington, J.K. Rose and K. Jacobson, 1987, Effect of mutations in three domains of the vesicular stomatitis viral glycoprotein on its lateral diffusion in the plasma membrane, *J. Cell Biol.* **105**, 69–75.
158. Shaw, S., G.E. Gunther-Luce, R. Quinones, R.E. Gress, T.A. Springer and M.E. Sanders, 1986, Two antigen-independent adhesion pathways used by human cytotoxic T cell clones, *Nature* **323**, 262–264.
159. Soderquist, M.E. and A.G. Walton, 1980, Structural changes in proteins adsorbed on polymer surfaces, *J. Colloid Interface Sci.* **75**, 386–397.
160. Springer, T.A., 1990, Adhesion receptors of the immune system, *Nature* **346**, 425–434.
161. Staunton, D.E., M.L. Dustin, H.P. Erickson and T.A. Springer, 1990, The arrangement of the immunoglobulin-like domains of ICAM-1 and the binding sites for LFA-1 and rhinovirus, *Cell* **61**, 243–254.
162. Stolberg, J. and S.E. Fraser, 1988, Acetylcholine receptors and concanavalin A binding sites on culture *Xenopus* muscle cells. Electrophoresis, diffusion and aggregation, *J. Cell Biol.* **107**, 1397–1408.
163. Sugimoto, Y., 1981, Effect on the adhesion and locomotion of mouse fibroblasts by their interaction with differently charged substrates. A quantitative study by ultrastructural methods, *Exp. Cell Res.* **135**, 39–45.
164. Sung, K.L.P., C. Dong, G.W. Schmid-Schönbein, S. Chien and R. Skalak, 1988, Leukocyte relaxation properties, *Biophys. J.* **54**, 331–336.
165. Sung, K.L.P., L.A. Sung, M. Crimmins, S.J. Burakoff and S. Chien, 1986, Determination of junction avidity of cytolytic T cell and target cell, *Science* **234**, 1405–1408.
166. Tangelder, G.J. and K.E. Arfors, 1991, Inhibition of leukocyte rolling in venules by protamine and sulfated polysaccharides, *Blood* **77**, 1565–1571.
167. Taniguchi, N., I. Nanba and S. Kozuyumi, 1974, Characterization of glycosaminoglycans in human leucocytes, *Biochem. Med.* **11**, 217–226.
168. Tank, D.W., E.S. Wu and W.W. Webb, 1982, Enhanced molecular diffusibility in muscle membrane blebs: release of lateral constraints, *J. Cell Biol.* **92**, 207–212.
169. Tha, S.P., J. Shuster and H.L. Goldsmith, 1986, Interaction forces between red cells agglutinated by antibody. II – Measurement of hydrodynamic force of breakup, *Biophys. J.* **50**, 1117–1126.

170. Tissot, O., A. Pierres, C. Foa, M. Delaage and P. Bongrand, 1992, Motion of cells sedimenting on a solid surface in a laminar shear flow, *Biophys. J.* **61**, 204–215.
171. Tozeren, A., 1990, Cell-cell conjugation – transient analysis and experimental implication, *Biophys. J.* **58**, 641–652.
172. Tozeren, A., K.L.P. Sung and S. Chien, 1989, Theoretical and experimental studies on cross bridge migration during cell disaggregation, *Biophys. J.* **55**, 479–487.
173. Tran-Son-Tay, R., D. Needham, A. Yeung and R.M. Hochmuth, 1991, Time-dependent recovery of passive neutrophils after large deformation, *Biophys. J.* **60**, 856–866.
174. Unanue, E.R., W.D. Perkins and M.J. Karnovsky, 1972, Ligand-induced movement of lymphocyte membrane macromolecules. I – Analysis by immunofluorescence and ultrastructural radioautography, *J. Exp. Med.* **136**, 885–906.
175. Valentine, R.C. and N.M. Green, 1967, Electron microscopy of an antibody-hapten complex, *J. Mol. Biol.* **27**, 615–617.
176. Van Oss, C.J., 1991, Interaction forces between biological and other polar entities in water: How many different primary forces are there?, *J. Disp. Sci. Technol.* **12**, 201–220.
177. Van Oss, C.J., M.K. Chaudury and R.J. Good, 1987, Monopolar surfaces, *Adv. Colloid Surface Sci.* **28**, 35–64.
178. Vogel, K.G. and R.O. Kelley, 1977, Cell surface glycosaminoglycans: Identification and organization in cultured human embryo fibroblasts, *J. Cell Physiol.* **92**, 469–480.
179. Vogler, E.A., 1988, Thermodynamics of short term cell adhesion in vitro, *Biophys. J.* **53**, 759–769.
180. Wade, W.F., J.H. Freed and M. Edidin, 1989, Translational diffusion of class II major histocompatibility complex molecules is constrained by their cytoplasmic domains, *J. Cell Biol.* **109**, 3325–3331.
181. Wagner, H. and M. Rollinghoff, 1974, T cell-mediated cytotoxicity: discrimination between antigen recognition, lethal hit and cytolysis phase, *Eur. J. Immunol.* **4**, 745–750.
182. Wegener, A.M.K., F. Letourneur, A. Hoeveler, T. Brocker, F. Luton and B. Malissen, 1992, The T cell receptor/CD3 complex is composed of at least two autonomous transduction molecules, *Cell* **68**, 83–95.
183. Weiller, N.K., 1974, Visualization of concanavalin A binding sites with scanning electron microscopy, *J. Cell Biol.* **63**, 699–707.
184. Weiss, P. and B. Garber, 1952, Shape and movements of mesenchyme cells as function of the physical structure of the medium. Contribution to a quantitative morphology, *Proc. Nat. Acad. Sci. USA* **38**, 264–280.
185. Wier, M. and M. Edidin, 1988, Constraint of the translational diffusion of a membrane glycoprotein by its external domain, *Science* **242**, 412–414.
186. Willingham, M.C. and I. Pastan, 1975, Cyclic AMP modulates microvillus formation and agglutinability in transformed and normal mouse fibroblasts, *Proc. Nat. Acad. Sci. USA* **72**, 1203–1267.
187. Winzler, R.J., 1970, Carbohydrates in cell surface, *Int. Rev. Cytol.* **29**, 77–125.
188. Woods, A., M. Hook, L. Kjellen, C.G. Smith and D.A. Rees, 1984, Relationship of heparan sulfate proteoglycans to the cytoskeleton and extracellular matrix of cultured fibroblasts, *J. Cell Biol.* **99**, 1743–1753.
189. Yanagishita, M. and V.C. Hascall, 1992, Cell surface heparan sulfate proteoglycans, *J. Biol. Chem.* **267**, 9451–9454.
190. Zhang, F., B. Crise, B. Su, Y. Hou, J.K. Rose, A. Bothwell and K. Jacobson, 1991, Lateral diffusion of membrane-spanning and glycosylphosphatidylinositol-linked proteins: Towards establishing rules governing the lateral mobility of membrane molecules, *J. Cell Biol.* **119**, 75–84.
191. Zimmerman, G.A., S.M. Prescott and T.M. McIntyre, 1992, Endothelial cell interactions with granulocytes: Tethering and signaling molecules, *Immunol. Today* **13**, 93–100.
192. Zurkhov, S.N., 1965, Kinetic concept of the strength of solids, *Int. J. Fract. Mech.* **1**, 311–323.
193. Kaplanski, G., C. Farnarier, O. Tissot, A. Pierres, A.M. Benociel, M.C. Alessi, S. Kaplanski and P. Bongrand, 1992, *Biophys. J.* **64**,

This Page Intentionally Left Blank

Cell Membranes and the Cytoskeleton

P. JANMEY

*Experimental Medicine Division, Brigham and Women's Hospital,
Biomedical and Biological Sciences, Harvard Medical School,
Boston MA 02115, USA*

Contents

1. Introduction	807
2. The cell membrane	808
3. The cytoskeleton	808
3.1. Actin filaments	809
3.2. Microtubules	810
3.3. Intermediate filaments	811
4. Membrane/cytoskeletal interactions independent of chemical binding	812
5. Examples of cytoskeletal/membrane interactions in intact cells	813
5.1. Erythrocytes	813
5.2. Spectrin/actin network of platelets	816
5.3. Relation between 2-D and 3-D networks	816
5.4. Lymphocytes	818
5.5. Epithelial cells	818
6. Relation between the cytoskeleton and lipid membrane asymmetry	819
7. Actin/membrane interactions	820
7.1. Actin/lipid binding	820
7.2. Binding of actin to structures in cell membranes	821
8. Tubulin and microtubules	827
9. Intermediate filaments	829
9.1. Intermediate filament/lipid binding	829
9.2. Intermediate filament/membrane receptor binding	830
10. Membrane-bound motor molecules	831
11. Binding of transmembrane receptors to the cytoskeleton	833
12. Volume regulation	834
13. Regulation of the cytoskeleton by membrane lipids	835
14. Conclusion	838
Acknowledgment	838
References	838

1. Introduction

The interplay between the three-dimensional protein network called the cytoskeleton and the two-dimensional lipid bilayer which forms the cell membrane is a central feature of cell biology and a richly complex physical and chemical phenomenon. The complexity of the membrane/cytoskeleton boundary derives in part from the intricacy of the interface between two soft materials and in part from the number of distinct molecules and chemical interactions that occur at this interface and influence its physical properties and chemical composition. The importance of the field and the volume of contributions to it have motivated many reviews [1, 2] and a recent book devoted to this topic [3].

In the diversity of interactions between membrane constituents and components of the cytoskeleton, several themes reappear in different contexts.

- The binding of the major cytoskeletal fiber proteins themselves (except for some intermediate filaments) to phospholipids appears generally to be relatively weak and transient. Direct biochemical interactions of actin filaments, microtubules, and some types of intermediate filaments with purified lipids have been documented *in vitro*, but whether these interactions dominate the membrane/cytoskeletal interface is uncertain.
- Rather than linking cytoskeletal filaments directly to the lipid bilayer, intact cells assemble complexes of various proteins at points where the cytoskeleton attaches to the membrane. Some components in these linkages span the lipid bilayer, some penetrate into the cytoplasmic face of the bilayer, some bind preferentially to specific phospholipid headgroups, and others bind cytoskeletal filaments either directly to the lipid bilayer or indirectly to proteins bound to the membrane.
- In some cases the transmembrane proteins to which cytoskeletal filaments link are enzymes or ion transporters. The activity of these complexes is sometimes related to the extent of their attachment to the cytoskeleton and can alter the structure of both the membrane and the cytoskeletal network.
- Some types of cells possess two types of protein network linked to the membrane, a two dimensional lamina similar to that of the red cell and a three dimensional gel network linked either to the lipid bilayer or to the 2-D protein network.
- Motor molecules previously thought to produce motion primarily or exclusively between different protein assemblies, as in the sarcomere of the muscle, have now been shown to bind directly to purified lipids and to the plasma membrane of cells.

- Clustering of lipids and proteins within the membrane may be an important mechanism regulating their ability to produce biochemical and structural changes in the cell.
- Acidic phospholipids, particularly phosphoinositides appear to be especially important for interacting with cytoskeletal proteins, both by linking proteins to the bilayer and by biochemically regulating the activity of enzymes and cytoskeletal binding proteins.

This chapter will attempt to summarize current understanding of the biophysical properties of the cytoskeleton/membrane interface and to describe examples of each of the different classes of interaction between protein biopolymers and lipid membranes in cells. In particular, some biological processes that illustrate the importance of cytoskeletal/membrane interactions in normal and pathologic functioning of cells will be described.

2. The cell membrane

The physical and chemical properties of lipid bilayers are discussed in other chapters of this volume and in recent extensive reviews [4, 5]. The general character of lipids in biological membranes includes a diversity in the structures of both the hydrophobic chains in the interior of the bilayer and the hydrophilic headgroups which extend into the extracellular or cytoplasmic aqueous space. The headgroups of membrane phospholipids can form non-covalent bonds with peripheral membrane binding proteins, often apparently through electrostatic attractions, and in some cases even covalent bonds from the phospholipid to specific residues in particular proteins. It has been argued that the chemical heterogeneity of lipids *in vivo* precludes large scale phase transitions as being important mediators of cell function. On the other hand, there is abundant evidence that the distribution of different lipids in the membrane bilayer is not random, and that the physical consequences of the redistribution of lipids may be important in cell structure and transmembrane signalling. The non-random distribution of lipids in the membrane is found both between the inner and outer leaflet of the bilayer and within a single lipid monolayer. In cell membranes, charged lipids reside mainly in the inner monolayer, and clustering of acidic lipids is implicated in binding to specific intracellular proteins. The essential difference between the cell membrane and lipid bilayer vesicles is the presence of proteins bound to both sides of the bilayer surface and penetrating into or through the membrane itself. The nature and consequence of these protein-lipid interactions are reviewed elsewhere [5–7].

3. The cytoskeleton

Nearly all cells contain some form of filamentous protein polymer in their interior. Eukaryotic cells often possess an intricate three-dimensional network of interpenetrating and partly crosslinked filaments whose length, concentration, and attachments to each other or to the cell membrane are remodeled in response to specific signals.

This reversible assembly and spatial organization of biopolymers is intimately related to the cell's ability to maintain its shape or to alter it as it moves or is otherwise activated. The network of filamentous proteins, often operationally defined as that part of a cell which remains insoluble when the membrane is disrupted by detergents, is generally called the cytoskeleton. The filaments in this skeleton are composed of three types of protein polymer – microfilaments, intermediate filaments and microtubules – and the many accessory proteins that bind to them. The structures of the basic filament types and their subunits are shown in fig. 1. A detailed description of the properties of the cytoskeleton and the methods used to study the protein constituents can be found in several recent books devoted to the subject [8–11].

3.1. Actin filaments

Microfilaments are linear polymers of the globular protein actin. The globular monomer (G-actin) polymerizes into filamentous (F-) actin which appears in electron micrographs as two right-handed helices wound around each other with a repeat distance of approximately 36 nm [12]. Actin is an acidic protein with an isoelectric point of about 5.4, and approximately 11 net negative charges at neutral pH, depending on the actin isoform. The linear charge density of an actin filament, therefore, is approximately $-4.1/\text{nm}$, and can vary depending on the isoform, the phosphorylation state of nucleotides bound to it, and the number of bound divalent cations. The charge density is not uniform over the whole filament, and in particular, a cluster of negative charges is concentrated at a distinct site on the filament exterior near its contact site with several actin binding proteins [12]. The polyelectrolyte nature of F-actin is likely to be relevant to its interaction with membrane phospholipids. The polymerization of actin *in vivo* causes the hydrolysis of 1 actin-bound ATP for each subunit added to the filament. Since actin polymerization is rapidly reversible, the ATP hydrolysis associated with actin assembly accounts for up to 40% of a cell's total ATP turnover [13]. The physiologic role of this ATP hydrolysis remains unknown. ATP hydrolysis is not required for actin polymerization since ADP-bound actin also polymerizes, and the ATP is hydrolyzed only after the subunit has added onto the filament [14].

Actin filaments have a diameter of 7 nm [12] and can reach lengths of 30–100 μm *in vitro* [15], and at least several microns *in vivo*. Because these filaments are so long, they form semi-dilute solutions at extremely low volume fraction ($< 0.05\%$) [16, 17] in which rotational diffusion of the filaments is greatly retarded due to solute-solute interactions. At physiologic concentrations (5–20 mg/ml) F-actin forms viscoelastic networks with shear moduli on the order of 100–1000 Pa [17–20]. Although they appear very stiff in electron and light micrographs [21], actin filaments are remarkably flexible on a μm length scale and display many features of Rouse–Zimm coils in solution [17, 22, 23]. Possibly this flexibility or its alteration plays some role in the physiologic function of actin. Nearly all mechanically relevant properties of actin filaments – length, stiffness, concentration, lateral or orthogonal aggregation – can be regulated by one or more of scores of actin binding proteins found in the cytoplasm of most cells. The characterization of these many actin binding proteins is reviewed elsewhere [24].

Structure of Cytoskeletal Filaments

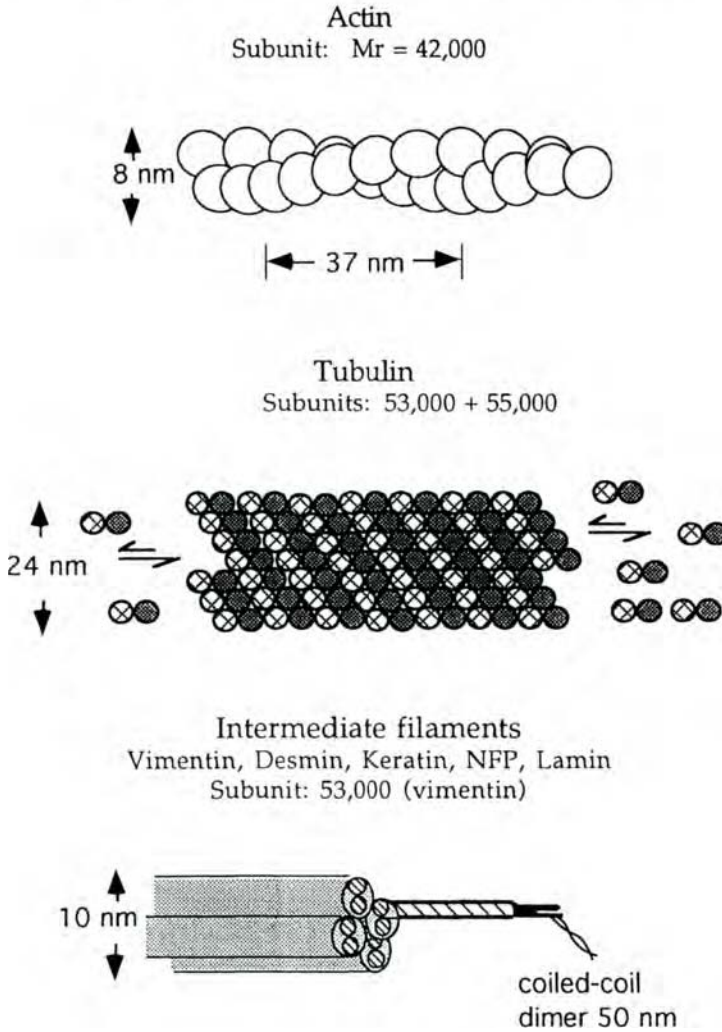


Fig. 1. Structure of the three major types of cytoskeletal filaments.

3.2. Microtubules

Microtubules are formed from the complex polymerization of tubulin α/β heterodimers into hollow cylinders of approximately 25 nm diameter which can be more than 100 μm long. The walls of the microtubule are composed of 5 nm-diameter linear protofilaments arranged in parallel. The number of protofilaments in a microtubules is typically 13, but can vary between 10 and at least 16. The iso-

electric points of α - and β -tubulins are 5.3 and 5.1, respectively, and at neutral pH, tubulin dimers carry approximately 30 net negative charges. Based on the packing of tubulin in the microtubule, each linear protofilament has a linear charge density of approximately $-3.8/\text{nm}$, which depends on the tubulin isoform and the nature of ions bound to the microtubule. Like actin, the tubulin subunits bind nucleoside triphosphates and hydrolyze them after they polymerize. Unlike actin, which binds most purine nucleotides, tubulin binds GTP rather than ATP. Another contrast with actin is that the thermodynamics of polymerization and especially the rates of disassembly of microtubules depend strongly on the nature of the nucleotide bound to the end of the microtubule [25]. GDP-bound subunits at the end of a filament dissociate very rapidly, but a cap of GTP-bound subunits at the ends of the microtubule can protect GDP-bound subunits farther away from the end from fragmenting or dissociating. This feature of tubulin polymerization has led to the concept of the dynamic instability of microtubules as an aspect of their physiologic function. As might be expected from their greater diameter and tubular structure, microtubules are much stiffer than actin filaments. Like actin filaments, microtubules also form viscoelastic networks *in vitro*, but these networks have much lower shear moduli at comparable weight fractions of polymer [26]. Also like actin filaments, microtubule stability, structure and polymerization are affected by microtubule associated proteins (MAPS), the properties of which are reviewed elsewhere [27].

3.3. Intermediate filaments

As their name implies, intermediate filaments (IFs) are thicker than microfilaments and thinner than microtubules. They are approximately 10 nm in diameter and many microns long, in cells often ranging from the plasma membrane to the nucleus [28]. They also form viscoelastic networks at low protein concentration *in vitro* [29, 30] and are thought to provide mechanical strength to the cell *in vivo*. Intermediate filaments differ from microfilaments and microtubules in several respects. Unlike actin and tubulin, which have only a few closely related isoforms in the same species and are very strongly conserved in evolution, intermediate filaments are formed from polymers of proteins that vary greatly among different cell types of the same species and between different species. Whereas actin and tubulin are acidic proteins, different intermediate filament proteins can be either acidic or basic, and the importance of linear charge density on intermediate filaments is not certain. Numerous unicellular eukaryotic cells, such as Dictyostelium slime molds, which possess actin and tubulin filament systems very similar to those of mammalian cells do not appear to contain intermediate filaments at all. The intermediate filament subunit proteins fall into several classes, reviewed in [31], which have in common a high degree of α -helical secondary structure. IF polymerization, unlike that of actin and tubulin, does not involve nucleotide hydrolysis or any other obvious irreversible reaction. Although IFs turn over *in vivo* and *in vitro*, the kinetics of their assembly and disassembly appear to be quite different and much slower than those of actin filaments or microtubules. Furthermore the mechanical properties of IFs differ from those of MTs or actin filaments. Individual IFs appear more flexible in electron micrographs, and networks of IF filaments become stronger as they are deformed (a property termed

strain-hardening), with shear moduli 100 times greater at 50% strain than at 1%, whereas actin filament and microtubule networks are very fragile and rupture at low strains (10–20%) [30]. IF-associated proteins that control IF polymerization or direct their binding to other cellular structures have been described (reviewed in [32]), but the nature of these interactions has been less thoroughly studied compared to MAPs or actin binding proteins.

4. Membrane/cytoskeletal interactions independent of chemical binding

A simple interaction between the cytoskeleton and the cell membrane arises from steric considerations. If a gel forms within a bilayer vesicle, the bending fluctuations of the bilayer that occur in empty liposomes are resisted by the elasticity of the gel. This has been observed in experiments where actin was polymerized within phospholipid vesicles [33–35]. The elastic modulus of purified cytoskeletal filament networks at physiologically relevant concentrations are on the order of 10–1000 Pa in shear deformation [30, 36] over a large range of frequency between at least 0.01 and 100 rad/s. Therefore such networks would present a strong barrier to surface deformation occurring on this time scale, although large scale deformations of both membrane and cytoplasm can occur on a slower time scale. This effect would be reinforced by specific attachments between the gel and the membrane but are also significant in the absence of attachments. Outward movements of the bilayer away from the gel on the other hand are much more strongly inhibited by the gel if the membrane is attached to it. However, even in the absence of attachments, the lifting of the bilayer away from an interior polymer network will be retarded by limitations to water flow required to fill the space between the gel and the membrane. The permeability coefficients for water through different liquid-crystalline phospholipid bilayers range from 10^{-4} to 10^{-2} cm/s [37], but changes in local cell structure, such as formation of blebs, can occur more rapidly than would be expected if water had to diffuse across the cell membrane into the newly formed structure [38]. The permeability of biological membranes to water varies from one cell type to another, and in some cells such as renal epithelial cells is very low. In these and other cells, water flow is mediated by specific hormone-sensitive transmembrane water channels [37].

Water transport through the cytoskeleton is also impeded by the biopolymer network, and in the case of actin filament networks, the rate of water flow depends very strongly on the structure of the network. The volume flow (J_v) of water through an actin network surrounded by a semi-permeable membrane obeys the relation

$$J_v = L_p(1 - \varepsilon)P_f \quad (1)$$

where L_p is a constant that depends on the permeability of the membrane and P_f is the osmotic stress. The parameter ε varies from 0 to 1 depending on the concentration of actin and the degree of its polymerization and crosslinking. In an actin gel crosslinked by filamin (ABP) water flow ceases below a critical osmotic pressure estimated to be several mosm [39]. Disruption of the normally restricted movement

of water through both the cell membrane and the cytoskeleton may be involved in the pathologic formation of cell blebs in metabolically poisoned cells and in cells genetically lacking the actin-crosslinking protein ABP [38].

A further interaction between cytoskeletal filaments and the cell membrane not requiring direct binding involves the generation of cell protrusions. Liposomes loaded with either actin [33–35] or tubulin [40] undergo shape changes superficially resembling some aspects of cell motion when the proteins inside the liposomes polymerize. These transformations are particularly dramatic in the case of microtubules [40]. The finding that the changes in liposome structure depend on parameters such as the length and degree of crosslinking of actin filaments by substoichiometric amounts of actin binding proteins [34] suggests that a significant aspect of the effect of protein polymers on the lipid bilayer is primarily mechanical. Of course, direct biochemical interactions between protein polymers and the lipid bilayer are also crucial *in vivo*, and a specific example of the consequence of disrupting the link between F-actin and the membrane is cited in section 5.1. A model in which a small bundle of actin filaments elongates near a membrane boundary has been proposed to explain the protrusion of filopods, which are long rodlike extensions of the cell surface [41]. In this model, the polymerizing filaments are not directly attached to the membrane but serve to rectify the random bending fluctuations of the lipid bilayer because of the mechanical resistance they provide. Using experimental values of membrane tension (0.035 dyne/cm) and the elongation rate of polymerizing actin (0.7 $\mu\text{m/s}$) this model can account for experimentally observed rates of filopod extension (0.1 $\mu\text{m/s}$).

A different steric interaction results from the constraint that the membrane surface places on the configurational freedom of long polymers. A lattice model for the arrangement of microtubules within a membrane-bounded space has been developed based on the geometry and dimensions of the axon [42]. Calculations using this model show that a non-random distribution of microtubule density near the surface of the membrane, approximating that found *in vivo*, can result from purely statistical considerations.

5. Examples of cytoskeletal/membrane interactions in intact cells

5.1. Erythrocytes

The best studied cytoskeletal/membrane complex is that of the red blood cell. Since human and other mammalian erythrocytes lack a three-dimensional cytoskeletal framework or a nucleus, the biochemical and structural analysis of the proteins that form the scaffolding underneath the lipid bilayer of the membrane can be much better characterized than in other cell types. A schematic diagram of the red cell cytoskeleton is shown in fig. 2. The two-dimensional protein network underneath the membrane is composed mainly of the proteins spectrin, actin, and band 4.1. Spectrin is a heterodimer composed of two high molecular weight, largely alpha-helical polypeptide chains, which form larger oligomers through head-to-head binding of the dimers. Spectrin tetramers are joined by a protein called band 4.1 to short actin filaments containing approximately 10 subunits largely stabilized by tropomyosin. The

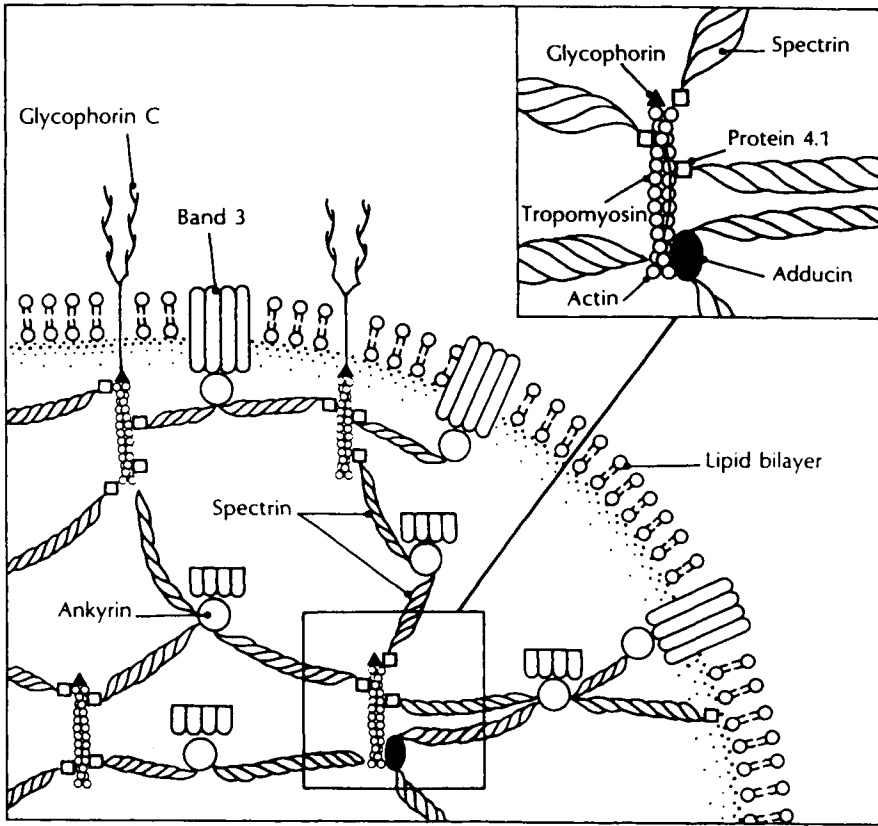


Fig. 2. Schematic model of the orientation of proteins of human erythrocyte membranes. Proteins of the spectrin-actin junction not shown in this model include protein 4.9 and tropomodulin. From ref. [257].

The details of this complex have recently been reviewed [43]. The binding of spectrin to actin is facilitated by 4.1, but spectrin itself has domains homologous to actin binding sites in other proteins [44], and actin crosslinking activity *in vitro* [45].

The spectrin-actin network is linked to the red cell phospholipid bilayer membrane in several ways. Band 4.1 binds to the transmembrane protein glycophorin by an interaction stabilized by PIP₂ [46]. 4.1 also binds directly to PS [47, 48], a phospholipid found predominantly in the cytoplasmic leaflet of the membrane bilayer. A second link from the spectrin-actin network to the membrane is via the protein ankyrin [49], a multidomain protein with binding sites for spectrin and for the anion exchanger (band 3) a major component of the red cell membrane [50]. A third potential link is via band 4.9 (dematin) which binds and bundles actin *in vitro* [51, 52]. Dematin also binds a 55 kDa protein recently shown to bind tightly to the erythrocyte membrane by virtue of extensive covalent linkage to palmitate [53]. This latter protein has kinase activity and sequence homology to the SH3 domain of src.

Phosphorylation of band 4.9 by this membrane bound kinase ablates its actin binding activity. Ankyrin [54] and 4.1 [55] can also be phosphorylated, and activation of kinases may be a mechanism for disrupting membrane/cytoskeletal linkages in some cases. A fourth regulatable link between the proteins of this network is adducin [56–58], a ligand for calmodulin [58] and a substrate for protein kinase C [56], which binds much tighter to the spectrin-actin complex than to either protein alone [57]. That adducin functions as a regulated actin binding protein is also suggested by the similarity of part of its sequence to that of an actin binding motif in spectrin and actin gelation proteins [59].

In addition to proteins mediating the linkage of the spectrin-actin network to membrane-bound proteins, the 2-D cytoskeleton may also be stabilized by direct, but weaker binding between the lipid bilayer and hydrophobic domains of spectrin, ankyrin, and 4.1, as judged by fluorescence quenching by the hydrophobic molecule 2-bromostearate [60]. Penetration of spectrin into the headgroup domain of DMPC monolayers has also recently been documented using specular reflection of neutrons [61].

Maintaining a link between the protein network and the lipid bilayer is essential for the maintenance of red cell shape and for the rapid flickering motions of intact red cell membranes [62]. A number of disorders including hereditary spherocytosis and elliptocytosis are caused by decreased expression or mutation of spectrin, ankyrin, or 4.1 [63]. As implied by the names of these diseases, the link between protein network and lipid membrane is thought to determine the characteristic shape of the cell, although how this occurs is not known. One interesting feature related to shape determination is that at least under some conditions, the surface area of both the lipid membrane and the spectrin-actin network separately are larger than the surface area of the intact structure. The remarkable flexibility of the spectrin-actin cytoskeleton has recently been demonstrated by visualization of the thermal motions of the skeleton of a red cell ghost immediately after removal of the lipid [64]. The protein network first expands to a nearly spherical shape, independent of the original shape of the ghost, and exhibits large scale undulations, consistent with a persistence length of ~ 10 nm for spectrin. If the ionic strength is increased, the skeletons decrease in size and become stiffer, due apparently to a reorganization of spectrin/spectrin contacts and possibly the formation of 3-dimensional crosslinks. The mechanics of the red cell skeleton have been extensively studied [62, 65] and the results of measurements, largely using deformation in microcapillaries are summarized elsewhere [66]. Such measurements have also permitted an estimation of the force density of association between the lipid bilayer and the spectrin-actin network as 40–50 Pa [67].

The structural consequences of rupturing the link between the spectrin-actin network and the membrane have been treated theoretically and predict a redistribution of the spectrin-actin network and the formation of purely lipid regions in the membrane [68]. Focal uncoupling of the spectrin network from the membrane has been observed experimentally. One dramatic consequence of such uncoupling is seen in deoxygenated sickled red cells, where under appropriate conditions hemoglobin polymerizes beneath sites where the membrane has detached from the cytoskeleton

and forms long spikes that protrude as much as 30 microns from the cell body. Such spikes contain band 3, but no spectrin [69, 70]. The formation of these spicules is an interesting example of cell protrusion linked to protein polymerization without an apparent necessity for either a motor molecule or ATP hydrolysis. The formation of these protrusions may have implications for actin- and tubulin-based forms of motility also.

5.2. Spectrin-actin network of platelets

While originally thought to be a structure unique to red blood cells, a 2-dimensional spectrin-actin lattice has now been identified in many cell types. The structures of these networks and the nature of their links to the membrane are similar with some interesting variations. One example of a 2-D membrane lattice is found in the platelet. The existence of such a network was first inferred from the finding that shells of detergent-insoluble material rich in actin sedimented and were visible in the electron microscope [71, 72]. Figure 3 shows a high-resolution electron micrograph of the membrane skeleton of a resting platelet [73] and its striking similarity to both the red cell skeleton and, interestingly, to a molecular dynamics simulation of a membrane skeleton modeled as a triangulated tethered surface [74].

5.3. Relation between 2-D and 3-D networks

Linkages between 2-D and 3-D networks in different cells are numerous and varied. For example, the resting platelet contains in addition to its 2-D spectrin-actin network a 3-D skeleton formed of an actin-based filamentous core linked to the membrane by actin cables [75], often by lateral association of the actin cables with the spectrin-actin lattice [73]. This lattice, in turn, is held to the membrane by links between ABP (filamin) and the transmembrane glycoprotein GPIb [76–78]. The GPIb/ABP link is found in interstices of the spectrin-actin lattice, and it is thought that the 3-D actin network holds the 2-D network in compression in resting cells. The transmembrane fibrin receptor complex GPIIb/IIIa is also associated with the platelet membrane skeleton [79]. Under appropriate extraction conditions, the 2-D sheet can be separated from the 3-D cytoskeleton formed by the filament core and the filament bundles emanating from it [73]. Platelet activation is associated with an explosive burst of actin polymerization, a release of the contacts between the 2-D and 3-D networks, and extension of long protrusions away from the platelet core. The extensive and concentrated actin network is now connected to the expanded surface area of the activated platelet by several links. Some ABP-GPIb contacts are maintained or formed at new sites, and biochemically distinct linkages between the fibrin receptor GPIIb/IIIa and the actin network are present, mediated by a number of proteins including talin, alpha-actinin and vinculin, in structures possibly analogous to those in focal adhesions [80] (section 7.2.1).

In other cell types, different links between the 2-D and 3-D networks have been described [81, 82]. An important and versatile link between the 2-D and 3-D networks appears to be ankyrin. In addition to its binding to spectrin and the anion

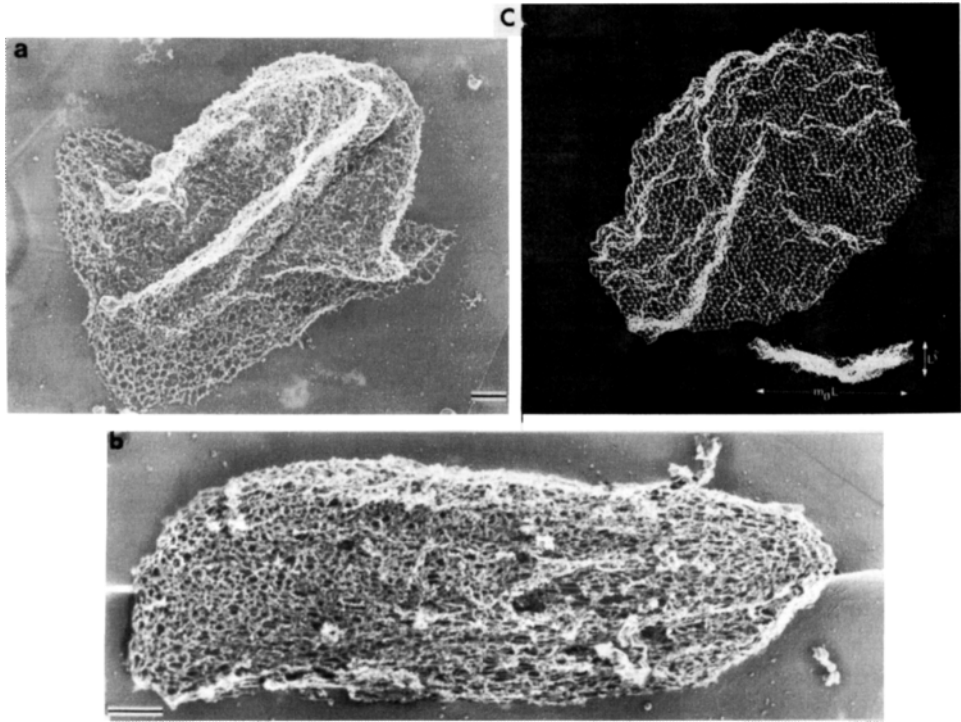


Fig. 3. High resolution electron micrographs of two-dimensional spectrin-actin networks derived from resting platelets (a) and red blood cells (b) compared to a perspective and side view of a molecular model of a large tethered membrane composed of 4219 monomers (c). a and b from ref. [73]; c from ref. [74].

exchanger in red blood cells, ankyrin has also been reported to associate with tubulin and the transmembrane proteins uvomorulin (E-cadherin) in epithelial cells [83], GP85 in lymphoma cells [84] and the voltage-dependent sodium channel in brain [85, 86].

Spectrin or its non-red blood cell analog fodrin has been reported to bind other cytoskeletal proteins such as the actin- and lipid-binding protein calpactin, but with low enough affinity to cast doubt on the specificity of the interaction [87]. Another ligand for spectrin is plectin, which would provide a link between the membrane lattice and intermediate filaments [88]. Spectrin also associates with the epidermal growth factor receptor [89] and may be a ligand for a component of the malarial parasite *Plasmodium falciparum* which causes disruption of the red cell membrane [90]. Although there are many potential ligands for spectrin, it is not clear which can bind simultaneously, and it is likely that there are large differences in affinity among

them. For example, the binding of spectrin itself to F-actin is relatively weak, but is increased by one order of magnitude by 4.1 [91].

From the biochemical and ultrastructural data obtained recently in this developing field, there is evidence for potential specific links from the spectrin-actin lattice to all three of the intracellular filament networks. The physical characteristics of such a composite material remain to be measured.

5.4. *Lymphocytes*

An example of the dynamic interaction of actin and tubulin polymers with the plasma membrane is seen in lymphocytes. In cells of the lymphoblastic cell line KE37 a migrating contractile acto-myosin ring constricts the cytoplasm at one end, causing it to flow toward the other end where membrane veils form as actin polymerizes underneath [92]. In the absence of microtubules, the ring migrates back and forth along the whole length of the cell, and the veil formation occurs alternatively at both ends. Microtubule formation elongates the cell and prevents migration of the ring past the centrosomal region so that veil formation occurs only at one end, giving the cell a distinct polarity. Native B lymphocytes exhibit localized membrane fluctuations corresponding to transverse displacements of 131 ± 22 nm with frequency 0.3–15 Hz, as measured by a novel optical method based on point dark field microscopy [93]. Colchicine, which depolymerizes microtubules, decreased the amplitude of the fluctuations to 88 ± 14 nm, whereas cytochalasin B, which depolymerizes actin increased the amplitude to 184 ± 31 nm. Although in these two cases of membrane movement, actin filaments and microtubules appear to be intimately involved in altering membrane structure, the nature of their attachment to the membrane and the signals to which they respond are unknown.

5.5. *Epithelial cells*

A morphologically well-studied cell-cell junction at sites where epithelial cells contact each other is the desmosome. The molecular organization of the desmosome is only partly understood. A related structure at the basal ends of epithelial cells where they attach to the extracellular matrix is called the hemi-desmosome. Both structures are characterized by a dense plaque of proteins attached to the plasma membrane from which intermediate filaments originate or to which they attach laterally (fig. 4). The biochemical composition of these two types of contacts differs, and the attachment of intermediate filaments to these membrane sites may be mediated by different proteins [94]. Since filaments attach to adjacent plaques on both sides of a cell-cell contact, and since the intermediate filament network spans the entire cell volume, these junction/intermediate filament complexes form a continuous three-dimensional network within a multicellular tissue which can transmit and resist mechanical forces. Other types of cell attachments relevant to epithelial cells are adherens junctions and focal contacts to which actin filaments attach, and these structures are discussed in more detail in section 7.2.

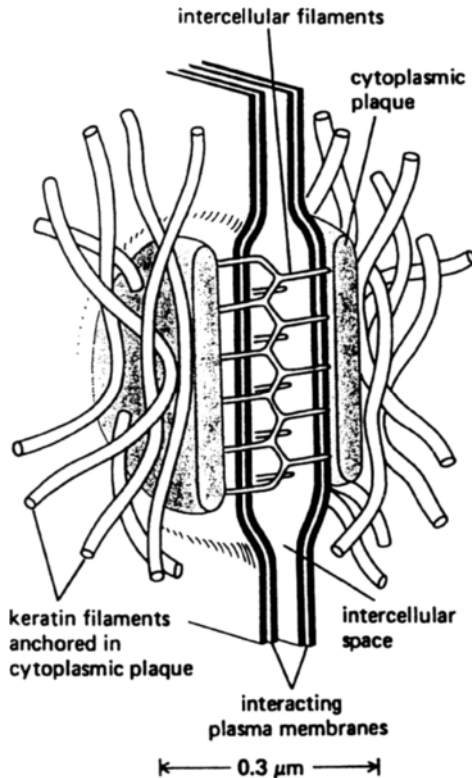


Fig. 4. Schematic drawing of a spot desmosome showing the anchoring of intermediate filaments to a complex of proteins bound to the intracellular face of the cell membrane and connected to the neighboring cell by intercellular filaments. From ref. [258].

6. Relation between the cytoskeleton and lipid membrane asymmetry

A striking feature of biological membranes is that the distribution of different phospholipid headgroups varies greatly between the inner and outer leaflet. Generally, there are more acidic headgroups facing the cytoplasm than the extracellular space. This asymmetry is maintained by several factors including specific lipid transfer enzymes (flippases), membrane voltage, and electrostatic binding to intracellular proteins, including components of the cytoskeleton [95]. In red blood cells, both the presence of a spectrin-actin membrane cytoskeleton and an ATP-dependent aminophospholipid pump are required to generate and maintain the cells' phospholipid distribution [96]. Aminophospholipid translocation from the outer to the inner leaflet requires coordination between a cytoskeletal and a membrane protein [97]. However, the asymmetry does not result simply from the binding of phospholipids to the membrane skeleton, since heat treatment of human erythrocytes at 50°C disrupted both the spectrin self-association and the binding of actin to the skeleton, but did not affect the phospholipid distribution [98].

The importance of the lipid asymmetry for the physiologic function of human red cells is illustrated by the finding that antibodies against PS and cardiolipin found in the blood of a patient with autoerythrocyte sensitization syndrome redistributed more than 50% of the PS to the outer leaflet of both the patient's red cells and homologous red cells from a healthy donor and disrupted the red cell cytoskeleton [99]. On the other hand, labeling of red cell cytoskeletal proteins by a photoactivatable phospholipid analog incorporated into the membrane of erythrocytes from patients with chronic myelogenous leukemia or sickle cell disease, which have symmetric lipid distributions, was similar to that of normal red cell membrane proteins, suggesting that the spectrin network does not directly account for the lipid asymmetry of these cells [100].

The transverse distribution of lipids in the platelet membrane is also related to the actin cytoskeleton in a complex manner. The aminophospholipids PE and PS added to platelets incorporated into the membrane and redistributed transversely at a rapid rate (10–40 min half-time) relative to PC. During the time that there was an excess of exogenous lipid in the outer leaflet, the platelets transformed from their resting discoid shape to a small central body with long pseudopods associated with actin polymerization. The shape change reversed when PE or PS redistributed to the inner leaflet [101]. This structural change may be related to the direct and specific binding of PS but not PC to the platelet cytoskeleton [102]. Similarly, the highly acidic lipid PIP_2 , which is thought to be localized entirely to the inner leaflet of the plasma membrane binds so tightly to the cytoskeleton of activated platelets that it resists extraction with organic solvents under conditions where all other lipids are solubilized [103, 104].

The lateral distribution of lipids is also affected by the cytoskeleton. In the developing optic nerve axonal membrane, staining with three different sterol-specific probes was spatially heterogeneous. The patchy staining was not reduced at increased temperatures, but was reduced by Mg^{2+} . Portions of the membrane not stained by the sterol dyes were preferentially observed in association with filaments extending from microtubules to the cell membrane [105, 106]. Renal proximal tubule cells, which control the flow of water, ions and other solutes across the epithelium, also present an interesting relation between the cytoskeleton and formation and maintenance of a non-uniform lipid distribution. In this case, the cell membrane is polarized into apical and basolateral membrane domains with different lipid compositions and very different transport properties. The apical membrane in particular has a very low water permeability. The maintenance of this polarized structure depends on an intact actin cytoskeleton. Ischemic injury to these cells causes disruption of the actin cytoskeleton and its links to the membrane which precede loss of surface membrane polarity [107, 108].

7. Actin/membrane interactions

7.1. Actin/lipid binding

Actin monomers and filaments are negatively charged at physiologic pH and have some areas of hydrophobic residues on their surfaces. Interactions of G- and F-actin

have been reported with charged and uncharged lipid monolayers and bilayers. Actin filaments bind positively charged phospholipid vesicles, presumably mainly by electrostatic attractions [109]. This interaction has recently been exploited to immobilize and orient actin filaments on lipid monolayers for electron microscopy [110]. A feature of this interaction observed in solution is that positively charged liposomes composed of a mixture of PC and sterylamine cause the polymerization of actin in solutions that otherwise maintain monomeric actin [109]. Actin polymerization is also driven by other positively charged molecules such as myelin basic protein, poly-lysine and the myosin head, but whether such processes occur *in vivo* is not known.

An interaction under approximately physiologic solution conditions has also been shown between F-actin and unilamellar PC or PG vesicles in mM concentrations of divalent cations. The association of F-actin with these bilayers appears to require stabilization by soluble cation-mediated electrostatic forces and leads to alignment of actin filaments on the bilayer surface as well as changes in the permeability and microviscosity of the lipid bilayer [111]. Incorporation of cholesterol into liposomes decreases their affinity for actin [112]. The binding affinity and chemical specificity of these actin/lipid binding reactions remain to be determined. The effects of divalent cations suggest that salt bridges between the actin filaments and the phospholipids may be important.

The association of F-actin with DMPC bilayers on a solid support has also been detected by total internal reflection fluorescence microscopy (TIRF). These measurements established two important features of actin/lipid binding by showing that the strength of the actin/lipid interaction can depend strongly on the filament length. Long F-actin filaments bound to a bilayer surface were nearly totally released by addition to the soluble phase of the actin binding protein severin, which cleaves the non-covalent bonds between filament subunits and stoichiometrically decreases the average filament length. If applicable also to cells, this result suggests that the binding of actin filaments to the membrane may result from the cooperative interaction of many weak binding sites, and that actin filaments bound to a surface remain capable of reacting with at least some actin binding proteins in the soluble phase (cytosol) [113].

In summary, a direct binding of actin filaments with purified phospholipid monolayers and bilayer vesicles has been observed. Under various conditions, actin can bind neutral, positively, or negatively charged lipids, suggesting that these interactions may not be of high specificity. The binding is also likely to be of low affinity, since it can easily be disrupted by changes in the filament length, and because lipid binding assays such as differential sedimentation and gel filtration chromatography, which detect specific interactions with some actin binding proteins (see section 13) yield generally negative results for actin.

7.2. Binding of actin to structures in cell membranes

Binding of actin to isolated biological membranes appears to be tight and specific. Liver membranes, depleted of their endogenously-bound actin, bind both G- and

F-actin as well as a non-polymerizable actin derivative [114]. Binding of G- and F-actin are mutually competitive, saturable, and inhibited by ATP. Since membrane bound actin does not bind phalloidin nor appear to be filamentous in electron microscopy, the state of the actin bound to the membrane may differ for that of actin polymers. Platelet membranes also bind actin in a form that resists removal by actin severing proteins such as gelsolin and does not appear filamentous in EM [71, 115]. The molecules responsible for binding actin to the membranes of liver and other cell types remain largely unknown.

Beside direct binding of actin to the lipid bilayer, at least five chemically distinct links binding the actin network to the cell membrane have been documented and some of them are shown schematically in fig. 5.

- Transmembrane proteins that bind actin.
- Proteins that bind both F-actin and the cytoplasmic face of the lipid bilayer.
- Proteins that bind actin and insert into the membrane through a covalently bound lipid moiety.
- Proteins that bind both F-actin and a transmembrane protein.
- Proteins that bind F-actin and another protein that binds to the membrane.

In some cases the links between actin and the proteins bound to the membrane are weak and fleeting, which has made biochemical characterization difficult even in cases where immunofluorescence studies have shown clear colocalization of actin and its accessory proteins at sites of membrane attachment. In other cases the binding of actin to its membrane-bound ligand is of high affinity and sensitive to the state of activation of surface receptors. There are also reports of enzymatically catalyzed covalent links between intracellular actin filaments and extracellular proteins at sites where both ligands bind to transmembrane receptor complexes [116]. In addition to protein-protein interactions at the interface, protein complexes at sites where activated membrane receptors have clustered or where the membrane adheres to another surface

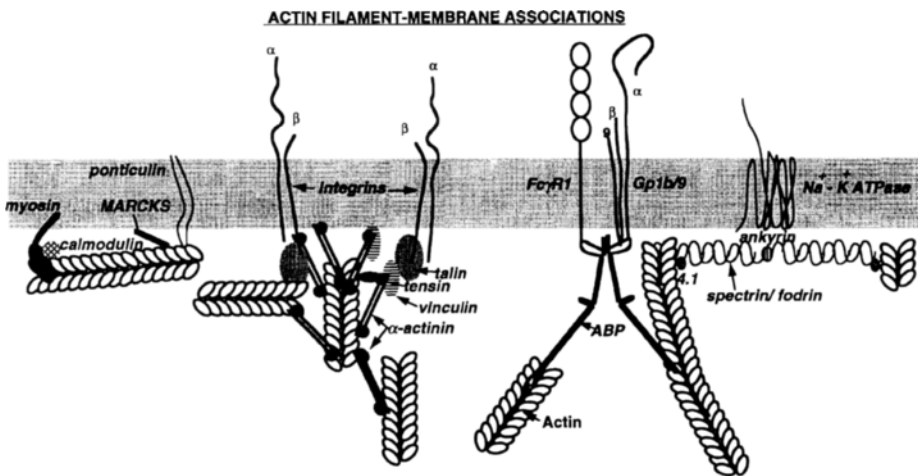


Fig. 5. Schematic representation of protein structures involved in linking actin filaments to the cell membrane.

are probably stabilized by recruitment of specific lipids which either diffuse into such sites or are formed *in situ* by enzymes known to be activated when specific receptors are occupied by extracellular ligands.

A major challenge for understanding membrane cytoskeletal interactions is to distinguish between colocalization of proteins at the membrane and formation of mechanically significant bonds. One aspect of this problem is the determination of the force required to break the contact between two cells held together by specific transmembrane junctions [117, 118].

7.2.1. Focal adhesions

The most thoroughly studied and possibly the most complicated connection between the actin network and the cell membrane is the complex of proteins and lipids that forms at sites where cells attach to the extracellular matrix or to artificial surfaces [119–125]. Such membrane-cytoskeletal links are observed in non-adherent cells also and are especially well studied in the platelet, where the actin links to the fibrin/fibronectin receptor GPIIb/IIIa. The transmembrane proteins mediating these contacts are members of the integrin family, which bind fibronectin or other EM proteins by their extracellular domains and attach to bundles of actin filaments by their intracellular domains. Integrins are heterodimeric complexes of *a*- and *b*-chains in which both chains span the bilayer once, and the cytoplasmic domain of the *b*-chain is responsible for linkage of the integrin to the actin system. The proteins thought to be responsible for linking actin filaments to integrins are shown schematically in fig. 6a. Which proteins are absolutely required for formation of focal adhesions is still under discussion, and the order in which these proteins bind integrins, actin or each other is only partly elucidated.

The proteins talin and alpha-actinin have both been demonstrated to bind the intracellular domains of the integrin *b*-chain. Alpha-actinin is a major constituent of focal adhesions as judged by immuno-localization [121, 126–129]. Alpha-actinin is well characterized as an actin crosslinking protein, which is regulated by Ca, in non-muscle cells, and which forms actin filament aggregates ranging from bundles to open networks, depending on the isoform [130]. Recently, a direct binding of alpha-actinin to some integrin types has also been documented [127, 128], and the importance of this protein *in vivo* is suggested by the finding that injection of alpha-actinin fragments into living cells causes a disruption of their cytoskeleton [129]. The affinity of alpha-actinin for certain membrane lipids, most notably diacylglycerol and palmitate is also likely to contribute to its binding at focal adhesions [131]. The recent finding that alpha-actinin also binds PIP₂ with very high affinity, and that the F-actin crosslinking function of some alpha-actinin isoforms requires PIP₂ [132] raises further interesting possible functions for this protein as a cytoskeleton/membrane linker.

Talin was also identified as a protein bound to integrins, primarily the fibronectin receptor, in several cell types [80, 133–136]. The binding of talin to integrins may be under the control of phosphorylation caused for example by interleukin 1 beta [136], and its function as a linker protein can be reversed by the calcium dependent protease calpain [135]. Originally, it was thought that talin was linked to actin filaments only

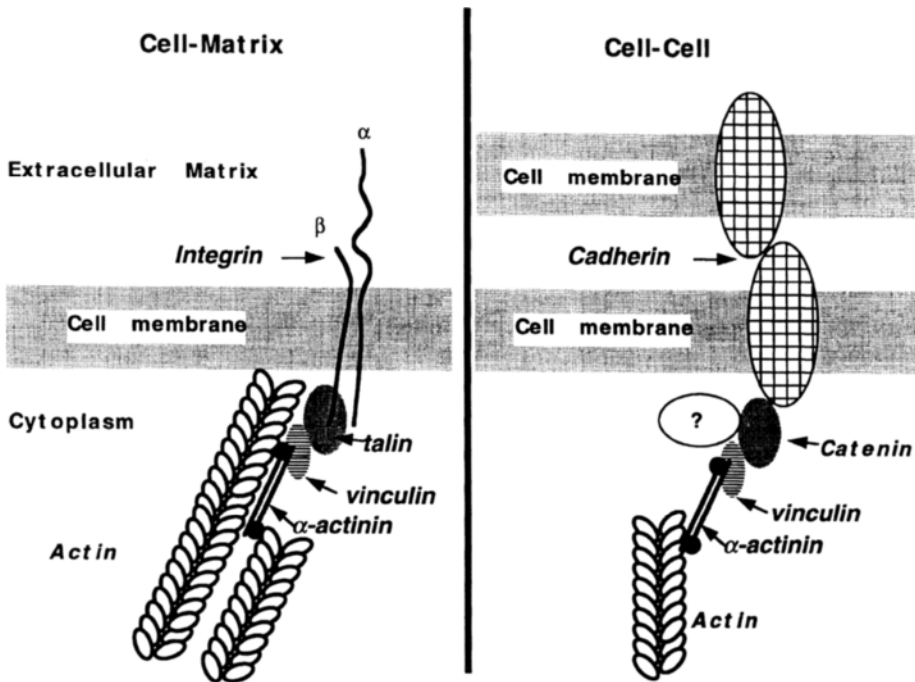


Fig. 6. A scheme depicting some of the proposed intermolecular interactions in cell-matrix (a) and cell-cell (b) adherens-type junctions. In cell/matrix connections, the transmembrane integrin complex binds extracellular matrix filaments on one side of the cell and talin (or perhaps alpha-actinin) in the cytoplasm. Talin also binds to vinculin or alpha-actinin, and these proteins or perhaps talin itself binds to F-actin. Interactions of proteins with phospholipids in the inner monolayer of the membrane are also observed but not depicted in this scheme. In cell-cell contacts a cadherin receptor binds to a yet unknown plaque component which plays a role similar to that of talin in cell-matrix contacts. Vinculin, alpha-actinin and actin function much as they do in cell-matrix contacts.

through other proteins such as vinculin and alpha-actinin, but more recently talin has been shown to bind directly to actin [137–139]. There are therefore two independent links of actin filaments to integrins, talin and alpha-actinin, and both are found in the same focal adhesions sites. A further property shared with alpha-actinin is the affinity of talin for phospholipids. The platelet talin homolog P235 bound mixtures of DMPC, DMPG and DMPS in an electrostatic interaction [140], and talin can link F-actin to negatively charged phospholipid vesicles [139]. In this sense talin may differ from alpha-actinin, in that alpha-actinin/lipid interactions appear to have a hydrophobic component. A further interesting relation between these two proteins is that talin augments the gelation of actin by alpha-actinin, although it does not appear to cause gelation of actin itself [141].

A third major protein component of focal adhesions and other cytoskeleton/membrane attachments is vinculin. The function of this protein is still unclear, but various interesting properties have been observed. There is differing evidence concerning

the binding of vinculin to actin [142, 143] but clearer evidence that it associates with the cytoskeleton of stimulated platelets, for example [144]. Vinculin also binds both talin [134] and alpha-actinin [145] and is a ligand for the recently described component of focal contacts paxillin [146]. Furthermore, vinculin may be linked directly to lipid bilayers in several ways. A portion of the protein can be covalently linked to either myristic [147] or palmitic acid [148]. In addition, vinculin also binds phospholipid bilayers non-covalently [149–154] with an apparent two step mechanism involving both electrostatic interactions with acidic headgroups and insertion into the hydrophobic domain of the monolayers (reviewed in [150, 152]). As with other components of the focal adhesion, vinculin illustrates the apparent redundancy of contacts mediating the actin/membrane connection. Vinculin may bind the lipid bilayer directly through one of several mechanisms and may bind actin directly. Alternatively, vinculin may also bind to one of several proteins such as talin or alpha-actinin which themselves may bind either directly to lipids or to the intracellular domain of integrin. These proteins or their complexes may then bind actin. The importance of vinculin to the *in vivo* function of cells is demonstrated by the recent finding that cells genetically devoid of vinculin are capable of forming transient protrusions, but unable to form stable contact with surfaces or directed locomotion [155].

In addition to the relatively abundant components of focal adhesions which include actin, vinculin, talin and alpha-actinin, several other proteins are found preferentially associated with these structures. These proteins include tensin, zyxin, ezrin, filamin [156], dystrophin [157], and paxillin (for review see ref. [124]). These less abundant proteins may be responsible for regulation of the larger focal contact complex.

7.2.2. Adherens junctions/cadherins

Sites at which cells attach to other cells differ in several respects from sites at which they attach to surfaces. The transmembrane proteins mediating cell attachment are members of a superfamily of adhesion molecules termed cadherins [158–160]. Some members of the cadherin family form cell-cell contact sites which involve recruitment of actin filaments to the contact site. Many of the proteins mediating attachment of actin to the intracellular domain of cadherins remain to be characterized. Three cytoplasmic proteins found attached to different classes of cadherins have been termed catenins [158, 161]. These catenins are presumed to mediate attachment of the actin filament network to cadherins. Some similarity between the proteins in this structure and those in focal contacts is suggested by the recent finding that catenin alpha is homologous to vinculin [162], and several proteins found in focal adhesions also appear in adherens junctions, with the notable exception of talin [134] (fig. 6b). Actin filaments link to adherens junctions by both their sides and ends. The binding of actin filament barbed ends to the complex of cadherin-bound proteins is likely to involve radixin, a barbed-end capping protein homologous to band 4.1 and localized in cell-cell contact sites [163]. Cadherin-mediated membrane cytoskeleton linkages appear to be highly variable among different cell types. Depending in part on the types of cadherin and catenins expressed, these contacts link cell membranes to either the actin network or the intermediate filament network [159] (see section 9.2).

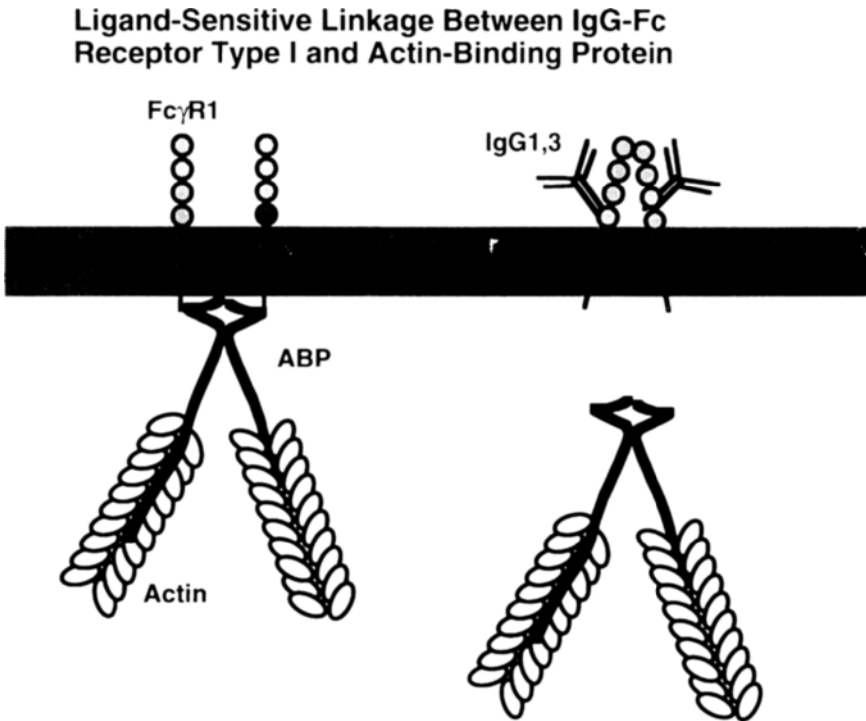


Fig. 7. Ligand sensitive linkage between IgG-Fc receptor type 1 and actin binding protein.

7.2.3. ABP binding to GPIb/IX and the Fc-receptor

Of all the links between transmembrane proteins and actin filaments, the most direct and, in some respects, the most specifically documented is that between the platelet receptor for von Willebrand factor (GPIb/IX) and actin binding protein (ABP or filamin) (see fig. 5). A site at the C-terminus of the ABP homodimer near the self-association site [78, 164, 165] binds to a site in the intracellular domain of GPIb [76, 77]. The other end of the elongated ABP molecule contains an actin binding site, so that each GPIb membrane protein can be linked to two actin filaments within the 2-D or 3-D actin network of the cell. In phagocytes, a different ABP-mediated membrane-actin linkage has been found. In a myeloid cell line, the intracellular domain of the high-affinity receptor for the Fc domain of immunoglobulin G (Fc γ R1) binds to ABP [166]. In unstimulated cells, all of the Fc γ R1 is bound to ABP. When the receptor binds ligand (IgG), changes in cell surface structure occur concomitant with dissociation of the ABP link to the receptor (see fig. 7). The rapid and specific release of activated receptors from their bonds to the cytoskeleton is likely to be a common mechanism by which signals received at the cell surface initiate changes in cell shape.

7.2.4. 5' nucleotidase

The ectoenzyme 5' nucleotidase has a somewhat enigmatic role in binding actin to the extracellular matrix [152]. The hydrophobic form of the enzyme is linked to the membrane through a glycosyl-phosphatidyl inositol linkage, common to many extracellularly disposed membrane proteins that lack transmembrane domains [167]. The extracellular domain of 5' nucleotidase binds the extracellular matrix proteins fibronectin and laminin [168]. When reconstituted into phospholipid bilayer vesicles, the membrane bound protein also binds F-actin, but not actin monomers [168, 169]. Furthermore, stimulation of a tumor cell line with insulin caused an increase of membrane-bound actin that was associated with 5' nucleotidase [170]. How this apparently direct link between actin filaments and a protein bound to the outer leaflet of the membrane through a lipid moiety can occur is not obvious, but the possibility for direct signalling from the outer membrane to promote actin polymerization has recently been observed in a different system (see section 10).

7.2.5. Other direct actin/membrane linking proteins

Several proteins have been reported to bind actin filaments directly to the cytoplasmic face of the plasma membrane. The most thoroughly documented of these is ponticulin, a small glycoprotein found in the membrane of *Dictyostelium discoidium*. Ponticulin binds directly to the sides of actin filaments and has additional function of promoting actin polymerization by stabilization of actin oligomers that serve as nucleation for further actin polymerization [171, 172]. Another example of direct actin/membrane link is the MARCKS protein. Directly after translation MARCKS is ligated to myristic acid, which recruits it to the plasma membrane of macrophages and other cell types [173]. MARCKS also has at least one actin binding site and causes bundling of actin filaments [174]. A number of stimuli that either activate protein kinase C or raise intracellular calcium release MARCKS from the cell membrane and reverse its actin binding properties. A similar combination of actin binding and subcellular localization is seen in the abundant lymphocyte protein LSP1 [175]. This protein also associates significantly with the cell membrane and binds actin. When lymphocytes are activated, surface receptors aggregate into patches and caps in a process thought to involve the actin cytoskeleton. The finding that LSP1 co-caps with the B-cell mIgM receptor suggest that it might mediate association of actin with these receptors. Other candidate proteins linking F-actin to the cell membrane surface include a 58 kDa membrane protein in Ascites tumor cell microvilli [176] and a 50 kDa protein in hepatocyte membranes [177].

8. Tubulin and microtubules

Tubulin is often a major component of cell membrane fractions prepared by mechanical disruption of cells and separation of membrane-bound from soluble components by centrifugation. Purified tubulin can also bind purified phospholipid bilayers. That such binding might have physiologic significance is supported by the finding that phosphorylation of tubulin by a calmodulin-dependent protein kinase enhances its

association with membranes. Dephosphorylation of tubulin reverses the interaction of tubulin with lipids [178]. The transient binding of tubulin to the membrane, regulated by a kinase localized or activated at specific sites, may provide a means to alter the physical properties of the cell membrane in response to appropriate signals.

Most examples of microtubule/membrane binding described involve the binding and translocation of membrane-bounded organelles along microtubule tracks [179]. The biochemistry of these interactions, which may have features in common with the binding of microtubules to the outer cell membrane have been reviewed elsewhere [180, 181]. Proteins linking microtubules to the plasma membrane also have been found, and in some cases biochemical binding studies confirm the observations based on immunocytochemistry and microscopy. A common example of microtubule/plasma membrane association is the peripheral band of microtubules found in platelets of many but not all species and in the red blood cells of birds and fish. The organization of the chicken red blood cell cytoskeleton is shown in fig. 8. In addition to the vimentin intermediate filament network linking the nucleus to the spectrine-actine lattice, these cells contain a marginal band of microtubules running along their periphery [182]. Several proteins have been identified as candidates for linking the microtubules to the membrane [183, 184]. One of these proteins may be identical or related to ezrin [184], a protein with sequence homology to band 4.1 of erythrocytes and associated with actin/membrane contacts in microvilli [185]. Another attachment of microtubules may be to ankyrin [49]. The function of the marginal band in platelets and red cells is unclear, since platelets lacking microtubules still undergo normal activation and in red cells the volume change in response to osmotic pressure changes is independent of the integrity of the microtubule marginal band [183].

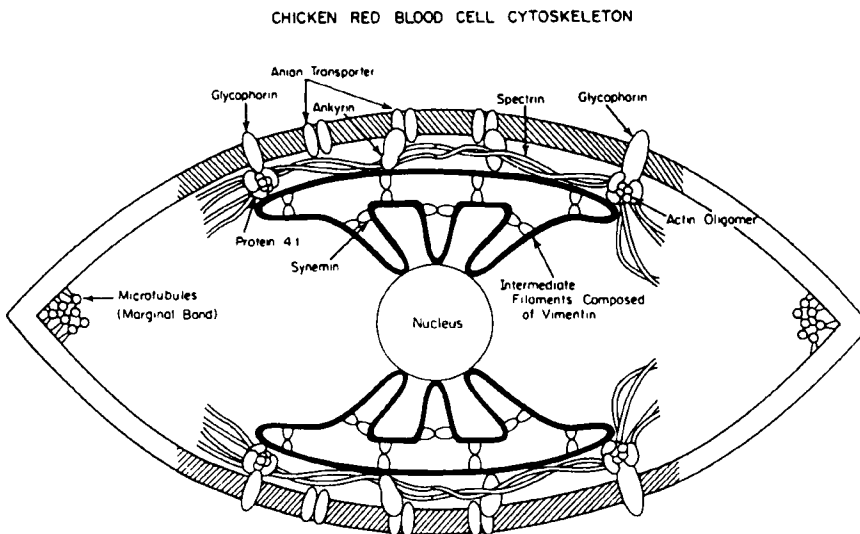


Fig. 8. Proposed arrangement of proteins forming the cytoskeleton of a chicken red blood cell. Note the marginal band of microtubules which is absent from mature mammalian red cells. From ref. [182].

Another example of microtubule/membrane binding is found in the trypanosomatid *crithidia fasciculata* which contains a ring of parallel microtubules that enclose the cell body and attach to the membrane by crosslinks visible in the EM. Three different proteins have been identified that may hold this structure together and to the membrane. Somewhat surprisingly, one of these has been identified as a glycolytic enzyme, glyceraldehyde 3-phosphate dehydrogenase [186]. Another enzyme involved in intermediate metabolism, a flagellar creatine kinase, also can associate with both phospholipids and tubulin, and therefore may have properties suitable for a microtubule/membrane linker [187].

A transient interaction of tubulin with the membrane may be mediated by the binding of tubulin dimers to the alpha subunit of some trimeric GTPases [188, 189]. These G-proteins function in signal transduction by interacting with the cytoplasmic face of transmembrane receptors and facilitating the activation of intracellular enzymes. The binding of G proteins to microtubules may be part of a mechanism to move or target them to specific sites in the membrane.

9. Intermediate filaments

9.1. Intermediate filament/lipid binding

Just as IF structure differs from that of actin filaments or microtubules in many respects, the interaction of IF with lipids differs in being more thoroughly documented and apparently stronger and more specific in nature. The intermediate filament proteins keratin and vimentin, for example, are often heavily contaminated with non-covalently bound lipid during their purification [190]. Keratins from cultured mouse mammary epithelial cells retain a relatively high amount of radiolabeled lipid in a high ratio of polar to non-polar lipids that survive SDS-polyacrylamide gel electrophoresis. Under the same extraction conditions, actin filaments retain very little lipid, and most of that is in the form of neutral lipid [191]. Vimentin through its non-helical N-terminal portion binds strongly to acidic phospholipid vesicles *in vitro*, causing aggregation of PS liposomes and leakage of PI vesicles at protein/phospholipid molar ratios as low as 1 : 500. The effects of monovalent and divalent cations on these interactions suggest that there is an electrostatic component to this binding [192]. A theory for the kinetics of these interactions has been developed [193]. Purified delipidated vimentin also binds neutral lipids such as cholesterol and cholesterol esters *in vitro*, apparently through its helical rod portion, and binding to phospholipid vesicles is enhanced if they contain cholesterol or 1,2-dioleoyl glycerol [190], although in some experiments the presence of a negative phospholipid in the vesicle is also required for stable binding.

In immunofluorescence studies of fixed cells, lipids have also been specifically colocalized with IFs. In human umbilical vein endothelial and other cell types, the glycosphingolipids globoside and ganglioside GM3 are associated with vimentin intermediate filaments, but not with F-actin or microtubules [194, 195]. Cholesterol ester liquid droplets have also been reported to bind intermediate filaments in adrenal cells, and this interaction may be important for transporting cholesterol from the cell

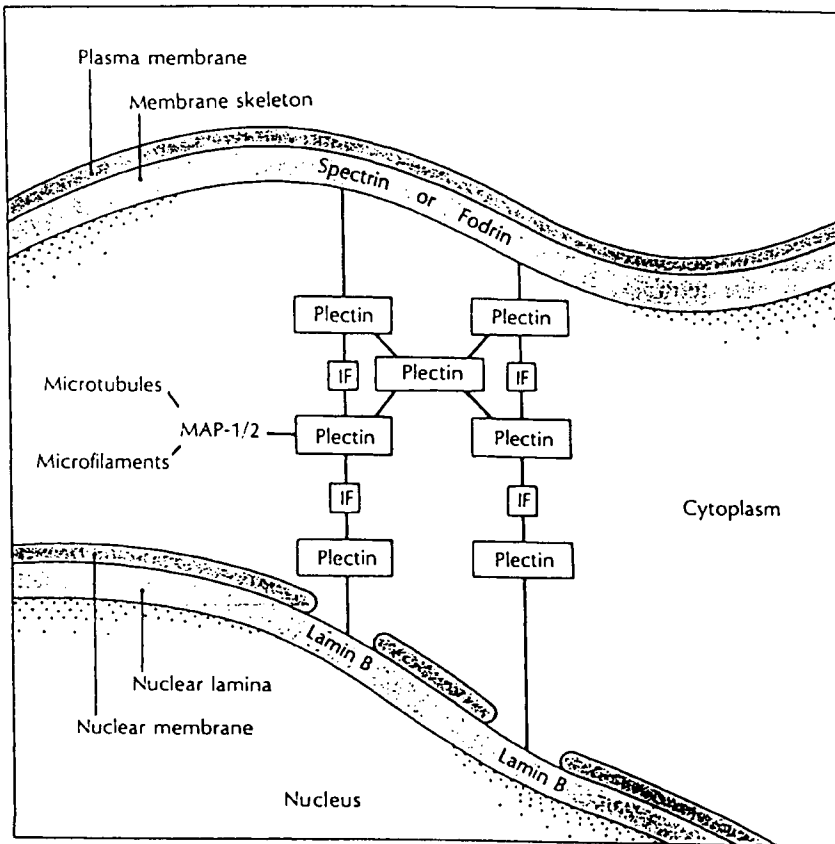


Fig. 9. Schematic view of the varied functions of plectin in the organization of the cytoskeleton. From ref. [32].

membrane to the mitochondria, also bound to IF's, [196] to supply substrate for steroid hormone synthesis [197].

9.2. Intermediate filament/membrane receptor binding

As with the other classes of cytoskeletal filaments, tight and specific binding of IFs to protein complexes at the cell membrane are also inferred to be crucial for some aspects of cell signalling and control of morphology. Several different structures have been identified as sites for IF/membrane linkages, based largely on microscopic and immunologic studies. The best known of these IF/membrane links are the desmosomes and hemidesmosomes, discussed in section 4.4. Proteins identified in these structures are thought to form the specific links from the IF to the membrane adhesion site, but biochemical characterization and reconstitution of the complete complex has not been achieved. Some of the proteins in desmosomes, such as

the desmoplakins have some structural similarity to intermediate filament proteins themselves. Other proteins that may be involved in linking IFs to desmosomes are discussed in recent reviews [28, 198].

Other types of links between IFs and the cell membrane also have been reported. In non-epithelial cells, IFs may attach to the spectrin-actin membrane skeleton by binding either spectrin or ankyrin [32]. In addition to possible direct binding of IF subunits to the membrane skeleton, such binding may also be mediated by proteins such as plectin, a 300 kDa protein that binds not only IFs, but also MAPS and spectrin-related molecules [88]. Some MAPS, in turn also bind ankyrin [49]. This complex arrangement is shown schematically in fig. 9 and illustrates how all three cytoskeletal polymers can bind as an integrated unit to specific sites at the plasma membrane and also why a coherent biochemical elucidation of these interactions is so difficult. The continuous link between the plasma membrane and the nuclear membrane formed mainly by intermediate filaments is thought to be a significant aspect of some forms of cell response to mechanical or chemical signals received at the cell surface [199–202].

10. Membrane-bound motor molecules

A particularly interesting class of proteins linking the cell membrane to the cytoskeleton are mechanochemical enzymes. These proteins provide not only a reversible link between protein filaments and the lipid bilayer, but also the potential to move the membrane surface relative to the interior framework of the cell. One example of such an enzyme is myosin I [203–206]. Structural characterization of the microvilli forming the brush border of intestinal epithelial cells revealed structures protruding from a crosslinked actin filament core bundle to the overlaying plasma membrane [207]. Biochemical characterization and sequence analysis of these structures [208, 209] revealed that they are complexes of calmodulin with an ATPase with primary structure homologous to that of myosin I, an enzyme related to the conventional myosin of muscles (termed myosin II), which lacks the ability to assemble into thick filaments, but can translocate actin filaments in the presence of ATP. Similar myosin I proteins have been found in many other cell types and appear to be preferentially located near the membrane at the front of moving cells [210–213]. Myosin I molecules contain 2 actin binding sites, one of which is ATP-sensitive, and a site which binds tightly to acidic phospholipids [210]. Myosin I isoforms are likely to have numerous functions in the cell, and some cell types possess multiple related myosin I gene products. One of the major roles proposed for myosin I is to move the cell membrane during locomotion. A schematic diagram showing how this is proposed to occur is shown in fig. 10. The possibility that such a displacement of membrane can occur *in vivo* is suggested by the finding that myosin I bound to an immobilized phospholipid bilayer can move actin filaments across the phospholipid surface *in vitro* [214]. However, how a motor molecule bound to a fluid lipid bilayer can apply force to protein networks is not obvious.

A second class of motor molecules moves on microtubules. Most of the evidence on this system has been obtained from studies, reviewed elsewhere [179, 215], of

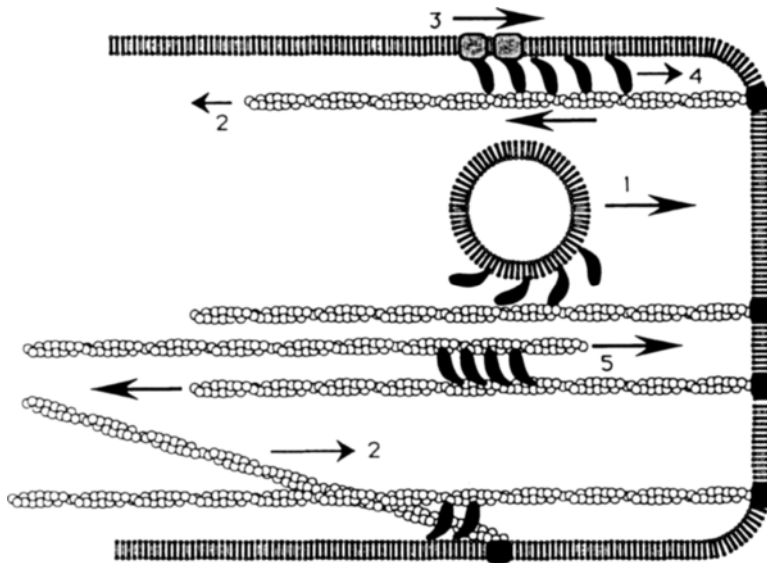


Fig. 10. Schemes for myosin-I-membrane interactions. From ref. [210]. 1, Membrane-bound myosin-I moves organelles along actin filaments within the cytoplasm; 2, myosin-I tethered in the membrane proteins or a second actin filament produces a contraction on actin filaments. This could cause contraction of actin filaments tethered to cell structures such as the plasma membrane [30, 31], or concentrate actin filaments into an area of activity; 3, myosin-I causes the movement of the plasma membrane relative to the actin filaments. The direction of movement would be determined by the polarity of the actin filaments. At the cell periphery, in microvilli or filopodia the direction of this movement would be expected to be centrifugal, 4, Myosin-I and associated membrane molecules may be free to diffuse in the plane of the membrane. An interaction of myosin-I with tethered cortical actin filaments may serve to move myosin-I along the actin filaments, concentrating them in a region of activity. 5, Myosin-I has already been shown to cause contraction of actin filaments relative to each other, *in vitro* [14, 21, 22]. A network of actin filament in the cytoplasm could be contracted in this way.

the movement of small intracellular membrane-bounded organelles on microtubule tracks. In addition, the same microtubule/motor system can be used to draw large membrane sheets along microtubules. One example of this is the formation of two-dimensional polygonal networks of membrane by the movement of membrane-bound kinesin on microtubules [216]. If the kinesin is bound to a sufficiently large and fluid membrane, rather than a small sphere, the movement of kinesin along the microtubule drags the membrane-bound kinesin ligand along, distorting the membrane. This sort of mechanism may function in the formation of the endoplasmic reticulum.

A third class of motion linked to membrane cytoskeletal interactions is represented by the movement of glycoproteins or beads attached to the cell surface [217–221]. One property of this type of motion is that a bead needs to be attached to a particular point on the cell surface for sufficient time for some kind of contact to form, presumably with the cytoskeleton. Only then does its motion on the cell surface become different from that of the bulk membrane lipid. The molecular details of this move-

ment, which is generally rearward, have not yet been fully elucidated. However, one important clue comes from studies with cells of the slime mold *Dictyostelium discoideum* which lack the large conventional myosin II motor. In these cells, rearward bead movement still occurs, but the spatial pattern of the motion is different [218]. Another striking form of motion involving the membrane/cytoskeletal interface occurs when beads bearing a positive surface charge are placed on the surface of nerve growth cones. If the bead's charge density is sufficiently high, it begins to move along the surface of the cell at speeds and in a direction uncorrelated with the dominant rearward flow of the bulk cytoplasm [222]. As the bead moves on the surface, it leaves behind a trail of newly polymerized actin, similar to that associated with propulsion of the infectious bacterium *Listeria* in the cytoplasm [223]. In this example, a physical perturbation of the outer leaflet of the cell membrane by electrostatic charge on the bead is apparently sufficient to trigger submembrane actin polymerization and a reordering of the cytoskeleton that allows surface motion to occur.

11. Binding of transmembrane receptors to the cytoskeleton

Often, the evidence that a free or activated receptor is bound to the cytoskeleton comes from studies showing that the receptor is insoluble in non-ionic detergent extracts, or that it is immobilized based on fluorescence recovery measurements after photobleaching (FRAP). How specific or mechanically strong such interactions are cannot generally be judged from such measurements, and different receptors become immobilized by very different mechanisms. For example, the tetrameric high-affinity receptor for IgE in rat basophilic leukemia cells aggregates and associates with the cytoskeleton when it is activated [224–227]. The activation of such cells normally causes simultaneous actin polymerization, and clustering and insolubilization of the receptor. However, these two events are not causally related because drugs such as cytochalasin B which prevent the actin polymerization do not affect receptor solubility [224]. The components of the cell membrane alone are sufficient to cause the insolubility of activated IgE receptors [225]. Moreover, disrupting the cytoplasmic domains of any of the components of the receptor by site-directed mutagenesis failed to prevent the receptor's apparent association with the cytoskeleton. Even the extracellular domain bound to the outer leaflet of the membrane via a glycosylphosphatidylinositol link became detergent-insoluble as long as the receptor was aggregated [226]. These results suggest that this type of receptor becomes non-specifically enmeshed in the membrane skeleton when the membrane proteins are aggregated by ligands.

In contrast, other types of transmembrane protein interactions with the cytoskeleton are easily disrupted by alteration of their cytoplasmic domains. Removal of as few as 6 amino acids from one of the two chains that form the heterodimeric class II major histocompatibility complex increased its lateral diffusion constant three fold, and complete removal of the cytoplasmic portion of the complex increased it by a factor of 10. The critical amino acid sequence is rich in basic residues which could

interact either directly with the negatively charged actin filaments or microtubules to account for the limited mobility of the wild-type protein [228]. In most cases neither the biochemical affinity of a receptor for the cytoskeleton nor the mechanical strength of the bond between the two have been measured. One exception is the point contact between red blood cells measured by pulling an agglutinin bound to a rigid surface away from its transmembrane ligand on a red blood cell held in a microcapillary. The force required to rupture this contact in a short time was $1-2 \times 10^{-6}$ dyne, for three different ligand pairs, as measured by the deformation of the cell surface [117]. Biochemical analysis showed that rupture resulted from removal of the transmembrane ligand from the lipid bilayer of the cell membrane and not from breakage of the protein-protein bond between the two ligands.

12. Volume regulation

The cell's volume is also maintained by structures at the membrane/cytoskeletal interface. Normally, in living cells the surface area of the lipid membrane is far in excess of the amount needed for the volume it encloses. Therefore, large volume increases can be accommodated before the elastic limit of the bilayer is reached. Cells maintain a relatively constant volume in the presence of a wide range of osmotic conditions by utilizing several mechanisms. The cytoskeletal network, like any viscoelastic material, can itself provide some resistance to osmotic swelling and deswelling. However, *in vitro* data suggest that such a direct contribution to preventing volume change is likely to be minimal under physiologic conditions. For example, resting neutrophils have the characteristics of viscoelastic liquids rather than solids [229–231], and although they might respond slowly to osmotic shocks, their material properties provide no mechanism to maintain a constant shape for prolonged times. The elastic moduli of living cells and of purified actin, vimentin, or microtubule networks at the concentrations present *in vivo* are on the order of several hundred Pa and are time-dependent, decreasing at longer times, on the order of minutes or hours [30, 33], whereas intact cells can maintain constant volume and cell integrity after transfer to solutions with osmolarity differences corresponding to several hundred thousand Pa and can maintain this volume for very long times. Rather than using a passive resistance to volume changes which would be governed by the viscoelasticity of the cytoskeleton, cells maintain their volume actively by regulating the influx and outflow of ions and water through a variety of channels, some of which pump ions against a gradient at the expense of ATP hydrolysis.

Although the elasticity of the cytoskeleton seems unlikely to resist physiologically reasonable osmolarity gradients, the cytoskeletal network is nevertheless intimately involved in volume regulation [232–234]. Cells genetically devoid of specific actin-crosslinking proteins which normally increase the shear modulus of actin networks *in vitro* and which may link the network to cell membrane receptors *in vivo* show a marked increase in volume changes in response to osmotic gradients and a decreased capacity to return to their resting volumes [235]. Secondly, agents which disrupt either microtubules or actin filaments also eliminate volume regulation by

neutrophils [236]. The mechanism for this link between the cytoskeleton and volume regulation is unknown, but at least two hypotheses have been put forward. First, several classes of ion channels have been reported to be directly linked to the cytoskeleton [85, 86, 237], and the activity of the Na^+ channel depends on the gel state of actin networks *in vitro* [238]. Second, although the cytoskeleton is not strong enough to prevent osmotically driven volume changes, an intact crosslinked network nevertheless exerts a restoring stress as long as it is stretched or compressed in relation to its resting shape. Such an elastic effect may serve as a memory for the cell to return to its resting volume at which the cytoskeletal strain reaches a minimum. In both cases the cytoskeleton must be tightly coupled to the cell membrane, either directly to transmembrane ion channels or to stable membrane-bound anchors.

13. Regulation of the cytoskeleton by membrane lipids

The boundary between the cell membrane and cytoplasm is not only a physical constraint and a surface for contact and adhesion, but it is also an interface at which a great deal of chemistry occurs. Chemical reactions in this environment can either alter the membrane-cytoskeletal interface itself, or produce second messengers for reactions elsewhere in the cell. An example of how contact between the actin-based cytoskeleton and the acidic polyphosphoinositides PIP and PIP_2 may lead to changes in the state of actin polymerization is outlined in fig. 11. The actin binding protein

TRANSMEMBRANE SIGNALLING, GELSOLIN AND THE ACTIN CYCLE

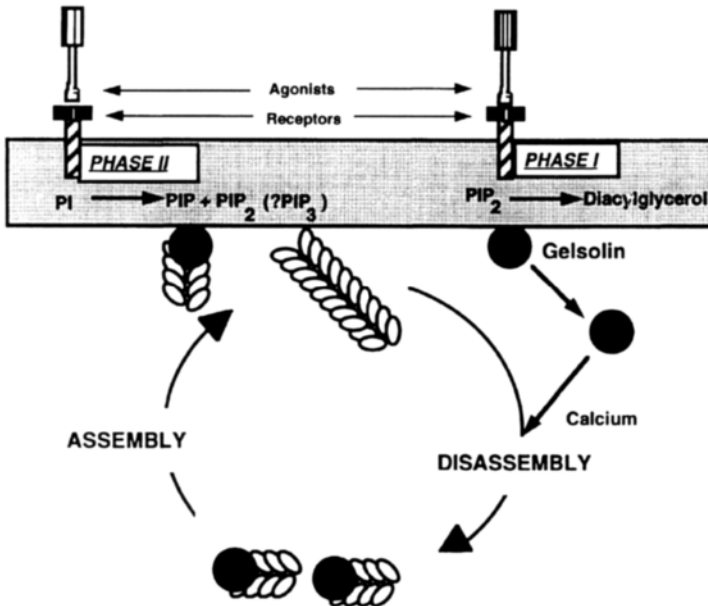


Fig. 11. Transmembrane signalling, gelsolin, and the actin cycle. Adapted from ref. [259].

gelsolin, which severs filaments and binds to their fast-growing 'barbed' ends in the presence of elevated cytosolic Ca^{2+} , binds to PIP and PIP_2 through two distinct poly-basic domains of similar structure [239, 240]. This interaction releases bound actin filaments and exposes barbed ends onto which further sub-membrane actin polymerization occurs. Similarly, the positively charged actin monomer sequestering protein profilin also binds PPI's and releases actin monomers providing material to fuel the rapid polymerization of actin from ends liberated by PPI-bound gelsolin [241–243]. If these and other actin and PPI-binding proteins are coordinately inactivated by receptor-mediated PPI turnover, they could provide a mechanism whereby actin polymerizes directly at the membrane/cytosol interface [244, 245]. Such actin polymerization is an immediate consequence of many types of cell activation and is implicated in the generation of directed forces in cell motility.

The plausibility of such mechanisms is strengthened by the finding that increases in some PPI levels – notably PIP_3 – sometimes correlate with increased actin polymerization [246, 247], although bulk levels of PPI's do not show a simple correlation with the states of gelsolin or profilin [248], which is not surprising given the vast excess of these lipid species to the proteins in most cell types. Local changes in PPI concentration generated by specific receptor activation are required to produce the localized and transient actin polymerization observed when cells are signalled to move. Often this signalling involves two aspects: activation of phospholipase C which lowers PIP and PIP_2 levels by hydrolysis to diacylglycerol and IP_2 or IP_3 , and activation of PI and PIP kinases, which restore PPI levels by phosphorylation at different sites on the inositol ring to produce isomers of PIP and PIP_2 . An initial activation of PLC would reduce PIP_2 levels, elevate intracellular Ca^{2+} (via IP_3 -activated storage release) and lead to actin filament severing by gelsolin and capping of barbed ends, thus solating the cortical actin network. Subsequent or consequent restoration of PPI's, often to levels greater than those of the pre-stimulated cell, would remove the gelsolin cap from actin, release actin sequestered by profilin and allow rapid actin polymerization. The evidence for these pathways is reviewed elsewhere [244].

Currently, at least 10 cytoskeletal proteins have been reported to bind PPI's, and many of these interactions are well described in a recent review [152]. A common finding in PPI- and actin binding proteins is a polybasic domain adjacent to or interrupted by a hydrophobic region [239]. These sequences bear a superficial resemblance to the stretches of basic amino acids often found at the immediate cytoplasmic domain of transmembrane proteins [228]. A synthetic peptide based on one of the PPI-binding sites of gelsolin undergoes a coil to helix transition in the presence of small amounts of PIP_2 [249]. Such a peptide/lipid interaction is likely to alter the structure of both ligands. An important aspect of the binding of PPI's to actin binding proteins is that the PPI's must be associated within the lipid bilayer in clusters of approximately 5–10 molecules in order to exert their effect on the proteins (fig. 12). Since at least some of the enzymes that use PPI's as their substrates also require clustering, the competition for substrate and the changes in lipid structure caused by the binding of peripheral membrane proteins is an efficient mechanism to

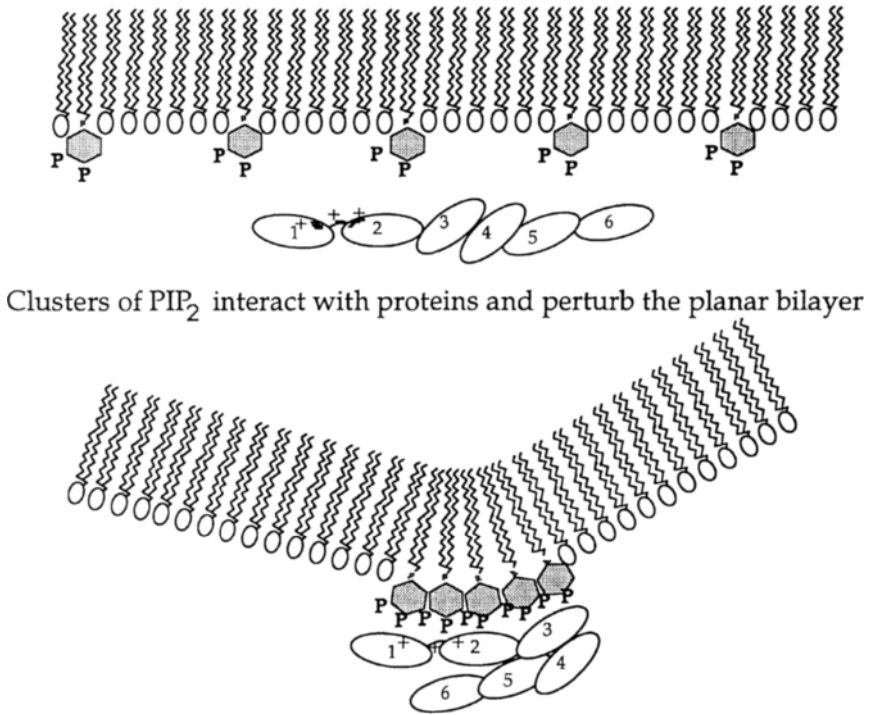


Fig. 12. Binding of gelsolin to PIP₂ requires clustering of PIP₂ headgroups within mixed lipid bilayers.

regulate enzymatic activity [243, 250]. Moreover, clustering of trace lipids with unusually large headgroups and surface charges is likely to cause a change in the shape of the plasma membrane at the site where cytoskeletal proteins bind or where lipases and lipid kinases are activated. As an example, the initial phase of platelet activation by thrombin is associated with the hydrolysis of nearly 50% of the total PIP₂ into diacylglycerol and IP₃ [251, 252]. In this reaction, membrane sites enriched in the phospholipid with the largest head group and surface charge would, within seconds, be enriched in a lipid with no headgroup. The imbalance in surface areas of the inner and outer leaflet resembles that caused when PS or PE are added to the outer leaflet of platelets in the experiment described in section 5.3, which leads to large scale shape transitions. A coordinated interaction between local and reversible structuring of the membrane lipid bilayer and changes in the extent of filament assembly and architecture is likely to be an integral part of many forms of cell shape change and motility. The coupling between cytoskeletal proteins and remodelling of membrane lipid structure is supported by the finding that numerous enzymes associated with reactions essential for signalling through the PPI-pathway are localized or regulated by the cytoskeleton [253–256].

14. Conclusion

The boundary between the cell membrane and its protein networks exhibits the properties expected for soft materials composed of multiple chemically distinct components. Both the mechanical and the biochemical properties of proteins and lipids at this interface determine its structure and dynamics. A key feature of the interactions among the membrane components is that few if any of them are of very high affinity and long lived. This ensures a rapid accommodation to environmental changes and makes detailed physical and chemical characterization difficult. The interface reacts to physical stresses used to measure it, and biologically important contacts dissociate during attempts to purify their component parts. Nevertheless, a large number of molecules have been identified as important for determining the structure of the cytoskeleton-membrane surface. The integrity of these structures is necessary for proper adherence of cells to the substratum or to each other and for the generation of forces during motility. As more biochemical data accumulate, a pattern of apparent redundancy emerges. Proteins linking different filaments of the cytoskeleton to the membrane may do so by binding to both proteins and lipids in the membrane. Structurally homologous surface receptors may bind to any of the different filament types in the cytoskeleton depending on the accessory proteins localized or activated at sites of attachment. How the variety of biochemical interactions determine the physical properties of the cell surface and how they participate in such processes as cell adhesion or motility remains a major unanswered question in cell biology.

Acknowledgment

I am grateful to Tom Stossel and Vitauts Kalnins for their helpful comment on this manuscript.

References

1. Luna, E.J. and A.L. Hitt, 1992, Cytoskeleton-plasma membrane interactions, *Science* **258**, 955–964.
2. Stossel, T., 1993, On the crawling of animal cells, *Science* **260**, 1086–1094.
3. Mooseker, M. and J. Morrow, 1991, *Ordering the Membrane-Cytoskeleton Trilayer* (Academic Press, San Diego) p. 245.
4. Kleinfeld, A., 1987, Current views of membrane structure, in: *Membrane Structure and Function*, Vol. 29, eds R. Klausner, C. Kempf and J. van Renswoude (Academic Press, San Diego) pp. 1–25.
5. Bloom, M., E. Evans and O. Mouritsen, 1991, Physical perspectives of the fluid lipid-bilayer component of cell membranes – a perspective, *Q. Rev. Biophys.* **24**, 293–397.
6. McLaughlin, S., 1989, The electrostatic properties of membranes, *Annu. Rev. Biophys. Biophys. Chem.* **18**, 113–136.
7. Sackmann, E., 1990, Molecular and global structures and dynamics of membranes and lipid bilayers, *Can. J. Phys.* **68**, 999–1012.
8. Amos, L.A. and W.B. Amos, 1991, *Molecules of the Cytoskeleton* (Guilford Press, New York).
9. Bershadsky, A.D. and J.M. Vasiliev, 1988, *Cytoskeleton* (Plenum, New York).
10. Carraway, V. and C.A.C. Carraway, 1992, *The Cytoskeleton: A Practical Approach* (IRL Press, New York).
11. Schliwa, M., 1987, *The Cytoskeleton: An Introductory Survey*, (Springer, Vienna) p. 326.
12. Holmes, K., D. Popp, W. Gebhard and W. Kabsch, 1990, Atomic model of the actin filament, *Nature* **347**, 44–49.

13. Daniel, J., I. Molish, L. Robkin and H. Holmsen, 1986, Nucleotide exchange between cytosolic ATP and F-actin-bound ADP may be a major energy-utilizing process in unstimulated platelets, *Eur. J. Biochem.* **156**, 677–684.
14. Carlier, M., 1989, Role of nucleotide hydrolysis in the dynamics of actin filaments and microtubules, *Int. Rev. Cytol.* **115**, 139–170.
15. Burlacu, S., P.A. Janmey and J. Borejdo, 1992, Distribution of actin filament lengths measured by fluorescence microscopy, *Am. J. Physiol.* **C5**, 69–77.
16. Janmey, P.A., J. Peetermans, K.S. Zaner, T.P. Stossel and T. Tanaka, 1986, Structure and mobility of actin filaments as measured by quasielastic light scattering, viscometry, and electron microscopy, *J. Biol. Chem.* **261**, 8357–8362.
17. Müller, O., H. Gaub, M. Bärmann and E. Sackmann, 1991, Viscoelastic moduli of sterically and chemically cross-linked actin networks in the dilute and semi-dilute regime: Measurements by an oscillating disk rheometer, *Macromolecules* **24**, 3111–3120.
18. Hvidt, S. and P. Janmey, 1990, Elasticity and flow properties of actin gels, *Makromol. Chem. Macromol. Symp.* **39**, 209–213.
19. Janmey, P.A., S. Hvidt, J. Peetermans, J. Lamb, J.D. Ferry and T.P. Stossel, 1988, Viscoelasticity of F-actin and F-actin/gelsolin complexes, *Biochemistry* **27**, 8218–8227.
20. Janmey, P.A., S. Hvidt, J. Lamb and T.P. Stossel, 1990, Resemblance of actin-binding protein/actin gels to covalently crosslinked networks, *Nature* **345**, 89–92.
21. Gittes, F., B. Mickey, J. Nettleton and J. Howard, 1993, Flexural rigidity of microtubules and actin filaments measured from thermal fluctuations in shape, *J. Cell Biol.* **120**, 923–934.
22. Schmidt, C.F., M. Baermann, G. Isenberg and E. Sackmann, 1989, Chain dynamics, mesh size, and diffusive transport in networks of polymerized actin. A quasielastic light scattering and microfluorescence study, *Macromolecules* **22**, 3638–3649.
23. Kas, J., H. Strey, M. Barmann and E. Sackmann, 1993, Measurement of the wave-vector-dependent bending stiffness of freely flickering actin filaments, *Europhys. Lett.* **21**, 865–870.
24. Hartwig, J. and D. Kwiatkowski, 1991, Actin-binding proteins, *Curr. Opin. Cell Biol.* **3**, 87–97.
25. Hill, T.L., 1984, Introductory analysis of the GTP-cap phase-change kinetics at the end of a microtubule, *Proc. Nat. Acad. Sci. USA* **81**, 6728–6732.
26. Sato, M., W.H. Schwartz, S.C. Selden and T.D. Pollard, 1988, Mechanical properties of brain tubulin and microtubules, *J. Cell Biol.* **106**, 1205–1211.
27. Olmsted, J., 1986, Microtubule-associated proteins, *Annu. Rev. Cell Biol.* **2**, 421–458.
28. Goldman, R. and P. Steiner, 1990, *Cellular and Molecular Biology of Intermediate Filaments* (Plenum, New York).
29. Leterrier, J.-L. and J. Eyer, 1987, Properties of highly viscous gels formed by neurofilaments *in vitro*, *Biochem. J.* **245**, 93–101.
30. Janmey, P.A., U. Euteneuer, P. Traub and M. Schliwa, 1991, Viscoelastic properties of vimentin compared with other filamentous biopolymer networks, *J. Cell Biol.* **113**, 155–160.
31. Stewart, M., 1990, Intermediate filaments: Structure, assembly and molecular interactions, *Curr. Opin. Cell Biol.* **2**, 91–100.
32. Foisner, R. and T. Wiche, 1991, Intermediate filament-associated proteins, *Curr. Opin. Cell Biol.* **3**, 75–81.
33. Janmey, P., C. Cunningham, G. Oster and T. Stossel, 1992, Cytoskeletal networks and osmotic pressure in relation to cell structure and motility, in: *Swelling Mechanics: From Clays to Living Cells and Tissues*, ed. T. K. Karalis (Springer, Heidelberg) pp. 333–346.
34. Cortese, J.D., B. Schwab, C. Frieden and E.L. Elson, 1989, Actin polymerization induces a shape change in actin-containing vesicles, *Proc. Nat. Acad. Sci. USA* **86**, 5773–5777.
35. Bärmann, M., J. Käs, H. Kurzmeier and E. Sackmann, 1992, A new cell model – actin networks encaged by giant vesicles, in: *Structure and Conformation of Amphiphilic Membranes*, ed. R. Lipowsky (Springer, Berlin).
36. Janmey, P.A., 1991, Mechanical properties of cytoskeletal polymers, *Curr. Opin. Cell Biol.* **3**, 4–11.
37. Verkman, A., 1992, Water channels in cell membranes, *Annu. Rev. Physiol.* **54**, 97–108.

38. Cunningham, C.C., J.B. Gorlin, D.J. Kwiatkowski, J.H. Hartwig, P.J. Janmey, H.R. Byers and T.P. Stossel, 1992, Actin-binding protein requirement for cortical stability and efficient locomotion, *Science* **255**, 325–327.
39. Ito, T., K.S. Zaner and T.P. Stossel, 1987, Nonideality of volume flows and phase transitions of F-actin solutions in response to osmotic stress, *Biophys. J.* **51**, 745–753.
40. Miyamoto, H. and H. Hotani, 1988, Polymerization of microtubules within liposomes produces morphological change of their shapes, in: *Dynamics of Microtubules*, ed. H. Hotani (Taniguchi Foundation).
41. Peskin, C., G. Odell and G. Oster, 1993, Cellular motions and thermal fluctuations: The Brownian ratchet, *Biophys. J.* **65**, 316.
42. Malev, V., D. Gromov, Y.Y. Komissarchik and M. Brudnaya, 1992, Interfacial models of nerve fiber cytoskeleton, *Biophys. J.* **63**, 1101–1117.
43. Bennett, V., 1990, Spectrin-based membrane skeleton: a multipotential adaptor between plasma membrane and cytoplasm, *Physiol. Rev.* **70**, 1029–1065.
44. Byers, T.J., C.A. Husain, R.R. Dubreuil, D. Branton and L.S. Goldstein, 1989, Sequence similarity of the amino-terminal domain of *Drosophila* beta spectrin to alpha actinin and dystrophin, *J. Cell Biol.* 1633–1641.
45. Schanus, E., S. Booth, B. Hallaway and A. Rosenberg, 1985, The elasticity of spectrin-actin gels at high protein concentration, *J. Biol. Chem.* **260**, 3724–3730.
46. Anderson, R.A. and V.T. Marchesi, 1985, Regulation of the association of membrane skeletal Protein 4.1 with glycophorin by a polyphosphoinositide, *Nature* **318**, 295–298.
47. Rybicki, A., R. Heath, B. Lubin and R. Schwartz, 1988, Human erythrocyte Protein 4.1 is a phosphatidylserine binding proteins, *J. Clin. Invest.* **81**, 255–260.
48. Cohen, A.M., S.C. Liu, J. Lawler, L. Derick and J. Palek, 1988, Identification of the protein 4.1 binding site to phosphatidylserine vesicles, *Biochemistry* **27**, 614–619.
49. Bennett, V. 1992, Ankyrins, *J. Biol. Chem.* **267**.
50. Willardson, B.M., B.J. Thevenin, M.L. Harrison, W.M. Kuster, M.D. Benson and P.S. Low, 1989, Localization of the ankyrin-binding site on erythrocyte membrane protein, Band 3, *J. Biol. Chem.* **264**, 15893–15899.
51. Husain, C.A., A. Levin and D. Branton, 1988, Abolition of actin-bundling by phosphorylation of human erythrocyte Protein 4.9, *Nature* **334**, 718–721.
52. Husain, C.A., W. Faquin, C.C. Wu and D. Branton, 1989, Purification of erythrocyte dematin (protein 4.9) reveals an endogenous protein kinase that modulates actin-bundling activity, *J. Biol. Chem.* **264**, 8985–8991.
53. Ruff, P., D.W. Speicher and C.H. Husain, 1991, Molecular identification of a major palmitoylated erythrocyte membrane protein containing the src homology 3 motif, *Proc. Nat. Acad. Sci. USA* **88**, 6595–6599.
54. Cianci, C.D., M. Giorgi and J.S. Morrow, 1988, Phosphorylation of ankyrin down-regulates its cooperative interaction with spectrin and Protein 3, *J. Cell Biochem.* **37**, 301–315.
55. Faquin, W.C., S.B. Chahwala, L.C. Cantley and D. Branton, 1986, Protein kinase C of human erythrocytes phosphorylates Bands 4.1 and 4.9, *Biochim. Biophys. Acta* **887**, 142–149.
56. Bennett, V., K. Gardner and J.P. Steiner, 1988, Brain adducin: A protein kinase C substrate that may mediate site-directed assembly at the spectrin-actin junction, *J. Biol. Chem.* **263**, 5860–5869.
57. Gardner, K. and V. Bennett, 1987, Modulation of spectrin-actin assembly by erythrocyte adducin, *Nature* **328**, 359–362.
58. Mische, S., M.S. Mooseker and J.S. Morrow, 1987, Erythrocyte adducin: A calmodulin-regulated actin-bundling protein that stimulates spectrin-actin binding, *J. Cell Biol.* **105**, 2837–2845.
59. Joshi, R., D.M. Gilligan, E. Otto, T. McLaughlin and V. Bennett, 1991, Primary structure and domain organization of human alpha and beta adducin, *J. Cell Biol.* **115**, 665–675.
60. Kahana, E., J.C. Pinder, K.S. Smith and W.B. Gratzler, 1992, Fluorescence quenching of spectrin and other red cell membrane cytoskeletal proteins. Relation to hydrophobic binding sites, *Biochem. J.* 75–80.

61. Johnson, S.J., T.M. Bayerl, W. Weihan, H. Noack, J. Penfold, R.K. Thomas, D. Kanellas, A.R. Rennie and E. Sackmann, 1991, Coupling of spectrin and polylysine to phospholipid monolayers studied by specular reflection of neutrons, *Biophys. J.* **60**, 1017–1025.
62. Zeman, K., H. Engelhard and E. Sackmann, 1990, Bending undulations and elasticity of the erythrocyte membrane: Effects of cell shape and membrane organization, *Eur. Biophys. J.* **18**, 203–219.
63. Palek, J., 1987, Hereditary elliptocytosis, spherocytosis and related disorders: Consequences of a deficiency or a mutation of membrane skeletal proteins, *Blood Rev.* **1**, 147–168.
64. Svoboda, K., C. Schmidt, D. Branton and S. Block, 1992, Conformation and elasticity of the isolated red blood cell membrane skeleton, *Biophys. J.* **63**, 784–793.
65. Elgsaeter, A., B.T. Stokke, A. Mikkelsen and D. Branton, 1986, The molecular basis of erythrocyte shape, *Science* **234**, 1217–1223.
66. Evans, E.A., 1989, Structure and deformation properties of red blood cells: Concepts and quantitative methods, *Methods Enzymol.* **173**, 3–35.
67. Lerche, D., M.M. Kozlov and W. Meier, 1991, Time-dependent elastic extensional RBC deformation by micropipette aspiration: Redistribution of the spectrin network?, *Eur. Biophys. J.* **19**, 301–309.
68. Kozlov, M.M., L.V. Chernomordik and V.S. Markin, 1990, A mechanism of formation of protein-free regions in the red cell membrane: The rupture of the membrane skeleton, *J. Theoret. Biol.* **144**, 347–365.
69. Liu, S.C., L.H. Derick, M.A. Duquette and J. Palek, 1989, Separation of the lipid bilayer from the membrane skeleton during discocyte-echinocyte transformation of human erythrocyte ghosts, *Eur. J. Cell Biol.* **49**, 358–365.
70. Liu, S.C., L.H. Derick, S. Zhai and J. Palek, 1991, Uncoupling of the spectrin-based skeleton from the lipid bilayer in sickled red cells, *Science* **252**, 574–576.
71. Fox, J.E., J.K. Boyles, M.C. Berndt, P.K. Steffen and L. K. Anderson, 1988, Identification of a membrane skeleton in platelets, *J. Cell Biol.* **106**, 1525–1538.
72. Fox, J.E., C.C. Reynolds, J.S. Morrow and D.R. Phillips, 1987, Spectrin is associated with membrane-bound actin filaments in platelets and is hydrolyzed by the Ca^{2+} -dependent protease during platelet activation, *Blood* **69**, 537–545.
73. Hartwig, J.H. and M. DeSisto, 1991, The cytoskeleton of the resting human blood platelet: structure of the membrane skeleton and its attachment to actin filaments, *J. Cell Biol.* **112**, 407–425.
74. Abraham, F. and D. Nelson, 1990, Diffraction from polymerized membranes, *Science* **249**, 393–397.
75. Takeuchi, K., K. Kuroda, M. Ishigami and T. Nakamura, 1990, Actin cytoskeleton of resting bovine platelets, *Exp. Cell Res.* **186**, 374–380.
76. Okita, L., D. Pidar, P. Newman, R. Montgomery and T. Kunicki, 1985, On the association of glycoprotein Ib and actin-binding protein in human platelets, *J. Cell Biol.* **100**, 317–321.
77. Fox, J., 1985, Identification of actin-binding protein as the protein linking the membrane skeleton to glycoproteins on platelet plasma membrane, *J. Biol. Chem.* **260**, 11970–11977.
78. Ezzell, R.M., D.M. Kenney, S. Egan, T.P. Stossel and J.H. Hartwig, 1988, Localization of the domain of actin-binding protein that binds to membrane glycoprotein Ib and actin in human platelets, *J. Biol. Chem.* **263**, 13303–13309.
79. Suzuki, H., K. Tanoue and H. Yamazaki, 1991, Morphological evidence for the association of plasma membrane glycoprotein IIb/IIIa with the membrane skeleton in human platelets, *Histochemistry* **96**, 31–39.
80. Beckerle, M.C., D.E. Miller, M.E. Bertagnolli and S.J. Locke, 1989, Activation-dependent redistribution of the adhesion plaque protein talin, in intact human platelets, *J. Cell Biol.* **109**, 3333–3346.
81. Lehtonen, E., G. Ordonez and I. Reima, 1988, Cytoskeleton in preimplantation mouse development *Cell Differ.* **24**, 165–177 [published erratum appears in **25**, 79].
82. Mangeat, P.H., 1988, Interaction of biological membranes with the cytoskeletal framework of living cells, *Biol. Cell* **64**, 261–281.

83. Nelson, W.J. and R.W. Hammerton, 1989, A membrane-cytoskeletal complex containing Na⁺, K⁺-ATPase, ankyrin, and fodrin in Madin-Darby canine kidney (MDCK) cells: Implications for the biogenesis of epithelial cell polarity, *J. Cell Biol.* **108**, 893-902.
84. Bourguignon, L.Y., E.L. Kalomiris and V.B. Lokeshwar, 1991, Acylation of the lymphoma transmembrane glycoprotein, GP85, may be required for GP85-ankyrin interaction, *J. Biol. Chem.* **266**, 11761-11765.
85. Srinivasan, Y., L. Elmer, J. Davis, V. Bennett and K. Angelides, 1988, Ankyrin and spectrin associate with voltage-dependent sodium channels in brain, *Nature* **333**, 177-180.
86. Srinivasan, Y., M. Lewallen and K.J. Angelides, 1992, Mapping the binding site on ankyrin for the voltage-dependent sodium channel from brain, *J. Biol. Chem.* **267**, 7483-7489.
87. Cheney, R.E. and M.B. Willard, 1989, Characterization of the interaction between calpactin I and fodrin (non-erythroid spectrin), *J. Biol. Chem.* **264**, 18068-18075.
88. Herrmann, H. and G. Wiche, 1987, Plectin and IFAB 300k are homologous proteins binding to microtubule-associated proteins 1 and 2 and to the 240 kilodalton subunit of spectrin, *J. Biol. Chem.* **262**, 1320-1325.
89. Kwiatkowska, K., I.A. Khrebtukova, D.A. Gudkova, G.P. Pinaev and A. Sobota, 1991, Actin-binding proteins involved in the capping of epidermal growth factor receptors in A431 cells, *Exp. Cell Res.* **196**, 255-263.
90. Ruangjirachuporn, W., R. Udomsangpetch, J. Carlsson D. Drenckhahn, P. Perlmann and K. Berzins, 1991, Plasmodium falciparum: analysis of the interaction of antigen Pf155/RESA with the erythrocyte membrane, *Exp. Parasitol.* **73**, 62-72.
91. Cohen, C.M. and C. Korsgren, 1980, Band 4.1 causes spectrin-actin gels to become thixotropic, *Biochem. Biophys. Res. Commun.* **97**, 1429-1435.
92. Bornens, M., M. Paintrand and C. Celati, 1989, The cortical microfilament system of lymphoblasts displays a periodic oscillatory activity in the absence of microtubules: Implications for cell polarity, *J. Cell Biol.* **109**, 1071-1083.
93. Mittelman, L., S. Levin and R. Korenstein, 1991, Fast cell membrane displacements in B lymphocytes. Modulation by dihydrocytochalasin B and colchicine, *FEBS Lett.* **293**, 207-210.
94. Jones, J. and K. Green, 1991, Intermediate filament-plasma membrane interactions, *Curr. Opin. Cell Biol.* **3**, 127-132.
95. Maksymiwi, R., S.F. Sui, H. Gaub and E. Sackmann, 1987, Electrostatic coupling of spectrin dimers to phosphatidylserine containing lipid lamellae, *Biochemistry* **26**, 2983-2990.
96. Gupta, C.M., 1990, Is there any role of membrane bilayer-skeleton interaction in maintaining the transmembrane phospholipid asymmetry in erythrocytes?, *Biotechnol. Appl. Biochem.* **12**, 506-511.
97. Connor, J. and A.J. Schroit, 1990, *Biochemistry* **29**, 37-43.
98. Gudi, S.R., A. Kumar, V. Bhakuni, S.M. Gokhale and C.M. Gupta, 1990, Membrane skeleton-bilayer interaction is not the major determinant of membrane phospholipid asymmetry in human erythrocytes, *Biochim. Biophys. Acta.* **1023**, 63-72.
99. Strunecka, A., L. Krpejsova, J. Palecek, J. Macha, M. Maturova, L. Rosa and A. Paleckova, 1990, Transbilayer redistribution of phosphatidylserine in erythrocytes of a patient with autoerythrocyte sensitization syndrome (psychogenic purpura), *Folia Haematol. (Leipzig)* **117**, 829-841.
100. Pradhan, D., P. Williamson and R.A. Schlegel, 1991, Bilayer/cytoskeleton interactions in lipid-symmetric erythrocytes assessed by a photoactivable phospholipid analogue, *Biochemistry* **30**, 7754-7758.
101. Sune, A. and A. Bienvenue, 1988, Relationship between the transverse distribution of phospholipids in plasma membrane and shape change of human platelets, *Biochemistry* **27**, 6794-6800.
102. Comfurius, P., E.M. Bevers and R.F. Zwaal, 1989, Interaction between phosphatidylserine and the isolated cytoskeleton of human blood platelets, *Biochim. Biophys. Acta* **983**, 212-216.
103. Livne, A., M.A. Packham, M.A. Guccione and J.F. Mustard, 1988, Aggregation-related association of lipid with the cytoskeleton of rabbit and human platelets prelabeled with [3H]palmitic acid. Similar effects of adenosine diphosphate- and thrombin-induced aggregation, *J. Clin. Invest.* **81**, 288-299.

104. Vickers, J., R. Kinlough-Rathbone and J. Mustard, 1987, Phosphatidylinositol 4,5-bisphosphate is selectively retained by platelet-fibrin clots formed by thrombin, *Biochem. J.* **245**, 649–653.
105. Fields, R.D. and S.G. Waxman, 1988, Regional membrane heterogeneity in premyelinated CNS axons: factors influencing the binding of sterol-specific probes, *Brain Res.* **443**, 231–242.
106. Fields, R.D., J.A. Black and S.G. Waxman, 1987, Filipin-cholesterol binding in CNS axons prior to myelination: evidence for microheterogeneity in premyelinated axolemma, *Brain Res.* **404**, 21–32.
107. Molitoris, B.A., 1991, New insights into the cell biology of ischemic acute renal failure, *J. Am. Soc. Nephrol.* **1**, 1263–1270.
108. Molitoris, B.A., 1991, Ischemia-induced loss of epithelial polarity: potential role of the actin cytoskeleton [editorial], *Am. J. Physiol.* **F7**, 69–78.
109. Laliberte, A. and C. Gicquaud, 1988, Polymerization of actin by positively charged liposomes, *J. Cell Biol.* **106**, 1221–1227.
110. Ward, R.J., J.F. Menetret, F. Pattus and K. Leonard, 1990, Method for forming two-dimensional paracrystals of biological filaments on lipid monolayers, *J. Electron Microsc. Tech.* **14**, 335–341.
111. St Onge, D. and C. Gicquaud, 1989, Evidence of direct interaction between actin and membrane lipids, *Biochem. Cell Biol.* **67**, 297–300.
112. Okimasu, E., K. Nobori, S. Kobayashi, E. Suzuki, S. Terada and K. Utsumi, 1987, Inhibitory effect of cholesterol on interaction between cytoplasmic actin and liposomes, and restorative effect of high osmotic pressure, *Cell Struct. Funct.* **12**, 187–195.
113. Schmidt, C., 1988, Dynamik und Struktur polymerer aktin Netzwerke und ihre Wechselwirkung mit Modellmembranen, PhD Thesis, Technischen Universität München.
114. Tranter, M., S. Sugrue and M. Schwartz, 1991, Binding of actin to liver cell membranes: The state of membrane-bound actin, *J. Cell Biol.* **112**, 891–901.
115. Fox, J.E. and J.K. Boyles, 1988, The membrane skeleton – a distinct structure that regulates the function of cells, *Bioessays* **8**, 14–18.
116. Wang, D.L., A.E. Annamalai, S. Ghosh, A.M. Gewirtz, and R.W. Colman, 1990, Human platelet factor V is crosslinked to actin by FXIIIa during platelet activation by thrombin, *Thromb. Res.* **57**, 39–57.
117. Evans, E., D. Berk and A. Leung, 1991, Detachment of agglutinin-bonded red blood cells, I. Forces to rupture molecular-point attachments, *Biophys. J.* **59**, 838–848.
118. Evans, E., D. Berk, A. Leung and N. Mohandas, 1991, Detachment of agglutinin-bonded red blood cells, II. Mechanical energies to separate large contact areas, *Biophys. J.* **59**, 849–860.
119. Burridge, K., K. Fath, T. Kelly, G. Nuckolls and C. Turner, 1988, Focal adhesions: Transmembrane junctions between the extracellular matrix and the cytoskeleton, *Annu. Rev. Cell Biol.* **4**, 487–525.
120. Burridge, K. and K. Fath, 1989, Focal contacts: Transmembrane links between the extracellular matrix and the cytoskeleton, *Bioessays* **10**, 104–108.
121. Burridge, K., G. Nuckolls, C. Otey, F. Pavalko, K. Simon and C. Turner, 1990, Actin-membrane interaction in focal adhesions, *Cell Differ. Dev.* **32**, 337–342.
122. Fath, K.R., C.J. Edgell and K. Burridge, 1989, The distribution of distinct integrins in focal contacts is determined by the substratum composition, *J. Cell Sci.* **67**–75.
123. Rahilly, M.A., D.M. Salter and S. Fleming, 1991, Composition and organization of cell-substratum contacts in normal and neoplastic renal epithelium, *J. Pathol.* **165**, 163–171.
124. Turner, C.E. and K. Burridge, 1991, Transmembrane molecular assemblies in cell-extracellular matrix interactions, *Curr. Opin. Cell Biol.* **3**, 849–853.
125. Bailey, J. and D. Gingell, 1988, Contacts of chick fibroblasts on glass: Results and limitations of quantitative interferometry, *J. Cell Sci.* **215**–224.
126. Mueller, S.C., T. Kelly, M.Z. Dai, H.N. Dai and W.T. Chen, 1989, Dynamic cytoskeleton-integrin associations induced by cell binding to immobilized fibronectin, *J. Cell Biol.* **3455**–3464.
127. Otey, C.A., F.M. Pavalko and K. Burridge, 1990, An interaction between alpha-actinin and the beta 1 integrin subunit *in vitro*, *J. Cell Biol.* **111**, 721–729.
128. Pavalko, F.M., C.A. Otey, K.O. Simon and K. Burridge, 1991, Alpha-actinin: A direct link between actin and integrins, *Biochem. Soc. Trans.* **19**, 1065–1069.
129. Pavalko, F.M. and K. Burridge, 1991, Disruption of the actin cytoskeleton after microinjection of proteolytic fragments of alpha-actinin, *J. Cell Biol.*, **114**, 481–491.

130. Meyer, R.K. and U. Aebi, 1990, Bundling of actin filaments by α -actinin depends on its molecular length, *J. Cell Biol.* **110**, 2013–2024.
131. Burn, P., A. Rotman, R.K. Meyer and M.M. Burger, 1985, Diacylglycerol in large α -actinin/actin complexes and in the cytoskeleton of activated platelets, *Nature* **314**, 469–472.
132. Fukami, K., K. Furuhashi, M. Inagaki, T. Endo, S. Hatano and T. Takenawa, 1992, Requirement of phosphatidylinositol 4,5-bisphosphate for α -actinin function, *Nature* **359**, 150–152.
133. Drenckhahn, D., M. Beckerle, K. Burridge and J. Otto, 1988, Identification and subcellular location of talin in various cell types and tissues by means of [125I]vinculin overlay, immunoblotting and immunocytochemistry, *Eur. J. Cell Biol.* **46**, 513–522.
134. Nuckolls, G.H., C.E. Turner and K. Burridge, 1990, Functional studies of the domains of talin, *J. Cell Biol.* **110**, 1635–1644.
135. Turner, C.E., F.M. Pavalko and K. Burridge, 1989, The role of phosphorylation and limited proteolytic cleavage of talin and vinculin in the disruption of focal adhesion integrity, *J. Biol. Chem.* **264**, 11938–11944.
136. Qwarnstrom, E.E., S.A. MacFarlane, R.C. Page and S.K. Dower, 1991, Interleukin 1 beta induces rapid phosphorylation and redistribution of talin: A possible mechanism for modulation of fibroblast focal adhesion, *Proc. Nat. Acad. Sci. USA* **88**, 1232–1236.
137. Muguruma, M., S. Matsumura and T. Fukazawa, 1990, Direct interactions between talin and actin, *Biochem. Biophys. Res. Commun.* **171**, 1217–1223.
138. Isenberg, G. and W.H. Goldmann, 1992, Actin-membrane coupling: A role for talin [news], *J. Muscle Res. Cell Motil.* **13**, 587–589.
139. Kaufmann, S., J. Kas, W.H. Goldmann, E. Sackmann and G. Isenberg, 1992, Talin anchors and nucleates actin filaments at lipid membranes. A direct demonstration, *FEBS Lett.* **314**, 203–205.
140. Heise, H., T. Bayerl, G. Isenberg and E. Sackmann, 1991, Human platelet P-235, a talin-like actin binding protein, binds selectively to mixed lipid bilayers, *Biochim. Biophys. Acta.* **1061**, 121–131.
141. Muguruma, M., S. Matsumura and T. Fukazawa, 1992, Augmentation of α -actinin-induced gelation of actin by talin, *J. Biol. Chem.* **267**, 5621–5624.
142. Ruhnau, K. and A. Wegner, 1988, Evidence for direct binding of vinculin to actin filaments, *FEBS Lett.* **228**, 105–108.
143. Otto, J.J., 1986, The lack of interaction between vinculin and actin, *Cell Motil. Cytoskeleton* **6**, 48–55.
144. Asijee, G.M., A. Sturk, T. Bruin, J.M. Wilkinson and C.J. Ten, 1990, Vinculin is a permanent component of the membrane skeleton and is incorporated into the (re)organising cytoskeleton upon platelet activation, *Eur. J. Biochem.* **189**, 131–136.
145. Wachstock, D.H., J.A. Wilkins and S. Lin, 1987, Specific interaction of vinculin with α -actinin, *Biochem. Biophys. Res. Commun.* **146**, 554–560.
146. Turner, C.E., J.J. Glenney and K. Burridge, 1990, Paxillin: A new vinculin-binding protein present in focal adhesions, *J. Cell Biol.* **111**, 1059–1068.
147. Kellie, S. and N.M. Wigglesworth, 1987, The cytoskeletal protein vinculin is acylated by myristic acid, *FEBS Lett.* **213**, 428–432.
148. Burn, P. and M.M. Burger, 1987, The cytoskeletal protein vinculin contains transformation-sensitive, covalently bound lipid, *Science* **235**, 476–479.
149. Meyer, R., 1989, Vinculin-lipid interaction: A model for focal contact formation, *Eur. J. Cell Biol.* **50**, 491–499.
150. Niggli, V. and M. Burger, 1987, Interaction of the cytoskeleton with the plasma membrane, *J. Membr. Biol.* **100**, 97–121.
151. Niggli, V., L. Sommer, J. Brunner and M.M. Burger, 1990, Interaction in situ of the cytoskeletal protein vinculin with bilayers studied by introducing a photoactivatable fatty acid into living chicken embryo fibroblasts, *Eur. J. Biochem.* **187**, 111–117.
152. Isenberg, G., 1991, Actin-binding protein – lipid interactions, *Cell Motil. Cytoskeleton* **12**, 136–144.
153. Burn, P., 1988, Amphitropic proteins: A new class of membrane proteins, *Trends Biochem. Sci.* **13**, 79–83.

154. Burn, P., A. Kupfer and S.J. Singer, 1988, Dynamic membrane-cytoskeletal interactions: Specific association of integrin and talin arises *in vivo* after phorbol ester treatment of peripheral blood lymphocytes, *Proc. Nat. Acad. Sci. USA* **85**, 497–501.
155. Samuels, M., R. Ezzell, T. Cardozo, D. Critchley, J.-L. Coll and E. Adamson, 1993, Expression of chicken vinculin complements the adhesion-defective phenotype of a mutant mouse-f9 embryonal carcinoma cell, *J. Cell Biol.* **121**, 909–921.
156. Pavalko, F.M., C.A. Otey and K. Burridge 1989, Identification of a filamin isoform enriched at the ends of stress fibers in chicken embryo fibroblasts, *J. Cell Sci.* 109–118.
157. Kramarcy, N.R. and R. Sealock, 1990, Dystrophin as a focal adhesion protein. Colocalization with talin and the Mr 48,000 sarcolemmal protein in cultured *Xenopus* muscle, *FEBS Lett.* **274**, 171–174.
158. Wheelock, M.J. and K.A. Knudsen, 1991, Cadherins and associated proteins, *In Vivo* **5**, 505–513.
159. Magee, A. and R. Buxton, 1991, Transmembrane molecular assemblies regulated by the greater cadherin family, *Curr. Opin. Cell. Biol.* **3**, 854–861.
160. Ozawa, M., H. Hoschutsky, K. Herrenknecht and R. Kemler, 1990, A possible new adhesive site in the cell-adhesion molecule uvomorulin, *Mech. Dev.* **33**, 49–56.
161. Ozawa, M., H. Baribault and R. Kemler, 1989, The cytoplasmic domain of the cell adhesion molecule uvomorulin associates with three independent proteins structurally related in different species, *EMBO J.* **8**, 1711–1717.
162. Herrenknecht, K., M. Ozawa, C. Eckerskorn, F. Lottspeich, M. Lenter and R. Kemler, 1991, The uvomorulin-anchorage protein alpha catenin is a vinculin homologue, *Proc. Nat. Acad. Sci. USA* **88**, 9156–9160.
163. Funayama, N., A. Nagafuchi, N. Sato, S. Tsukita and S. Tsukita, 1991, Radixin is a novel member of the Band 4.1 family, *J. Cell Biol.* **115**, 1039–1048.
164. Aakhus, A.M., J.M. Wilkinson and N.O. Solum, 1991, Glycoprotein Ib- and actin-binding regions in human platelet actin-binding protein, *Biochem. Soc. Trans.* **19**, 1133–1134.
165. Gorlin, J., R. Yamin, S. Egan, M. Stewart, T. Stossel, D. Kwiatkowski and J. Hartwig, 1990, Human endothelial actin-binding protein (ABP-280, non-muscle filamin): A molecular leaf spring, *J. Cell Biol.* **111**, 1089–1105.
166. Ohta, Y., T.P. Stossel and J.H. Hartwig, 1991, Ligand-sensitive binding of actin-binding protein to immunoglobulin G Fc receptor I (Fc gamma RI), *Cell* **67**, 275–282.
167. Low, M., 1989, The glycosyl-phosphatidylinositol anchor of membrane proteins, *Biochim. Biophys. Acta* **988**, 427–454.
168. Stochaj, U., J. Dieckhoff, J. Mollenhauer, M. Cramer and H.G. Mannherz, 1989, Evidence for the direct interaction of chicken gizzard 5'-nucleotidase with laminin and fibronectin, *Biochim. Biophys. Acta* **992**, 385–392.
169. Dieckhoff, J., B. Niggemeyer, R. Lietzke and H.G. Mannherz, 1987, Reconstitution of purified chicken gizzard 5'-nucleotidase in phospholipid vesicles. Evidence for its transmembraneous character and the existence of functional domains on both sides of the phospholipid bilayer, *Eur. J. Biochem.* **162**, 451–459.
170. Vedeler, A., I.F. Pryme and J.E. Hesketh, 1991, Insulin induces changes in the subcellular distribution of actin and 5'-nucleotidase, *Mol. Cell Biochem.* **108**, 67–74.
171. Wuestehube, L. and E. Luna, 1987, F-actin binds to the cytoplasmic surface of Ponticulin, a 17-kD Integral glycoprotein from *Dictyostelium discoideum* plasma membranes, *J. Cell Biol.* **105**, 1741–1751.
172. Shariff, A. and E. Luna, 1990, *Dictyostelium discoideum* plasma membranes contain an actin-nucleating activity that requires ponticulin, an integral membrane glycoprotein, *J. Cell Biol.* **110**, 681–692.
173. Thelen, M., A. Rosen, A.C. Nairn and A. Aderem, 1991, Regulation by phosphorylation of reversible association of a myristoylated protein kinase C substrate with the plasma membrane, *Nature* **351**, 320–322.
174. Hartwig, J., M. Thelen, A. Rosen, P. Janmey, A. Nairn and A. Aderem, 1992, The MARCKS protein is an actin filament crosslinking protein regulated by protein kinase C-mediated phosphorylation and by calcium/calmodulin, *Nature* **356**, 618–622.

175. Jongstra-Bilen, J., P.A. Janmey, J.H. Hartwig, S. Galea and J. Jongstra, 1992, The lymphocyte-specific protein LSP1 binds to F-actin and to the cytoskeleton through its C-terminal basic domain, *J. Cell Biol.* **118**, 1443–1453.
176. Liu, Y., K. Carraway and C. Carraway, 1989, Isolation and characterization of a 58kDa membrane- and microfilament-associated protein from ascites tumor cell microvilli, *J. Cell Biol.* **264**, 1208–1214.
177. Bärmann, M., J. Wadsack and M. Frimner, 1986, A 50 kDa actin-binding protein in plasma membranes of rat hepatocytes and of rat liver tumors, *Biochim. Biophys. Acta* **859**, 110–116.
178. Hargreaves, A., F. Wandosell and J. Avila, 1986, Phosphorylation of tubulin enhances its interaction with membranes, *Nature* **323**, 827–828.
179. Kelly, R., 1990, Associations between microtubules and intracellular organelles, *Curr. Opin. Cell Biol.* **2**, 105–108.
180. Severin, F.F., 1991, Microtubule-associated proteins, *Biokhimiia* **56**, 963–976.
181. Duden, R., W.C. Ho, V.J. Allan and T.E. Kreis, 1990, What's new in cytoskeleton-organelle interactions? Relationship between microtubules and the Golgi-apparatus, *Pathol. Res. Pract.* **186**, 535–541.
182. Woods, C. and E. Lazarides, 1988, The erythroid membrane skeleton: Expression and assembly during erythropoiesis, *Annu. Rev. Med.* **39**, 107–122.
183. Stetzkowski-Marden, F., C. Deprette and R. Cassoly, 1991, Microtubular-marginal band in the avian erythrocyte: studies of cell swelling kinetics and identification of tubulin-binding proteins of plasma membrane skeleton which co-localize with the microtubular marginal band, in: *The Living Cell in Four Dimensions*, ed. C. Troyanowsky (American Institute of Physics, New York) pp. 244–250.
184. Birgbauer, E. and F. Solomon, 1989, A marginal band-associated protein has properties of both microtubule- and microfilament-associated proteins, *J. Cell Biol.* 1609–1620.
185. Gould, K.L., A. Bretscher, F.S. Esch and T. Hunter, 1989, cDNA cloning and sequencing of the protein-tyrosine kinase substrate, ezrin, reveals homology to Band 4.1, *EMBO J.* **8**, 4133–4142.
186. Bramblett, G.T., R. Kambadur and M. Flavin, 1989, Immunocytochemical studies with antibodies to three proteins prominent in the isolated microtubule cytoskeleton of a trypanosomatid, *Cell Motil. Cytoskeleton* **13**, 145–157.
187. Quest, A.F. and B.M. Shapiro, 1991, Membrane association of flagellar creatine kinase in the sperm phosphocreatine shuttle, *J. Biol. Chem.* **266**, 19803–19811.
188. Wang, N. and M.M. Rasenick, 1991, Tubulin-G protein interactions involve microtubule polymerization domains, *Biochemistry* **30**, 10957–10965.
189. Bereznikova, A.V., A.B. Gareeva, N.A. Kochanova, K.M. Popov, T.V. Bulargina and E.S. Severin, 1990, Interaction of alpha-subunit of the GTP-binding protein Go with cytoskeleton, *Biokhimiia* **55**, 1229–1236.
190. Traub, P., G. Perides, S. Kuhn and A. Scherbarth, 1987, Efficient interaction of nonpolar lipids with intermediate filaments of the vimentin type, *Eur. J. Cell Biol.* **43**, 55–64.
191. Asch, H.L., E. Mayhew, R.O. Lazo and B.B. Asch, 1990, Lipids noncovalently associated with keratins and other cytoskeletal proteins of mouse mammary epithelial cells in primary culture, *Biochim. Biophys. Acta* **1034**, 303–308.
192. Horkovics, K.S., and P. Traub, 1990, Specific interaction of the intermediate filament protein vimentin and its isolated N-terminus with negatively charged phospholipids as determined by vesicle aggregation, fusion, and leakage measurements, *Biochemistry* **29**, 8652–8657.
193. Horkovics, K.S. and P. Traub, 1991, A mathematical model for protein-induced lipid vesicle leakage: Interaction of the intermediate filament protein vimentin and its isolated N-terminus with phosphatidylinositol vesicles, *J. Theoret. Biol.* **153**, 89–110.
194. Gillard, B.K., J.P. Heath, L.T. Thurmon and D.M. Marcus, 1991, Association of glycosphingolipids with intermediate filaments of human umbilical vein endothelial cells, *Exp. Cell Res.* **192**, 433–444.
195. Gillard, B., L. Thurmon and D. Marcus, 1992, Association of glycosphingolipids with intermediate filaments of mesenchymal, epithelial, glial, and muscle cells, *Cell Motil. Cytoskeleton* **21**, 255–271.

196. Almahbobi, G., L.J. Williams and P.F. Hall, 1992, Attachment of mitochondria to intermediate filaments in adrenal cells: Relevance to the regulation of steroid synthesis, *Exp. Cell Res.* **200**, 361–369.
197. Almahbobi, G. and P.F. Hall, 1990, The role of intermediate filaments in adrenal steroidogenesis, *J. Cell Sci.* 679–687.
198. Schwartz, M., K. Owaribe, J. Kartenbeck and W. Francke, 1990, Desmosomes and hemi-desmosomes: Constitutive molecular components, *Annu. Rev. Cell Biol.* **6**, 461–491.
199. Hintner, H., U. Stanzl, K. Dahlback, B. Dahlback and S.M. Breathnach, 1989, Vitronectin shows complement-independent binding to isolated keratin filament aggregates, *J. Invest. Dermatol.* **93**, 656–661.
200. French, S.W., H. Kawahara, Y. Katsuma, M. Ohta and S.H. Swierenga, 1989, Interaction of intermediate filaments with nuclear lamina and cell periphery, *Electron. Microsc. Rev.* **2**, 17–51.
201. Chopra, H., J.S. Hatfield, Y.S. Chang, I.M. Grossi, L.A. Fitzgerald, C.Y. O’Gara, L.J. Marnett, C.A. Diglio, J.D. Taylor and K.V. Honn, 1988, Role of tumor cytoskeleton and membrane glycoprotein IRGpIIb/IIIa in platelet adhesion to tumor cell membrane and tumor cell-induced platelet aggregation, *Cancer Res.* **48**, 3787–3800.
202. Chopra, H., S.E. Fligel, J.S. Hatfield, K.K. Nelson, C.A. Diglio, J.D. Taylor and K.V. Honn, 1990, An *in vivo* study of the role of the tumor cell cytoskeleton in tumor cell-platelet-endothelial cell interactions, *Cancer Res.* **50**, 7686–7696.
203. Korn, E.D. and J.E. Hammer, 1990, Myosin I, *Curr. Opin. Cell Biol.* **2**, 57–61.
204. Collins, K., J. Sellers and P. Matsudaira, 1991, Myosin I: A new insight into the mechanism and cellular significance of actin-based motility, *Adv. Biophys.* **27**, 221–226.
205. Pollard, T.D., S.K. Doberstein and H.G. Zot, 1991, Myosin-I, *Annu. Rev. Physiol.* **53**, 653–681.
206. Cheney, R.E. and M.S. Mooseker, 1992, Unconventional myosins, *Curr. Opin. Cell Biol.* **4**, 27–35.
207. Drenckhahn, D. and R. Dermietzel, 1988, Organization of the actin filament cytoskeleton in the intestinal brush border: A quantitative and qualitative immunoelectron microscope study, *J. Cell Biol.* **107**, 1037–1048.
208. Mooseker, M.S. and T.R. Coleman, 1989, The 110-kD protein-calmodulin complex of the intestinal microvillus (brush border myosin I) is a mechanoenzyme, *J. Cell Biol.* **108**, 2395–2400.
209. Garcia, A., E. Coudrier, J. Carboni, J. Anderson, J. Vandekerckhove, M. Mooseker, D. Louvard and M. Arpin, 1989, Partial deduced sequence of the 110-kD-calmodulin complex of the avian intestinal microvillus shows that this mechanoenzyme is a member of the myosin I family, *J. Cell Biol.* 2895–2903.
210. Adams, R.J. and T.D. Pollard, 1989, Binding of myosin I to membrane lipids, *Nature* **340**, 565–568.
211. Adams, R.J. and T.D. Pollard, 1989, Membrane-bound myosin-I provides new mechanisms in cell motility, *Cell Motil. Cytoskeleton* **14**, 178–182.
212. Baines, I.C. and E.D. Korn, 1990, Localization of myosin IC and myosin II in *Acanthamoeba castellanii* by indirect immunofluorescence and immunogold electron microscopy, *J. Cell Biol.* 1895–1904.
213. Miyata, H., B. Bowers and E.D. Korn, 1989, Plasma membrane association of *Acanthamoeba* myosin I, *J. Cell Biol.* 1519–1528.
214. Zot, H.G., S.K. Doberstein and T.D. Pollard, 1992, Myosin-I moves actin filaments on a phospholipid substrate: Implications for membrane targeting, *J. Cell Biol.* **116**, 367–376.
215. Schroer, T.A. and M.P. Sheetz, 1991, Functions of microtubule-based motors, *Annu. Rev. Physiol.* **53**, 629–652.
216. Vale, R.D. and H. Hotani, 1988, Formation of membrane networks *in vitro* by kinesin-driven microtubule movement, *J. Cell Biol.* 2233–2241.
217. Kucik, D.F., E.L. Elson and M.P. Sheetz, 1989, Forward transport of glycoproteins on leading lamellipodia in locomoting cells [see comments], *Nature* **340**, 315–317.
218. Jay, P.Y. and E.L. Elson, 1992, Surface particle transport mechanism independent of myosin II in *Dictyostelium*, *Nature* **356**, 438–440.
219. Kucik, D.F., S.C. Kuo, E.L. Elson and M.P. Sheetz, 1991, Preferential attachment of membrane glycoproteins to the cytoskeleton at the leading edge of lamella, *J. Cell Biol.* **114**, 1029–1036.

220. Qian, H., M.P. Sheetz and E.L. Elson, 1991, Single particle tracking. Analysis of diffusion and flow in two-dimensional systems, *Biophys. J.* **60**, 910–921.
221. Sheetz, M.P., S. Turney, H. Qian and E.L. Elson, 1989, Nanometre-level analysis demonstrates that lipid flow does not drive membrane glycoprotein movements [see comments], *Nature* **340**, 284–288.
222. Forscher, P., C. Lin and C. Thompson, 1992, Novel form of growth cone motility involving site-directed actin filament assembly, *Nature* **357**, 515–518.
223. Theriot, J., T. Mitchison, L. Tilney and D. Portnoy, 1992, The rate of actin-based motility of intracellular *listeria-monocytogenes* equals the rate of actin polymerization, *Nature* **357**, 257–260.
224. Apgar, J.R., 1990, Antigen-induced cross-linking of the IgE receptor leads to an association with the detergent-insoluble membrane skeleton of rat basophilic leukemia (RBL-2H3) cells, *J. Immunol.* **145**, 3814–3822.
225. Apgar, J.R., 1991, Association of the crosslinked IgE receptor with the membrane skeleton is independent of the known signaling mechanisms in rat basophilic leukemia cells, *Cell Regul.* **2**, 181–191.
226. Mao, S.Y., G. Alber, J. Rivera, J. Kochan and H. Metzger, 1992, Interaction of aggregated native and mutant IgE receptors with the cellular skeleton, *Proc. Nat. Acad. Sci. USA* **89**, 222–226.
227. Seagrave, J., J.R. Pfeiffer, C. Wofsy and J.M. Oliver, 1991, Relationship of IgE receptor topography to secretion in RBL-2H3 mast cells, *J. Cell Physiol.* **148**, 139–151.
228. Wade, W., J. Freed and M. Edidin, 1989, Translational diffusion of class II major histocompatibility complex molecules is constrained by their cytoplasmic domains, *J. Cell Biol.* **109**, 3325–3331.
229. Hochmuth, R.M. and D. Needham, 1990, The viscosity of neutrophils and their transit times through small pores, *Biorheology* **27**, 817–828.
230. Evans, E. and A. Yeung, 1989, Apparent viscosity and cortical tension of blood granulocytes determined by micropipet aspiration, *Biophys. J.* **56**, 151–160.
231. Downey, G.P., E.L. Elson, B. Schwab, S.C. Erzurum, S.K. Young and G.S. Worthen, 1991, Biophysical properties and microfilament assembly in neutrophils: Modulation by cyclic AMP, *J. Cell Biol.* **114**, 1179–1190.
232. Hallows, K.R., C.H. Packman and P.A. Knauf, 1991, Acute cell volume changes in anisotonic media affect F-actin content of HL-60 cells, *Am. J. Physiol.* **C1154**–1161.
233. Cornet, M., E. Delpire and R. Gilles, 1988, Relations between cell volume control, microfilaments and microtubules networks in T2 and PC12 cultured cells, *J. Physiol. (Paris)* **83**, 43–49.
234. Ziyadeh, F.N., J.W. Mills and A. Kleinzeller, 1992, Hypotonicity and cell volume regulation in shark rectal gland: role of organic osmolytes and F-actin, *Am. J. Physiol.* **F468**–479.
235. Cantiello, H.F., A.G. Prat, J.V. Bonventre, C.C. Cunningham, J.H. Hartwig and D.A. Ausiello, 1993, Actin-binding protein contributes to cell volume regulatory ion channel activation in melanoma cells, *J. Biol. Chem.* **268**, 4596–4599.
236. Linshaw, M.A., C.A. Fogel, G.P. Downey, E.W. Koo and A.I. Gotlieb, 1992, Role of cytoskeleton in volume regulation of rabbit proximal tubule in dilute medium, *Am. J. Physiol.* **262**, F144–150.
237. Edelstein, N.G., W.A. Catterall and R.T. Moon, 1988, Identification of a 33-kilodalton cytoskeletal protein with high affinity for the sodium channel, *Biochemistry* **27**, 1818–1822.
238. Cantiello, H.F., J.L. Stow, A.G. Prat and D.A. Ausiello, 1991, Actin filaments regulate epithelial Na⁺ channel activity, *Am. J. Physiol.* **261**, C882–888.
239. Yu, F.-X., H.-Q. Sun, P. Janmey and H. Yin, 1992, Identification of a polyphosphoinositide binding sequence in an actin monomer binding domain of gelsolin, *J. Biol. Chem.* **267**, 14616–14621.
240. Janmey, P., J. Lamb, P. Allen and P. Matsudaira, 1992, Phosphoinositide-binding peptides derived from the sequences of gelsolin and villin, *J. Biol. Chem.* **267**, 11818–11823.
241. Lassing, I. and V. Lindberg, 1985, Specific interaction between phosphatidylinositol 4,5 bisphosphate and profilactin, *Nature* **314**, 604–606.
242. Lassing, I. and U. Lindberg, 1988, Evidence that the phosphatidylinositol cycle is linked to cell motility, *Exp. Cell Res.* **174**, 1–15.
243. Goldschmidt-Clermont, P.J., L.M. Machesky, J.J. Baldassare and T.D. Pollard, 1990, The actin-binding protein profilin binds to PIP2 and inhibits its hydrolysis by phospholipase C, *Science* **247**, 1575–1578.

244. Stossel, T.P., 1989, From signal to pseudopod. How cells control cytoplasmic actin assembly, *J. Biol. Chem.* **264**, 18261–18264.
245. Janmey, P.A., 1991, Gel-sol transitions of the cytoplasm and its regulation, in: *The Living Cell in Its Four Dimensions*, ed. C. Troyanowsky (American Institute of Physics).
246. Traynor, K.A., B.L. Thompson, A.L. Harris, P. Taylor, G.M. Omann and L.A. Sklar, 1989, Transient increase in phosphatidylinositol 3,4-bisphosphate and phosphatidylinositol trisphosphate during activation of human neutrophils, *J. Biol. Chem.* **264**, 15668–15673.
247. Eberle, M., K.A. Traynor, L.A. Sklar and J. Norgauer, 1990, Is there a relationship between phosphatidylinositol trisphosphate and F-actin polymerization in human neutrophils?, *J. Biol. Chem.* **265**, 16725–16728.
248. Dadabay, C.Y., E. Patton, J.A. Cooper and L.J. Pike, 1991, Lack of correlation between changes in polyphosphoinositide levels and actin/gelsolin complexes in A431 cells treated with epidermal growth factor, *J. Cell Biol.* **112**, 1151–1156.
249. Xian, W., T.M. Garver, W.H. Braunlin and P.A. Janmey, 1992, NMR and CD conformational studies of a 20 amino acid PIP₂-binding site on gelsolin, *Faseb. J.* **6**, A87.
250. Goldschmidt, C.P., J.W. Kim, L.M. Machesky, S.G. Rhee and T.D. Pollard, 1991, Regulation of phospholipase C- γ 1 by profilin and tyrosine phosphorylation, *Science* **251**, 1231–1233.
251. Rittenhouse, S.E., 1983, Human platelets contain phospholipase C that hydrolyzes polyphosphoinositides, *Proc. Nat. Acad. Sci. USA* **80**, 5417–5420.
252. Rittenhouse, S.E. and J.P. Sasson, 1985, Mass changes in myoinositol trisphosphate in human platelets stimulated by thrombin. Inhibitory effects of phorbol ester, *J. Biol. Chem.* **260**, 8657–8660.
253. Grondin, P., M. Plantavid, C. Sultan, M. Breton, G. Mauco and H. Chap, 1991, Interaction of pp60c-src, phospholipase C, inositol-lipid, and diacylglycerol kinases with the cytoskeletons of thrombin-stimulated platelets, *J. Biol. Chem.* **266**, 15705–15709.
254. Banno, Y., T. Nakashima, T. Kumada, K. Ebisawa, Y. Nonomura and Y. Nozawa, 1992, Effects of gelsolin on human platelet cytosolic phosphoinositide-phospholipase C isozymes, *J. Biol. Chem.* **267**, 6488–6494.
255. Payraastre, B., P. van Bergen en Henegouwen, M. Breton, J. den Hartigh, M. Plantavid, A.J. Verkleij and J. Boonstra, 1991, Phosphoinositide kinase, diacylglycerol kinase, and phospholipase C activities associated to the cytoskeleton: effect of epidermal growth factor, *J. Cell Biol.* **115**, 121–128.
256. van Belzen, N., M. Spaargaren, A.J. Verkleij and J. Boonstra, 1990, Interaction of epidermal growth factor receptors with the cytoskeleton is related to receptor clustering, *J. Cell Physiol.* **145**, 365–375.
257. Bennett, V., 1990, Spectrin: A structural mediator between diverse plasma membrane proteins and the cytoplasm, *Curr. Opin. Cell Biol.* **2**, 51–56.
258. Alberts, B., D. Bray, J. Lewis, M. Raff, K. Roberts and J. Watson, 1983, *Mol. Biol. Cell* (New York, Garland) p. 685.
259. Stossel, T., 1991, Actin-membrane interactions in eukaryotic mammalian cells, in: *Ordering the Membrane-Cytoskeleton Trilayer*, eds M. Mooseker and B. Morrow (Academic Press, San Diego) pp. 97–107.

This Page Intentionally Left Blank

Electroporation and Electrofusion of Membranes

D.S. DIMITROV

*Section on Membrane Structure and Function, National Cancer Institute,
National Institutes of Health, Bethesda, Maryland 20892, USA
Central Laboratory of Biophysics,
Bulgarian Academy of Sciences, Sofia 1113, Bulgaria*

Contents

1. Introductory remarks	854
1.1. Membrane fusion ensures specific, controlled transfer of molecules in life processes and is important for biotechnology and biomedical research	854
1.2. Manifestations of cell fusion were observed nearly two centuries ago, while electrofusion was discovered in the late 1970's	854
1.3. Electric fields can induce fusion of a wide variety of membranes	855
2. Polarization of membranes underlies their destabilization, adhesion and fusion	855
2.1. Polarization is due to restricted motion of charges	855
2.2. Interaction of electric fields with polarized membranes induces mechanical stresses ...	856
2.3. Forces exerted on polarized membranes can induce structural rearrangements, approach of membranes and their fusion	856
3. High voltage pulses electroporate membranes	857
3.1. High voltage pulses can permeabilize membranes	857
3.2. The devices for electroporation are conceptually simple	858
3.3. The transmembrane voltage induced by the external electric fields is accurately described by a simple formula	859
3.4. Intramembrane field strength is much higher than the strength of the applied electric field	860
3.5. Membranes are electroporated when the transmembrane voltage exceeds a threshold value	861
3.6. Transfer of molecules by electroporation is asymmetric	861
3.7. The threshold voltage of electroporation decreases with an increase in intramembrane mechanical stresses (membrane tension)	861
3.8. The electromechanical models of electroporation describe membrane rupture as mediated by intramembrane stresses induced by the field	864
3.9. The energy-based approaches describe formation and expansion of pores as overcoming energy barriers	866
4. Mutual attraction and adhesion of the cells in AC fields is due to dielectrophoresis	867
4.1. Formation of 'pearl chains' of cells in AC fields is due to dielectrophoresis	867
4.2. The dielectrophoretic force exerted on individual cells can be accurately measured	868
4.3. The intercellular attraction force increases with decreasing the intermembrane separation and is proportional to the square of the field intensity	870
4.4. The attraction of cells induced by AC fields can affect fusion efficiency	871

5. Electroporative pulses induce fusion of adhered membranes	872
5.1. Electrofusion is induced at the same threshold voltages as electroporation	872
5.2. Devices for electrofusion are very similar to those for electroporation	874
5.3. Long-lived fusogenic states exist after membrane electroporation	874
5.4. Fusion is localized and results in formation of intracellular vesicles	875
5.5. The cell cytoskeleton is reorganized during electrofusion	877
5.6. Assays based on fluorescence dyes allow accurate measurement of fusion kinetics	879
5.7. Fusion occurs after a lag time (delay) following the application of the fusogenic trigger	879
5.8. Delays in electrofusion decrease with an increase in the field strength and are proportional to the solution viscosity	880
5.9. Rates of fusion can provide information for the time course of membrane merging and fusion pore expansion	880
5.10. Fusion yields and delays are related but may reflect different properties of the fusing membranes	883
6. Kinetic pathways of membrane fusion resemble coalescence in colloid systems	884
6.1. 'Fusion' of lipid monolayers on liquid surfaces is by diffusion or intermixing driven by surface pressure gradients	884
6.2. Fusion of bilayers requires overcoming the intramembrane attraction	886
6.3. The molecular mechanism of bilayer fusion is unknown	890
6.4. Fusion of cell membranes can be qualitatively described but the molecular rearrangements remain unclear	890
7. Fusion in life processes involves specialized proteins but kinetically can be similar to electrofusion	892
8. New approaches are needed to understand molecular mechanisms of fusion	893
Acknowledgement	893
List of symbols	893
References	895

1. Introductory remarks

1.1. Membrane fusion ensures specific, controlled transfer of molecules in life processes and is important for biotechnology and biomedical research

Fusion of membranes is a physical process which was of critical importance for the rapid evolution of life on earth and is involved in a variety of life processes today. One could imagine that billions of years ago the mechanical and/or electrical interactions in the ancient ocean mediated close apposition and destabilization of membranes which resulted in their fusion. Fusion of parts of the same membrane led to cell division and fusion of different membranes resulted in cell fusion. Both phenomena led to transfer and exchange of molecules which contributed to the rapid acceleration of the evolution of life on earth. One could further speculate that the 'first' fusion reactions were non-specific and any membranes could fuse provided appropriate conditions, including molecular contact, membrane destabilization and proper composition. Subsequently, specialized proteins appeared which led to the specific fusion of membranes and to controlled transfer of molecules. Today, the specific fusion of membranes seems to be the predominant mode of fusion in biological systems; however, the ability of membranes to fuse non-specifically, e.g., by external electric fields, provides information about the fundamental mechanisms of fusion and is important for biotechnology, medicine and research in biology.

1.2. Manifestations of cell fusion were observed nearly two centuries ago, while electrofusion was discovered in the late 1970's

The first manifestations of a fusion phenomenon were observed almost two centuries ago by the German biologist Johannes Muller (see [1]). He discovered multinucleated giant cells in histological specimen while studying pathological conditions. By the turn of the nineteenth century, the medical literature contained several reports of 'polykaryocytosis' as symptomatic of a variety of diseases, including tuberculosis, variola, varicella, and rubeola. This raised the question whether these giant cells originated from successive mitoses or from fusion of mononucleated cells [2]. Later fusion was clearly established [3] as a mode of their formation, but it was not until the 1960's, when the studies of fusion 'exploded'. During a relatively short period of time a number of interesting fusion phenomena were discovered and characterized by using light microscopy (for history see [1]): (i) viruses can induce formation of giant multinucleated cells (syncytia) [4–6], (ii) during fertilization the acrosomal membrane interdigitates and then coalesces with the egg membranes [7], (iii) mononucleated myoblasts fuse to form myotubes, at least in vitro [8, 9], and (iv) cell hybrids can be formed in vitro by spontaneous cell fusion [10, 11]. The interest in studying fusion

grew in the next decades mainly because of its importance for production of hybrid cells. In the early 1970's polyethylene glycol was introduced as a fusion agent for plant protoplasts [12, 13] and animal cells [14] (see also the chapter of K. Arnold in this book). In the late 1970's groups from Japan and Germany reported that cell fusion can be also induced by external electric fields (electrofusion) [15–18].

1.3. Electric fields can induce fusion of a wide variety of membranes

During the last decade numerous studies have shown that external electric fields can induce fusion of a wide variety of cell and artificial membranes (for review see [19–23]). This experimental observation is a demonstration of an inherent ability of membranes to fuse if appropriate conditions are provided and indicates the existence of properties of membrane systems, related to fusion, which are largely independent of the type of membranes. These properties include membrane stability and adhesion. Membranes are designed by nature to be stable and resist external constraints. They must be destabilized, i.e. they must be forced to change their structure to molecular conformations appropriate for fusion. The destabilized membranes must be at close apposition to allow merging of their lipid matrix. Therefore, understanding of fusion mechanisms requires understanding mechanisms of membrane destabilization and establishment of contact. External direct current (DC) fields can destabilize membranes and induce formation of pores (electroporation) (for recent review see [23]). External alternating current (AC) fields can induce membrane approach and contact predominantly by a process termed dielectrophoresis [24]. In the following chapter, I will focus on membrane fusion induced by electric fields (electrofusion) but I will also discuss electroporation and dielectrophoresis which are closely related to electrofusion.

I first briefly discuss polarization as one of the basic mechanisms of interactions of membranes with electric fields, leading to electroporation, dielectrophoresis and electrofusion, and then summarize observations on electroporation and dielectrophoresis related to electrofusion. In the rest of the chapter, I focus on observations of electrofusion and on the current concepts of its mechanisms. Why electrofusion may be important for understanding biological fusion is also briefly discussed.

2. Polarization of membranes underlies their destabilization, adhesion and fusion

2.1. Polarization is due to restricted motion of charges

External electric fields can induce formation of pores in membranes, move cells by dielectrophoresis and fuse membranes. All these phenomena are based on the same physical process: the polarization of material in electric fields. The polarization of membranes or any other material results from the fundamental interaction of electric fields with charges. Electric fields exert forces on charges which can either move if they are free to do so or accumulate if they are limited in their motion. The free motion of charges depends on the conductivity of the material while the charge

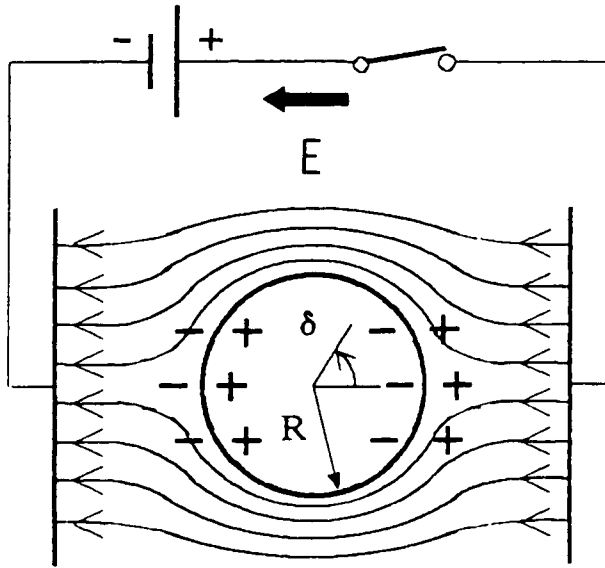


Fig. 1. Membranes restrict motion of charges and lead to cell polarization by external electric fields. The induced transmembrane voltage is maximal at the cell poles and minimal at the equator. Adapted from [37].

redistribution in a limited space is characterized by its polarizability. Figure 1 illustrates schematically how cells can be polarized due to the restricted motion of ions imposed by the plasma membranes.

2.2. Interaction of electric fields with polarized membranes induces mechanical stresses

The interaction of the external electric fields with the polarized material results in forces which can then induce motions inside particles or motion of the particles as whole. The motions inside the material can result in structural rearrangements or even mechanical fracture in the material, which for membranes can subsequently lead to their electroporation and electrofusion. The motion of the particles as a whole can occur even in the absence of a net charge, but only in non-uniform electric fields. It is a consequence of the interaction of the redistributed charges which have zero net charge but locally interact with electric fields of different strength, which leads to a net force exerted on the particle. This phenomenon, termed dielectrophoresis [24], can also occur in homogeneous external fields if there are other particles yielding local non-uniformities of the electric field. This leads to mutual attraction of the particles, to their approach and eventually to adhesion.

2.3. Forces exerted on polarized membranes can induce structural rearrangements, approach of membranes and their fusion

The magnitude and the type of motion depends on the electric field, the nature and geometry of the material. Membranes have low polarizability (relative dielectric constant about 2) and low conductivity (specific membrane conductance about 1 mS/cm^2 , which corresponds to a 'bulk' conductivity of about 1 nS/cm), surrounded by a medium of high dielectric constant (about 80) and high conductivity (about 0.1 S/cm). Application of external fields to membrane systems leads to motion of ions in the medium surrounding the membranes, accumulation of charges at the membrane surfaces and membrane polarization. The charges at the membrane surfaces create electric field inside the membrane which is commonly of much higher strength than the field in the surrounding medium. The electric field inside the membrane interacts with the polarized membrane material which results in intramembrane motions and structural rearrangements. At sufficiently high field strengths these events can lead to formation of pores and discharge of the membrane surfaces by ionic currents through the pores. If another membrane is at close apposition, the molecular rearrangements can also result in fusion by mutual diffusion of the lipid molecules which leads to their intermixing and membrane merging. The molecular contact needed for fusion can be enhanced by the mutual attraction of the two polarized membranes. While this qualitative description of the interactions of membranes with electric fields leading to electroporation, mutual approach and fusion probably reflects basic features of those phenomena, the quantitative modeling and understanding of their molecular mechanisms are very complicated and far from clear. In the next two sections I describe basic experimental approaches and observations, as well as attempts for theoretical modeling of electroporation and dielectrophoresis.

3. High voltage pulses electroporate membranes

3.1. High voltage pulses can permeabilize membranes

In the late 1960's and the early 1970's it was found that application of high voltage direct current (DC) pulses to cell suspensions leads to killing of bacteria and yeasts [25], lysis of erythrocytes and protoplasts [26], release of catecholamines and ATP from chromaffin granules [27] and transcellular ion flow in bacteria [28] (for early electroporation data see [22]). This was originally attributed to electric breakdown of the cell membrane, which implies irreversible rupture of the membrane [26]. Later it was shown that the membrane permeability changes can be transient in nature [27] and that they can be analyzed in terms of reversible dielectric breakdown [29]. The first electroporative gene transfer into living cells with the subsequent actual expression of the foreign gene [30] led to explosive development of the studies on interactions of membranes with high voltage pulses. The term electroporation was introduced by Neumann [30] and presently generally accepted to refer not only to the phenomenon of formation of pores but also to all pore related events caused by exposure of membranes to high field strengths [31]. How actually electropores may look like is shown in fig. 2.

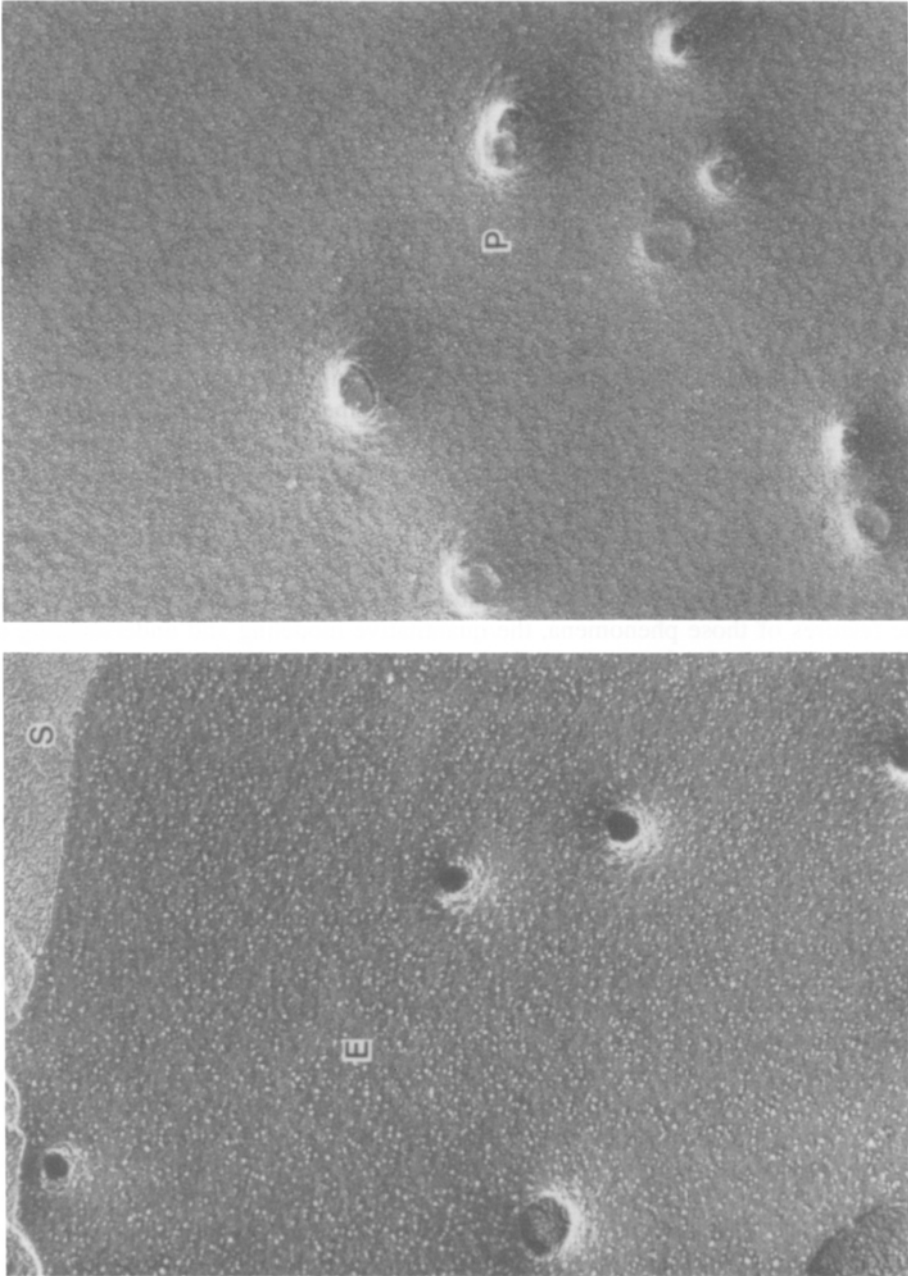


Fig. 2. Left panel: external (E) membrane face of an electroporated human red blood cell frozen at 40 ms after the application of a high voltage pulse. Right panel: protoplasmic (P) membrane face of an electroporated erythrocyte frozen at 220 ms after the pulse. 60,000 \times . Borrowed from [157].

3.2. The devices for electroporation are conceptually simple

One of the reasons for the success of the electroporation as a method of choice for gene transfer and studies of membrane behavior in electric fields is the conceptual simplicity of the experimental devices used to induce electroporation. They consist of two electrodes embedded in the cell suspension (see, e.g., fig. 1, where only one cell is shown). The electrodes are connected to a high voltage pulse generator which allows to control the voltage and duration of the electric pulse. The gene DNA or any other water soluble substance, which should be transferred into cells, is in the medium. The pulse application results in formation of pores in the cell membrane. This leads to exchange of molecules between the medium and the cytoplasm by diffusion, electroosmosis or other mechanisms. The membranes resealed after the pulse and the substance of interest is entrapped inside the cells.

3.3. The transmembrane voltage induced by the external electric fields is accurately described by a simple formula

Presently there are a wide variety of protocols, electrode configurations, media composition and pulse generators which can be used to electroporate a number of cells (for recent review see [23]). Let us consider a membrane which forms a spherical shell as shown in fig. 1. The application of an external electric field leads to currents of ions, which accumulate at the membrane surfaces and give rise to induced surface potentials on both sides of the membrane. This results in creation of a voltage V across the membrane. The basic relationship which is mostly used to estimate this transmembrane voltage induced by a rectangular pulse of field strength E is

$$V = V_m [1 - \exp(-\tau/t_p)], \quad (1)$$

where V_m is the maximal value of the transmembrane voltage, τ is the duration of the pulse and t_p is the characteristic polarization time. For spherical membranes of radius R , V_m and the charging time constant t_p are given by [32, 33]

$$V_m = 1.5ER \cos \delta, \quad (2)$$

$$t_p = RC_m(r_i + 0.5r_0), \quad (3)$$

where δ is the angle between E and the radius vector, see fig. 1, C_m is the membrane capacitance, r_i and r_0 are resistivities inside and outside the cell, and the membrane conductance was neglected (see also [34]). Applicability of eq. (2) to membrane systems was confirmed by using voltage sensitive dyes [35–37], see fig. 3. For the system, used by Kinoshita and his collaborators [37], the radius of the sea urchin eggs is 5×10^{-3} cm, a typical electric field strength E is 100 V/cm, the membrane capacitance C_m is $1 \mu\text{F}/\text{cm}^2$, the resistivity of the Ca^{2+} -free sea water r_0 is 20 ohm-cm, and the intracellular resistivity r_i is 200 ohm-cm. The maximal induced transmembrane voltage V_m as calculated by using eq. (2) is 0.75 V and the charging time t_p

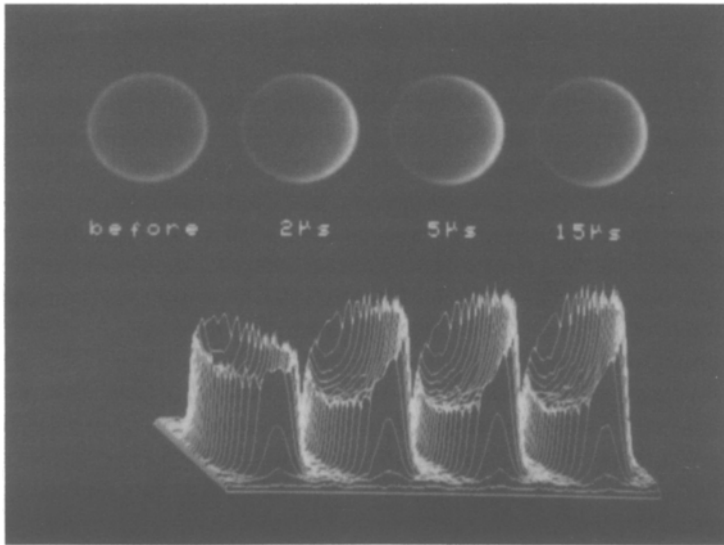


Fig. 3. Induction of surface potential in a sea urchin egg as monitored by a potential sensitive dye. Snapshots were taken with an exposure time of $0.3 \mu\text{s}$ under a pulsed laser fluorescence microscope at the indicated times after the onset of an external electric field of 100 V/cm . Intensity profiles are shown at the bottom. The positive electrode was on the right side of the cell. From [37].

calculated from eq. (3) is $1 \mu\text{s}$. The above values are typical for a wide variety of systems.

3.4. Intramembrane field strength is much higher than the strength of the applied electric field

The above relationships show that the cell radius is very important parameter in electroporation. Since the transmembrane voltage V is proportional to the cell radius, cells of larger radii can be electroporated at smaller strengths E than smaller cells. Another interesting prediction of eq. (2) is that the electric field strength inside the membrane E_m is much stronger than the applied field E . An estimate of E_m ($E_m = V_m/d$, d being membrane thickness) shows that the membrane amplifies the external field by a factor of R/d which can be of the order of 100 or more.

It is also seen from eq. (2) that the induced transmembrane voltage depends on the position along the membrane. At the poles, at $\delta = 0$, the induced voltage is maximal, while at $\delta = 90^\circ$ it is equal to zero. This leads to a variation in the pore size and in the number of pores along the cell surface. Since V_m changes its sign when δ equals $\pi/2$ and $3\pi/2$, see fig. 1 and eq. (2), and the inherent preexisting transmembrane voltage V_i does not, the actual potential which is the sum of both, will be larger on the one half of the spherical membrane than on the other one.

The charging time t_p is another important parameter in electroporation. It increases with an increase in the resistivities and the cell radius. The pulse duration should

be always longer than the charging time in order to get maximal transmembrane voltage.

3.5. Membranes are electroporated when the transmembrane voltage exceeds a threshold value

Electroporation is a threshold phenomenon. Substances can be exchanged through electroporated membranes only if the transmembrane voltage exceeds a certain critical value which for cells is in the range from several hundreds mV to 1–2 V [22, 37–40]. The threshold voltage depends on the pulse duration [39–41]. An increase in the pulse duration needed for electroporation leads to a decrease in the critical voltage (fig. 4a). The pulse duration needed for electroporation at constant transmembrane voltage decreases with an increase in temperature (fig. 4b). The activation energy for the data shown in fig. 4b is 15 kcal/mol. Once the transmembrane voltage reaches its critical value, the poration takes place within microseconds [37, 38, 42]. Longer electric pulses produce larger pores [43]. The fast recovery of cell membranes after poration occurs within milliseconds while the complete recovery may last for seconds, minutes [35, 37, 44] or even hours [45] (fig. 5a). The reseal of electropores in lipid domains also may take seconds [36, 46]. The rate of pore reseal increases with increasing temperature (fig. 5b). The activation energy for the reseal (28 kcal/mol [44]) is somewhat higher than that for the formation of pores. Pulses of very long duration or/and high voltage can lead to irreversible membrane destabilization with subsequent membrane fragmentation. Loading of cells with water soluble molecules vary widely within the cell population (fig. 6), which may indicate variations of membrane properties and/or size between individual cells.

3.6. Transfer of molecules by electroporation is asymmetric

Permeation of ions and fluorescence dyes through the porated membranes have often be found to be asymmetric [47–50]. In some cases, e.g., in sea urchin eggs the dye and Ca^{2+} permeation was much higher on the negative-electrode side, whereas the dye burst was seen mainly on the positive side in liposomes [37]. It was suggested that the inherent physiological potential is added to the induced transmembrane potential and this is the cause of the asymmetric formation of pores [48]. This explanation, however, can not be applied to the sea urchin eggs where the higher potential is on the positive side. The electroosmotic flow can also cause asymmetric transfer of molecules due to the negative surface charge of the plasma membranes [49, 50]. This explains the motion of molecules from the negative toward the positive electrode but can not explain the observations that molecule transfer was observed long after the removal of the electric field. Further studies are needed for elucidation of the mechanisms of the asymmetric electroporation.

3.7. The threshold voltage of electroporation decreases with an increase in intramembrane mechanical stresses (membrane tension)

An interesting observation which can provide clues for the mechanism of electroporation is that the critical voltage needed for poration of cell membranes decreases

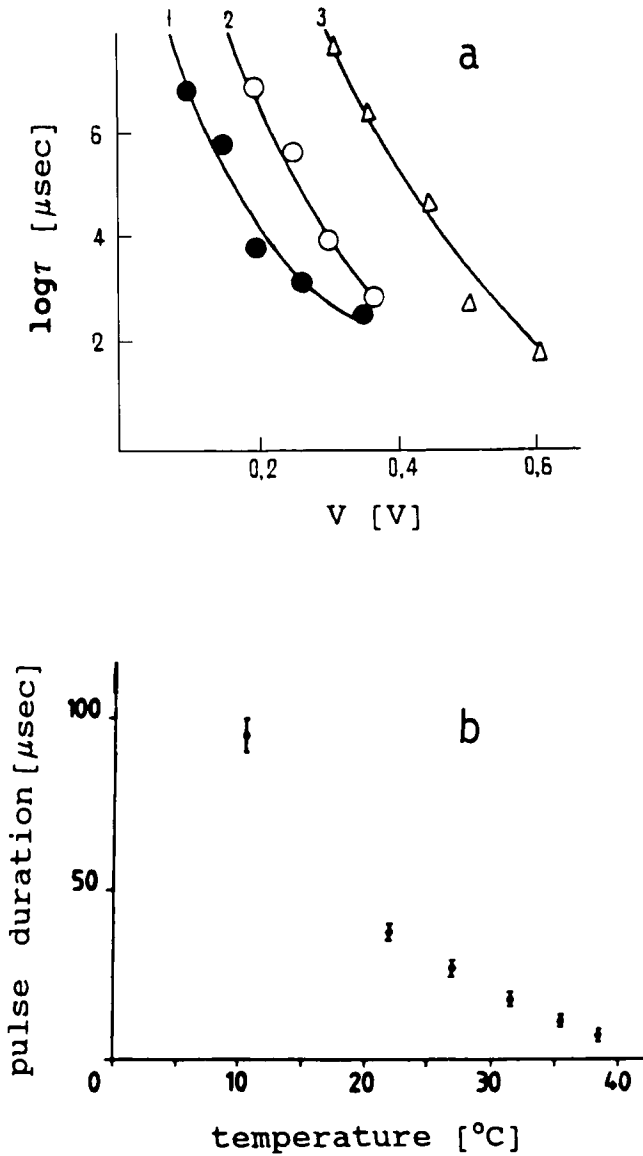


Fig. 4. (a) The duration of the electric pulse τ needed to disrupt lipid bilayer membranes decreases with increasing the transmembrane voltage V . Empty circles indicate bilayers of phosphatidylcholine, solid circles show the data for the same bilayers but in the presence of 4×10^{-4} g/l lysophosphatidylethanolamine, and the empty triangles correspond to bilayers from phosphatidylethanolamine. The continuous lines are a theoretical prediction from an energy-based stochastic approach for electroporation [41]. From [65]. (b) The pulse duration τ needed for electroporation decreases with the increasing temperature T . The transmembrane voltage applied across the pea protoplast membranes was 1.7 V. From [40].

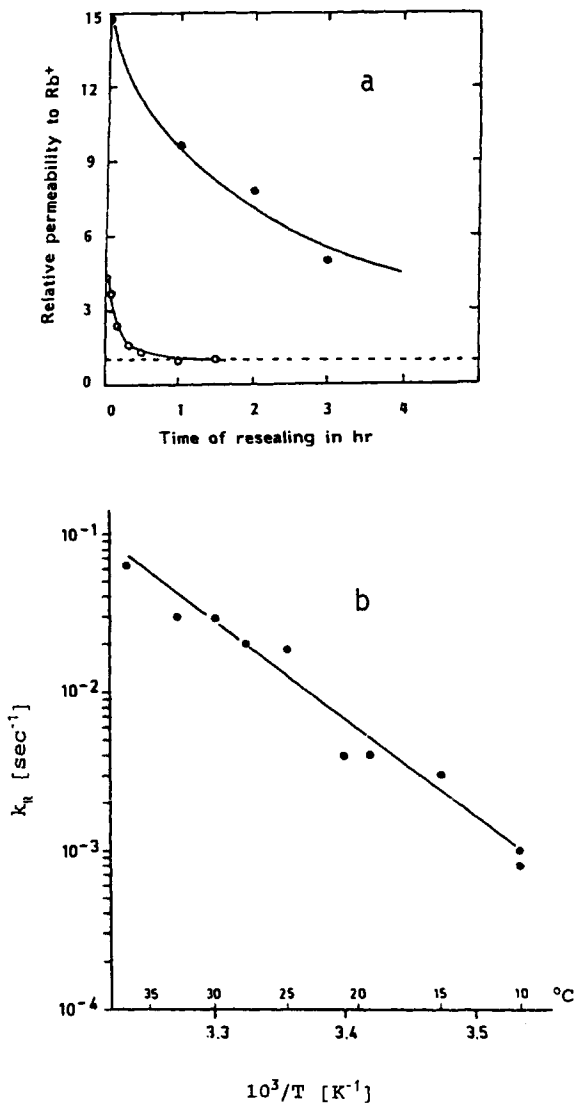


Fig. 5. (a) Restoration of membrane permeability occurs within minutes to hours. (Lower curve) Erythrocytes became leaky to Rb^+ , but not to sucrose, after a treatment with a 4 kV/cm pulse for 2 μs . Restoration of the membrane permeability took more than 30 min. (Upper curve) Red blood cells became transiently permeable to sucrose after treatment with high voltage pulses (3.7 kV/cm) for longer periods of time (20 μs). Restoration of the membrane permeability against Rb^+ took more than 20 hr. From [45]. (b) The rate of pore resealing increases with an increase in temperature. Human erythrocytes were subjected to electrical pulse ($E = 6$ kV/cm, $t = 40$ μs) and their permeabilities were measured at different times after the pulse. Then the rate constants of resealing, k_R , were calculated and plotted as function of the temperature. From the slope of the Arrhenius plot a mean value of 28.1 ± 1.8 kcal/mole was calculated for the activation energy. From [44].

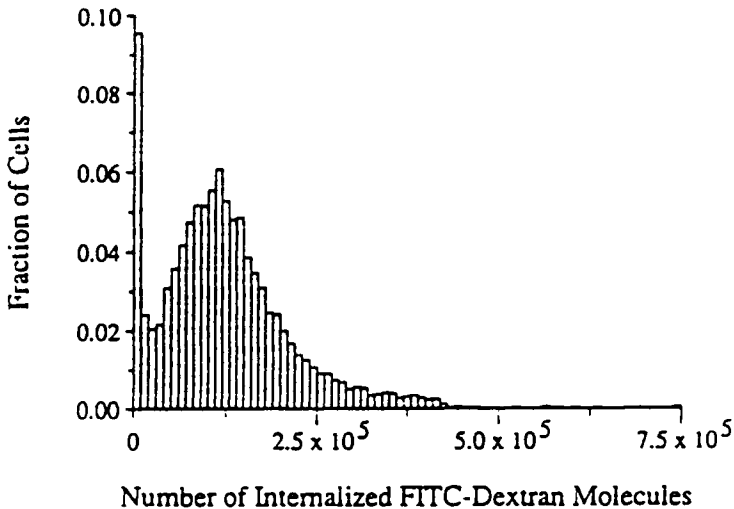


Fig. 6. Population distribution of the number of FITC-dextran molecules taken up by cells subjected to a single $50 \mu\text{s}$ pulse of 8 kV/cm strength. The average of this distribution corresponds to 1.4×10^5 molecules of FITC-dextran. The wide distribution around this mean value is clearly indicated by the graphical display. From [158].

with an increase in the membrane tension controlled by osmotic forces [51, 52]. Needham and Hochmuth [53] developed a new experimental approach based on micropipette technique which allows to set precisely the membrane tension and measure the critical voltage of membrane permeabilization. They found that for lipid vesicles the square of the critical transmembrane voltage is linearly related to the membrane tension (fig. 7). At zero membrane tension, the critical membrane voltage increased from 1.1 to 1.8 V with an increase in cholesterol content. These results indicate that the electric fields induce stresses in the membranes, which are equivalent to stresses induced by external mechanical pressures as those in the micropipettes and that those stresses depend on the lipid composition, especially on the presence of cholesterol. How stresses lead to formation of pores in membranes, however, is a question which remains to be answered.

3.8. *The electromechanical models of electroporation describe membrane rupture as mediated by intramembrane stresses induced by the field*

Two main theoretical approaches were developed to describe electroporation – electromechanical and energetic. They originated from theories in the physics of condensed matter and physical chemistry of thin liquid films. The electromechanical approach considers membranes as elastic [51, 53–55] or viscoelastic bodies [56, 57] and applies the principles of elasticity and of physical chemistry of thin liquid films. The basic conclusion from this approach is the existence of a critical transmembrane voltage above which the membrane is unstable and eventually ruptures. The derived value for the critical voltage is in good agreement with the experimental data.

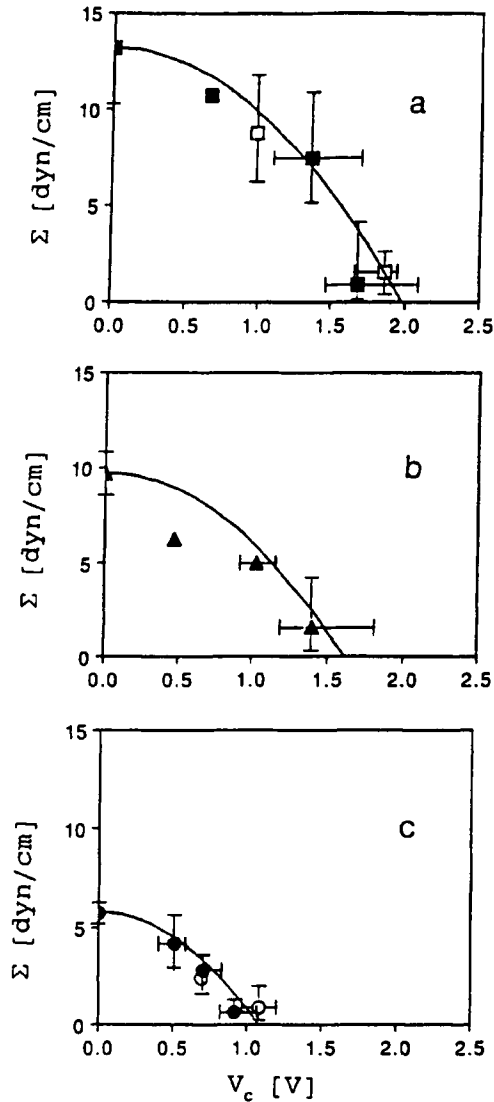


Fig. 7. Critical voltages for membrane permeabilization V_c as function of applied membrane tension Σ . (a) vesicles composed of a mixture of stearylphosphatidylcholine (SOPC) and cholesterol (1 : 1) containing small amounts (5%) of charged lipid, dioleoylphosphatidylglycerol (DOPG), in conducting solutions (10 mM NaCl plus sucrose/glucose) (filled symbols); vesicles from SOPC:cholesterol (1 : 1) in solutions of low conductivity (1 mM NaCl plus glucose) (open symbols), (b) vesicles from erythrocyte lipids in conducting solutions, (c) vesicles from SOPC containing small amounts of DOPG in conductive solutions (filled symbols); vesicles from SOPC in solutions of low conductivity (open symbols). The solid curves are plots of an equation based on the electromechanical model of membrane rupture. From [53].

One problem with the initial development of this approach [51, 54] was that at the critical voltage the membrane thickness should be reduced by about 40%. For an incompressible membrane this implies that the membrane surface area is capable of an extraordinary expansion which is not confirmed by data [53]. Two different solutions to this problem were suggested. In one of them the surface tension of the two surfaces of the membrane was explicitly taken into account [56] and the rupture of the membrane was considered to be due to the instability of thermal fluctuations of the membrane surface shape represented as a superposition of surface waves. This led to the prediction that the average membrane thickness may not be changed significantly but the membrane can be ruptured locally by the growing surface shape instabilities. Another solution of the problem of large membrane thicknesses change was the following. The membrane tension [53] or the mechanical stresses in the membrane [55] induced by the external electric field were calculated and it was postulated that the membrane ruptures at certain critical tension which corresponds to small membrane area changes. This approach does not predict theoretically the critical voltage but rather postulates its existence as an inherent property of the membrane which can be measured accurately. In principle this property could be calculated by using the theories of fracture mechanics or other theories of material failure.

While ingenious and inherently correct the later approach does not allow to theoretically predict the dependence of the critical voltage on the pulse duration. An approach based on the viscoelastic behavior of the membranes was suggested to explain this dependence [56]. According to the viscoelastic model of membrane electroporation, the external electric field leads to growth of unstable undulations of the membrane surface with a rate proportional to the membrane viscosity. The membrane ruptures when the amplitude of the fastest growing perturbation becomes equal to the membrane thickness. The predictions of the viscoelastic model and its generalizations [58] are in good agreement with data for cell membranes [39, 40] and bilayer lipid membranes [41]. The calculated concentration of pores is also close to that observed for erythrocyte membranes by Chang, which is $8/\mu\text{m}^2$ [59]. It must be pointed out that models based on surface shape instabilities could describe only initial stages of pore formation. Whether those pores expand and rupture irreversibly the membranes cannot be predicted by these models, at least at this stage of their development.

3.9. The energy-based approaches describe formation and expansion of pores as overcoming energy barriers

A conceptually different approach for describing the formation and expansion of pores induced by electric fields is based on energy considerations [41, 60–66]. It was assumed that the free energy of the pores is a sum of two components – one is due to the surface energy and the other one is due to the pore edge energy (line tension). While the surface energy component tends to expand the pores, the edge energy component tends to close them. When the pore radius exceeds a critical value equal to the ratio of the surface energy density to the pore edge energy, the pore expands spontaneously until the membrane ruptures. Pores with radii smaller than the critical one have to overcome an energy barrier in order to increase their

radii above the critical one. This takes time which is inversely proportional to the Boltzmann's factor $\exp(-E_a/kT)$, where E_a is the height of the energy barrier, k is Boltzmann's constant and T is the absolute temperature. The application of external electric fields leads to a decrease in the pore energy due to the polarization of water in the pore which is higher than that of the membrane material. This decreases the energy barrier with a factor which is proportional to the square of the transmembrane voltage. The decrease of the energy barrier leads to shorter periods of time needed to overcome that barrier and reach the critical pore radius. The stochastic mechanism of pore expansion by overcoming energy barriers can describe a number of experimental data for bilayer lipid membranes (for review see [64–66]). However, like the electromechanical model it is phenomenological and does not allow to distinguish between hydrophobic and hydrophilic pores or other structures. It is assumed that the pores allowing transfer of molecules are hydrophilic pores, which originate from hydrophobic pores. The details of the mechanism of conversion to hydrophilic pores is unknown.

It seems reasonable to assume that the formation of hydrophilic pores results from the growth of unstable shape undulations of the membrane surfaces and partially by conversion of hydrophobic pores. The creation of pores by the electric field does not preclude the possibility that preexisting pores can serve as 'nucleation' sites for formation of larger pores [67]. The relative contribution of each of these two mechanisms of initial formation of pores depends on the phase state of the membranes and the pulse strength.

Several other approaches for describing the formation of pores and the kinetics of electroporation were suggested [34, 62, 63, 68]. While some of these models suggest plausible molecular rearrangements during electroporation, rigorous experimental prove is lacking.

The above considerations mainly apply to the formation and expansion of pores in lipid membranes. This does not exclude the possibility for pore formation through integral proteins or at the lipid-protein interface [44, 68] (fig. 8). How actually the pores are formed is not clear yet.

4. Mutual attraction and adhesion of the cells in AC fields is due to dielectrophoresis

4.1. Formation of 'pearl chains' of cells in AC fields is due to dielectrophoresis

Nearly one century ago, Kerr observed electric field-mediated formation of 'pearl chains' linking many suspended particles (mentioned by O'Konski [69]). Liebensy observed the same phenomenon with erythrocytes [70]. Figure 9 shows an example of aligned cells in electric fields. Pearl chain formation can be considered as a special case of the movement of particles in non-homogeneous fields because one particle distorts the field acting on the other and vice versa. Movement of cells will take place if the gradient of the square of the electric field strength does not vanish (fig. 10) and if the force is strong enough to overcome the thermal motion. The motion of particles in non-homogeneous fields was termed dielectrophoresis [24]. Krasny-Ergen [71] applied the principal of minimal potential energy to study theoretically

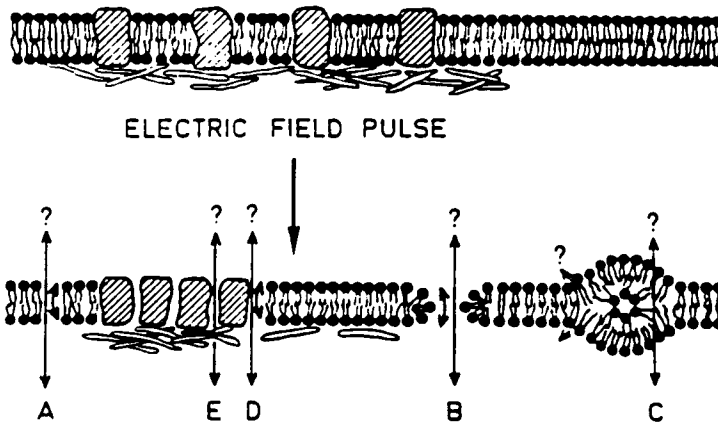


Fig. 8. Schematic view of the various types of membrane alterations and defects following electroporation. The scheme illustrates the concept that the field pulse might perturb integral and/or peripheral (membrane skeletal) proteins and thereby affect the organization of the lipid domains. Leakes (⊓) and flip sites (⊔) could be located in (A) hydrophobic pores, (B) hydrophilic pores, (C) nonlamellar phases, or (D) areas of a mismatch between lipid and integral proteins. Leaks could also be formed between aggregated proteins (E). From [44].

the pearl chain formation. Later this effect was investigated thoroughly by Schwan and coworkers [72, 73] and Pohl [24].

4.2. *The dielectrophoretic force exerted on individual cells can be accurately measured*

The dielectrophoretic force F acting on a spherical particle of radius R in an inhomogeneous field of strength E can be represented as

$$\vec{F} = 2\pi R^3 \varepsilon_0 K_e \nabla E^2 \quad (4)$$

where ε_0 is the permittivity of free space and K_e is an effective net polarizability of the cell.

The cell polarizability K_e was measured for a wide variety of cells by using several different approaches [24, 74–77]. The dynamic method for measuring K_e is based on measuring the rate of motion of single cells in a cylindrically symmetrical system and calculating the force F by using the Stokes formula [74, 78]. The basic advantage of this method is that it allows accurate measurement of K_e for individual cells. It was found that K_e depends on the solution conductivity [24, 79], the frequency of the electric field [24, 77, 80], calcium ions [79], the type of cells [24, 76, 77] and surface charge [81]. A typical value for pea protoplasts (radius 15 μm) at solution conductivity 0.47 mS/m and frequency 1 MHz is $K_e = 110$. One of the basic conclusions is that in the radio frequency range most of the living cells behave as highly conductive spheres and the dielectrophoretic force can be

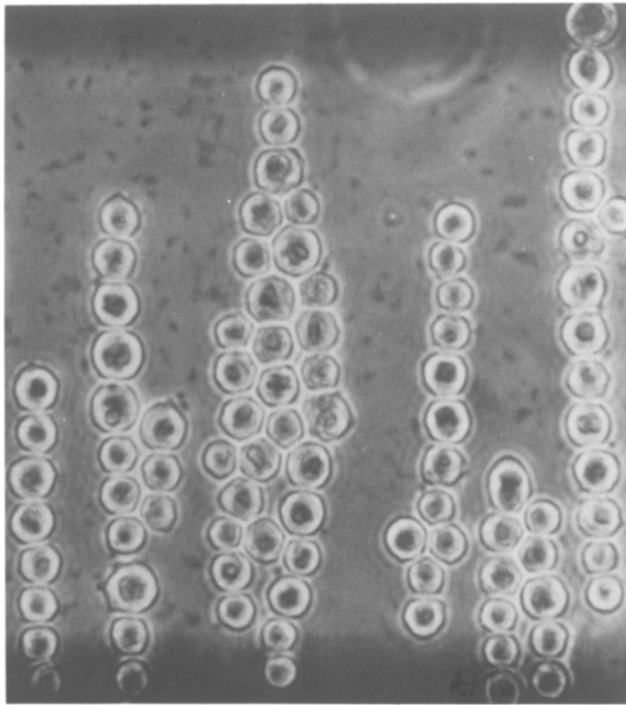


Fig. 9. Formation of pearl chains by dielectrophoresis of mouse leukemic lymphoblasts as observed by phase contrast. The applied AC field was of 0.8 kV/cm strength and 100 kHz frequency. From [117].

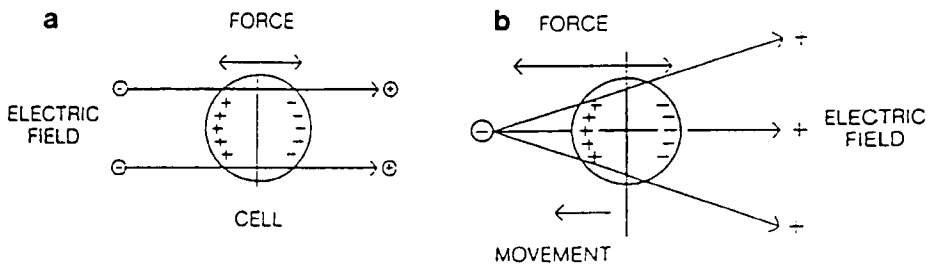


Fig. 10. Charge separation and force on a cell in (a) a homogeneous and (b) an inhomogeneous electric field. From [159].

estimated by assuming that the cell polarizability K_e is of the order of the relative permittivity of the surrounding medium (for water solutions of the order of 10 to 100).

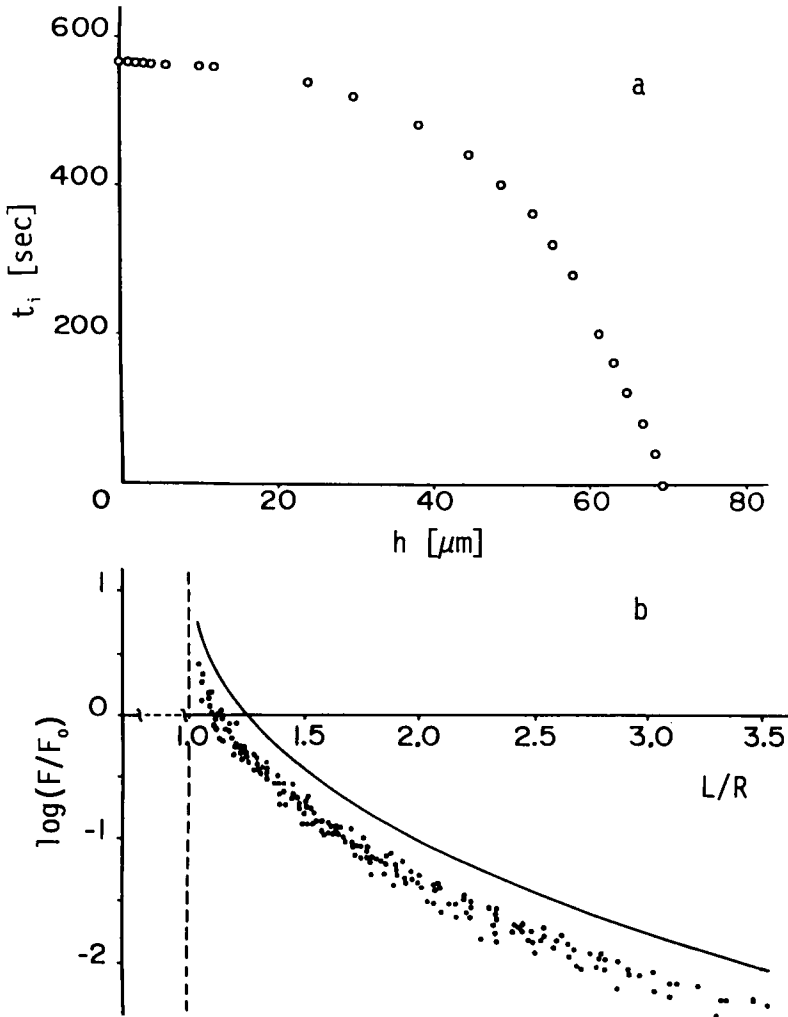


Fig. 11. (a) Dependence of the intermembrane separation h on time $t_i = t_c - t$ during mutual dielectrophoresis of cells, t_c is the time required to make contact ($t = t_c$ at $h = 0$); (b) Force F of mutual attraction as a function of the dimensionless separation $L/R = 1 + h/2R$ calculated from the experimental data in the range of 1 to 10 MHz (points) and theoretical prediction for highly conductive spheres (continuous line). $F_0 = \epsilon_0 \epsilon_r E^2 R^2$, ϵ_r is the relative permittivity. From [82].

4.3. *The intercellular attraction force increases with decreasing the intermembrane separation and is proportional to the square of the field intensity*

Similar considerations are valid for the interaction of two cells in AC fields. The interaction force in the radio frequency range can be estimated by assuming that the cells behave as highly conductive spheres. The calculations are, however, very com-

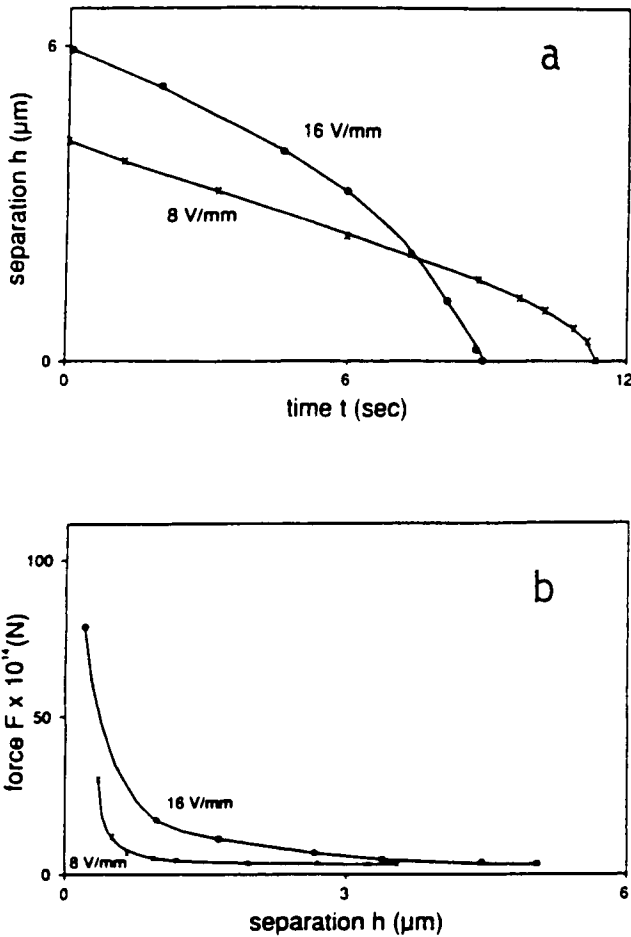


Fig. 12. (a) Dependence of separation h on time t for erythrocyte ghosts in 60 Hz AC fields for two different field strengths, 8 V/mm and 16 V/mm; (b) Calculated force of attraction F as function of separation. From [83].

plicated and can be evaluated only numerically [82]. Their evaluation showed very good agreement with the experimental data [82] (fig. 11). The data for the force of attraction in the low frequency (60 Hz) [83] and the radio-frequency (0.1–10 MHz) range [82] was obtained from the measured rates of approach of the cells. It was found that i) the force of mutual attraction increases strongly with decreasing the separation distance, ii) the membranes deform at close apposition to form almost plane-parallel surfaces, and iii) the force of attraction is proportional to the square of the electric field strength (fig. 12).

4.4. *The attraction of cells induced by AC fields can affect fusion efficiency*

The equilibrium separation between the membranes is determined by the balance of the dielectrophoretic force and the repulsive intermembrane forces (hydration, electrostatic, steric). Therefore any increase in the AC field strength leads to a decrease in the intermembrane separation. Another important parameter is the contact area between the membranes. Any increase in the contact area leads to a higher probability of fusion. The increase in the force of attraction induced by the external AC field results in an increase of the contact area and the membrane tension. Therefore, increasing the intensity of the AC fields can enhance fusion by increasing the probability for fusion. Very high AC field strengths, however, may result in heat generation and turbulent flows, which decrease the fusion efficiency. Hence, an optimal AC field strength exists at which the fusion efficiency is maximal.

After removing the AC field, the cells commonly separate, driven by Brownian motion. This indicates that AC fields lead to reversible cell aggregation and are not sufficient to overcome the energy barriers preventing adhesion and fusion of membranes. In several instances, however, it was observed that AC fields can induce permanent adhesion of red blood cells [74, 78, 84]. This was originally attributed to fusion, but later was found to be tight adhesion or in the best case probably semi-fusion. Therefore, electric fields of higher intensity should be applied to induce real fusion. They should, however, be applied for short periods of time to avoid heat generation and turbulent flows, which can disrupt the cell aggregates. How membranes can be fused by such high voltage pulses is discussed next.

5. **Electroporative pulses induce fusion of adhered membranes**

5.1. *Electrofusion is induced at the same threshold voltages as electroporation*

In 1979 Senda et al. published a paper describing an interesting observation [15]. When an electric field was applied by microelectrodes to two plant protoplasts, brought at close contact by using a micromanipulator, the cells underwent morphological changes until they formed a single fusion product as observed by light microscopy. At about the same time three other research groups fused cells by high voltage electric pulses but using different approaches to bring the cells at close contact. The Berg's group used polyethylene glycol (PEG) to aggregate cells and then stimulated yeast protoplast fusion by electric field [17]. The evidence for fusion was genetic because the pulses led to formation of viable hybrids which grew on minimal media to form prototrophic colonies. Neumann et al. [16] achieved cell agglutination by rolling the cell suspension in plastic tubes, while Zimmermann and Scheurich [18] used AC fields to bring plant protoplasts at close approach by dielectrophoresis. Figure 13 shows an example of electrofusion as observed by a fluorescent dye redistribution assay [85].

The common and striking feature of these observations of electrofusion was that the magnitude of the transmembrane voltage needed for fusion was about the same (of the order of 1 V) as that for electroporation, while electrofusion was insensitive

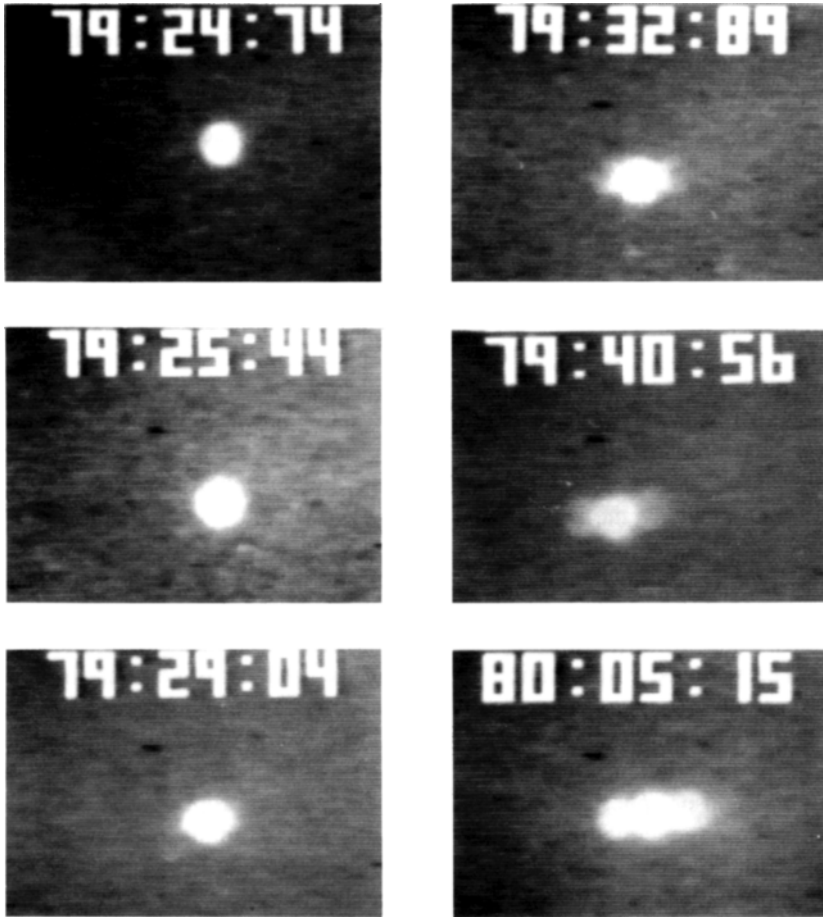


Fig. 13. Electrofusion of erythrocyte ghosts as demonstrated by a fluorescence dye redistribution assay [85]. One cell, originally labeled with DiI, is surrounded by two originally unlabeled cells which are not visible under fluorescence. The labeled cell does not show any indication of dye transfer before the pulse (79 : 24 : 74). The high-voltage electric pulse (strength 0.3 kV/mm, duration 0.9 ms) is applied at 79 : 25 : 44. The first appearance of fluorescence as small 'horns' on the originally unlabeled cells can be seen about 4 sec later (at 79 : 29 : 04). The horns increase in length (79 : 32 : 89) until reaching the end of the originally unlabeled membranes (79 : 40 : 56) and the state of uniform fluorescence brightness at 80 : 05 : 15. The width of the alphanumeric is 50 μm . From [85].

to the way the cells were brought into contact. Later it was demonstrated that not only the absolute value of the transmembrane voltage correlates with that needed for electroporation, but also the entire functional dependence of the pulse voltage on its duration is the same (fig. 14) [40]. These observations led to conclusions important both for the design of protocols for efficient fusion and for understanding its mechanisms.

5.2. *Devices for electrofusion are very similar to those for electroporation*

Since electrofusion is so similar to electroporation with respect to the characteristics of the electric pulses, the devices used for electrofusion are very similar to those used for electroporation. The main difference is in the way the cells are brought at close contact. A wide variety of approaches has been used to induce cell contact, including mechanical by utilizing micromanipulators and centrifugation; chemical, by utilizing PEG and other agglutinating substances, and electric, by using AC fields. The cells can also make contact spontaneously or the contact can be achieved by increasing the cell concentration. One of the most used and convenient way to induce cell adhesion is by dielectrophoresis [24, 86]. In the rest of this chapter I discuss predominantly electrofusion of cells brought at close approach by dielectrophoresis not only because it is widely used but also because it allows fine regulation of the separation between membranes.

An electrofusion device consists of a generator and a chamber. The generator typically has three main components: 1) high voltage generator for DC pulses of short duration, 2) AC generator for inducing dielectrophoresis, and 3) electronic switch which switches the DC and AC fields. The DC pulses can be either exponentially decaying, squared or radio frequency modulated. The AC field is commonly in the MHz range, but low frequency electric fields (60 Hz) were also used. The generator output is connected to the working chamber which has two electrodes, commonly made from platinum. The size and configuration of the electrodes vary widely. The simplest configuration consists of two plane-parallel electrodes embedded in the cell suspension. In this case the cell concentration should be relatively high. The separation between the cells should be of the order of their diameters or less to allow for efficient mutual dielectrophoresis to occur. For diluted cell suspensions cylindrical or spherical electrodes may be more appropriate. Those electrodes create non-homogeneous fields which move the cells leading to an increase of the cell concentration near the electrodes (if the dielectrophoresis is positive which is the common case for biological cells). Excellent reviews for different electrode configurations and generators can be found in the book of Chang et al. [23].

5.3. *Long-lived fusogenic states exist after membrane electroporation*

The classic protocol for inducing fusion is to bring the cells at close approach (e.g., by dielectrophoresis) first and then to apply the high voltage DC pulse. It was, however, occasionally observed that cells still can be fused if the pulse is applied first and then the cells are brought at contact [87, 88]. In 1986 Sowers' and Teissie's groups studied thoroughly this phenomenon and found that erythrocyte ghosts [89] and Chinese hamster ovary cells [90] can be fused by the pulse-first protocol. The efficiency of fusion is, however, somewhat lower than that for the contact-first protocol [91] and multiple pulses must be applied [92]. These observations led to the concept of existence of long-lived fusogenic states [89] or transient permeant structures [90]. The life-time of these states is in the range of seconds to minutes and therefore pores surrounded solely by lipid molecules in liquid-crystalline state are unlikely candidates for such states because their life-time is much shorter. In cell membranes, however,

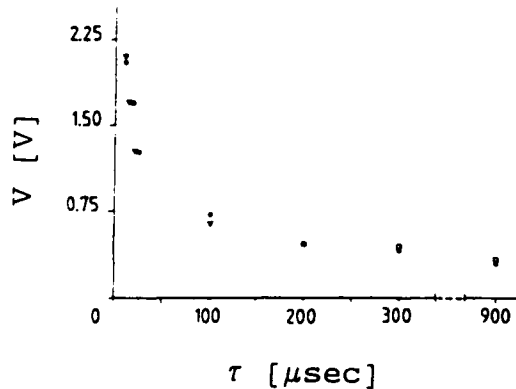


Fig. 14. Correlation between the threshold transmembrane voltage V of electrofusion (triangles), of electroporation (circles) and of cell destruction (squares) as function of the pulse duration τ . The square of the threshold voltage is inversely proportional to the pulse duration in agreement with the fluctuation wave mechanism of electroporation. From [40].

proteins could be involved or lipid domains in solid state or both. In support of this hypothesis are the observations that the long-lived fusogenic state is laterally immobile within the time scale of the experiments which is of the order of minutes [90, 92]. A ^{31}NMR study of the membrane phospholipid organization in Chinese hamster ovary cells following electroporation suggests that the organization of the polar heads is altered [93]. This can lead to an increase in the surface hydrophobicity, which was observed experimentally for plant protoplasts [94]. The increase in the surface hydrophobicity can result in a decrease of the repulsive hydration forces, enhanced membrane contact and fusion [95, 96].

5.4. Fusion is localized and results in formation of intracellular vesicles

While the nature of the long-lived fusogenic state remains unclear, morphological and kinetic studies revealed other important characteristics of the electrofusion process. It was frequently observed that fusion of large cells was accompanied by formation of intracellular vesicles [97]. Probably intracellular vesicles are also formed during fusion of smaller cells but the limit of resolution of the light microscopy does not allow to identify them when their diameters is smaller than $0.2\text{--}1\ \mu\text{m}$. Electron microscopy studies provided further evidence that fusion is initiated locally [98, 99] and involves small areas (probably nm or tens of nms). The initial fusion sites then can expand resulting in formation of intracellular vesicles or other structures with a characteristic periodic pattern [100] (fig. 15). This led to the proposition of an ultrastructural model of electrofusion by Stenger and Hui [98] (fig. 16). According to this model, the membranes are at close apposition (about 15 nm) before the pulse application. The DC pulse leads to their local destabilization. The destabilized areas make local contact and fuse. It is interesting to note that periodic structures leading to local contacts were observed when erythrocytes were adhered by polyionic

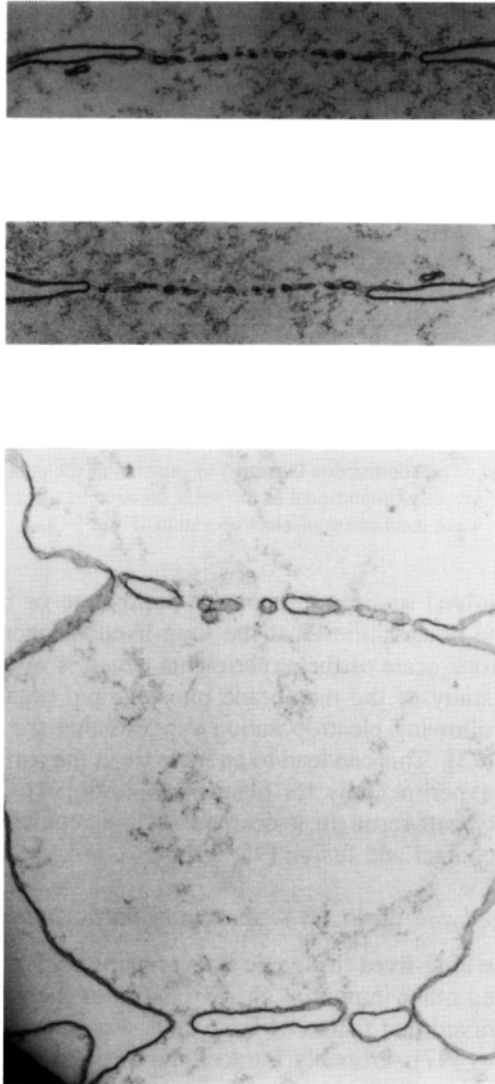


Fig. 15. Formation of intracellular vesicles after electrofusion of erythrocyte ghosts induced with a single pulse ($E = 0.4$ kV/cm, decay half-time = 1.2 ms) as revealed by thin section electron microscopy. Left panel: two stable diaphragm fusion zones shared between three erythrocyte ghosts in a pearl chain (oriented left-right); Middle and right panels: two other representative examples of stable planar diaphragm fusion zones indicating periodicity and heterogeneity in fusion pore diameters. From [100].

macromolecules [101, 102]. Therefore one might speculate that local contacts are due not only to the existence of local perturbation (destabilization) of the membranes but they can arise during the subsequent approach of the membranes. A mechanism based on the instability and growth of membrane undulations, represented as a superposition

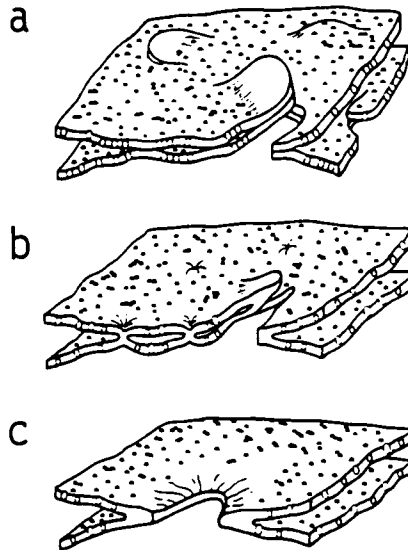


Fig. 16. An ultrastructural model of electrofusion. (a) Within 100 ms of pulse application, the aqueous layer between the membranes is perturbed and localized membrane contacts are formed. The membranes are also perturbed. (b) By about 2 sec membrane continuity is established. (c) Within 10 sec following pulse application, permanent lumina are formed. From [98].

of waves, was suggested to explain these and other observations [57, 103]. This mechanism is discussed in more details later.

It should also be noted that the observation of intracellular vesicles following fusion suggests an explanation how the excess membrane is removed after fusion if the total volume of the fused cells is kept constant. Probably fusion initiates at different points in the intermembrane contact area including its perimeter. The expansion of the locally fused membranes then leads to formation of vesicles inside the cell which removes the constraint imposed by the incompressibility of the membranes.

5.5. *The cell cytoskeleton is reorganized during electrofusion*

One might think that not only the incompressibility of the membranes but also the intracellular filamentous proteins, known as cytoskeleton, can impose constraints impeding the morphological changes leading to rounding of the cells and formation of single fusion products consisting of two or more cells. By utilizing immunofluorescence microscopy it was shown that in Chinese hamster ovary cells the microfilaments were not affected by the DC pulses, but the microtubules disappeared during the first minutes after the pulse and then reformed during the subsequent incubation [104]. In another type of cells (CV-1), however, all three components of the cytoskeleton, microtubules, microfilaments and intermediate filaments underwent significant reorganization during electrofusion [105]. The microtubules played an active role in the nuclear movement during cell fusion [105] (fig. 17). Another

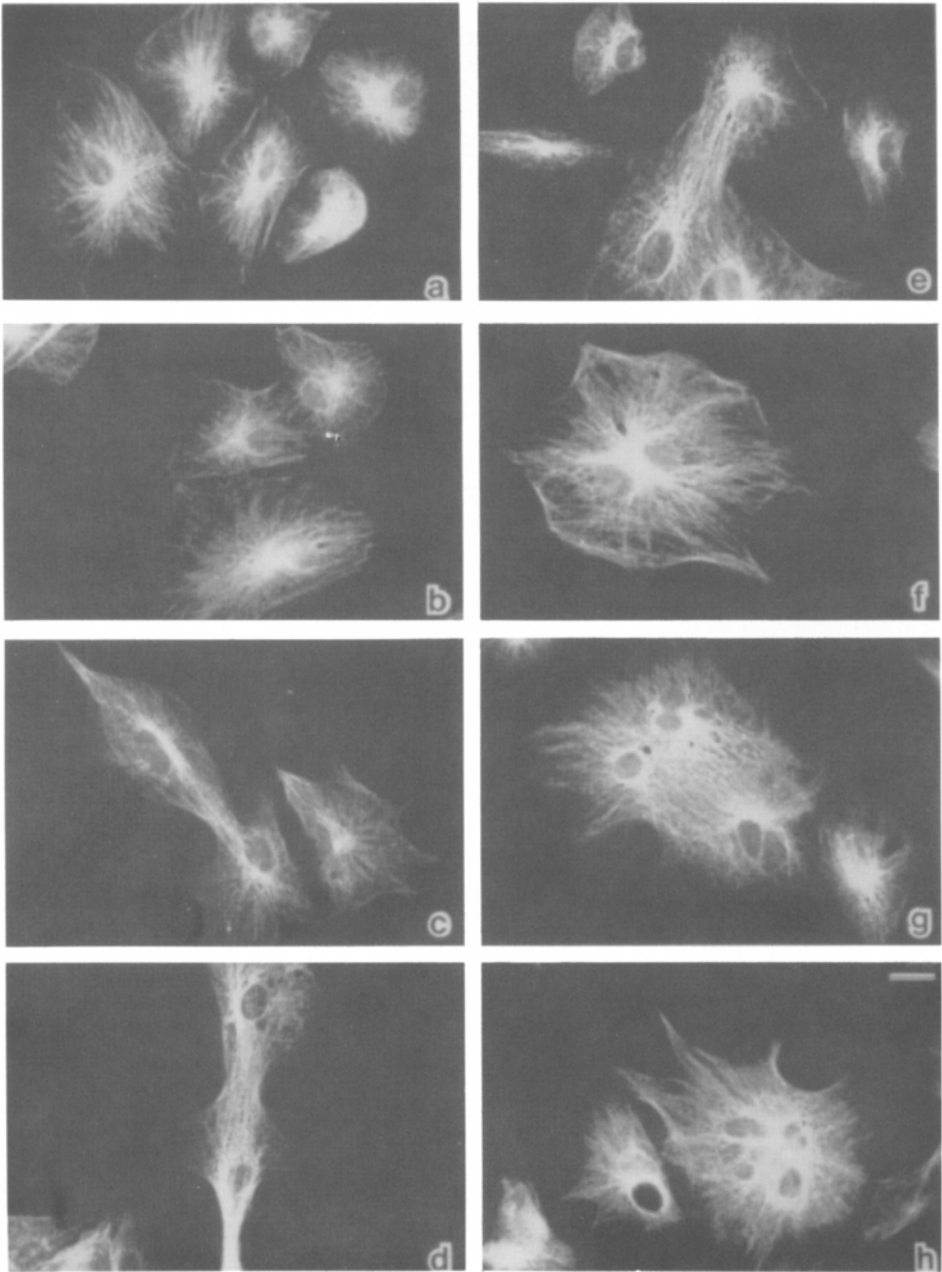


Fig. 17. Distribution of microtubules in cells at various stages of electrofusion. (a) Before electric treatment, (b) after 5 min, (c) 15 min, (d,e) 30 min, (f) 2 h, (g,h) 3 h. Scale bar = 25 μm . From [105].

observation supports the notion for the role of the cytoskeleton in fusion and raises the question for the limits of light microscopy in detection of fusion. I found that while at room temperature fusion of erythrocyte ghosts, as indicated by a fluorescent dye redistribution assay, commonly does not lead to rounding of the fused cells and formation of giant cells, the exposure of the ghosts at 37°C and higher temperatures leads to formation of significant number of giant cells (unpublished). A more extensive study [100] indicated that the disruption of the spectrin network, which can be considered as a rudimentary cytoskeleton, leads to formation of giant cells. The occurrence of fusion and lack of morphological changes observable under the light microscope for erythrocyte ghosts with intact spectrin network shows that in many cases fusion may not be detected by utilizing only light microscopy. Whether cytoskeleton affects the very act of membrane fusion remains to be elucidated.

5.6. Assays based on fluorescence dyes allow accurate measurement of fusion kinetics

The development of fusion assays based on fluorescence dyes provided more accurate monitoring of fusion than the light microscopy and led to the possibility to measure the kinetics of membrane electrofusion in real time. There are two different approaches utilizing fluorescent dyes. The first one is based on the redistribution of the dye from a labeled membrane to an originally unlabeled membrane observed by fluorescence microscopy. The second one relies on formation of fluorescence complexes upon mixing of the fusing membranes. The dye redistribution assay was used both with membrane soluble (commonly DiI) and water soluble (commonly FITC-dextran) dyes [85, 87], while the fluorescent complex formation assay was used utilizing the water soluble terbium (Tb) ions and dipicolinic acid (DPA) which upon mixing form the fluorescent Tb-DPA complex [99, 106]. The Tb/DPA assay allows continuous monitoring of fusion in cell suspensions by a spectrofluorometer, while the dye redistribution assay monitors fusion of single cells. By combining the dye redistribution assay with a videomicroscope the spatial and temporal development of the fluorescence in the originally unlabeled cells can be precisely monitored. This allowed to find and extensively characterized the lag times (delays) following the application of the fusogenic pulse. Because the delays are an important source of information about the life-time of intermediates in fusion leading to understanding its kinetic mechanisms I next discuss delays in fusion in more details.

5.7. Fusion occurs after a lag time (delay) following the application of the fusogenic trigger

The delay is the time period between the triggering of fusion and the membrane coalescence [107]. From an experimental point of view the delay is the lag time between the application of the trigger of fusion and the first indication of fusion. Measuring delays requires answering several questions. When is exactly the trigger applied? What is the response time of the measuring system? What is the minimal increase in the signal which should be assumed as an indication of fusion? In electrofusion the moment of trigger application can be precisely located in time. The

time resolution of videomicroscopy systems is of the order of tens of milliseconds. For assays based on fluorescent dyes redistribution the first indication of fusion is the increase in the fluorescence in the originally unlabeled membrane near the membrane contact due to the diffusion of the dye. This time is also of the order of tens of milliseconds. Therefore, delays in electrofusion can be measured by assays, based on fluorescent dyes redistribution monitored by videomicroscopy, with an accuracy of the order of tens of milliseconds.

Delays in fusion vary widely for different systems. They can be less than 5 ms for the neurotransmitter release [108] or minutes and hours for cell fusion induced by the HIV-1 envelope proteins [109–112]. For planar-planar bilayer fusion [113] the lifetimes of the events leading to fusion ('waiting time' for fusion) are in the range of seconds to minutes. Even for the same system, but for different experimental conditions, the delays can vary by orders of magnitude. For instance, delays in viral fusion are in the range of milliseconds to minutes [114–116].

5.8. Delays in electrofusion decrease with an increase in the field strength and are proportional to the solution viscosity

A systematic study of delays in electrofusion of erythrocyte ghosts [85] showed that they decreased from 4 to 0.3 s with an increase in (i) the pulse strength from 0.25 to 1 kV/mm (fig. 18a), (ii) the pulse duration in the range 0.073–1.8 ms, and (iii) the dielectrophoretic force which brings the membranes at close apposition before triggering fusion. They increased proportionally to the increase in the solution viscosity (fig. 18b). The delays decreased 2–3 times with an increase in temperature from 21 to 37°C. The Arrhenius plot yielded straight lines. The calculated activation energy, 17 kcal/mol, does not depend on the pulse strength [85] and is similar to that found for the fusion yield of mouse lymphoma cells [117] and electroporation [40].

The data for delays in electrofusion of erythrocyte ghosts [85] can be described by an empirical formula [107]

$$\text{Delay} = C\mu \exp(E_a/R_gT), \quad (5)$$

where C is a constant which does not depend on the activation energy E_a and the solution viscosity μ , R_g is the gas constant and T the absolute temperature. The constant C is inversely proportional to the driving force of the fusion reaction and proportional to the system resistance to fusion. Therefore, it depends on all the factors which determine the driving force and the fusion resistance. The activation energy does not depend on the strength of the fusogen. Typical values of C are in the range 10–1000 Pa⁻¹ and of the activation energy E_a is 10–30 kcal/mol. A more refined theoretical analysis of the delays in fusion is presented elsewhere [118].

5.9. Rates of fusion can provide information for the time course of membrane merging and fusion pore expansion

While the delays reflect the life-time of the intermediates before the actual intermixing of the membrane components, the rates of fusion provide information for the

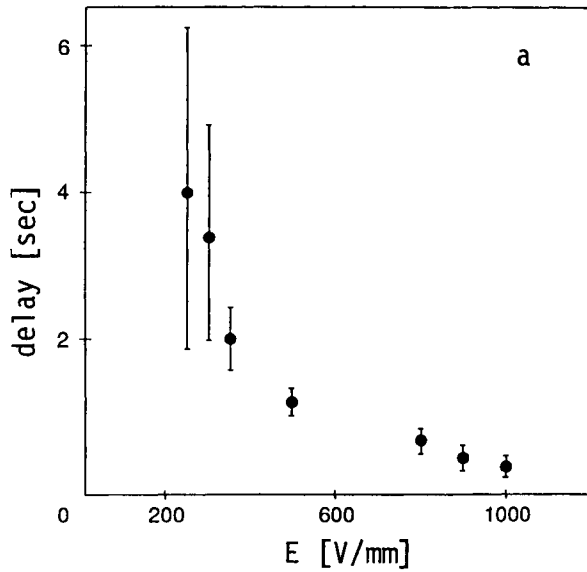


Fig. 18(a). The delay in electrofusion of erythrocyte ghosts decreases with increasing the pulse strength. From [85].

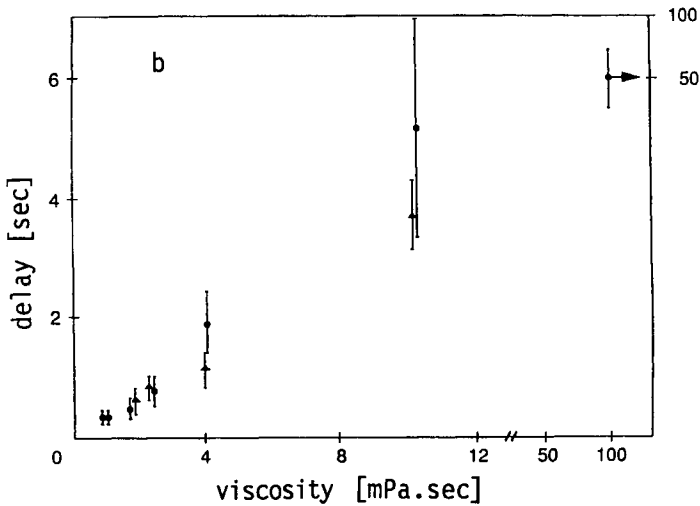


Fig. 18(b). The delay in electrofusion is proportional to the solution viscosity. From [85].

subsequent stages of the fusion process. Rates of fusion are commonly measured by taking the derivatives of the fluorescence changes with respect to time. For indi-

vidual cells they reflect the rate of diffusion of the dye through the intermembrane junction after membrane merging. There are two limiting cases: 1) the dye transfer through the intermembrane junction is fast compared to the lateral diffusion in the originally unlabeled membrane and 2) the transfer through the intermembrane junction is slower than the diffusion.

In the first case the rate of dye transfer is entirely determined by the diffusion coefficient of the dye in the originally unlabeled membrane and the membrane geometry. This is the case, e.g., shown in fig. 19, borrowed from the study of electrofusion of erythrocyte ghosts (see also fig. 13) [85]. The plot of the square of the distance between the diffusion front and the membrane contact zone versus time is linear. The slope gives $4D$, D being the diffusion coefficient, which for this particular case is equal to $0.55 \times 10^{-8} \text{ cm}^2/\text{s}$. This is one method of measuring the lateral diffusion of fluorescent dyes. Therefore in this case the increase in fluorescence in the initial stage of the membrane transfer is not a measure of rate of fusion. It only shows that the rate of dye transfer through intermembrane junctions is faster than the rate of diffusion. After the diffusion front reaches the far end of the cell, the fluorescence intensity continues to increase until reaching the final equilibrium state. This stage also depends on the diffusion. The case of fast dye transfer through intermembrane junctions occurs when the total length of membrane contact by junctions is larger than the contact perimeter. For example, if the intermembrane

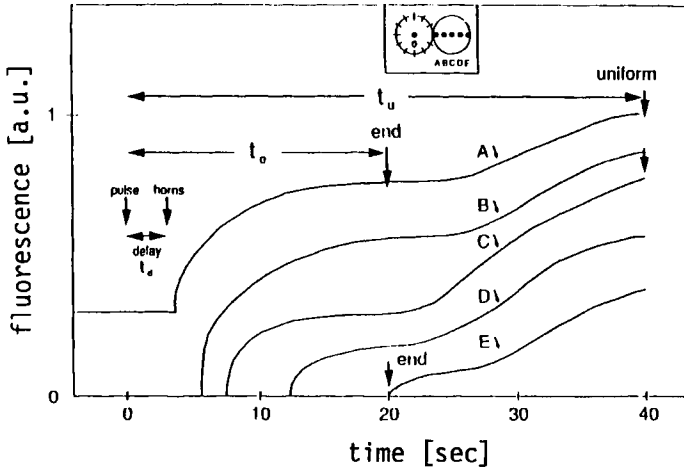


Fig. 19. An example of kinetics of dye redistribution to an originally unlabeled membrane following application of a high voltage pulse. The space locations of the points of measurement are shown in the inset. The distances from the contact with the labeled membrane are (in μm) A, 0 (the contact); B, 1.7; C, 3.3 (the center of the erythrocyte ghost); D, 5; and E, 6.6 (the far end of the membrane). The fluorescence intensity is normalized to that at the center of the labeled membrane (point O in the inset). The fluorescence intensity at the membrane contact (point A in the inset) is higher than zero even before the pulse because of the close proximity of the labeled membrane. The increase in fluorescence begins after a delay at a point in time that coincides with a characteristic appearance of the fluorescence as 'horns' (see fig. 13). The dye diffuses until reaching the far ends of the membranes (after time t_e) and an almost uniform redistribution (after time t_u). From [85].

junctions are channels, fast dye transfer occurs when the product of the number of channels and their average perimeter is larger than the perimeter of the membrane contact.

When the rate of dye transfer through the fusion junction is lower than the diffusion rate, the increase of fluorescence is uniform. It depends only on the time and the properties of the fusion junctions. The rate of increase reflects the number and size of the fusion junctions and their change with time. When the number and size of the fusion junctions are constant, the fluorescence increase should be linear with time in the beginning of the dye transfer. Any differences from the linear relationship could be attributed to changes of the size and number of the fusion junctions, including creation of new or closing of 'old' junctions. Therefore, fluorescence changes after delays may contain important information about intermediates in fusion and their evolution with time. Unfortunately, this important process has not been quantitated yet.

For a population of cells, the rate of fusion can be defined in at least two ways. Either it is the number of cells fused per unit time or it is the total fluorescence change per unit time. In the first case fusion rates can be measured simply by counting the number of cells fused as a function of time. Evidently, in this case the rate of fusion is given by the individual differences in the lag times (delays). It will be equal to the number of fused cells which have delays within a time interval divided by that time interval.

The spectrofluorimetric assays measure rates of fusion by monitoring the fluorescence increase over time [106]. In this case, in addition to the contribution of variations in delays, there will be also an effect of the rate of dye transfer to the unlabeled cells. For instance, the water soluble dye can be transferred through pores by electroosmosis within ms [50]. Therefore, when using contents mixing assays the measured rates of fluorescence increase can be higher than the actual rates of fusion. This can be the reason for the high rates and lack of delays in the kinetic curves obtained by using water soluble dyes [99, 106].

5.10. Fusion yields and delays are related but may reflect different properties of the fusing membranes

Fusion yields are commonly defined as the maximal number of fused labeled cells normalized to the total number of labeled cells [87]. At that time the fusion rate is zero. Sometimes, for convenience fusion yield can be considered as a function of time. Then it reflects the number of cells so far fused until a given time. The rate of fusion at that time is the derivative of the fusion yield with respect to time. Further I discuss only the maximal fusion yield.

For a population of cells, the change of the parameters of the system, which lead to decrease of the delay, cause commonly an increase in fusion yields. For example, in electrofusion of erythrocyte ghosts, the increase in pulse strength and duration, decreases the delay and increases the fusion yield [85]. This means that under stronger pulses more cells acquire the property to fuse. Those which would have fused anyway do it faster. Several experimental results, however, indicate

that while fusion yields and delays are related they may reflect different physical parameters [85]:

- 1) Under strong pulses practically all cells fuse, i.e. the fusion yield is near 100% and further increase in the pulse strength does not lead to an increase in the fusion yield. The delay can be increased, however, several fold with a further increase of the pulse strength.
- 2) For weak pulses, the delay does not change significantly. The fusion yield, however, increases several fold with the increase of the pulse strength.
- 3) The fusion yield changes significantly, while the delay does not, in buffers of different ionic strength.

With respect to the effect of ionic strength on fusion yield, there are inconsistencies between several reports. Fibroblasts fused with higher yield in solutions of higher ionic strength [119], erythrocyte ghosts show a maximum at 20–30 mM phosphate buffer saline, while chinese hamster ovary cells showed lower fusion yields in high ionic strength solutions [120, 121]. Similar inconsistencies exist for the effect of calcium ions. Mouse leukemic lymphoblasts (L5178Y) required Ca^{2+} for their fusion [117], while chinese hamster ovary cells electrofusion was reduced by increasing calcium ion concentration in the range from 0 to 1 mM [120]. The important role of calcium ions in biological systems, for fusion and the phase state of membranes has been known for years, but what is the molecular mechanism of its action on fusion is still unknown [122]. More refined studies of the effect of Ca^{2+} on electrofusion may provide critical information needed for understanding its role in fusion.

6. Kinetic pathways of membrane fusion resemble coalescence in colloid systems

In what follows I present a current understanding of the kinetic mechanisms of electrofusion. I begin with a brief description of very simple systems – fusion of monolayers; then consider fusion of lipid bilayers, and finally I present a plausible qualitative description how cell membranes may fuse.

6.1. *'Fusion' of lipid monolayers on liquid surfaces is by diffusion or intermixing driven by surface pressure gradients*

Bubbles (or drops) in foams (or emulsions) are inherently unstable and tend to coalesce ('fuse'). The driving force for the fusion reaction is the higher free energy of the individual bubbles than the fused bubbles. Assuming that the final volume of two fused bubbles of equal radii, R , and surface tensions, σ , is equal to the sum of the volumes of the individual bubbles, the surface free energy is $(2 - 2^{2/3})4\pi\sigma R^2$ times larger than that after fusion. The large excess in free energy leads to rapid fusion of the bubbles. The fusion rate, however, decreases with increasing the initial separation between the bubbles, the viscosity of the liquid and the density of the monolayers from surface active substances, particularly lipids, which cover the bubble surfaces. At high monolayer densities fusion may never occur in spite of the gain in free energy. Numerous experimental and theoretical studies have shown that there are

two major types of resistance to coagulation and coalescence (in particular, fusion) in colloid systems – hydrodynamic and energetic (for review see, e.g., the books of Scheludko [123], and Dukhin, Rulev and Dimitrov [124]).

The hydrodynamic resistance is due predominantly to the viscosity of the liquid between the bubble surfaces and determines the rate of the so-called ‘fast coalescence’. In the case of ‘pure’ (without energy barriers) fast coalescence, e.g., bubbles in the absence of surfactants, the driving force of the fusion reaction $F = -dG/dh$ (G being the free energy and h being the reaction coordinate, e.g., separation between the bubbles) is always positive. The overall rate of fusion is solely determined by the balance of the driving force and the viscous resistance of the liquid layer between the bubbles. The fusion rate decreases with an increase in viscosity and a decrease in surface tension.

The energy barriers are due to repulsive forces between the bubble surfaces and/or to structural reorganizations of the lipid molecules during the very act of fusion. They lead to the so-called ‘slow coalescence’. The fusion rate in this case is proportional to the probability of overcoming the energy barriers by thermal fluctuations. An example are bubbles with surfaces covered by lipid monolayers of high density. External factors, e.g., electric fields, can be needed to decrease the energy barriers in order to induce fusion. After overcoming the energy barriers, the system can reach the final equilibrium state by a kinetic pathway determined by its hydrodynamic resistance.

To understand kinetic mechanisms of fusion one needs to know how the interplay between the fusion driving force and the system resistance determines the kinetic pathways leading to fusion. It is reasonable to assume that the system utilizes the *fastest* pathway to reach equilibrium. Thirty years ago, Scheludko (see in [123]) suggested that the most rapid kinetic pathway leading to fast coalescence is the growth of thermal fluctuations of the shape of the interacting surfaces, represented as a superposition of surface fluctuation waves. The fluctuation wave mechanism of bubble and drop coalescence was further developed by Ivanov, Scheludko and their collaborators [125, 126] to include the viscous resistance of the liquid film as a whole and the physical properties of the surfactants. Ivanov and Dimitrov [126] found that the viscosity of the monolayer and the surface diffusion of its molecules [127] are critical for the rate of growth of the fluctuation waves and succeeded to explain why the critical separation at which the bubbles fuse is affected by the monolayer density, a phenomenon which was observed in a variety of foam and emulsion systems.

Further studies of the dynamic properties of lipid monolayers have shown that in addition to the surface diffusion, there is another process by which the lipid molecules can move very rapidly under the action of differences in surface pressures arising from differences in the monolayer densities; this is the so-called Marangoni effect (see, e.g., [128]). The Marangoni effect leads to much faster lateral motion of the lipid molecules than the surface diffusion and is strongly affected by the type of lipid molecules, their escape into the bulk of the liquid, the liquid viscosity and the presence of protein molecules [128–130]. For example, for dipalmitoyllecithin monolayers the Marangoni ‘diffusion’ coefficient was measured to be in the range of 350 to 3400 cm²/s [128], which is about 9 orders of magnitude higher than the

respective surface diffusion coefficient. However, since the Marangoni effect depends on the thickness of the liquid support, for approaching bubbles at separations of about 10 nm it can result in 'only' 10^3 -fold faster rate of lipid molecules motion than the diffusion. Another interesting phenomenon is the monolayer collapse. It was shown that the kinetics of monolayer collapse can be described by a Maxwell type of viscoelastic body [131]. The escape of the lipid molecules in the third dimension under high pressures may lead to fusion with another monolayers if they are at close approach.

For very high monolayer densities, the energy barriers determine the life-time of the film separating the bubbles. The process of rupture of this film, consisting of two adhered monolayers, was elegantly described by Derjaguin and his collaborators [132–134], who calculated the energy barriers by using the concept of linear tension (edge energy). It must be emphasized that Derjaguin [134] considered bilayer membranes which are metastable because they are under tension, and that the tension is the driving force for their rupture. Therefore, liposomes may not be described by this approach, because in most cases they are not under tension. For the current concepts of thin film dynamics and instability see [135, 136].

The lessons to be learned from the studies of these 'simple' systems are: 1) there are two major kinetic mechanisms for the fusion process to develop – (i) growth of surface shape instabilities and (ii) overcoming energy barriers, 2) in both cases the properties of the thin liquid layer between the surfaces, and those of the monolayers are critical for the kinetics of fusion, and 3) the fusion *per se* is diffusion of the lipid molecules and Marangoni effect, and therefore is determined by the type of the lipid molecules and the interactions with their environment.

6.2. Fusion of bilayers requires overcoming the intramembrane attraction

While fusion of lipid monolayers is 'simply' intermixing of their molecules driven by concentration and surface pressure gradients, i.e. by lateral diffusion and Marangoni effect, fusion of lipid bilayers could be more complicated because of their three-dimensional structure (for a current view on the structure, dynamics and conformations of bilayers see the reviews of Sackmann [137] and Lipowsky [138]). The strong mutual attraction of the two leaflets in the bilayer leads to restrictions in the ability of the outer leaflets to intermix. Therefore formation of intermediate structures may be needed to overcome the energy barrier due to the internal bilayer interactions [139]. While this fundamental difference between monolayers and bilayers could lead to different molecular mechanisms, the major kinetic pathways of fusion of monolayers and bilayers may be similar. The liquid layer between the approaching surfaces and the surface properties of monolayers and bilayers are essentially the same. Even the Van der Waals forces and the bending rigidity, which depend on the thickness of the bilayer, may not differ significantly, provided that the physico-chemical environment is the same. These similarities indicate that the kinetics of the intermembrane interactions leading to fusion might be qualitatively the same as for monolayers covering bubble (or drop) surfaces. The fusion *per se* ultimately requires intermixing of the lipid molecules and therefore should involve 'monolayer type' of

lateral diffusion and Marangoni effect. Based on these arguments and the similarity of the phenomenological equations which describe the mechanics of monolayers and bilayers, I proposed that fusion of bilayer membranes may follow similar kinetic pathways as fusion of monolayers in colloid systems, and that the knowledge gained in colloid and surface chemistry should be used to describe some features of fusion of bilayer and cell membranes [57, 103, 140–142].

The overall fusion process could be divided into two major processes. The first one is the ‘adhesion’ step. It leads to establishment of close molecular contact. The second one is the ‘destabilization’ step. It results in overcoming the internal resistance of the bilayers to fuse due to their intramembrane interactions. While the adhesion step is commonly followed by the destabilization step, fusion could also occur if the membranes are first destabilized and then adhered, albeit at lower efficiency.

There are two major kinetic pathways which can lead to ultimate molecular contact (fig. 20) [142]. The first one is by a continuous, gradual, approach of the two

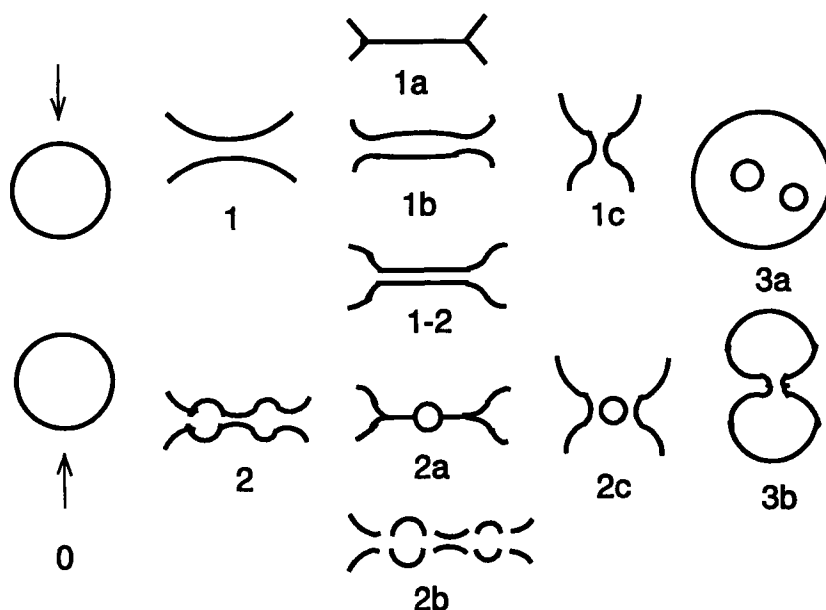


Fig. 20. A sketch of kinetic pathways of electrofusion of membranes. (0) Two membranes approach each other under the action of a driving force due to intermembrane attraction or external fields, e.g., electric. (1) The membranes approach each other by gradually changing their shapes to almost flat membranes which surround a liquid layer of almost uniform thickness. (2) Fast localized membrane approach due to unstable shape undulations. (1a) A single bilayer membrane formed by ‘semi-fusion’ of two membranes which can expand to reach an equilibrium state. (1b) Non-uniform ‘non-wavy’ liquid layer between approaching membranes. (1–2) A liquid layer between membranes which has a uniform thickness. (2a) Localized ‘semi-fusion’ of membranes and formation of ‘lenses’. (2b) Destabilization of the membranes and formation of pores. (1c, 2c) Fusion of membranes and formation of intracellular vesicles or other structures. (3a,b) Post-membrane fusion phenomena leading to final fusion products.

From [142].

membranes (fig. 20; 1). It commonly occurs when the attractive intermembrane forces are not very strong and the system reaches equilibrium without development of instabilities of the liquid layer between the membranes. This pathway can lead to formation of a single bilayer by 'semi-fusion' of the outer leaflets of the interacting bilayers (fig. 20; 1a) [113, 143], formation of a flat liquid layer between the two bilayers (fig. 20; 1b) or initiate an expansion of the liquid layer between the bilayers (fig. 20; 1, 2). The second major kinetic pathway is by a 'discontinuous' decrease of the separation between the two bilayers due to the growth of unstable fluctuations of the membrane shape (fig. 20; 2). It occurs when the driving force is large, e.g., after application of high voltage electric pulses. While the average thickness of the liquid layer between the membranes does not significantly change with time, the growth of the membrane shape instabilities results in the establishment of local contacts where the separation between the membranes is very small (fig. 20; 2a, 2b). These local contacts can either expand to reach a final equilibrium state (fig. 20; 1a; 1, 2) or they can lead to destabilization of the membranes (fig. 20; 2b).

The membrane destabilization can be induced by the molecular interactions at the local contact, especially when the two membranes are under tension, or by external forces arising, e.g., from electric fields. In the first case the merging of the membranes obviously follows their destabilization or occurs simultaneously. When external electric pulses are applied and the membranes are not at molecular contact, the membranes could be destabilized (fig. 20; 2b), but fuse only after making contact. Depending on the strength and duration of the electric pulse and the separation between the membranes, these membranes could fuse during the pulse or after the pulse. In any case fusion of the membranes could result in formation of small vesicles (fig. 20; 2c) or other membrane formations (fig. 20; 1c). The final stage of the fusion process is the expansion of the fusion pore (fig. 20; 1c; 2c), commonly driven by the membrane tension, until reaching the final equilibrium shape of the fused membranes. The fused membranes can surround a rounded cell (fig. 20; 3a) or the fusion product can preserve the overall morphology of the cells before fusion (fig. 20; 3b).

Theoretical formulas were derived to describe the kinetics of each of these kinetic pathways [57, 141]. Without going into mathematical details, I will discuss several estimates which allow to predict the conditions under which each of the stages could occur and estimate its rate. The time to reach contact by a continuous approach of the membranes (fig. 20; 1) increases with increasing the liquid viscosity and the total area of contact, and with decreasing the driving force and the separation between the membranes. The same is valid for the discontinuous membrane approach (fig. 20; 2), except that the contact area in this case should be substituted by the area of the fastest growing undulation (wave), which is of the order of the square of its characteristic length (wave length). Because of the dependence of that area on the intermembrane forces and other physical parameters and the non-linear character of the functional relationships between those parameters, the characteristic time of the wave growth could be much shorter than the rate of approach of the membranes as a whole. An estimate of the ratio of the two characteristic times (of continuous and discontinuous membrane approach) leads to the formula $F/h\Sigma$, where F is the force

which drives the membrane approach, h the intermembrane separation and Σ the membrane tension. For $F = 10^{-6}$ dyn, $h = 10$ nm and $\Sigma = 1$ mdyn/cm, this ratio is of the order of 1000. This means that under those conditions it is 1000-fold faster to establish local contact by unstable fluctuational waves than to gradually approach the membranes. Therefore, in this case the kinetic pathway is by discontinuous approach (fig. 20; 2). For liquid viscosity equal to 0.01 P the time of this type of approach for the above example is 10 s. Similar considerations apply for tension free membranes where the time of localized approach is determined by the bending rigidity. In this case ($\Sigma = 0$) another formula is valid where Σ should be replaced by a dimensional factor proportional to the bending rigidity K .

The local membrane contact could expand by a rate which is determined by the liquid viscosity, membrane tension, contact angle and the thickness of the liquid layer between the membranes [140, 141, 144]. This rate can be very low which could lead to very long times of establishment of uniform liquid layer between the adhering membranes. Similar theoretical considerations and formulas apply for expansion of membranes consisting of one bilayer surrounded by two monolayers of bilayers (fig. 20; 1a, 2a) [140]. The rate of expansion in all these cases, U , can be estimated by the formula: $U = h\Sigma/4\mu l$, where h is the thickness of the mobile layer between the two monolayers (or bilayers), e.g., the solvent in the case of supported bilayer lipid membranes, μ is its viscosity, Σ is the tension of the two interacting monolayers (or bilayers), which drives the expansion, and l is the length of the perimeter of contacting monolayers (or bilayers) along which the tension is applied. This formula predicts times of expansion of the order of seconds for supported bilayer lipid membranes. More sophisticated formulas are presented in [140, 144]. For solvent free membranes, where h is zero or very small, expansion may not occur or may be very slow.

The destabilization of the membranes may occur either by the fluctuation wave mechanism or by overcoming energy barriers or by both mechanisms as discussed before (sections 3.8 and 3.9). It leads to formation of pores, defects or other structures. The shape of the lipid molecules can affect the stability of those structures [113].

The interaction of two pores or a pore and a membrane may lead to intermixing of the lipid molecules and to their fusion. The interaction between the two membranes can contribute to their destabilization due to an increase in the intramembrane electric field strength. External electric fields can destabilize the membrane-membrane contact much faster than the liquid layer between the membranes because of the greater transmembrane voltage across the membranes [58]. Therefore one might expect that, depending on the electric field strength, the adhered membranes can be either first destabilized and then they interact to fuse, or they may form a close (molecular contact) and then fuse. Probably in most cases the membranes are first destabilized and then they fuse. This is supported by theoretical considerations indicating that after formation of pores the rate of local membrane approach may increase significantly due to their permeabilization [145] and the increase in the force of local attraction due to electric currents [146]. Direct experimental evidence supporting this conclusion is, however, lacking.

The intermixing of the membranes, i.e. the very act of fusion, is very fast. An estimate, based on the lateral diffusion of lipids leads to times $\tau_f = l_D^2/4D$ of the order of microseconds if the characteristic distance l_D is about 5 nm and the diffusion coefficient D is of the order of 10^{-8} cm²/s. Surface pressure differences between the two bilayers (Marangoni effect) can lead to even shorter times of intermixing.

The intermixing of lipids from the two interacting membranes leads to formation of fusion junctions, which can transform into fusion pores. The fusion pores can either expand (fig. 20; 2c), stabilize (fig. 20; 3b) or in rare cases close. For liquid crystalline membranes under tension the expansion of the fusion pores can be relatively fast process with a rate proportional to the membrane tension Σ and inversely proportional to the liquid viscosity μ and the radius of curvature of the membranes R_c [142]. The rate of expansion could be also affected by the membrane viscosity. Numerical estimates of the characteristic time of expansion τ_e , based on the formula $\tau_e = \mu R_c / \Sigma$ [142], give a reasonable value of 10 ms when $\mu = 0.01$ P, $\Sigma = 0.01$ dyn/cm and $R_c = 0.1$ mm. When the membranes are not under tension, the driving force for the fusion pore expansion is zero or very small. The time of expansion therefore could be very long. High membrane viscosities may also increase the expansion times. Under conditions favoring very long times of expansion, the fusion pores may stabilize or even close thus returning the system back to the initial stage of two separate membranes.

The duration of the fusion process as a whole is a sum of the durations of each stage. While the times for membrane destabilization and intermixing are very short, the initial (adhesion) and latest (expansion) stages can be very long and therefore rate determining. This indicates one of the fundamental problems for studying mechanisms of fusion. Fusion itself is very rapid and localized while the 'background' processes (adhesion and expansion) are slow and involve large parts of the membranes.

6.3. *The molecular mechanism of bilayer fusion is unknown*

Because of the very small amount of membrane lipid involved in fusion pores and their very short life-times direct measurement of the intermediate structures in fusion of lipid bilayers is very difficult if not impossible. Some progress was made by using NMR for fusion of membranes in lipid suspensions [147–149]. Whether this is relevant to fusion of lipid bilayers remains to be seen. The lack of direct experimental measurements of lipid bilayer fusion hinders the understanding of the molecular mechanisms of fusion. In contrast, there are several theoretical models which try to calculate intermediate structures requiring minimal activation energy for their formation [139, 150, 151]. These models are helpful in the design of new experiments for better understanding of the molecular rearrangements during fusion.

6.4. *Fusion of cell membranes can be qualitatively described but the molecular rearrangements remain unclear*

Unlike lipid bilayers, cell membranes are highly heterogeneous, contain significant amounts of proteins, glycoproteins and glycolipids, are surrounded by surface layers

of adsorbed molecules, and are attached to the cytoskeleton (for a current view on the structure and dynamics of cell membranes and nice cartoons, see the review of Sackmann [137]). The high level of complexity of cell membranes leads to difficulties in modeling fusion. Nevertheless, phenomenological models could be still helpful for understanding certain aspects of electrofusion.

The following picture for the kinetic pathways of cell electrofusion emerges from the comparison of the experimental data with the theoretical models. The cells, held at close apposition by dielectrophoresis or other interactions, are unable to fuse because of the inherent stability of the membranes and the repulsive forces between them. The application of high voltage pulses leads to at least two effects: 1) further approach of the membranes [152, 153] and 2) their destabilization. The membrane destabilization and formation of pores or other structures enhances the local approach of the membranes by (i) providing the driving force due to the high free energy state, which can reduce or eliminate the repulsive intermembrane forces and (ii) decreasing the local hydrodynamic resistance which increases the rate of local approach. The excess free energy of the pores (or defects, or unknown structures) can be either dissipated as thermal motion without formation of fusion junction or can be utilized in the rearrangements of the lipid molecules leading to fusion. Efficient fusion occurs when the membranes are at close approach or brought rapidly at close approach after the pulse before the free energy of the (activated) 'fusogenic state' has been dissipated. On the one hand, membrane proteins can enhance the fusion reaction if they stabilize the state of high free energy by not allowing rapid dissipation of energy, increase membrane binding and/or provide an appropriate environment for the structural rearrangements of the lipid molecules. On the other hand, they can decrease the efficiency of the fusion reaction by creating additional (mainly steric) resistance to local membrane approach. Which effect will dominate depends on the specific lipid and protein composition and on the phase state of the membranes.

The high free energy of the activated membranes is probably localized in electropores. Two pores apposing each other are the most efficient kinetic pathway of fusion because the driving force is high and the hydrodynamic resistance is small. Such pores are also predominantly formed when the membranes are at close apposition. This does not exclude the possibility, however, that pores in one of the membranes can destabilize locally the opposing membrane albeit at low efficiency. This is probably the case when the two membranes are brought in contact after the pulse, because the geometric probability for two pores being apposing each other is very low due to the low pore concentration in the membranes. This may be one of the causes for the low efficiency of fusion in this case.

Because of the high free energy of the membranes after the pulse the liquid film between them can be destabilized, which can lead to a rapid localized approach until reaching molecular contact. Thus the molecular contact may occur during the pulse if the duration of the pulse is longer than the time needed to make contact. If the approach is slow, the membrane contact may occur after the pulse. The occurrence of molecular contacts does not necessarily lead to merging of the two membranes. Energy barriers for the molecular rearrangements of the lipid molecules from a pore (or another) configuration to a fusion junction should be overcome to initiate fusion.

The height of these barriers is of the same magnitude as that for lateral mobility of lipid molecules and therefore one might speculate that the lipid rearrangements kinetically resemble the lateral lipid diffusion in membranes. Energy barriers may also exist before the occurrence of molecular contact if the free energy of the pores is not sufficient to overcome the repulsive intermembrane forces.

Fusion of membranes occurs after overcoming those energy barriers and leads to local continuity of the membranes, i.e. to fusion junctions. The formation of fusion junctions may lead or may not lead to continuity of the cell cytoplasm, i.e. to the formation of a fusion pore. Depending on the structure of the fusion intermediates, fusion pores may form simultaneously with formation of fusion junctions, may form later or may never form. Since for cell membranes the molecular structure of the intermediates is not known and it is difficult, if not impossible, to describe this structure theoretically, one might only speculate how and when formation of fusion pores occurs.

The fusion pores can stabilize, reverse to the initial prefusion state ('flickering') or expand. The expansion of fusion pores may lead to 'fusion' with other pores, rounding of the fused cells and eventually formation of giant cells (syncytia), when many cells fuse. Alternatively, the cells may retain their shape if the fusion pores do not expand, because of constraints arising, e.g., from the cytoskeleton or other factors which remain to be elucidated.

7. Fusion in life processes involves specialized proteins but kinetically can be similar to electrofusion

Electrofusion provides a convenient way to study fundamental mechanisms of membrane fusion, which may help to understand the fusion mechanisms in biological systems. While the major requirements for electrofusion and biological fusion (close contact, destabilization, overcoming energy barriers and appropriate structural rearrangements) are the same, fusion in biological systems is tightly controlled by specific protein interactions and full understanding of its mechanisms requires understanding the structure and conformational changes of the fusion proteins.

The biological fusion process which is best understood in terms of molecular structure and conformational changes of fusion proteins is viral fusion [154, 155]. Viral fusion is caused by proteins which undergo conformational changes to expose hydrophobic peptides after activation by low pH or interaction with receptor molecules. The exposure of the hydrophobic fusion peptide to the water environment results in an increase in the free energy of the peptide and its immediate environment possibly including the surfaces of the interacting membranes. This leads to a high free energy state which could be similar to that of a fusogenic electropore in electrofusion. Therefore, the kinetic pathways of viral fusion after activation of the viral proteins could be similar to those of electrofusion. The existence of a high energy state of the viral fusion protein leads to local mutual approach of the lipid bilayers and destabilization of the membranes and of the liquid layer between them. The lipid matrix of the membrane then undergoes localized structural rearrangements resulting in lipid intermixing. An indication that this stage of viral fusion is also similar to

that in electrofusion is the magnitude of the activation energy which in both cases is of the order of the activation energy of the lateral mobility of the lipid molecules (15–25 kcal/mol) [85, 156]. After the formation of fusion junctions and pores, they can either expand and lead to formation of giant cells or stabilize and preserve the morphology of aggregated cells [85, 100].

The comparison between electrofusion and virus fusion may lead to the discovery of new important parameters affecting the kinetics of viral fusion. For example, by analogy with electrofusion one might predict that delays in viral fusion should increase with increasing the viscosity of the liquid between the membranes. This was confirmed experimentally for fusion of Sendai virus [118]. A detailed comparison between electrofusion and viral fusion is made elsewhere [107].

The above considerations could be applied to a wide variety of biological processes involving fusion, including exo- and endocytosis, fertilization, cell division, intracellular transport and myoblast formation.

8. New approaches are needed to understand molecular mechanisms of fusion

Electrofusion is a multistep process, which requires close apposition of the membranes, their destabilization and appropriate structural rearrangements of the lipid matrix. While the kinetic mechanisms of fusion could be understood in terms of phenomenological models, the molecular mechanisms are unknown and new approaches are needed for their elucidation. Understanding mechanisms of electrofusion is not only of practical importance for its optimization but also may help in understanding fundamental mechanisms of fusion in biological systems.

Acknowledgement

I would like to thank I. Ivanov, who taught me in science and how to think about theory, instability of liquid films and dynamics of interfacial systems; A. Scheludko and R. Jain for the many exciting discussions of fluctuation waves and membrane instability; D. Zhelev, who shaped my way of thinking about electrofusion by a critical evaluation of the experimental data and theories; N. Stoicheva, R. Mutafchieva, M. Angelova, P. Doinov and G. Sharkov for interesting discussions; A. Sowers for his original suggestions and R. Blumenthal for the intellectual environment and inspiration to measure and analyze delays in fusion. I am grateful to M. Apostolova for critique and logic. I appreciate the helpful comments of R. Lipowsky.

List of symbols

AC alternating current

C proportionality constant in eq. (5)

C_m membrane capacitance

d membrane thickness

D diffusion coefficient

DC direct current

DiI 1,1'-dihexadecyl-3,3,3',3'-tetramethylindocarbocyanine perchlorate

- E electric field strength
 E_a activation energy
 F driving force
 $F_0 = \varepsilon_0 E_r E^2 R^2$
 FITC fluorescein isothiocyanate
 G free energy of intermembrane interaction
 h separation between surfaces including membrane surfaces
 k Boltzmann's constant
 k_R rate constant of pore resealing
 K membrane rigidity
 K_e effective net cell polarizability
 l length of perimeter of contacting monolayers or bilayers
 l_D characteristic diffusion length in fusion
 $L = h/2 + R$
 r_i intracellular electric resistivity
 r_o extracellular electric resistivity
 R radius of cells or other spherical particles
 R_c curvature radius of membranes
 R_g gas constant
 t time
 t_c time required to make membrane contact
 t_e time needed for a fluorescence dye to diffuse to the far ends of originally unlabeled membranes after fusion
 t_p charging time
 t_u time needed to reach an uniform redistribution of fluorescence dyes after membrane fusion
 T absolute temperature
 U rate of expansion of membrane contact
 V transmembrane voltage
 V_c critical transmembrane voltage needed for electroporation
 V_i inherent transmembrane voltage (at $E = 0$)
 V_m maximal transmembrane voltage
 δ angle between radius vector and electric field vector
 ε_0 permittivity of free space
 E_r relative permittivity
 μ liquid viscosity
 Σ membrane tension
 σ surface tension
 τ pulse duration
 τ_e characteristic time of fusion pore expansion
 τ_f characteristic fusion time

References

1. Ringertz, N.R. and R.E. Savage, 1976, *Cell Hybrids* (Academic Press, New York).
2. Langhans, T., 1868, *Über Resenzellen mit wandständigen Kernen in Tuberkelen und die fibrose Form des Tuberkels*, *Arch. Pathol. Anat. Physiol. Klin. Med.* **42**, 382–404.
3. Lewis, W.H., 1927, The formation of giant cells in tissue culture and their similarity to those in tuberculous lesions, *Am. Rev. Tuberc.* **15**, 616–628.
4. Okada, Y., 1958, The fusion of Ehrlich's tumor cells caused by HVJ virus *in vitro*, *Biken's J.* **1**, 103–110.
5. Hoggan, M.D. and B. Roizman, 1959, The isolation and properties of a variant of herpes simplex virus producing multinucleate giant cells in monolayer cultures in the presence of antibody, *Am. J. Hyg.* **70**, 208–219.
6. Okada, Y., 1962, Analysis of giant polynuclear cell formation caused by HVJ virus from Ehrlich's ascites tumor cells, I. Microscopic observation of giant polynuclear cell formation, *Exp. Cell Res.* **26**, 98–107.
7. Colwin, L.H. and A.L. Colwin, 1960, Formation of sperm entry holes in the vitelline membrane of *Hydroides hexagonus* (Annelida) and evidence of their lytic origin, *J. Biophys. Biochem. Cytol.* **7**, 315–320.
8. Holtzer, H., J. Abbott and J. Lash, 1958, The formation of multi-nucleate myotubes, *Anat. Rec.* **131**, 567.
9. Capers, C.R., 1960, Multinucleation of skeletal muscle *in vitro*, *J. Biophys. Biochem. Cytol.* **7**, 559–566.
10. Barski, G., S. Sorieul and F. Cornefert, 1961, "Hybrid" type cells in combined cultures of two different mammalian cell strains, *J. Nat. Cancer Inst.* **26**, 1269–1291.
11. Sorieul, S. and R. Ephrussi, 1961, Karyological demonstration of hybridization of mammalian cells *in vitro*, *Nature* **190**, 653–654.
12. Bonnett, H.T. and T. Eriksson, 1974, Transfer of algal chloroplasts into protoplasts of higher plants, *Planta* **120**, 71–79.
13. Kao, K.N. and M.R. Michayluk, 1974, A method for high-frequency intergeneric fusion of plant protoplasts, *Planta* **115**, 355–367.
14. Pontecorvo, G., 1975, Production of indefinitely multiplying mammalian somatic cell hybrids by polyethylene glycol (PEG) treatment, *Somatic Cell Genet.* **1**, 397–400.
15. Senda, M., J. Takeda, S. Abe and T. Nakamura, 1979, Induction of cell fusion of plant protoplasts by electrical stimulation, *Plant Cell Physiol.* **20**, 1441–1443.
16. Neumann, E., G. Gerisch and K. Opatz, 1980, Cell fusion induced by high electric impulses applied to *Dictyostelium*, *Naturwissenschaften* **67**, 414–415.
17. Weber, H., W. Forster, H.-E. Jacob and H. Berg, 1981, Microbiological implications of electric field effects, *Z. Allg. Microbiol.* **21**, 555–562.
18. Zimmermann, U. and P. Scheurich, 1981, High frequency fusion of plant protoplasts by electric fields, *Planta* **151**, 26–32.
19. Berg, H., W. Forster and J. Hans-Egon, 1987, Electric field effects on biological membranes: Electroincorporation and electrofusion, in: *Bioelectrochemistry II. Membrane Phenomena*, eds G. Milazzo and M. Blank (Plenum Press, New York) pp. 135–166.
20. Sowers, A.E., 1987, *Cell Fusion* (Plenum Press, New York).
21. Zimmermann, U., W.M. Arnold and W. Mehrle, 1988, Biophysics of electroinjection and electrofusion, *J. Electrostatics* **21**, 309–345.
22. Neumann, E., A.E. Sowers and C.A. Jordan, 1989, *Electroporation and Electrofusion in Cell Biology* (Plenum Press, New York).
23. Chang, D.C., B.M. Chassy, J.A. Saunders and A.E. Sowers, 1992, *Guide to Electroporation and Electrofusion* (Academic Press, San Diego).
24. Pohl, H.A., 1978, *Dielectrophoresis* (Cambridge Univ. Press, London).
25. Sale, A.J.H. and W.A. Hamilton, 1967, Effects of high electric fields on microorganisms, I. Killing of bacteria and yeasts, *Biochim. Biophys. Acta* **148**, 781–788.
26. Sale, A.J.H. and W.A. Hamilton, 1968, Effects of high electric fields on microorganisms, III. Lysis of erythrocytes and protoplasts, *Biochim. Biophys. Acta* **163**, 37–43.

27. Neumann, E. and K. Rosenheck, 1972, Permeability changes induced by electric pulses in vesicular membranes, *J. Membr. Biol.* **10**, 279–290.
28. Zimmermann, U., J. Schulz and G. Pilwat, 1973, Transcellular flow in *Escherichia coli* B and electrical sizing of bacteria, *Biophys. J.* **13**, 1005–1013.
29. Zimmermann, U., G. Pilwat and F. Riemann, 1974, Reversibler dielektrischer Durchbruch von Zellmembranen in elektrostatischen Feldern, *Z. Naturforsch.* **29c**, 304–305.
30. Neumann, E., M. Schaefer-Ridder, Y. Wang and P.H. Hofschneider, 1982, Gene transfer into mouse lymphoma cells by electroporation in high electric fields, *EMBO J.* **1**, 841–845.
31. Weaver, J.C. and K.T. Powell, 1989, Theory of electroporation, in: *Electroporation and Electrofusion in Cell Biology*, eds E. Neumann, A.E. Sowers and C.A. Jordan (Plenum Press, New York) pp. 111–126.
32. Schwan, H.P., 1957, Electrical properties of tissue and cell suspensions, *Adv. Biol. Med. Phys.* **5**, 147–209.
33. Schwan, H.P., 1989, Dielectrophoresis and rotation of cells, in: *Electroporation and Electrofusion in Cell Biology*, eds E. Neumann, A.E. Sowers and C.A. Jordan (Plenum Press, New York) pp. 3–21.
34. Neumann, E., 1989, The relaxation hysteresis of membrane electroporation, in: *Electroporation and Electrofusion in Cell Biology*, eds E. Neumann, A.E. Sowers and C.A. Jordan (Plenum Press, New York) pp. 61–82.
35. Kinoshita, K.Jr., I. Ashikawa, N. Saita, H. Yoshimura, H. Itoh, K. Nagayama and A. Ikegami, 1988, Electroporation of cell membrane visualized under a pulsed-laser fluorescence microscope, *Biophys. J.* **53**, 1015–1019.
36. Hibino, M., M. Shigemori, H. Itoh, K. Nagayama and K. Kinoshita, 1991, Membrane conductance of an electroporated cell analyzed by submicrosecond imaging of transmembrane conductance, *Biophys. J.* **59**, 209–220.
37. Kinoshita, K., M. Hibino, H. Itoh, M. Shigemori, K. Hirano, Y. Kirino and T. Hayakawa, 1992, Events of membrane electroporation visualized on a time scale from microsecond to seconds, in: *Guide to Electroporation and Electrofusion*, eds D.C. Chang, B.M. Chassy, J.A. Saunders and A.E. Sowers (Academic Press, Orlando) pp. 29–46.
38. Kinoshita, K.Jr. and T.Y. Tsong, 1977, Voltage-induced pore formation and hemolysis of human erythrocytes, *Biochim. Biophys. Acta* **471**, 479–497.
39. Benz, R. and U. Zimmermann, 1980, Relaxation studies on cell membranes and lipid bilayers in the high electric field range, *Bioelectrochem. Bioenerg.* **7**, 723–739.
40. Zhelev, D.V., D.S. Dimitrov and P. Doinov, 1988, Correlation between physical parameters in electrofusion and electroporation of protoplasts, *Bioelectrochem. Bioenerg.* **20**, 155–167.
41. Abidor, I.G., V.B. Arakelyan, L.V. Chernomordik, Yu.A. Chizmadzhev, V.F. Pastushenko and M.R. Tarnsevich, 1979, Electrical breakdown of bilayer lipid membranes, I. The main experimental facts and their qualitative discussion, *Bioelectrochem. Bioenerg.* **6**, 37–52.
42. Tsong, T.Y., 1989, Electroporation of cell membranes: Mechanisms and applications, in: *Electroporation and Electrofusion in Cell Biology*, eds E. Neumann, A.E. Sowers and C.A. Jordan (Plenum Press, New York) pp. 149–163.
43. Kinoshita, K.Jr. and T.Y. Tsong, 1977, Formation and resealing of pores of controlled sizes in human erythrocyte membrane, *Nature* **268**, 438–441.
44. Deuticke, B. and K. Schwister, 1989, Leaks induced by electrical breakdown in the erythrocyte membrane, in: *Electroporation and Electrofusion in Cell Biology*, eds E. Neumann, A.E. Sowers and C.A. Jordan (Plenum Press, New York) pp. 127–148.
45. Serpersu, E.H., Jr.K. Kinoshita and T.Y. Tsong, 1985, Reversible and irreversible modification of erythrocyte membrane permeability by electric field, *Biochim. Biophys. Acta* **812**, 779–785.
46. Teissie, J. and T.Y. Tsong, 1981, Electric field induced transient pores in phospholipid bilayer vesicles, *Biochemistry* **20**, 1548–1554.
47. Rossignol, D.P., G.L. Decker, W.J. Lennarz, T.Y. Tsong and J. Teissie, 1983, Induction of calcium-dependent, localized cortical granule breakdown in sea-urchin eggs by voltage pulsation, *Biochim. Biophys. Acta* **763**, 346–355.
48. Mehrle, W., U. Zimmermann and R. Hampp, 1985, Evidence for asymmetrical uptake of fluorescent dyes through electroporeabilized membranes of *Avena mesophyll* protoplasts, *FEBS Lett.* **185**, 89–94.

49. Sowers, A.E., 1988, Fusion events and nonfusion contents mixing events induced in erythrocyte ghosts by an electric pulse, *Biophys. J.* **54**, 619–626.
50. Dimitrov, D.S. and A.E. Sowers, 1990, Membrane electroporation – fast molecular exchange by electroosmosis, *Biochim. Biophys. Acta* **1022**, 381–392.
51. Zimmermann, U., G. Pilwat, A. Pequeux and R. Gilles, 1980, Electromechanical properties of human erythrocyte membranes: the pressure dependence of potassium permeability, *J. Membr. Biol.* **54**, 103–113.
52. Zhelev, D.V., D.S. Dimitrov and I. Tsoneva, 1988, Electrical breakdown of protoplasts membranes under different osmotic pressures, *Bioelectrochem. Bioenerg.* **19**, 217–225.
53. Needham, D. and R.M. Hochmuth, 1989, Electro-mechanical permeabilization of lipid vesicles: Role of membrane tension and compressibility, *Biophys. J.* **55**, 1001–1009.
54. Crowley, J.M., 1973, Electrical breakdown of bimolecular lipid membranes as an electromechanical instability, *Biophys. J.* **13**, 711–724.
55. Bryant, G. and J. Wolfe, 1987, Electromechanical stresses produced in the plasma membranes of suspended cells by applied electric fields, *J. Membr. Biol.* **96**, 129–139.
56. Dimitrov, D.S., 1984, Electrical breakdown of lipid bilayers and cell membranes – a thin viscoelastic film model, *J. Membr. Biol.* **78**, 53–60.
57. Dimitrov, D.S. and R.K. Jain, 1984, Membrane stability, *Biochim. Biophys. Acta* **779**, 437–468.
58. Dimitrov, D.S., D.V. Zhelev and R.K. Jain, 1985, Stability of viscoelastic membrane systems modeled as multilayered thin films, *J. Theoret. Biol.* **113**, 353–377.
59. Chang, D.C., 1992, Structure and dynamics of electric-field-induced membrane pores as revealed by rapid-freezing electron microscopy, in: *Guide to Electroporation and Electrofusion*, eds D.C. Chang, J.A. Saunders, B.M. Chassy and A. E. Sowers (Academic Press, Orlando) pp. 9–27.
60. Derzhanski, A., A.G. Petrov and M.D. Mitov, 1979, Electric field induced pores in erythrocyte membrane – a discussion, in: *Proceedings of the Fifth School on Biophysics of Membrane Transport* (Wroclaw, Poland) pp. 285–286.
61. Weaver, J.C. and R.A. Mintzer, 1981, Decreased membrane stability due to transmembrane potentials, *Phys. Lett.* **86A**, 57–59.
62. Sugar, I.P., 1981, The effects of external fields on the structure of lipid bilayers, *J. Physiol. (Paris)* **77**, 1035–1042.
63. Sugar, I.P. and E. Neumann, 1984, Stochastic model for electric field-induced membrane pores: Electroporation, *Electroporation Biophys. Chem.* **19**, 211–225.
64. Sugar, I.P., 1989, Stochastic model of electric field-induced membrane pores, in: *Electroporation and Electrofusion in Cell Biology*, eds E. Neumann, A.E. Sowers and C.A. Jordan (Plenum Press, New York) pp. 97–110.
65. Chernomordik, L.V. and Y.A. Chizmadzhev, 1989, Electrical breakdown of lipid bilayer membranes: phenomenology and mechanism, in: *Electroporation and Electrofusion in Cell Biology*, eds E. Neumann, A.E. Sowers and C.A. Jordan (Plenum Press, New York) pp. 83–95.
66. Weaver, J.C. and A. Barnett, 1992, Progress toward a theoretical model for electroporation mechanism: membrane electrical behavior and molecular transport, in: *Guide to Electroporation and Electrofusion*, eds D.C. Chang, B.M. Chassy, J.A. Saunders and A.E. Sowers (Academic Press, Orlando) pp. 91–117.
67. Kashchiev, D. and D. Exerova, 1983, Bilayer lipid membrane permeation and rupture due to hole formation, *Biochim. Biophys. Acta* **732**, 133–145.
68. Tsong, T.Y., 1992, Time sequence of molecular events in electroporation, in: *Guide to Electroporation and Electrofusion*, eds D.C. Chang, B.M. Chassy, J.A. Saunders and A.E. Sowers (Academic Press, Orlando) pp. 47–61.
69. O’Konski, C.T., 1981, A history of electro-optics, in: *Molecular Electro-Optics*, ed. S. Krause (Plenum Press, New York) pp. 1–25.
70. Liebesny, P., 1938, Athermic short-wave therapy, *Arch. Phys. Ther. (Leipzig)* **19**, 736.
71. Krasny-Ergen, W., 1936, Nicht-thermische Wirkungen elektrischer Schwingungen auf Kolloide, *Hochfrequenztech. Elektroakust.* **48**, 126–133.
72. Schwan, H.P. and L.D. Sher, 1969, Alternating-current field-induced forces and their biological implications, *J. Electrochem. Soc.* **116**, 170–174.

73. Takashima, S. and H.P. Schwan, 1985, Alignment of microscopic particles in electric fields and its biological implications, *Biophys. J.* **467**, 513–518.
74. Dimitrov, D.S., I. Tsoneva, N. Stoicheva and D. Zhelev, 1984, An assay for dielectrophoresis: Applications to electromagnetically induced membrane adhesion and fusion, *J. Biol. Phys.* **12**, 26–30.
75. Stoicheva, N., I. Tsoneva and D.S. Dimitrov, 1985, Protoplast dielectrophoresis in axisymmetric fields, *Z. Naturforsch.* **40c**, 735–739.
76. Dimitrov, D.S. and D.V. Zhelev, 1987, Dielectrophoresis of individual cells. Experimental methods and results, *Bioelectrochem. Bioenerg.* **17**, 549–557.
77. Iglesias, F.J., C. Santamaria, M.C. Lopez and A. Dominguez, 1989, Dielectrophoresis: Behavior of microorganisms and effect of electric fields on orientation phenomena, in: *Electroporation and Electrofusion in Cell Biology*, eds E. Neumann, A.E. Sowers and C.A. Jordan (Plenum Press, New York) pp. 37–57.
78. Tsoneva, I., D.V. Zhelev and D.S. Dimitrov, 1986, Red blood cell dielectrophoresis is axisymmetric fields, *Cell Biophys.* **8**, 89–101.
79. Stoicheva, N. and D.S. Dimitrov, 1986, Dielectrophoresis of single protoplasts: Effects of increased conductivity caused by calcium ions, *Stud. Biophys.* **111**, 17–21.
80. Stoicheva, N. and D.S. Dimitrov, 1986, Frequency effects in protoplasts dielectrophoresis, *Electrophoresis* **7**, 339–341.
81. Stoicheva, N., D.S. Dimitrov and A. Ivanov, 1987, Chloroplast dielectrophoresis: Effects of frequency and surface charge, *Eur. Biophys. J.* **14**, 253–256.
82. Zhelev, D.V., P. Kuzmin and D.S. Dimitrov, 1991, Mutual dielectrophoresis of cells, *Bioelectrochem. Bioenerg.* **26**, 193–203.
83. Dimitrov, D.S., M.A. Apostolova and A.E. Sowers, 1990, Attraction, deformation and contact of erythrocyte membranes induced by low frequency electric fields, *Biochim. Biophys. Acta* **1023**, 389–397.
84. Scheurich, P., U. Zimmermann, M. Mischel and I. Lamprecht, 1980, Membrane fusion and deformation of red blood cells by electric fields, *Z. Naturforsch.* **35c**, 1081–1085.
85. Dimitrov, D.S. and A.E. Sowers, 1990, A delay in membrane fusion: Lag times observed by fluorescence microscopy of individual fusion events induced by an electric field pulse, *Biochemistry* **29**, 8337–8344.
86. Zimmermann, U., 1982, Electric field-mediated fusion and related electrical phenomena, *Biochim. Biophys. Acta* **694**, 227–277.
87. Sowers, A.E., 1984, Characterization of electric field-induced fusion in erythrocyte ghost membranes, *J. Cell Biol.* **99**, 1989–1996.
88. Zimmermann, U., K.-H. Buchner and W.M. Arnold, 1984, Electrofusion of cells: Recent developments and relevance for evolution, in: *Charge and Field Effects in Biosystems*, eds M.J. Allen and P.N.R. Usherwood (Abacus Press, Normal, Ill) pp. 293–318.
89. Sowers, A.E., 1986, A long-lived fusogenic state is induced in erythrocyte ghosts by electric pulses, *J. Cell Biol.* **102**, 1358–1362.
90. Teissie, I. and M.P. Rols, 1986, Fusion of mammalian cells in culture is obtained by creating the contact between cells after their electroporabilization, *Biochem. Biophys. Res. Commun.* **140**, 258–266.
91. Wu, Y., J.G. Montes and R.A. Sjodin, 1992, Determination of electric field threshold for electrofusion of erythrocyte ghosts. Comparison of pulse-first and contact-first protocols, *Biophys. J.* **61**, 810–815.
92. Sowers, A.E., 1989, The mechanism of electroporation and electrofusion in erythrocyte membranes, in: *Electroporation and Electrofusion in Cell Biology*, eds E. Neumann A.E. Sowers and C.A. Jordan (Plenum Press, New York) pp. 229–256.
93. Lopez, A., M.P. Rols and J. Teissie, 1988, 31-P NMR analysis of membrane phospholipid organization in viable reversibly electroporabilized Chinese Hamster Ovary cells, *Biochemistry* **27**, 1222–1228.
94. Hahn-Hagerdal, B., K. Hosono, A. Zachrisson and C.H. Bornman, 1986, Polyethylene glycol and electric field treatment of plant protoplasts: characterization of some membrane properties, *Physiol. Plants* **67**, 359–364.

95. Ohki, S., 1987, Physicochemical factors underlying lipid membrane fusion, in: *Cell Fusion*, ed. A.E. Sowers (Plenum Press, New York) pp. 331–352.
96. Ohki, S. and K. Arnold, 1990, Surface dielectric constants, surface hydrophobicity and membrane fusion, *J. Membr. Biol.* **114**, 195–203.
97. Vienken, J., U. Zimmermann, R. Ganser and H. Hampp, 1983, Vesicle formation during electrofusion of mesophyll protoplasts of *Kalanchoe daigremontiana*, *Planta* **157**, 331–335.
98. Stenger, D.A. and S.W. Hui, 1986, Kinetics of ultrastructural changes during electrically-induced fusion of human erythrocytes, *J. Membr. Biol.* **93**, 43–53.
99. Stenger, D.A. and S.A. Hui, 1989, Electrofusion Kinetics: Studies using electron microscopy and fluorescence contents mixing, in: *Electroporation and Electrofusion in Cell Biology*, eds E. Neumann, A.E. Sowers and C.A. Jordan (Plenum Press, New York) pp. 167–180.
100. Chernomordik, L.V. and A.E. Sowers, 1991, Evidence that the spectrin network and a nonosmotic force control the fusion product morphology in electrofused erythrocyte ghosts, *Biophys. J.* **60**, 1026–1037.
101. Coakley, W.T. and D. Gallez, 1989, Membrane-membrane contact: Involvement of interfacial instability in the generation of discrete contacts, *Biosci. Rep.* **9**, 675–691.
102. Coakley, T.W., H. Darmani and A.J. Baker, 1991, Membrane contact induced between erythrocytes by polycations, lectins and dextran, in: *Cell and Model Membrane Interactions*, ed. S. Ohki (Plenum Press, New York) pp. 25–45.
103. Dimitrov, D.S., 1982, Instability of thin liquid films between membranes, *Colloid Polym. Sci.* **260**, 1137–1144.
104. Blangero, C., M.P. Rols and J. Teissie, 1989, Cytoskeletal reorganizations during electric field-induced fusion of Chinese hamster ovary cells grown in monolayers, *Biochim. Biophys. Acta* **981**, 295–302.
105. Zheng, Q. and D.C. Chang, 1992, Dynamics of cytoskeletal reorganization in CV-1 cells during electrofusion, in: *Guide to Electroporation and Electrofusion*, eds D.C. Chang, B.M. Chassy, J.A. Saunders and A.E. Sowers (Academic Press, Orlando) pp. 179–198.
106. Stenger, D.A. and S.W. Hui, 1988, Human erythrocyte electrofusion kinetics monitored by aqueous contents mixing, *Biophys. J.* **53**, 833–838.
107. Dimitrov, D.S., 1992, Membrane fusion kinetics, in: *Guide to Electroporation and Electrofusion*, eds D.C. Chang, B.M. Chassy, J.A. Saunders and A.E. Sowers (Academic Press, Orlando) pp. 155–166.
108. Heuser, J.E., T.S. Reese, M.J. Dennis, Y. Jan, L. Jan and L. Evans, 1979, Synaptic vesicle exocytosis captured by quick freezing and correlated with quantal transmitter release, *J. Cell Biol.* **81**, 275–300.
109. Dimitrov, D.S., H. Golding and R. Blumenthal, 1991, Initial steps in HIV-1 envelope glycoprotein mediated cell fusion monitored by a new assay based on redistribution of fluorescence markers, *AIDS Res. Human Retrovir.* **7**, 799–805.
110. Dimitrov, D.S., K. Hillman, J. Manischewitz, R. Blumenthal and H. Golding, 1992, Kinetics of interaction of sCD4 with cells expressing HIV-1 envelope and inhibition of syncytia formation, *AIDS* **60**, 249–256.
111. Dimitrov, D.S., R. Willey, M. Martin and R. Blumenthal, 1992, Kinetics of HIV-1 interactions with sCD4 and CD4⁺ cells: Implications for inhibition of virus infection and initial steps of virus entry into cells, *Virology* **187**, 398–4060.
112. Sato, H., J. Ornstein, D. Dimitrov and M. Martin, 1992, Cell-to-cell spread of HIV-1 occurs within minutes and may not involve the participation of virus particles, *Virology* **186**, 712–724.
113. Chernomordik, L.V., G.B. Melikyan and Yu.A. Chizmadzhev, 1987, Biomembrane fusion: A new concept derived from model studies using two interacting planar lipid bilayers, *Biochim. Biophys. Acta* **906**, 309–352.
114. Morris, S.J., D.P. Sarkar, J.M. White and R. Blumenthal, 1989, Kinetics of pH-dependent fusion between 3T3 fibroblasts expressing influenza hemagglutinin and red blood cells, *J. Biol. Chem.* **264**, 3972–3978.
115. Hoekstra, D. and J.W. Kok, 1989, Entry mechanisms of enveloped viruses. Implications for fusion of intracellular membranes, *Biosci. Rep.* **9**, 273–305.

116. Spruce, A.E., A. Iwata, J.M. White and W. Almers, 1989, Patch clamp studies of single cell-fusion events mediated by a viral fusion protein, *Nature* **342**, 555–558.
117. Ohno-Shosaku, T. and Y. Okada, 1985, Electric pulse-induced fusion of mouse lymphoma cells: roles of divalent cations and membrane lipid domains, *J. Membr. Biol.* **85**, 269–280.
118. Dimitrov, D.S. and R. Blumenthal, 1991, Kinetics of intermembrane interactions leading to fusion, in: *Cell and Model Membrane Interactions*, ed. S. Ohki (Plenum Press, New York) pp. 115–133.
119. Sukharev, S.I., I.N. Bandrina, A.I. Barbul, L.I. Fedorova, I.G. Abidor and A.V. Zelenin, 1990, Electrofusion of fibroblasts on the porous membrane, *Biochim. Biophys. Acta* **1034**, 125–131.
120. Blangero, C. and J. Teissie, 1985, Ionic modulation of electrically-induced fusion of mammalian cells, *J. Membr. Biol.* **86**, 247–253.
121. Rols, M.-P. and J. Teissie, 1989, Ionic-strength modulation of electrically induced permeabilization and associated fusion of mammalian cells, *Eur. J. Biochem.* **179**, 109–115.
122. Papahadjopoulos, D., S. Nir and N. Duzgunes, 1990, Molecular mechanisms of calcium-induced membrane fusion, *J. Bioenerg. Biomembr.* **22**, 157–179.
123. Scheludko, A., 1967, *Colloid Chemistry* (North Holland, Amsterdam).
124. Dukhin, S.S., N.N. Rulyov and D.S. Dimitrov, 1986, *Coagulation and Dynamics of Thin Layers* (Naukova Dumka, Kiev).
125. Ivanov, I.B., B.P. Radoev, E. Manev and A. Scheludko, 1970, *Trans. Faraday Soc.* **66**, 1262–1273.
126. Ivanov, I.B. and D.S. Dimitrov, 1974, Hydrodynamics of thin liquid films. Effects of surface viscosity on thinning and rupture of foam films, *Colloid Polym. Sci.* **252**, 982–990.
127. Radoev, B.P., D.S. Dimitrov and I.B. Ivanov, 1974, Hydrodynamics of thin liquid films. Effects of surfactants on the rate of thinning, *Colloid Polym. Sci.* **252**, 50–55.
128. Dimitrov, D.S., I. Panaiotov, P. Richmond and L. Ter-Minassian-Saraga, 1978, Dynamics of insoluble monolayers, I. Dilational or elastic modulus, friction coefficient and Marangoni effect for dipalmitoyllecithin, *J. Colloid Interface Sci.* **65**, 483–494.
129. Panaiotov, I., D.S. Dimitrov and L. Ter-Minassian-Saraga, 1979, Dynamics of insoluble monolayers, II. Viscoelastic behavior and Marangoni effect for mixed protein phospholipid films, *J. Colloid Interface Sci.* **72**, 49–53.
130. Panaiotov, I., D.S. Dimitrov and M. Ivanova, 1979, Influence of bulk-to-surface diffusion interchange on dynamic surface tension excess at uniformly compressed interface, *J. Colloid Interface Sci.* **69**, 318–325.
131. Dimitrov, D.S., I. Panaiotov, Ts. Ivanova and G. Georgiev, 1977, Surface pressure relaxation of dipalmitoyllecithin monolayers, *Ann. Univ. Sofia Fac. Chem.* **72**, 119–130.
132. Derjaguin, B.V. and Yu.V. Gutop, 1962, *Colloid J.* **24**, 431–437.
133. Derjaguin, B.V. and A.V. Prokhorov, 1981, *J. Colloid Interface Sci.* **81**, 108–115.
134. Derjaguin, B.V., 1986, *Stability Theory of Colloids and Thin Films* (Nauka, Moscow).
135. Ivanov, I.B., 1988, *Thin Liquid Films* (Marcel Dekker, New York).
136. Ivanov, I.B. and D.S. Dimitrov, 1988, Thin film drainage, in: *Thin Liquid Films*, ed. I.B. Ivanov (Marcel Dekker, New York).
137. Sackmann, E., 1990, Molecular and global structure and dynamics of membranes and lipid bilayers, *Can. J. Phys.* **68**, 999–1012.
138. Lipowsky, R., 1991, The conformation of membranes, *Nature* **349**, 475–481.
139. Siegel, D.P., 1993, Modeling protein-induced fusion mechanisms: insights from the relative stability of lipidic structures, in: *Viral Fusion Mechanisms*, ed. J. Bentz (CRC Press, Boca Raton, Florida).
140. Dimitrov, D.S., 1981, A hydrodynamic theory of the bilayer membrane formation, *Biophys. J.* **36**, 21–25.
141. Dimitrov, D.S., 1983, Dynamic interactions between approaching surfaces of biological interest, *Prog. Surf. Sci.* **14**, 295–424.
142. Dimitrov, D.S., 1986, Approach and instability of membranes: Physicochemical mechanisms and applications to adhesion, fusion, dielectrophoresis, electroporation and liposome formation, in: *Proc. 8th School Bioph. Membrane Transport*. Mierki. Polland, Vol. 1, pp. 51–82.
143. Song, L., Q.F. Ahkong, G. Georgescauld and J.A. Lucy, 1991, Membrane fusion without cytoplasmic fusion (hemi-fusion) in erythrocytes that are subjected to electrical breakdown, *Biochim. Biophys. Acta* **1065**, 54–62.

144. Ivanov, I.B., D.S. Dimitrov and B.P. Radoev, 1978, Hydrodynamics of thin liquid films. Rate of expansion of the perimeter of the three-phase contact line, *J. Colloid Interface Sci.* **63**, 166–168.
145. Dimitrov, D.S., I.B. Ivanov and T.T. Traykov, 1984, Influence of permeability on the rate of mutual approach of membranes, *J. Membr. Sci.* **17**, 79–87.
146. Kuzmin, P.I., V.F. Pastushenko, I.G. Abidor, S.I. Sukharev, A.I. Barbul and Y.A. Chizmadzhev, 1988, Theoretical analysis of a cell electrofusion mechanism, *Biol. Membrany* **5**, 600–612.
147. Laggner, P., 1988, X-Ray studies on biological membranes using synchrotron radiation, *Top. Current Chem.* **145**, 173–202.
148. Laggner, P. and M. Kriechbaum, 1991, Phospholipid phase transitions: Kinetics and structural mechanisms, *Chem. Phys. Lipids* **57**, 121–145.
149. Tate, M.W., E. Shyamsunder and S.M. Gruner, 1992, Kinetics of the lamellar-inverse hexagonal phase transition determined by time-resolved X-ray diffraction, *Biochemistry* **31**, 1081–1092.
150. Sugar, I.P., W. Forster and E. Neumann, 1987, Model of cell electrofusion: Membrane electroporation, pore coalescence and percolation, *Biophys. Chem.* **26**, 321–335.
151. Kozlov, M.M. and V.S. Markin, 1983, Possible mechanism of membrane fusion, *Biophysics* **28**, 255–261.
152. Dimitrov, D.S. and D.V. Zhelev, 1988, Fluctuation wave mechanism of membrane electrofusion, *Colloid Polym. Sci.* **76**, 26–31.
153. Hui, S.W. and D.A. Stenger, 1992, Effects of intercellular forces on electrofusion, in: *Guide to Electroporation and Electrofusion*, eds D.C. Chang, B.M. Chassy, J.A. Saunders and A.E. Sowers (Academic Press, Orlando) pp. 167–178.
154. Blumenthal, R., 1987, Membrane fusion, *Curr. Top. Membr. Transp.* **29**, 203–254.
155. Blumenthal, R. and D.S. Dimitrov, 1995, Membrane fusion, in: *Handbook of Physiology Section on Cell Physiology*, eds J. F. Hoffman and J. C. Jamieson (Oxford University Press, New York).
156. Sarkar, D.P., S.J. Morris, O. Eidelman, J. Zimmerberg and R. Blumenthal, 1989, Initial stages of influenza hemagglutinin-induced cell fusion monitored simultaneously by two fluorescent events: Cytoplasmic continuity and lipid mixing, *J. Cell Biol.* **109**, 113–122.
157. Chang, D.C. and T.S. Reese, 1990, Changes in membrane structure induced by electroporation as revealed by rapid-freezing electron microscopy, *Biophys. J.* **58**, 1–12.
158. Bartoletti, D.C., G.I. Harrison and J.C. Weaver, 1989, The number of molecules taken up by electroporated cells: quantitative determination, *FEBS Lett.* **256**, 4–10.
159. Hofmann, G.A., 1989, Cells in electric fields. Physical and practical electronic aspects of electro cell fusion and electroporation, in: *Guide to Electroporation and Electrofusion*, eds D.C. Chang, B.M. Chassy, J.A. Saunders and A.E. Sowers (Academic Press, Orlando, FL) pp. 389–407.

This Page Intentionally Left Blank

Cation-Induced Vesicle Fusion Modulated by Polymers and Proteins

K. ARNOLD

*Institute of Medical Physics and Biophysics,
Department of Medicine,
University of Leipzig, Germany*

Contents

1. Introduction	905
2. Cellular and artificial fusion processes – an introduction	906
2.1. Artificial and natural cell-cell fusion	906
2.2. Intracellular fusion	906
2.3. Virus-cell fusion	907
2.4. Vesicle fusion	909
3. Monitoring of vesicle fusion	910
3.1. Mixing of membrane lipids	911
3.2. Intermixing of vesicle content	912
4. Aggregation mechanisms	913
4.1. Cation-induced aggregation	913
4.2. Hydration repulsion	917
4.3. Hydrophobic attraction	920
4.4. Steric forces	921
4.5. Effect of cations and polymers on water layers between membranes	925
5. Fusion of vesicles – facts and models	927
5.1. Cation-induced fusion	927
5.2. Polarity decrease of bilayer surfaces	930
5.3. Modulation of cation-induced fusion by poly(ethylene glycol)	932
5.4. Polyanion-induced fusion	935
5.5. Cation-induced fusion modulated by proteins	937
6. Molecular mechanisms of vesicle fusion processes	940
6.1. Correlation of intramembrane and intermembrane interactions	940
6.2. Role of non-bilayer structures	942
6.3. Hydrophobic point defects	943
6.4. Role of proteins	945
7. Concluding remarks	947
Acknowledgments	948
References	949

1. Introduction

Membrane fusion is an important cell-physiological event that occurs in various intra- and intercellular processes, such as exocytosis, endocytosis, membrane genesis, viral infection, and fertilization. Hundreds of fusion events can occur every minute in a living cell. The diversity of cellular fusion processes could indicate that very different mechanisms are used by the cell to realize the fusion of membranes. This view is also supported by the large number of different cellular components involved in the triggering and temporal and spatial control of fusion. For instance, Ca^{2+} is required for exocytosis processes but it is not necessary for virus-cell fusion where the fusion of some viruses is triggered by low pH. However, the biophysical investigations of membrane fusion processes suggested that some general molecular mechanisms appear in all fusion processes. It will be shown in this chapter that a hydrophobic contact between the fusing membranes has to be created in order to initiate fusion of membranes. Another general requirement for fusion is the occurrence of packing defects among lipid molecules at the point of fusion.

The physical theories of membrane stability are relatively well established. However, a full understanding of membrane fusion processes requires not only a description of membrane stability but particularly of its transient instability. During the fusion event, drastic reorganizations in membrane structure must occur in order to allow the close approach and merging of membranes followed by the reconstitution of a new membrane. Because membranes serve as a relatively impermeable barrier, this function has to be maintained during the fusion process despite the transient destabilization. Therefore, research on membrane fusion is especially challenged to give an explanation of the interplay of membrane integrity and membrane destabilization. It's not surprising that investigations of fusion mechanisms have fertilized the development of theories of membrane stability, e.g., in respect to the role of the hydrophilicity and hydrophobicity of the membrane surface.

Studies of molecular mechanisms of membrane fusion processes have concentrated on areas that are relatively accessible to experimentation. At present virus-cell fusion represents the only example of a biological fusion where the molecular components involved in the fusion event are relatively well known. In an attempt to gain an understanding of the complex processes of cellular and subcellular fusion processes, much biophysical work has been devoted to studies of relatively simple model membranes such as lipid vesicles. As recognized in almost all fields of membrane research, both approaches are necessary for an understanding of the very complex processes of membrane fusion, the study of the fusion of real biological systems as well as of model systems. The last of these efforts is well covered by recent reviews [1–6].

This chapter has its focus on applications of phospholipid vesicles for the elucidation of molecular mechanisms of membrane fusion. Rather than presenting a complete review of work on vesicle fusion, basic biophysical concepts are demonstrated for fusion processes induced by cations, polymers and cation-binding proteins. Biological fusion processes are briefly reviewed to define the components involved in fusion processes. Fluorescence techniques that are frequently used to monitor the fusion are described. Before the fusion of vesicles is discussed, the aggregation of vesicles is considered with emphasis on the realization of a close approach of the membranes, recognized as a requirement for fusion. Some current models of vesicle fusion are discussed in the last sections of this chapter.

2. Cellular and artificial fusion processes – an introduction

The different types of fusion processes have been extensively reviewed [7, 8] and have found entry in textbooks on cell biology. Here the basic phenomena and components involved in these processes will be discussed briefly to emphasize the role of Ca^{2+} and proteins for fusion processes.

2.1. Artificial and natural cell-cell fusion

The early experimental work about fusion was mainly stimulated by the prospects that the development of techniques for the artificial fusion of cells can provide for the study of fundamental cell-biological processes and biotechnology (for a historical review see [9]). It is only about 30 years ago that Barski et al. [10] produced the first hybrid cells, after the occurrence of multinucleated cells have been observed by histologists and pathologists for many years. The next advance was the development of methods for the selection of hybrid cells from the culture medium and the increase of the yield of hybrid cells. Harris and Watkins [11] had found that UV-inactivated hemagglutinating virus of Japan, now called Sendai virus, is able to induce the fusion of cells. The hybrid cells had the property to divide and grow. The technique was considerably refined and improved and contributions to studies in virology and immunology became possible. Kohler and Milstein [12] applied this technique for the production of hybridoma cells. After the fusogenic properties of poly(ethylene glycol) (PEG) had been discovered [13], the Sendai virus was replaced by this more easily prepared fusogen in the hybridoma technique. In recent years, chemical (poly(ethylene glycol)) and physical (electrofusion) induction of cell-cell fusion have been used extensively in modern biotechnology.

Important natural intercellular fusion events include sperm-egg fusion and the formation of multinucleated muscle cells by fusion of myoblasts.

2.2. Intracellular fusion

Intracellular transport processes involve specific fusion processes between intracellular membrane vesicles and with the plasma membrane. Exocytosis is the process in which a stored secretory product (e.g., neurotransmitters, hormones such as insulin,

digestive enzymes) is released from the cell into the extracellular space by fusion of the membrane of the secretory vesicle with the cell membrane. The following stages can be distinguished in an exocytosis reaction [14, 15]: transport of vesicles to the plasma membrane, adhesion of vesicles, semifusion of plasma and vesicle membrane and fusion of membranes accompanied by the mixing of vesicle content with the extracellular medium (fig. 1). Much evidence was accumulated that the increase in intracellular concentration of Ca^{2+} is the intracellular signal for exocytosis in a wide variety of secretory cells. Calcium may enter the cell through voltage-dependent Ca^{2+} channels (e.g., neurotransmitter release in the synaptic terminal) or through receptor-operated Ca^{2+} channels activated by hormones [16–19].

Although the requirement for Ca^{2+} in regulated exocytosis has been well recognized, the molecular mechanisms by which Ca^{2+} acts, remain largely unknown. An involvement of specific proteins in the process can be expected because the single stages of exocytosis have to be correlated in time and location. Several proteins were identified which could take an active part in exocytosis, but their exact function is still unclear (for recent reviews see [20–23]). The cytosolic Ca^{2+} activity is increased from a resting value of $0.1 \mu\text{M}$ to an activated value of $1\text{--}10 \mu\text{M}$. A determination of the actual intracellular concentration is not a trivial matter because of the high buffering capacity in cells and the possibility that highly localized increases of Ca^{2+} can induce fusion. A study on depolarized chromaffin cells estimated, that the Ca^{2+} entry into the cytosolic space can reach up to $340 \mu\text{M}$ in one second during a short depolarization [24]. The micromolar Ca^{2+} sensitivity indicates that high-affinity Ca^{2+} -binding proteins might mediate the trigger effect of Ca^{2+} . The finding that intracellular calcium concentration microdomains of the order of 200 to $300 \mu\text{M}$ occur against the cytoplasmic surface of the plasmalemma during neurotransmitter secretion supported the view that low affinity calcium-binding sites are activated at the active zone [25].

Endocytosis is the process of internalization of soluble (pinocytosis) or particulate (phagocytosis) substances from the extracellular environment. This process starts with the invagination of the plasma membrane and is finished with the formation of an endocytotic vesicle. The last stage of the process is the fusion of the invaginated plasma membrane with itself (fig. 1). The receptor-mediated endocytosis is a special endocytotic pathway. Various viruses (e.g., influenza virus) and serum lipoproteins enter the cell on this way. Relatively little is known about the molecular mechanisms of the fusion processes in endocytosis [20]. It has to be assumed that this process requires metabolic energy.

Within a cell numerous fusion events occur mediating the flow of cellular components between different cell organelles. These include fusion of early endocytotic vesicles and fusion of vesicles transporting materials from endoplasmic reticulum to Golgi apparatus, between Golgi stacks, and from endosomes to Golgi apparatus. It appears that many distinct proteins either membrane-associated or solved in the cytoplasm are involved in each intracellular fusion event [20, 26–28].

2.3. Virus-cell fusion

An example of biological membrane fusion in which the role of proteins is well established is given by the interaction of enveloped viruses with their host cells [29].

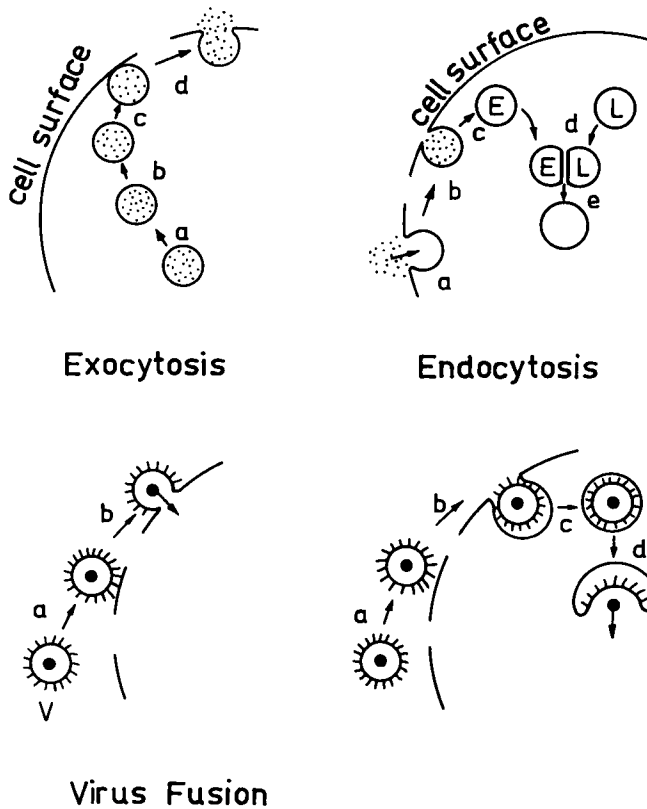


Fig. 1. Schematic drawing of the morphology and sequence of reactions of exocytosis, endocytosis and viral fusion. Different reactions are shown as follows: Exocytosis: (a, b) approach of an exocytosis vesicle, (c) triggering of adhesion, (d) fusion of vesicle and plasma membrane and discharge of vesicle content. Endocytosis: (a) Invagination of the plasma membrane, (b) fusion of the invaginated plasma membrane with itself and (c) motion of the endocytotic vacuole. Another fusion reaction can follow such as the fusion of endocytotic vacuole (E) with a lysosome (L) (d, e). Virus fusion: The direct fusion of an enveloped virus with the plasma membrane is given in the left part. The binding of the virus on the cell surface (a) is followed by the fusion of the virus envelope with the membrane (b) delivering the genome into the cytosol of host cells. In the receptor-mediated endocytosis (a-c) of virus (right part) the virus envelope fuses with the limiting membrane of the endocytotic vacuole (endosome) (d).

Animal viruses consist of a membrane or envelope which surrounds the nucleocapsid. The lipids of the envelope bilayer are derived from the plasma membrane of the host cell. Glycoproteins are incorporated in the envelope. For most viruses the protein composition of the envelope is very simple as it contains only a few proteins which are well characterized. Thus virus fusion provides a good model system to study the molecular mechanisms of protein function in membrane fusion (recent reviews: [2, 20, 28, 30]).

Fusion of the viral membrane with a cellular target membrane represents the key event in the infectious entry of the genetic material of the given virus in the cell. There are two classes of viruses in respect to the entry mechanism. Viruses with low pH-dependent activity (e.g., influenza virus, vesicular stomatitis virus) fuse with the membrane of acidic endosomes after their uptake by receptor-mediated endocytosis (fig. 1). Viruses with pH-independent activity fuse with the plasma membrane, e.g., Sendai virus, HIV (fig. 1). The pH dependence of virus fusion is a property of the viral fusion protein. The hemagglutinin of influenza virus is the best characterized fusion protein and models of the pH-dependent conformational change and penetration of a hydrophobic segment of hemagglutinin in the target membrane were given [20, 29, 30]. Synthetic peptides have been synthesized that mimic fusion regions of the viral protein and their interaction with liposomes and cells was studied [30, 31–34].

2.4. Vesicle fusion

The discussion of the natural fusion processes has shown, that the elucidation of the molecular mechanisms of membrane fusion cannot be restricted to the action of a few membrane components. Moreover, only some specific molecular components were identified to be involved in fusion processes. This specificity can result from phospholipids, glycolipids, cholesterol, membrane proteins, cytosolic proteins, metal ions such as Ca^{2+} , metabolic processes and components of the cytoskeleton. Another source of specificity is the trigger mechanism. Except the already mentioned increase of intracellular Ca^{2+} and H^+ other triggers such as changes of osmotic pressure, synthesis of unsaturated fatty acids, alterations of specific phospholipids such as phosphatidylinositol and specific proteins were discussed. The complexity of this problem requires the use of model systems which allow the separate investigation of single parts of the 'fusion machinery'.

Phospholipid vesicles and planar bilayer membranes (BLM) are the most simple model systems. Much of our current knowledge on molecular mechanisms has been obtained from studies on phospholipid vesicles. These systems have the advantage that the properties can be manipulated in a wide range (phospholipid composition, electrolyte composition, pH, incorporation of fusion effectors, size of vesicles, fluidity, nonbilayer structures). The recent success in efficiently reconstituting fusogenic proteins such as hemagglutinin of influenza virus in vesicle systems (called virosomes) shows that vesicles may serve as a valuable fundamental model for characterizing protein-membrane interactions that may lead to fusion. The potential role of calcium ions and changes in pH as triggers of membrane fusion and the modulatory role of phospholipid head groups and soluble proteins have been investigated in vesicle systems.

However, fusion requirements for vesicles are often far from those observed for biological fusion. For example, Ca^{2+} -induced fusion of vesicles occurs at much higher calcium concentrations compared with the fusion behaviour of secretory vesicles. Other limitations are (i) the lack of recognition molecules, if phospholipid vesicles are used in the simplest form and (ii) lack of postfusion stability [27]. Biological fusion processes underlay a control which removes the stimulus to fusion

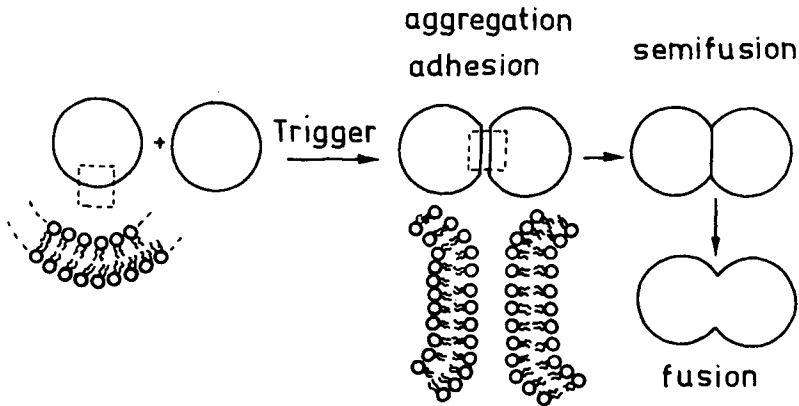


Fig. 2. Fusion reaction of two phospholipid vesicles. The first step is the aggregation and adhesion of the vesicles and the second the fusion of bilayers. In some systems, the aggregation/adhesion is followed by the semifusion (formation of one bilayer) before complete fusion with intermixing of vesicle contents occurs.

after the membrane fusion is completed. In vesicle systems the stimulus continues to act on the vesicles after their fusion until the system reaches the final state which can considerably deviate from the state of fused vesicles. For example stacked bilayers and cochleate structures are formed in the Ca^{2+} -induced fusion of acidic vesicles, or the vesicles are transformed to the hexagonal phase [35].

It was found that the following stages occur in a fusion reaction of vesicles (fig. 2): aggregation of vesicles, molecular contact of bilayers, local destabilization of bilayers at the site of contact and intermixing of vesicle contents. Mixing of lipids of the outer monolayers can occur in the region of bilayer contact before the complete fusion, accompanied by the mixing of vesicle contents, appears. A process where the destabilization results in the formation of one bilayer between the two vesicles, causing intermixing of membrane lipids without intermixing of vesicle contents, was considered as semifusion [1].

3. Monitoring of vesicle fusion

As can be seen from figs 1 and 2 membrane fusion reactions are very complex processes. It is necessary to introduce criteria which must be met to assure that a real membrane fusion has occurred. For example, mixing of membrane components or increase in vesicle size may be the result of membrane fusion, but can also result from the exchange of membrane components between apposing membranes. It was found that the following three criteria are sufficient to define a vesicle fusion: (i) merging of membranes, (ii) intermixing of vesicle contents, and (iii) maintaining of the barrier function of membranes [27, 36]. In most vesicle fusion processes an increase in the vesicle permeability is observed due to postfusion instability as

discussed before. In respect to the requirements of the fusion criteria it is important that the leakage occurs after the merging of lipids and intermixing of the aqueous contents of vesicles, even when the time delay between these processes is very short.

In principle, many biophysical methods developed for studies of physical and morphological properties of membranes can be used to detect fusion processes. Light scattering, electron microscopy, DSC, NMR and ESR spectroscopy and fluorescence techniques have been applied. Fluorescence methods provide the advantage of high sensitivity and time resolution. A certain disadvantage results from the use of probe molecules. The application of fluorescence methods in respect to the requirements of the fusion criteria was critically reviewed [36–38].

3.1. *Mixing of membrane lipids*

Lipid mixing has been measured by monitoring the concentration-dependent properties of membrane-associated probes, usually a fluorescence probe [39, 40]. Such probes should meet the following requirements: (i) slow or almost no interchange between membranes in the absence of fusion, (ii) low perturbation of membrane packing and structure and the probes should be present at sufficiently low surface density, (iii) the fusogenic agent should not directly change the fluorescence properties and (iv) high quantum yield of fluorescence. The head-group-labeled N-(7-nitro-2,1,3-benzoxadiazol-4-yl) phosphatidylethanolamine (NBD-PE) and N-(lissamine rhodamine B sulfonyl) phosphatidylethanolamine (Rh-PE) meet many of these requirements. The use of these probes for the monitoring of the mixing of lipids is based on resonance energy transfer between NBD as energy donor group and Rh as energy acceptor group. Since resonance energy transfer depends on the proximity of the donor and acceptor group, the change in surface concentration of the probes during membrane fusion can be detected as a change of fluorescence intensities [41].

The lipid mixing assay based on resonance energy transfer can be used in two versions. In the probe dilution assay both probes are incorporated in one population of vesicles and their dilution into a population of unlabeled vesicles is monitored as a change in resonance energy transfer resulting in an increase of NBD fluorescence and decrease of Rh fluorescence (fig. 3). In a similar manner other concentration-dependent fluorescence properties can be used. The fluorescence of Octadecyl-rhodamine-B-chlorid (R_{18}) incorporated in one vesicle population at a self-quenching surface concentration increases as the probe is diluted in unlabeled vesicles [40]. The ratio of the excimer/monomer fluorescence of pyrene-labeled phospholipids is decreased after dilution [42]. The sensitivity of fluorescence lifetimes of fluorescence probes was also used [43].

In the other version of the lipid mixing assay based on resonance energy transfer each probe is incorporated in a separate population of vesicles (Probe mixing assay). The decrease of the donor fluorescence or the increase of the acceptor fluorescence is monitored [44]. Both fluorescence assays can provide the extent and the kinetics of fusion quantitatively, provided that the changes of the resonance energy transfer occur only due to fusion. In the probe dilution assay, the fluorescence-labeled vesicles are usually prepared with 0.6 mol% each of NBD-PE and Rh-PE in the bilayer and

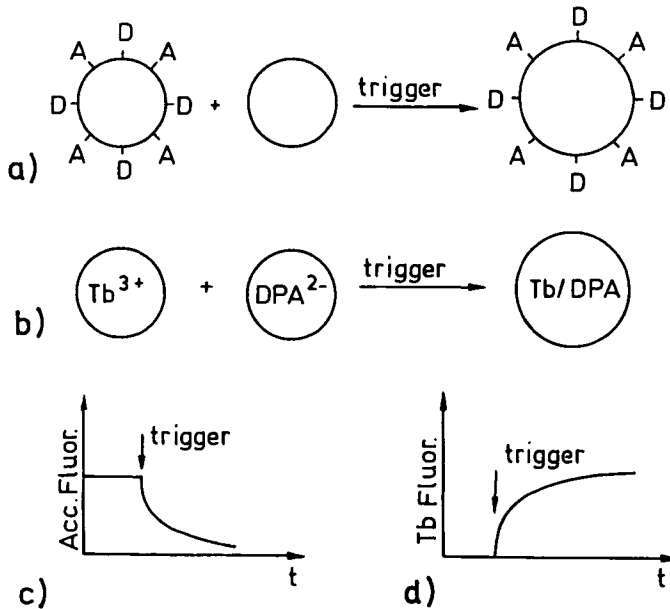


Fig. 3. Schematic representation of fluorescence fusion assays described in the text. (a) Resonance energy transfer assay for mixing of bilayer lipids and (b) assay for mixing of internal contents. D and A denote donor and acceptor fluorescence molecules. The time courses of the acceptor fluorescence in the probe dilution assay and of the Tb fluorescence in the internal content mixing assay are given in (c) and d), respectively.

labeled and unlabeled vesicles are mixed at a ratio of 1:1. Complete fusion would be expected to result in a bilayer containing 0.3 mol% each of the fluorescent probes. The fluorescence intensity of such vesicles is related to a fusion extent of 100%. The fluorescence intensity of the initial state of vesicles is taken as the zero level of fusion.

3.2. Intermixing of vesicle content

The most adequate assays of membrane fusion are those monitoring the intermixing of aqueous contents. A fluorescence assay based on complex formation between dipicolinic acid (DPA) and Tb^{3+} has been used extensively [45]. Each one of the pair of reactants is encapsulated in different populations of vesicles (fig. 3). To prevent the binding of Tb^{3+} to negatively charged phospholipids, a weak chelator is additionally entrapped, usually citrate. The fluorescence intensity of Tb^{3+} complexed with DPA is increased by four orders of magnitude.

In order to detect the intermixing of vesicle contents only, the reactions resulting from vesicle leakage are quenched by EDTA and Ca^{2+} which are added to the medium outside the vesicles. 100% maximal fluorescence in the fusion experiment indicates the fluorescence that would be obtained if all the encapsulated Tb were to

react with DPA. Under certain circumstances this value can be determined from the fluorescence obtained upon lysis of the vesicles with detergent. With a modification of the Tb/DPA assay the kinetics of the release of vesicle contents can be measured [46].

In a similar manner as described for the reactions of fluorophores, enzymatic reactions were used to monitor the intermixing of vesicle contents. Enzymes and substrate molecules are entrapped in different populations of vesicles and an inhibitor is solved in the external medium. Enzymatic activities were also used to measure the fusion of intracellular organelles, exocytosis processes and the fusion of phospholipid vesicles with cells.

4. Aggregation mechanisms

4.1. Cation-induced aggregation

4.1.1. DLVO-theory

The aggregation behaviour of colloidal particles can be adequately described by the DLVO (Derjaguin–Landau–Verwey–Overbeek) theory [47, 48]. In this theory the total free energy is considered to consist of the sum of the repulsive electric double layer energy and the attractive Van der Waals energy.

Considering the free energy of interaction between two planar parallel surfaces, the rate of decay with distance d of the Van der Waals interaction energy per unit area may be expressed as

$$F \simeq - \frac{H}{12\pi d^2} \quad (1)$$

where H is the Hamaker constant of the membrane for intermediate separations d which are of the order of the membrane thickness. Usually the Hamaker constants of biological membranes are higher compared to those of bilayer membranes due to the presence of proteins.

The electrostatic interaction energy is difficult to evaluate. However, the following approximation formula for low surface potentials and larger separations can be used (linear approximation)

$$F = F_0 \exp(-\kappa d) \quad (2)$$

where the Debye length $1/\kappa$ is a measure of the effective thickness of the diffuse double layer. F_0 and κ are functions of the surface charge density and the electrolyte composition. At higher surface potentials and smaller separations, numerical calculations of the Poisson–Boltzmann equation are necessary to obtain the exact interaction energy. More extended considerations were given [47, 77].

The total free energy is then used to predict the aggregation behaviour. Due to the combination of an attractive and repulsive force, that energy can usually have a local minimum as a function of surface separation (fig. 4). The energy minimum

at contact is known as the primary minimum. In more concentrated electrolyte solutions a secondary minimum with free energy F' , separated by an energy barrier F^* from the primary minimum, can occur. As the surface potential or surface charge approaches zero the particles experience only the Van der Waals interaction and attract each other at all positions. However, at short distances of bilayer separation this attraction is prevented by additional repulsive interactions of short range (e.g., hydration repulsion), not involved in the DLVO theory (see below).

The depth of the secondary energy minimum F' determines the stability of the membrane suspension. Stable aggregates will be only formed if $F'/kT \gg 1$. It was shown by direct measurements of forces between charged bilayers that beyond 3 nm separation the forces are in good agreement with the predictions of the DLVO theory, especially in relation to the influence of electrolyte composition, pH and surface charge.

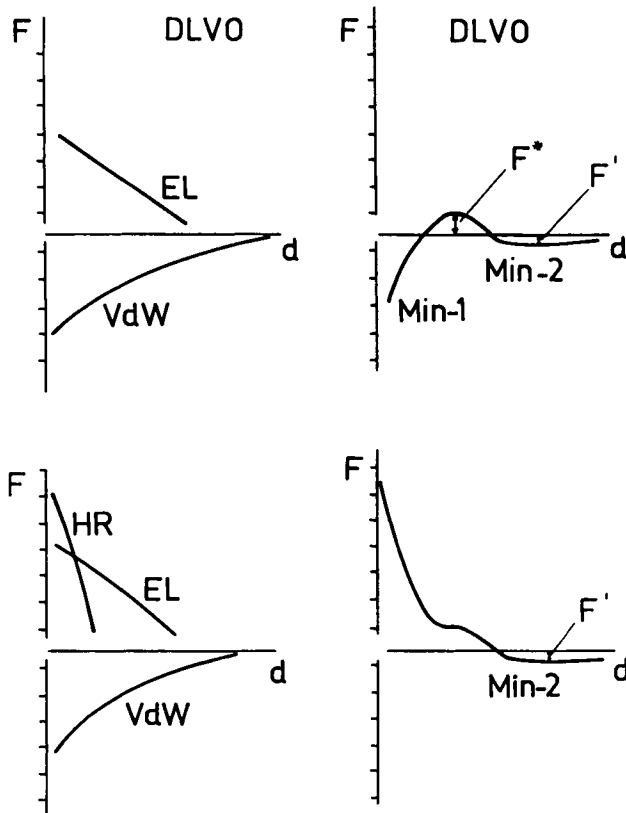


Fig. 4. Free energy F of two lipid bilayers as a function of membrane separation d (F on a logarithmic scale) for a vesicle suspension, involving electrostatic (EL), Lifshitz–Van der Waals (VdW) and hydration repulsion (HR) interaction. The classical DLVO plot with the primary minimum (Min-1) of attraction, the maximum of repulsion (F^*) and the secondary minimum (Min-2) of attraction F' is given on the right side (above). The combination of the hydration repulsion, the EL repulsion and VdW attraction is given below (adapted from Van Oss [210]).

4.1.2. Kinetics of aggregation

Studies on cation-induced fusion of acidic vesicles have shown that the kinetics of the process can be modeled as a two-step process involving aggregation followed by the fusion step [49, 50]



It is assumed that the aggregation products V_2 are dimers which are formed from vesicles V_1 with a rate constant C_{11} . The dimers can dissociate (rate constant D_{11}) or fuse (rate constant f_{11}). The slower of the two steps becomes rate-limiting. The kinetic analysis of fusion has proved to be extremely important in defining the role of specific components. It is essential to determine whether a component is effective in the step promoting aggregation or fusion. Some systems can be manipulated by changing external conditions that either aggregation or fusion controls the overall rate of the reaction. In accordance with the DLVO theory the rate constant C_{11} is a function of the energy barrier F^* [48]:

$$C_{11} = 8kTN_A 10^{-3} \exp[-F^*/kT]/3\eta. \quad (4)$$

C_{11} is the rate constant introduced by Verwey and Overbeek (the expressions are different by a factor 2) and η is the dynamic viscosity. N_A is Avogadro's number. The description of the time course of Ca^{2+} -induced fusion of small unilamellar PS vesicles by a mass action model has indicated that aggregation is the rate-limiting step [49, 50]. Calculations of the energy barrier from eq. 4 using experimental rate constants of aggregation give values of F^* in the order of 1–10 kT [50]. These values are much lower than those expected from DLVO theory in the presence of fusogenic cation concentrations. The inclusion of repulsive hydration forces in the calculations would further increase the energy barrier. One has to assume that in addition to the effect of charge neutralization structural changes of approaching bilayers (e.g., deformations, instabilities and formation of spikes) and cation bridges lower the energy barrier [50, 51]. This point will be discussed later.

4.1.3. Properties of cation-induced vesicle aggregation

In contrast to fusion, the aggregation can be a reversible process after the triggers are removed. In addition to the forces between vesicles, the aggregation is influenced by the vesicle concentration.

The electrostatic repulsion is very sensitive to the electrolyte composition and diminishes at higher monovalent concentrations. Aggregation of negatively charged vesicles was observed at high concentrations of monovalent cations [52, 53]. The binding of monovalent cations to the phospholipid head group, resulting in a partial compensation of the head group charge, contributes to the reduction of the electrostatic repulsion besides the screening effect. The ability of monovalent cations to fuse vesicles is very low compared to divalent cations. Only very recently lipid mixing was reported to occur for small unilamellar vesicles consisting of acidic phospholipids with fully saturated fatty acids [54]. Divalent cations are very effective

in reducing the repulsion, mainly by direct binding to the phospholipid headgroup. Slow aggregation processes are observed at submillimolar concentrations of divalent cations due to the formation of intervesicular salt linkages [55]. Fast aggregation of negatively charged vesicles on a time scale of seconds occurs at millimolar concentrations of divalent cations, e.g., 1–2 mM Ca^{2+} and 4–5 mM Mg^{2+} for small unilamellar PS vesicles in 100 mM NaCl and pH 7.4. Larger cation concentrations are required for aggregation of large unilamellar PS vesicles because the electrostatic repulsion energy is approximately proportional to the vesicle diameter. The rate constants were about the same when the medium contained 2 mM and 5 mM Ca^{2+} with small and large unilamellar PS vesicles, respectively.

Figure 5 shows the PS vesicle aggregation induced by trivalent (La^{3+}), divalent (Ca^{2+}) and monovalent (Na^+ , H^+) cations and polyamines (spermine $^{4+}$, spermidine $^{3+}$, putrescine $^{2+}$). It was found that the threshold concentrations of cations for aggregation are well correlated with the surface potentials determined from measurements of electrophoretic mobilities. At the points of aggregation the surface potentials are reduced from about -83 mV in the absence of cations to about -40 mV [52, 56]. Because of the differences in binding affinities of divalent cations the threshold concentrations for aggregation increase in the sequence $\text{Mn}^{2+} < \text{Ba}^{2+} < \text{Ca}^{2+} < \text{Sr}^{2+} < \text{Mg}^{2+}$ [52]. At high monovalent salt concentrations Ca^{2+} is more effective than Ba^{2+} . The reductions of surface potentials as a function of mono- and divalent cations are rather well described by the Gouy–Chapman–Stern theory by explicitly considering the different binding affinities of cations.

From the above results, it is likely that the membrane surface potential has a good correlation with the extent of vesicle aggregation. However, one would not expect that close aggregation necessary for fusion can occur at surface potentials in the order of -40 mV, because of the relatively high electrostatic repulsion. For

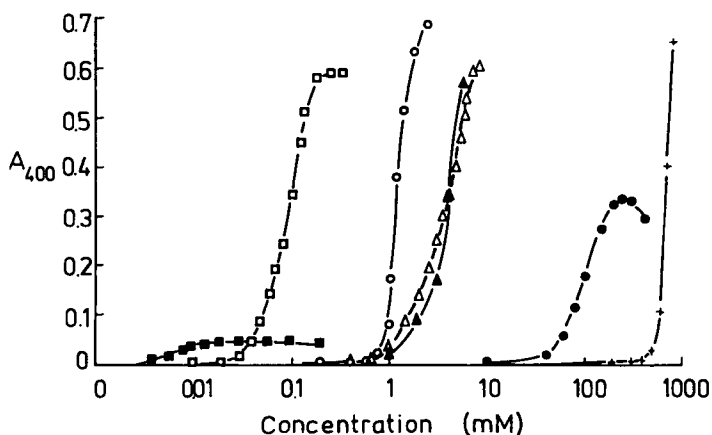


Fig. 5. Turbidity of small unilamellar PS vesicles suspended in 0.1 M NaCl buffer solution, pH 7.4 ($0.1 \mu\text{moles lipid/ml}$ except for La^{3+} $0.01 \mu\text{moles lipid/ml}$) as a function of concentration of La^{3+} (■), spermine $^{4+}$ (□), Ca^{2+} (○), spermidine $^{3+}$ (Δ), H^+ (▲), putrescine $^{2+}$ (●) and Na^+ (+). (Data taken from refs [56, 73].)

fusogenic cations, such as Tb^{3+} , La^{3+} , Mn^{2+} , Ca^{2+} and H^+ vesicle fusion occurs when the surface potential is reduced to approximately -40 mV. For non-fusogenic cations (e.g., Na^+ , K^+ and partly Mg^{2+}) and polyamines the vesicle fusion is not observed even when the concentrations of ions are increased far beyond the threshold concentration for aggregation and the surface potentials become lower in magnitude than -40 mV. The discrepancy results from the fact that the surface potentials were measured under conditions of isolated surfaces instead of aggregated surfaces. It was shown that PS bilayers undergoing aggregation and fusion exhibit an enhanced binding affinity for fusogenic cations such as Ca^{2+} [57–59]. An intermembrane $\text{Ca}(\text{PS})_2$ complex is formed between interacting bilayers. This complex reduces the surface potentials, and, in addition changes the hydration properties of the PS surfaces resulting in a dehydrated space between the bilayers (see below). This effect contributes to the decrease of the energy barrier F^* which increases the rate constant of aggregation, see eq. (4) above. It seems that vesicle fusion is determined by the mode of binding of cations in the aggregated state.

Unlike Ca^{2+} , PS large unilamellar vesicles cannot be fused by Mg^{2+} , although the vesicles aggregate [60]. This specificity of Ca^{2+} over Mg^{2+} probably arises during the approach of the bilayers. It was found that Mg^{2+} is not able to form unhydrated interbilayer complexes.

4.2. Hydration repulsion

The close approach of membranes below 3 nm is ruled by a complex interplay of repulsive and attractive forces of short range. As discussed by Parsegian and Rand (this volume and references given there) a repulsive hydration force presumably results from the strong binding of water to hydrophilic groups of membrane surfaces. The range of the hydration forces determined from measurements of lipid bilayers is about 1–3 nm. With decreasing separation the interaction energy grows exponentially with a characteristic decay length of 0.08–0.64 nm [61].

$$F = +F_0 \exp(-d/\lambda) \quad (5)$$

where λ is the decay length of the interaction energy. Higher decay lengths may occur at high ionic strength. The hydration repulsion dominates the interaction of bilayer membranes at separations less than about 3 nm. As bilayers approach contact, repulsive pressures can increase to the order of 1000 atm. That shows that the hydration repulsion is an enormous barrier to approaching bilayers and prevents the coalescence in the primary minimum. For example, the work E required to bring two small unilamellar vesicles (diameter 300 Å) to within a separation of 13 Å has been estimated to be of the order of $10 kT$, corresponding to a statistical weight, $\exp(-E/kT) \sim 10^{-4}$ [62].

Figure 4 is a plot of bilayer interaction energies with the consideration of electric double layer repulsion, Van der Waals attraction and hydration repulsion. The exponentially decaying hydration repulsion is followed by a more gradual electrostatic repulsion, followed by the Van der Waals attraction. A secondary minimum may appear at a separation of about 5 nm depending on the electrostatic repulsion. A region

of weak attraction was found at 5 nm and 6 nm for DOPE and DOPC, respectively, deposited on mica using a surface forces apparatus [63]. As already discussed above a stable contact between bilayers will be achieved if the energy of the secondary minimum is deep enough ($F' \gg kT$). For the estimation of this energy one has to take into consideration that the energy of this minimum, i.e. the energy of attraction is less than the Van der Waals attraction at this separation.

Because of the relatively low Van der Waals attraction of membranes, aggregation can only occur if a large contact area can be provided. The stacks of bilayers in a multilayer vesicle represent such a system. Experiments have confirmed that these vesicles take up a definite volume of water forming a water layer of definite thickness between bilayers. With decreasing surface charge, the bilayer separation is shifted to shorter values [64]. For uncharged multilayer vesicles prepared from PC a distance of about 2.5 nm was measured [62]. Because of the smaller area of contact stable aggregates are not formed for small vesicles.

The magnitude of the hydration repulsion at a given distance varies among lipid species over more than one order of magnitude. It is influenced by head group, chain composition and temperature [65]. The hydration repulsion of PE is much smaller than the repulsion of PC, and the gel phase has a reduced repulsion compared to the liquid crystalline state. As discussed below, the vesicle-vesicle fusion is strongly related to the hydration repulsion. In the presence of PE in phospholipid vesicles, fusion is promoted.

The origins of hydration repulsion between bilayer membranes are yet unclear [66]. There are indications for both directions of interpretation, the correlation to the orientation of water as well as to the thermal fluctuations of the liquid-like surface (steric force). The term polar repulsion is used by Van Oss to characterize the short range repulsion between surfaces in water [67]. He has developed a semiquantitative description of these forces involving data of the polar properties of the surface, such as surface and interfacial tensions. Because in fusion processes repulsive forces have to be overcome, probably by changes of the surface properties, this description could adequately take into consideration the primary surface changes.

It was found that surfaces of many water-soluble polymers (poly(ethylene glycol), polysaccharides), proteins, nucleic acids, phospholipid bilayers and cells are very strong proton acceptors (strong electron donors in the Lewis acid-base interaction) and weak proton donors due to the existence of proton acceptor groups on these surfaces (e.g., $-\text{COO}^-$, $-\text{OPO}_2\text{O}^-$, $-\text{O}-$, $-\text{SO}_3^-$, $-\text{SO}_4^-$). Such surfaces were termed as negatively monopolar by Van Oss [67–71]. Positively monopolar are surfaces with strong proton donor properties resulting from groups such as $-\text{NH}_3^+$. By means of contact angle measurements with different polar and apolar liquids the monopolarity can be determined for any given system [67].

The water molecules of hydration are bound to negatively monopolar surfaces with hydrogen atoms pointing to the proton acceptor group. This property is mediated to the next layers of water and it decreases in layers which are more distant from the surface. The water molecules are bound to a positively monopolar surface with lone pairs of electrons directed to the surface. As shown by Van Oss the interaction of

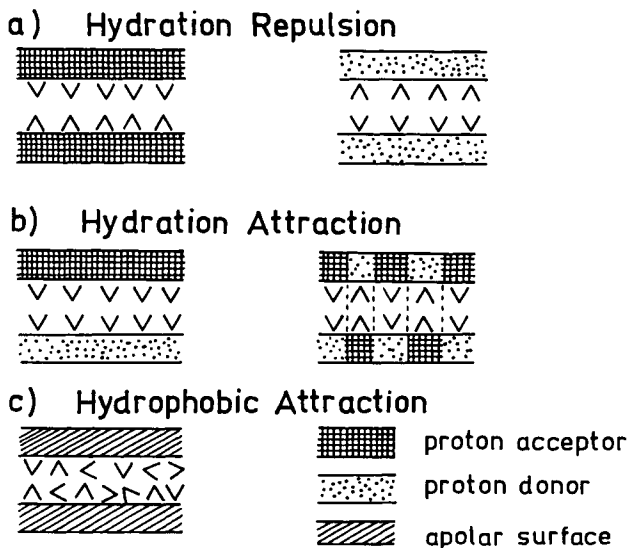


Fig. 6. (a) Hydration repulsion and (b) hydration attraction between polar surfaces, each of which is characterized by proton acceptor or proton donor properties or a combination of both. (c) Hydrophobic attraction between apolar surfaces. The polarization of water molecules immediately at the surface is schematically indicated.

monopolar surfaces of identical monopolarity results in a strong hydration repulsion. This is schematically illustrated in fig. 6a.

Most interestingly, hydration attraction can appear for surfaces of opposite monopolarity (fig. 6b). These surfaces bind water in opposite directions. Rand et al. [65] have used an idea, similar to this model of hydration attraction, to explain the reduced repulsion of PE bilayers compared to PC bilayers. Different to PC the PE head group bears polar groups of opposite monopolarity (phosphate, amine). If the amine and phosphate groups are sitting on opposite surfaces in complementary positions, an attraction could result (fig. 6b). Because the groups are in thermal motion, configurations of opposite groups of repulsive as well as attractive nature could occur. However, the resulting interaction could be less repulsive.

Very recently it was shown that Ca^{2+} very strongly reduces the proton acceptor capacity or monopolarity of the phospholipid bilayer surface [68]. The reduction of the monopolarity simultaneously changes the mode of hydration of the surface. In other words, Ca^{2+} increases the hydrophobicity of the surface. It is one of the most important properties of polar interactions that the magnitude and sign of the forces can be strongly influenced by small changes of surface properties, such as the binding of Ca^{2+} . Beside the effect of Ca^{2+} binding on the electrostatic repulsion discussed before, the reduction of the hydrophilicity of the surface is very important for the close approach of membranes and results in the formation of the interbilayer complexes.

4.3. Hydrophobic attraction

It had long been suspected that other attractive forces in addition to Van der Waals attraction could play a role in surface interaction. Recent studies have increasingly implicated the hydrophobic interaction in the fusion of membranes [72–76]. The hydrophobic interaction is the attractive counterpart to the hydration repulsion. A hydrophobic surface is different from a polar surface in the sense that it cannot bind water via ionic or hydrogen bonds (fig. 6c). Van der Waals attraction still exists between water and a hydrophobic surface.

Similar to the hydrophobic attraction of molecules in water, the hydrophobic attraction of surfaces results from the entropically unfavourable orientation of water at hydrophobic surfaces [77]. The hydrophobic attraction of surfaces tends to be much stronger than the Van der Waals attraction. This was concluded from measurements of the interaction of mica surfaces coated with surfactant monolayers exposing the hydrocarbon groups to the water phase [78]. These studies have found that the force is of long range, decaying exponentially with a characteristic length of 1–2 nm in the range 0–10 nm followed by a more gradual decay beyond 10 nm [77]. Thus the hydrophobic interaction energy can be described by the empirical law

$$F = -2\gamma \exp(-d/\lambda') \quad (6)$$

for surface separations d in the range 0–10 nm, where λ' is the corresponding decay length. The attractive energy is proportional to the interfacial tension γ of the surface with water. As expected the interaction energy increases with increasing hydrophobicity. Typical values for saturated hydrocarbons are about 50 mJm⁻². Other expressions, including polar components of the interfacial tension, were given by Van Oss et al. [69].

For unstressed phospholipid bilayers the attraction seems to be well described by the Van der Waals interaction. However, the attraction becomes stronger and longer ranged compared to the Van der Waals attraction, as the bilayers are stressed or the temperature is increased. Stress of the bilayers can expose parts of the hydrophobic chains to the water. Osmotic stress or high curvature of membranes were recognized to promote fusion processes. The interaction of a hydrophobic region of a membrane (e.g., hydrophobic segment of a fusion protein) with a target membrane bilayer is thought to destabilize the target membrane and increase the hydrophobicity of the membrane surface [33]. These regions of membranes coalesce to form a single membrane.

The hydration repulsion and hydrophobic attraction are interdependent and therefore not additive, because both arise from the structure of water (provided that the hydration repulsion of phospholipid bilayers does not exclusively arise from thermal fluctuations). When both, polar and hydrophobic groups are present on a surface, the resulting interaction is not necessarily the sum of the separate components [77]. That could explain why a very small increase of the bilayer area can enhance attraction remarkably [79].

4.4. Steric forces

Steric stabilization is a term that was used to explain the phenomenon of stabilization of hydrophobic particles in water by means of adsorption or covalent attachment of polar polymers. Napper [80] has provided a very extensive discussion of the theoretical concepts of this field. Macromolecular structures at cell surfaces have a great impact on cell-cell interactions, e.g., the erythrocytes are stabilized by the glycocalyx surface layer in suspension. During the approach of another surface, complex rearrangements and interactions of the surface layer take place resulting in repulsion as well as attraction dependent on the properties of the layer and the solution.

It has been reported that several water-soluble polymers are able to induce the aggregation and fusion of cells and phospholipid vesicles (for a recent review [81]). These effects of solvated polymers are strongly dependent on the mode of interaction of the polymer with the surface. Therefore, mainly the molecular mechanisms of the adsorption or exclusion processes of polymers are to be discussed. After this, mechanisms of the aggregation process can be derived from the knowledge of polymer adsorption. In fusion processes induced by both charged and uncharged polymers, membranes are brought into close contact by quite different interactions of polymers with surfaces [81]. Such studies could also contribute to the understanding of the mechanisms of protein-induced fusion.

Different possibilities of polymer-surface interaction are shown in fig. 7. Steric repulsion and attraction (fig. 7b), bridging attraction (fig. 7b) and depletion attraction (fig. 7c) will be discussed in the following.

4.4.1. Steric repulsion

The adsorption or covalent attachment of polar polymers in such a manner that the polymer chains extend into the aqueous phase leads to a repulsion of surfaces due

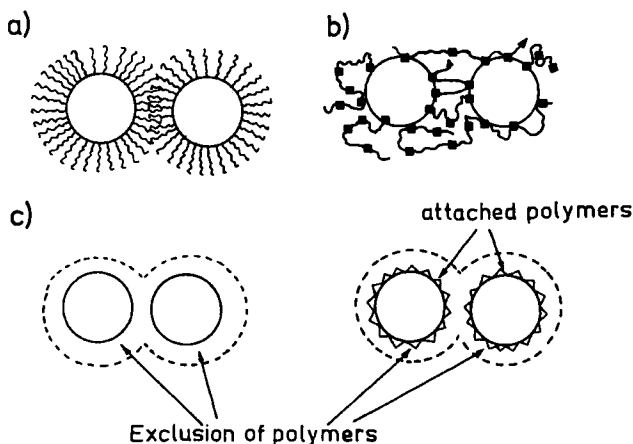


Fig. 7. (a) Polymer-induced steric repulsion, (b) bridging attraction and (c) depletion attraction of lipid vesicles (see text for explanations).

to steric hindrance, changes in the conformational entropy and excluded volume effects [80]. For charged polymers an additional contribution results from the electrostatic repulsion. The interaction energy of layers of polymer molecules may be approximated as [77].

$$F(d) = 36\Gamma kT \exp(-d/R_g) \quad (7)$$

where R_g denotes the unperturbed radius of gyration of the polymer molecule and Γ is the number of chains per unit area. As an example, if the segment length is 1.0 nm, the segment molecular weight is 200 and the polymer molecular weight is 10^6 , then $R_g \simeq 29$ nm is obtained. Equation (7) was derived for low surface coverage. At high coverage the adsorbed polymer chains are so close to each other that they must extend away from the surface much farther than R_g . The range of the repulsive force is then many times R_g . In the case of grafted polymers, the shape of the surface layer becomes brushlike.

More recently the importance of polar (hydration) repulsion between the polymer layers was realized as a mechanism of steric repulsion [71, 82, 83]. A strong repulsion was reported between solid surfaces coated with polyoxyethylene-containing surfactants or poly(ethylene glycol) using the surfaces force apparatus [84, 85] and X-ray diffraction studies of multilayer vesicles [86]. It was shown that poly(ethylene glycol) molecules experience a very strong repulsion in water due to the action of the hydration force [81, 82].

However, it should be emphasized that the repulsive effect of attached polymers can only occur if the polymers have a high solubility in the medium in which the cells or vesicles are suspended. In poor solvents segments of polymer can attract each other due to Van der Waals interaction. If two polymer-coated surfaces approach under these conditions the attraction between the outermost segments of layers results in a surface attraction. On further approach repulsion occurs due to the steric overlapping of polymer segments. Aggregates which were formed by the segment-segment attraction cannot lead to the close surface contact necessary for fusion.

4.4.2. Bridging attraction

If the interaction between polymer segments and the surfaces is attractive, cross-binding of surfaces occurs readily under appropriate circumstances (fig. 7b). As a rule this bridging mechanism can only occur at low polymer concentrations when the surfaces are covered to a lesser extent. At high polymer concentrations strong electrostatic, steric or polar repulsive forces due to the coverage of the surface prevent the mutual approach of the surfaces. Charged polymers are very potent candidates for the aggregation of phospholipid vesicles by formation of polymer bridges. Electrostatic attraction between the charged groups of the polymer and the membrane surfaces can overcome repulsive components.

That is the way in which positively charged polypeptides (e.g., polylysine) aggregate negatively charged vesicles. Another type of electrostatic interaction between

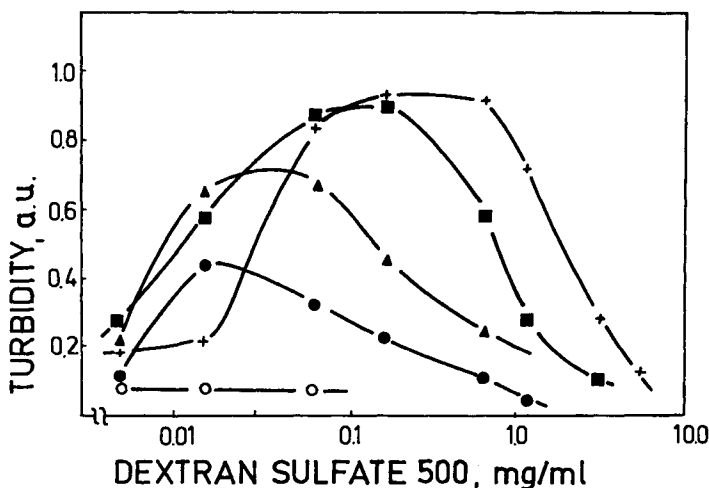


Fig. 8. Turbidity of small unilamellar DMPC/egg-PE vesicles (10 mol% egg-PE) as a function of dextran sulfate (MW 500,000) concentration for 0 (+), 50 (■), 100 (▲), 150 (●) and 200 mM (○) NaCl in the presence of 2.0 mM CaCl_2 and 10 mM HEPES at pH 7.4 and above T_C (30°C). The system exhibits aggregation properties typical for a bridging attraction. A maximum of aggregation appears. Furthermore, the adsorption of the negatively charged polymer to the vesicle surface is mediated by the formation of phosphate- Ca^{2+} -sulfate bridges between polymers and PC/PE head groups [203]. Because of the involvement of electrostatic interactions, the aggregation diminishes with increasing NaCl concentration.

sites of equal sign, especially negatively charged surfaces and polymers, is the formation of cation bridges between the polymer and the surface (fig. 8).

The important point in the bridging mechanism is that even for a relatively small adsorption energy per each binding site of the polymer, the cumulative action of the binding sites along a polymer chain will result in a substantial energy of surface interaction, especially for polymers of high molecular weight. This effect, in fact, explains why the adsorption of polymers tends to be irreversible. If a previously adsorbed segment of polymer desorbs, the mass of segments that remains attached will tend to draw back this segment. It should be recognized that such principles are directly applicable to adsorption processes of proteins.

4.4.3. Depletion attraction

If mutual repulsion between the free polymer and the membrane surface occurs, polymer molecules are excluded from the surface. A depletion layer, characterized by a depletion profile is formed in the vicinity of the surface (fig. 7c). As demonstrated experimentally polar polymers such as poly(ethylene glycol), dextran and other polysaccharides are repelled by phospholipid bilayers [87–90] and biological membranes [83, 91–93].

Once two depleted surfaces are closer from each other than the thickness of the depletion layer, surfaces are pushed together due to the higher osmotic pressure of

polymers dissolved in the bulk relative to the osmotic pressure in the center of the gap (depletion flocculation). This is opposite to the behaviour predicted in the case of polymer adsorption, as discussed before. The depletion attraction is effective if the repulsion between the polymer molecules as well as between the polymer molecules and the particle surface is higher than the particle-particle repulsion. Therefore, a critical polymer concentration is necessary to bring particles together close enough for aggregation, close contact and fusion.

The influence of poly(ethylene glycol) on the Ca^{2+} -induced aggregation of small PS vesicles is given in fig. 9. The aggregation occurs for Ca^{2+} concentration larger than or equal 1 mM Ca^{2+} in the absence of poly(ethylene glycol). Addition of poly(ethylene glycol) reduces the threshold concentration of Ca^{2+} for aggregation. Without Ca^{2+} , vesicle aggregation starts at about 15 wt% poly(ethylene glycol) 6000. Compared to the PC vesicles, the poly(ethylene glycol) concentrations for the aggregation of PS vesicles are higher due to the electrostatic repulsion of PS vesicles. The combined effect of Ca^{2+} and poly(ethylene glycol) results from the reduction of the electrostatic repulsion by Ca^{2+} and the increase of the attractive component from poly(ethylene glycol)-induced depletion attraction. Similar influences of surface charges and ions were found for many other vesicles [94–98]. A theoretical treatment of the depletion effect on the adsorption of cations on the vesicle surface has demonstrated that the actions of Ca^{2+} and poly(ethylene glycol) are not simply additive [99]. Poly(ethylene glycol) enhances the interaction of the lipid surface with cations favouring vesicle aggregation.

Evans and Needham [100] have directly measured the depletion energy of two interacting bilayer surfaces in concentrated dextran solutions. They successfully verified the following equation, originally derived by Asakura and Oosawa [101], for the depletion free energy per unit area at bilayer separations smaller than R_g

$$F = -cR_g kT, \quad (8)$$

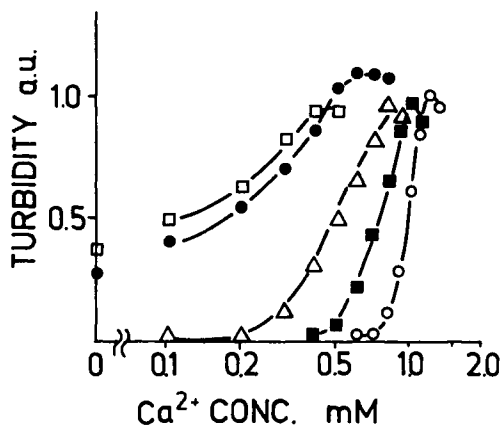


Fig. 9. Turbidity of small unilamellar PS vesicles as a function of Ca^{2+} concentration in the presence of 0 (\circ), 5 (\blacksquare), 10 (\blacktriangle), 15 (\bullet) and 20 (\square) wt% poly(ethylene glycol) 6000 at pH 7.0. The vesicle suspension contains 0.1 M NaCl, 4 mM TES and 0.02 mM EDTA.

c is the bulk polymer concentration. It is assumed that the attractive force acts uniformly over a distance of R_g , i.e. that the polymers are pushed out from the gap for separations smaller than R_g .

Depletion attraction can also occur if part of the polymer molecules attach themselves to the particle surface (fig. 7c). A depletion layer resulting from the repulsion between free and attached polymers occurs between the polymer surface layer and the bulk polymer. Such phenomena were observed for the effect of dextran on the aggregation of erythrocytes [83, 91]. In some cases depletion attraction was followed by depletion repulsion at higher concentrations. It is assumed that this mechanism appears when the surface concentration of the polymer is higher than its bulk concentration [83].

An inhibition of Ca^{2+} -induced aggregation of didodecylphosphate vesicles in the presence of high molecular weight poly(ethylene glycol) 20000 was described [102]. An explanation for this effect is a bad solubility of poly(ethylene glycol) under the conditions of the experiment. The clouding temperature of poly(ethylene glycol) 20000 is 103 °C in water. Above this temperature a phase separation occurs with formation of a concentrated polymer phase and a dilute polymer phase. In the presence of phosphate ions this temperature can decrease below 40 °C for phosphate concentrations higher 1 M. These conditions are comparable to those near the vesicle surface bearing the phosphate ions. Since the experiments were carried out at 40 °C the depletion effect of poly(ethylene glycol) at the vesicle surface did not occur. For poly(ethylene glycol) 8000 the same effect was observed at 52 °C providing further support for a role of clouding in poly(ethylene glycol)-mediated aggregation [103].

Polysaccharide chains are usually considered to be highly polar, since they have no obvious nonpolar moieties in them. However, conformations can be realized in the chains wherein all the hydroxyl groups are disposed in one side of the chain and the hydrogens disposed in the other [104]. Such an amphiphilic surface is present in linear oligomeric dextrans but not dextrans, cellulose and xylans. This finding is of relevance to cell surface polysaccharides, glycoproteins and lectin-sugar interactions, since it suggests contributions from hydrophobic components in such interactions.

Therefore, the interaction of polar polymers with membrane surfaces can be much more complex than discussed here.

4.5. *Effect of cations and polymers on water layers between membranes*

Among the structural events thought to contribute to fusion, bilayer dehydration has been proposed [88, 95, 105, 106]. If we try to understand the mechanisms of fusion at a molecular scale, all the components of the intermediate state of membrane fusion must be considered, including the water layer.

There are different experimental approaches to the study of hydration. Very recently reviews about these methods were given [61, 107]. Water adsorption isotherms specify the work necessary to transfer water from the bulk to the regions between membranes. Calorimetry detects the changed thermodynamical properties of the interbilayer water. From the dielectric relaxation measurements the dipole relaxation times of water molecules are derived. Small-angle X-ray and neutron diffraction

allow the determination of the thickness of the water layer and the location of water molecules. Spectroscopic methods as nuclear magnetic resonance (NMR), infrared and Raman spectroscopy are sensitive to the orientational and dynamical properties of the water motion.

The ^2H -NMR spectroscopy of deuterated water ($^2\text{H}_2\text{O}$) in phospholipid/water dispersions has some significant advantages, because this method can provide information about both the ordering of water molecules, i.e. the structure of hydration layers and the dynamics of the water molecules [105, 108–111]. The total number of water molecules is determined from the quadrupolar splitting of the $^2\text{H}_2\text{O}$ NMR signal. This information is comparable to the measurement of the thickness of the water layer by use of X-ray diffraction studies.

Figure 10 shows the number of water molecules, incorporated between bilayers, per phospholipid molecule, as a function of the poly(ethylene glycol) concentration. PC multilamellar vesicles suspended in $^2\text{H}_2\text{O}$ were used for the ^2H NMR spectroscopy. The water content is effectively reduced by poly(ethylene glycol) due to depletion attraction of bilayers as discussed in 4.4.3. At 50 wt% poly(ethylene glycol), a concentration used in artificial cell fusion, the number of water molecules is reduced from 23 to approximately 8 water molecules per phospholipid. That means that the trapped and partly the bound water molecules are extracted. The critical concentration of poly(ethylene glycol) for the vesicle fusion is about 30 wt%. Less than 11 water molecules/lipid are incorporated between bilayers under these conditions. This value of hydration is in close agreement with measurements based on X-ray diffraction studies [112, 113].

Summarizing the results of NMR studies of different lipids it can be concluded that definite numbers of water molecules/lipid are influenced in their behaviour by

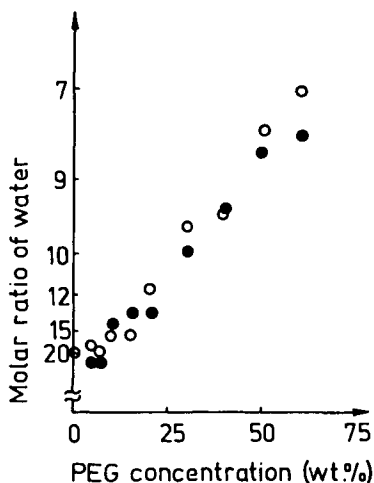


Fig. 10. Number of water molecules per lipid molecule incorporated between bilayers of multilamellar egg lecithin vesicles prepared in deuterated water as a function of the concentration of poly(ethylene glycol) 20,000. The quadrupole splittings measured by ^2H -NMR spectroscopy of $^2\text{H}_2\text{O}$ were used for the calculation of the content of water. Poly(ethylene glycol) was directly added (○) or separated from the dispersion by a dialysis membrane (●). (Data taken from [110].)

the bilayer surface. These water molecules show restricted motion, are partially oriented and were classified as 'bound' water [110]. About 12 water molecules/lipid were found to be 'bound' in multilamellar PC vesicles. Presumably, these molecules of water are important to membrane structural integrity, and their perturbation is expected to have consequences in respect to the bilayer properties [105, 113]. A rapid transfer of lipids between bilayers was observed at low water content. The thickness of the water layer determined from X-ray diffraction studies is about 5 Å at the critical concentration of poly(ethylene glycol) for fusion [113]. These authors have concluded that bilayers at this 5 Å separation are essentially in molecular contact due to the thermal motion of phospholipid headgroups which can extend 2–3 Å in the aqueous space between bilayers.

In contrast to poly(ethylene glycol), addition of millimolar concentrations of Ca^{2+} to multilamellar PS vesicles or small unilamellar PS vesicles changes the $^2\text{H}_2\text{O}$ NMR spectrum completely. The quadrupole splitting vanishes and the singlet observed is a strong indication that Ca^{2+} displaces water of hydration forming a dehydrated or probably anhydrous Ca-PS complex [114]. A comparable effect was found for some tri-valent cations but not for Mg^{2+} where a residual hydration is still observed. Studies of a DMPA/ Ca^{2+} system have also demonstrated that the DMPA molecules are highly dehydrated [115]. It was possible to show in this study that some water molecules are strongly immobilized in the complex.

The combined addition of poly(ethylene glycol) and Ca^{2+} to small unilamellar PS vesicles at concentrations higher than the critical concentration for aggregation and fusion (figs 9 and 14) results also in the formation of unhydrous Ca^{2+} /PS complexes (Ohki and Arnold, unpublished). Other situations leading to partial or complete dehydration at the point of contact between membranes are PE bilayers which are not well hydrated [116], PC bilayers at close contact as a result of localized out-of-plane thermal fluctuations [117] and freezing and thawing [118] and dielectrophoresis [119].

5. Fusion of vesicles – facts and models

5.1. Cation-induced fusion

Table 1 provides a summary of fusion experiments done with different phospholipids, mixtures of phospholipids, and types of vesicles and cations. The fusogenic behaviour of Ca^{2+} , Mg^{2+} , Na^+ and H^+ is only indicated. The list is most probably incomplete and only some representative examples of references and systems are given. Since the first identification of vesicle fusion [120] the cation-induced fusion of PS vesicles was most extensively studied. There is a specific concentration for each fusogenic cation at which the rate of vesicle fusion starts to increase. Such a concentration is defined as the 'fusion threshold' concentration of the cation.

Not all cations are able to induce fusion. For monovalent cations, except for H^+ , fusion seems to appear for very special conditions only despite the high capability for vesicle aggregation (see above). Lipid mixing of small unilamellar vesicles composed of PS or PG of specific fatty acid composition (DPPS, DMPG) induced

Table 1
Ion-induced fusion of various lipid vesicles and their threshold concentrations (adapted from Ohki and Arnold, 1989). The vesicle types are small unilamellar (SUV), large unilamellar (LUV), and multilamellar (MLV) vesicles.

Lipids	Types	Threshold Conc.*	References
OPS	SUV	H ⁺ , pH < 3.5	[193, 52]
PS	LUV	H ⁺ , pH 2.0	[122, 194]
PC, gel state	SUV	H ⁺ , pH < 4.0	[195]
DPPS, DPMG	SUV	300 mM Na ⁺	[54]
		Li ⁺ > Na ⁺ > K ⁺ > Cs ⁺	
PS	SUV	> 1 mM Ca ²⁺	[120]
PS	LUV	2.4 mM Ca ²⁺	[60, 188]
		no fusion for Mg ²⁺	
PA	SUV	0.2 mM Ca ²⁺ , Mg ²⁺	[196]
PA	LUV	0.03–0.1 mM Ca ²⁺	[197]
		Mg ²⁺ > Ca ²⁺	
PG	SUV	5 mM Ca ²⁺ , 20 mM Mg ²⁺	[198]
PG	MLV	10 mM Ca ²⁺	[196]
PI	LUV	no fusion up to 50 mM Ca ²⁺	[197]
CL	SUV	Ca ²⁺ , Mg ²⁺	[199]
CL	LUV	10 mM Ca ²⁺	
PE	SUV,LUV	2 mM Ca ²⁺ , 3 mM Mg ²⁺	[148, 116]
PS/PC (1 : 1)	SUV	Ca ²⁺ < Mg ²⁺ 3–5 mM Ca ²⁺	[200, 188]
PS/PC, PS/PE	SUV	Ca(PS/PC) > Ca(PS/PE) > Ca(PS)	
PS/PC, PS/PE	LUV	Ca(PS/PC) > Mg(OPS/PE)	[188]
PS/PC, PS/PC/PE	SUV	Ca(PS/PC) > Ca(PS/PC/PE)	[152]
CL/PC (1 : 1)	LUV	9 mM Ca ²⁺	[208, 51, 209]
CL/PE	SUV	Ca ²⁺	[192]
PE/oleic acid	SUV	H ⁺ , pH < 6.5	[189]
PS, PE/PA	LUV	inhibition of	[190, 191]
+ glycolipids		Ca ²⁺ -ind. fusion	[202]

* In most cases, the vesicles were suspended in 0.1 M NaCl

by monovalent cations was very recently described [54]. These systems were not studied with respect to the intermixing of internal contents which would assure that real fusion occurs. The cation efficiency of lipid mixing decreases in the order Li⁺ > Na⁺ > K⁺ > Cs⁺. H⁺ is the only monovalent cation that causes fusion of a broad range of phospholipids. PS vesicles are fused below pH 4.0 [52, 121, 122]. Results for small unilamellar PS vesicles are given in fig. 11. The studies of the pH-induced vesicle fusion have strong relations to intracellular fusion processes. Polyamines which are also involved in intracellular fusion processes, induce aggregation but not fusion of large unilamellar vesicles composed of PS, PA and mixtures of PA with PC at physiological concentrations. The presence of a high mole fraction of PE in acidic vesicles enables fusion. However, polyamines are very effective modulators of Ca²⁺-induced vesicle fusion [123].

Tri- and divalent cations fuse small unilamellar PS vesicles at very specific concentrations (fig. 11). The sequence of threshold concentrations of fusion is the same found for the aggregation of vesicles. Increasing the monovalent salt concentration

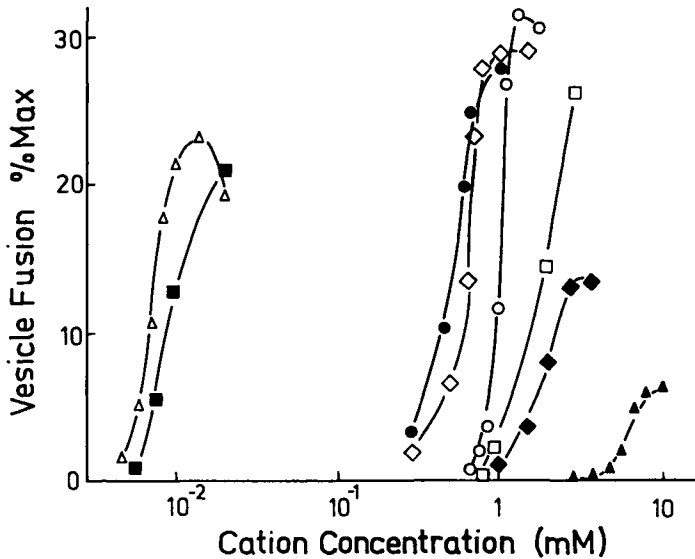


Fig. 11. Fusion of small unilamellar PS vesicles in 0.1 M NaCl, pH 7.4, with various cation concentrations. Fusion was monitored by the fluorescence content mixing assay (TbCl_3/DPA). The concentration of PS was $50 \mu\text{M}$ for all divalent cations and $5 \mu\text{M}$ for the trivalent cations. (La^{3+} (Δ), Tb^{3+} (\blacksquare), Mn^{2+} (\bullet), Ba^{2+} (\diamond), Ca^{2+} (\circ), Sr^{2+} (\blacklozenge), Mg^{2+} (\blacktriangle), H^+ (\square)). (Data taken from [73].)

results in a very rapid aggregation compared to fusion. For the PA vesicle-cation systems, vesicle fusion similar to those given in fig. 11 is observed and the fusion threshold concentrations of fusogenic ions are about one order of magnitude smaller than those obtained for the PS systems. The large unilamellar vesicles composed of different acidic phospholipids fuse at higher cation concentrations compared to small unilamellar vesicles, in agreement with the higher concentrations for aggregation. There is an absolute specificity for Ca^{2+} over Mg^{2+} in inducing the fusion of large unilamellar vesicles. The ability of Mg^{2+} to cause aggregation of large unilamellar vesicles without fusion provides an interesting case of the fusion reaction (compare eq. (3)). For example, fusion of large unilamellar PS vesicles is aggregation-limited, when induced by Ca^{2+} alone, but when induced by Ca^{2+} plus Mg^{2+} , limited by fusion.

In respect to the threshold concentration of Ca^{2+} , the efficiency to fuse large unilamellar vesicles composed of different acidic phospholipids decreases in the sequence $\text{PA} > \text{PS} > \text{cardiolipin} > \text{PG}$ and the Ca^{2+} concentrations vary from approximately 0.2 mM for PA through 2 mM for PS to 15 mM for PG. Large unilamellar PI vesicles are resistant to Ca^{2+} -induced fusion although aggregation occurs. Because of the difficulty to prepare stable PE vesicles, the fusion was only studied at high pH or at lower pH in the presence of low ionic strength saline. Fusion induced by Ca^{2+} and Mg^{2+} occurs at low ionic strength, and upon acidification [116, 124].

There is an obvious difference of the fusion reaction observed with PE if compared to other lipids. Two distinct sequential processes, i.e. aggregation and destabilization leading to the merging of bilayer lipids and intermixing of contents, can be usually shown to be independent. In the case of large unilamellar PS vesicles, with Mg^{2+} the vesicles can be made to aggregate reversibly, but they will not fuse unless Ca^{2+} is present to initiate membrane destabilization. However, in the case of PE the two processes seem not to be separable [116]. Conditions which lead to aggregation are accompanied by merging of lipids and contents. PE can be considered as forming a metastable bilayer which, under conditions of close interbilayer contact lead to fusion events.

Large unilamellar PS/PC (1 : 1) vesicles do not fuse in the presence of Ca^{2+} . When PE is substituted for PC the vesicles fuse. The inhibitory role of PC is particularly apparent in the Mg^{2+} -induced fusion of large unilamellar vesicles composed of PS and PE. Unlike pure large unilamellar PS vesicles, Mg^{2+} becomes fusogenic when PE is also present. This is presumably due to the instability and low hydration of pure PE bilayers. The ability of PE to form non-bilayer structures may be an important factor making such membranes fusogenic [116]. However, when PE is partly replaced by PC in the mixture, Mg^{2+} becomes again ineffective. Addition of glycolipids to acidic phospholipids results in a certain inhibition of Ca^{2+} -induced fusion. The inhibitory effect is enhanced for higher concentrations and larger headgroups indicating the occurrence of steric repulsions (compare 4.4).

5.2. Polarity decrease of bilayer surfaces

In studies of ion-induced vesicle fusion it was found that the extent of membrane fusion correlates well with the degree of the increase of interfacial tension of phospholipid monolayers [52, 56]. A theory was proposed from these findings that in order for two membranes to fuse, a certain degree of hydrophobicity of the membrane surfaces has to be attained [53, 75, 125]. Another physico-chemical property, which correlates well with the extent of cation-induced fusion, is the surface dielectric constant [74]. A review about the micropolarity effects at water/lipid interfaces was recently given [126].

According to Kimura and Ikegami [127] the wavelength at the maximum of the fluorescence spectrum of dansylphosphatidylethanolamine (DPE) is closely related to the dielectric constant of the medium. Since the fluorophore (dansyl group) of DPE, incorporated in phospholipid vesicles is localized in the glycerol backbone region of the bilayer, the observed changes in the fluorescent signal indicate the properties of the surface polar region. From the relationship between the wavelength at the fluorescence maximum in known dielectric media and the measured values of the emission spectra maxima of DPE in vesicles, the dielectric constant of the lipid polar region can be deduced [74].

The results of studies of the influence of cations on the surface dielectric constant of small unilamellar PS vesicles are given in fig. 12. The surface dielectric constants of small PC and PS unilamellar vesicle membranes are about $\epsilon = 35$ and 30, respectively. As the fusogenic ion concentration in the PS vesicle suspension solution increases the dielectric constant of the DPE environment decreases. There

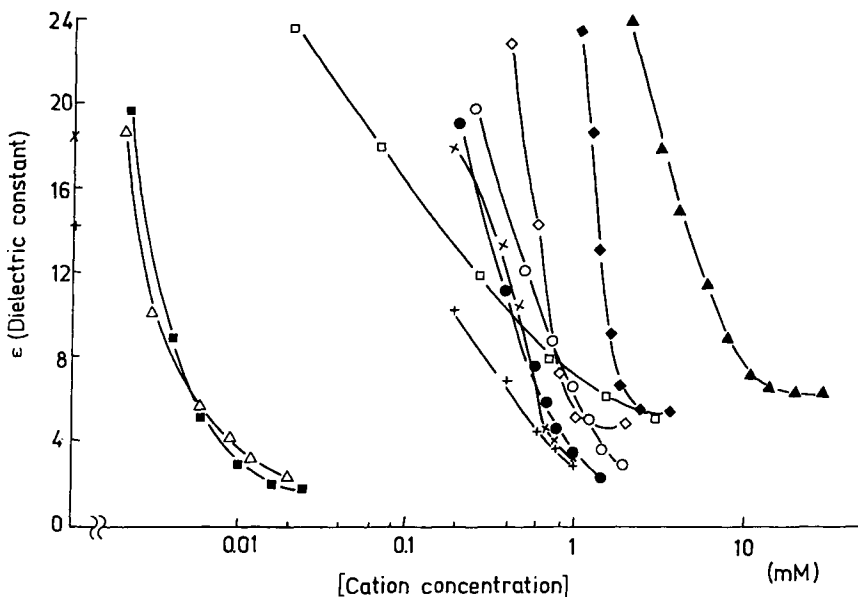


Fig. 12. Surface dielectric constant of small unilamellar PS vesicles suspended in 0.1 M NaCl buffer containing various fusogenic concentrations of La^{3+} (Δ), Tb^{3+} (\blacksquare); Mn^{2+} (\bullet); Ba^{2+} (\diamond); Ca^{2+} (\circ), Sr^{2+} (\blacklozenge); Mg^{2+} (\blacktriangle); H^+ (\square) and various Ca^{2+} concentrations in the presence of 10 wt% poly(ethylene glycol) 6000 (\times) and 15 wt% poly(ethylene glycol) 6000 ($+$) (adapted from [74]).

is a good correlation between the extent of vesicle fusion and the degree of decrease in dielectric constant. At the concentration corresponding to the fusion threshold concentration the dielectric constant has about the same value (~ 12) for all fusogenic ions examined. The surface dielectric constants are reduced to as low as 4 as these fusogenic ions exceed their fusion threshold concentrations. On the other hand, in the Mg^{2+} case the dielectric constant did not change further. For nonfusogenic ions (Na^+ , K^+ , polyamines) no shift in the spectra maxima was observed, although a great deal of aggregation of small unilamellar PS vesicles was observed. Contrary to other monovalent cations, as the concentration of hydrogen ion is increased (pH is decreased) a gradual decrease of the dielectric constant with respect to H^+ concentration occurs compared to the strong fusogenic cations.

The lowering of the surface dielectric constant indicates the increase in hydrophobicity of the bilayer surface. The very low values of the dielectric constant for strong fusogenic ions suggest that these ions may form nearly anhydrous complexes of cation and lipid polar groups. On the other hand, although Mg^{2+} can induce fusion of small unilamellar PS vesicles, the surface dielectric constant was not reduced below 11. This result supports other findings discussed before that Mg^{2+} may not remove membrane-bound water thoroughly enough to produce such anhydrous Mg-PS complexes.

As a membrane surface attains a certain hydrophobicity, two interacting membranes can become closely bound due to the reduction of hydration repulsion and the increase of hydrophobic attraction. However, such a close apposition of membranes may not be sufficient to induce membrane fusion. The most susceptible site for an instability of these membranes may be the boundary between the close contact and non-contact regions due to greater physical stresses and perturbation of lipid packing [73, 75]. As shown in fig. 13 the membrane curvature has a maximum in this region. Also this region is exerted by an additional asymmetrical force (line tension) which becomes larger as the size of vesicles becomes smaller.

Below, the good correlation between the poly(ethylene glycol)-induced vesicle fusion and the decrease of the surface dielectric constant in these systems will be discussed. However, it cannot be expected that close correlation of fusion extent with the decrease of surface dielectric constant is a property of all fusion systems. Especially in systems where the fusion event is strongly localized in small areas, the delocalized fluorescence probe is unable to detect these changes of surface properties. Moreover, when molecules contributing a high surface energy or defects to a membrane, are mixed with the lipid composing vesicle membranes, the fusion can start at an overall lower surface hydrophobicity if these molecules are located at the fusion site [75, 128, 129]. The application of the method is restricted to the occurrence of large areas of contacting membranes. Very recently a fluorescence method was developed for the detection of the polarity decrease at the adhesive junction between two model membranes [130].

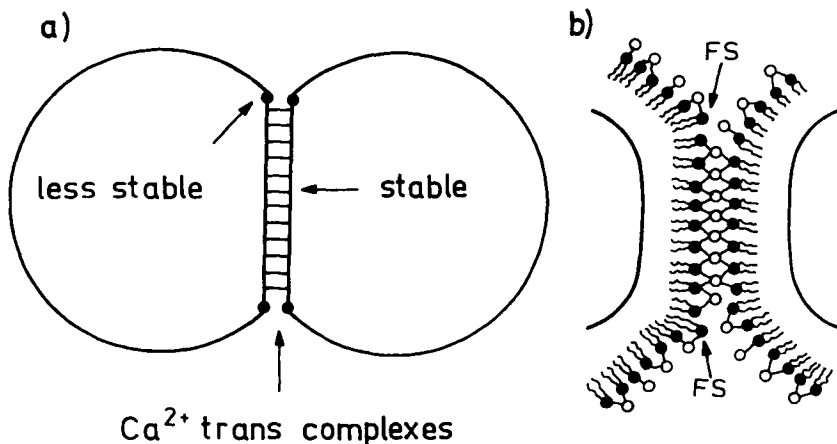


Fig. 13. Schematic diagrams of the adhesion of acidic vesicles by fusogenic concentrations of cations. The deformation of vesicles is shown in (a). A destabilization results from the increase in bilayer curvature due to strong adhesion. The formation of Ca²⁺ cis and Ca²⁺ trans complexes is indicated in (b). FS stands for the fusion site where the bilayer molecules are energetically unstable (adapted from [73] and [75]).

5.3. Modulation of cation-induced fusion by poly(ethylene glycol)

Unlike other uncharged polymers, poly(ethylene glycol) itself is able to induce fusion of small unilamellar vesicles prepared from charged as well as uncharged phospholipids. The threshold concentrations of poly(ethylene glycol) needed for fusion are dependent on the molecular weight and vesicle composition and amounts about 20–30 wt% for poly(ethylene glycol) 6000 [73–75, 94, 96, 113, 128, 129, 131–134]. Poly(ethylene glycol) is even capable of inducing fusion between PC vesicles in spite of the fact that this lipid is strongly hydrated and usually inhibits fusion of acidic vesicles that are mixed with PC. Dextran can induce fusion of larger vesicles, but at a much lower rate than poly(ethylene glycol) [96, 135]. Poly(ethylene glycol) is considered to force vesicles together due to the depletion attraction as discussed in 4.4.3 and 4.5.

At the threshold concentrations of poly(ethylene glycol) 6000 for fusion of small unilamellar PC and PS vesicles, the surface dielectric constant is reduced to about 16 and 12, respectively [73, 75, 76]. This dielectric constant of 12 for small unilamellar PS vesicles is approximately the same value as those for cation-induced fusion. However, for small unilamellar PC vesicles, it decreased to only 16 indicating that the membrane surfaces are still more hydrophilic when fusion occurs. Vesicles are flattened due to the withdrawal of free water from the vesicles by poly(ethylene glycol) and fusion could occur at the highly curved boundaries as proposed by MacDonald [133] and Ohki and Arnold, [73, 74]. Thus, two lipid vesicles might fuse due to the disruption of lipid packing exposing hydrophobic regions. The detergent-like properties of poly(ethylene glycol) are another possibility of the bilayer destabilization [136]. Lentz et al. [128] have found that high bilayer curvature encourages fusion of closely apposed membrane bilayers. However, the most highly curved vesicles did not mix their contents but ruptured and resealed, leading to the formation of larger vesicles in a manner different from vesicle fusion.

Burgess et al. [113, 137] have observed that poly(ethylene glycol) does not induce fusion of large unilamellar vesicles composed of a single synthetic PC (DPPC) but that it does cause close contact and rapid lipid transfer between these vesicles. PE-containing large unilamellar vesicles (DLPE/DOPC) did fuse and the concentration of poly(ethylene glycol) required to induce fusion decreased as the percentage of PE increased [113]. Large unilamellar DPPC vesicles can be induced to fuse when they contain small amounts of certain amphipathic compounds such as lyso-PC, platelet activating factor and palmitic acid [128, 129]. The common property of these additives is the positive intrinsic curvature. These fusogenic amphipaths disrupt the normal lamellar lipid packing within their immediate environment, especially the interfacial region of the membrane. This imperfect packing could expose hydrophobic regions of the membrane to water and thereby raise the surface energy of the bilayer [128]. In contrast to the usual assumption that fusion is promoted by additives favouring nonbilayer structures, the ability of these amphipaths to enhance fusion is better correlated with the tendency to change lipid packing. Lentz et al. [128] have found that for these promoters of fusion the changes in dielectric constant do not correlate with the ability of a bilayer to be fused by poly(ethylene glycol).

Figure 14 presents the results of the application of the NBD-Rh probe dilution assay (see 3.1 for the application of this method) on fusion of small unilamellar PS vesicles induced by Ca^{2+} in the presence of various poly(ethylene glycol) concentrations in the vesicle suspension. The application of the terbium/dipicolinic acid assay has given similar results [74]. When the poly(ethylene glycol) concentration was increased, the concentration of Ca^{2+} required to induce the same extent of PS vesicle fusion was decreased. These results are in agreement with measurements of the fusion of PS and PS/PE vesicles under the influence of Ca^{2+} , Mg^{2+} and poly(ethylene glycol) [44]. An enhancement of the Ca^{2+} -induced fusion by poly(ethylene glycol) was also found for didodecylphosphate vesicles [102].

As found for the cation- and poly(ethylene glycol)-induced fusion, the surface dielectric constant is reduced to about 12 at the threshold concentrations of Ca^{2+} in the presence of various poly(ethylene glycol) concentrations. An example is given in fig. 10. An increase of the concentration of Ca^{2+} or poly(ethylene glycol) beyond the threshold concentration decreases the surface dielectric constant to 4 indicating that again unhydrous complexes are formed, even at Ca^{2+} concentrations much lower than in the poly(ethylene glycol)-free vesicle suspension. The important point of these experiments is that relatively low Ca^{2+} concentrations are able to induce vesicle fusion, once the bilayers were brought in close contact. In this respect the

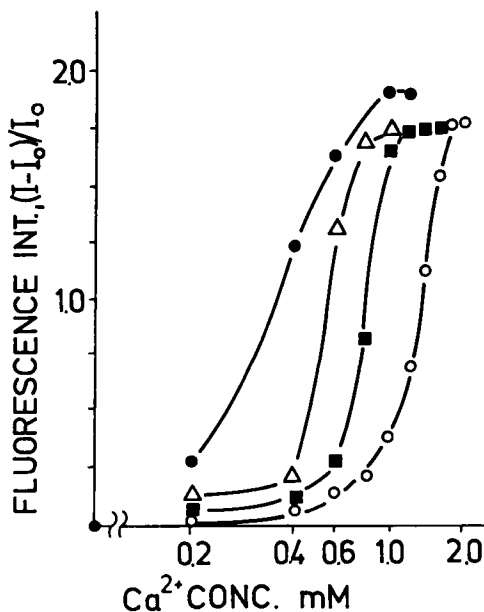


Fig. 14. Ca^{2+} -induced fusion of small unilamellar PS vesicles suspended in 0.1 M NaCl/pH 7.4 and various poly(ethylene glycol) 6000 concentrations. Fusion was monitored by use of the probe dilution assay (NBD-PE/Rh-PE) in the presence of 0 wt% (○), 5 wt% (■), 10 wt% (△) and 15 wt% (●) poly(ethylene glycol). The degree of fusion was calculated from $F = (I_{525} - I_{525}^0)/I_{525}^0$ where I_{525} and I_{525}^0 were the fluorescence intensities of NBD-PE at 525 nm with and without fusogen, respectively.

The fluorescence was excited at 460 nm (from [74].)

Table 2
Polyanion-induced fusion of vesicles (adapted from [81]).

Polyanion	Lipid and	vesicle type	References
Dextran sulfate	PC, PC/PE (+ calcium)	SUV	[203]
	PC (+ calcium)	SUV/LUV	[204]
	PC/Stearylamine	SUV	[205]
	PC/chol/DEBDA[OH]	REV	[206]
Heparin	PC (+ calcium)	SUV/LUV	[204]
DNA	PC/chol/DEBDA[OH]	REV	[206]
PASP	PC/chol/DEBDA[OH]	REV	[207]

Abbreviations: REV, reverse-phase evaporated vesicles; PASP, poly(aspartic acid); DEBDA[OH], a quaternary ammonium detergent (see [206]).

action of poly(ethylene glycol) on Ca^{2+} -induced fusion exhibits a similarity to the effects of Ca^{2+} -binding proteins on natural fusion processes.

These findings may give reasons for the high Ca^{2+} requirements for vesicle fusion compared to intracellular fusion. Part of the reason is probably the necessity to reduce the surface charge of acidic vesicles and the low concentration of vesicles that is used in fusion experiments. All factors that contribute to the decrease of electrostatic repulsion and enhance the rate of vesicle aggregation potentially decrease the Ca^{2+} requirement. The high ability of poly(ethylene glycol) to promote aggregation and close approach of vesicles due to depletion attraction allows the high affinity trans complex of Ca^{2+} and acidic phospholipids to form more easily because of the increase of the thermal collision rate between vesicle surfaces.

5.4. Polyanion-induced fusion

First reports about fusion of phospholipid vesicles in the presence of anionic polymers listed in table 2 were given very recently. Glycosaminoglycans comprise negatively charged polymers such as heparin and chondroitin sulfate which are important components of the extracellular matrix. Dextran sulfate has a structure very similar to glycosaminoglycans and this polymer was used instead of glycosaminoglycans in many investigations. The interest in this polymer increased because it was used as a potent drug against HIV infection [138]. Studies of the fusion of virions with lipid vesicles and erythrocyte membranes have given some insights into the mechanism of the action of dextran sulfate and glycosaminoglycans [139–141].

The binding of glycosaminoglycans to phospholipid vesicles was investigated by microelectrophoretic experiments [139, 142]. These polyanions bind to neutral phospholipid vesicles (PC, PC/PE) only in the presence of Ca^{2+} . If positively charged stearylamine or other detergents (table 2) are incorporated in the vesicles, binding occurs without Ca^{2+} . Negatively charged phospholipids such as PS do not bind the polyanions, even in the presence of millimolar concentrations of Ca^{2+} . The use of this divalent cation is biologically relevant because it occurs in relatively high concentrations (about 3 mM) in the extracellular space.

As discussed by Kim and Nishida [143] divalent cations can form bridges between the phosphate group of the lipids and the negatively charged sites of the polyanion.

If positively charged amphiphiles are incorporated in the bilayer the surface potential of the vesicles becomes positive and a binding also occurs in the absence of Ca^{2+} . It can be concluded that a positive surface potential, resulting from Ca^{2+} adsorption or incorporation of positively charged amphiphiles, is a prerequisite for the binding of the polyanions.

The aggregation induced by polyanions is assumed to be mediated by a bridging mechanism of the polyanion between adjacent vesicles as discussed above (section 4.4.2 and fig. 8). At high concentrations of the polymer a disaggregation occurs. The polyanion concentration necessary for maximum aggregation is slightly lower than the polyanion concentration for saturation of polymer adsorption. As expected the bridging mechanism can only occur at low polymer concentrations where the surface of vesicles is covered to a lesser extent.

So far fusion of vesicles induced by polyanions was only measured by use of lipid mixing assays. More precisely, the mixing of lipids could be established. It cannot be concluded that a real fusion in terms of the fusion criteria occurs before the mixing of vesicle contents can be demonstrated in these systems (see section 3). The application of the internal content mixing assay failed to show the intermixing of internal contents due to a strong leakage of internal contents indicating the occurrence of defects in the bilayer. Therefore, a more probable interpretation of the lipid mixing is that lipid vesicles ruptured and resealed, leading to the formation of larger vesicles.

Several experiments with PC vesicles and Ca^{2+} /dextran sulfate demonstrated that an almost dehydrated complex is formed in the aggregated state at temperatures below the phase transition temperature. As revealed by differential scanning calorimetry measurements the phase transition temperature of DMPC vesicles is increased by about 10°C [81, 144, 145]. Possibly, the dehydrating effect of the cation combined with a lateral fixation of the lipid molecules by the polymer causes the increase of the phase transition temperature. The measurement of the surface dielectric constants gives dielectric constants as low as observed for PS vesicles in the presence

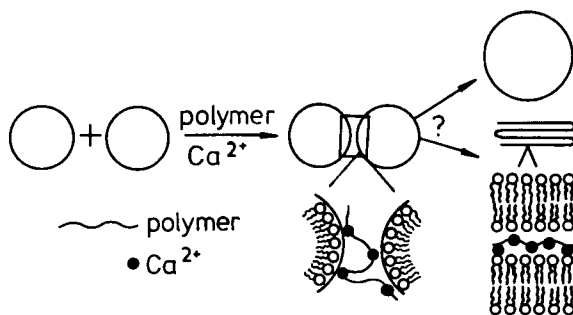


Fig. 15. Model of the combined action of Ca^{2+} and polyanions on aggregation and lipid mixing of PC vesicles. The aggregation of vesicles is mediated by a bridging mechanism of polyanions and Ca^{2+} . The intermediate stages, occurring after the aggregation process, could not be identified. The most probable interpretation of lipid mixing is that lipid vesicles rupture and resealed, resulting in the formation of larger vesicles and stacked bilayer arrangements. A complete conversion into almost unhydrous complexes of stacked bilayers occurs at optimum concentrations of Ca^{2+} and polyanions for aggregation.

of Ca^{2+} (O. Zschörnig, unpublished results). The reduced influence of Mg^{2+} on the phase transition and the dielectric constant is also shared by the PS/cation and PC/cation/polyanion system. The formation of stacked bilayer arrangements at high Ca^{2+} concentrations observed by freeze fracture electron microscopy indicates another common behaviour of both systems (W. Richter, unpublished results).

A conceptual model of the combined action of Ca^{2+} and polyanions on PC vesicle aggregation and lipid mixing is given in fig. 15. The mixing of lipids of the outer monolayers can already occur in the aggregated state resulting from the close approach of the surfaces due to the formation of an unhydrated complex. These properties are worth to be mentioned because PC was exclusively considered to prevent aggregation and close approach of vesicle surfaces in other fusion systems.

5.5. Cation-induced fusion modulated by proteins

Although little is known about natural fusion processes, it is generally accepted that proteins are involved in the different stages of membrane fusion. They have to bring together the correct membranes for fusion, thus providing for fusion specificity. The recognition has to be followed by an approach of the membranes into close contact where the proteins have to generate the perturbations required for fusion. When the intermembrane fusion takes place, the target for the initial contact is the ectoplasmic site (egg-sperm fusion, myoblast fusion). In exocytosis, proteins localized on the endoplasmic site are the first target. Exoplasmic and endoplasmic fusion are different since the two surfaces have different lipid and protein composition and the intra- and extracellular compartments have different ionic compositions, e.g., Ca^{2+} concentrations. The complexity of intracellular processes may be increased as soon as metabolic energy is involved at several stages of fusion.

Besides fusion-inducing viral proteins, no other intrinsic membrane proteins of fusion activity have been identified so far (recent reviews: [20–22, 28, 146, 147]). A present challenge is to identify endogenous proteins that mediate fusion processes. Indirect evidence suggests that cytosolic Ca^{2+} -binding proteins called annexins are involved in fusion. The first protein of this family originally isolated from chromaffine cells was synexin (annexin VII). However, it became evident that the annexins are not fusion factors but they may have a modulating role. These proteins have Ca^{2+} -specific aggregation activity. Studies of the effect of these Ca^{2+} -binding proteins on the fusion of vesicles have given some insights in the specific role of proteins and Ca^{2+} in fusion mechanisms. In the following the aggregation and fusion abilities of Ca^{2+} -binding proteins, and charged polypeptides are discussed.

5.5.1. Charged polypeptides

Protein-induced aggregation and fusion can involve both electrostatic and hydrophobic interactions between the protein and the participating membranes. Charged polypeptides aggregate membranes mainly by electrostatic interaction.

Polylysine-induced fusion has been reported [148–151]. The extents of aggregation and fusion depend on the fraction of negatively charged lipids in the vesicles and the relative amount of polylysine. It was found that this polycation crosslinks negatively

charged vesicles. Similar to the effect of charged polymers on vesicles (figs 7 and 15) the aggregating activity of polylysine shows a maximum effect which then declines at higher concentrations. Once the vesicles are aggregated, excess polylysine inhibits close approach and fusion due to steric and electrostatic effects [150]. Optimal aggregation and fusion occur when charge neutralization is possible without complete coverage of the vesicles with polypeptides.

The fusion activity of charged polypeptides is usually pH-dependent. Fusion of PC/PS vesicles induced by polylysine increases strongly below pH 4.0 suggesting that it correlates with the protonation of the PS-carboxyl group. In other cases such as the fusion of vesicles induced by polyhistidine, changes of the protein properties are responsible for the pH dependence [152]. It can be concluded that for fusion to occur each component of the lipid-polypeptide-lipid complex has to be optimized for close aggregation. Therefore, the major function of the charged polypeptides in vesicle fusion is the promotion of aggregation through charge neutralization of the aggregated system.

Bondeson and Sundler have extended these measurements by identifying both the amino acid and phospholipid specificities in the interactions [151]. At neutral pH a strong aggregation of acidic vesicles detected by lipid intermixing was found after addition of poly(L-lysine) and poly(L-histidine). However, when the incubation with the peptides at neutral pH was followed by acidification, complete membrane fusion, i.e. intermixing of vesicle contents, occurred. The appearance of a maximum of lipid mixing which decreases at higher concentration confirms the formation of polymer bridges as the aggregation mechanism. The authors favour the idea that acidification triggers fusion mainly by acting on the phospholipid head groups.

The basic peptides may lead to partial headgroup dehydration due to a tight interaction between the charges of the polymer and phospholipid head group increasing the sensitivity toward a proton-induced fusion. The ratio of lysine residues to DPPA headgroups in the aggregated complex was determined to be greater than unity [153, 154].

5.5.2. Ca^{2+} -dependent protein-induced fusion

The aggregation and fusion of acidic vesicles occurs at millimolar Ca^{2+} concentrations. However, Ca^{2+} -dependent natural fusion processes require micromolar Ca^{2+} concentrations only.

A simple explanation for this discrepancy in the Ca^{2+} threshold is that other factors increasing the fusion activity of Ca^{2+} , are involved. Some water-soluble proteins were identified which are able to associate with vesicles in the presence of Ca^{2+} , thereby lowering the threshold of Ca^{2+} concentration for aggregation and fusion.

Synexin was the first cytosolic protein whose activity on Ca^{2+} -induced vesicle fusion was studied. Without Ca^{2+} , synexin is not able to induce aggregation and fusion. This system was established as a membrane model which has a sensitivity to Ca^{2+} comparable to biological membranes [45, 155, 156]. The activities of synexin are triggered by Ca^{2+} , but not by Mg^{2+} . Negatively charged phospholipid vesicles of different compositions can be aggregated by synexin/ Ca^{2+} , but fusion is inhibited by addition of PC. In general, synexin enhances the initial rate of fusion and lowers

the Ca^{2+} threshold. The largest effect by synexin is observed in the case of PA/PE vesicles. In this system the initial rate is increased by two orders of magnitude, and the Ca^{2+} threshold is lowered from about 1 mM to 10 μM . Synexin-mediated fusion always required a phospholipid composition itself susceptible to fusion at some Ca^{2+} concentration. Thus fusion is still controlled by the phospholipid composition [147, 157]. In respect to the threshold concentration of Ca^{2+} , the efficiency to fuse large unilamellar vesicles composed of different acidic phospholipids changes in the same sequence as observed in the absence of synexin.

From the analysis of the two-step kinetics (compare eq. (3)) of synexin-facilitated fusion was concluded, that synexin increases the aggregation rate constant, while the fusion rate constant is unchanged [158]. At relatively low Ca^{2+} concentrations, negatively charged liposomes aggregate in the presence of synexin. Ca^{2+} appears to bind to synexin at two different sites with different affinities [159]. The site of highest affinity regulates the binding of the protein to the surface. Ca^{2+} concentrations of about 1 μM are necessary. Aggregation of vesicles is not promoted until Ca^{2+} is increased above 10 μM . A second Ca^{2+} -binding site comes into play at this concentration which was recognized to provide binding sites for a Ca^{2+} -mediated self-aggregation of synexin. Vesicles can be crosslinked by the formation of a complex bridge consisting of (acidic lipid)- Ca^{2+} -(synexin)_n- Ca^{2+} -(acidic lipid). The actual number of synexin molecules that self-aggregate to form this structure is unknown. In contrast to synexin, some other annexins can crosslink vesicles in their monomeric form.

Contrary to the Ca^{2+} -dependent polymers and cationic polypeptides which directly link vesicle surfaces (fig. 7), synexin shows a stable maximum aggregating effect, even at high concentrations. This indicates different mechanisms of bridging. The common property of these systems is the existence of multiple binding sites of the polymers and proteins. Annexins with multiple binding sites aggregate vesicles either in their monomeric or polymeric form involving annexin-annexin interactions. After the first contact of the vesicles, a closer approach of these vesicles can result from subsequent binding of annexin monomers or polymers. However, in order to enable intervesicle phospholipid-phospholipid contact, annexins must be displaced from the region of closest contact.

This model made some assumptions about the mode of binding of annexins to membrane surfaces. It was assumed that a high flexibility of the attachment of annexins to surfaces occurs, and interbilayer distances relevant to the formation of the Ca^{2+} trans complex can be realized. The finding that the polycation spermine displaces bound annexins suggests that annexin binding is largely ionic in nature [157]. It has been suggested that synexin can undergo a conformational change which makes it possible to insert completely into the lipid bilayer [160]. However, under conditions where aggregation and fusion of vesicles do not occur such membrane-embedded domains could not be identified [147]. It cannot be excluded that other modes of binding could exist under conditions where annexins mediate vesicle aggregation and fusion.

The recent crystallization and X-ray diffraction analysis of annexin V in the absence of phospholipids [161, 162] have led to a plausible model of the interaction

of this annexin with phospholipid bilayers [147]. Further structural characterization is necessary for a thorough understanding of the mechanism of annexin binding and its effect on fusion (see section 6.4).

Amphiphilic proteins, consisting of a polar and hydrophobic part, can facilitate aggregation and fusion of vesicles by the penetration of the hydrophobic part in one vesicle and binding of a polycationic or Ca^{2+} -binding site to the adjacent vesicle.

A cluster of arginine and lysine residues with interspersed electrically neutral amino acids can bind a significant fraction of cytoplasmic protein to the acidic vesicle membrane if the cluster contains more than five basic residues [163]. Many proteins were found acting in this way on vesicle aggregation and fusion (insulin, colicin, cardiotoxin). However, the structure of the protein may preclude several of the basic residues in the cluster from interacting with acidic lipids. The relatively rigid helix structure of melittin may constrain the basic residues to point away from the surface. Such proteins will adsorb strongly to bilayer membranes by means of hydrophobic interaction. The fusogenic abilities of basic amphipathic α -helical peptides depend on the content of α -helical structures of the peptides in the presence of vesicles [164]. Some of them require special conditions to become amphiphilic. Low pH and Ca^{2+} are triggers known to induce the required conformational changes. Proteins of a high solubility in water at physiological pH can change their conformation through exposure of the hydrophobic regions at acidic pH. The conformational change is followed by a penetration of the hydrophobic part in the hydrophobic core of the bilayer. The insertion of protein segments may provide the perturbation of bilayer stability necessary for the formation of transient intermediates for bilayer merging and fusion. The pH-induced fusion of acidic vesicles by lysozyme exhibits properties of such a mechanism [165].

6. Molecular mechanisms of vesicle fusion processes

6.1. Correlation of intramembrane and intermembrane interactions

As already mentioned above, a close contact between membranes is a prerequisite to fusion to occur. Therefore, the evaluation of forces leading to the approach of membranes is a central problem of the investigation of fusion mechanisms. However, a close contact of membranes does not necessarily result in a membrane fusion, even if the attractive forces are further increased. Membrane fusion can only occur, when the close approach of membranes is accompanied by such changes of the intramembrane interactions inducing perturbations of the membrane structure relevant for the fusion process. Thus, the interactions have to be discussed from both points of view, the approach of membranes and the perturbation of membranes.

The electrostatic, steric and solvation interactions are candidates for such interactions because they act between membranes as well as within the membrane. For instance, addition of Ca^{2+} to negatively charged bilayer membranes reduces the electrostatic repulsion. At the same time the repulsion between headgroups is reduced and the phospholipids are more closely packed. The strong hydration of PC headgroups leads to a higher distance of separation of PC molecules in the bilayer and

an increase of the bilayer-bilayer repulsion. Furthermore, in addition to promoting aggregation by lowering the hydration repulsion, this could also have the effect of destabilizing the bilayer.

It was also found that the lateral distribution of lipids and proteins is changed in reconstituted and natural membranes when membranes are approaching.

The structural changes that can occur on approach of bilayers within the hydration regions have been summarized by Rand [166] as follows: (i) the hydrocarbon chains can crystallize due to dehydration, for instance by the formation of the Ca^{2+} trans complex, (ii) the intrabilayer lateral pressure increases, (iii) lateral segregation of bilayer components can occur in mixed bilayers and (iv) disruption of the bilayer and a complete rearrangement of its molecules is possible.

Considerable interest has been directed to the possible relationship between calcium-induced lateral segregation and calcium-mediated interaction of bilayers prepared from a mixture of anionic lipids with PC or PE [59, 95, 167]. Limited, and possibly reversible, rapid lateral redistributions of anionic lipids accompany the calcium-mediated interaction, lipid mixing and fusion of PC/PS as well as PC/PA vesicles [167]. The accumulation of fusion-competent lipids in the area of closest approach can result in a closer apposition and a sequence of other structural alterations can follow. This mechanism was discussed to occur for the more weakly hydrated PE in the fusion region. In addition to promoting aggregation by lowering the hydration repulsion, this could also have the effect of destabilizing the bilayer, since these lipids promote the formation of non-lamellar phases [166]. The interaction between vesicles itself has changed the phospholipid composition of the contact region.

It was discussed above that the affinity for Ca^{2+} of apposed PS bilayers far exceeds that of the isolated surface and that a strong adhesion of vesicles results. Spherical vesicles will necessarily flatten against each other and the attractive energy of adhesion is transformed into the stresses that develop as the bilayers deform by changing their curvatures and by increasing their surface area and bilayer tension [106, 168]. The intravesicular pressure is also increased. If no volume loss occurs, high adhesion energies can produce tensions that exceed critical levels of bilayer stability (fig. 13). The contact area could break and the vesicles fuse in such a way that the area/volume ratio becomes high enough to remove the stress [169]. If volume loss occurs the tension in the bilayer is reduced which can lead to stable adhesion of vesicles. Observations of PS vesicle rupture showed that critical tension was always reached before volume loss could reduce it. PS/PC vesicles can respond with a stable adhesion without rupture and fusion, probably due to a lower adhesion energy.

The stresses discussed here are identical to those that would result from osmotic stress. Ca^{2+} -induced fusion of vesicles with planar membranes can occur only if accompanied by the disruptive force of osmotic swelling [170]. These findings have emphasized a possible role of osmotic forces in cellular fusion processes. Osmotic pressure is viewed as the crucial step driving the bilayer destabilization, possibly in conjunction with non-lamellar structures [171].

Fusion can also be driven by internal packing forces. This is observed when the temperature of small unilamellar PC vesicles is lowered much below the chain melting temperature. The curved bilayers of small unilamellar vesicles become

highly stressed as the chains now attempt to line up and pack into less curved bilayers. Since these changes favour larger vesicles they may lead to rupture.

6.2. Role of non-bilayer structures

The essential step in fusion is the rearrangement of the lipid molecules of the two apposed membranes to form a single, continuous membrane.

The reduction of the hydration repulsion allows critically close apposition of interacting vesicles. The observation that most biological membranes contain large amounts of lipids which prefer the formation of nonlamellar phases has led to the suggestion that nonbilayer structures are of relevance for membrane fusion. Conformational rearrangement of the acyl chains from bilayer packing to some other phases such as hexagonal phase [172–174] or cubic phases [175] may be important in the membrane fusion process. This is quite plausible, considering the mechanism of the lamellar/hexagonal phase transition. Similar to bilayer fusion, close apposition of L_α -phase bilayers is required for phase transition to occur. However, the structural transitions of phospholipid bilayers during membrane fusion are expected to occur locally at the area of intermembrane contact. Therefore, these phases are not generated in bulk during membrane fusion. Fusion may involve a small defect possessing some characteristics of these non-bilayer phases. Thus, the formation of long-range order that can be detected by microscopic or spectroscopic techniques is precluded.

Transitions between lamellar (L_α), inverted cubic ($I_{||}$), and inverted hexagonal ($H_{||}$) phases appear to occur by formation of discrete intermediate structures (Seddon and Templer, this volume). Siegel has developed a theory describing the formation of the intermediate structures [176, 177]. Briefly, the theory predicts that short-lived 'inverted micellar intermediates' and long-lived metastable structures called 'interlamellar attachment' are formed. Formation of inverted micellar intermediates is analogous to a subcritical fluctuation and should begin at temperatures well below the transition temperature from L_α to $H_{||}$. The interlamellar attachments can be visualized directly by time-resolved cryotransmission electron microscopy with resolutions in the time regime of seconds [178].

Using vesicles made of N-monomethylated dioleoyl-phosphatidylethanolamine (DOPE-Me), Ellens et al. [175] found increased fusion to occur in the temperature range in which the N-monomethylated dioleoylphosphatidylethanolamine would form an isotropic or inverted cubic phase in a lipid dispersion. When the temperature was above the transition temperature T_H for formation of the $H_{||}$ phase, lysis of vesicles developed. In the temperature range where fusion was observed, formation of interlamellar attachments appeared. These structures did not occur at temperatures above T_H .

In accordance with the theory of the $L_\alpha/H_{||}$ phase transition proposed by Siegel the initial step is the formation of the inverted micellar intermediates. These inverted micellar intermediates are also formed at temperatures below T_H . In this state, lipids can exchange in the outer monolayers. This sort of lipid exchange should be observed whenever an inverted micellar intermediate can form and the system is in the vicinity of the $L_\alpha/H_{||}$ transition. The inverted micellar intermediate can easily go back to

the apposed bilayers. A mixing of outer monolayer lipids was frequently observed in studies using lipid mixing assays.

These micelles may then aggregate in the plane of the two apposed membranes and transform either to an $H_{||}$ phase or to the interlamellar attachment, i.e. channels between the bilayers. These channels then expand allowing membrane fusion with non-leaky mixing of the aqueous contents. Theory shows that it is difficult for the interlamellar attachment to revert to the inverted micellar intermediate structure. If the lipid has a strong tendency for $H_{||}$ phase formation then the vesicles will rupture and release their contents. Mixing of vesicle contents without leakage can occur for conditions if interlamellar attachment formation is favoured. Interlamellar attachment formation has a chance to occur when the ratio of the areas of the lipid head groups at the lipid-water interfaces of the L_{α} and $H_{||}$ phases at equilibrium is in the right range ($\simeq 1.2$).

The studies of PE systems are remarkably compatible with the prediction of this model [175, 178, 179]. The importance of this mechanism is that it is a contact-mediated transition focusing the structural destabilization where it is needed [106]. This is less clear in the case of lipid systems with ion-induced $L_{\alpha}/H_{||}$ transitions like the cardiolipin/PC system. It was shown above that fusion can be induced by cations in anionic lipid systems by mechanisms that have nothing to do with $H_{||}$ -phase formation, e.g., the Ca^{2+} /PS system. In anionic vesicle systems that form a $H_{||}$ phase upon addition of cations, it is unclear whether fusion occurs via interlamellar attachments or via a mechanism related to that in PS vesicle fusion. This indicates that intermembrane intermediates different from inverted micellar intermediates and interlamellar attachments should be formed in the Ca^{2+} -induced vesicle fusion. However, it can be suspected from these findings that the difficulty in the structural analysis of the fusion mechanism is not that intermembrane intermediates do not exist but rather that it is difficult to detect these structures since their lifetime is rather short.

Because of the uncertainties of the existence of intermediates based on equilibrium structures such as 'inverted micells' and 'hexagonal phase', Papahadjopoulos et al. [180] proposed to introduce intermediates of much simpler configurations that share some features with the above structures. This proposal emphasizes the transient and unstable, perhaps even stochastic character of the intermediate. Such possible intermediates are shown in fig. 16.

6.3. Hydrophobic point defects

The formation of a fully dehydrated contact between the bilayers, induced by Ca^{2+} , Ca^{2+} /poly(ethylene glycol) and Ca^{2+} /dextran sulfate was described above. However, a number of other systems, where fusion was observed, do not exhibit complete dehydration. This was shown for poly(ethylene glycol)-induced fusion and fusion of bilayers supported on mica surfaces [76, 79, 181].

Ohki proposed that the increased hydrophobicity of the bilayer surface is responsible for membrane fusion [72]. As was shown by measurements of the interfacial tension and the surface dielectric constant, fusogenic concentrations of divalent

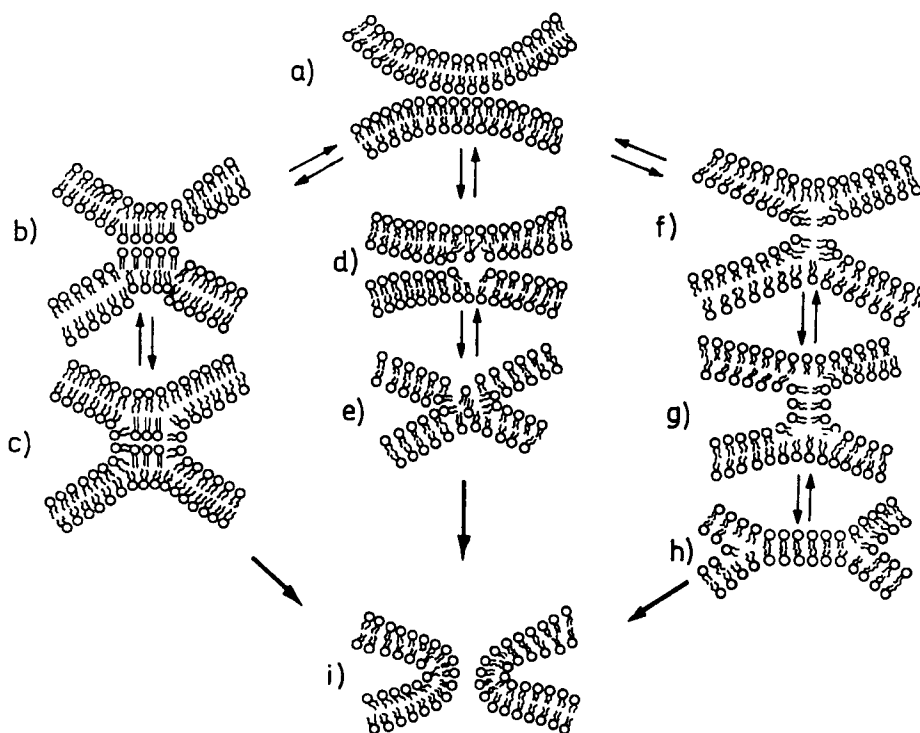


Fig. 16. Hypothetical stages in the molecular rearrangement of phospholipids during fusion of vesicles, BLM's and bilayers deposited on mica surfaces. (a) local approach of apposed bilayers; (b) formation of hydrophobic point defects located at the boundary between regions of contacting and non-contacting bilayers. Parts of acyl chains are exposed to water; (c) fusion of outer monolayers to minimize hydrocarbon-water contact; (d) fluctuations in molecular packing of lipids and formation of a hydrophobic contact; (e) collapse of the outer monolayers; (f) local out-of-plane fluctuations of lipids and formation of hydrophobic contacts; (g) stalk formation and contact outer monolayers; (h) monolayer fusion; (i) fused bilayers. (Adapted from [2, 73, 76, 77, 117, 180, 182]).

cations make the surface more hydrophobic. Other factors such as the degree of vesicle curvature, temperature and membrane expansion due to osmotic swelling or vesicle deformation in the process of adhesion (fig. 13), all have a similar correlation between the surface hydrophobicity and the tendency of bilayers to fuse. It is reasonable to assume that these influences increase the probability that nonpolar fatty acyl chains are transiently exposed to water (fig. 16). Hydrophobic point defects formed in this way can then provide the source for localized hydrophobic attraction between two membranes which have such defects. The effect of divalent cations on fusion of acidic vesicles is consistent with the concept of point defects since the fusion site is located at the boundary between regions of contacting (e.g., Ca^{2+} trans complex) and non-contacting bilayers (e.g., Ca^{2+} cis complex) (figs 13 and 16b).

The hydration barrier preventing close contact between bilayers is replaced by an

attractive force, one order of magnitude larger than the Van der Waals attraction as discussed above.

Hui et al. [182] have observed that point defects occur in membranes (mixtures of egg-PC and soybean PE) induced to fuse by freezing and thawing. In the resulting multilayers, numerous lipidic particles were observed. From these findings a model of bilayer fusion has been suggested as given in figs 16d and 16e.

A model of fusion based on the assumption that out-of-plane thermal fluctuations of apposed bilayers lead to local overcoming of hydration repulsion was proposed from observations on BLM interactions [117, 183]. The energy of hydration repulsion is proportional to the area of contact and could be sufficiently small in case of a localized approach of small areas of bilayers. Local fluctuations of bilayers can cause bending and close approach of bilayers (fig. 16f). A repulsion of the apposed polar heads of lipid molecules in the region of close contact may induce the rupture of interacting outer monolayers resulting in the formation of the monolayer stalk (fig. 16g) which can develop into monolayer fusion (fig. 16h). At this stage the monolayer fusion may be completely reversible.

If the stalk formation is favoured the stalk will expand leading to an irreversible formation of a bilayer separating inner volumes of vesicles. This process is facilitated by negative spontaneous curvature of the interacting outer monolayers. In the model of the stalk formation it is assumed that fusion is completed by destabilization and rupture of the bilayer [183].

The monolayer fusion of planar bilayer lipid membranes discussed before occurs spontaneously after close approach of the bilayers [184, 185]. A fusion of the outer monolayers was also observed when lipid bilayers deposited on mica surfaces are brought into contact by an external pressure of about 10–100 atm [63, 76, 79, 181]. The adhesion of the bilayers can be progressively increased if they are stressed to expose more hydrophobic groups. Only a small increase in the exposed hydrocarbon area is required to increase the adhesion energy, indicating a complex behaviour of the polarity of a surface composed of hydrophilic and hydrophobic groups as discussed in section 4.3.

Fusion of the outer monolayers starts locally at the weakest or most highly stressed point of the two apposing bilayers when they are still at a finite distance. Intermediate arrangements of lipids similar to the formation of a stalk were observed for bilayers deposited on mica surfaces [76]. The final state of the process is the formation of a bilayer after the fusion of outer monolayers occurred (fig. 16h).

This fusion exhibits a single basic mechanism in which the bilayers do not overcome the hydration repulsion. Localized bilayer deformations allow these repulsive forces to be 'bypassed' via strong hydrophobic attraction.

6.4. Role of proteins

Proteins have been recognized to play a crucial role in bringing about membrane fusion. To clarify molecular details of the mechanisms involved, phospholipid vesicles can serve as a valuable model for characterizing early protein-membrane interactions, that may lead eventually to fusion. In section 5.5.1 vesicle aggregation and

fusion processes induced by charged polypeptides were discussed. These studies have revealed that a combination of electrostatic interactions and penetration of hydrophobic segments of the protein into the acyl chain region appear to be of major importance in inducing the fusion process. A deep penetration of peptide moieties into the external bilayer leaflets may result in the perturbation of the lipid packing necessary for fusion. Therefore, studies of correlations between fusion and protein penetration have attracted much attention [165].

By analogy with the hemagglutinin of influenza virus, fusion probably involves the hydrophobic attachment to both bilayers. The fusion of influenza virus with cells does not require Ca^{2+} , but rather is mediated directly by hemagglutinin. Since the hemagglutinin is already an integral protein of the virus envelope, it only needs to expose a hydrophobic moiety to bridge the two membranes. An acidic-induced conformational change resulting in exposure of the conserved hydrophobic N-terminus of the hemagglutinin-2 subunit appears to be the essential feature of this fusion reaction. Hydrophobic photolabelling of the segment indicates that the peptide inserts into phospholipid bilayers as an amphiphilic helix [186]. It was speculated that the penetration of a hydrophobic or amphiphilic peptide into a lipid bilayer at the site of contact induces the formation of structures similar to the inverted micellar intermediates. The fusion may also occur in a local protrusion of the bilayer formed at the area of hydrophobic contact mediated by the protein. Molecular modeling of the fusion peptide assemblies has shown that a cone-shaped structure may be formed that could stabilize a highly curved bilayer [187]. This state shares some properties with the stalk mechanism given in fig. 16. However, the models are being actively discussed [211].

The studies of the effects of Ca^{2+} -binding proteins on vesicle fusion published so far have revealed that the rate of vesicle aggregation is only increased resulting in an increase of the fusion rate (section 5.5.2). It can be assumed that the fusion of bilayers is realized by the action of the cations without any involvement of proteins. This model is supported by the finding that the effect of different cations on fusion agrees with the sequence of fusion activity observed in the protein-free vesicle system. If the cation is unable to fuse the vesicles the addition of the protein may result in an aggregation of the vesicles, but vesicle fusion does not occur. As already discussed in section 5.5, the proteins have to be excluded from the fusion site in order to allow the close approach of bilayers necessary for the cation-induced fusion. In this respect the poly(ethylene glycol)- and protein-induced fusion have a common property. In both cases the aggregator is excluded from the region of contact where fusion of bilayers occurs. Their function in the fusion reaction is mainly based on the formation of a state of apposed membranes.

Tentative models of arrangements of Ca^{2+} -binding proteins in regions close to the fusion site are given in fig. 17. From the experiments it is likely that protein monomers as well as dimers mediate initial aggregation of vesicles [147]. If the proteins do not penetrate into the bilayers the distance of bilayer separation is of the order of the diameter of the proteins which can be estimated to be about 4 nm for annexins. The contact between bilayer phospholipids would be minimal. In the case of PS vesicles the formation of the trans complex for Ca^{2+} in the region of contact

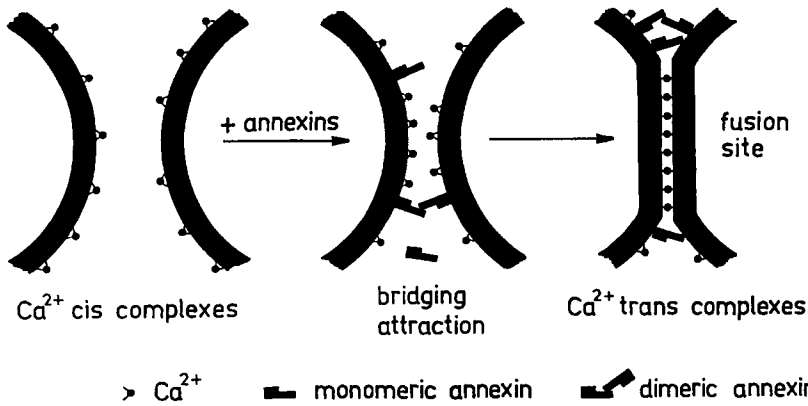


Fig. 17. Model of Ca^{2+} -dependent aggregation and fusion of vesicles mediated by Ca^{2+} -binding proteins, e.g., annexin VII. Ca^{2+} forms cis-complexes with the lipid surface at large distances of bilayer separation (left part). Ca^{2+} -trans complexes can be formed in the aggregated state (right part). Ca^{2+} -binding sites of the protein are involved in the lipid-protein interaction and protein-protein interaction (not indicated in the scheme). Protein monomers and protein associates are able to make a contact with two bilayers resulting in vesicle aggregation. Fusion occurs in protein-free regions of contacting bilayers. The fusion step is characterized by properties very similar to the Ca^{2+} -induced fusion of vesicles in the absence of proteins (adapted from Meers et al. [147].)

may initiate the fusion process in the same manner as described for the Ca^{2+} -induced fusion of PS vesicles. Because it should be expected that the Ca^{2+} -trans complex is only effective at lower distances of bilayer separation other additional processes have to come into the play. Either conformational changes of the proteins or deformations of the protein-free regions enable a closer approach of bilayers or both mechanisms occur simultaneously. Molecular models of the fusion reaction per se should follow the routes discussed for the Ca^{2+} -induced fusion (e.g., fig. 16). Further studies are needed for a thorough understanding of the mechanism of bilayer fusion induced by Ca^{2+} -binding proteins [212].

7. Concluding remarks

Studies on cation-induced fusion of lipid bilayer membranes and the role of polymers and Ca^{2+} -binding proteins in membrane fusion were reviewed. The basic finding of these studies was that membrane surface hydrophobicity is one of the important factors contributing to membrane fusion. A hydrophobic interaction of membranes results when hydrophobic groups of the membrane are exposed to water. As discussed above such hydrophobic areas are formed by binding of cations to bilayer surfaces, local packing strains induced by osmotic stresses, inhomogeneous binding of cations and penetration of proteins into the bilayer. Thus, the physical mechanism of fusion is based on a balance of attractive interactions, such as hydrophobic attraction and short-range repulsive interactions, such as hydration repulsion. All factors

which either increase the hydrophobicity of the surface or decrease the hydration repulsion would tend to increase the probability of fusion.

The hypothesis on the role of hydrophobic interactions in the fusion process has stimulated the development of methods for the direct measurement of the hydrophilicity/hydrophobicity of vesicle surfaces. The measurement of the surface dielectric constant discussed in this chapter is able to provide data about the changes of surface properties relevant to the fusion process. Because the fusion event can occur in a very small area of the surface, experimental methods have to be developed by which one can detect such local changes of these properties of the surface.

The surface hydrophobicity may not be sufficient to induce membrane fusion. Two closely apposed membranes are usually stable. In addition a destabilization of the contact region is necessary resulting in structural transitions. Simple molecular models for the mechanism of lipid membrane fusion were presented incorporating various elements, such as point defects, stalk formation, non-bilayer intermediates, and the boundary between contact and non-contact regions. However, further studies would be necessary in order to elucidate the importance of each mechanism in any given system. Future experimental work should reveal the fundamental similarities and differences in the ways in which fusion occurs in vesicle systems.

Ca^{2+} ions and proteins are essential components of natural fusion processes. Studies of the interaction of these components with bilayer membranes and of the influence on the bilayer fusion have allowed us to identify several essential features that probably relate to their actions in the membrane fusion process. For instance it was shown above, that the lipid composition has a great influence on the fusion extent. The fusion of vesicles composed of PS and PE is efficiently triggered by Ca^{2+} . Therefore, it is not surprising that this phospholipid composition was found in the cytoplasmic monolayers of plasma membranes and vesicles involved in intracellular fusion processes [213]. On the other hand, the outer monolayer of cells contains PC and SM. Thus normally the outer monolayer of cells is not fusion-competent. However, much more components are involved in biological fusion processes. Fusion pores have been detected with electrophysiological techniques in two important natural fusion processes, regulated exocytosis of mast cell granules and fusion mediated by the influenza hemagglutinin. This finding supports the idea that natural fusion processes are highly localized events. Thus, protein-mediated pore formation seems to be a common property for viral and cellular fusion events [211]. Further detailed studies of the role of cytoplasmic and membrane components are needed for a better understanding of the physical mechanisms of membrane fusion processes.

Acknowledgments

This work was supported by a grant of Deutsche Forschungsgemeinschaft (SFB 197, A 10). I thank Drs A. Herrmann, S. Ohki, C.J. Van Oss and O. Zschörnig for many valuable discussions and Anett Dombrowski and Tino Engländer for expert secretarial assistance.

References

1. Düzgünes, N., 1985, Membrane fusion, in: *Subcellular Biochemistry*, Vol. 11, ed. D.B. Roodyn (Plenum, New York) pp. 195–286.
2. Blumenthal, R., 1987, Membrane Fusion, *Curr. Top. Membr. Transp.* **29**, 203–254.
3. Sowers, A.E., 1987, *Cell Fusion* (Plenum, New York).
4. Ohki, S., D. Doyle, T.D. Flanagan, S.W. Hui and E. Mayhew (eds), 1988, *Molecular Mechanisms of Membrane Fusion* (Plenum, New York).
5. Lucy, J.A. and Q.F. Ahkong, 1989, Membrane fusion; fusogenic agents and osmotic forces, in: *Subcellular Biochemistry*, Vol. 14, eds J.R. Harris and A.-H. Etémadi (Plenum, New York) pp. 189–228.
6. Wilschut, J. and D. Hoekstra (eds), 1991, *Membrane Fusion* (Marcel Dekker, New York).
7. Poste, G. and A.C. Allison, 1973, Membrane fusion, *Biochim. Biophys. Acta* **300**, 421–465.
8. Poste, G. and G.L. Nicolson (eds), 1978, *Membrane Fusion* (Elsevier, Amsterdam).
9. Littlefield, J.W., 1987, The early history of mammalian somatic cell fusion, in: *Cell Fusion*, ed. A.E. Sowers (Plenum, New York).
10. Barski, G., S. Sorienel and F. Cornefert, 1960, Production dans des cultures in vitro de deux souches cellulaires en association de cellules de caractere "hybride", *C.R. Acad. Sci.* **251**, 1825–1827.
11. Harris, H. and J.F. Watkins, 1965, Hybrid cells derived from mouse and man: Artificial heterokaryons of mammalian cells from different species, *Nature (London)* **205**, 640–646.
12. Kohler, G. and C. Milstein, 1975, Continuous cultures of fused cells secreting antibody of predefined specificity, *Nature (London)* **256**, 495–497.
13. Pontecorvo, G., 1975, Production of mammalian somatic cell hybrids by means of poly (ethylene glycol) treatment, *Somatic Cell Genet.* **1**, 397–400.
14. Palade, G., 1975, Intracellular aspects of the process of protein synthesis, *Science* **189**, 347–358.
15. Hiram, Y. and A. Nir, 1984, On mechanical aspects, *J. Theoret. Biol.* **111**, 91–113.
16. Neher, E., 1992, Ion channels for communication between and within cells, *Science* **256**, 498–502.
17. Penner, R. and E. Neher, 1989, The patch clamp technique in the study of secretion, *TINS* **12**, 159–163.
18. Sakman, B., 1992, Elementary steps in synaptic transmission revealed by currents through single ion channels, *Science* **256**, 503–512.
19. Chow, R.H., L. von Rüden and E. Neher, 1992, Delay in vesicle fusion revealed by electrochemical monitoring of single secretory events in adrenal chromaffin cells, *Nature* **356**, 60–63.
20. Stegmann, T., R.W. Doms and A. Helenius, 1989, Protein-mediated membrane fusion, *Annu. Rev. Biophys. Biophys. Chem.* **18**, 187–211.
21. Zaks, W.J. and C.E. Creutz, 1990, Evaluation of the annexins as potential mediators of membrane fusion in exocytosis, *J. Bioenerg. Biomembr.* **22**, 97–120.
22. Burgoyne, R.D., 1990, Secretory vesicle-associated proteins and their role in exocytosis, *Annu. Rev. Physiol.* **52**, 647–659.
23. Morgan, A. and R.D. Burgoyne, 1992, Exo 1 and Exo 2 proteins stimulate calcium-dependent exocytosis in permeabilized adrenal chromaffin cells, *Nature* **355**, 833–836.
24. Artalejo, C.R., A.G. Garcia and D. Aunis, 1987, Chromaffin cell calcium channel kinetics measured isotopically through fast calcium, strontium, and barium fluxes, *J. Biol. Chem.* **262**, 915–926.
25. Llinas, R., M. Sugimori and R.B. Silver, 1992, Microdomains of high calcium concentration in a presynaptic terminal, *Science* **256**, 677–679.
26. Schatz, G., 1989, Biological cold fusion, *Nature* **339**, 336.
27. Wilschut, J., 1989, Intercellular membrane fusion, *Curr. Opin. Cell Biol.* **1**, 639–647.
28. White, J.M., 1990, Viral and cellular membrane fusion proteins, *Ann. Rev. Physiol.* **52**, 675–697.
29. White, J.M., M. Kielian and A. Helenius, 1983, Membrane fusion proteins of enveloped animal viruses, *Q. Rev. Biophys.* **16**, 151–195.
30. Hoekstra, D., 1990, Membrane fusion of enveloped viruses: Especially a matter of protein, *J. Bioenerg. Biomembr.* **22**, 121–155.
31. Srinivas, S.K., R.V. Srinivas, G.M. Anantharamaiah, J.P. Segrest and R.W. Compans, 1992, Membrane interactions of synthetic peptides corresponding to amphipathic helical segments of the human immunodeficiency virus type-1 envelope glycoprotein, *J. Biol. Chem.* **267**, 7121–7127.

32. Ohnishi, S., 1988, Fusion of viral envelopes with cellular membranes, in: *Membrane Fusion in Fertilization. Cellular Transport and Viral Infection*, eds N. Düzgünes and F. Bronner (Academic Press, New York) pp. 257–296.
33. Düzgünes, N., M.C. Padraso de Lima, C.E. Larsen, L. Stamatatos, D. Flasher, D.R. Alford, D.S. Friend and S. Nir, 1991, Fusion of influenza, sendai and simian immunodeficiency viruses with cell membranes and liposomes, in: *Cell and Model Membrane Interactions*, ed. S. Ohki (Plenum, New York) pp. 179–197.
34. Düzgünes, N. and S.A. Shavnin, 1992, Membrane destabilization by N-terminal peptides of viral envelope proteins, *J. Membr. Biol.* **128**, 71–80.
35. Papahadjopoulos, D., 1978, Calcium-induced phase changes and fusion in natural and model membranes, *Cell Surf. Rev.* **5**, 765–790.
36. Düzgünes, N., Th.M. Allen, J. Fedor and D. Papahadjopoulos, 1988, Why fusion assays disagree, in: *Molecular Mechanisms of Membrane Fusion*, eds Ohki et al. (Plenum, New York) pp. 543–555.
37. Düzgünes, N. and J. Bentz, 1988, Fluorescence assays for membrane fusion, in: *Spectroscopic Membrane Probes*, Vol. 1, ed. L.M. Loew (CRC Press, Boca Raton, FL) pp. 117–159.
38. Morris, J.S., D. Bradley, C.C. Gibson, P.D. Smith and R. Blumenthal, 1988, Use of membrane-associated fluorescence probes to monitor fusion of bilayer vesicles: Application to rapid kinetics using pyrene excimer/monomer fluorescence, in: *Spectroscopic Membrane Probes*, Vol. 1, ed. L.M. Loew (CRC Press, Boca Raton, FL) pp. 161–191.
39. Struck, D.K., D. Hoekstra and R.E. Pagano, 1981, Use of resonance energy transfer to monitor membrane fusion, *Biochemistry* **20**, 4093–4099.
40. Hoekstra, D., K. de Boer, T. Klappe and J. Wilschut, 1984, Fluorescence method for measuring the kinetics of fusion between biological membranes, *Biochemistry* **23**, 5675–5681.
41. Fung, B.K. and L. Stryer, 1978, Surface density determination in membranes by fluorescence energy transfer, *Biochemistry* **17**, 5241–5248.
42. Amselem, S., Y. Barenholz, A. Loyter, S. Nir and D. Lichtenbrg, 1986, Fusion of Sendai virus with negatively charged liposomes as studied by pyrene-labeled phospholipid liposomes, *Biochim. Biophys. Acta.* **860**, 301–313.
43. Parente, R.A. and B.R. Lentz, 1986, Fusion and phase separation monitored by life time changes of fluorescence phospholipid probe, *Biochemistry* **25**, 1021–1026.
44. Hoekstra, D., 1982, Kinetics of intermixing of lipids and mixing of aqueous contents during vesicle fusion, *Biochim. Biophys. Acta* **692**, 171–175.
45. Wilschut, J. and D. Papahadjopoulos, 1979, Ca^{2+} -induced fusion of phospholipid vesicles monitored by mixing of aqueous contents, *Nature* **281**, 690–692.
46. Bentz, J., D. Düzgünes and S. Nir, 1983, Kinetics of divalent cation-induced fusion of phosphatidylserine vesicles: Correlation between fusogenic capacities and binding affinities, *Biochemistry*, **22**, 3320–3330.
47. Derjaguin, B.V., N.V. Churaev and V.M. Muller, 1987, *Surface Forces* (Pergamon Press, New York).
48. Verwey, E.J.W. and J.Th.G. Overbeek, 1948, *Theory of Stability of Lyophobic Colloids* (Elsevier, Amsterdam).
49. Nir, S., J. Bentz and A.R. Portis, 1980, Effect of cation concentrations and temperature on the rates of aggregation of acidic phospholipid vesicles: Application to fusion, *Adv. Chem. Ser.* **188**, 75–106.
50. Nir, S., 1991, Modeling of aggregation and fusion of phospholipid vesicle, in: *Membrane Fusion*, eds J. Wilschut and D. Hoekstra (Marcel Dekker, New York) pp. 127–154.
51. Wilschut, J., S. Nir, J. Scholma and D. Hoekstra, 1985, Kinetics of Ca^{2+} -induced fusion of cardiolipin-phosphatidylcholine vesicles: Correlation between vesicle aggregation, bilayer destabilization and fusion, *Biochemistry* **24**, 4630–4636.
52. Ohki, S., N. Düzgünes and K. Leonards, 1982, Phospholipid vesicle aggregation: Effect of monovalent and divalent cations, *Biochemistry* **21**, 2127–2133.
53. Ohki, S., S. Roy, H. Ohshima and K. Leonards, 1984, Monovalent cation-induced phospholipid vesicle aggregation: Effect of ion binding, *Biochemistry* **23**, 6126–6132.

54. Eklund, K.K., 1990, Monovalent cation-induced fusion of acidic phospholipid vesicles, *Chem. Phys. Lipids* **52**, 199–206.
55. Shigematsu, M., T. Fujie, T. Inoue, Y. Murata, M. Tanaka and G. Sugihara, 1992, Abnormal aggregation of acidic phospholipid vesicles in the very low concentration range of divalent cations, *J. Colloid Interface Sci.* **149**, 536–541.
56. Ohki, S. and J. Duax, 1986, Interactions of polyamines with phosphatidylserine membranes, *Biochim. Biophys. Acta* **861**, 177–186.
57. Portis, A., C. Newton, W. Pangborn and D. Papahadjopoulos, 1979, Studies on the mechanism of membrane fusion: Evidence for an intermembrane Ca^{2+} -phospholipid complex, synergism with Mg^{2+} and inhibition by spectrin, *Biochemistry* **18**, 780–790.
58. Feigenson, G.W., 1986, On the nature of calcium binding between phosphatidylserine lamellae, *Biochemistry* **25**, 5819–5825.
59. Feigenson, G.W., 1989, Calcium ion binding between lipid bilayers: The four-component system of phosphatidylserine, phosphatidylcholine, calcium chloride, and water, *Biochemistry* **28**, 1270–1278.
60. Wilschut, J., N. Düzgünes and D. Papahadjopoulos, 1981, Calcium/magnesium specificity in membrane fusion: Kinetics of aggregation and fusion of phosphatidylserine vesicles and the role of bilayer curvature, *Biochemistry* **20**, 3126–3133.
61. Rand, P. and V.A. Parsegian, 1989, Hydration forces between phospholipid bilayers, *Biochim. Biophys. Acta* **988**, 351–376.
62. Lis, L.J., M. McAlister, N. Fuller, R.P. Rand and V.A. Parsegian, 1982, Interactions between neutral phospholipid bilayer membranes, *Biophys. J.* **37**, 657–666.
63. Wolfe, J., E. Perez, M. Bonanno and J.-P. Chapel, 1991, The interaction and fusion of bilayers formed from unsaturated lipids, *Eur. Biophys. J.* **19**, 275–281.
64. Parsegian, V.A. and R.P. Rand, 1983, Membrane interaction and deformation. Surface forces in biological systems, *Ann. NY Acad. Sci.* **416**, 1–12.
65. Rand, R.P., N. Fuller, V.A. Parsegian and D.C. Rau, 1988, Variation of hydration forces between neutral phospholipid bilayers: Evidence for hydration attraction, *Biochemistry* **27**, 7711–7722.
66. Israelachvili, J.N. and H. Wennerström, 1990, Hydration or steric forces between amphiphilic surfaces?, *Langmuir* **6**, 873–876.
67. Van Oss, C.J., M.K. Chaudhury and R.J. Good, 1987, Monopolar surfaces, *Adv. Colloid Interface Sci.* **28**, 35–64.
68. Van Oss, C.J., 1988, Polar interfacial interactions, hydration pressure and membrane fusion, in: *Molecular Mechanism of Membrane Fusion*, eds S. Ohki, D. Doyle, T.D. Flanagan, S.W. Hui and E. Mayhew (Plenum, New York) pp. 113–122.
69. Van Oss, C.J., M.K. Chaudhury and R.J. Good, 1988, Interfacial Lifshitz–Van der Waals and polar interactions in macroscopic systems, *Chem. Rev.* **88**, 927–941.
70. Van Oss, C.J. and R.J. Good, 1988, On the mechanism of “hydrophobic” interactions, *J. Disp. Sci. Technol.* **9**, 355–362.
71. Van Oss, C.J., 1990, Surface free energy contribution to cell interactions, in: *Biophysics of the Cell Surface*, eds R. Glaser and D. Gingell (Springer, Berlin) pp. 131–152.
72. Ohki, S., 1984, Effects of divalent cations, temperature, osmotic pressure gradient, and vesicle curvature on phosphatidylserine vesicle fusion, *J. Membr. Biol.* **77**, 265–275.
73. Ohki, S. and K. Arnold, 1990, Phospholipid vesicle fusion induced by cations and poly(ethylene glycol), in: *Biophysics of the Cell Surface*, eds R. Glaser and D. Gingell (Springer, Berlin) pp. 193–219.
74. Ohki, S. and K. Arnold, 1990, Surface dielectric constant, surface hydrophobicity and membrane fusion, *J. Membr. Biol.* **114**, 195–203.
75. Ohki, S., 1991, Physico-chemical factors underlying membrane adhesion and fusion, in: *Cell and Model Membrane Interaction*, ed. S. Ohki (Plenum, New York) pp. 267–283.
76. Helm, C.A., J.N. Israelachvili and P.M. McGuiggan, 1992, Role of hydrophobic forces in bilayer adhesion and fusion, *Biochemistry* **31**, 1794–1805.
77. Israelachvili, J.N., 1991, *Intermolecular and Surface Forces* (Academic Press, New York).
78. Pashley, R.M., P.M. McGuiggan, B.W. Ninham and D.F. Evans, 1985, *Science* **229**, 1088–1089.

79. Helm, C.A., J.N. Israelachvili and P.M. McGuiggan, 1989, Molecular mechanisms and forces involved in the adhesion and fusion of amphiphilic bilayers, *Science* **246**, 919–922.
80. Napper, D.H., 1983, *Polymeric Stabilization of Colloidal Dispersions* (Academic Press, New York).
81. Arnold, K., M. Krumbiegel, O. Zschörnig, D. Barthel and S. Ohki, 1991, Influence of polar polymers on the aggregation and fusion of membranes, in: *Cell and Model Membrane Interactions*, ed. S. Ohki (Plenum, New York) pp. 63–87.
82. Van Oss, C.J., K. Arnold, R.J. Good, K. Gawrisch and S. Ohki, 1992, Interfacial tension and the osmotic pressure of solutions of polar polymers, *J. Macromol. Sci. Chem.* **A27**, 563–580.
83. Van Oss, C.J., K. Arnold and W.T. Coakley, 1990, Depletion flocculation and depletion stabilization of erythrocytes, *Cell Biophys.* **17**, 1–10.
84. Klein, J. and P.F. Luckham, 1984, Forces between two adsorbed poly(ethylene oxide) layers in a good aqueous solvent in the range 0–100 nm, *Macromolecules* **17**, 1041–1048.
85. Claesson, P.M. and C.G. Golander, 1987, Direct measurements of steric interactions between mica surfaces covered with electrostatically bound low-molecular-weight polyethylene oxide, *J. Colloid Interface Sci.* **117**, 366–374.
86. Arnold, K., Y.M. Lvov, M. Szögyi and S. Györgyi, 1986, Effect of poly(ethylene oxide)-containing surfactants on membrane-membrane interaction, *Stud. Biophys.* **113**, 7–14.
87. Arnold, K., O. Zschörnig, W. Herold and D. Barthel, 1987, Effect of PEG on the electrophoretic mobility of liposomes, *Mol. Cryst. Liq. Cryst.* **152**, 357–362.
88. Arnold, K., A. Herrmann, K. Gawrisch and L. Pratsch, 1988, Water-mediated effects of PEG on membrane properties and fusion, in: *Molecular Mechanisms of Membrane Fusion*, eds S. Ohki, D. Doyle, T.D. Flanagan, S.W. Hui and E. Mayhew (Plenum, New York) pp. 255–272.
89. Arnold, K., O. Zschörnig, L. Pratsch, E. Donath, D. Barthel and A. Herrmann, 1988, Exclusion of PEG from membrane surfaces and aggregation of liposomes and lipoproteins, *Stud. Biophys.* **127**, 113–120.
90. Arnold, K., O. Zschörnig, D. Barthel and W. Herold, 1990, Exclusion of poly(ethylene glycol) from liposome surfaces, *Biochim. Biophys. Acta* **1022**, 303–310.
91. Bäumler, H. and E. Donath, 1987, Does dextran indeed significantly increase the surface potential of human red blood cells, *Stud. Biophys.* **120**, 113–122.
92. Pratsch, L. and E. Donath, 1988, Poly(ethylene glycol) depletion layers on human red blood cell surfaces measured by electrophoresis, *Stud. Biophys.* **123**, 101–108.
93. Arnold, K. and O. Zschörnig, 1988, Aggregation of human plasma low density lipoproteins by means of poly(ethylene glycol), *Biomed. Biochim. Acta* **47**, 949–954.
94. Tilcock, C.T.S. and D. Fisher, 1982, The interaction of phospholipid membranes with poly(ethylene glycol). Vesicle aggregation and lipid exchange, *Biochim. Biophys. Acta* **688**, 645–652.
95. Hoekstra, D., 1982, Role of lipid phase separation and membrane hydration in phospholipid vesicle fusion, *Biochemistry* **21**, 2833–2840.
96. Boni, L.T., J.S. Hah, S.W. Hui, P. Mukherjee, J.T. Ho and C.Y. Jung, 1984, Aggregation and fusion of unilamellar vesicles by poly(ethylene glycol), *Biochim. Biophys. Acta* **775**, 409–418.
97. Yamazaki, M., S. Ohnishi and T. Ito, 1989, Osmoelastic coupling in biological structures: Decrease in membrane fluidity and osmophobic association of phospholipid vesicles in response to osmotic stress, *Biochemistry* **28**, 3710–3715.
98. Yamazaki, M. and T. Ito, 1990, Deformation and instability in membrane structure of phospholipid vesicles caused by osmophobic association: Mechanical stress model for the mechanisms of poly(ethylene glycol)-induced membrane fusion, *Biochemistry* **29**, 1309–1314.
99. Raudino, A. and P. Bianciardi, 1991, Polymer-mediated electrostatic interactions between charged lipid assemblies and electrolyte solutions: A tentative model of the poly(ethylene glycol)-induced cell fusion, *J. Theoret. Biol.* **149**, 1–20.
100. Evans, E.A. and D. Needham, 1988, Intrinsic colloidal attraction/repulsion between lipid bilayers and strong attraction induced by non-adsorbing polymers, in: *Molecular Mechanisms of Membrane Fusion*, eds S. Ohki, D. Doyle, T.D. Flanagan, S.W. Hui and E. Mayhew (Plenum, New York) pp. 83–99.
101. Asakura, S. and F. Oosawa, 1958, Interaction between particles suspended in solutions of macromolecules, *J. Polym. Sci.* **33**, 183–192.

102. Rupert, L.A.M., J.B.F.N. Engberts and D. Hoekstra, 1988, Effect of poly(ethylene glycol) on the Ca^{2+} -induced fusion of, *Biochemistry* **27**, 8232–8239.
103. Fonteijn, T.A.A., J.B.F.N. Engberts and D. Hoekstra, 1991, On the mechanism of membrane fusion: Use of synthetic surfactant vesicles as a novel model system, in: *Cell and Model Membrane Interaction*, ed. S. Ohki (Plenum, New York) pp. 215–228.
104. Sundari, C.S., B. Ramau and Balasubramaniau, 1991, Hydrophobic surfaces in oligosaccharides: linear dextrans are amphiphilic chains, *Biochim. Biophys. Acta* **1065**, 35–41.
105. Arnold, K., L. Pratsch and K. Gawrisch, 1983, Effect of poly(ethylene glycol) on phospholipid hydration and polarity of the external phase, *Biochim. Biophys. Acta* **728**, 121–128.
106. Rand, R.P. and V.A. Parsegian, 1986, Mimicry and mechanism in phospholipid models of membrane fusion, *Annu. Rev. Physiol.* **48**, 201–212.
107. Gawrisch, K., V.A. Parsegian and P. Rand, 1989, Membrane hydration, in: *Biophys of the Cell Surface*, eds R. Glaser and D. Gingell (Springer, Berlin) pp. 61–73.
108. Salsbury, N.J., A. Darke and D. Chapman, 1972, Deuteron magnetic resonance studies of water associated with phospholipids, *Chem. Phys. Lipids* **8**, 142–151.
109. Finer, E.G. and A. Darke, 1974, Phospholipid hydration studied by deuteron magnetic resonance spectroscopy, *Chem. Phys. Lipids* **12**, 1–16.
110. Arnold, K. and K. Gawrisch, 1993, Effect of fusogenic agents on membrane hydration: A deuterium nuclear magnetic resonance approach, *Methods Enzymol.* **222**, 143–157.
111. Gawrisch, K., D. Ruston, J. Zimmerberg, V.A. Parsegian, R.P. Rand and N. Fuller, 1992, Membrane dipole potentials, hydration forces, and the ordering of water at the membrane surface, *Biophys. J.* **61**, 1213–1223.
112. McIntosh, T.J., A.D. Magid and S.A. Simon, 1987, Steric repulsion between phosphatidylcholine bilayers, *Biochemistry* **26**, 7325–7332.
113. Burgess, S.W., T.J. McIntosh and B.R. Lentz, 1992, Modulation of poly(ethylene glycol)-induced fusion by membrane hydration: Importance of interbilayer separation, *Biochemistry* **31**, 2653–2661.
114. Hauser, H., E.G. Finer and A. Darke, 1977, Crystalline anhydrous Ca-phosphatidylserine bilayers, *Biochem. Biophys. Res. Comm.* **76**, 267–274.
115. Laroche, G., E.J. Dufourc, J. Dufourc and M. Pérolet, 1991, Structure and dynamics of dimyristoylphosphatidic acid/calcium complexes by ^2H -NMR, infrared, and Raman spectroscopies and small-angle X-ray diffraction, *Biochemistry* **30**, 3105–3114.
116. Allen, T.M., K. Hong and D. Papahadjopoulos, 1990, Membrane contact, fusion and hexagonal (H_{II}) transitions in phosphatidyl-ethanolamine liposomes, *Biochemistry* **29**, 2976–2985.
117. Leikin, S.L., M.M. Kozlov, L.V. Chernomordik, V.S. Markin and Y.A. Chizmadzhev, 1987, Membrane fusion: Overcoming the hydration barrier and local restructuring, *J. Theoret. Biol.* **129**, 411–425.
118. MacDonald, R.I. and R.C. MacDonald, 1983, Lipid mixing during freeze-thawing of liposome membranes as monitored by fluorescence energy transfer, *Biochim. Biophys. Acta* **735**, 243–251.
119. Zimmermann, U., 1982, Electric field-mediated fusion and related electrical phenomena, *Biochim. Biophys. Acta* **694**, 227–277.
120. Papahadjopoulos, D., G. Poste, B.E. Schaffer and W.J. Vail, 1974, Membrane fusion and molecular segregation in phospholipid vesicles, *Biochim. Biophys. Acta* **352**, 10–28.
121. Düzgünes, N., R.M. Straubinger, P.A. Baldwin, D.S. Friend and D. Papahadjopoulos, 1985, Proton-induced fusion of oleic acid phosphatidylethanolamine liposomes, *Biochemistry* **24**, 3091–3098.
122. Ellens, H., J. Bentz and F.C. Szoka, 1985, H^{+} - and Ca^{2+} -induced fusion and destabilization of liposomes, *Biochemistry* **24**, 3099–3106.
123. Hong, K., F. Schuber and D. Papahadjopoulos, 1983, Polyamines: Biological modulators of membrane fusion, *Biochim. Biophys. Acta* **732**, 469–472.
124. Ellens, H., J. Bentz and F.C. Szoka, 1986, Fusion of phosphatidylethanolamine-containing liposomes and the mechanism of the L- H_{II} phase transition, *Biochemistry* **25**, 4141–4147.
125. Ohki, S., 1988, Surface tension, hydration energy and membrane fusion, in: *Molecular Mechanics of Membrane Fusion*, eds S. Ohki, D. Doyle, T.D. Flanagan, S.W. Hui and E. Mayhew (Plenum, New York) pp. 123–138.

126. Tocanne, J.-F. and J. Teissié, 1990, Ionization of phospholipids and phospholipid-supported interfacial lateral diffusion of protons in membrane model systems, *Biochim. Biophys. Acta* **1031**, 111–142.
127. Kimura, Y. and A. Ikegami, 1985, Local dielectric properties around polar regions of lipid bilayers, *J. Membr. Biol.* **85**, 225–231.
128. Lentz, B.R., G.F. McIntyre, D.J. Parks, J.C. Yates and D. Massenburg, 1992, Bilayer curvature and certain amphipaths promote poly(ethylene glycol)-induced fusion of dipalmitoylphosphatidylcholine unilamellar vesicles, *Biochemistry* **31**, 2643–2653.
129. Lentz, B.R., J. Prevratil, D. Parks and J.R. Wu, 1992, Fluorescent probes reveal altered interfacial properties in membranes that can be induced to fuse by PEG, *Biophys. J.* **61**, A497.
130. Brewer, G.J., 1992, Polarity decrease at the adhesive junction between two model membranes containing gangliosides, *Biochemistry* **31**, 1809–1815.
131. Blow, A.M.J., G.M. Botham, D. Fisher, A.H. Goodall, C.P.S. Tilcock and J.A. Lucy, 1978, Water and calcium ions in cell fusion induced by PEG, *FEBS Lett.* **94**, 305–310.
132. Hui, S.W. and L.T. Boni, 1991, Membrane Fusion induced by polyethylene glycol, in: *Membrane Fusion*, eds J. Wilschut and D. Hoekstra (Marcel Dekker, New York) pp. 231–253.
133. MacDonald, R.I., 1985, Membrane fusion due to dehydration by polyethylene glycol, dextran or sucrose, *Biochemistry* **24**, 4058–4066.
134. Parente, R.A. and B.R. Lentz, 1986, Rate and extent of poly(ethylene glycol)-induced large vesicle fusion monitored by bilayer and internal content mixing, *Biochemistry* **25**, 6678–6688.
135. Parente, R.A. and B.R. Lentz, 1984, Phase behavior of large unilamellar vesicles composed of synthetic phospholipids, *Biochemistry* **23**, 2353–2362.
136. Arnold, K., A. Herrmann, L. Pratsch and K. Gawrisch, 1985, The dielectric properties of aqueous solutions of poly(ethylene glycol) and their influence on membrane structure, *Biochim. Biophys. Acta* **815**, 515–518.
137. Burgess, S.W., D. Massenburg, J.C. Yates and B.R. Lentz, 1991, Poly(ethylene glycol)-induced lipid mixing but not fusion between synthetic phosphatidylcholine large unilamellar vesicles, *Biochemistry* **30**, 4193–4200.
138. Mitsuya, H., D.J. Looney, S. Kuno, R. Ueno, F. Wong-Staal and S. Broder, 1988, Dextran sulfate suppression of viruses in the HIV family: Inhibition of virion binding to CD⁴⁺ cells, *Science* **240**, 646–649.
139. Arnold, K., T.D. Flanagan and S. Ohki, 1990, Influence of dextran sulfate on the fusion of Sendai virus with liposomes, *Biomed. Biochim. Acta* **49**, 633–635.
140. Ohki, S., K. Arnold, N. Srinivasakumar and T.D. Flanagan, 1992, Effect of anionic polymers on fusion of Sendai virus with human erythrocyte ghosts, *Antiviral Res.* **18**, 163–177.
141. Herrmann, A., T. Korte, K. Arnold and B. Hillebrecht, 1992, The influence of dextran sulfate on influenza virus fusion with erythrocyte membranes, *Antiviral Res.* **19**, 295–311.
142. Krumbiegel, M. and K. Arnold, 1990, Microelectrophoresis studies of the binding of glycosaminoglycans to phosphatidylcholine liposomes, *Chem. Phys. Lipids* **54**, 1–7.
143. Kim, Y.C. and T. Nishida, 1977, Nature of interaction of dextran sulfate with lecithin dispersions and lysolecithin micelles, *J. Biol. Chem.* **252**, 1243–1249.
144. Grudzev, A.D., V.V. Khrantsov, L.M. Weiner and V.G. Budker, 1982, Fluorescence polarization study of the interaction of biopolymers with liposomes, *FEBS Lett.* **137**, 227–230.
145. Bichenkov, E.E., V.G. Budker, I.K. Korobeinicheva, E.V. Savchenko and V.V. Filimonov, 1988, DNA interaction with phosphatidylcholine liposomes. Melting of DNA and phase transition of the lipid membrane in the complex (Russian), *Biol. Membrany (Moscow)* **5**, 843–851.
146. Creutz, E.C., W.J. Zaks, H.C. Hamann and W.H. Martin, 1987, The role of Ca²⁺-dependent membrane-binding proteins in the regulation and mechanism of exocytosis, in: *Cell Fusion*, ed. A.E. Sowers (Plenum, New York).
147. Meers, P., K. Hong and D. Papahadjopoulos, 1991, Annexin-phospholipid interactions in membrane fusion, in: *Cell and Model Membrane Interactions*, ed. S. Ohki (Plenum, New York) pp. 115–134.
148. Stollery, J.G. and W.J. Vail, 1977, Interaction of divalent cations or basic proteins with phosphatidylethanolamine vesicles, *Biochim. Biophys. Acta* **471**, 372–390.

149. Gad, A.E., B.C. Silver and G.D. Eytan, 1982, Polycation-induced fusion of negatively charged vesicles, *Biochim. Biophys. Acta* **690**, 124–132.
150. Walter, A., C.J. Steer and R. Blumenthal, 1986, Polylysine induces pH-dependent fusion of acidic phospholipid vesicles: A model for polycation-induced fusion, *Biophys. Biochim. Acta* **861**, 319–330.
151. Bondeson, J. and R. Sundler, 1990, Promotion of acidic-induced membrane fusion by basic peptides. Amino acid and phospholipid specificities, *Biochim. Biophys. Acta* **1026**, 186–194.
152. Uster, P.S. and D.W. Deamer, 1985, pH-dependent fusion of liposomes using titrable polycations, *Biochemistry* **24**, 1–8.
153. Hartmann, W. and H.-J. Galla, 1978, Binding of polylysine to charged bilayer membranes – Molecular organization of a lipid-peptide complex, *Biochim. Biophys. Acta* **509**, 474–490.
154. Takahashi, H., S. Matuoka, S. Kato, K. Ohki and I. Hatta, 1991, Electrostatic interaction of poly(L-lysine) with, *Biochim. Biophys. Acta* **1069**, 229–234.
155. Hong, K. and N. Düzgünes and D. Papahadjopoulos, 1982, Modulation of membrane fusion by calcium-binding proteins, *Biophys. J.* **37**, 297–305.
156. Hong, K., P.R. Meers, N. Düzgünes and D. Papahadjopoulos, 1991, Fusion of liposomes induced and modulated by proteins and polypeptides, in: *Membrane Fusion*, eds J. Wilschut and D. Hoekstra (Marcel Dekker, New York).
157. Meers, P., D. Daleke, K. Hong and D. Paphadjopoulos, 1991, Interactions of annexins with membrane phospholipids, *Biochemistry* **30**, 2903–2908.
158. Meers, P., J. Bentz, D. Alford, S. Nir, D. Paphadjopoulos and K. Hong, 1988, Synexin enhances the aggregation rate but not the fusion rate of liposomes, *Biochemistry* **27**, 4430–4439.
159. Creutz, C.E. and D.C. Sterner, 1983, Calcium dependence of the binding of synexin to isolated chromaffin granules, *Biochem. Biophys. Res. Commun.* **114**, 355–364.
160. Meers, P., T. Mealy, N. Pavlotsky and A.I. Tauber, 1992, Annexin I-mediated vesicular aggregation: mechanism and role in human neutrophils, *Biochemistry* **31**, 6372–6382.
161. Huber, R., J. Römisch and E.-P. Paques, 1990, The crystal and molecular structure of human annexin V, an anticoagulant protein that binds to calcium and membranes, *EMBO J.* **9**, 3867–3874.
162. Huber, R., M. Schneider, I. Mayr, J. Römisch and E.-P. Paques, 1990, The calcium binding sites in human annexin V by crystal structure analysis at 2.0 Å resolution, *FEBS Lett.* **275**, 15–21.
163. Mosior, M. and McLaughlin, 1992, Binding of basic peptides to acidic lipids in membranes: Effects of inserting alanine(s) between the, *Biochemistry* **31**, 1767–1773.
164. Lee, S., R. Aoki, O. Oishi, H. Aoyagi and N. Yamasaki, 1992, Effect of amphipathic peptides with different α -helical contents on liposome fusion, *Biochim. Biophys. Acta* **1103**, 157–162.
165. Arnold, K., D. Hoekstra and S. Ohki, 1992, Association of lysozyme to phospholipid surfaces and vesicle fusion, *Biochim. Biophys. Acta* **1124**, 88–94.
166. Rand, R.P., 1981, Interacting phospholipid bilayers: Measured forces and induced structural changes, *Annu. Rev. Biophys. Bioeng.* **10**, 277–314.
167. Silvius, J.R., 1990, Calcium-induced phase separations and interactions of phosphatidylcholine/ionic phospholipid vesicles, *Biochemistry* **29**, 2930–2938.
168. Evans, E.A. and V.A. Parsegian, 1983, Energetics of membrane deformation and adhesion in cell and vesicle aggregation, *Ann. NY Acad. Sci.* **416**, 13–33.
169. Kachar, B., N. Fuller and R.P. Rand, 1986, Morphological responses to calcium-induced interaction of phosphatidylserine-containing vesicles, *Biophys. J.* **50**, 779–788.
170. Cohen, F.S., M.H. Akabas, J. Zimmerberg and A. Finkelstein, 1984, Parameters affecting the fusion of unilamellar phospholipid vesicles with planar bilayer membranes, *J. Cell Biol.* **98**, 1054–1062.
171. Lucy, J.A. and Q.F. Ahkong, 1986, An osmotic model for the fusion of biological membranes, *FEBS Lett.* **199**, 1–11.
172. Cullis, P.R. and M.J. Hope, 1978, Effects of fusogenic agents on membrane structure of erythrocyte ghosts and the mechanism of membrane fusion, *Nature* **271**, 672–675.
173. Verkley, A.J., C. Mombers, W.J. Gerritsen, L. Leunissen-Bijvelt and R.P. Cullis, 1979, Fusion of phospholipid vesicles in, *Biochim. Biophys. Acta* **555**, 358–361.
174. Siegel, D.P., 1984, Inverted micellar structures in bilayer membranes, *Biophys. J.* **45**, 399–420.

175. Ellens, H., D.P. Siegel, D. Alford, P.L. Yeagle, L. Boni, L.J. Lis, P.J. Quinn and J. Bentz, 1989, Membrane fusion and inverted phases, *Biochemistry* **28**, 3692–3703.
176. Siegel, D.P., 1986, Inverted micellar intermediates and the transitions between lamellar, cubic, and inverted hexagonal lipid phases, II. Implications for membrane-membrane interactions and membrane fusion, *Biophys. J.* **49**, 1171–1183.
177. Siegel, D.P., 1987, Membrane-membrane interactions via intermediates in lamellar-to-inverted hexagonal phase transitions, in: *Cell Fusion*, ed. A.E. Sowers (Plenum, New York) pp. 181–207.
178. Siegel, D.P., J.L. Burns, M.H. Chestnut and Y. Talmon, 1989, Intermediates in membrane fusion and bilayer/nonbilayer phase transitions imaged by time-resolved cryo-transmission electron microscopy, *Biophys. J.* **56**, 161–169.
179. Siegel, D.P., J. Bansbach, D. Alford, H. Ellens, L.J. Lis, P.J. Quinn, P.L. Yeagle and J. Bentz 1989, Physiological levels of diacylglycerols in phospholipid membranes induce membrane fusion and stabilize inverted phases, *Biochemistry* **28**, 3703–3709.
180. Papahadjopoulos, D., S. Nir and N. Düzgünes, 1990, Molecular mechanisms of calcium-induced membrane fusion, *J. Bioenerg. Biomembr.* **22**, 157–179.
181. Horn, R.G., 1984, Direct observation of the force between two lipid bilayers and observation of their fusion, *Biochim. Biophys. Acta* **778**, 224–228.
182. Hui, S.W., T.P. Stewart, L.T. Boni and P.L. Yeagle, 1981, Membrane fusion through point defects in bilayers, *Science* **212**, 921–923.
183. Chernomordik, L.V., G.B. Melikyan and Yu.A. Chizmadzhev, 1987, Biomembrane fusion: A new concept derived from model studies using two interacting planar lipid bilayers, *Biochim. Biophys. Acta* **906**, 309–352.
184. Neher, E., 1974, Asymmetric membranes resulting from the fusion of two black lipid bilayers, *Biochim. Biophys. Acta* **373**, 327–336.
185. Chernomordik, L.V., M.M. Kozlow, G.B. Melikyan, I.G. Abidor, V.S. Markin, and Yu.A. Chizmadzhev, 1985, The shape of lipid molecules and monolayer membrane fusion, *Biophys. Biochim. Acta* **812**, 643–655.
186. Harter, C., P. James, T. Bächli, G. Semenza and J. Brunner, 1989, Hydrophobic binding of the ectodomain of influenza hemagglutinin to membranes occurs through the “fusion peptide”, *J. Biol. Chem.* **264**, 6459–6464.
187. Guy, H.R., S.R. Durell, C. Schoch and R. Blumenthal, 1992, Analyzing the fusion process of influenza hemagglutinin by mutagenesis and molecular modeling, *Biophys. J.* **62**, 95–97.
188. Düzgünes, N. and S. Ohki, 1981, Fusion of small unilamellar liposomes with phospholipid planar membranes and large single-bilayer vesicles, *Biochim. Biophys. Acta* **640**, 734–747.
189. Düzgünes, N., J. Wilschut, R. Fraley and D. Papahadjopoulos, 1981, Studies on the mechanism of membrane fusion: Role of head group composition in calcium and magnesium-induced fusion of mixed phospholipid vesicles, *Biochim. Biophys. Acta* **642**, 182–195.
190. Hoekstra, D. and N. Düzgünes, 1986, Ricinus communis agglutinin-mediated agglutination and fusion of glycolipid-containing phospholipid vesicles. Effect of carbohydrate headgroup size, calcium ions, and spermine, *Biochemistry* **25**, 1321–1330.
191. Düzgünes, N. and D. Hoekstra, 1986, Agglutination and fusion of glycolipid-phospholipid vesicles mediated by lectins and calcium ions, *Stud. Biophys.* **111**, 5–10.
192. Hope, M.J., D.C. Walker and P.R. Cullis, 1983, Calcium and pH-induced fusion of small unilamellar vesicles consisting of phosphatidylethanolamine and negatively charged phospholipids. A freeze-fracture study, *Biochem. Biophys. Res. Commun.* **110**, 15–22.
193. Papahadjopoulos, D., W.J. Vail, C. Newton, S. Nir, K. Jacobson, G. Poste and R. Lazo, 1977, Studies on membrane fusion, III. Role of calcium-induced phase changes, *Biochim. Biophys. Acta* **465**, 579–598.
194. Bondeson, J., J. Wijkander and R. Sundler, 1984, Proton-induced membrane fusion. Role of phospholipid composition and protein-mediated intermembrane contact, *Biochim. Biophys. Acta* **777**, 21–27.
195. Massari, S., E. Folena, V. Ambrosin, G. Schiavo and R. Colonna, 1991, pH-dependent lipid packing, membrane permeability and fusion in phosphatidylcholine vesicles, *Biochim. Biophys. Acta* **1067**, 131–138.

196. Papahadjopoulos, D., W.J. Vail and G. Poste, 1976, Studies on membrane fusion, II. Induction of fusion in pure phospholipid membranes by calcium and other divalent cations, *Biochim. Biophys. Acta* **465**, 579–598.
197. Sundler, R. and D. Papahadjopoulos, 1981, Control of membrane fusion by phospholipid head groups, I. Phosphatidate/phosphatidylinositol specificity, *Biochim. Biophys. Acta* **649**, 743–750.
198. Rosenberg, J., N. Düzgünes and C. Kayatar, 1983, Comparison of two liposome fusion assays monitoring the intermixing of aqueous contents and of membrane components, *Biochim. Biophys. Acta* **735**, 173–180.
199. Vail, W.J. and J.G. Stollery, 1979, Phase changes of cardiolipin vesicles mediated by divalent cations, *Biochim. Biophys. Acta* **551**, 74–84.
200. Ohnishi, S. and T. Ito, 1974, Calcium-induced phase separations in phosphatidylserine-phosphatidylcholine membranes, *Biochemistry* **13**, 881–887.
201. Hoekstra, D., A. Yaron, A. Carmel and G. Scherphof, 1979, Fusion of phospholipid vesicles containing a trypsin-sensitive fluorogenic substrate and trypsin, *FEBS Lett.* **106**, 176–180.
202. Sundler, R. and J. Wijkander, 1983, Protein-mediated intermembrane contact specifically enhances Ca^{2+} -induced fusion of phosphatidate-containing membranes, *Biochim. Biophys. Acta* **730**, 391–394.
203. Arnold, K., S. Ohki and M. Krumbiegel, 1990, Interaction of dextran sulfate with phospholipid surfaces and liposome aggregation and fusion, *Chem. Phys. Lipids* **55**, 301–307.
204. Budker, V.G., Yu.Ya. Markushin, T.E. Vakrusheva, E.V. Kiseleva, T.V. Maltseva and V.N. Sidorov, 1990, Ca^{2+} -mediated interaction of negatively charged polysaccharides with phosphatidylcholine vesicles (Russian), *Biol. Membrany (Moscow)* **7**, 419–427.
205. Zschörnig, O., K. Arnold, W. Richter and S. Ohki, 1992, Dextran sulfate-dependent fusion of liposomes containing cationic stearylamine, *Chem. Phys. Lipids* **63**, 15–22.
206. Keren-Zur, M., M. Beigel and A. Loyter, 1989, Induction of fusion in aggregated and nonaggregated liposomes bearing cationic detergents, *Biochim. Biophys. Acta* **983**, 253–258.
207. Beigel, M., M. Keren-Zur, Y. Laster and A. Loyter, 1988, Poly(aspartic acid)-dependent fusion of liposomes bearing the quaternary ammonium detergent [[(1,1,3,3-Tetramethylbutyl) cresoxy] ethoxy] ethyl] dimethylbenzylammonium hydroxide, *Biochemistry* **27**, 660–666.
208. Wilschut, J., M. Holsappel and R. Jansen, 1982, Ca^{2+} -induced fusion of cardiolipin/phosphatidylcholine vesicles monitored by mixing of aqueous vesicle contents, *Biochim. Biophys. Acta* **690**, 297–301.
209. Wilschut, J., 1991, Membrane fusion in lipid vesicle systems, in: *Membrane Fusion*, eds J. Wilschut and D. Hoekstra (Marcel Dekker, New York) pp. 89–126.
210. Van Oss, C.J., 1989, Energetics of cell-cell and cell-biopolymer interactions, *Cell Biophys.* **14**, 1–16.
211. White, J.M., 1992, Membrane fusion, *Science* **259**, 917–924.
212. Creutz, C.E., 1992, The annexins and exocytosis, *Science* **258**, 924–931.
213. Devaux, P.F., 1991, Static and dynamic lipid asymmetry in cell membrane, *Biochemistry* **30**, 1163–1173.

This Page Intentionally Left Blank

Author Index

- Aakhus, A.M., 845
Abbas, A.K., 796
Abbott, J., *see* Holtzer, H., 895
Abe, S., *see* Senda, M., 895
Abidor, I.G., 896
Abidor, I.G., *see* Chernomordik, L.V., 956
Abidor, I.G., *see* Kuzmin, P.I., 901
Abidor, I.G., *see* Sukharev, S.I., 900
Abney, J.R., 299, 350, 351, 398
Abney, J.R., *see* Scalettar, B.A., 356
Abra, R.M., *see* Fielding, R.M., 517
Abraham, F., 841
Abraham, F.F., 601
Abricossova, I.I., *see* Derjaguin, B.V., 598
Absolom, D.R., 796
Absolom, D.R., *see* Neumann, A.W., 801
Acheson, A., *see* Rutishauser, U., 802
Adam, C.G., 688
Adam, G.W., *see* Johnson, S.J., 598
Adams, G.E., *see* Israelachvili, J.N., 687
Adams, R.J., 847
Adamson, A.W., 753, 796
Adamson, E., *see* Samuels, M., 845
Aderem, A., *see* Hartwig, J., 845
Aderem, A., *see* Thelen, M., 845
Aebi, U., *see* Meyer, R.K., 844
Afshar-Rad, T., 597
Aggerbeck, L.P., *see* Gulik-Krzywicki, T., 150
Aghion, J., *see* Picard, G., 204
Aguerre-Chariol, O., *see* Bivas, I., 301, 398, 459
Aharony, A., *see* Stauffer, D., 356
Ahkong, Q.F., *see* Lucy, J.A., 949, 955
Ahkong, Q.F., *see* Song, L., 900
Ahle, S., 63
Ahlers, M., *see* Darst, S.A., 211
Ahuja, R.C., *see* Kinnunen, P.K.J., 205
Akabas, M.H., *see* Cohen, F.S., 955
Akersson, T., *see* Kjellander, R., 641, 690
Akiyama, M., *see* Mannock, D.A., 155
Alber, G., *see* Mao, S.Y., 848
Albert, S.O., *see* Robbin, R., 802
Alberts, A., 93
Alberts, B., 62, 457, 596, 849
Albrecht, G., *see* Panaiotov, I.I., 210
Albrecht, O., 202, 203, 299, 303
Albrecht, P., *see* Ourisson, G., 95
Alder, B.J., 351
Alecio, M.R., 351
Alegria, G., *see* Popovic, Z.D., 210
Alessi, M.C., *see* Kaplanski, G., 803
Alexander, A.E., *see* Fort, T., 203
Alford, D., *see* Ellens, H., 154, 956
Alford, D., *see* Meers, P., 955
Alford, D., *see* Siegel, D.P., 157, 956
Alford, D.R., *see* Düzgünes, N., 950
Alicata, D.A., *see* Rayner, M.D., 687
Alkhalaf, W., 519
Allan, V.J., *see* Duden, R., 846
Allen, P., *see* Janmey, P., 848
Allen, T.M., 517, 518, 953
Allen, T.M., *see* Papahadjopoulos, D., 518
Allen, T.M., *see* Düzgünes, N., 950
Allison, A.C., *see* Poste, G., 949
Almahbobi, G., 847
Almeida, P.F., *see* Vaz, W.L.C., 357
Almeida, P.F.F., 302, 351
Almers, W., *see* Spruce, A.E., 900
Alonso, A., *see* Burger, K.N.J., 160
Als-Nielsen, J., 205, 206
Als-Nielsen, J., *see* Böhm, C., 206
Als-Nielsen, J., *see* Helm, C.A., 205
Als-Nielsen, J., *see* Kenn, R.M., 209
Als-Nielsen, J., *see* Kjaer, K., 205
Als-Nielsen, J., *see* Möhwald, H., 209
Als-Nielsen, J., *see* Vaknin, D., 206
Alving, C.R., 517
Ambrose, E.J., *see* Easty, G.C., 798
Ambrosin, V., *see* Massari, S., 956
Ammann, A., 600
Amos, L.A., 838
Amos, W.B., *see* Amos, L.A., 838
Amselem, S., 950
Anantharamaiah, G.M., *see* Srinivas, S.K., 949
Andelman, D., 155, 208, 400, 461
Andelman, D., *see* Guttman, G., 641
Andelman, D., *see* Harden, J.L., 642
Andelman, D., *see* Kawakatsu, T., 461
Andelman, D., *see* Leibler, S., 303, 461, 641

- Andelman, D., *see* Pincus, P., 600, 641
 Andelman, D., *see* Safran, S.A., 461, 720
 Anderson, C.M., 351
 Anderson, D.M., 150, 151
 Anderson, D.M., *see* Ström, P., 151
 Anderson, J., *see* Garcia, A., 847
 Anderson, L., *see* Fox, J.E., 841
 Anderson, R.A., 840
 Andersson, S., 150
 Andersson, S., *see* Hyde, S.T., 150
 Andrade, J.D., 796
 André, P., 796
 André, P., *see* Mège, J.L., 801
 Angelides, K., *see* Srinivasan, Y., 842
 Angelova, M.I., 720
 Annamalai, A.E., *see* Wang, D.L., 843
 Antippa, A.F., 205
 Aoki, R., *see* Lee, S., 955
 Aoyagi, H., *see* Lee, S., 955
 Apell, H.-J., *see* Knoll, W., 304
 Appgar, J.R., 848
 Apostolova, M.A., *see* Dimitrov, D.S., 898
 Appel, J., *see* Porte, G., 152, 397
 Appell, J., *see* Larché, F., 641
 Arakawa, T., 687
 Arakelyan, V.B., *see* Abidor, I.G., 896
 Araujo, C., *see* Thewalt, J., 95
 Arbuns, C.K., *see* Picker, L.J., 801
 Arends, J., *see* Schackenraad, J.M., 802
 Arfors, K.E., *see* Tangelder, G.J., 802
 Arnett, E.M., 154
 Arnold, K., 952, 953, 954, 955, 957
 Arnold, K., *see* Herrmann, A., 954
 Arnold, K., *see* Krumbiegel, M., 954
 Arnold, K., *see* Ohki, S., 899, 951, 954
 Arnold, K., *see* van Oss, C.J., 952
 Arnold, K., *see* Zschörnig, O., 957
 Arnold, W.M., *see* Zimmermann, U., 895, 898
 Arnott, S., 796
 Arpin, M., *see* Garcia, A., 847
 Artalejo, C.R., 949
 Arvidson, G., *see* Eriksson, P.-O., 152, 156
 Arvidson, G., *see* Gutman, H., 156
 Arvidson, G., *see* Lindblom, G., 157, 354
 Arvidson, G., *see* Sjölund, M., 157
 Asa, D., *see* Foxall, C., 799
 Asakura, S., 952
 Asch, B.B., *see* Asch, H.L., 846
 Asch, H.L., 846
 Ashikawa, I., *see* Kinoshita, K.Jr., 896
 Ashurst, W.T., *see* Levesque, D., 354
 Asijee, G.M., 844
 Atherton, A., 796
 Atiard, P., 599
 Attard, P., 640, 689, 690
 Ault, K.A., 796
 Ault, K.A., *see* Abbas, A.K., 796
 Aunis, D., *see* Artalejo, C.R., 949
 Ausiello, D.A., *see* Cantiello, H.F., 848
 Austin, R.H., *see* Vaz, W.L.C., 357
 Avila, J., *see* Hargreaves, A., 846
 Axelrod, D., 351
 Axelrod, D., *see* Koppel, D.E., 204
 Babbar, S., *see* Mayhew, E.G., 518
 Bächli, T., *see* Harter, C., 956
 Backer, J.M., 458
 Bader, H., 601
 Bader, H., *see* Sackmann, E., 298, 601
 Baermann, M., *see* Schmidt, C.F., 839
 Baier, R.E., 796
 Bailey, A., *see* Afshar-Rad, T., 597
 Bailey, J., 843
 Bailey, S.M., 719
 Baines, I.C., 847
 Baird, B., *see* Ryan, T.A., 802
 Baker, A.J., *see* Coakley, T.W., 899
 Bakker-Woudenberg, I., 518
 Balasubramaniau, *see* Sundari, C.S., 953
 Baldassare, J.J., *see* Goldschmidt-Clermont, P.J.,
 848
 Baldwin, J.M., *see* Henderson, R., 94
 Baldwin, P.A., *see* Düzgünes, N., 953
 Ballamy, W.D., 204
 Balthasar, D.M., 209
 Baltimore, D., *see* Darnell, J., 62, 596
 Bandrina, I.N., *see* Sukharev, S.I., 900
 Bangham, A.D., 516
 Banno, Y., 849
 Banschbach, J., *see* Siegel, D.P., 157, 159, 956
 Barak, L.S., *see* Schlessinger, J., 802
 Barber, B.H., *see* Christink, E.R., 797
 Barbul, A.I., *see* Kuzmin, P.I., 901
 Barbul, A.I., *see* Sukharev, S.I., 900
 Bareman, J.P., 208
 Barenholz, Y., *see* Amselem, S., 950
 Barenholz, Y., *see* Gatt, S., 519
 Barenholz, Y., *see* Lasic, D.D., 517
 Baribault, H., *see* Ozawa, M., 845
 Bärmann, M., 839, 846
 Bärmann, M., *see* Kas, J., 839
 Bärmann, M., *see* Müller, O., 839
 Barnes, I.S., *see* Hyde, S.T., 153
 Barnett, A., *see* Weaver, J.C., 897
 Barois, P., 151
 Barrantes, F.J., *see* Criado, M., 352
 Barry, E.L.R., *see* Mosher, D.F., 801
 Barski, G., 895, 949

- Barthel, D., *see* Arnold, K., 952
 Bartle, E.A., *see* Seddon, J.M., 152
 Bartoletti, D.C., 901
 Barton, P.G., 155
 Barton, P.G., *see* Findlay, E.J., 641
 Bassereau, P., 719
 Bassereau, P., *see* Larché, F., 641
 Bassereau, P., *see* Porte, G., 152, 397, 602
 Batchelor, M.T., *see* Attard, P., 689
 Baumgärtner, A., *see* Lipowsky, R., 600
 Baumgartner, H.R., 796
 Bäumlner, H., 952
 Bausch, R., 600
 Bayerl, T., 299, 300
 Bayerl, T., *see* Heise, H., 303, 844
 Bayerl, T., *see* Johnson, S.I., 304
 Bayerl, T., *see* Johnson, S.K., 62
 Bayerl, T., *see* Koechy, T., 300
 Bayerl, T., *see* König, S., 300, 397, 601
 Bayerl, T., *see* Reindl, H., 302
 Bayerl, T.M., 206, 598
 Bayerl, T.M., *see* Johnson, S.J., 598, 841
 Bayerl, Th., *see* Reinl, H., 303
 Béal, D., *see* Joliot, P., 353
 Beblík, G., 398, 720
 Bech, J., 689
 Beck, K., 204
 Beck, K., *see* Peters, R., 203
 Beckerle, M., *see* Drenckhahn, D., 844
 Beckerle, M.C., 841
 Beckett, L.A., *see* Carpén, O., 797
 Beckmann, E., *see* Henderson, R., 94
 Beigel, M., 957
 Beigel, M., *see* Keren-Zur, M., 957
 Belaya, M.L., 299, 598
 Bell, G.I., 753, 796
 Bell, G.I., *see* Bongrand, P., 797
 Bell, G.I., *see* Capo, C., 753, 797
 Bell, G.I., *see* Michl, J., 801
 Bell, G.M., 207
 Bell, R.M., *see* Bishop, W.R., 62
 Bellocq, A.M., *see* Safinya, C.R., 151, 689, 719
 Ben Shaul, Y., 796
 Ben-Avraham, D., *see* Havlin, S., 353
 Ben-Naim, A., 397
 Ben-Shaul, A., 397, 398
 Ben-Shaul, A., *see* Fattal, D., 399
 Ben-Shaul, A., *see* Gelbart, W.M., 401
 Ben-Shaul, A., *see* Szleifer, I., 153, 299, 398, 489
 Benattar, J.J., *see* Daillant, J., 206
 Bender, J.R., *see* Pardi, R., 801
 Bennet, V., 62
 Bennett, V., 840, 849
 Bennett, V., *see* Gardner, K., 840
 Bennett, V., *see* Joshi, R., 840
 Bennett, V., *see* Srinivasan, Y., 842
 Bennett, W., *see* Bjorkman, P., 797
 Bennett, W.S., *see* Steitz, T.A., 687
 Benociel, A.M., *see* Kaplanski, G., 803
 Benoliel, A.M., *see* André, P., 796
 Benoliel, A.M., *see* Bongrand, P., 797
 Benoliel, A.M., *see* Capo, C., 753
 Benoliel, A.M., *see* Capo, C., 797
 Benoliel, A.M., *see* Foa, C., 799
 Benoliel, A.M., *see* Horoyan, M., 800
 Benoliel, A.M., *see* Mège, J.L., 801
 Bensimon, D., 641
 Bensimon, D., *see* Fourcade, B., 458
 Bensimon, D., *see* Michalet, X., 461
 Bensimon, D., *see* Mutz, M., 300, 461
 Benson, M.D., *see* Willardson, B.M., 840
 Bentz, J., 160, 950
 Bentz, J., *see* Düzgünes, N., 950
 Bentz, J., *see* Ellens, H., 154, 953, 956
 Bentz, J., *see* Meers, P., 955
 Bentz, J., *see* Nir, S., 950
 Bentz, J., *see* Siegel, D.P., 157, 956
 Benvegnu, D.J., 462
 Benveniste, M., *see* Livnek, E., 800
 Benz, R., 896
 Beran, M.J., 351
 Bercovier, J.H., *see* Gatt, S., 519
 Berendsen, H.J.C., *see* Edholm, O., 400
 Berendsen, H.J.C., *see* Egberts, E., 400, 601
 Berendsen, H.J.C., *see* Marrink, S.-J., 689
 Berendsen, H.J.C., *see* Marrink, S.J., 601
 Berendsen, H.J.C., *see* van der Ploeg, P., 400
 Bereznikova, A.V., 846
 Berg, E.L., *see* Picker, L.J., 801
 Berg, H., 93, 895
 Berg, H., *see* Weber, H., 895
 Berg, P., *see* Fraley, R.T., 518
 Bergelson, L.D., *see* Margolis, L.B., 800
 Berk, D., 753
 Berk, D., *see* Evans, E., 753, 798, 843
 Berke, G., 796
 Berke, G., *see* Kalina, M., 800
 Berkowitz, M.L., 689
 Berkowitz, M.L., *see* Marrink, S.-J., 689
 Berkowitz, M.L., *see* Marrink, S.J., 601
 Berkowitz, M.L., *see* Raghavan, K., 689
 Berman, L.E., *see* Schmidt, C.F., 462
 Berndl, K., 301, 457, 460, 516, 602, 721
 Berndl, K., *see* Seifert, U., 457, 721
 Berndl, K., *see* Wortis, M., 458
 Berndt, M.C., *see* Fox, J.E., 841
 Berridge, M.J., 160

- Bershadsky, A.D., 838
 Bertagnolli, M.E., *see* Beckerle, M.C., 841
 Berzins, K., *see* Ruangjirachuporn, W., 842
 Bessis, M., 62
 Best, L., *see* Jähnig, F., 397
 Beveridge, T.J., *see* Gorby, Y.A., 93
 Bevers, E.M., *see* Comfurius, P., 842
 Bevilacqua, M.P., 796
 Bezanilla, F., *see* Zimmerberg, J., 687
 Bezrukov, S.M., *see* Keller, S.L., 687
 Bhakuni, V., *see* Gudi, S.R., 842
 Bianciardi, P., *see* Raudino, A., 952
 Bibo, A.M., 209
 Bibo, A.M., *see* Kenn, R.M., 209
 Bichenkov, E.E., 954
 Bienvenue, A., *see* Sune, A., 842
 Bieri, B.E., 796
 Bilderback, D.H., *see* Caffrey, M., 158
 Biltonen, R., *see* Freire, E., 352
 Biltonen, R.L., 351
 Biltonen, R.L., *see* Estep, T.N., 352
 Biltonen, R.L., *see* Thompson, T.E., 356
 Binder, K., *see* Kreer, M., 208
 Binder, K., *see* Scheringer, M., 208
 Binnig, G., 207
 Birch, G., *see* Weiner, N., 490
 Birgbauer, E., 846
 Birgenau, R.J., 208
 Bishop, W.R., 62
 Biswas, A., 400
 Bivas, I., 301, 398, 399, 459
 Bivas, I., *see* Faucon, J.F., 398, 459, 720
 Bivas, I., *see* Petrov, A.G., 300, 397, 489
 Bjorkman, P., 797
 Black, J.A., *see* Fields, R.D., 843
 Black, P.H., *see* Robbin, R., 802
 Blackwell, M.F., 351
 Blake, T.D., 598
 Blakemore, R.P., 93
 Blakemore, R.P., *see* Gorby, Y.A., 93
 Blanckenhagen, P., *see* Als-Nielsen, J., 205
 Blangero, C., 899, 900
 Blankenburg, R., 210
 Blankenburg, R., *see* Darst, S.A., 211
 Blankschtein, D., *see* Naor, A., 400
 Blaurock, A.E., 151
 Bloch, K., 94, 95
 Bloch, K., *see* Dahl, C.E., 95
 Block, S., *see* Svoboda, K., 841
 Block, S.M., *see* Svoboda, K., 462
 Blomqvist, K., *see* Thuren, T., 211
 Bloom, M., 93, 95, 298, 401, 461, 517, 753, 838
 Bloom, M., *see* Bayerl, T.M., 598
 Bloom, M., *see* Davis, J.H., 94, 303
 Bloom, M., *see* Ipsen, J.H., 397
 Bloom, M., *see* Lafleur, M., 397
 Bloom, M., *see* Mouritsen, O.G., 94, 303, 398, 399
 Bloom, M., *see* Nezil, F.A., 94, 397, 460
 Bloom, M., *see* Thewalt, J., 95
 Blossey, R., *see* Bausch, R., 600
 Blow, A.M.J., 954
 Blume, G., *see* Cevc, G., 490
 Blumenthal, R., 901, 949
 Blumenthal, R., *see* Dimitrov, D.S., 899, 900
 Blumenthal, R., *see* Guy, H.R., 956
 Blumenthal, R., *see* Morris, J.S., 950
 Blumenthal, R., *see* Morris, S.J., 899
 Blumenthal, R., *see* Sarkar, D.P., 901
 Blumenthal, R., *see* Walter, A., 955
 Bo, L., 459
 Boal, D.H., 462, 463
 Boccara, N., *see* Meunier, J., 150, 641
 Boden, N., 154
 Boggs, J.M., 151, 156
 Bogner, J.R., 518
 Bohanon, T.M., *see* Lin, B., 209
 Böhm, C., 206
 Böhm, C., *see* Brezesinski, G., 209
 Böhm, C., *see* Kenn, R.M., 209
 Bohorques, M., 204
 Bolton, J.R., *see* Picard, G., 204
 Bonanno, M., *see* Wolfe, J., 951
 Bonavida, B., *see* Grimm, E., 799
 Bondeson, J., 955, 956
 Bongrand, P., 797
 Bongrand, P., *see* André, P., 796
 Bongrand, P., *see* Bell, G.I., 753, 796
 Bongrand, P., *see* Capo, C., 753, 797
 Bongrand, P., *see* Foa, C., 799
 Bongrand, P., *see* Horoyan, M., 800
 Bongrand, P., *see* Kaplanski, G., 803
 Bongrand, P., *see* Mège, J.L., 801
 Bongrand, P., *see* Tissot, O., 803
 Boni, L., *see* Ellens, H., 154, 956
 Boni, L.T., 156, 952
 Boni, L.T., *see* Hui, S.W., 954, 956
 Bonnett, H.T., 895
 Bonventre, J.V., *see* Cantiello, H.F., 848
 Boonstra, J., *see* Payrastre, B., 849
 Boonstra, J., *see* van Belzen, N., 849
 Booth, S., *see* Schanus, E., 840
 Bopp, P., *see* Schlenkrich, M., 208
 Borejdo, J., *see* Burlacu, S., 839
 Borgström, B., 160
 Born, G.V.R., *see* Atherton, A., 796
 Bornens, M., 842
 Bornman, C.H., *see* Hahn-Hagerdal, B., 898

- Boroske, E., 460, 519
 Bosio, L., *see* Daillant, J., 206
 Bösterling, B., *see* Stier, A., 159
 Botham, G.M., *see* Blow, A.M.J., 954
 Bothorel, P., *see* Angelova, M.I., 720
 Bothorel, P., *see* Bivas, I., 301, 398, 459
 Bothorel, P., *see* Faucon, J.F., 398, 459, 720
 Bothorel, P., *see* Meleard, P., 459, 460
 Bothwell, A., *see* Zhang, F., 803
 Botos, P., *see* Shyamsunder, E., 155
 Bottega, R., *see* Epan, R.M., 157
 Bouchaud, J.-P., 351
 Bouchaud, J.-P., *see* Lavergne, J., 353
 Bougis, P., *see* Vainio, P., 211
 Bouligand, Y., 150
 Bourguignon, L.Y., 842
 Bouvier, P., *see* Rohmer, M., 95
 Bowen, P.J., 203
 Bowers, B., *see* Miyata, H., 847
 Boyanov, A.I., *see* Hinz, H.-J., 156
 Boyanov, A.I., *see* Koynova, R.D., 151
 Boyanov, A.I., *see* Tenchov, B.G., 156
 Boyer, B.P., *see* Haywood, A.M., 753
 Boyer, C., *see* André, P., 796
 Boyles, J.K., *see* Fox, J.E., 841, 843
 Bozic, B., 458
 Brackenbury, A., *see* Cunningham, B.A., 753
 Bradley, D., *see* Morris, J.S., 950
 Brainsma, R., 301
 Bramblett, G.T., 846
 Brandley, B.K., *see* Foxall, C., 799
 Branton, D., *see* Byers, T.J., 840
 Branton, D., *see* Elgsacter, A., 841
 Branton, D., *see* Faquin, W.C., 840
 Branton, D., *see* Husain, C.A., 840
 Branton, D., *see* Svoboda, K., 462, 841
 Braunlin, W.H., *see* Xian, W., 849
 Bray, D., *see* Alberts, A., 93
 Bray, D., *see* Alberts, B., 62, 457, 596, 849
 Bray, J., *see* Dawson, R.M.C., 157
 Breathnach, S.M., *see* Hintner, H., 847
 Brenner, H., *see* Goldman, A.J., 799
 Brentel, I., *see* Lindblom, G., 157, 160
 Breton, M., *see* Grondin, P., 849
 Breton, M., *see* Payrastré, B., 849
 Bretscher, A., *see* Gould, K.L., 846
 Brewer, G.J., 954
 Brezesinski, G., 202, 209
 Brezesinski, G., *see* Dietrich, A., 209
 Brezesinski, G., *see* Nuhn, P., 209
 Brian, A.A., *see* McConnell, H.M., 210
 Brickmann, J., *see* Schlenkrich, M., 208
 Brienne, M.J., *see* Mutz, M., 300
 Briggs, M.S., 210
 Brochard, F., 301, 460, 599
 Brochard, F., *see* Andelman, D., 208
 Brocker, T., *see* Wegener, A.M.K., 803
 Broder, S., *see* Mitsuya, H., 954
 Brook, D.E., *see* Buxbaum, R., 797
 Broseta, D., *see* Moore, B., 209
 Brudnaya, M., *see* Malev, V., 840
 Bruggeman, D.A.G., 351
 Bruin, T., *see* Asijee, G.M., 844
 Bruinsma, R., 152, 460
 Brumen, M., *see* Heinrich, V., 460
 Brumen, M., *see* Svetina, S., 459, 721
 Brumm, Th., *see* Reinl, H., 303
 Brunette, E., *see* Stribling, R., 519
 Brunner, J., *see* Harter, C., 956
 Brunner, J., *see* Niggli, V., 844
 Bryant, A., *see* Smith, D.P.E., 207
 Bryant, G., 897
 Buas, M., 351
 Buchner, K.-H., *see* Zimmermann, U., 898
 Budil, D.E., *see* Shin, Y.-K., 356
 Budker, V.G., 957
 Budker, V.G., *see* Bichenkov, E.E., 954
 Budker, V.G., *see* Grudzev, A.D., 954
 Bueldt, G., 299
 Buferne, M., *see* André, P., 796
 Bulargina, T.V., *see* Bereznikova, A.V., 846
 Buldt, G., 206
 Bultmann, T., 351
 Buoncore, L., *see* Rose, J.K., 519
 Burakoff, S.J., *see* Bierer, B.E., 796
 Burakoff, S.J., *see* Sung, K.L.P., 802
 Burger, K.N.J., 160
 Burger, M., *see* Niggli, V., 844
 Burger, M.M., *see* Burn, P., 844
 Burgess, S.W., 953, 954
 Burgoyne, R.D., 949
 Burgoyne, R.D., *see* Morgan, A., 949
 Burkhardt, T.W., 601, 719
 Burlacu, S., 839
 Burn, P., 844, 845
 Burns, J.L., *see* Siegel, D.P., 154, 956
 Burrige, K., 843
 Burrige, K., *see* Drenckhahn, D., 844
 Burrige, K., *see* Fath, K.R., 843
 Burrige, K., *see* Nuckolls, G.H., 844
 Burrige, K., *see* Otey, C.A., 843
 Burrige, K., *see* Pavalko, F.M., 843, 845
 Burrige, K., *see* Turner, C.E., 843, 844
 Burton, A.C., *see* Rand, R.P., 688
 Busscher, H.J., *see* Schackenraad, J.M., 802
 Butcher, E.C., *see* Picker, L.J., 801
 Butko, P., *see* Rand, R.P., 687
 Butler, K.W., *see* Mantsch, H.H., 158

- Butt, H.-J., 687
 Buxbaum, R., 797
 Buxton, R., *see* Magee, A., 845
 Buxton, R.S., *see* Magee, A.I., 753
 Byers, H.R., *see* Cunningham, C.C., 840
 Byers, T.J., 840

 Cabane, B., *see* Kékicheff, P., 151, 154
 Cadenhead, D.A., 202, 203
 Cadenhead, D.A., *see* Balthasar, D.M., 209
 Cadenhead, D.A., *see* Heckl, W.M., 204
 Cadenhead, D.A., *see* Rice, D.K., 209
 Caffrey, M., 153, 157, 158, 159
 Cafiso, D., *see* Langner, M., 690
 Caille, A., 202
 Caille, M., 602
 Caille, M., *see* Slater, G., 356
 Cameron, D.G., *see* Mantsch, H.H., 158
 Canham, P.B., 457, 597
 Cantiello, H.F., 848
 Cantley, L.C., *see* Faquin, W.C., 840
 Cantor, R.S., 207, 401
 Capers, C.R., 895
 Capo, C., 753, 797
 Capo, C., *see* André, P., 796
 Capo, C., *see* Bongrand, P., 797
 Capo, C., *see* Foa, C., 799
 Capo, C., *see* Horoyan, M., 800
 Capo, C., *see* Mège, J.L., 801
 Carboni, J., *see* Garcia, A., 847
 Cardini, G., *see* Bareman, J.P., 208
 Cardozo, T., *see* Samuels, M., 845
 Carey, M.C., *see* Patton, J.S., 160
 Carignano, M.A., 400
 Carlier, M., 839
 Carlsson D., *see* Ruangjirachuporn, W., 842
 Carmel, A., *see* Hoekstra, D., 957
 Carnie, S.L., 690
 Carpén, O., 797
 Carr, I., 797
 Carraway, C., *see* Liu, Y., 846
 Carraway, C.A.C., *see* Carraway, V., 838
 Carraway, K., *see* Liu, Y., 846
 Carraway, V., 838
 Carslaw, H.S., 351
 Carvell, M., 688
 Cassiman, J.J., *see* David, G., 798
 Cassoly, R., *see* Stetzkowski-Marden, F., 846
 Castle, W.B., *see* Jandl, J.H., 753
 Cates, M.E., 152
 Catterall, W.A., *see* Edelstein, N.G., 848
 Caulfield, J.P., *see* Carpén, O., 797
 Cavalier-Smith, T., 93, 94
 Celati, C., *see* Bornens, M., 842

 Ceska, T.A., *see* Henderson, R., 94
 Cevc, G., 150, 151, 152, 155, 156, 206, 298, 301, 351, 462, 489, 490, 596, 598, 689, 690
 Cevc, G., *see* Gonzalez, P., 490
 Cevc, G., *see* Seddon, J.M., 153, 155, 205, 688
 Chahwala, S.B., *see* Faquin, W.C., 840
 Chan, W.K., *see* Schneider, M.B., 356
 Chance, S.M., *see* New, R.R.C., 517
 Chang, D.C., 895, 897, 901
 Chang, D.C., *see* Zheng, Q., 899
 Chang, E.L., 155
 Chang, E.L., *see* Lo, S.-L., 94
 Chang, E.L., *see* Yager, P., 155
 Chang, H., 158
 Chang, Y.S., *see* Chopra, H., 847
 Chap, H., *see* Grondin, P., 849
 Chapel, J.-P., *see* Wolfe, J., 951
 Chapman, D., *see* Haris, P.I., 298
 Chapman, D., *see* Pink, D.A., 355, 399
 Chapman, D., *see* Salisbury, N.J., 953
 Chapman, D.L., 640
 Charvolin, J., 149, 150, 152
 Charvolin, J., *see* Hendrikx, Y., 154
 Charvolin, J., *see* Holmes, M.C., 154
 Charvolin, J., *see* Rançon, Y., 154
 Charvolin, J., *see* Sadoc, J.F., 150, 160
 Chassy, B.M., *see* Chang, D.C., 895
 Chaudhury, M.K., *see* van Oss, C.J., 803, 951
 Chazotte, B., 351
 Chazotte, B., *see* Gupte, S.S., 353
 Chazotte, B., *see* Hackenbrock, Ch.R., 63
 Chen, S.C., 158
 Chen, W.T., *see* Mueller, S.C., 843
 Chen, Y.-L., 205
 Chen, Y.L.E., 207
 Cheney, R.E., 842, 847
 Cherng, S.L., *see* Scott, H.L., 399
 Chernomordik, L.V., 897, 899, 956
 Chernomordik, L.V., *see* Abidor, I.G., 896
 Chernomordik, L.V., *see* Kozlov, M.M., 841
 Chernomordik, L.V., *see* Leikin, S.L., 953
 Chernousov, M.A., *see* Mosher, D.F., 801
 Cherry, R.J., *see* Anderson, C.M., 351
 Cherry, R.J., *see* Peters, R., 355
 Chestnut, M.H., *see* Siegel, D.P., 154, 956
 Chien, S., 797
 Chien, S., *see* Dong, C., 798
 Chien, S., *see* Schmid-Schönbein, G.W., 802
 Chien, S., *see* Skalak, R., 753
 Chien, S., *see* Sung, K.L.P., 802
 Chien, S., *see* Tozeren, A., 753, 803
 Chin, Y., *see* Allen, T.M., 518
 Chiruvolu, S., *see* Bailey, S.M., 719
 Chizmadzhev, Y.A., *see* Abidor, I.G., 896

- Chizmadzhev, Y.A., *see* Chernomordik, L.V., 897, 899, 956
- Chizmadzhev, Y.A., *see* Kuzmin, P.I., 901
- Chizmadzhev, Y.A., *see* Leikin, S.L., 953
- Chonn, A., *see* Allen, T.M., 517
- Chopra, H., 847
- Chow, R.H., 949
- Chowdry, B.Z., 158
- Christenson, H.K., 689
- Christenson, H.K., *see* Claesson, P.M., 689
- Christiansson, A., *see* Wieslander, Å., 160
- Christink, E.R., 797
- Chuang, D., 63
- Chung, H.S., 351
- Churaev, N.V., *see* Derjaguin, B.V., 599, 690, 950
- Cianci, C.D., 840
- Claesson, P.M., 689, 952
- Claesson, P.M., *see* Christenson, H.K., 689
- Clare, D.M., *see* Davis, J.H., 94, 303
- Clark, N.A., *see* Gruner, S.M., 154
- Clark, N.A., *see* Safinya, C.R., 151, 689, 719
- Clark, N.A., *see* Smith, G.S., 206
- Clark, W.R., *see* Smith, B.A., 204
- Clegg, R.M., 351
- Clegg, R.M., *see* Vaz, W.L.C., 357
- Clerc, M., 154
- Coakley, T.W., 899
- Coakley, W.T., 754, 899
- Coakley, W.T., *see* van Oss, C.J., 952
- Coe, T.J., *see* Scott, H.L., 399
- Cohen, A.M., 840
- Cohen, C.M., 842
- Cohen, F.S., 955
- Cohen, M.H., 352
- Cohen, M.H., *see* Grest, G.S., 353
- Cohen, M.H., *see* Turnbull, D., 356, 357
- Cohn, Z.A., *see* Detmers, P.A., 798
- Coleman, T.R., *see* Mooseker, M.S., 847
- Coll, J.-L., *see* Samuels, M., 845
- Collins, K., 847
- Collins, L.R., *see* Woodle, M.C., 518
- Colman, R.W., *see* Wang, D.L., 843
- Colombo, M., *see* Parsegian, V.A., 687
- Colombo, M.F., 687
- Colonna, R., *see* Massari, S., 956
- Colwin, A.L., *see* Colwin, L.H., 895
- Colwin, L.H., 895
- Combs, L.L., *see* Bell, G.M., 207
- Comfurius, P., 842
- Compans, R.W., *see* Srinivas, S.K., 949
- Connor, J., 842
- Conti, F., *see* Heinemann, S.H., 302
- Cook, G.M.W., 797
- Cook-Röder, J., 601, 719
- Cooper, E.R., 490
- Cooper, J.A., *see* Dadabay, C.Y., 849
- Coorssen, J.R., 689
- Copeland, B.R., 352
- Corless, J.M., 159
- Corne, S.A., *see* Boden, N., 154
- Cornefert, F., *see* Barski, G., 895, 949
- Cornelius, F., 517
- Cornell, D.G., *see* Dluhy, R.A., 206
- Cornet, M., 848
- Corri, W.D., 797
- Cortese, J.D., 839
- Costa, E., *see* Chuang, D., 63
- Costello, M.J., *see* Corless, J.M., 159
- Coudrier, E., *see* Garcia, A., 847
- Cowley, A.C., 597, 641, 688
- Cox, R.G., *see* Goldman, A.J., 799
- Cozens-Roberts, C., 753, 797
- Craievich, A.F., *see* Doucet, J., 206
- Cramer, M., *see* Stochaj, U., 845
- Crawford, M.A., 95
- Creutz, C.E., 955, 957
- Creutz, C.E., *see* Zaks, W.J., 949
- Creutz, E.C., 954
- Criado, M., 352
- Criado, M., *see* Vaz, W.L.C., 357
- Crimmins, M., *see* Sung, K.L.P., 802
- Crise, B., *see* Zhang, F., 803
- Critchley, D., *see* Samuels, M., 845
- Crommelin, D.J.A., *see* Nassander, U.K., 517
- Crommelin, D.J.A., *see* Storm, G., 517
- Crowley, J.M., 897
- Cudd, A., *see* Nicolau, C., 518
- Cullen, J., 160
- Cullis, P.R., 95, 153, 159, 955
- Cullis, P.R., *see* de Kruijff, B., 153, 159
- Cullis, P.R., *see* Gruner, S.M., 157
- Cullis, P.R., *see* Hope, M.J., 156, 956
- Cullis, P.R., *see* Hornby, A.P., 157
- Cullis, P.R., *see* Lafleur, M., 397
- Cullis, R.P., *see* Verkleij, A.J., 955
- Cunningham, B.A., 753
- Cunningham, C., *see* Janmey, P., 839
- Cunningham, C.C., 840
- Cunningham, C.C., *see* Cantiello, H.F., 848
- Curtis, A.S.G., 797
- D'Amico, K., *see* Tate, M.W., 159
- Dadabay, C.Y., 849
- Dahl, C.E., 95
- Dahl, J.S., *see* Dahl, C.E., 95
- Dahlback, B., *see* Hintner, H., 847
- Dahlback, K., *see* Hintner, H., 847

- Dai, H.N., *see* Mueller, S.C., 843
 Dai, M.Z., *see* Mueller, S.C., 843
 Daillant, J., 206
 Daleke, D., *see* Meers, P., 955
 Dalziel, A.W., *see* Chowdry, B.Z., 158
 Dan, N., 399
 Daniel, J., 839
 Danielsen, M., *see* Felgner, P., 518
 Darke, A., *see* Finer, E.G., 953
 Darke, A., *see* Hauser, H., 953
 Darke, A., *see* Salisbury, N.J., 953
 Darmani, H., *see* Coakley, T.W., 899
 Darnell, J., 62, 596
 Darst, S.A., 211
 Das, S., 157, 689
 David, F., 600, 641, 720
 David, F., *see* Bensimon, D., 641
 David, G., 798
 Davies, R.J., 210
 Davis, H.T., *see* Anderson, D.M., 151
 Davis, H.T., *see* Löfgren, H., 205
 Davis, J., *see* Srinivasan, Y., 842
 Davis, J.H., 94, 303
 Davis, J.H., *see* Vist, M.R., 95, 357, 461
 Dawidowicz, E.A., *see* Backer, J.M., 458
 Dawson, R.M.C., 157
 Day, A.R., *see* Garboczi, E.J., 352
 de B. Costa, S.M., 204
 de Biasio, R.L., 798
 de Boer, K., *see* Hoekstra, D., 950
 de Brabander, M., *see* Geerts, H., 352
 de Bradander, M., 352
 de Gennes, P.-G., 152, 299, 400, 459, 518, 597, 599, 600, 601, 641, 690, 798
 de Gennes, P.-G., *see* Andelman, D., 208
 de Gennes, P.-G., *see* Joanny, J.F., 599, 753
 de Grado, W.F., *see* Briggs, M.S., 210
 de Haas, G.H., *see* Dijkman, R., 211
 de Haas, G.H., *see* Ransac, S., 211
 de Jong, W.H., *see* Nassander, U.K., 517
 de Jong, W.H., *see* Storm, G., 517
 de Koker, R., *see* McConnell, H.M., 208
 de Koning, B., *see* Den Engelsen, D., 205
 de Kruijff, B., 153, 159
 de Kruijff, B., *see* Cullis, P.R., 95, 153, 159
 de Kruijff, B., *see* Dekker, C.J., 157
 de Kruijff, B., *see* Noordam, P.C., 157
 de Kruijff, B., *see* Tournois, H., 160
 de Mey, J., *see* Geerts, H., 352
 de Petris, S., 798
 de Rosa, M., 94
 de Rosa, M., *see* Gulik, A., 94, 159
 de Rosa, M., *see* Luzzati, V., 94, 159
 de Rosa, M., *see* Vaz, W.L.C., 357
 de Verteuil, F., *see* Caille, A., 202
 de Vries, M.S., *see* Garboczi, E.J., 352
 DeGrip, W.J., *see* Gruner, S.M., 154
 DeSisto, M., *see* Hartwig, J.H., 841
 Deamer, D.W., 93
 Deamer, D.W., *see* Morowitz, H.J., 93
 Deamer, D.W., *see* Uster, P.S., 955
 Debs, R., *see* Stribling, R., 519
 Debye, P., 640
 Decker, G.L., *see* Rossignol, D.P., 896
 Defendi, V., *see* Corri, W.D., 797
 Degovics, G., *see* Laggner, P., 155
 Degovics, G., *see* Lohner, K., 155
 Deisenhofer, J., 94
 Deizhanski, A.I., *see* Petrov, A.G., 300
 Dekker, C.J., 157
 Dekker, N., *see* Dijkman, R., 211
 Delaage, M., *see* Tissot, O., 803
 Delacroix, H., *see* Mariani, P., 150
 Delbrück, M., *see* Saffman, P.G., 355
 Delpire, E., *see* Cornet, M., 848
 Dembo, M., 753, 798
 Dembo, M., *see* Bell, G.I., 753, 796
 den Engelsen, D., 205
 den Hartigh, J., *see* Payraastre, B., 849
 Denicolò, I., *see* Doucet, J., 206
 Denning, S.M., *see* Haynes, B.F., 799
 Dennis, M.J., *see* Heuser, J.E., 899
 Depieds, R., *see* Bongrand, P., 797
 Depieds, R., *see* Capo, C., 797
 Deprette, C., *see* Stetzkowski-Marden, F., 846
 Derick, L., *see* Cohen, A.M., 840
 Derick, L.H., *see* Liu, S.-C., 62, 841
 Derjaguin, B.V., 598, 599, 688, 690, 798, 900, 950
 Dermietzel, R., *see* Drenckhahn, D., 847
 Derzhanski, A., 897
 Derzhanski, A., *see* Bivas, I., 399
 Derzhanski, A., *see* Petrov, A.G., 303
 Derzko, Z., 352
 Derzko, Z.I., *see* Vaz, W.L., 753
 Derzko, Z.I., *see* Vaz, W.L.C., 204
 Desmezeaud, M., *see* Alkhalaf, W., 519
 Detmers, P.A., 798
 Deuling, H.J., 457
 Deuticke, B., 896
 Devaux, P.F., 62, 352, 957
 Devaux, P.F., *see* Farge, E., 460
 Dewhirst, M., *see* Needham, D., 518
 Dhathathreyan, A., *see* Kozarac, Z., 210
 di Meglio, J.-M., 398
 Dieckhoff, J., 845
 Dieckhoff, J., *see* Stochaj, U., 845
 Dietrich, A., 209

- Dietrich, A., *see* Brezesinski, G., 209
 Diglio, C.A., *see* Chopra, H., 847
 Dijkman, R., 211
 Dilger, J.P., *see* Elliott, J.R., 399
 Dill, K.A., 399, 400
 Dill, K.A., *see* Stigter, D., 400
 Dimitrov, D.S., 897, 898, 899, 900, 901
 Dimitrov, D.S., *see* Blumenthal, R., 901
 Dimitrov, D.S., *see* Dukhin, S.S., 900
 Dimitrov, D.S., *see* Ivanov, I.B., 900, 901
 Dimitrov, D.S., *see* Panaiotov, I., 900
 Dimitrov, D.S., *see* Radoev, B.P., 900
 Dimitrov, D.S., *see* Sato, H., 899
 Dimitrov, D.S., *see* Stoicheva, N., 898
 Dimitrov, D.S., *see* Tsoneva, I., 898
 Dimitrov, D.S., *see* Zhelev, D.V., 896, 897, 898
 Dimon, P., *see* Safinya, C.R., 151, 689, 719
 Dluhy, R.A., 206
 Dluhy, R.A., *see* Hunt, R.D., 206
 Dluhy, R.A., *see* Mitchell, M.L., 206
 Döbereiner, H.-G., 303, 458, 460
 Döbereiner, H.-G., *see* Miao, L., 459, 721
 Döbereiner, H.-G., *see* Seifert, U., 300, 458
 Doberstein, S.K., *see* Pollard, T.D., 847
 Doberstein, S.K., *see* Zot, H.G., 847
 Dobner, B., *see* Nuhn, P., 209
 Doershnik, C.M., *see* Picker, L.J., 801
 Doi, M., 798
 Doinov, P., *see* Zhelev, D.V., 896
 Dolan, A.K., 798
 Dominguez, A., *see* Iglesias, F.J., 898
 Doms, R.W., *see* Stegmann, T., 949
 Donath, E., *see* Arnold, K., 952
 Donath, E., *see* Bäumlner, H., 952
 Donath, E., *see* Pratsch, L., 952
 Dong, C., 798
 Dong, C., *see* Sung, K.L.P., 802
 Donnay, G., 159
 Doolittle, R.F., *see* Kyte, J., 94
 Dörfler, H.-D., *see* Nuhn, P., 209
 Dörfler, H.-D., *see* Rettig, W., 209, 210
 Dorn, K., *see* Bader, H., 601
 Doucet, J., 151, 206
 Dowbenko, D., *see* Foxall, C., 799
 Dower, S.K., *see* Qwarnstrom, E.E., 844
 Dowling, T., *see* Barois, P., 151
 Downey, G.P., 848
 Downey, G.P., *see* Linshaw, M.A., 848
 Downing, D.T., *see* Wertz, P.W., 490
 Downing, K.H., *see* Henderson, R., 94
 Doyle, D., *see* Ohki, S., 949
 Drenckhahn, D., 844, 847
 Drenckhahn, J., *see* Ruangjirachuporn, W., 842
 Driessen, A.J.M., 63
 Duax, J., *see* Ohki, S., 951
 Dubois, M., 688
 Dubois-Violette, E., 149
 Dubreuil, R.R., *see* Byers, T.J., 840
 Ducharme, D., 205
 Ducharme, D., *see* Antippa, A.F., 205
 Ducker, W.A., 687
 Duda, G., *see* Motschmann, H., 205
 Duden, R., 846
 Dufourc, E.J., *see* Laroche, G., 953
 Dufourc, J., *see* Laroche, G., 953
 Dukhin, S.S., 900
 Dunne, L.J., *see* Bell, G.M., 207
 Duplantier, B., 461, 641
 Duquette, M.A., *see* Liu, S.C., 841
 Durell, S.R., *see* Guy, H.R., 956
 Durrant, J.A., *see* Adam, C.G., 688
 Dustin, M.L., 753
 Dustin, M.L., *see* Carpén, O., 797
 Dustin, M.L., *see* Kishimoto, T.K., 753
 Dustin, M.L., *see* Staunton, D.E., 802
 Dutta, P., 205
 Dutta, P., *see* Lin, B., 209
 Dutton, G., 519
 Dutton, P.L., *see* Popovic, Z.D., 210
 Duwe, H.-P., *see* Sackmann, E., 457
 Duwe, H.P., 300, 398, 459, 597
 Duwe, H.P., *see* Engelhardt, H., 398, 459
 Duwe, H.P., *see* Lösche, M., 203
 Duwe, H.T., 489
 Duwe, M.P., 398
 Düzgünes, D., *see* Bentz, J., 950
 Düzgünes, N., 949, 950, 953, 956
 Düzgünes, N., *see* Hoekstra, D., 956
 Düzgünes, N., *see* Hong, K., 955
 Düzgünes, N., *see* Ohki, S., 950
 Düzgünes, N., *see* Papahadjopoulos, D., 900, 956
 Düzgünes, N., *see* Rosenberg, J., 957
 Düzgünes, N., *see* Wilschut, J., 951
 Dyatovitskaya, E.V., *see* Margolis, L.B., 800
 Dyson, F.J., 93
 Dzhavakhidze, P.G., 689
 Earnshaw, J.C., 205
 Easty, D.M., *see* Easty, G.C., 798
 Easty, G.C., 798
 Eberle, M., 849
 Ebisawa, K., *see* Banno, Y., 849
 Eckerskorn, C., *see* Herrenknecht, K., 845
 Edelman, G.M., *see* Cunningham, B.A., 753
 Edelstein, N.G., 848
 Edgell, C.J., *see* Fath, K.R., 843
 Edholm, O., 397, 399, 400
 Edidin, M., 798

- Edidin, M., *see* Wade, W., 803, 848
 Edidin, M., *see* Wier, M., 803
 Edidin, M., *see* Yechiel, E., 357
 Edwards, S.F., *see* Doi, M., 798
 Edwards, S.F., *see* Dolan, A.K., 798
 Egan, S., *see* Ezzell, R.M., 841
 Egan, S., *see* Gorlin, J., 845
 Egberts, E., 400, 601
 Egger, M., *see* Weisenhorn, A.L., 207
 Eggert, W., *see* Cevc, G., 152
 Eggl, P., *see* Sackmann, E., 298, 601
 Ehrlich, S., *see* Dutta, P., 205
 Eibl, H., *see* Harlos, K., 151
 Eibl, H., *see* Knoll, W., 304
 Eibl, H., *see* Pascher, I., 206
 Eibl, H., *see* Stümpel, J., 151
 Eibl, H., *see* Träuble, H., 154, 203, 301
 Eidelman, O., *see* Sarkar, D.P., 901
 Eikenberry, E.F., *see* Tate, M.W., 149
 Einstein, A., 352, 798
 Eisenberg, D., 94
 Eisenberg, M., 688
 Eklund, K.K., 951
 Ekwall, P., 153
 el Soda, M., *see* Alkhalaf, W., 519
 El-Meshad, N., *see* Tahir-Kheli, R.A., 356
 Elder, M., 151, 206
 Elgsaeter, A., 841
 Elgsaeter, A., *see* Stokke, B.T., 463
 Elias, H., 798
 Elias, P.M., 95
 Ellens, H., 154, 953, 956
 Ellens, H., *see* Bentz, J., 160
 Ellens, H., *see* Siegel, D.P., 157, 956
 Ellington Jr., J.C., *see* McIntosh, T.J., 688
 Elliott, J.R., 399
 Elmer, L., *see* Srinivasan, Y., 842
 Elson, E., *see* Axelrod, D., 351
 Elson, E., *see* Kucik, D.F., 353
 Elson, E., *see* Qian, H., 355
 Elson, E.L., *see* Cortese, J.D., 839
 Elson, E.L., *see* Downey, G.P., 848
 Elson, E.L., *see* Jay, P.Y., 847
 Elson, E.L., *see* Koppel, D.E., 204
 Elson, E.L., *see* Kucik, D.F., 847
 Elson, E.L., *see* N.O. Petersen, W.B. McConnau-
 gley, 801
 Elson, E.L., *see* Pasternak, C., 801
 Elson, E.L., *see* Peterson, N.O., 300
 Elson, E.L., *see* Qian, H., 848
 Elson, E.L., *see* Schlessinger, J., 802
 Elson, E.L., *see* Sheetz, M.P., 356, 848
 Elwenspoeck, M., *see* Boroske, E., 460, 519
 Emeis, C.A., 352
 Endo, T., *see* Fukami, K., 844
 Engberts, J.B.F.N., *see* Fonteijn, T.A.A., 953
 Engberts, J.B.F.N., *see* Rupert, L.A.M., 953
 Engel, A., *see* Engel, J., 798
 Engel, J., 798
 Engelhard, H., *see* Zeman, K., 841
 Engelhard, V.H., *see* Norment, A.M., 801
 Engelhardt, H., 300, 398, 459, 462
 Engelhardt, H., *see* Duwe, M.P., 398
 Engelhardt, H., *see* Sackmann, E., 457
 Engelhardt, H., *see* Zeman, K., 301
 Engelhardt, H., *see* Zilker, A., 458
 Engelman, D.M., *see* Lewis, B.A., 400
 Ennis, J., 400
 Epand, R.M., 157
 Epand, R.M., *see* Chang, H., 158
 Ephrussi, R., *see* Sorieul, S., 895
 Erickson, C.A., 798
 Erickson, H.P., *see* Staunton, D.E., 802
 Ericsson, B., *see* Hyde, S.T., 150
 Eriksson, J.C., *see* Ljunggren, S., 153
 Eriksson, P.-O., 152, 156
 Eriksson, P.-O., *see* Lindblom, G., 157
 Eriksson, T., *see* Bonnett, H.T., 895
 Ernst, M.H., 352
 Erzurum, S.C., *see* Downey, G.P., 848
 Esch, F.S., *see* Gould, K.L., 846
 Estep, T.N., 352
 Euteneuer, U., *see* Janmey, P.A., 839
 Evans, E., 63, 299, 301, 352, 459, 460, 462, 597,
 599, 600, 601, 687, 688, 718, 720, 721, 753,
 843, 848
 Evans, E., *see* Berk, D., 753
 Evans, E., *see* Bloom, M., 93, 298, 401, 461,
 517, 753, 838
 Evans, E., *see* Buxbaum, R., 797
 Evans, E., *see* Kwok, R., 299, 687, 719
 Evans, E., *see* Merkel, R., 63, 300
 Evans, E., *see* Needham, D., 461
 Evans, E., *see* Rand, R.P., 688
 Evans, E., *see* Sackmann, E., 516
 Evans, E.A., 300, 397, 457, 458, 459, 462, 597,
 600, 642, 687, 688, 690, 753, 798, 799, 841,
 952, 955
 Evans, E.A., *see* Waugh, R., 462
 Evans, D.F., *see* Pashley, R.M., 689, 951
 Evans, D.F., *see* Tsao, Y.-H., 688, 690
 Evans, L., *see* Heuser, J.E., 899
 Everson, G., *see* Carr, I., 797
 Ewen, B., 206
 Ewert, U., *see* Shin, Y.-K., 356
 Exerova, D., *see* Kashchiev, D., 897
 Eyer, J., *see* Leterrier, J.-L., 839
 Eyring, E., 799

- Eyring, H., *see* Zwolinsky, B. J., 489
 Eytan, G.D., *see* Gad, A.E., 955
 Ezzell, R., *see* Samuels, M., 845
 Ezzell, R. M., 841
- Fahn, C., *see* Sackmann, E., 298, 601
 Fainstein, V., *see* Lopez-Berestein, G., 517
 Fan, D., *see* Fidler, I.J., 517
 Faquin, W., *see* Husain, C.A., 840
 Faquin, W.C., 840
 Farago, B., *see* Pfeiffer, W., 355
 Farge, E., 460
 Farnarier, C., *see* Kaplanski, G., 803
 Farrall, A.J., *see* Thewalt, J.L., 95
 Faruqi, A.R., *see* Radiman, S., 151
 Fath, K., *see* Burridge, K., 843
 Fath, K.R., 843
 Fattal, D., 399
 Faucon, J.F., 398, 459, 720
 Faucon, J.F., *see* Angelova, M.I., 720
 Faucon, J.F., *see* Meleard, P., 459, 460
 Feder, J., 352
 Feder, T., *see* Rädler, J., 301
 Feder, T.J., *see* Rädler, J., 598
 Fedor, J., *see* Düzgünes, N., 950
 Fedorova, L.I., *see* Sukharev, S.I., 900
 Fehder, P.L., *see* Emeis, C.A., 352
 Feigel'man, M.V., *see* Belaya, M.L., 598
 Feigenson, G.W., 641, 688, 951
 Feigenson, G.W., *see* Florine, K.I., 688
 Feigenson, G.W., *see* Swanson, J.E., 641
 Feiglman, M.V., *see* Belaya, M.L., 299
 Feire, E., *see* Snyder, B., 356
 Feld, M.K., *see* Grinnell, F., 799
 Felder, S., *see* Livnek, E., 800
 Felgner, P., 518
 Fendler, J.H., 517
 Fennie, C., *see* Foxall, C., 799
 Fenzl, W., 599
 Fenzl, W., *see* Cevc, G., 462, 598
 Fernandez, M.S., 156, 203
 Ferry, J.D., *see* Janmey, P.A., 839
 Feynman, R.P., 599
 Fidler, I.J., 517
 Fidler, I.J., *see* Lopez-Berestein, G., 517
 Fielding, R.M., 517
 Fields, R.D., 843
 Filimonov, V.V., *see* Bichenkov, E.E., 954
 Finch, S.A.E., *see* Stier, A., 159
 Findlay, E.J., 641
 Finegold, L., 158
 Finer, E.G., 953
 Finer, E.G., *see* Hauser, H., 953
 Fink, C.A., *see* Simon, S.A., 688
 Finkelstein, A., *see* Cohen, F.S., 955
 Fischer, A., 205, 207, 209, 301
 Fischer, A., *see* Lösche, M., 203
 Fischer, A., *see* Sackmann, E., 301
 Fischer, T.M., 458, 461
 Fisher, D., *see* Blow, A.M.J., 954
 Fisher, D., *see* Tilcock, C.P.S., 156
 Fisher, D., *see* Tilcock, C.T.S., 952
 Fisher, G.W., *see* de Biasio, R.L., 798
 Fisher, L.R., *see* Francis, G.W., 799
 Fisher, M.E., 601
 Fisher, M.E., *see* Huse, D.A., 601
 Fisher, M.E., *see* Lipowsky, R., 599
 Fitzgerald, L.A., *see* Chopra, H., 847
 Flanagan, I., 799
 Flanagan, T.D., *see* Arnold, K., 954
 Flanagan, T.D., *see* Ohki, S., 949, 954
 Flasher, D., *see* Düzgünes, N., 950
 Flavin, M., *see* Bramblett, G.T., 846
 Fleming, S., *see* Rahilly, M.A., 843
 Fligiel, S.E., *see* Chopra, H., 847
 Florine, K.I., 688
 Flörshheimer, M., 205, 209
 Flory, P., 302
 Flory, P.J., 400, 799
 Flory, P.J., *see* Dill, K.A., 399
 Flugge, W., 753
 Flynn, G., *see* Weiner, N., 490
 Foa, C., 799
 Foa, C., *see* André, P., 796
 Foa, C., *see* Mège, J.L., 801
 Foa, C., *see* Tissot, O., 803
 Fogden, A., 153, 641
 Fogel, C.A., *see* Linshaw, M.A., 848
 Fogerty, F.J., *see* Mosher, D.F., 801
 Foisner, R., 839
 Foldvari, M., 490
 Folena, E., *see* Massari, S., 956
 Fonteijn, T.A.A., 953
 Fontell, K., 149, 152
 Fontell, K., *see* Gutman, H., 156
 Forrester, J.V., *see* Curtis, A.S.G., 797
 Forscher, P., 848
 Förster, G., *see* Brezesinski, G., 202
 Förster, G., *see* Nuhn, P., 209
 Forster, W., *see* Berg, H., 895
 Forster, W., *see* Sugar, I.P., 901
 Forster, W., *see* Weber, H., 895
 Fort, T., 203
 Fourcade, B., 458, 460, 461
 Fourcade, B., *see* Miao, L., 457, 721
 Fourcade, B., *see* Michalet, X., 461
 Fourcade, B., *see* Wortis, M., 458
 Fox, J., 841

- Fox, J.E., 841, 843
 Fox, K.K., *see* Fontell, K., 152
 Foxall, C., 799
 Fraley, R., *see* Düzgünes, N., 956
 Fraley, R.T., 518
 Francis, G., *see* Rand, R.P., 687
 Francis, G.W., 799
 Francke, W., *see* Schwartz, M., 847
 Frankel, R.B., *see* Blakemore, R.P., 93
 Frankel, R.B., *see* Mann, S., 93
 Franks, N.P., 150
 Fraser, S.E., *see* Stolberg, J., 802
 Frederik, P.M., *see* Lasic, D.D., 517
 Freed, J., *see* Wade, W., 848
 Freed, J.H., *see* Naycem, A., 354
 Freed, J.H., *see* Shin, Y.-K., 356
 Freed, J.H., *see* Wade, W.F., 803
 Freire, E., 352
 Freire, E., *see* Biltonen, R.L., 351
 French, S.W., 847
 Frey, E., 301
 Frey, W., *see* Sackmann, E., 301
 Frieden, C., *see* Cortese, J.D., 839
 Friend, D.S., *see* Düzgünes, N., 950, 953
 Frimmer, M., *see* Bärman, M., 846
 Froines, J.R., *see* de B. Costa, S.M., 204
 Frojmovic, M., 799
 Fromherz, P., 298, 462, 489
 Fromherz, P., *see* Fernandez, M.S., 156, 203
 Fründ, R., *see* Hinz, H.-J., 156
 Fujie, T., *see* Shigematsu, M., 951
 Fukami, K., 844
 Fukazawa, T., *see* Muguruma, M., 844
 Fuller, N., *see* Gawrisch, K., 689, 953
 Fuller, N., *see* Kachar, B., 688, 955
 Fuller, N., *see* Lis, L.J., 800, 951
 Fuller, N., *see* Parsegian, V.A., 597, 640
 Fuller, N., *see* Rand, R.P., 156, 157, 951
 Fuller, N.L., *see* Cowley, A.C., 597, 641, 688
 Fuller, N.L., *see* Gawrisch, K., 689
 Fuller, N.L., *see* Horn, R.G., 207
 Fuller, N.L., *see* Lis, L.J., 688
 Fuller, N.L., *see* Parsegian, V.A., 687, 688, 753
 Fuller, N.L., *see* Rand, R.P., 687, 688, 689
 Funayama, N., 845
 Fung, B.K., 950
 Fuoss, R.M., 642
 Fürst, W., 63, 298
 Fürth, R., 352
 Furuhashi, K., *see* Fukami, K., 844

 Gabert, J., *see* André, P., 796
 Gabizon, A., 517, 518
 Gabizon, A., *see* Lasic, D.D., 518
 Gabizon, A., *see* Martin, F., 518
 Gabizon, A., *see* Papahadjopoulos, D., 518
 Gad, A.E., 955
 Gadek, T.R., *see* Felgner, P., 518
 Gaenslar, K., *see* Stribling, R., 519
 Gaffney, B.J., *see* Chen, S.C., 158
 Gaines, G.L., 202
 Gaines Jr., G.L., *see* Ballamy, W.D., 204
 Galea, S., *see* Jongstra-Bilen, J., 846
 Galindo, J.R., *see* Foa, C., 799
 Galindo, J.R., *see* Mège, J.L., 801
 Galla, H.-J., 204, 300, 301, 352
 Galla, H.-J., *see* Hartmann, W., 955
 Galla, H.-J., *see* Heithier, H., 204
 Galla, H.-J., *see* Xue You Han, K. Gietzen, 302
 Gallet, F., *see* Muller, P., 209
 Gallez, D., *see* Coakley, W.T., 899
 Gally, H.U., *see* Bueldt, G., 299
 Gally, H.U., *see* Buldt, G., 206
 Gambacorta, A., *see* de Rosa, M., 94
 Gambacorta, A., *see* Gulik, A., 94, 159
 Gambacorta, A., *see* Luzzati, V., 94, 159
 Gambacorta, A., *see* Vaz, W.L.C., 357
 Gamble, R.A., *see* Francis, G.W., 799
 Gancet, C., *see* Ransac, S., 211
 Ganser, R., *see* Vienken, J., 899
 Gao, X., 519
 Garber, B., *see* Weiss, P., 803
 Garboczi, E.J., 352
 Garcia, A., 847
 Garcia, A.G., *see* Artalejo, C.R., 949
 Gardam, M., 352
 Gardner, K., 840
 Gardner, K., *see* Bennett, V., 840
 Gareeva, A.B., *see* Bereznikova, A.V., 846
 Garoff, S., *see* Safran, S.A., 208
 Garrod, D.R., *see* Steinberg, M.S., 754
 Garrouste, F., *see* Capo, C., 753, 797
 Garver, T.M., *see* Xian, W., 849
 Gasmi, L., *see* Curtis, A.S.G., 797
 Gatt, S., 519
 Gaub, H., *see* Maksymiw, R., 302, 303, 842
 Gaub, H., *see* Müller, O., 839
 Gaub, H.E., *see* Moy, V.T., 209
 Gaub, H.E., *see* Radmacher, M., 690
 Gaub, H.E., *see* Weisenhorn, A.L., 207
 Gawrisch, K., 689, 953
 Gawrisch, K., *see* Arnold, K., 952, 953, 954
 Gawrisch, K., *see* van Oss, C.J., 952
 Gebauer, D., 489
 Gebhard, W., *see* Holmes, K., 838
 Gebhardt, C., 299, 461, 641
 Gebhardt, C., *see* Krbec, R., 299
 Gebhardt, C., *see* Sackmann, E., 299

- Gee, M.L., *see* Chen, Y.L.E., 207
 Geerts, H., 352
 Geerts, H., *see* de Bradander, M., 352
 Gelb, N.A., *see* Robbin, R., 802
 Gelbart, W.M., 401
 Gelbart, W.M., *see* Ben-Shaul, A., 397, 398
 Gelbart, W.M., *see* Szleifer, I., 153, 299, 398, 489
 Gelfand, M., *see* Fisher, M.E., 601
 Gelles, J., 352
 Gennis, R.B., 93, 298, 799
 Geogallas, A., *see* Pink, D.A., 355
 Geogopoulos, P., *see* Dutta, P., 205
 Georgallas, A., 202
 Georges, A., *see* Bouchaud, J.-P., 351
 Georgescauld, G., *see* Song, L., 900
 Georgiev, G., *see* Dimitrov, D.S., 900
 Georgiou, G.N., *see* Anderson, C.M., 351
 Gerber, Ch., *see* Binnig, G., 207
 Gerber, Ch., *see* Smith, D.P.E., 207
 Gerisch, G., *see* Neumann, E., 895
 Germain, C., *see* Doucet, J., 206
 Gerritsen, W.J., *see* Verkleij, A.J., 955
 Gershfeld, N.L., *see* Horn, L.W., 203
 Gershfeld, N.L., *see* Tajima, K., 208
 Gerson, D.F., *see* Schürch, S., 802
 Geshfeld, N., 203
 Gesztes, A., 490
 Gesztes, A., *see* Foldvari, M., 490
 Geuens, S., *see* Geerts, H., 352
 Geurts, J., *see* Juergens, E., 299
 Gewirtz, A.M., *see* Wang, D.L., 843
 Ghosh, R.N., 352
 Ghosh, S., *see* Wang, D.L., 843
 Gibson, C.C., *see* Morris, J.S., 950
 Gicquaud, C., *see* Laliberte, A., 843
 Gicquaud, C., *see* St Onge, D., 843
 Gierasch, L.M., *see* Briggs, M.S., 210
 Gilani, S., *see* Huang, S.K., 518
 Gillard, B., 846
 Gilles, R., *see* Cornet, M., 848
 Gilles, R., *see* Zimmermann, U., 897
 Gilligan, D.M., *see* Joshi, R., 840
 Gimbrone, M.A., *see* Bevilacqua, M.P., 796
 Gingell, D., 799
 Gingell, D., *see* Bailey, J., 843
 Gingell, D., *see* Francis, G.W., 799
 Gingell, D., *see* LeNeveu, D.M., 688, 753
 Gingell, R.P., *see* LeNeveu, D.M., 718
 Ginsberg, R.C., *see* Svenson, C.E., 517
 Giorgi, M., *see* Cianci, C.D., 840
 Girardet, M., *see* Lipowsky, R., 462, 601
 Gittes, F., 839
 Gladden, L.F., *see* Hollewand, M.P., 353
 Glaser, M., 461
 Glaser, R., 62
 Gleason, M., *see* Melancon, P., 63
 Glenney, J.J., *see* Turner, C.E., 844
 Glick, B., *see* Melancon, P., 63
 Gliozzi, A., *see* de Rosa, M., 94
 Gokhale, S.M., *see* Gudi, S.R., 842
 Golan, D.E., 63
 Golan, D.E., *see* Alecio, M.R., 351
 Golander, C.G., *see* Claesson, P.M., 952
 Gold, J.M., *see* Arnett, E.M., 154
 Goldfine, H., 160
 Golding, H., *see* Dimitrov, D.S., 899
 Goldman, A.J., 799
 Goldman, R., 839
 Goldmann, W.H., *see* Isenberg, G., 844
 Goldmann, W.H., *see* Kaufmann, S., 304, 844
 Goldschmidt, C.P., 849
 Goldschmidt-Clermont, P.J., 848
 Goldsmith, H.L., *see* Tha, S.P., 802
 Goldstein, L.S., *see* Byers, T.J., 840
 Goldstein, R.E., 640, 641, 690
 Goldstein, R.E., *see* Duplantier, B., 641
 Golstein, P., 799
 Golstein, P., *see* Bongrand, P., 797
 Gómez-Fernández, J.C., *see* Ortiz, A., 160
 Gompper, G., 459, 600, 601, 720
 Gondol, D., *see* Habazettl, J., 304
 Gonzalez, P., 490
 Good, R.J., 799
 Good, R.J., *see* van Oss, C.J., 803, 951, 952
 Goodall, A.H., *see* Blow, A.M.J., 954
 Goodsaid-Zalduondo, F., *see* Vaz, W.L.C., 357
 Goodwin, G.C., *see* Davies, R.J., 210
 Gorbi, A.L., *see* Kishimoto, T.K., 753
 Gorby, Y.A., 93
 Gordon, P., 352
 Gorlin, J., 845
 Gorlin, J.B., *see* Cunningham, C.C., 840
 Gotlieb, A.L., *see* Linshaw, M.A., 848
 Gotto, A.M., *see* Vainio, P., 211
 Gould, K.L., 846
 Gould, S.A.C., *see* Weisenhorn, A.L., 207
 Gould, S.J., 94
 Gouy, G., 640
 Grainger, D.W., 211, 302
 Granfeldt, M.K., 690
 Gratzner, W.B., *see* Kahana, E., 840
 Green, B.R., *see* Webb, M.S., 357
 Green, D.E., 159
 Green, K., *see* Jones, J., 842
 Green, N.M., *see* Valentine, R.C., 803
 Greenwood, J.A., 799
 Gregonis, D.E., *see* Andrade, J.D., 796

- Gregoriadis, G., 489, 517
 Gresalfi, T., *see* Eisenberg, M., 688
 Gress, R.E., *see* Shaw, S., 802
 Grest, G.S., 353
 Grest, G.S., *see* Petsche, I.B., 601
 Grest, G.S., *see* Schmidt, C.F., 462
 Grimm, E., 799
 Grinnell, F., 799
 Grinstein, G., 602
 Gripon, J.C., *see* Alkhalaf, W., 519
 Groebner, G., *see* Stohrer, T., 299
 Gromov, D., *see* Malev, V., 840
 Grondin, P., 849
 Gross, D., 63
 Grossi, I.M., *see* Chopra, H., 847
 Grotehans, S., 600
 Grotehans, S., *see* Lipowsky, R., 598
 Gruber, E.E., 599
 Grudzev, A.D., 954
 Gruen, D.W.R., 301, 399, 598, 689
 Gruen, D.W.R., *see* Hladky, S.B., 400
 Gruler, H., 461
 Gruler, H., *see* Albrecht, O., 202, 203, 299, 303
 Gruler, H., *see* Gebhardt, C., 299, 461, 641
 Gruler, H., *see* Krbecek, R., 299
 Grundy, M., 206
 Gruner, A., 298
 Gruner, S.M., 95, 153, 154, 157, 158, 159, 689
 Gruner, S.M., *see* Anderson, D.M., 150
 Gruner, S.M., *see* Gawrisch, K., 689
 Gruner, S.M., *see* Keller, S.L., 687
 Gruner, S.M., *see* Kirk, G.L., 157, 689
 Gruner, S.M., *see* Lewis, R.N.A.H., 155
 Gruner, S.M., *see* Mannock, D.A., 155
 Gruner, S.M., *see* Nayaran, O., 153
 Gruner, S.M., *see* Rand, R.P., 157, 689
 Gruner, S.M., *see* Shyamsunder, E., 155, 159
 Gruner, S.M., *see* Tate, M.W., 149, 156, 159, 901
 Gruner, S.M., *see* Turner, D.C., 153, 689
 Grünewald, B., 158
 Grünewald, S., *see* Brezesinski, G., 202
 Gualian, M., *see* Brainsma, R., 301
 Guccione, M.A., *see* Livne, A., 842
 Gudi, S.R., 842
 Gudkova, D.A., *see* Kwiatkowska, K., 842
 Guggenheim, E.A., 302
 Guinier, A., *see* Caille, M., 602
 Guldbbrand, L., 208, 599, 688, 690
 Gulik, A., 94, 159
 Gulik, A., *see* Luzzati, V., 94, 150, 159
 Gulik, A., *see* Vargas, R., 151
 Gulik-Krzywicki, T., 150, 688
 Gumpert, J., *see* Meyer, H.W., 159
 Gunning, B.E.S., 159
 Gunstone, F.D., *see* Barton, P.G., 155
 Gunther-Luce, G.E., *see* Shaw, S., 802
 Gupta, C.M., 842
 Gupta, C.M., *see* Gudi, S.R., 842
 Gupte, S.S., 353
 Gupte, S.S., *see* Hackenbrock, Ch.R., 63
 Gutheil, M., *see* Nuhn, P., 209
 Gutman, H., 156
 Gutop, Yu.V., *see* Derjaguin, B.V., 900
 Guttman, G., 641
 Guy, H.R., 94, 956
 Györgyi, S., *see* Arnold, K., 952

 Haas, H., 204, 210
 Haas, N.S., 156
 Habazettl, J., 304
 Hackenbrock, C.R., *see* Chazotte, B., 351
 Hackenbrock, C.R., *see* Gupte, S.S., 353
 Hackenbrock, Ch.R., 63
 Häckl, W., 721
 Hafeman, D.G., 210
 Hah, J.S., *see* Boni, L.T., 952
 Hahn-Hagerdal, B., 898
 Hajduk, D.A., *see* Gawrisch, K., 689
 Hale, L.P., *see* Haynes, B.F., 799
 Hall, A.K., *see* Rutishauser, U., 802
 Hall, D.G., *see* Carvell, M., 688
 Hall, P.F., *see* Almahbobi, G., 847
 Hallaway, B., *see* Schanus, E., 840
 Hallmann, D., *see* Vaz, W.L.C., 357
 Hallows, K.R., 848
 Halperin, B.I., 208
 Halperin, B.I., *see* Nelson, D.R., 300
 Hamann, H.C., *see* Creutz, E.C., 954
 Hamilton, W.A., *see* Sale, A.J.H., 895
 Hammer, D., *see* Dembo, M., 753, 798
 Hammer, D.A., 753, 799
 Hammer, G.G., *see* Schlessinger, J., 802
 Hammer, J.E., *see* Korn, E.D., 847
 Hammerling, U., *see* Lipscomb, M.F., 800
 Hammerton, R.W., *see* Nelson, W.J., 842
 Hammond, K., 490
 Hamori, C.J., 517
 Hampp, H., *see* Vienken, J., 899
 Hampp, R., *see* Mehrle, W., 896
 Hanert, C.E., *see* Thewalt, J.L., 95
 Hans-Egon, J., *see* Berg, H., 895
 Hänsch, T.W., *see* Hörber, J.K.H., 207
 Hansen, C., *see* Allen, T.M., 518
 Hansma, H.G., *see* Weisenhorn, A.L., 207
 Hansma, P.K., *see* Weisenhorn, A.L., 207
 Hansson, E., *see* Fontell, K., 152
 Hanusse, P., *see* Bivas, I., 301, 398, 459
 Harbich, W., 598, 719

- Harbich, W., *see* Helfrich, W., 150, 719
 Harbich, W., *see* Servuss, R.M., 720
 Harbich, W., *see* Wiese, W., 458, 721
 Hård, S., 205
 Harden, J.L., 303, 642
 Hardt, S.L., 63
 Hargreaves, A., 846
 Haris, P.I., 298
 Harlos, K., 151
 Harlos, K., *see* Pascher, I., 206
 Harlos, K., *see* Seddon, J.M., 150, 688
 Harlos, K., *see* Stümpel, J., 151
 Harlos, K., *see* Watts, A., 151
 Harris, A.K., 799
 Harris, A.L., *see* Traynor, K.A., 849
 Harris, H., 949
 Harris, J., 208
 Harris, J.M., *see* de B. Costa, S.M., 204
 Harrison, A.K., 353
 Harrison, G.I., *see* Bartoletti, D.C., 901
 Harrison, M.L., *see* Willardson, B.M., 840
 Harter, C., 956
 Hartmann, W., 955
 Hartmann, W., *see* Galla, H.-J., 204, 352
 Hartmann, W., *see* Galla, H.J., 300
 Hartung, J., 721
 Hartung, R., *see* Cevc, G., 152
 Hartwig, J., 839, 845
 Hartwig, J., *see* Gorlin, J., 845
 Hartwig, J.H., 841
 Hartwig, J.H., *see* Cantiello, H.F., 848
 Hartwig, J.H., *see* Cunningham, C.C., 840
 Hartwig, J.H., *see* Ezzell, R.M., 841
 Hartwig, J.H., *see* Jongstra-Bilen, J., 846
 Hartwig, J.H., *see* Ohta, Y., 845
 Harvey, N., *see* Arnett, E.M., 154
 Hascall, V.C., *see* Yanagishita, M., 803
 Hasegawa, A., *see* Foxall, C., 799
 Hashin, Z., 353
 Hatano, S., *see* Fukami, K., 844
 Hatfield, J.S., *see* Chopra, H., 847
 Hatta, I., 303
 Hatta, I., *see* Takahashi, H., 955
 Hauge, E.H., *see* Ernst, M.H., 352
 Hauser, H., 151, 203, 953
 Hauser, H., *see* Oldani, D., 203
 Hauser, H., *see* Paltauf, F., 203
 Hauser, M., *see* Cevc, G., 598
 Hausner, G.G., *see* Hui, S.W., 207
 Havlin, S., 353
 Hayakawa, T., *see* Kinoshita, K., 896
 Haydon, D.A., *see* Elliott, J.R., 399
 Haydon, D.A., *see* Hladky, S.B., 399
 Haynes, B.F., 799
 Haywood, A.M., 753
 Heath, J.P., *see* Gillard, B.K., 846
 Heath, R., *see* Rybicki, A., 840
 Heckl, W.M., 204, 207, 210
 Heckl, W.M., *see* Hörber, J.K.H., 207
 Hedman, K., 799
 Heenan, R., *see* Schurtenberger, P., 152
 Heimbürg, T., 156
 Heinemann, S.H., 302
 Heinrich, R., *see* Heinrich, V., 460
 Heinrich, V., 460
 Heinz, B., *see* Morowitz, H.J., 93
 Heise, H., 303, 844
 Heithier, H., 204
 Helenius, A., 489
 Helenius, A., *see* Stegmann, T., 949
 Helenius, A., *see* White, J.M., 949
 Helfrich, *see* Sackmann, E., 516
 Helfrich, P., 399
 Helfrich, W., 150, 153, 298, 300, 301, 397, 400, 457, 458, 459, 460, 462, 489, 517, 596, 597, 599, 600, 601, 641, 689, 718, 719, 720, 799
 Helfrich, W., *see* Beblík, G., 398, 720
 Helfrich, W., *see* Boroske, E., 460, 519
 Helfrich, W., *see* Harbich, W., 598, 719
 Helfrich, W., *see* Hartung, J., 721
 Helfrich, W., *see* Klösgen, B., 720
 Helfrich, W., *see* Kozlov, M.M., 720
 Helfrich, W., *see* Kummrow, M., 300, 459, 720
 Helfrich, W., *see* Mutz, M., 459, 596, 597, 719
 Helfrich, W., *see* Niggemann, G., 720
 Helfrich, W., *see* Ou-Yang, Z.-C., 460
 Helfrich, W., *see* Servuss, R.-M., 462, 598
 Helfrich, W., *see* Servuss, R.M., 719, 720
 Helfrich, W., *see* Wiese, W., 458, 460, 721
 Helfrich, W., *see* Winterhalter, M., 400, 641
 Heller, H., 400
 Helm, C., 719
 Helm, C.A., 204, 205, 207, 951, 952
 Helm, C.A., *see* Chen, Y.L.E., 207
 Helm, C.A., *see* Kjaer, K., 205
 Helm, C.A., *see* Lösche, M., 208
 Helm, C.A., *see* Miller, A., 203
 Hemperly, J.J., *see* Cunningham, B.A., 753
 Henderson, R., 94
 Hendriks, Y., 154
 Henkart, P.A., 799
 Henkel, T., *see* Knoll, W., 304
 Hennig, A., *see* Elias, H., 798
 Henon, S., 204
 Heremans, A., *see* David, G., 798
 Herold, W., *see* Arnold, K., 952
 Herrenknecht, K., 845
 Herrenknecht, K., *see* Ozawa, M., 845

- Herrington, K.L., *see* Kaler, E.W., 461
 Herrmann, A., 954
 Herrmann, A., *see* Arnold, K., 952, 954
 Herrmann, H., 842
 Herron, J.N., 205
 Hersh, E.M., *see* Lopez-Berestein, G., 517
 Hesketh, J.E., *see* Vedeler, A., 845
 Heuser, J.E., 899
 Hewison, L.A., *see* Coakley, W.T., 754
 Heyn, S.-P., *see* Weisenhorn, A.L., 207
 Hibbs, A.R., *see* Feynman, R.P., 599
 Hibino, M., 896
 Hibino, M., *see* Kinoshita, K., 896
 Hickel, W., 203
 Hiemenz, P.C., 641
 Hiergeist, C., 600, 601
 Higgs, P.G., 642
 Hilfer, R., *see* Scheringer, M., 208
 Hill, T.L., 839
 Hillard, I.E., 303
 Hillebrecht, B., *see* Herrmann, A., 954
 Hillman, K., *see* Dimitrov, D.S., 899
 Hintner, H., 847
 Hinz, H.-J., 156
 Hinz, H.-J., *see* Koynova, R., 158
 Hinz, H.-J., *see* Kutenreich, H., 156
 Hiram, Y., 949
 Hiramoto, Y., 799
 Hirano, K., *see* Kinoshita, K., 896
 Hirshfeld, C.L., 210, 303
 Hitchcock, P., *see* Elder, M., 151, 206
 Hitt, A.L., *see* Luna, E.J., 838
 Hladky, S.B., 399, 400
 Ho, J.T., *see* Boni, L.T., 952
 Ho, W.C., *see* Duden, R., 846
 Hochmuth, R.M., 848
 Hochmuth, R.M., *see* Needham, D., 897
 Hochmuth, R.M., *see* Tran-Son-Tay, R., 803
 Hodges, R.S., *see* Davis, J.H., 94, 303
 Hoekstra, D., 899, 949, 950, 952, 956, 957
 Hoekstra, D., *see* Arnold, K., 955
 Hoekstra, D., *see* Düzgünes, N., 956
 Hoekstra, D., *see* Fonteijn, T.A.A., 953
 Hoekstra, D., *see* Rupert, L.A.M., 953
 Hoekstra, D., *see* Struck, D.K., 950
 Hoekstra, D., *see* Wilschut, J., 949, 950
 Hoeveler, A., *see* Wegener, A.M.K., 803
 Hoffmann, H., *see* Hofmann, S., 641
 Hofmann, G.A., 901
 Hofmann, S., 641
 Hofschneider, P.H., *see* Neumann, E., 896
 Hogan, J., *see* Caffrey, M., 153
 Hogan, J.L., *see* Seddon, J.M., 152
 Hoggan, M.D., 895
 Holak, T.A., *see* Habazettl, J., 304
 Holifield, B., *see* de Bradander, M., 352
 Hollenbeck, P., *see* Geerts, H., 352
 Hollewand, M.P., 353
 Holm, M., *see* Felgner, P., 518
 Holmes, K., 838
 Holmes, K.V., *see* Lipscomb, M.F., 800
 Holmes, M.C., 154
 Holmes, M.C., *see* Boden, N., 154
 Holmgren, A., *see* Nilsson, A., 156
 Holmsen, H., *see* Daniel, J., 839
 Holowka, D., *see* Ryan, T.A., 802
 Holsappel, M., *see* Wilschut, J., 957
 Holtzer, H., 895
 Hong, K., 953, 955
 Hong, K., *see* Allen, T.M., 953
 Hong, K., *see* Meers, P., 954, 955
 Höning, D., 204
 Honkanen, R.E., *see* Rigler, M.W., 160
 Honn, K.V., *see* Chopra, H., 847
 Hook, H., *see* Hedman, K., 799
 Hook, M., *see* Woods, A., 803
 Hope, M.J., 156, 956
 Hope, M.J., *see* Cullis, P.R., 95, 153, 159, 955
 Hope, M.J., *see* de Kruijff, B., 153, 159
 Hopkins, C.R., 63
 Hopkins, C.R., *see* de Bradander, M., 352
 Hopter, R., *see* Lopez-Berestein, G., 517
 Hörber, J.K.H., 207
 Hori, M., *see* Yonezawa, F., 357
 Horkovics, K.S., 846
 Horn, L.W., 203
 Horn, R., 688
 Horn, R., *see* Israelachvili, J.N., 153, 489
 Horn, R.G., 207, 597, 688, 799, 956
 Hornby, A.P., 157
 Horne, R.W., *see* Bangham, A.D., 516
 Horoyan, M., 800
 Horvath, L.I., *see* Brezesinski, G., 202
 Hoschutzky, H., *see* Ozawa, M., 845
 Hosono, K., *see* Hahn-Hagerdal, B., 898
 Hotani, H., *see* Miyamoto, H., 840
 Hotani, H., *see* Vale, R.D., 847
 Hou, Y., *see* Scullion, B.F., 802
 Hou, Y., *see* Zhang, F., 803
 Howard, J., *see* Gittes, F., 839
 Hristova, K., *see* Needham, D., 518
 Hsi, S.C., *see* Mantsch, H.H., 158
 Hsiung, H., *see* Rasing, Th., 205
 Hsu, L., 461
 Huang, C., *see* Lin, H., 155
 Huang, C., *see* Wang, Z., 155
 Huang, C., *see* Xu, H., 158
 Huang, C.H., *see* McIntosh, T.J., 688

- Huang, H.W., 399
 Huang, J.S., *see* Turner, D.C., 689
 Huang, K.S., *see* Lasic, D.D., 518
 Huang, L., *see* Gao, X., 519
 Huang, S.K., 518
 Huang, S.K., *see* Papahadjopoulos, D., 518
 Huber, R., 955
 Hübner, W., 206
 Hüchel, E., *see* Debye, P., 640
 Hughes, B.D., 353
 Hui Bon Hoa, G., *see* Kornblatt, J.A., 687
 Hui, S.A., *see* Stenger, D.A., 899
 Hui, S.-W., 353
 Hui, S.-W., *see* Sen, A., 156
 Hui, S.W., 207, 901, 954, 956
 Hui, S.W., *see* Boni, L.T., 156, 952
 Hui, S.W., *see* Ohki, S., 949
 Hui, S.W., *see* Stenger, D.A., 899
 Hummel, B., *see* Caffrey, M., 159
 Hunt, R.D., 206
 Hunter, T., *see* Gould, K.L., 846
 Hupfer, B., *see* Bader, H., 601
 Husain, C.A., 840
 Husain, C.A., *see* Byers, T.J., 840
 Husain, C.H., *see* Ruff, P., 840
 Huse, D.A., 601
 Husson, F., *see* Luzzati, V., 687
 Hvidt, S., 839
 Hvidt, S., *see* Janmey, P.A., 839
 Hyde, S.T., 150, 153
 Hyde, S.T., *see* Andersson, S., 150
 Hyde, S.T., *see* Barois, P., 151
 Hyde, S.T., *see* Fogden, A., 153
 Hynes, R.O., 800
- Ibel, K., *see* Knoll, W., 302
 Ice, G.E., *see* Lin, B., 209
 Ichinose, Y., *see* Fidler, I.J., 517
 Iglesias, F.J., 898
 Ikegami, A., *see* Kimura, Y., 954
 Ikegami, A., *see* Kinoshita, K., Jr., 896
 Imainzumi, S., *see* Hatta, I., 303
 Inagaki, M., *see* Fukami, K., 844
 Inczedy-Marcsek, M., *see* Kuttentreich, H., 156
 Inman, R., *see* Jacobson, K., 753
 Inoue, T., *see* Shigematsu, M., 951
 Inverardi, L., *see* Pardi, R., 801
 Ipsen, I., *see* Evans, E.A., 642
 Ipsen, J., *see* Evans, E., 600
 Ipsen, J.H., 95, 210, 303, 353, 397
 Irvine, R.F., *see* Dawson, R.M.C., 157
 Isenberg, G., 62, 844
 Isenberg, G., *see* Heise, H., 303, 844
 Isenberg, G., *see* Kaufmann, S., 304, 844
- Isenberg, G., *see* Schmidt, C.F., 839
 Ishigami, M., *see* Takeuchi, K., 841
 Ishihara, A., *see* Jacobson, K., 753
 Ishihara, A., *see* Lee, G.M., 354
 Ishihara, A., *see* de Bradander, M., 352
 Israelachvili, J., 688, 753, 800
 Israelachvili, J., *see* Kuhl, T., 519
 Israelachvili, J., *see* Marra, J., 206
 Israelachvili, J.I., 687
 Israelachvili, J.N., 153, 159, 206, 207, 300, 397, 489, 598, 599, 640, 687, 689, 690, 951
 Israelachvili, J.N., *see* Bailey, S.M., 719
 Israelachvili, J.N., *see* Chen, Y.L.E., 207
 Israelachvili, J.N., *see* Helm, C., 719
 Israelachvili, J.N., *see* Helm, C.A., 207, 951, 952
 Israelachvili, J.N., *see* Horn, R.G., 207, 597, 688, 799
 Israelachvili, J.N., *see* Marra, J., 462, 597, 688
 Israelachvili, J.N., *see* Sirota, E.B., 641
 Ito, T., 840
 Ito, T., *see* Ohnishi, S., 957
 Ito, T., *see* Yamazaki, M., 952
 Itoh, H., *see* Hibino, M., 896
 Itoh, H., *see* Kinoshita, K., Jr., 896
 Ivanov, A., *see* Stoicheva, N., 898
 Ivanov, I.B., 900, 901
 Ivanov, I.B., *see* Dimitrov, D.S., 901
 Ivanov, I.B., *see* Radoev, B.P., 900
 Ivanova, M., *see* Panaiotov, I., 900
 Ivanova, Ts., *see* Dimitrov, D.S., 900
 Iwata, A., *see* Spruce, A.E., 900
- Jackson, P.H., *see* Boden, N., 154
 Jacob, H.-E., *see* Weber, H., 895
 Jacobson, K., 753
 Jacobson, K., *see* de Bradander, M., 352
 Jacobson, K., *see* Papahadjopoulos, D., 956
 Jacobson, K., *see* Scullion, B.F., 802
 Jacobson, K., *see* Vaz, W.L.C., 357
 Jacobson, K., *see* Zhang, F., 803
 Jacobson, K.A., *see* Derzko, Z., 352
 Jacobson, K.A., *see* Lee, G.M., 354
 Jacobson, K.A., *see* Vaz, W.L., 753
 Jacobson, K.A., *see* Vaz, W.L.C., 204
 Jacrot, B., *see* Zaccai, G., 150
 Jaeger, J.C., *see* Carslaw, H.S., 351
 Jaehnig, F., 299, 301
 Jäger, J., *see* Lücken, U., 720
 Jähnig, F., 353, 397, 399
 Jähnig, F., *see* Strehlow, U., 158
 Jähnig, F., *see* Vaz, W.L.C., 357
 Jahnke, L.L., 95
 Jain, M.K., 210
 Jain, R.K., *see* Dimitrov, D.S., 897

- Jakobsson, E., *see* Helfrich, P., 399
 James, P., *see* Harter, C., 956
 Jamieson, G.A., 62
 Jan, K.-M., *see* Skalak, R., 753
 Jan, L., *see* Heuser, J.E., 899
 Jan, Y., *see* Heuser, J.E., 899
 Jandi, J.H., 753
 Janiak, M.J., 156, 205, 641
 Janke, W., 600, 720
 Janke, W., *see* Kleinert, H., 720
 Janmey, P., 839, 848
 Janmey, P., *see* Hartwig, J., 845
 Janmey, P., *see* Hvidt, S., 839
 Janmey, P., *see* Yu, F.-X., 848
 Janmey, P.A., 839, 849
 Janmey, P.A., *see* Burlacu, S., 839
 Janmey, P.A., *see* Jongstra-Bilen, J., 846
 Janmey, P.A., *see* Xian, W., 849
 Janmey, P.J., *see* Cunningham, C.C., 840
 Jansen, R., *see* Wilschut, J., 957
 Janzen, J., *see* Evans, E., 753
 Jay, P.Y., 847
 Jekott, J.J., *see* Woodle, M.C., 518
 Jenkins, J.T., 460
 Jenkins, J.T., *see* Schneider, M.B., 459
 Jenkins, J.T., *see* Schneider, M.D., 301
 Joanny, J.-F., *see* Harden, J.L., 642
 Joanny, J.-F., *see* Higgs, P.G., 642
 Joanny, J.-F., *see* Pincus, P., 600, 641
 Joanny, J.F., 599, 753
 Joanny, J.F., *see* Andelmann, D., 208
 Johansson, J., *see* Edholm, O., 399
 Johansson, L.B.-A., *see* Lindblom, G., 354
 Johansson, S., *see* Hedman, K., 799
 Johnson, E.A., *see* Arnett, E.M., 154
 Johnson, K.L., 800
 Johnson, S.I., 304
 Johnson, S.J., 598, 841
 Johnson, S.K., 62
 Johnston, N.C., *see* Goldfine, H., 160
 Joliot, A., *see* Joliot, P., 353
 Joliot, P., 353
 Joliot, P., *see* Lavergne, J., 353
 Jolley, K.W., *see* Boden, N., 154
 Jones, G., *see* Rothstein, T.L., 802
 Jones, J., 842
 Jones, M.N., *see* Davies, R.J., 210
 Jones, M.N., *see* Hammond, K., 490
 Jongstra, J., *see* Jongstra-Bilen, J., 846
 Jongstra-Bilen, J., 846
 Jönsson, B., 400
 Jonsson, B., 689, 690
 Jonsson, B., *see* Attard, P., 690
 Jonsson, B., *see* Granfeldt, M.K., 690
 Jönsson, B., *see* Guldbrand, L., 208, 599
 Jonsson, B., *see* Guldbrand, L., 688, 690
 Jönsson, B., *see* Kjellander, R., 641
 Jonsson, B., *see* Kjellander, R., 690
 Jordan, C.A., *see* Neumann, E., 895
 Josephs, R., *see* Shen, B.W., 62
 Joshi, R., 840
 Jovin, T.M., 353
 Jovin, T.M., *see* Criado, M., 352
 Jovin, T.M., *see* Vaz, W.L.C., 357
 Juergens, E., 299
 Jülicher, F., 458, 459, 460, 461, 489, 600
 Jung, C.Y., *see* Boni, L.T., 952
 Jürg Waser, *see* Kuhn, H., 93
 Kabat, E.A., 800
 Kabsch, W., *see* Holmes, K., 838
 Kachar, B., 95, 159, 688, 955
 Kachar, B., *see* Pinto da Silva, P., 159
 Kachar, B., *see* Rand, R.P., 688
 Kaes, J., 301, 517
 Kaes, J., *see* Berndl, K., 301, 516
 Kaes, J., *see* Duwe, H.P., 300, 398
 Kaes, J., *see* Kaufmann, S., 304
 Kahana, E., 840
 Kaler, E.W., 461
 Kalina, M., 800
 Kallabis, H., 602
 Kalomiris, E.L., *see* Bourguignon, L.Y., 842
 Kam, Z., *see* Livnek, E., 800
 Kambadur, R., *see* Bramblett, G.T., 846
 Kamp, D., *see* Hickel, W., 203
 Kandler, O., 94
 Kandler, O., *see* Wheelis, M.L., 93
 Kandler, O., *see* Woese, C.R., 93
 Kanellas, D., *see* Johnson, S.I., 304
 Kanellas, D., *see* Johnson, S.J., 841
 Kanellas, K., *see* Johnson, S.K., 62
 Kao, K.N., 895
 Kapitza, H.G., *see* Vaz, W.L.C., 357
 Kaplan, L., *see* Northfelt, D.W., 518
 Kaplanski, G., 803
 Kaplanski, S., *see* Kaplanski, G., 803
 Karcher, H., 461
 Kardar, M., *see* Abraham, F.F., 601
 Karlström, G., *see* Ipsen, J.H., 95, 210, 353
 Karnovsky, M.J., *see* Abbas, A.K., 796
 Karnovsky, M.J., *see* Unanue, E.R., 803
 Karplus, M., *see* Pastor, R.W., 400
 Kartenbeck, J., *see* Schwartz, M., 847
 Kas, J., 839
 Kas, J., *see* Kaufmann, S., 844
 Käs, J., 458, 460, 721
 Käs, J., *see* Berndl, K., 457, 602, 721

- Käs, J., *see* Bärmann, M., 839
 Käs, J., *see* Duwe, H.P., 459, 597
 Käs, J., *see* Duwe, H.T., 489
 Käs, J., *see* Döbereiner, H.-G., 303, 458
 Kashchiv, D., 897
 Katchalsky, A., *see* Fuoss, R.M., 642
 Kato, S., *see* Takahashi, H., 955
 Katsuma, Y., *see* French, S.W., 847
 Kauertz, M.T., *see* Op den Kamp, J.A.F., 302
 Kaufmann, S., 304, 844
 Kaupp, U.B., 63
 Kawaguchi, M., *see* Chen, Y.-L., 205
 Kawahara, H., *see* French, S.W., 847
 Kawakatsu, T., 461
 Kawakatsu, T., *see* Andelman, D., 461
 Kawasaki, K., *see* Andelman, D., 461
 Kawasaki, K., *see* Kawakatsu, T., 461
 Kay, R.L., *see* Liu, N.I., 155
 Kayatar, C., *see* Rosenberg, J., 957
 Kaye, R.D., *see* Seddon, J.M., 155, 205, 688
 Keane, D.T., *see* Gruner, S.M., 157
 Keating, M., *see* Lopez-Berestein, G., 517
 Keira, T., *see* Ranck, J.L., 151
 Kékicheff, P., 151, 154, 640
 Kékicheff, P., *see* Hendriks, Y., 154
 Kékicheff, P., *see* Shubin, V.E., 641
 Keller, D.J., 208
 Keller, D.J., *see* Moy, V.T., 209
 Keller, S.L., 687
 Kelley, R.O., *see* Vogel, K.G., 803
 Kellie, S., 844
 Kellner, B.M.J., *see* Cadenhead, D.A., 202, 203
 Kelly, R., 846
 Kelly, T., *see* Burridge, K., 843
 Kelly, T., *see* Mueller, S.C., 843
 Kemler, R., *see* Herrenknecht, K., 845
 Kemler, R., *see* Ozawa, M., 845
 Kendall, K., *see* Johnson, K.L., 800
 Kenn, R.M., 209
 Kenn, R.M., *see* Möhwald, H., 209
 Kenney, D.M., *see* Ezzell, R.M., 841
 Kenworthy, A.K., *see* Simon, S.A., 688
 Keren-Zur, M., 957
 Keren-Zur, M., *see* Beigel, M., 957
 Ketterson, J.B., *see* Dutta, P., 205
 Khrantsov, V.V., *see* Grudzev, A.D., 954
 Khrebtukova, I.A., *see* Kwiatkowska, K., 842
 Kielian, M., *see* White, J.M., 949
 Killian, J.A., *see* de Kruijff, B., 159
 Kim, I.C., 353
 Kim, I.C., *see* Torquato, S., 356
 Kim, J.T., 155, 156
 Kim, J.W., *see* Goldschmidt, C.P., 849
 Kim, M.W., *see* Rasing, Th., 205
 Kim, Y.C., 954
 Kimball, B., *see* Detmers, P.A., 798
 Kimball, G.E., *see* Eyring, E., 799
 Kimura, Y., 954
 King, J.S., *see* Law, B.A., 519
 King, M.D., *see* Sachse, J.H., 355
 King, R.N., *see* Andrade, J.D., 796
 Kinloch, A.J., 860
 Kinlough-Rathbone, R., *see* Vickers, J., 843
 Kinnunen, P.K.J., 205
 Kinnunen, P.K.J., *see* Thuren, T., 211
 Kinnunen, P.K.J., *see* Vainio, P., 211
 Kinoshita, K., 896
 Kinoshita, K., *see* Hibino, M., 896
 Kinoshita, K., Jr., 896
 Kinoshita, Jr., K., *see* Serpersu, E.H., 896
 Kiometzis, M., 641
 Kirby, C., 519
 Kirino, Y., *see* Kinoshita, K., 896
 Kirk, G.L., 157, 689
 Kirk, G.L., *see* Gruner, S.M., 157
 Kirstein, S., 204
 Kiseleva, E.V., *see* Budker, V.G., 957
 Kishimoto, T.K., 753
 Kiso, M., *see* Foxall, C., 799
 Kitson, N., *see* Thewalt, J., 95
 Kjaer, K., 205
 Kjaer, K., *see* Als-Nielsen, J., 206
 Kjaer, K., *see* Böhm, C., 206
 Kjaer, K., *see* Helm, C.A., 205
 Kjaer, K., *see* Kenn, R.M., 209
 Kjaer, K., *see* Möhwald, H., 209
 Kjaer, K., *see* Vaknin, D., 206
 Kjellander, R., 208, 598, 599, 640, 641, 688, 689, 690
 Kjellander, R., *see* Attard, P., 690
 Kjellén, L., *see* Hedman, K., 799, 803
 Klappe, T., *see* Hoekstra, D., 950
 Kleemann, W., 353
 Klein, J., 599, 952
 Klein, J., *see* Luckham, P.F., 599, 800
 Klein, M.L., *see* Bareman, J.P., 208
 Klein, W., *see* Reynolds, P.J., 355
 Kleinert, H., 720
 Kleinert, H., *see* Janke, W., 600
 Kleinert, H., *see* Kiometzis, M., 641
 Kleinfeld, A., 838
 Kleinzeller, A., *see* Ziyadeh, F.N., 848
 Klom, J.P.G., *see* Dekker, C.J., 157
 Klösgen, B., 720
 Klösgen, B., *see* Hartung, J., 721
 Klösgen, B., *see* Helfrich, W., 459, 720
 Knauf, P.A., *see* Hallows, K.R., 848
 Knobler, C.M., *see* Bibo, A.M., 209

- Knobler, C.M., *see* Moore, B., 209
 Knoll, A.H., 93, 94
 Knoll, W., 302, 303, 304
 Knoll, W., *see* Hickel, W., 203
 Knoll, W., *see* Lösche, M., 203
 Knoll, W., *see* Mortensen, K., 299
 Knoll, W., *see* Motschmann, H., 205
 Knoll, W., *see* Pfeiffer, W., 355
 Knoll, W., *see* Reiter, H., 204
 Knoll, W., *see* Schmidt, G., 209
 Knudsen, K.A., *see* Wheelock, M.J., 845
 Knutton, S.K., 800
 Kobayashi, S., *see* Okimasu, E., 843
 Koch, G.L.E., *see* Flanagan, I., 799
 Kochan, J., *see* Mao, S.Y., 848
 Kochanova, N.A., *see* Bereznikova, A.V., 846
 Koechy, T., 300
 Koel, K.W., *see* Kaupp, U.B., 63
 Koethe, G., *see* Stohrer, T., 299
 Kohler, G., 949
 Kok, J.W., *see* Hoekstra, D., 899
 Kolinski, A., *see* Milik, M., 400
 Kolodney, M.S., 800
 Komissarchik, Y.Y., *see* Malev, V., 840
 Komura, S., 462
 König, H., *see* Kandler, O., 94
 König, S., 300, 397, 601
 Koo, E.W., *see* Linshaw, M.A., 848
 Kopito, R.R., 62
 Koppel, D.E., 204, 800
 Koppel, D.E., *see* Axelrod, D., 351
 Korb, J.P., *see* Keller, D.J., 208
 Korenstein, R., *see* Mittelman, L., 842
 Korn, E.D., 847
 Korn, E.D., *see* Baines, I.C., 847
 Korn, E.D., *see* Miyata, H., 847
 Kornberg, R.D., *see* Darst, S.A., 211
 Kornblatt, J.A., 687
 Kornyshev, A.A., 598, 689
 Kornyshev, A.A., *see* Cevc, G., 598
 Kornyshev, A.A., *see* Dzhavakhidze, P.G., 689
 Kornyshev, A.A., *see* Leikin, S., 689, 690
 Korobeinicheva, I.K., *see* Bichenkov, E.E., 954
 Korsgren, C., *see* Cohen, C.M., 842
 Korte, T., *see* Herrmann, A., 954
 Koshy, K.M., *see* Boggs, J.M., 151
 Kosterlitz, J.M., 207
 Koth, Chr., *see* Rettig, W., 209, 210
 Kourilsky, F.M., *see* LeBouteiller, P.P., 800
 Kovacs, G.J., *see* Popovic, Z.D., 210
 Koynova, R., 158
 Koynova, R., *see* Hinz, H.-J., 156
 Koynova, R., *see* Kuttenreich, H., 156
 Koynova, R.D., 151, 152
 Koynova, R.D., *see* Tenchov, B.G., 156
 Kozak, J.J., *see* McCarthy, J.E., 354
 Kozarac, Z., 210
 Kozlov, H.M., *see* Helfrich, W., 400
 Kozlov, M.M., 400, 689, 690, 720, 841, 901
 Kozlov, M.M., *see* Helfrich, W., 721
 Kozlov, M.M., *see* Leikin, S.L., 953
 Kozlov, M.M., *see* Lerche, D., 462, 841
 Kozlov, M.M., *see* Chernomordik, L.V., 956
 Kozuymi, S., *see* Taniguchi, N., 802
 Kraemer, P.H., 800
 Krajewski-Bertrand, M.-A., 95
 Kramarcy, N.R., 845
 Kramer, D., *see* Szleifer, I., 153, 299, 398, 489
 Krasny-Ergen, W., 897
 Kraus, M., 602
 Krbecsek, R., 299
 Kreer, M., 208
 Kreis, T.E., *see* Duden, R., 846
 Kremer, K., *see* Kreer, M., 208
 Kremer, K., *see* Lipowsky, R., 150
 Kriechbaum, M., *see* Laggner, P., 159, 901
 Kroll, D.M., *see* Gompfer, G., 459, 600, 601, 720
 Kroll, D.M., *see* Zia, R.K.P., 600
 Krop, B., *see* Ranck, J.L., 158
 Krpejsova, L., *see* Strunecka, A., 842
 Krstić, R.V., 490
 Krug, H., *see* Peterson, I.R., 207, 301
 Krumbiegel, M., 954
 Krumbiegel, M., *see* Arnold, K., 952, 957
 Kubalek, E.W., *see* Darst, S.A., 211
 Kucik, D.F., 353, 847
 Kuhl, T., 519
 Kuhn, H., 93
 Kuhn, S., *see* Traub, P., 846
 Kukan, B., *see* Evans, E.A., 798
 Kumada, T., *see* Banno, Y., 849
 Kumar, A., *see* Gudi, S.R., 842
 Kummrow, M., 300, 459, 720
 Kummrow, M., *see* Niggemann, G., 720
 Kunicki, T., *see* Okita, L., 841
 Kuno, S., *see* Mitsuya, H., 954
 Kuo, A.L., 353
 Kuo, S.C., *see* Edidin, M., 798
 Kuo, S.C., *see* Kucik, D.F., 847
 Kupfer, A., 800
 Kupfer, A., *see* Burn, P., 845
 Kuroda, K., *see* Takeuchi, K., 841
 Kurrle, A., 302, 399
 Kurzmeier, H., *see* Bärmann, M., 839
 Kuschel, F., *see* Brezesinski, G., 202
 Kusner, R., 461
 Kusner, R., *see* Hsu, L., 461

- Kussakov, M., *see* Derjaguin, B.V., 598
 Kuster, W.M., *see* Willardson, B.M., 840
 Kutner, R., *see* van Beijeren, H., 357
 Kутtenreich, H., 156
 Kутtenreich, H., *see* Hinz, H.-J., 156
 Kuzmin, P., *see* Zhelev, D.V., 898
 Kuzmin, P.I., 901
 Kwiatkowska, K., 842
 Kwiatkowski, D., *see* Gorlin, J., 845
 Kwiatkowski, D., *see* Hartwig, J., 839
 Kwiatkowski, D.J., *see* Cunningham, C.C., 840
 Kwok, R., 299, 687, 719
 Kwok, R., *see* Evans, E., 687
 Kyte, J., 94

 LaCelle, P.L., *see* Meiselman, H.J., 801
 Lackie, J.M., *see* Curtis, A.S.G., 797
 Lacorbère, M., *see* Schubert, D., 802
 Lafleur, M., 397
 Laggner, P., 155, 158, 159, 901
 Laggner, P., *see* Koynova, R.D., 152
 Laggner, P., *see* Kутtenreich, H., 156
 Laggner, P., *see* Lohner, K., 155
 Lake, J.A., 93
 Lake, J.A., *see* Rivera, M.C., 93
 Lalanne, J., *see* Bivas, I., 398, 459
 Laliberte, A., 843
 Lallane, J.L., *see* Bivas, I., 301
 Lamb, H., 353
 Lamb, J., *see* Janmey, P., 848
 Lamb, J., *see* Janmey, P.A., 839
 Lambert, M., *see* Doucet, J., 151
 Lamprecht, I., *see* Scheurich, P., 898
 Landau, L.D., 298, 462, 601
 Landauer, R., 353
 Lang, C.A., *see* Hörber, J.K.H., 207
 Langer, J.S., 303
 Langer, S.A., *see* Seifert, U., 460, 602
 Langer, T.S., 302
 Langevin, D., 205
 Langevin, D., *see* Meunier, J., 150, 641
 Langhans, T., 895
 Langlet, C., 800
 Langmuir, I., 641
 Langmuir, I.K., 202
 Langner, M., 690
 Langworthy, T.A., 94
 Larché, F., 641
 Laroche, G., 953
 Larsen, C.E., *see* Düzgünes, N., 950
 Larson, R.S., *see* Kishimoto, T.K., 753
 Larsson, K., 149
 Larsson, K., *see* Andersson, S., 150
 Larsson, K., *see* Gulik-Krzywicki, T., 150

 Larsson, K., *see* Hyde, S.T., 150
 Lasch, J., 490
 Lasch, J., *see* Wohlrab, W., 490
 Lash, J., *see* Holtzer, H., 895
 Lasic, D.D., 516, 517, 518
 Lasic, D.D., *see* Hamori, C.J., 517
 Lasic, D.D., *see* Huang, S.K., 518
 Lasic, D.D., *see* Kuhl, T., 519
 Lasic, D.D., *see* Mayhew, E.G., 518
 Lasic, D.D., *see* Needham, D., 518
 Lasic, D.D., *see* Papahadjopoulos, D., 518
 Lasic, D.D., *see* Vaage, J., 518
 Lasic, D.D., *see* Woodle, M.C., 517
 Lasky, L.A., *see* Foxall, C., 799
 Lässig, M., 600
 Lässig, M., *see* Hiergeist, C., 601
 Lassing, I., 848
 Laster, Y., *see* Beigel, M., 957
 Lauffenburger, D.A., *see* Cozens-Roberts, C., 753, 797
 Lauffenburger, D.A., *see* Hammer, D.A., 753, 799
 Lauffer, M.A., 354
 Lavergne, J., 353
 Lavergne, J., *see* Joliot, P., 353
 Law, B.A., 519
 Lawall, R., *see* Motschmann, H., 205
 Lawler, J., *see* Cohen, A.M., 840
 Lawrence, M.B., 800
 Lawrence, M.D., 753
 Laxhuber, L., *see* Helm, C.A., 204
 Laxhuber, L.A., *see* Kjaer, K., 205
 Lazarides, E., 62
 Lazarides, E., *see* Woods, C., 846
 Lazo, R., *see* Papahadjopoulos, D., 956
 Lazo, R.O., *see* Asch, H.L., 846
 Le Blanc, R.M., *see* Picard, G., 204
 LeBouteiller, P.P., 800
 Le Chrom, C., *see* Picard, G., 204
 Le Doussal, P., 601
 Le Sage, R., *see* Picard, G., 204
 LeNeveu, D.M., 489, 687, 688, 718, 753
 Lear, J.D., *see* Briggs, M.S., 210
 Leathes, J.B., 354
 Leblanc, R.M., *see* Antippa, A.F., 205
 Leblanc, R.M., *see* de B. Costa, S.M., 204
 Leblanc, R.M., *see* Ducharme, D., 205
 Leblanc, R.M., *see* Picard, G., 204
 Leckband, D., *see* Kuhl, T., 519
 Lee, A.G., 152, 153, 210, 303
 Lee, B.K., *see* Rau, D.C., 687
 Lee, G.M., 354
 Lee, S., 955
 Lee, S.B., 354

- Leermakers, F.A.M., 399, 400
 Leesnitzer, *see* Gupte, S.S., 353
 Leeuwen, J.M.J., *see* Ernst, M.H., 352
 Lehninger, A., 800
 Lehtonen, E., 841
 Lei, N., *see* Schmidt, C.F., 462
 Leibler, L., *see* Joanny, J.F., 599, 753
 Leibler, S., 300, 303, 461, 489, 599, 641, 642
 Leibler, S., *see* Anderson, D.M., 150
 Leibler, S., *see* Bensimon, D., 641
 Leibler, S., *see* David, F., 600
 Leibler, S., *see* Goldstein, R.E., 641, 690
 Leibler, S., *see* Lipowsky, R., 462, 596, 600, 718, 753
 Leibler, S., *see* Peliti, L., 597
 Leikin, S., 687, 689, 690
 Leikin, S., *see* Kozlov, M.M., 690
 Leikin, S.L., 953
 Leikin, S.L., *see* Kornyshev, A.A., 689
 Leiserowitz, L., *see* Böhm, C., 206
 Lekkerkerker, H.N.W., 400, 641
 Lemonnier, F.A., *see* LeBouteiller, P.P., 800
 Lenaz, G., 354
 Lennarz, W.J., *see* Rossignol, D.P., 896
 Lennon, J.F., *see* Brochard, F., 301, 460, 599
 Lenter, M., *see* Herrenknecht, K., 845
 Lentz, B.R., 954
 Lentz, B.R., *see* Burgess, S.W., 953, 954
 Lentz, B.R., *see* Parente, R.A., 950, 954
 Leonard, K., *see* Ward, R.J., 843
 Leonards, K., *see* Ohki, S., 950
 Lerche, D., 462, 841
 Letellier, L., *see* Ranck, J.L., 158
 Letierrier, J.-L., 839
 Letourneur, F., *see* Wegener, A.M.K., 803
 Leung, A., *see* Evans, E., 753, 843
 Leung, A., *see* Evans, E.A., 753, 798
 Leunissen-Bijvelt, L., *see* Verkleij, A.J., 955
 Levadny, V.G., *see* Belaya, M.L., 299
 Levadny, V.G., *see* Dzhavakhidze, P.G., 689
 Levadnyl, V.G., *see* Belaya, M.L., 598
 Levelut, A.M., *see* Clerc, M., 154
 Levelut, A.M., *see* Doucet, J., 151
 Lever, M.J., 155
 Levesque, D., 354
 Levin, A., *see* Husain, C.A., 840
 Levin, S., *see* Mittelman, L., 842
 Levine, Y.K., 800
 Levine, Y.K., *see* Franks, N.P., 150
 Lewallen, M., *see* Srinivasan, Y., 842
 Lewis, B.A., 400
 Lewis, G.N., 302
 Lewis, J., *see* Alberts, A., 93
 Lewis, J., *see* Alberts, B., 62, 457, 596, 849
 Lewis, R.N.A.H., 155, 158
 Lewis, R.N.A.H., *see* Balthasar, D.M., 209
 Lewis, R.N.A.H., *see* Mannock, D.A., 155, 158
 Lewis, R.N.A.H., *see* Rice, D.K., 209
 Lewis, R.N.A.H., *see* Sen, A., 156
 Lewis, T.J., *see* Bowen, P.J., 203
 Lewis, W.H., 895
 Lichtenbrg, D., *see* Amselem, S., 950
 Lichtenheld, M.G., *see* Podack, E.R., 801
 Lichtman, M.A., *see* Meiselman, H.J., 801
 Lidin, S., *see* Andersson, S., 150
 Liebesny, P., 897
 Liepinsh, E., *see* Otting, G., 687
 Lietzke, R., *see* Dieckhoff, J., 845
 Lifshitz, E.M., *see* Landau, L.D., 298, 462, 601
 Lifson, S., *see* Fuoss, R.M., 642
 Liggett, D., *see* Stribling, R., 519
 Lin, B., 209
 Lin, C., *see* Forscher, P., 848
 Lin, H., 155
 Lin, H., *see* Wang, Z., 155
 Lin, H., *see* Xu, H., 158
 Lin, M., *see* Dutta, P., 205
 Lin, S., *see* Wachstock, D.H., 844
 Lindberg, U., *see* Lassing, I., 848
 Lindberg, V., *see* Lassing, I., 848
 Lindblom, G., 94, 149, 157, 160, 354
 Lindblom, G., *see* Eriksson, P.-O., 152, 156
 Lindblom, G., *see* Gutman, H., 156
 Lindblom, G., *see* Nilsson, A., 156
 Lindblom, G., *see* Sjölund, M., 157
 Lindblom, G., *see* Wennerstrom, H., 357
 Lindblom, G., *see* Wieslander, Å., 160
 Lindman, B., *see* Wennerström, H., 397
 Linse, P., *see* Guldbrand, L., 208, 599, 688
 Linseisen, F.M., *see* Thewalt, J.L., 95
 Linshaw, M.A., 848
 Lipka, G., *see* Chowdry, B.Z., 158
 Lipowsky, R., 95, 150, 300, 303, 397, 458, 461, 462, 489, 516, 596, 598, 599, 600, 601, 602, 718, 719, 753, 900
 Lipowsky, R., *see* Ammann, A., 600
 Lipowsky, R., *see* Berndl, K., 301, 457, 516, 602, 721
 Lipowsky, R., *see* Cook-Röder, J., 601, 719
 Lipowsky, R., *see* Grotehans, S., 600
 Lipowsky, R., *see* Hiergeist, C., 601
 Lipowsky, R., *see* Jülicher, F., 458, 459, 489, 600
 Lipowsky, R., *see* Komura, S., 462
 Lipowsky, R., *see* Leibler, S., 599, 642
 Lipowsky, R., *see* Lässig, M., 600
 Lipowsky, R., *see* Netz, R.R., 596, 599, 601, 719
 Lipowsky, R., *see* Sackmann, E., 516

- Lipowsky, R., *see* Seifert, U., 300, 457, 458, 598, 721, 753
 Lipowsky, R., *see* Zia, R.K.P., 600
 Lipscomb, M.F., 800
 Lis, L.J., 597, 688, 800, 951
 Lis, L.J., *see* Ellens, H., 154, 956
 Lis, L.J., *see* Siegel, D.P., 157, 956
 Lis, W.T., *see* Lis, L.J., 597
 Litovitz, T.A., *see* Macedo, P.B., 354
 Litster, J.D., *see* Birgenau, R.J., 208
 Littlefield, J.W., 949
 Littman, D.R., *see* Norment, A.M., 801
 Liu, N.I., 155
 Liu, S.C., 62, 841
 Liu, S.C., *see* Cohen, A.M., 840
 Liu, Y., 846
 Livne, A., 842
 Livnek, E., 800
 Ljunggren, S., 153
 Linas, R., 949
 Lloyd, C.W., *see* Rees, D.A., 801
 Lo, S.-L., 94
 Locke, S.J., *see* Beckerle, M.C., 841
 Lodish, H., *see* Darnell, J., 62, 596
 Lodish, H.F., *see* Kopito, R.R., 62
 Löfgren, H., 205
 Lohner, K., 155, 157
 Lohner, K., *see* Lagner, P., 155, 158
 Lokersee, A.F., *see* Bakker-Woudenberg, I., 518
 Lokeshwar, V.B., *see* Bourguignon, L.Y., 842
 Longley, W., 150
 Longmire, K., *see* Frojmovic, M., 799
 Looney, D.J., *see* Mitsuya, H., 954
 Loosley-Millman, M.E., 490, 688
 Lopez, A., 898
 Lopez, M.C., *see* Iglesias, F.J., 898
 Lopez-Berestein, G., 517
 Lories, V., *see* David, G., 798
 Lösche, M., 202, 203, 208, 209
 Lösche, M., *see* Fischer, A., 209
 Lösche, M., *see* Heckl, W.M., 210
 Lösche, M., *see* Helm, C.A., 204
 Lösche, M., *see* Vaknin, D., 206
 Loth, H., 490
 Lottspeich, F., *see* Herrenknecht, K., 845
 Lourtie, I., *see* Melo, E.C.C., 354
 Louvard, D., *see* Garcia, A., 847
 Low, M., 845
 Low, P.S., *see* Willardson, B.M., 840
 Lowry, M.R., *see* Adam, C.G., 688
 Loyter, A., *see* Amselem, S., 950
 Loyter, A., *see* Beigel, M., 957
 Loyter, A., *see* Keren-Zur, M., 957
 Lubensky, T.C., *see* MacKintosh, F.C., 461
 Lubin, B., *see* Rybicki, A., 840
 Lücken, U., 720
 Luckham, P., *see* Afshar-Rad, T., 597
 Luckham, P.F., 599, 800
 Luckham, P.F., *see* Klein, J., 599, 952
 Lucy, J.A., 949, 955
 Lucy, J.A., *see* Blow, A.M.J., 954
 Lucy, J.A., *see* Song, L., 900
 Luisi, P.L., 152
 Luisi, P.L., *see* Scartazzini, R., 152
 Luke, J.C., 460
 Luna, E., *see* Shariff, A., 845
 Luna, E., *see* Wuestehube, L., 845
 Luna, E.J., 838
 Luna, M., *see* Lopez-Berestein, G., 517
 Lundberg, G., *see* Fogden, A., 153
 Lundmark, M., *see* Pascher, I., 151
 Lundquist, M., 209
 Lurquin, P., 518
 Luscher, M.A., *see* Christink, E.R., 797
 Luton, F., *see* Wegener, A.M.K., 803
 Lutton, E.S., 152
 Luzzati, V., 94, 149, 150, 152, 159, 687
 Luzzati, V., *see* Gulik, A., 94, 159
 Luzzati, V., *see* Gulik-Krzywicki, T., 688
 Luzzati, V., *see* Mariani, P., 150
 Luzzati, V., *see* Ranck, J.L., 151
 Luzzati, V., *see* Tardieu, A., 151, 152
 Luzzati, V., *see* Vargas, R., 151
 Lvov, Y.M., *see* Arnold, K., 952
 Lyle, I.G., *see* Carvell, M., 688
 Lyle, I.G., *see* Davies, R.J., 210
 Lyle, I.G., *see* Hammond, K., 490
 Ma, S.M., *see* Andrade, J.D., 796
 Mabrey, S., 156, 302, 354
 MacDonald, A.G., 155
 MacDonald, R.C., *see* MacDonald, R.I., 953
 MacDonald, R.I., 953, 954
 MacFarlane, S.A., *see* Qwarnstrom, E.E., 844
 MacIntosh, T.J., *see* Needham, D., 518
 MacKay, A., *see* Thewalt, J., 95
 MacKintosh, F.C., 461
 MacKintosh, F.C., *see* Safran, S.A., 461
 Macedo, P.B., 354
 Macha, J., *see* Strunecka, A., 842
 Machesky, L.M., *see* Goldschmidt, C.P., 849
 Machesky, L.M., *see* Goldschmidt-Clermont, P.J., 848
 Mackay, A.L., 150
 Madan, K.H., *see* Templer, R.H., 152
 Madeira, V.M.C., *see* Vaz, W.L.C., 357
 Mage, M., *see* Rothstein, T.L., 802
 Magee, A.I., 753, 845

- Magid, A.D., *see* McIntosh, T.J., 597, 688, 689, 953
- Magid, A.D., *see* Simon, S.A., 688, 689
- Magid, L., *see* Strey, R., 152
- Magid, L.J., *see* Schurtenberger, P., 152
- Magin, R.L., *see* Caffrey, M., 159
- Mahanta, J., 719
- Mahanty, J., 598, 640, 690, 753
- Mak, N., *see* Lewis, R.N.A.H., 158
- Makita, A., 800
- Maksymiw, R., 302, 303, 842
- Malev, V., 840
- Malhotra, V., *see* Melancon, P., 63
- Malissen, B., *see* André, P., 796
- Malissen, B., *see* Wegener, A.M.K., 803
- Malkina, A.D., *see* Derjaguin, B.V., 598
- Maltseva, T.V., *see* Budker, V.G., 957
- Malukutka, S., 299
- Manev, E., *see* Ivanov, I.B., 900
- Mangeat, P.H., 841
- Manischewitz, J., *see* Dimitrov, D.S., 899
- Mann, D.M., *see* Rutishauser, U., 802
- Mann, S., 93
- Mannherz, H.G., *see* Dieckhoff, J., 845
- Mannherz, H.G., *see* Stochaj, U., 845
- Mannock, D.A., 155, 158
- Mannock, D.A., *see* Lewis, R.N.A.H., 155
- Mannock, D.A., *see* Sen, A., 156
- Mannock, D.A., *see* Turner, D.C., 153
- Mantsch, H.H., 158, 298
- Mao, S.Y., 848
- Marcelja, S., 207, 299, 598, 640, 641, 688, 689
- Marcelja, S., *see* Gruen, D.W.R., 301, 598, 689
- Marcelja, S., *see* Kékicheff, P., 640
- Marcelja, S., *see* Kjellander, R., 208, 598, 599, 640, 641, 688, 689, 690
- Marcelja, S., *see* Langner, M., 690
- Marčelja, S., 354, 398, 399
- Marčelja, S., *see* Israelachvili, J.N., 153, 489
- Marchase, B., *see* McClay, D.R., 801
- Marchesi, V.T., *see* Anderson, R.A., 840
- Marchesi, V.T., *see* Speicher, D.W., 62
- Marcus, D., *see* Gillard, B., 846
- Margolis, L.B., 800
- Margulis, L., 94
- Mariani, P., 150
- Mariani, P., *see* Luzzati, V., 150
- Mariani, P., *see* Vargas, R., 151
- Marignan, J., *see* Bassereau, P., 719
- Marignan, J., *see* Larché, F., 641
- Marignan, J., *see* Porte, G., 152, 397, 602
- Markin, V.S., *see* Chernomordik, L.V., 956
- Markin, V.S., *see* Kozlov, M.M., 841, 901
- Markin, V.S., *see* Leikin, S.L., 953
- Markushin, Yu.Ya., *see* Budker, V.G., 957
- Marnett, L.J., *see* Chopra, H., 847
- Marques, C., *see* Harden, J.L., 642
- Marqusee, J.A., *see* Dill, K.A., 399
- Marra, J., 206, 207, 462, 597, 688
- Marra, J., *see* Horn, R.G., 207, 597, 688
- Marra, J., *see* Israelachvili, J., 688
- Marrink, S.-J., 601, 689
- Marsh, D., 151, 153, 155, 299, 303, 354, 596
- Marsh, D., *see* Cevc, G., 150, 206, 298, 351, 489, 596, 689, 690
- Marsh, D., *see* Heimburg, T., 156
- Marsh, D., *see* Sachse, J.H., 355
- Marsh, D., *see* Seddon, J.M., 150, 155, 205, 688
- Marsh, D., *see* Watts, A., 151
- Marsh, D.E., *see* Crawford, M.A., 95
- Martin, F., 518
- Martin, F., *see* Weiner, N., 490
- Martin, F.J., *see* Huang, S.K., 518
- Martin, F.J., *see* Lasic, D.D., 518
- Martin, F.J., *see* Martin, F., 518
- Martin, F.J., *see* Mayhew, E.G., 518
- Martin, F.J., *see* Northfelt, D.W., 518
- Martin, F.J., *see* Papahadjopoulos, D., 518
- Martin, F.J., *see* Vaage, J., 518
- Martin, F.J., *see* Woodle, M.C., 518
- Martin, M., *see* Dimitrov, D.S., 899
- Martin, M., *see* Sato, H., 899
- Martin, W.H., *see* Creutz, E.C., 954
- Martinez-Palomo, A., 800
- Martins, J.M., 354
- Maschke, W., *see* Watts, A., 151
- Mason, J.T., 158
- Mason, R., *see* Elder, M., 151, 206
- Massari, S., 956
- Massenburg, D., *see* Burgess, S.W., 954
- Massenburg, D., *see* Lentz, B.R., 954
- Mateo, P.L., *see* Mabrey, S., 302, 354
- Mathur, R., *see* Tahibi, A., 519
- Matsudaira, P., *see* Collins, K., 847
- Matsudaira, P., *see* Janmey, P., 848
- Matsumura, S., *see* Muguruma, M., 844
- Mattai, J., 155
- Mattai, J., *see* Goldfine, H., 160
- Mattai, J., *see* Kim, J.T., 155, 156
- Mattes, H.D., *see* Lösche, M., 208
- Matuoka, S., *see* Takahashi, H., 955
- Maturova, M., *see* Strunecka, A., 842
- Mauco, G., *see* Grondin, P., 849
- Max, J.-J., *see* Ducharme, D., 205
- Maxwell, J.C., 354
- May, R., *see* Porte, G., 602
- May, S., 400
- Mayer, C., *see* Stohrer, T., 299

- Mayhew, E., *see* Asch, H.L., 846
 Mayhew, E., *see* Huang, S.K., 518
 Mayhew, E., *see* Ohki, S., 949
 Mayhew, E., *see* Papahadjopoulos, D., 518
 Mayhew, E., *see* Vaage, J., 518
 Mayhew, E.G., 518
 Mayr, I., *see* Huber, R., 955
 Mayrovitz, H.N., 801
 McAlister, M., *see* Lis, L.J., 688, 951
 McCalden, T., 517
 McCarthy, J.E., 354
 McClay, D.R., 801
 McConnell, H.M., 208, 210
 McConnell, H.M., *see* Benvegna, D.J., 462
 McConnell, H.M., *see* Copeland, B.R., 352
 McConnell, H.M., *see* Devaux, P., 352
 McConnell, H.M., *see* Hafeman, D.G., 210
 McConnell, H.M., *see* Keller, D.J., 208
 McConnell, H.M., *see* Kleemann, W., 353
 McConnell, H.M., *see* Moy, V.T., 209
 McConnell, H.M., *see* Owicki, J.C., 299, 354, 355, 398
 McConnell, H.M., *see* Recktenwald, D.J., 355
 McConnell, H.M., *see* Rice, P.A., 210, 303
 McConnell, H.M., *see* Rubenstein, J.L.R., 355
 McConnell, H.M., *see* Seul, M., 204
 McConnell, H.M., *see* Shimshick, E.J., 302, 356
 McConnell, H.M., *see* Smith, B.A., 204
 McConnell, H.M., *see* Smith, L.M., 356
 McConnell, H.M., *see* Subramaniam, S., 203, 211
 McConnell, H.M., *see* Tamm, L.K., 211
 McConnell, H.M., *see* Weis, R.M., 204, 357
 McConnell, H.M., *see* Weiss, R.M., 203
 McConnell, H.M., *see* Wu, S., 302
 McConnell, H.M., *see* Wu, S.H.-W., 461
 McDermott, D.C., *see* Johnson, S.J., 598
 McElhaney, R.N., *see* Balthasar, D.M., 209
 McElhaney, R.N., *see* Lewis, R.N.A.H., 155, 158
 McElhaney, R.N., *see* Mannock, D.A., 155, 158
 McElhaney, R.N., *see* Mantsch, H.H., 298
 McElhaney, R.N., *see* Rice, D.K., 209
 McElhaney, R.N., *see* Sen, A., 156
 McElhaney, R.N., *see* Turner, D.C., 153
 McGrath, M., *see* Curtis, A.S.G., 797
 McGuiggan, P.M., *see* Chen, Y.L.E., 207
 McGuiggan, P.M., *see* Helm, C.A., 207, 719, 951, 952
 McGuiggan, P.M., *see* Pashley, R.M., 689, 951
 McHugh, L.L., *see* Rothstein, T.L., 802
 McIlroy, P.M., *see* Cantor, R.S., 207
 McIntosh, J., *see* Simon, S.A., 688
 McIntosh, T.J., 597, 688, 689, 953
 McIntosh, T.J., *see* Blaurock, A.E., 151
 McIntosh, T.J., *see* Burgess, S.W., 953
 McIntosh, T.J., *see* Lasic, D.D., 517
 McIntosh, T.J., *see* Longley, W., 150
 McIntosh, T.J., *see* Needham, D., 461, 518
 McIntosh, T.J., *see* Simon, S.A., 688, 689
 McIntosh, T.J., *see* Wilkinson, D.A., 158
 McIntyre, G.F., *see* Lentz, B.R., 954
 McIntyre, T.M., *see* Zimmerman, G.A., 803
 McIver, D.J.L., *see* Schürch, S., 802
 McKeever, P.E., 801
 McKeown-Longo, P.J., 801
 McKintosh, F.C., *see* Harden, J.L., 303
 McLaughlin, *see* Mosior, M., 955
 McLaughlin, S., 203, 301, 838
 McLaughlin, S., *see* Eisenberg, M., 688
 McLaughlin, S.G.L., 641, 690
 McLaughlin, S.G.L., *see* Langner, M., 690
 McLaughlin, T., *see* Joshi, R., 840
 McLonnanaghey, M.D., *see* Peterson, N.O., 300
 Mcalister, M., *see* Lis, L.J., 800
 Meadows, R., *see* Templer, R.H., 154
 Mealy, T., *see* Meers, P., 955
 Meers, P., 954, 955
 Meers, P.R., *see* Hong, K., 955
 Meers, P.R., *see* Tank, D., 356
 Mège, J.L., 801
 Mège, J.L., *see* Bongrand, P., 797
 Mège, J.L., *see* Foa, C., 799
 Mehra, T., *see* Allen, T.M., 518
 Mehrishi, J.N., 801
 Mehrle, W., 896
 Mehrle, W., *see* Zimmermann, U., 895
 Mehta, K.R., *see* Lopez-Berestein, G., 517
 Meier, W., *see* Lerche, D., 462, 841
 Meinhart, M., *see* Janke, W., 600
 Meiselman, H.J., 801
 Melancon, P., 63
 Melard, P., *see* Faucon, J.F., 398
 Meleard, P., 459, 460
 Méléard, P., *see* Faucon, J.F., 459, 720
 Méléard, Ph., *see* Angelova, M.I., 720
 Melikyan, G.B., *see* Chernomordik, L.V., 899, 956
 Meller, P., *see* Blankenburg, R., 210
 Meller, P.H., *see* Darst, S.A., 211
 Melo, E.C.C., 354
 Melo, E.C.C., *see* Bultmann, T., 351
 Melo, E.C.C., *see* Martins, J.M., 354
 Melo, E.C.C., *see* Vaz, W.L.C., 357
 Menetret, J.F., *see* Ward, R.J., 843
 Merkel, R., 63, 300
 Metcalfe, M., *see* Evans, E., 688, 718
 Metcalfe, M., *see* Evans, E.A., 798
 Metzger, H., *see* Mao, S.Y., 848

- Meunier, J., 150, 641
 Meunier, J., *see* Daillant, J., 206
 Meunier, J., *see* Henon, S., 204
 Meyer, D., *see* Baumgartner, H.R., 796
 Meyer, H.W., 159
 Meyer, R., 844
 Meyer, R., *see* Hinz, H.-J., 156
 Meyer, R.K., 844
 Meyer, R.K., *see* Burn, P., 844
 Mezei, M., 490
 Mezei, M., *see* Foldvari, M., 490
 Mezei, M., *see* Gesztes, A., 490
 Miao, L., 457, 459, 721
 Miao, L., *see* Fourcade, B., 460
 Miao, L., *see* Seifert, U., 300, 458
 Miao, L., *see* Wortis, M., 458
 Michalet, X., 458, 461
 Michayluk, M.R., *see* Kao, K.N., 895
 Michel, H., *see* Deisenhofer, J., 94
 Michl, J., 801
 Mickey, B., *see* Gittes, F., 839
 Middleton, S.R., 203
 Mikkelsen, A., *see* Elgsaeter, A., 841
 Mikkelsen, A., *see* Stokke, B.T., 463
 Miklavic, S.J., *see* Granfeldt, M.K., 690
 Milik, M., 400
 Miller, A., 202, 203
 Miller, A., *see* Knoll, W., 304
 Miller, D.E., *see* Beckerle, M.C., 841
 Miller, K.W., *see* Lever, M.J., 155
 Miller, V.M., *see* Derjaguin, B.V., 690
 Mills, J.W., *see* Ziyadeh, F.N., 848
 Milner, S., 301
 Milner, S.T., 401, 460, 601, 719
 Milon, A., *see* Krajewski-Bertrand, M.-A., 95
 Milstein, C., *see* Kohler, G., 949
 Milton, G.W., 354
 Mingins, J., *see* Seddon, J.M., 152
 Minton, A.P., 354
 Mintzer, R.A., *see* Weaver, J.C., 897
 Mische, S., 840
 Mischel, M., *see* Scheurich, P., 898
 Mishal, Z., *see* LeBouteiller, P.P., 800
 Mitchell, D.J., 400, 641
 Mitchell, D.J., *see* Atiard, P., 599
 Mitchell, D.J., *see* Attard, P., 640, 690
 Mitchell, D.J., *see* Fogden, A., 641
 Mitchell, D.J., *see* Israelachvili, J.N., 397
 Mitchell, M.L., 206
 Mitchell, M.L., *see* Hunt, R.D., 206
 Mitchison, J.M., 688
 Mitchison, T., *see* Theriot, J., 848
 Mitov, M.D., *see* Derzhanski, A., 897
 Mitov, M.D., *see* Faucon, J.F., 398, 459, 720
 Mitov, M.D., *see* Meleard, P., 459, 460
 Mitov, M.D., *see* Petrov, A.G., 300
 Mitsuya, H., 954
 Mittelman, L., 842
 Mittler-Neher, S., *see* Knoll, W., 304
 Miyamoto, H., 840
 Miyata, H., 847
 Möbius, D., *see* Hönig, D., 204
 Möbius, D., *see* Kinnunen, P.K.J., 205
 Möbius, D., *see* Kozarac, Z., 210
 Möbius, D., *see* Vogel, V., 203
 Moeremans, M., *see* Geerts, H., 352
 Mohandas, N., *see* Evans, E., 753, 843
 Möhwald, H., 209
 Möhwald, H., *see* Als-Nielsen, J., 206
 Möhwald, H., *see* Brezesinski, G., 209
 Möhwald, H., *see* Böhm, C., 206
 Möhwald, H., *see* Dietrich, A., 209
 Möhwald, H., *see* Fischer, A., 209
 Möhwald, H., *see* Flörsheimer, M., 205, 209
 Möhwald, H., *see* Haas, H., 204, 210
 Möhwald, H., *see* Heckl, W.M., 204, 210
 Möhwald, H., *see* Heithier, H., 204
 Möhwald, H., *see* Helm, C.A., 204, 205
 Möhwald, H., *see* Hörber, J.K.H., 207
 Möhwald, H., *see* Kenn, R.M., 209
 Möhwald, H., *see* Kirstein, S., 204
 Möhwald, H., *see* Kjaer, K., 205
 Möhwald, H., *see* Lösche, M., 202, 203, 208, 209
 Möhwald, H., *see* Miller, A., 202, 203
 Möhwald, H., *see* Peschke, J., 210, 399
 Möhwald, H., *see* Riegler, J., 303
 Möhwald, H., *see* Steitz, R., 207
 Möhwald, H., *see* Vanderlick, K.T., 208
 Molish, I., *see* Daniel, J., 839
 Molitoris, B.A., 843
 Mollenhauer, J., *see* Stochaj, U., 845
 Mombers, C., *see* Verkleij, A.J., 955
 Montagne, J.B., *see* Schulman, J.H., 641
 Montes, J.G., *see* Wu, Y., 898
 Montgomery, R., *see* Okita, L., 841
 Montroll, E.W., 354
 Moon, R.T., *see* Edelstein, N.G., 848
 Moore, B., 209
 Mooseker, M., 838
 Mooseker, M., *see* Garcia, A., 847
 Mooseker, M.S., 847
 Mooseker, M.S., *see* Cheney, R.E., 847
 Mooseker, M.S., *see* Mische, S., 840
 Moreau, H., *see* Ransac, S., 211
 Morgan, A., 949
 Morgan, J., 93
 Morgan, J.R., *see* Williams, B.D., 517

- Morowitz, H.J., 93
 Morris, E.R., *see* Arnott, S., 796
 Morris, J.S., 950
 Morris, S.J., 899
 Morris, S.J., *see* Sarkar, D.P., 901
 Morrison, I.E.G., *see* Anderson, C.M., 351
 Morrow, J., *see* Mooseker, M., 838
 Morrow, J.S., *see* Cianci, C.D., 840
 Morrow, J.S., *see* Fox, J.E., 841
 Morrow, J.S., *see* Mische, S., 840
 Mortensen, K., 299
 Moscona, A., *see* Ben Shaul, Y., 796
 Mosher, D.F., 801
 Mosher, D.F., *see* McKeown-Longo, P.J., 801
 Mosior, M., 955
 Motschmann, H., 205
 Motschmann, H., *see* Reiter, H., 204
 Mountcastle, D.B., *see* Estep, T.N., 352
 Mouritsen, O., *see* Bloom, M., 298, 517, 838
 Mouritsen, O.G., 94, 207, 299, 303, 398, 399
 Mouritsen, O.G., *see* Bloom, M., 93, 95, 401, 461, 753
 Mouritsen, O.G., *see* Ipsen, J.H., 95, 210, 303, 353, 397
 Mouritsen, O.G., *see* Sperotto, M.M., 356, 399
 Moy, V.T., 209
 Moy, V.T., *see* Keller, D.J., 208
 Moy, V.T., *see* McConnell, H.M., 208
 Moynihan, D., *see* Caffrey, M., 153
 Mueller, S.C., 843
 Muguruma, M., 844
 Mukherjee, P., *see* Boni, L.T., 952
 Mulakutla, S., 158
 Müller, K., *see* Laggner, P., 155, 158
 Müller, K., *see* Lohner, K., 155
 Müller, O., 839
 Muller, P., 209
 Muller, V.M., *see* Derjaguin, B.V., 599, 798, 950
 Müller, W., *see* Herron, J.N., 205
 Müller-Krumbhaar, H., *see* Jülicher, F., 600
 Müller-Landau, F., *see* Cadenhead, D.A., 202
 Mullins, W.W., *see* Gruber, E.E., 599
 Munger, G., *see* Picard, G., 204
 Murakami, S., 160
 Murata, Y., *see* Shigematsu, M., 951
 Murray, B., *see* Cunningham, B.A., 753
 Murthy, A.K., *see* Kaler, E.W., 461
 Mustard, J., *see* Vickers, J., 843
 Mustard, J.F., *see* Livne, A., 842
 Muthy, A.K., *see* Kaler, E.W., 461
 Mutz, M., 300, 459, 461, 596, 597, 719
 Mutz, M., *see* Fourcade, B., 458
 Myers, J., *see* Ryan, T.A., 802
 Myers, M.C., *see* Warner, R.R., 490
 Nagafuchi, A., *see* Funayama, N., 845
 Nagano, M., *see* Murakami, S., 160
 Nagayama, K., *see* Hibino, M., 896
 Nagayama, K., *see* Kinoshita, K.Jr., 896
 Naghizadeh, J., *see* Dill, K.A., 399
 Nagle, J.F., 209, 302, 354
 Nagle, J.F., *see* Wilkinson, D.A., 158
 Nagle, J.F., *see* Wilkinson, D.A.W., 302
 Nagle, J.F., *see* Yang, C.P., 158
 Nairn, A., *see* Hartwig, J., 845
 Nairn, A.C., *see* Thelen, M., 845
 Nakamura, T., *see* Senda, M., 895
 Nakamura, T., *see* Takeuchi, K., 841
 Nakashima, T., *see* Banno, Y., 849
 Nakatani, Y., *see* Krajewski-Bertrand, M.-A., 95
 Nallet, F., 641
 Nallet, F., *see* Strey, R., 152
 Nanba, I., *see* Taniguchi, N., 802
 Naor, A., 400
 Napper, D.H., 801, 952
 Naqvi, K.R., 354
 Nassander, U.K., 517
 Nayar, R., *see* Cullis, P.R., 159
 Nayaran, O., 153
 Nayeem, A., 354
 Needham, D., 95, 301, 461, 518, 897
 Needham, D., *see* Elliott, J.R., 399
 Needham, D., *see* Evans, E., 299, 459, 597, 599, 687, 688, 718, 753
 Needham, D., *see* Evans, E.A., 687, 952
 Needham, D., *see* Hochmuth, R.M., 848
 Needham, D., *see* Lasic, D.D., 518
 Needham, D., *see* McIntosh, T.J., 688
 Needham, D., *see* Rand, R.P., 688
 Needham, D., *see* Simon, S.A., 689
 Needham, D., *see* Tran-Son-Tay, R., 803
 Neher, E., 949, 956
 Neher, E., *see* Chow, R.H., 949
 Neher, E., *see* Heinemann, S.H., 302
 Neher, E., *see* Penner, R., 949
 Nehring, J., 302
 Neil, G.A., *see* Langlet, C., 800
 Nelson, D., 301, 462
 Nelson, D., *see* Abraham, F., 841
 Nelson, D., *see* Frey, E., 301
 Nelson, D.R., 300, 462, 601
 Nelson, D.R., *see* Halperin, B.I., 208
 Nelson, K.K., *see* Chopra, H., 847
 Nelson, W.J., 842
 Nemetz, A., *see* Reiter, H., 204
 Neng-Bo He, *see* Hui, S.W., 207
 Nettleton, J., *see* Gittes, F., 839
 Netz, R.R., 596, 599, 601, 719

- Neumann, A.W., 801
 Neumann, A.W., *see* Absolom, D.R., 796
 Neumann, E., 895, 896
 Neumann, E., *see* Sugar, I.P., 897, 901
 Neumann, R.D., *see* Hård, S., 205
 Neumann, R.D., *see* Löfgren, H., 205
 Neupert, W., *see* Pfaller, R., 63
 New, R.R.C., 517
 Newman, M.S., *see* Woodle, M.C., 518
 Newman, P., *see* Okita, L., 841
 Newton, C., *see* Papahadjopoulos, D., 956
 Newton, C., *see* Portis, A., 688, 951
 Nezil, F.A., 94, 397, 460
 Nicholls, P., *see* Rand, R.P., 687
 Nichols, B.W., *see* Oldani, D., 203
 Nichols, P.D., *see* Jahnke, L.L., 95
 Nicholson, G.L., *see* Singer, S.J., 356
 Nicklas, K., *see* Schlenkrich, M., 208
 Nicolau, C., 518
 Nicolson, G.L., *see* Poste, G., 949
 Niederberger, W., *see* Seelig, J., 397
 Nieuwenhuizen, T.M., *see* Lipowsky, R., 600
 Nieva, J.-L., *see* Burger, K.N.J., 160
 Niggemann, G., 720
 Niggemeyer, B., *see* Dieckhoff, J., 845
 Niggli, V., 844
 Nilsson, A., 156
 Ninham, B.W., 640
 Ninham, B.W., *see* Atiardi, P., 599
 Ninham, B.W., *see* Attard, P., 640, 690
 Ninham, B.W., *see* Barois, P., 151
 Ninham, B.W., *see* Fogden, A., 641
 Ninham, B.W., *see* Hyde, S.T., 153
 Ninham, B.W., *see* Israelachvili, J.N., 397
 Ninham, B.W., *see* Mahanta, J., 719
 Ninham, B.W., *see* Mahanty, J., 598, 690, 753
 Ninham, B.W., *see* Mahatny, J., 640
 Ninham, B.W., *see* Mitchell, D.J., 400, 641
 Ninham, B.W., *see* Pashley, R.M., 689, 951
 Nir, A., *see* Hiram, Y., 949
 Nir, S., 950
 Nir, S., *see* Amselem, S., 950
 Nir, S., *see* Bentz, J., 950
 Nir, S., *see* Düzgünes, N., 950
 Nir, S., *see* Meers, P., 955
 Nir, S., *see* Papahadjopoulos, D., 900, 956
 Nir, S., *see* Wilschut, J., 950
 Nishida, T., *see* Kim, Y.C., 954
 Nishizuka, Y., 160
 Nissen, H.-U., 159
 Nitsche, J.C.C., *see* Anderson, D.M., 151
 Noack, H., *see* Johnson, S.I., 304
 Noack, H., *see* Johnson, S.J., 841
 Noack, H., *see* Johnson, S.K., 62
 Nobori, K., *see* Okimasu, E., 843
 Nolte, D.D., 354
 Nonomura, Y., *see* Banno, Y., 849
 Noordam, P.C., 157
 Noppl, D., *see* Döbereiner, H.-G., 303, 458
 Norgauer, J., *see* Eberle, M., 849
 Norment, A.M., 801
 Northfelt, D.W., 518
 Northrop, J.P., *see* Felgner, P., 518
 Noyes, R.M., 354
 Nozawa, Y., *see* Banno, Y., 849
 Nuckolls, G., *see* Burrige, K., 843
 Nuckolls, G.H., 844
 Nuhn, P., 209
 Nunn, R.S., *see* Needham, D., 95, 301
 Nuydens, R., *see* Geerts, H., 352
 Nuydens, R., *see* de Bradander, M., 352
 Nyholm, P.-G., *see* Pascher, I., 151

 O'Brien, M.P., *see* Prestegard, J.H., 160
 O'Gara, C.Y., *see* Chopra, H., 847
 O'Konski, C.T., 897
 O'Leary, T.J., 354
 Odell, G., *see* Peskin, C., 840
 Odermatt, E., *see* Engel, J., 798
 Odijk, T., 600, 641
 Ohki, K., *see* Takahashi, H., 955
 Ohki, S., 209, 899, 949, 950, 951, 953, 954
 Ohki, S., *see* Arnold, K., 952, 954, 955, 957
 Ohki, S., *see* Düzgünes, N., 956
 Ohki, S., *see* van Oss, C.J., 952
 Ohki, S., *see* Zschörnig, O., 957
 Ohnesorge, F., *see* Weisenhorn, A.L., 207
 Ohnishi, S., 950, 957
 Ohnishi, S., *see* Yamazaki, M., 952
 Ohno-Shosaku, T., 900
 Ohshima, H., *see* Ohki, S., 950
 Ohta, M., *see* French, S.W., 847
 Ohta, Y., 845
 Oishi, O., *see* Lee, S., 955
 Okada, Y., 895
 Okada, Y., *see* Ohno-Shosaku, T., 900
 Okimasu, E., 843
 Okita, L., 841
 Oldani, D., 203
 Oliver, J.M., *see* Seagrave, J., 848
 Olmsted, J., 839
 Olsen, E., *see* Detmers, P.A., 798
 Olsson, U., *see* Strey, R., 152
 Omann, G.M., *see* Traynor, K.A., 849
 Oosawa, F., 599
 Oosawa, F., *see* Asakura, S., 952
 Op den Kamp, J.A.F., 62, 302, 354
 Opatz, K., *see* Neumann, E., 895

- Orci, L., *see* Melancon, P., 63
 Ordonez, G., *see* Lehtonen, E., 841
 Orendi, H., *see* Reiter, H., 204
 Orger, B.H., *see* de B. Costa, S.M., 204
 Ornstein, J., *see* Sato, H., 899
 Ortiz, A., 160
 Oster, G., *see* Janmey, P., 839
 Oster, G., *see* Peskin, C., 840
 Osumi, M., *see* Murakami, S., 160
 Otey, C., *see* Burrige, K., 843
 Otey, C.A., 843
 Otey, C.A., *see* Pavalko, F.M., 843, 845
 Otlewski, J., *see* Habazettl, J., 304
 Otting, G., 687
 Otto, E., *see* Joshi, R., 840
 Otto, J., *see* Drenckhahn, D., 844
 Otto, J.J., 844
 Ou-Yang, Z.-C., 460, 461
 Ourisson, G., 95
 Ourisson, G., *see* Krajewski-Bertrand, M.-A., 95
 Ourisson, G., *see* Rohmer, M., 95
 Overbeek, J.Th.G., *see* Verwey, E.J.W., 599, 640, 690, 753, 950
 Owaribe, K., *see* Schwartz, M., 847
 Owicki, J.C., 299, 354, 355, 398
 Owicki, J.C., *see* Abney, J.R., 299, 350, 351, 398
 Ozawa, M., 845
 Ozawa, M., *see* Herrenknecht, K., 845
- Packham, M.A., *see* Livne, A., 842
 Packman, C.H., *see* Hallows, K.R., 848
 Padaso de Lima, M.C., *see* Düzgünes, N., 950
 Pagano, R.E., *see* Struck, D.K., 950
 Page, R.C., *see* Qwarnstrom, E.E., 844
 Pailthorpe, B.A., *see* Hughes, B.D., 353
 Paintrand, M., *see* Bornens, M., 842
 Palade, G., 949
 Palecek, J., *see* Strunecka, A., 842
 Paleckova, A., *see* Strunecka, A., 842
 Palek, J., 841
 Palek, J., *see* Cohen, A.M., 840
 Palek, J., *see* Liu, S.-C., 62
 Palek, J., *see* Liu, S.C., 841
 Pallas, N.R., 202
 Paltauf, F., 203
 Panaiotov, I., 900
 Panaiotov, I., *see* Dimitrov, D.S., 900
 Panaiotov, I.I., 210
 Pangborn, W., *see* Portis, A., 688, 951
 Pansu, B., *see* Dubois-Violette, E., 149
 Papahadjopoulos, D., 516, 518, 900, 950, 953, 956, 957
 Papahadjopoulos, D., *see* Allen, T.M., 953
 Papahadjopoulos, D., *see* Düzgünes, N., 950, 953, 956
 Papahadjopoulos, D., *see* Fraley, R.T., 518
 Papahadjopoulos, D., *see* Gabizon, A., 517
 Papahadjopoulos, D., *see* Hong, K., 953, 955
 Papahadjopoulos, D., *see* Huang, S.K., 518
 Papahadjopoulos, D., *see* Lasic, D.D., 518
 Papahadjopoulos, D., *see* Meers, P., 954, 955
 Papahadjopoulos, D., *see* Portis, A., 688, 951
 Papahadjopoulos, D., *see* Sundler, R., 957
 Papahadjopoulos, D., *see* Wilschut, J., 950, 951
 Paques, E.-P., *see* Huber, R., 955
 Parce, J.W., *see* Smith, L.M., 356
 Pardi, R., 801
 Parente, R.A., 950, 954
 Parham, P., *see* Norment, A.M., 801
 Parker, D., *see* Boden, N., 154
 Parks, D.J., *see* Lentz, B.R., 954
 Parsegian, A., *see* Gruner, A., 298
 Parsegian, A., *see* Rand, R.P., 719
 Parsegian, V.A., 597, 598, 640, 641, 687, 688, 689, 690, 753, 951
 Parsegian, V.A., *see* Colombo, M.F., 687
 Parsegian, V.A., *see* Cowley, A.C., 597, 641, 688
 Parsegian, V.A., *see* Evans, E., 688, 753
 Parsegian, V.A., *see* Evans, E.A., 600, 642, 798, 955
 Parsegian, V.A., *see* Gawrisch, K., 689, 953
 Parsegian, V.A., *see* Gruner, S.M., 689
 Parsegian, V.A., *see* Horn, R.G., 207, 597, 688
 Parsegian, V.A., *see* Keller, S.L., 687
 Parsegian, V.A., *see* Leikin, S., 687, 690
 Parsegian, V.A., *see* LeNeveu, D.M., 489, 687, 688, 718, 753
 Parsegian, V.A., *see* Lis, L.J., 597, 688, 800, 951
 Parsegian, V.A., *see* Loosley-Millman, M.E., 490, 688
 Parsegian, V.A., *see* Ninham, B.W., 640
 Parsegian, V.A., *see* Podgornik, R., 600, 642, 689
 Parsegian, V.A., *see* Prouty, M.S., 687
 Parsegian, V.A., *see* Rand, P., 951
 Parsegian, V.A., *see* Rand, R.P., 153, 156, 157, 207, 462, 489, 597, 687, 688, 689, 951, 953
 Parsegian, V.A., *see* Rau, D.C., 687
 Parsegian, V.A., *see* Sackmann, E., 516
 Parsegian, V.A., *see* Tsao, Y.-H., 688
 Parsegian, V.A., *see* Zimmerberg, J., 687
 Parsons, D.F., *see* Hui, S.W., 207
 Pascher, I., 151, 206
 Pascher, I., *see* Hauser, H., 151, 203
 Pascher, I., *see* Pearson, R.H., 151
 Pashley, R., *see* Israelachvili, J., 800
 Pashley, R.M., 689, 951
 Pashley, R.M., *see* Deamer, D.W., 93
 Pashley, R.M., *see* Ducker, W.A., 687

- Pashley, R.M., *see* Israelachvili, J.N., 689
 Pastan, I., *see* Schlessinger, J., 802
 Pastan, I., *see* Willingham, M.C., 803
 Pasternak, C., 801
 Pasternak, C.A., *see* Knutton, S.K., 800
 Pastor, R.W., 400
 Pastushenko, V.F., *see* Abidor, I.G., 896
 Pastushenko, V.F., *see* Kuzmin, P.I., 901
 Paton, W.D.M., *see* Lever, M.J., 155
 Patterson, L.K., *see* Bohorques, M., 204
 Patton, E., *see* Dadabay, C.Y., 849
 Patton, J.S., 160
 Patton, J.S., *see* Rigler, M.W., 160
 Pattus, F., *see* Vainio, P., 211
 Pattus, F., *see* Ward, R.J., 843
 Paudler, M., 205
 Paudler, M., *see* Herron, J.N., 205
 Pavalko, F., *see* Burrige, K., 843
 Pavalko, F.M., 843, 845
 Pavalko, F.M., *see* Otey, C.A., 843
 Pavalko, F.M., *see* Turner, C.E., 844
 Pavlotsky, N., *see* Meers, P., 955
 Pawson, D.L., *see* Donnay, G., 159
 Payrastre, B., 849
 Pearson, I.H., *see* Hauser, H., 151
 Pearson, R.H., 151
 Pearson, R.H., *see* Hauser, H., 203
 Pebay-Peyroula, E., *see* Seddon, J.M., 152
 Peetermans, J., *see* Janmey, P.A., 839
 Pelcovits, R.A., *see* Grinstein, G., 602
 Peliti, L., 597
 Peliti, L., *see* Nelson, D.R., 300, 462, 601
 Penfold, I., *see* Johnson, S.I., 304
 Penfold, J., *see* Bayerl, T., 299
 Penfold, J., *see* Bayerl, T.M., 206
 Penfold, J., *see* Grundy, M., 206
 Penfold, J., *see* Johnson, S.J., 841
 Penfold, J., *see* Johnson, S.K., 62
 Penfold, J., *see* Schurtenberger, P., 152
 Peng, J.B., *see* Dutta, P., 205
 Penner, R., 949
 Pequeux, A., *see* Zimmermann, U., 897
 Perez, E., *see* Wolfe, J., 951
 Perides, G., *see* Traub, P., 846
 Perkins, W.D., *see* Unanue, E.R., 803
 Perlmann, P., *see* Ruangjirachuporn, W., 842
 Perly, B., *see* Tabony, J., 356
 Pernot, P., *see* Ranck, J.L., 158
 Perrin, J., 355
 Peschke, J., 210, 399
 Pesci, A.I., *see* Duplantier, B., 641
 Pesci, A.I., *see* Goldstein, R.E., 640
 Peskin, C., 840
 Peters, R., 203, 355
 Peters, R., *see* Beck, K., 204
 Peters, W., *see* New, R.R.C., 517
 Petersen, N.O., 801
 Peterson, I.R., 207, 208, 301
 Peterson, I.R., *see* Bibo, A.M., 209
 Peterson, I.R., *see* Kenn, R.M., 209
 Peterson, I.R., *see* Steitz, R., 207
 Peterson, M.A., 301, 460
 Peterson, N.O., 300
 Pethica, B.A., *see* Middleton, S.R., 203
 Pethica, B.A., *see* Pallas, N.R., 202
 Petrov, A.G., 300, 303, 397, 489
 Petrov, A.G., *see* Derzhanski, A., 897
 Petsche, I.B., 601
 Petsche, I.B., *see* Schmidt, C.F., 462
 Pézolet, M., *see* Laroche, G., 953
 Pfaller, R., 63
 Pfanner, N., *see* Pfaller, R., 63
 Pfeiffer, J.R., *see* Seagrave, J., 848
 Pfeiffer, W., 355
 Pfeiffer, W., *see* Knoll, W., 304
 Pfeiffer, W., *see* Koenig, S., 300
 Pfeiffer, W., *see* König, S., 397, 601
 Pfeiffer, W., *see* Mortensen, K., 299
 Phillips, D.R., *see* Fox, J.E., 841
 Phillips, M.C., *see* Cadenhead, D.A., 203
 Phillips, M.C., *see* Cullen, J., 160
 Phillips, M.C., *see* Oldani, D., 203
 Phillips, M.C., *see* Paltauf, F., 203
 Piard, J.C., *see* Alkhalaf, W., 519
 Picard, G., 204
 Picker, L.J., 801
 Pidard, D., *see* Okita, L., 841
 Pieczonka, M.M., *see* Michl, J., 801
 Piepenstock, M., *see* Vaknin, D., 206
 Pierres, A., *see* Kaplanski, G., 803
 Pierres, A., *see* Tissot, O., 803
 Pierres, M., *see* Bongrand, P., 797
 Piersbacher, M.D., 801
 Pierschbacher, M.D., *see* Ruoslahti, E., 752
 Pieters, J., *see* Dekker, C.J., 157
 Pike, L.J., *see* Dadabay, C.Y., 849
 Pilwat, G., *see* Zimmermann, U., 896, 897
 Pinaev, G.P., *see* Kwiatkowska, K., 842
 Pincus, P., 600, 641
 Pincus, P., *see* Brainsma, R., 301
 Pincus, P., *see* Dan, N., 399
 Pincus, P., *see* de Gennes, P.-G., 601, 690
 Pincus, P., *see* Safran, S.A., 461, 720
 Pincus, P.A., *see* Safinya, C.R., 641
 Pincus, P.A., *see* Safran, S.A., 461
 Pinder, J.C., *see* Kahana, E., 840
 Pink, D., *see* Caille, A., 202
 Pink, D.A., 355, 399

- Pink, D.A., *see* Georgallas, A., 202
 Pinkall, U., *see* Karcher, H., 461
 Pinto da Silva, P., 159
 Planas, M.E., *see* Gonzalez, P., 490
 Plantavid, M., *see* Grondin, P., 849
 Plantavid, M., *see* Payrastré, B., 849
 Podack, E.R., 801
 Podgornik, R., 600, 642, 689, 690
 Podgornik, R., *see* Cevc, G., 689
 Podgornik, R., *see* Käs, J., 460
 Poëis, L.G., *see* Nassander, U.K., 517
 Pohl, H.A., 895
 Pokrovskii, V.L., 599
 Policova, Z., *see* Absolom, D.R., 796
 Pollard, T.D., 847
 Pollard, T.D., *see* Adams, R.J., 847
 Pollard, T.D., *see* Goldschmidt, C.P., 849
 Pollard, T.D., *see* Goldschmidt-Clermont, P.J., 848
 Pollard, T.D., *see* Sato, M., 839
 Pollard, T.D., *see* Zot, H.G., 847
 Pomeau, Y., 355
 Pontecorvo, G., 895, 949
 Popescu, M.C., *see* Svenson, C.E., 517
 Popielawski, J., 208
 Popov, K.M., *see* Bereznikova, A.V., 846
 Popovic, Z.D., 210
 Popp, D., *see* Holmes, K., 838
 Poppe, P.A., *see* Nassander, U.K., 517
 Porte, G., 152, 397, 602
 Porte, G., *see* Bassereau, P., 719
 Porte, G., *see* Larché, F., 641
 Porter, G., *see* de B. Costa, S.M., 204
 Porter, N.A., *see* McIntosh, T.J., 688
 Portis, A., 688, 951
 Portis, A.R., *see* Nir, S., 950
 Portnoy, D., *see* Theriot, J., 848
 Poste, G., 949
 Poste, G., *see* Papahadjopoulos, D., 953, 956, 957
 Powell, K.T., *see* Weaver, J.C., 896
 Pradhan, D., 842
 Prakash, M., *see* Dutta, P., 205
 Prat, A.G., *see* Cantiello, H.F., 848
 Pratsch, L., 952
 Pratsch, L., *see* Arnold, K., 952, 953, 954
 Prediger, E.A., *see* Cunningham, B.A., 753
 Prescott, S.M., *see* Zimmerman, G.A., 803
 Prestegard, J.H., 160
 Prevratil, J., *see* Lentz, B.R., 954
 Pribac, F., *see* Horn, R.G., 799
 Price, Z., *see* Grimm, E., 799
 Prokhorov, A.V., *see* Derjaguin, B.V., 900
 Prost, J., 150
 Prost, J., *see* Nallet, F., 641
 Prouty, M.S., 687
 Pryme, I.F., *see* Vedeler, A., 845
 Prywes, R., *see* Livnek, E., 800
 Puddington, L., *see* Scullion, B.F., 802
 Pumir, A., *see* Bensimon, D., 641
 Purcell, E.M., 93
 Purcell, E.M., *see* Berg, H.C., 93
 Puvvada, S., *see* Naor, A., 400
 Pyrak-Nolte, L.J., *see* Nolte, D.D., 354

 Qian, H., 355, 848
 Qian, H., *see* Sheetz, M.P., 848
 Quate, C.F., *see* Binnig, G., 207
 Quate, C.F., *see* Smith, D.P.E., 207
 Quest, A.F., 846
 Quian, H., *see* Sheetz, M.P., 356
 Quinn, J.A., *see* Cozens-Roberts, C., 753, 797
 Quinn, P.J., *see* Dawson, R.M.C., 157
 Quinn, P.J., *see* Ellens, H., 154, 956
 Quinn, P.J., *see* Koynova, R.D., 152
 Quinn, P.J., *see* Siegel, D.P., 157, 956
 Quinones, R., *see* Shaw, S., 802
 Qvarnstrom, E.E., 844

 Rabe, J., *see* Lösche, M., 203
 Rabe, J.P., *see* Smith, D.P.E., 207
 Radic, N., *see* Marcelja, S., 598, 689
 Radiman, S., 151
 Rädler, J., 301, 458, 459, 597, 598
 Radmacher, M., 690
 Radoev, B.P., 900
 Radoev, B.P., *see* Ivanov, I.B., 900, 901
 Radzihovsky, L., *see* Le Doussal, P., 601
 Raff, M., *see* Alberts, A., 93
 Raff, M., *see* Alberts, B., 62, 457, 596, 849
 Ragan, M.A., 94
 Raghavan, K., 689
 Raghavan, K., *see* Berkowitz, M.L., 689
 Rahilly, M.A., 843
 Ramachandran, C., *see* Weiner, N., 490
 Ramau, B., *see* Sundari, C.S., 953
 Ran, D.C., *see* Leikin, S., 690
 Ranavavare, S.B., *see* Nayeem, A., 354
 Ranck, J.L., 151, 158
 Raçon, Y., 154
 Rand, P., 951
 Rand, P., *see* Gawrisch, K., 953
 Rand, P., *see* Gruner, A., 298
 Rand, R., *see* Parsegian, V.A., 690
 Rand, R.D., *see* Lis, L.J., 800
 Rand, R.P., 153, 156, 157, 160, 207, 462, 489, 597, 687, 688, 689, 719, 951, 953, 955
 Rand, R.P., *see* Bech, J., 689

- Rand, R.P., *see* Coorssen, J.R., 689
 Rand, R.P., *see* Cowley, A.C., 597, 641, 688
 Rand, R.P., *see* Das, S., 157, 689
 Rand, R.P., *see* Gawrisch, K., 689, 953
 Rand, R.P., *see* Gruner, S.M., 689
 Rand, R.P., *see* Horn, R.G., 207, 597, 688
 Rand, R.P., *see* Kachar, B., 688, 955
 Rand, R.P., *see* Kozlov, M.M., 690
 Rand, R.P., *see* LeNeveu, D.M., 489, 678, 688, 718, 753
 Rand, R.P., *see* Leikin, S., 690
 Rand, R.P., *see* Lis, L.J., 597, 688, 951
 Rand, R.P., *see* Loosley-Millman, M.E., 490, 688
 Rand, R.P., *see* Parsegian, V.A., 597, 598, 640, 687, 688, 690, 753, 951
 Rand, R.P., *see* Tsao, Y.-H., 688
 Randal, M., *see* Lewis, G.N., 302
 Rando, R.R., *see* Alecio, M.R., 351
 Rangaraj, G., *see* Boggs, J.M., 151
 Rankin, A., *see* Carr, I., 797
 Ransac, S., 211
 Rao, M., *see* Boal, D.H., 462
 Rao, M., *see* Fourcade, B., 460
 Rao, M., *see* Miao, L., 457, 721
 Rao, M., *see* Wortis, M., 458
 Rasenick, M.M., *see* Wang, N., 846
 Rasing, Th., 205
 Rassow, J., *see* Pfaller, R., 63
 Ratnovsky, S.E., *see* Bierer, B.E., 796
 Rau, D.C., 687
 Rau, D.C., *see* Colombo, M.F., 687
 Rau, D.C., *see* Leikin, S., 687
 Rau, D.C., *see* Parsegian, V.A., 687
 Rau, D.C., *see* Podgornik, R., 689
 Rau, D.C., *see* Rand, R.P., 156, 688, 951
 Raudino, A., 952
 Rauscher, A., *see* Hofmann, S., 641
 Rawicz, B., *see* Evans, E., 721
 Rawicz, W., *see* Evans, E., 301, 459
 Rawicz, W., *see* Evans, E.A., 690
 Rawiso, M., *see* Kékicheff, P., 154
 Rayner, M.D., 687
 Recktenwald, D.J., 355
 Reddi, M.R., *see* Raghavan, K., 689
 Redemann, C., *see* Papahadjopoulos, D., 518
 Reed, R.A., 158
 Rees, A., *see* Arnott, S., 796
 Rees, D.A., 801
 Rees, D.A., *see* Woods, A., 803
 Reese, C.E., *see* Zwolinsky, B.J., 489
 Reese, T.S., *see* Chang, D.C., 901
 Reese, T.S., *see* Heuser, J.E., 899
 Reese, T.S., *see* Kachar, B., 95, 159
 Reese, T.S., *see* Rand, R.P., 688
 Reichert, A., *see* Grainger, D.W., 211, 302
 Reima, I., *see* Lehtonen, E., 841
 Reimer, D., *see* Stohrer, T., 299
 Reindl, H., 302
 Reinl, H., 303
 Reiter, H., 204
 Reiter, R., *see* Motschmann, H., 205
 Reman, F.C., *see* Tardieu, A., 151
 Renner, M., *see* Hinz, H.-J., 156
 Rennie, A., *see* Bayerl, T.M., 206
 Rennie, A., *see* Johnson, S.I., 304
 Rennie, A., *see* Johnson, S.K., 62
 Rennie, A.R., *see* Johnson, S.J., 598, 841
 Rennschuh, H., *see* Helfrich, W., 153
 Retter, U., *see* Vollhardt, D., 209
 Rettig, W., 209, 210
 Rettig, W., *see* Brezesinski, G., 202
 Rettig, W., *see* Dietrich, A., 209
 Reynolds, C.C., *see* Fox, J.E., 841
 Reynolds, P.J., 355
 Rhee, S.G., *see* Goldschmidt, C.P., 849
 Riaz, M., *see* Weiner, N., 490
 Ribl, H.O., *see* Darst, S.A., 211
 Riccio, T., *see* Eisenberg, M., 688
 Rice, D.K., 209
 Rice, P.A., 210, 303
 Rice, S.A., 208
 Rice, S.A., *see* Harris, J., 208
 Rice, S.A., *see* Popielawski, J., 208
 Richardson, R.M., *see* Grundy, M., 206
 Richmond, P., *see* Dimitrov, D.S., 900
 Richter, D., *see* Ewen, B., 206
 Richter, D., *see* König, S., 300, 397, 601
 Richter, D., *see* Lipowsky, R., 150
 Richter, W., *see* Juergens, E., 299
 Richter, W., *see* Meyer, H.W., 159
 Richter, W., *see* Zschörnig, O., 957
 Rieber, P., *see* Kurlle, A., 302, 399
 Riegler, H., *see* Herron, J.N., 205
 Riegler, H., *see* Paudler, M., 205
 Riegler, J., 303
 Riegler, J., *see* Peschke, J., 399
 Rienmann, F., *see* Zimmermann, U., 896
 Rietveld, A., *see* Cullis, P.R., 159
 Rietveld, A., *see* de Kruijff, B., 159
 Rigler, M.W., 160
 Rilfors, L., *see* Eriksson, P.-O., 152
 Rilfors, L., *see* Lindblom, G., 94, 149, 157
 Rilfors, L., *see* Sjölund, M., 157
 Rilfors, L., *see* Wieslander, Å., 160
 Ringertz, N.R., 895
 Ringold, G., *see* Felgner, P., 518
 Ringsdorf, H., *see* Bader, H., 601
 Ringsdorf, H., *see* Blankenburg, R., 210

- Ringsdorf, H., *see* Darst, S.A., 211
 Ringsdorf, H., *see* Grainger, D.W., 211, 302
 Ringsdorf, H., *see* Herron, J.N., 205
 Ringsdorf, H., *see* Sackmann, E., 298, 601
 Rittenhouse, S.E., 849
 Rivas, E., *see* Luzzati, V., 150
 Rivera, J., *see* Mao, S.Y., 848
 Rivera, M.C., 93
 Rivière, C., *see* Ransac, S., 211
 Robbin, R., 802
 Robbins, M.O., *see* Safran, S.A., 208
 Roberts, A.D., *see* Johnson, K.L., 800
 Roberts, K., *see* Alberts, A., 93
 Roberts, K., *see* Alberts, B., 62, 457, 596, 849
 Robinson, D.M., *see* Jamieson, G.A., 62
 Robkin, L., *see* Daniel, J., 839
 Rodriguez, B.E., *see* Kaler, E.W., 461
 Rodriguez, L., *see* Gonzalez, P., 490
 Roecker, C., *see* Fromherz, P., 298
 Roerdink, F.H., *see* Storm, G., 517
 Roetzer, H., *see* Knoll, W., 304
 Rohmer, M., 95
 Rohmer, M., *see* Ourisson, G., 95
 Roizman, B., *see* Hoggan, M.D., 895
 Rollinghoff, M., *see* Wagner, H., 803
 Rols, M.P., 900
 Rols, M.P., *see* Blangero, C., 899
 Rols, M.P., *see* Lopez, A., 898
 Rols, M.P., *see* Teissie, I., 898
 Roman, R., *see* Felgner, P., 518
 Romero-Rochin, V., *see* Duplantier, B., 641
 Romero-Rochin, V., *see* Goldstein, R.E., 640
 Römisch, J., *see* Huber, R., 955
 Rondelez, F., *see* Moore, B., 209
 Rondelez, F., *see* Prost, J., 150
 Rosa, L., *see* Strunecka, A., 842
 Rose, J.K., 519
 Rose, J.K., *see* Scullion, B.F., 802
 Rose, J.K., *see* Zhang, F., 803
 Rosen, A., *see* Hartwig, J., 845
 Rosen, A., *see* Thelen, M., 845
 Rosenberg, A., *see* Schanus, E., 840
 Rosenberg, J., 957
 Rosenheck, K., *see* Neumann, E., 896
 Roser, S.J., *see* Grundy, M., 206
 Rossignol, D.P., 896
 Roth, M., *see* Hendriks, Y., 154
 Rothman, J., *see* Melancon, P., 63
 Rothschild, K.J., *see* Gruner, S.M., 154
 Rothstein, T.L., 802
 Rotman, A., *see* Burn, P., 844
 Rougé, F., *see* André, P., 796
 Roux, D., 602, 641, 689
 Roux, D., *see* Cates, M.E., 152
 Roux, D., *see* Milner, S.T., 601, 719
 Roux, D., *see* Nallet, F., 641
 Roux, D., *see* Safinya, C.R., 151, 398, 689, 719
 Roux, D., *see* Strey, R., 152
 Roux, D., *see* Szleifer, I., 398, 489
 Roy, S., *see* Ohki, S., 950
 Ruangjirachuporn, W., 842
 Ruben, P.C., *see* Rayner, M.D., 687
 Rubenstein, J.L.R., 355
 Rubenstein, J.L.R., *see* Smith, L.M., 356
 Rucha, B.U., *see* Lösche, M., 203
 Ruckenstein, E., *see* Schiby, D., 689
 Rucknagel, D.C., *see* Schnitzer, B., 63
 Rueppel, D., 301
 Rueppel, D., *see* Fromherz, P., 298, 489
 Rueppel, D., *see* Sackmann, E., 299
 Ruff, P., 840
 Ruhnau, K., 844
 Rulyov, N.N., *see* Dukhin, S.S., 900
 Ruocco, M.J., 158
 Ruoslahti, E., *see* Piersbacher, M.D., 801
 Ruoslahti, E., 752
 Rupert, L.A.M., 953
 Russell, J., *see* Northfelt, D.W., 518
 Ruston, D., *see* Gawrisch, K., 689, 953
 Rutherford, J., *see* Carr, I., 797
 Ruths, J., *see* Paudler, M., 205
 Rutishauser, U., 802
 Ryan, T.A., 802
 Ryba, N.J.P., *see* Heimburg, T., 156
 Rybicki, A., 840
 Ryter, A., *see* Capo, C., 753, 797
 Sachse, J.H., 355
 Sackmann, E., 63, 94, 298, 299, 301, 401, 457, 458, 516, 601, 838, 900
 Sackmann, E., *see* Albrecht, O., 202, 203, 299, 303
 Sackmann, E., *see* Bayerl, T., 299, 300
 Sackmann, E., *see* Bayerl, T.M., 206
 Sackmann, E., *see* Berndl, K., 301, 457, 516, 602, 721
 Sackmann, E., *see* Bärmann, M., 839
 Sackmann, E., *see* Duwe, H.P., 300, 398, 459, 597
 Sackmann, E., *see* Duwe, H.T., 489
 Sackmann, E., *see* Duwe, M.P., 398
 Sackmann, E., *see* Döbereiner, H.-G., 303, 458
 Sackmann, E., *see* Engelhardt, H., 300, 398, 459, 462
 Sackmann, E., *see* Evans, E., 352
 Sackmann, E., *see* Fischer, A., 205, 207, 209, 301

- Sackmann, E., *see* Galla, H.-J., 204, 300, 301, 352
- Sackmann, E., *see* Gebhardt, C., 299, 461, 641
- Sackmann, E., *see* Heise, H., 303, 844
- Sackmann, E., *see* Johnson, S.I., 304
- Sackmann, E., *see* Johnson, S.J., 598, 841
- Sackmann, E., *see* Johnson, S.K., 62
- Sackmann, E., *see* Juergens, E., 299
- Sackmann, E., *see* Kaes, J., 301, 517
- Sackmann, E., *see* Kas, J., 839
- Sackmann, E., *see* Kaufmann, S., 304, 844
- Sackmann, E., *see* Knoll, W., 302, 303, 304
- Sackmann, E., *see* Koenig, S., 300
- Sackmann, E., *see* Krbecek, R., 299
- Sackmann, E., *see* Kurrle, A., 302, 399
- Sackmann, E., *see* Käs, J., 458, 460, 721
- Sackmann, E., *see* König, S., 397, 601
- Sackmann, E., *see* Lösche, M., 203
- Sackmann, E., *see* Maksymiw, R., 302, 303, 842
- Sackmann, E., *see* Merkel, R., 63, 300
- Sackmann, E., *see* Mortensen, K., 299
- Sackmann, E., *see* Müller, O., 839
- Sackmann, E., *see* Peterson, M.A., 301, 460
- Sackmann, E., *see* Pfeiffer, W., 355
- Sackmann, E., *see* Rueppel, D., 301
- Sackmann, E., *see* Rädler, J., 301, 458, 597, 598
- Sackmann, E., *see* Schmidt, C.F., 839
- Sackmann, E., *see* Sen-fang, Sui, 303
- Sackmann, E., *see* Träuble, H., 302, 356
- Sackmann, E., *see* Vaz, W.L.C., 357
- Sackmann, E., *see* Xue You Han, 302
- Sackmann, E., *see* Zeman, K., 301, 841
- Sackmann, E., *see* Zilker, A., 62, 301, 458
- Sadoc, J.F., 150, 160
- Sadoc, J.F., *see* Charvolin, J., 150, 152
- Sadoc, J.F., *see* Clerc, M., 154
- Saffman, P.G., 355
- Safinya, C.R., 151, 398, 641, 689, 719
- Safinya, C.R., *see* Roux, D., 602, 641, 689
- Safinya, C.R., *see* Schmidt, C.F., 462
- Safinya, C.R., *see* Smith, G.S., 206
- Safran, S.A., 208, 461, 720
- Safran, S.A., *see* Dan, N., 399
- Safran, S.A., *see* Milner, S., 301
- Safran, S.A., *see* Milner, S.T., 460
- Safran, S.A., *see* Safinya, C.R., 641
- Safran, S.A., *see* Szleifer, I., 153, 299, 398
- Safran, S.A., *see* Wang, Z.-G., 400
- Saita, N., *see* Kinoshita, K.Jr., 896
- Sakamoto, S., *see* Yonezawa, F., 357
- Sakman, B., 949
- Sakurai, J.D., *see* Tahibi, A., 519
- Sale, A.J.H., 895
- Salesse, C., *see* Blankenburg, R., 210
- Salesse, C., *see* Ducharme, D., 205
- Salesse, C., *see* Grainger, D.W., 211, 302
- Salsbury, N.J., 953
- Salter, D.M., *see* Rahilly, M.A., 843
- Salter, R.D., *see* Norment, A.M., 801
- Sammon, M.J., *see* Seul, M., 210
- Samraoui, B., *see* Bjorkman, P., 797
- Samuels, M., 845
- Sanchez, S., *see* Gonzalez, P., 490
- Sandermann, H., *see* Schumaker, G., 689
- Sanders, M.E., *see* Shaw, S., 802
- Sandhof, E., *see* Fürst, W., 63, 298
- Sankaram, M.B., 303, 355
- Sankaram, M.B., *see* Melo, E.C.C., 354
- Sankaram, M.B., *see* Thompson, T.E., 356
- Sano, M., *see* Kawaguchi, M., 205
- Santamaria, C., *see* Iglesias, F.J., 898
- Saper, M., *see* Bjorkman, P., 797
- Sarkar, D.P., 901
- Sarkar, D.P., *see* Morris, S.J., 899
- Sasson, J.P., *see* Rittenhouse, S.E., 849
- Sastry, V.S.S., *see* Nayeem, A., 354
- Sato, H., 899
- Sato, M., 839
- Sato, N., *see* Funayama, N., 845
- Saunders, J.A., *see* Chang, D.C., 895
- Saupe, A., *see* Nehring, J., 302
- Savage, R.E., *see* Ringertz, N.R., 895
- Savchenko, E.V., *see* Bichenkov, E.E., 954
- Sawyer, W.H., *see* Hughes, B.D., 353
- Saxman, K., *see* Dembo, M., 753, 798
- Saxton, M.J., 355
- Scalettar, B.A., 356
- Scalettar, B.A., *see* Abney, J.R., 351
- Scartazzini, R., 152
- Schackenraad, J.M., 802
- Schaefer, M., *see* Heller, H., 400
- Schaefer-Ridder, M., *see* Neumann, E., 896
- Schaffer, B.E., *see* Papahadjopoulos, D., 953
- Schanus, E., 840
- Schatz, G., 949
- Schechter, A.N., *see* Prouty, M.S., 687
- Schechter, E., *see* Ranck, J.L., 158
- Scheer, H., *see* Heckl, W.M., 210
- Scheludko, A., 900
- Scheludko, A., *see* Ivanov, I.B., 900
- Scherbarth, A., *see* Traub, P., 846
- Scheringer, M., 208
- Scherphof, G., *see* Hoekstra, D., 957
- Scheurich, P., 898
- Scheurich, P., *see* Zimmermann, U., 895
- Scheutjens, J.M.H.M., *see* Leermakers, F.A.M., 399, 400
- Schiavo, G., *see* Massari, S., 956

- Schiby, D., 689
 Schindler, M., *see* Koppel, D.E., 800
 Schlegel, R.A., *see* Pradhan, D., 842
 Schleicher, M., *see* Habazettl, J., 304
 Schlenkrich, M., 208
 Schlessinger, J., 802
 Schlessinger, J., *see* Axelrod, D., 351
 Schlessinger, J., *see* Koppel, D.E., 204
 Schlessinger, J., *see* Livnek, E., 800
 Schliwa, M., 838
 Schliwa, M., *see* Janmey, P.A., 839
 Schlossbauer, G., *see* Pfeiffer, W., 355
 Schlottmann, P., *see* Burkhardt, T.W., 601, 719
 Schmalzer, E.A., *see* Chien, S., 797
 Schmid-Schönbein, G.W., 802
 Schmid-Schönbein, G.W., *see* Chien, S., 797
 Schmid-Schönbein, G.W., *see* Dong, C., 798
 Schmid-Schönbein, G.W., *see* Sung, K.L.P., 802
 Schmidt, C., 843
 Schmidt, C., *see* Bayerl, T., 300
 Schmidt, C., *see* Svoboda, K., 841
 Schmidt, C.F., 462, 839
 Schmidt, C.F., *see* Svoboda, K., 462
 Schmidt, F., *see* Bayerl, T., 300
 Schmidt, G., 209
 Schmidt, G., *see* Knoll, W., 302, 303, 304
 Schmitt-Verhulst, A.M., *see* André, P., 796
 Schnapp, B.J., *see* Gelles, J., 352
 Schneider, M., *see* Huber, R., 955
 Schneider, M.B., 356, 459
 Schneider, M.D., 301
 Schnitzer, B., 63
 Schoch, C., *see* Guy, H.R., 956
 Schoellmann, G., *see* Vaz, W.L.C., 357
 Schoen, A.H., 150
 Schollmeier, M., *see* Sackmann, E., 298, 601
 Scholma, J., *see* Wilschut, J., 950
 Schomäcker, R., *see* Strey, R., 152
 Schroeder, A., 302
 Schroer, T.A., 847
 Schroit, A.J., *see* Connor, J., 842
 Schuber, F., *see* Hong, K., 953
 Schubert, D., 802
 Schulman, J.H., 641
 Schulten, K., *see* Heller, H., 400
 Schulz, J., *see* Zimmermann, U., 896
 Schumaker, G., 689
 Schürch, S., 802
 Schurman, B.L., *see* Biswas, A., 400
 Schurtenberger, P., 152
 Schuster, A., *see* Laggner, P., 155
 Schuster, A., *see* Lohner, K., 155
 Schwab, B., *see* Cortese, J.D., 839
 Schwab, B., *see* Downey, G.P., 848
 Schwan, H.P., 896, 897
 Schwan, H.P., *see* Takashima, S., 898
 Schwartz, E., *see* Elias, H., 798
 Schwartz, M., 847
 Schwartz, M., *see* Tranter, M., 843
 Schwartz, R., *see* Rybicki, A., 840
 Schwartz, W.H., *see* Sato, M., 839
 Schwister, K., *see* Deuticke, B., 896
 Scott, H.L., 303, 399
 Scott, H.L., *see* Nagle, J.F., 302
 Scriven, L.E., 150
 Scriven, L.E., *see* Anderson, D.M., 151
 Scriven, L.E., *see* Löfgren, H., 205
 Scullion, B.F., 802
 Seagrave, J., 848
 Sealock, R., *see* Kramarcy, N.R., 845
 Seddon, J., *see* Luzzati, V., 150
 Seddon, J.M., 149, 150, 152, 153, 155, 205, 688
 Seddon, J.M., *see* Cevc, G., 152
 Seddon, J.M., *see* Marsh, D., 151
 Seddon, J.M., *see* Templer, R.H., 152, 154
 Seed, B., *see* Bevilacqua, M.P., 796
 Seelig, A., *see* Seelig, J., 397
 Seelig, A.S.J., *see* Buldt, G., 206
 Seelig, J., 397
 Seelig, J., *see* Bueldt, G., 299
 Segrest, J.P., *see* Srinivas, S.K., 949
 Seifert, U., 300, 457, 458, 460, 461, 462, 489, 598, 602, 721, 753
 Seifert, U., *see* Berndl, K., 301, 457, 516, 602, 721
 Seifert, U., *see* Boal, D.H., 463
 Seifert, U., *see* Jülicher, F., 458, 460
 Seifert, U., *see* Kraus, M., 602
 Seifert, U., *see* Lipowsky, R., 462, 598, 719, 753
 Seifert, U., *see* Miao, L., 459, 721
 Seifert, U., *see* Wortis, M., 458
 Seitz, R., *see* Peterson, I.R., 301
 Selden, S.C., *see* Sato, M., 839
 Seleznev, S.A., *see* Petrov, A.G., 303
 Selig, J., 300
 Sellers, J., *see* Collins, K., 847
 Semenza, G., *see* Harter, C., 956
 Sen, A., 156
 Sen, A., *see* Mannoek, D.A., 158
 Sen-fang, Sui, 303
 Sen-fang, Sui, *see* Sackmann, E., 401
 Senda, M., 895
 Senden, T.J., *see* Ducker, W.A., 687
 Senden, T.J., *see* Kékicheff, P., 640
 Senfang Sui, *see* Maksymiw, R., 302
 Serafini, T., *see* Melancon, P., 63
 Serpersu, E.H., 896
 Servuss, R.-M., 462, 598

- Servuss, R.-M., *see* Beblík, G., 398
 Servuss, R.-M., *see* Helfrich, W., 301, 459, 599
 Servuss, R.M., 719, 720
 Servuss, R.M., *see* Beblík, G., 720
 Servuss, R.M., *see* Helfrich, W., 641, 719
 Servuss, R.M., *see* Mutz, M., 719
 Seul, M., 204, 210, 687
 Seul, M., *see* Hirshfeld, C.L., 210, 303
 Seul, M., *see* Subramaniam, S., 211
 Severin, E.S., *see* Bereznikova, A.V., 846
 Severin, F.F., 846
 Shapere, A., 93
 Shapiro, B.M., *see* Quest, A.F., 846
 Shariff, A., 845
 Sharma, D., *see* Picard, G., 204
 Shavnin, S.A., *see* Düzgünes, N., 950
 Shaw, S., 802
 Sheetz, *see* Kucik, D.F., 353
 Sheetz, M.P., 356, 458, 848
 Sheetz, M.P., *see* Edidin, M., 798
 Sheetz, M.P., *see* Gelles, J., 352
 Sheetz, M.P., *see* Koppel, D.E., 800
 Sheetz, M.P., *see* Kucik, D.F., 847
 Sheetz, M.P., *see* Qian, H., 355, 848
 Sheetz, M.P., *see* Schroer, T.A., 847
 Shen, B.W., 62
 Shen, Y.R., *see* Rasing, Th., 205
 Sher, L.D., *see* Schwan, H.P., 897
 Sherman, L.A., *see* Langlet, C., 800
 Shigematsu, M., 951
 Shigemori, M., *see* Hibino, M., 896
 Shigemori, M., *see* Kinoshita, K., 896
 Shih, M.C., *see* Lin, B., 209
 Shimojo, H., *see* Makita, A., 800
 Shimomura, M., *see* Kirstein, S., 204
 Shimshick, E.J., 302, 356
 Shin, Y.-K., 356
 Shipley, G.G., 149
 Shipley, G.G., *see* Cullen, J., 160
 Shipley, G.G., *see* Elder, M., 151, 206
 Shipley, G.G., *see* Goldfine, H., 160
 Shipley, G.G., *see* Haas, N.S., 156
 Shipley, G.G., *see* Janiak, M.J., 156, 205, 641
 Shipley, G.G., *see* Kim, J.T., 155, 156
 Shipley, G.G., *see* Malukutka, S., 299
 Shipley, G.G., *see* Mattai, J., 155
 Shipley, G.G., *see* Mulakutla, S., 158
 Shipley, G.G., *see* Reed, R.A., 158
 Shipley, G.G., *see* Ruocco, M.J., 158
 Shipman, C., *see* Weiner, N., 490
 Shoham, M., *see* Steitz, T.A., 687
 Shubin, V.E., 641
 Shubin, V.E., *see* Kékicheff, P., 640
 Shuster, J., *see* Tha, S.P., 802
 Shyamsunder, E., 155, 159
 Shyamsunder, E., *see* Tate, M.W., 149, 159, 901
 Sidorov, V.N., *see* Budker, V.G., 957
 Siegel, D.P., 153, 154, 157, 159, 602, 900, 955, 956
 Siegel, D.P., *see* Ellens, H., 154, 956
 Siemiarezuk, A., *see* Picard, G., 204
 Sigl, L., *see* Cevc, G., 462, 598
 Silver, B.C., *see* Gad, A.E., 955
 Silver, R.B., *see* Llinas, R., 949
 Silverstein, S.C., *see* Michl, J., 801
 Silvius, J.R., 153, 955
 Silvius, J.R., *see* Gardam, M., 352
 Simon, K., *see* Burridge, K., 843
 Simon, K.O., *see* Pavalko, F.M., 843
 Simon, S.A., 688, 689
 Simon, S.A., *see* McIntosh, T.J., 597, 688, 689, 953
 Simpson, D.J., 159
 Sinesky, M., 160
 Singer, M.A., *see* Finegold, L., 158
 Singer, S.J., 356
 Singer, S.J., *see* Burn, P., 845
 Singer, S.J., *see* Kupfer, A., 800
 Singer, S.J., *see* Sheetz, M.P., 458
 Sinha, S.K., *see* Safinya, C.R., 151, 689, 719
 Sinsheimer, R.L., *see* Weisenhorn, A.L., 207
 Sirota, E.B., 641
 Sirota, E.B., *see* Safinya, C.R., 398
 Sirota, E.B., *see* Smith, G.S., 206
 Sisk, R.B., *see* Bultmann, T., 351
 Sjodin, R.A., *see* Wu, Y., 898
 Sjölund, M., 157
 Sjölund, M., *see* Lindblom, G., 157, 160
 Skalak, R., 753
 Skalak, R., *see* Chien, S., 797
 Skalak, R., *see* Dong, C., 798
 Skalak, R., *see* Evans, E., 753
 Skalak, R., *see* Evans, E.A., 397, 687, 799
 Skalak, R., *see* Schmid-Schönbein, G.W., 802
 Skalak, R., *see* Sung, K.L.P., 802
 Sklar, L.A., *see* Eberle, M., 849
 Sklar, L.A., *see* Traynor, K.A., 849
 Skolnik, J., *see* Milik, M., 400
 Slater, G., 356
 Sleckman, B.P., *see* Bierer, B.E., 796
 Small, D.M., 149
 Small, D.M., *see* Janiak, M.J., 156, 205, 641
 Smith, B.A., 204
 Smith, B.A., *see* Rubenstein, J.L.R., 355
 Smith, B.A., *see* Smith, L.M., 356
 Smith, C.G., *see* Woods, A., 803
 Smith, D.P.E., 207
 Smith, E.B., *see* Lever, M.J., 155

- Smith, E.E., *see* Golstein, P., 799
 Smith, G.S., 206
 Smith, G.S., *see* Safinya, C.R., 151, 398, 689, 719
 Smith, K.S., *see* Kahana, E., 840
 Smith, L.M., 356
 Smith, P.D., *see* Morris, J.S., 950
 Smoluchowski, M.V., 356
 Snyder, B., 356
 So, P.T.C., 155
 So, P.T.C., *see* Gruner, S.M., 157
 So, P.T.C., *see* Nayaran, O., 153
 So, P.T.C., *see* Shyamsunder, E., 159
 Sobota, A., *see* Kwiatkowska, K., 842
 Soderquist, M.E., 802
 Soléau, S., *see* Angelova, M.I., 720
 Solomon, F., *see* Birgbauer, E., 846
 Solum, N.O., *see* Aakhus, A.M., 845
 Somerharju, P., *see* Thuren, T., 211
 Sommer, L., *see* Niggli, V., 844
 Sommerfeld, A., 356
 Sommers, W., *see* Als-Nielsen, J., 205
 Song, J., 459
 Song, J., *see* Evans, E., 460, 601
 Song, J., *see* Waugh, R.E., 459, 720
 Song, L., 900
 Sorienl, S., *see* Barski, G., 949
 Sorieul, S., 895
 Sorieul, S., *see* Barski, G., 895
 Sornette, D., 720
 Sotta, P., 154
 Soulié, J.M., *see* Ransac, S., 211
 Soumpasis, D.M., 356
 Sowers, A.E., 895, 897, 898, 949
 Sowers, A.E., *see* Chang, D.C., 895
 Sowers, A.E., *see* Chernomordik, L.V., 899
 Sowers, A.E., *see* Dimitrov, D.S., 897, 898
 Sowers, A.E., *see* Neumann, E., 895
 Spaargaren, M., *see* van Belzen, N., 849
 Sparrow, J.T., *see* Vainio, P., 211
 Spegt, P.A., *see* Luzzati, V., 152
 Speicher, D.W., 62
 Speicher, D.W., *see* Ruff, P., 840
 Spencer, H., *see* Schnitzer, B., 63
 Sperotto, M.M., 356, 399
 Spinke, J., *see* Knoll, W., 304
 Sprenger, I., *see* Döbereiner, H.-G., 303, 458
 Springer, T.A., 752, 802
 Springer, T.A., *see* Carpén, O., 797
 Springer, T.A., *see* Dustin, M.L., 753
 Springer, T.A., *see* Kishimoto, T.K., 753
 Springer, T.A., *see* Lawrence, M.B., 800
 Springer, T.A., *see* Lawrence, M.D., 753
 Springer, T.A., *see* Shaw, S., 802
 Springer, T.A., *see* Staunton, D.E., 802
 Springgate, M.W., *see* Owicki, J.C., 354, 398
 Spruce, A.E., 900
 Srinivas, R.V., *see* Srinivas, S.K., 949
 Srinivas, S.K., 949
 Srinivasakumar, N., *see* Ohki, S., 954
 Srinivasan, Y., 842
 Sripada, P.K., *see* Haas, N.S., 156
 Sripada, P.K., *see* Mattai, J., 155
 St Onge, D., 843
 Ställberg-Stenhagen, S., 209
 Stamatos, L., *see* Düzgünes, N., 950
 Stamm, M., *see* Motschmann, H., 205
 Stanley, H.E., 304
 Stanley, H.E., *see* Reynolds, P.J., 355
 Stanzl, U., *see* Hintner, H., 847
 Starkus, J.G., *see* Rayner, M.D., 687
 Stauffer, D., 356
 Staunton, D.E., 802
 Staunton, D.E., *see* Kishimoto, T.K., 753
 Steck, T.L., 462
 Steck, T.L., *see* Shen, B.W., 62
 Steer, C.J., *see* Walter, A., 955
 Steerenberg, P.A., *see* Nassander, U.K., 517
 Steerenberg, P.A., *see* Storm, G., 517
 Steffen, P.K., *see* Fox, J.E., 841
 Steger, H.F., *see* Pfaller, R., 63
 Stegmann, T., 949
 Stein, D.L., *see* Kirk, G.L., 689
 Steinberg, M.S., 754
 Steiner, J.P., *see* Bennett, V., 840
 Steiner, P., *see* Goldman, R., 839
 Steitz, R., 207
 Steitz, R., *see* Peterson, I.R., 207
 Steitz, T.A., 687
 Stengelin, S., *see* Bevilacqua, M.P., 796
 Stenger, D.A., 899
 Stenger, D.A., *see* Hui, S.W., 901
 Stenhagen, E., *see* Ställberg-Stenhagen, S., 209
 Stephenson, F.A., *see* Mason, J.T., 158
 Stephenson, F.A., *see* Xu, H., 158
 Sterling, I., *see* Karcher, H., 461
 Stern, O., 641
 Sterner, D.C., *see* Creutz, C.E., 955
 Stetzkowski-Marden, F., 846
 Stevens, J.D., 63
 Stevenson, D.K., *see* Hamori, C.J., 517
 Stevenson, G.V.W., *see* Anderson, C.M., 351
 Stewart, M., 839
 Stewart, M., *see* Gorlin, J., 845
 Stewart, T.P., *see* Hui, S.W., 956
 Steyer, A., *see* Pfeiffer, W., 355
 Stier, A., 159
 Stigter, D., 400

- Stigter, D., *see* Dill, K.A., 400
 Stochaj, U., 845
 Stohrer, T., 299
 Stoicheva, N., 898
 Stoicheva, N., *see* Dimitrov, D.S., 898
 Stokke, B.T., 463
 Stokke, B.T., *see* Elgsaeter, A., 841
 Stolberg, J., 802
 Stollery, J.G., 954
 Stollery, J.G., *see* Vail, W.J., 957
 Stopak, D., *see* Harris, A.K., 799
 Storm, G., 517
 Storm, G., *see* Bakker-Woudenberg, I., 518
 Storm, G., *see* Nassander, U.K., 517
 Storm, G., *see* Woodle, M.C., 518
 Stossel, T., 838, 849
 Stossel, T., *see* Gorlin, J., 845
 Stossel, T., *see* Janmey, P., 839
 Stossel, T.P., 849
 Stossel, T.P., *see* Cunningham, C.C., 840
 Stossel, T.P., *see* Ezzell, R.M., 841
 Stossel, T.P., *see* Ito, T., 840
 Stossel, T.P., *see* Janmey, P.A., 839
 Stossel, T.P., *see* Ohta, Y., 845
 Stoughton, R.B., 490
 Stow, J.L., *see* Cantiello, H.F., 848
 Straubinger, R.M., *see* Düzgünes, N., 953
 Strehlow, U., 158
 Strey, H., 462
 Strey, H., *see* Kas, J., 839
 Strey, H., *see* Peterson, M.A., 301, 460
 Strey, H., *see* Rädler, J., 301
 Strey, H., *see* Zilker, A., 62
 Strey, H.H., *see* Rädler, J., 598
 Strey, R., 152
 Stribling, R., 519
 Strobl, G.R., *see* Ewen, B., 206
 Ström, P., 151
 Strominger, J., *see* Bjorkman, P., 797
 Struck, D.K., 950
 Strunecka, A., 842
 Stryer, L., 62, 95
 Stryer, L., *see* Fung, B.K., 950
 Stuart, M.C.A., *see* Lasic, D.D., 517
 Stuehmer, W., *see* Heinemann, S.H., 302
 Stümpel, J., 151
 Stümpel, J., *see* Harlos, K., 151
 Stümpel, J., *see* Vaz, W.L.C., 357
 Sturk, A., *see* Asijee, G.M., 844
 Sturtevant, J.M., *see* Chen, S.C., 158
 Sturtevant, J.M., *see* Chowdry, B.Z., 158
 Sturtevant, J.M., *see* Mabrey, S., 156, 302, 354
 Su, B., *see* Zhang, F., 803
 Subramani, S., *see* Fraley, R.T., 518
 Subramaniam, S., 203, 211
 Suci, P.A., *see* Herron, J.N., 205
 Sugar, I.P., 897, 901
 Sugihara, G., *see* Shigematsu, M., 951
 Sugimori, M., *see* Llinas, R., 949
 Sugimoto, Y., 802
 Sugrue, S., *see* Tranter, M., 843
 Sui, S.F., *see* Maksymiw, R., 303, 842
 Sukharev, S.I., 900
 Sukharev, S.I., *see* Kuzmin, P.I., 901
 Sullivan, J., *see* Hsu, L., 461
 Sullivan, M., *see* Lopez-Berestein, G., 517
 Sullivan, M.M., *see* Williams, B.D., 517
 Sultan, C., *see* Grondin, P., 849
 Sumner, M.C.B., *see* Knutton, S.K., 800
 Sun, H.-Q., *see* Yu, F.-X., 848
 Sundari, C.S., 953
 Sundell, S., *see* Hauser, H., 151, 203
 Sundell, S., *see* Pascher, I., 151, 206
 Sundler, R., 957
 Sundler, R., *see* Bondeson, J., 955, 956
 Sune, A., 842
 Sung, K.-P., *see* Tozeren, A., 753
 Sung, K.L.P., 802
 Sung, K.L.P., *see* Chien, S., 797
 Sung, K.L.P., *see* Dong, C., 798
 Sung, K.L.P., *see* Schmid-Schönbein, G.W., 802
 Sung, K.L.P., *see* Tozeren, A., 803
 Sung, L.A., *see* Sung, K.L.P., 802
 Sunshine, J., *see* Rutishauser, U., 802
 Suzaki, E., *see* Okimasu, E., 843
 Suzuki, H., 841
 Svenson, C.E., 517
 Svetina, S., 300, 457, 458, 459, 516, 721
 Svetina, S., *see* Bozic, B., 458
 Svetina, S., *see* Heinrich, V., 460
 Svetina, S., *see* Käs, J., 460
 Svetina, S., *see* Waugh, R.E., 459, 720
 Svoboda, K., 462, 841
 Svoboda, K., *see* Schmidt, C.F., 462
 Swafford, J.A., *see* Carpén, O., 797
 Swalen, J.D., *see* Smith, D.P.E., 207
 Swann, M.M., *see* Mitchison, J.M., 688
 Swanson, J.E., 641
 Swierenga, S.H., *see* French, S.W., 847
 Szleifer, I., 153, 299, 398, 489
 Szleifer, I., *see* Ben-Shaul, A., 398
 Szleifer, I., *see* Carignano, M.A., 400
 Szögyi, M., *see* Arnold, K., 952
 Szoka, F.C., *see* Ellens, H., 953
 Szoka, F.C., *see* Woodle, M.C., 518
 Tabony, J., 356
 Tabor, D., *see* Israelachvili, J.N., 206

- Tahibi, A., 519
 Tahir-Kheli, R.A., 356
 Tajima, K., 208
 Takahashi, H., 955
 Takashima, S., 898
 Takeda, J., *see* Senda, M., 895
 Takeichi, M., 753
 Takenawa, T., *see* Fukami, K., 844
 Takeuchi, K., 841
 Talapov, A.L., *see* Pokrovskii, V.L., 599
 Talmon, Y., *see* Siegel, D.P., 154, 956
 Tamm, L., 211
 Tamm, L.K., 211
 Tanaka, M., *see* Shigematsu, M., 951
 Tanaka, T., *see* Janmey, P.A., 839
 Tandon, R.K., *see* Israelachvili, J., 800
 Tanford, C., 206, 298, 397, 596, 640
 Tangelder, G.J., 802
 Taniguchi, K., *see* Kawakatsu, T., 461
 Taniguchi, N., 802
 Tank, D., 356
 Tank, D.W., 802
 Tanoue, K., *see* Suzuki, H., 841
 Taraschi, T.F., *see* de Kruijff, B., 153, 159
 Tardieu, A., 151, 152
 Tardieu, A., *see* Charvolin, J., 149
 Tardieu, A., *see* Gulik-Krzywicki, T., 688
 Tardieu, A., *see* Ranck, J.L., 158
 Tarnsevich, M.R., *see* Abidor, I.G., 896
 Tate, M.W., 149, 156, 159, 901
 Tate, M.W., *see* Gawrisch, K., 689
 Tate, M.W., *see* Gruner, S.M., 157
 Tate, M.W., *see* Shyamsunder, E., 159
 Tauber, A.I., *see* Meers, P., 955
 Taupin, C., *see* de Gennes, P.-G., 152, 459, 597, 641
 Taylor, D.A., *see* Warner, R.R., 490
 Taylor, D.L., *see* de Biasio, R.L., 798
 Taylor, J.D., *see* Chopra, H., 847
 Taylor, P., *see* Traynor, K.A., 849
 Teissie, I., 898
 Teissie, J., 896
 Teissie, J., *see* Blangero, C., 899, 900
 Teissie, J., *see* Lopez, A., 898
 Teissie, J., *see* Rols, M.-P., 900
 Teissie, J., *see* Rossignol, D.P., 896
 Teissie, J., *see* Tocanne, J.-F., 954
 Telen, M.J., *see* Haynes, B.F., 799
 Templer, R.H., 152, 154
 ten Kate, M., *see* Bakker-Woudenberg, I., 518
 Ten, C.J., *see* Asijee, G.M., 844
 Tenchov, B., 157
 Tenchov, B., *see* Kutteneich, H., 156
 Tenchov, B.G., 156
 Tenchov, B.G., *see* Hinz, H.-J., 156
 Tenchov, B.G., *see* Koynova, R.D., 151, 152
 Ter-Minassian-Saraga, L., 210
 Ter-Minassian-Saraga, L., *see* Dimitrov, D.S., 900
 Ter-Minassian-Saraga, L., *see* Panaiotov, I., 900
 Ter-Minassian-Saraga, L., *see* Panaiotov, I.I., 210
 Terada, S., *see* Okimasu, E., 843
 Teubner, M., *see* Träuble, H., 154, 203
 Tha, S.P., 802
 Theilen, U., *see* Galla, H.-J., 204, 352
 Theilen, U., *see* Galla, H.J., 300
 Thelen, M., 845
 Thelen, M., *see* Hartwig, J., 845
 Theriot, J., 848
 Thevenin, B.J., *see* Willardson, B.M., 840
 Thewalt, J., 95
 Thewalt, J.L., 95
 Thom, D., *see* Rees, D.A., 801
 Thomas, R., *see* Johnson, S.I., 304
 Thomas, R., *see* Johnson, S.K., 62
 Thomas, R.K., *see* Bayerl, T., 299
 Thomas, R.K., *see* Bayerl, T.M., 206
 Thomas, R.K., *see* Johnson, S.J., 598, 841
 Thomas, S.C., *see* New, R.R.C., 517
 Thompson, B.L., *see* Traynor, K.A., 849
 Thomson, C., *see* Absolom, D.R., 796
 Thompson, C., *see* Forscher, P., 848
 Thompson, T.E., 356
 Thompson, T.E., *see* Almeida, P.F.F., 302, 351
 Thompson, T.E., *see* Bultmann, T., 351
 Thompson, T.E., *see* Estep, T.N., 352
 Thompson, T.E., *see* Melo, E.C.C., 354
 Thompson, T.E., *see* Sankaram, M.B., 303, 355
 Thompson, T.E., *see* Vaz, W.L.C., 357
 Thorpe, M.F., *see* Garboczi, E.J., 352
 Thorpe, M.F., *see* Xia, W., 357
 Thouless, D.J., *see* Kosterlitz, J.M., 207
 Thuren, T., 211
 Thurmon, L., *see* Gillard, B., 846
 Tiddy, G.J., *see* Adam, C.G., 688
 Tiddy, G.J., *see* Carvell, M., 688
 Tiddy, G.J.T., 149
 Tikhonov, A.N., *see* Margolis, L.B., 800
 Tilcock, C.P., *see* Cullis, P.R., 153
 Tilcock, C.P.S., 153, 156
 Tilcock, C.P.S., *see* Blow, A.M.J., 954
 Tilcock, C.P.S., *see* Cullis, P.R., 95, 153
 Tilcock, C.P.S., *see* Gruner, S.M., 157
 Tilcock, C.P.S., *see* Shyamsunder, E., 159
 Tilcock, C.T.S., 952
 Tilley, D., *see* Coakley, W.T., 754
 Tilney, L., *see* Theriot, J., 848
 Timasheff, S.N., *see* Arakawa, T., 687
 Tissot, O., 803

- Tissot, O., *see* Kaplanski, G., 803
 Titijevskaia, A.S., *see* Derjaguin, B.V., 598
 Toartelotte, M.E., 298
 Tocanne, J.-F., 954
 Todd, I., *see* Gingell, D., 799
 Toporov, Y.D., *see* Derjaguin, B.V., 798
 Toprakcioglu, C., *see* Radiman, S., 151
 Torbet, J., 690
 Torney, D.C., *see* Dembo, M., 753, 798
 Torquato, S., 356
 Torquato, S., *see* Kim, I.C., 353
 Torquato, S., *see* Lee, S.B., 354
 Torrie, G.M., *see* Carnie, S.L., 690
 Tournois, H., 160
 Tozeren, A., 753, 803
 Tozeren, H., *see* Schmid-Schönbein, G.W., 802
 Traeuble, H., 301, 302
 Tran-Son-Tay, R., 803
 Tranter, M., 843
 Traub, P., 846
 Traub, P., *see* Horkovics, K.S., 846
 Traub, P., *see* Janmey, P.A., 839
 Träuble, H., 154, 203, 356
 Traykov, T.T., *see* Dimitrov, D.S., 901
 Traynor, K.A., 849
 Traynor, K.A., *see* Eberle, M., 849
 Trinkaus, J.P., *see* Erickson, C.A., 798
 Tsao, Y.-H., 688, 690
 Tschopp, T.B., *see* Baumgartner, H.R., 796
 Tsoneva, I., 898
 Tsoneva, I., *see* Dimitrov, D.S., 898
 Tsoneva, I., *see* Stoicheva, N., 898
 Tsoneva, I., *see* Zhelev, D.V., 897
 Tsong, T.Y., 158, 896, 897
 Tsong, T.Y., *see* Kinosita, K.Jr., 896
 Tsong, T.Y., *see* Rossignol, D.P., 896
 Tsong, T.Y., *see* Serpersu, E.H., 896
 Tsong, T.Y., *see* Teissie, J., 896
 Tsukita, S., *see* Funayama, N., 845
 Tulkki, A.P., *see* Kinnunen, P.K.J., 205
 Turnbull, D., 356, 357
 Turnbull, D., *see* Cohen, M.H., 352
 Turner, C., *see* Burrige, K., 843
 Turner, C.E., 843, 844
 Turner, C.E., *see* Nuckolls, G.H., 844
 Turner, D.C., 153, 689
 Turner, D.C., *see* Gruner, S.M., 157
 Turner, D.C., *see* Lewis, R.N.A.H., 155
 Turner, D.C., *see* Mannock, D.A., 155
 Turner, D.C., *see* Nayaran, O., 153
 Turner, D.C., *see* Shyamsunder, E., 159
 Turner, D.C., *see* Tate, M.W., 149
 Turney, H., *see* Sheetz, M.P., 356
 Turney, S., *see* Sheetz, M.P., 848
 Tweet, A.G., *see* Ballamy, W.D., 204
 Udomsangpetch, R., *see* Ruangjirachuporn, W., 842
 Ueno, R., *see* Mitsuya, H., 954
 Uhr, J.W., *see* Lipscomb, M.F., 800
 Unanue, E.R., 803
 Unanue, E.R., *see* Abbas, A.K., 796
 Unanue, E.R., *see* Ault, K.A., 796
 Ungewickelt, E., *see* Ahle, S., 63
 Unkeless, J.C., *see* Michl, J., 801
 Unwin, P.N.T., *see* Henderson, R., 94
 Urumow, T., *see* Sackmann, E., 401
 Urumow, T., *see* Sen-fang, Sui, 303
 Usami, S., *see* Schmid-Schönbein, G.W., 802
 Uster, P.S., 955
 Utsumi, K., *see* Okimasu, E., 843
 Vaage, J., 518
 Vaheri, A., *see* Hedman, K., 799
 Vail, W.J., 957
 Vail, W.J., *see* Papahadjopoulos, D., 953, 956, 957
 Vail, W.J., *see* Stollery, J.G., 954
 Vainio, P., 211
 Vainio, P., *see* Thuren, T., 211
 Vaknin, D., 206
 Vakrusheva, T.E., *see* Budker, V.G., 957
 Vale, R.D., 847
 Valentine, R.C., 803
 van Beijeren, H., 357
 van Belzen, N., 849
 van Bergen en Henegouwen, P., *see* Payrastra, B., 849
 van Deenen, L.L.M., *see* de Kruijff, B., 159
 van Deenen, L.L.M., *see* Op den Kamp, J.A.F., 302
 van Echteld, C.J.A., *see* de Kruijff, B., 153, 159
 van Echteld, C.J.A., *see* Noordam, P.C., 157
 van Hoogevest, P., *see* de Kruijff, B., 159
 van Kessel, W.S.M., *see* Dekker, C.J., 157
 van Meer, G., 62
 van Oss, C.J., 803, 951, 952, 957
 van Oss, C.J., *see* Absolom, D.R., 796
 van Oss, C.J., *see* Neumann, A.W., 801
 van de Ven, T.G., *see* Frojmovic, M., 799
 van den Bergh, H., *see* David, G., 798
 van den Besselaar, A.M.H.P., *see* de Kruijff, B., 159
 van den Bosch, H., *see* de Kruijff, B., 159
 van der Ploeg, P., 400
 van der Ploeg, P., *see* Edholm, O., 400

- van der Schuerent, B., *see* David, G., 798
 van der Steen, A.T.M., *see* de Kruijff, B., 159
 Vandekerkhove, J., *see* Garcia, A., 847
 Vanderlick, K.T., 208
 Vargas, R., 151
 Vargas, R., *see* Luzzati, V., 150
 Vartio, T., *see* Hedman, K., 799
 Vasiliev, J.M., *see* Bershadsky, A.D., 838
 Vasilieva, E.Y., *see* Margolis, L.B., 800
 Vassal, L., *see* Alkhalaf, W., 519
 Vaz, W.L., 753
 Vaz, W.L.C., 204, 357
 Vaz, W.L.C., *see* Almeida, P.F.F., 302, 351
 Vaz, W.L.C., *see* Bultmann, T., 351
 Vaz, W.L.C., *see* Clegg, R.M., 351
 Vaz, W.L.C., *see* Criado, M., 352
 Vaz, W.L.C., *see* Jovin, T.M., 353
 Vaz, W.L.C., *see* Melo, E.C.C., 354
 Veatch, W., *see* Golan, D.E., 63
 Veatch, W.R., *see* Alecio, M.R., 351
 Vedeler, A., 845
 Venable, R.M., *see* Pastor, R.W., 400
 Verger, R., *see* Ransac, S., 211
 Verger, R., *see* Vainio, P., 211
 Verkleij, A., *see* Noordam, P.C., 157
 Verkleij, A.J., 159, 160, 955
 Verkleij, A.J., *see* Burger, K.N.J., 160
 Verkleij, A.J., *see* Cullis, P.R., 95, 153, 159
 Verkleij, A.J., *see* Payraastre, B., 849
 Verkleij, A.J., *see* de Kruijff, B., 153, 159
 Verkleij, A.J., *see* van Belzen, N., 849
 Verkman, A., 839
 Verméglio, A., *see* Joliot, P., 353
 Verméglio, A., *see* Lavergne, J., 353
 Verwey, E.J.W., 599, 640, 690, 753, 950
 Vickers, J., 843
 Vienken, J., 899
 Villalain, J., *see* Ortiz, A., 160
 Villalobo, A., 517
 Vincett, P.S., *see* Popovic, Z.D., 210
 Virtanen, J.A., *see* Kinnunen, P.K.J., 205
 Virtanen, J.A., *see* Thuren, T., 211
 Virtanen, J.A., *see* Vainio, P., 211
 Vist, M.R., 95, 357, 461
 Vitetta, E.S., *see* Lipscomb, M.F., 800
 Vodyanoy, I., *see* Keller, S.L., 687
 Vogel, H., *see* Jähnig, F., 397
 Vogel, H., *see* Vaz, W.L.C., 357
 Vogel, K.G., 803
 Vogel, V., 203
 Vogler, E.A., 803
 Voigt-Martin, I., *see* Peterson, I.R., 207, 301
 Voigt-Martin, I., *see* Steitz, R., 207
 Volberding, P.A., *see* Northfelt, D.W., 518
 Vollhardt, D., 209
 von Rüden, L., *see* Chow, R.H., 949
 von Tschärner, V., *see* Hafeman, D.G., 210
 Vreman, H.J., *see* Hamori, C.J., 517
 Wachstock, D.H., 844
 Wächterhäuser, G., 93
 Wack, D.C., 641
 Wade, C.G., *see* Kuo, A.L., 353
 Wade, W., 803, 848
 Wadsack, J., *see* Bärmann, M., 846
 Wagner, H., 803
 Wainwright, T.E., *see* Alder, B.J., 351
 Walker, D.C., *see* Hope, M.J., 956
 Wallach, D.F.H., *see* Tahibi, A., 519
 Walter, A., 955
 Walter, J., *see* Eyring, E., 799
 Walton, A.G., *see* Soderquist, M.E., 802
 Wandosell, F., *see* Hargreaves, A., 846
 Wang, D.L., 843
 Wang, L.L., *see* de Biasio, R.L., 798
 Wang, N., 846
 Wang, Y., *see* Neumann, E., 896
 Wang, Z., 155
 Wang, Z., *see* Lin, H., 155
 Wang, Z.-G., 400
 Wang, Z.G., *see* Turner, D.C., 153
 Ward, R.C., *see* Grundy, M., 206
 Ward, R.J., 843
 Warner, R.R., 490
 Warnock, R.A., *see* Picker, L.J., 801
 Warrender, N.A., *see* Seddon, J.M., 152
 Warrender, N.A., *see* Templer, R.H., 152, 154
 Watkins, J.F., *see* Harris, H., 949
 Watson, J., *see* Alberts, B., 849
 Watson, J.D., *see* Alberts, A., 93
 Watson, J.D., *see* Alberts, B., 62, 457, 596
 Watson, S.R., *see* Foxall, C., 799
 Watts, A., 151
 Watts, A., *see* Marsh, D., 354
 Watts, T.H., *see* McConnell, H.M., 210
 Waugh, R., 462
 Waugh, R., *see* Evans, E., 299, 460, 601
 Waugh, R.E., 459, 720
 Waugh, R.E., *see* Bo, L., 459
 Waugh, R.E., *see* Bozic, B., 458
 Waugh, R.E., *see* Song, J., 459
 Waxman, S.G., *see* Fields, R.D., 843
 Weaver, J.C., 896, 897
 Weaver, J.C., *see* Bartoletti, D.C., 901
 Webb, M.S., 357
 Webb, W.W., *see* Axelrod, D., 351
 Webb, W.W., *see* Ghosh, R.N., 352

- Webb, W.W., *see* Gross, D., 63
 Webb, W.W., *see* Koppel, D.E., 204
 Webb, W.W., *see* Ryan, T.A., 802
 Webb, W.W., *see* Schlessinger, J., 802
 Webb, W.W., *see* Schneider, M.B., 356, 459
 Webb, W.W., *see* Schneider, M.D., 301
 Webb, W.W., *see* Tank, D., 356
 Webb, W.W., *see* Tank, D.W., 802
 Webb, W.W., *see* Wack, D.C., 641
 Weber, H., 895
 Wegener, A.M.K., 803
 Wegner, A., *see* Ruhnau, K., 844
 Wegner, G., *see* Motschmann, H., 205
 Weidman, P., *see* Melancon, P., 63
 Weihan, W., *see* Johnson, S.J., 841
 Weiller, N.K., 803
 Weiner, L.M., *see* Grudzev, A.D., 954
 Weiner, N., 490
 Weis, R.M., 204, 357
 Weis, R.M., *see* McConnell, H.M., 210
 Weisenhorn, A.L., 207
 Weiss, A., 720
 Weiss, L., *see* Baier, R.E., 796
 Weiss, P., 803
 Weiss, R.M., 203
 Weisz, K., *see* Stohrer, T., 299
 Weitz, D., *see* Sirota, E.B., 641
 Wennerström, H., 357, 397, 600
 Wennerström, H., *see* Granfeldt, M.K., 690
 Wennerström, H., *see* Guldband, L., 208, 599, 688, 690
 Wennerström, H., *see* Ipsen, J.H., 95, 210, 353
 Wennerström, H., *see* Israelachvili, J.I., 687
 Wennerström, H., *see* Israelachvili, J.N., 300, 598, 690, 951
 Wennerström, H., *see* Jonsson, B., 689, 690
 Wennerström, H., *see* Jönsson, B., 400
 Wennerström, H., *see* Tsao, Y.-H., 690
 Wenz, M., *see* Felgner, P., 518
 Wertz, P.W., 490
 Wessel, G.M., *see* McClay, D.R., 801
 Wheelis, M.L., 93
 Wheelis, M.L., *see* Woese, C.R., 93
 Wheelock, M.J., 845
 White, J.M., 949, 957
 White, J.M., *see* Morris, S.J., 899
 White, J.M., *see* Spruce, A.E., 900
 White, L.R., *see* Hughes, B.D., 353
 White, L.R., *see* Israelachvili, J., 800
 White, S.H., *see* Wiener, M.C., 601
 Whitesell, L.G., *see* Arnett, E.M., 154
 Whitmarsh, J., *see* Blackwell, M.F., 351
 Whitt, M.A., *see* Rose, J.K., 519
 Wiche, G., *see* Herrmann, H., 842
 Wiche, T., *see* Foissner, R., 839
 Wiegel, F.W., 357
 Wiener, M.C., 601
 Wiener, M.C., *see* Yang, C.P., 158
 Wiener, O., 357
 Wier, M., 803
 Wiese, W., 458, 460, 721
 Wieslander, Å., 160
 Wieslander, Å., *see* Lindblom, G., 157, 160
 Wigglesworth, N.M., *see* Kellie, S., 844
 Wijkander, J., *see* Bondeson, J., 956
 Wijkander, J., *see* Sundler, R., 957
 Wikander, G., *see* Lindblom, G., 157, 160
 Wilczek, F., *see* Shapere, A., 93
 Wild, P., *see* Harris, A.K., 799
 Wildevuur, C.R.H., *see* Schackenraad, J.M., 802
 Wiley, D., *see* Bjorkman, P., 797
 Wilkins, J.A., *see* Wachstock, D.H., 844
 Wilkins, M.H.F., *see* Torbet, J., 690
 Wilkinson, D.A., 158
 Wilkinson, D.A., *see* Nagle, J.F., 209
 Wilkinson, D.A.W., 302
 Wilkinson, J.M., *see* Aakhus, A.M., 845
 Wilkinson, J.M., *see* Asijee, G.M., 844
 Willard, M.B., *see* Cheney, R.E., 842
 Willardson, B.M., 840
 Willey, R., *see* Dimitrov, D.S., 899
 Williams, B.D., 517
 Williams, D.B., *see* Christink, E.R., 797
 Williams, J.R., *see* Williams, B.D., 517
 Williams, K.E., *see* Williams, B.D., 517
 Williams, L.J., *see* Almabobi, G., 847
 Williams, N., *see* Weiner, N., 490
 Williamson, J.B.P., *see* Greenwood, J.A., 799
 Williamson, P., *see* Pradhan, D., 842
 Willingham, M.C., 803
 Willmore, T.J., 461
 Wilschut, J., 949, 950, 951, 957
 Wilschut, J., *see* Düzgünes, N., 956
 Wilschut, J., *see* Hoekstra, D., 950
 Wiltscheck, R., *see* Habazettl, J., 304
 Winch, P.J., *see* Earnshaw, J.C., 205
 Winkler, J., *see* Strey, R., 152
 Winsor, P.A., 152
 Winterhalter, M., 400, 641
 Winterhalter, M., *see* Kozlov, M.M., 400, 689
 Winzler, R.J., 803
 Wirthensohn, K., *see* Sackmann, E., 401
 Witten, T., *see* Sirota, E.B., 641
 Witten, T.A., *see* Milner, S.T., 401
 Wo Weihan, *see* Johnson, S.K., 62
 Wo wei han, *see* Johnson, S.I., 304
 Woese, C.R., 93, 94

- Woese, C.R., *see* Wheelis, M.L., 93
 Wofsy, C., *see* Seagrave, J., 848
 Wohlrab, W., 490
 Wohlrab, W., *see* Lasch, J., 490
 Wolfe, J., 951
 Wolfe, J., *see* Bryant, G., 897
 Wolfe, J., *see* Israelachvili, J.N., 159
 Wolfe, R.S., *see* Woese, C.R., 94
 Wong, P.T.T., 155
 Wong-Staal, F., *see* Mitsuya, H., 954
 Wonneberger, W., 303
 Woodle, M.C., 517, 518
 Woodle, M.C., *see* Papahadjopoulos, D., 518
 Woods, A., 803
 Woods, C., 846
 Woolley, P., *see* Träuble, H., 154, 203
 Worthen, G.S., *see* Downey, G.P., 848
 Wortis, M., 458
 Wortis, M., *see* Fourcade, B., 460
 Wortis, M., *see* Miao, L., 457, 459, 721
 Wortis, M., *see* Seifert, U., 300, 458
 Wright, S.D., *see* Detmers, P.A., 798
 Wu, C.C., *see* Husain, C.A., 840
 Wu, E.-S., *see* Tank, D., 356
 Wu, E.S., *see* Tank, D.W., 802
 Wu, J.R., *see* Lentz, B.R., 954
 Wu, N., *see* Needham, D., 518
 Wu, S., 302
 Wu, S.H.-W., 461
 Wu, Y., 898
 Wuestehube, L., 845
 Würz, U., *see* Heimburg, T., 156
 Wuthrich, K., *see* Otting, G., 687
 Wysolmerski, R.B., *see* Kolodney, M.S., 800
- Xia, W., 357
 Xian, W., 849
 Xu, H., 158
 Xue You Han, 302
- Yager, P., 155
 Yager, P., *see* Chang, E.L., 155
 Yamada, H., *see* Mannock, D.A., 155
 Yamada, K.M., *see* Schlessinger, J., 802
 Yamada, N., *see* Murakami, S., 160
 Yamasaki, N., *see* Lee, S., 955
 Yamazaki, H., *see* Suzuki, H., 841
 Yamazaki, M., 952
 Yamin, R., *see* Gorlin, J., 845
 Yanagishita, M., 803
 Yang, C.P., 158
 Yang, S.X., *see* Tsao, Y.-H., 688
 Yaron, A., *see* Hoekstra, D., 957
- Yates, J.C., *see* Burgess, S.W., 954
 Yates, J.C., *see* Lentz, B.R., 954
 Yeagle, P.L., *see* Ellens, H., 154, 956
 Yeagle, P.L., *see* Hui, S.W., 956
 Yeagle, P.L., *see* Siegel, D.P., 157, 956
 Yechiel, E., 357
 Yeung, A., *see* Evans, E., 460, 601, 848
 Yeung, A., *see* Evans, E.A., 799
 Yeung, A., *see* Tran-Son-Tay, R., 803
 Yin, H., *see* Yu, F.-X., 848
 Yonezawa, F., 357
 Yoshimura, H., *see* Kinoshita, K.Jr., 896
 Young, S.K., *see* Downey, G.P., 848
 Yu, F.-X., 848
 Yu, H., *see* Chen, Y.-L., 205
- Zaba, B.N., *see* Heckl, W.M., 210
 Zaccai, G., 150
 Zaccai, G., *see* Bueldt, G., 299
 Zaccai, G., *see* Buldt, G., 206
 Zachrisson, A., *see* Hahn-Hagerdal, B., 898
 Zaks, W.J., 949
 Zaks, W.J., *see* Creutz, E.C., 954
 Zaner, K.S., *see* Ito, T., 840
 Zaner, K.S., *see* Janmey, P.A., 839
 Zarda, P.R., *see* Skalak, R., 753
 Zasadzinski, J.A., *see* Bailey, S.M., 719
 Zasadzinski, J.A.N., *see* Kaler, E.W., 461
 Zeks, B., *see* Bozic, B., 458
 Zeks, B., *see* Cevc, G., 689
 Zeks, B., *see* Heinrich, V., 460
 Zeks, B., *see* Käs, J., 460
 Zeks, B., *see* Svetina, S., 300, 457, 458, 459, 516
 Zeks, B., *see* Waugh, R.E., 459
 Žekš, B., *see* Svetina, S., 721
 Žekš, B., *see* Waugh, R.E., 720
 Zelenin, A.V., *see* Sukharev, S.I., 900
 Zeman, K., 301, 841
 Zemb, Th., *see* Dubois, M., 688
 Zemlin, F., *see* Henderson, R., 94
 Zhai, S., *see* Liu, S.C., 841
 Zhang, F., 803
 Zhang, J., *see* Caffrey, M., 159
 Zhelev, D., *see* Dimitrov, D.S., 898
 Zhelev, D.V., 896, 897, 898
 Zhelev, D.V., *see* Dimitrov, D.S., 897, 898, 901
 Zhelev, D.V., *see* Tsoneva, I., 898
 Zheng, Q., 899
 Zia, R.K.P., 600
 Zia, R.K.P., *see* Fourcade, B., 460
 Zia, R.K.P., *see* Miao, L., 457, 721
 Zia, R.K.P., *see* Wortis, M., 458
 Ziegler, M., *see* Zilker, A., 301

- Zielinska, B., *see* Lipowsky, R., 462, 599
Zilker, A., 62, 301, 458
Zilker, A., *see* Boal, D.H., 463
Zilker, H., *see* Duwe, M.P., 398
Zimmerberg, J., 687
Zimmerberg, J., *see* Cohen, F.S., 955
Zimmerberg, J., *see* Gawrisch, K., 689, 953
Zimmerberg, J., *see* Sarkar, D.P., 901
Zimmerman, G.A., 803
Zimmerman, R.M., *see* Radmacher, M., 690
Zimmermann, U., 154, 895, 896, 897, 898, 953
Zimmermann, U., *see* Benz, R., 896
Zimmermann, U., *see* Mehrle, W., 896
Zimmermann, U., *see* Scheurich, P., 898
Zimmermann, U., *see* Vienken, J., 899
Zingg, W., *see* Absolom, D.R., 796
Zingg, W., *see* Neumann, A.W., 801
Ziyadeh, F.N., 848
Zlotnik, A., *see* Briggs, M.S., 210
Zograf, G., *see* Chen, Y.-L., 205
Zot, H.G., 847
Zot, H.G., *see* Pollard, T.D., 847
Zschörnig, O., 957
Zschörnig, O., *see* Arnold, K., 952
Zuckermann, M.J., *see* Caille, A., 202
Zuckermann, M.J., *see* Ipsen, J.H., 95, 210, 303, 353
Zuckermann, M.J., *see* Mouritsen, O.G., 207
Zuniga, M., *see* Edidin, M., 798
Zurkhov, S.N., 803
Zwaal, R.F., *see* Comfurius, P., 842
Zwanzig, R., *see* Harrison, A.K., 353
Zwolinsky, B.J., 489

Subject Index

- ABP (filamin) 812, 816, 826
acceptor fluorescence 911
accidental induced adhesion 695
accumulation tumours 511
acidic phospholipids 831
actin 10, 809, 810, 821, 833
actin cycle 835
actin filaments 809, 810, 821, 825, 834
actin-membrane interactions 820–827
actin polymerization 836
actin/spectrin network, *see* spectrin/actin network
activation energies for diffusion 315, 330, 346
activation energies for electrofusion 880
activation energies for electroporation 866, 867,
see also threshold voltage
activation energy for vesicle permeation 475
adaptin 47, 49
adenosine triphosphate, *see* ATP
adenylate cyclase 60
adhesion dynamics 727, 740
adhesion energies 447, 531, 693, 726, 737, 738
adhesion experiments on bilayers 527–536, 647–
670, 695–705, 729, 730
adhesion experiments on biomembranes 739,
741, 742, 748, 759, 762, 765
adhesion induced by cooling 702–705
adhesion induced by tension, *see* tension-induced
adhesion
adhesion-induced fusion 452
adhesion-induced rupture 452
adhesion of cells, *see* cell adhesion
adhesion of membrane bunches 578
adhesion of vesicles 446–452, 505
adhesion, spontaneous and induced 717
adhesion step in fusion 887
adhesion transition of vesicles 448–450
adhesion via dielectrophoresis 867–872
adhesive failure 726, 743–752, 795
adriamycin 502
adsorbed proteins 23, 287
adsorption of liposomes 498
aerosol 503
AFM, *see* atomic force microscopy
aggregate 218, 470, 525
aggregation mechanism for vesicles 913–927
aggregation rate constant for vesicles 915, 939
agro-food industry 514, 515
AIDS, *see* HIV infection
 α -actinin 823, 824
 α -adaptin, *see* adaptin
 α -helical structures 940
aminophospholipid 819
amphiphilic molecules 525, 645
amphiphilic peptides 81
amphiphilic solutes 139
amphotericin B 501
angular vesicles 714
ankyrin 10, 12, 814, 817, 828, 831
annexins 937
anomalous diffusion 315
anomalous roughness of bilayers 695, 712–715
anthracyclines 502
antibiotics 501
anticancer therapy 502
antiporters 26, 29
antivirals 501, 508
apparent binding area 775

- apparent contact angle, *see* effective contact angle
 applications of liposomes 480–486, 493–515
 archaeobacteria 72, 76, 77
 archaeobacterial membranes 76, 77
 area compressibility modulus 241, 243, 377, 416
 area expansivity 229
 area occupied by cholesterol 330
 area-difference-elasticity 411, 455–457
 artificial permeability barriers for vesicles 476
 asthma 503
 atmospheric oxygen and evolution 75
 atomic force microscopy (AFM) 186, 187, 648
 ATP (adenosine triphosphate) 809, 831, 834
 ATP-driven ion pumps 25, 26
 ATP-hydrolysis 25
 ATPases 26, 28, 54
 attractive electrostatic forces, *see* electrostatic forces and ion-ion correlations
 average radius of solid phase domains 335

 bacterial swimming 68
 band III (or band 3) protein 12, 20, 814
 bending elasticity 240–245, 373–388, 407–416, 469, 526
 bending energy 409–412
 bending energy threshold for adhesion, *see* threshold energy
 bending modes, *see* bending undulations
 bending modulus, *see* bending rigidity
 bending moment 220
 bending rigidity 241, 244, 379, 380, 382, 385, 409, 415, 526, 547, 551, 633, 733, 715, 716
 bending rigidity, electrostatic contribution, *see* electrostatic contribution to bending rigidities
 bending rigidity, experimental values 415, 715, 716
 bending rigidity for mixed bilayer 385
 bending rigidity, measurements of 246, 427, 715, 716
 bending rigidity, reduction by inhomogeneities 471
 bending rigidity, reduction by protrusions 585
 bending undulations 246, 426–429, 546–550, 866

 bicontinuous cubic phases 104, 147, 148
 bilayer → inverted hexagonal phase 240
 bilayer architecture 7, 225, 407
 bilayer asymmetry 24
 bilayer dimensions 649
 bilayer membrane 14–24, 109, 525, 656, 886, 909
 bilayer thickness 652
 bilayer-couple model 413
 bile salts 472, 503, *see also* edge-active molecules
 bimolecular rate constants 312
 binary systems, *see* lipid mixtures or lipid/protein mixtures
 binding of monovalent cations 915
 biocides 515
 biodistribution 498, 507, 508
 bioengineering, *see* liposomes
 biological adhesion, *see* adhesion of cells
 biological fusion, 854, 892, 906–909
 biological membranes, *see* biomembranes
 biomembranes 4–62, 70–92, 453–455, 494, 524, *see also* cell membranes or plasma membranes
 biomineralisation 497
 biopharmaceuticals 511
 biosynthesis of cholesterol 81
 biosynthesis of lipids 34, 35
 biosynthesis of membrane proteins 35, 36
 bivalent ions, *see* divalent ions
 Bjerrum length 612
 blisters 579
 Bloch- and Néel-walls 256
 blocked exchange between monolayers 381, 385, 386
 blood clearance of liposomes 505
 bond orientational order of chains, *see* orientational order
 bond orientational order of 2D lattice, *see* hexatic phase
 bond percolation 322
 Bonnet transformation 109
 bound shapes of vesicles 448–452
 bound water 926
 boundary layer around obstacles 332
 Bragg reflections from lyotropics 106
 brain lipids 92

- breathing mode 637
bridging attraction 921, 922, 936
Brownian motion 872
brush 506
buckling in bilayers 255–258
budding 52, 89, 424, 425, 437, 438, 717
budding transition 405, 406
bunches of membranes 536, 565–578, 699, 701–703
- c-AMP (cyclic adenosine monophosphate) 57
Ca²⁺ trans complexes 932
Ca²⁺-binding proteins 935
cadherins 726, 824, 825
calcium ions 657, 884
calcium solutions 611
calcium-induced fusion 249, 927–930
calcium-induced lateral segregation 941
calcium-induced lateral phase separation 296, 297
calorimetry 925
cancer therapy 502
carboxyl bond 228
cardiolipin 35
carcinoma 507
carriers for electron transfer 347
catenin alpha 825
cation bridges 915, 923
cation-induced aggregation 913
cation-induced fusion 915, 927, 933
cation-induced vesicle aggregation 915
cationic liposomes 512
cell 6
cell adhesion 740–752, 758–795
cell adhesion and surface charges 767
cell adhesion molecules 725, 760
cell coat 779
cell deformability 654, 770, *see also* micropipette aspiration
cell differentiation 30
cell membranes 2, 7, 782, 890, *see also* plasma membranes
cell motility 740
cell polarizability 868
cell-cell fusion 854, 872, 873, 906
cell-substrate adhesion 768, 769
- cellular evolution, *see* evolution of cells
cellulose 925
cerebrosides 14
chain branching 196
chain conformations 110, 238, 364, 369
chain conformations, probability distribution of 367–368
chain free energy 372, 373
chain length and phase behavior 137, 196
chain melting transition in bilayers 136, 141, 142, 221–224
chain melting transition in monolayers 165, 188, 194
chain melting transition, ionic strength dependence 252, 253
chain packing 359
chaperon 38
charged surfaces in liquids 540, 607
charge induced lipid protein interaction 292, 293
charge induced phase transition 251–254
charge regulation 544
charged amphiphilic membrane 607
charging time 860
cheese production 514
chemotaxis 68
chiral cubic phase 119
chirality 136
chirally pure lipids 194
CHOL, *see* cholesterol
cholates, *see* edge-active molecules
cholesterol (CHOL) 14, 74, 77, 80, 81, 82, 245, 274, 316, 497
cholesterol/lipid mixtures 85, 198, 327, 437, 438, 441
chondroitin sulfate 935
chromaffin cells 907
circulation times of liposomes 505
classification of cells 72–76
classification of defects 256
classification of lipids 14–19, 77
classification of membrane proteins 19–23
clathrin 46, 49
clathrin adaptor protein, *see* adaptin
Clausius Clapeyron equation 166
Clifford torus 430
close-packed cross-sectional area 330

- clouding temperature 925
- clustering of membrane proteins 54, 59
- cluster size in percolation 323
- co-ion concentration 614
- co-transporters 26
- coagulation of colloids 885
- coalescence of colloids 884, 885
- coarsening of domains 280
- coated pit 41, 49
- coated vesicles 41, 43
- cochleate structures 910
- coherence length 332
- cohesion of membrane bunches 572–578
- cohesive failure, *see* adhesion failure
- coions 541, 606
- collective protrusion modes 580–585
- colloid interactions 537, 734
- colloid particles 497
- colloid systems 884
- complete bud 439
- computer simulations 190, 552, 554, 556, 560, 571, 584, 585, 682
- configurational-entropic forces, *see* fluctuation-induced interactions
- conformal diffusion 435
- conformal transformations 430
- conformational transitions 237
- conjugate of adhering cells 758
- contact angle 695, 696, 765, 766, *see also* effective contact angle
- contact angle measurements 918
- contact angles of induced adhesion 696, 700
- contact areas of cells 794, 795
- contact curvature 447, 536
- contact potential 447
- contact probabilities of interacting membranes 558, 559, 572, 577
- contact rounding 695
- continuum hydrodynamic theories for protein diffusion 312, 313
- continuous shape transformations 422
- continuous unbinding transitions 556–559
- continuum percolation 325
- contour roughness 746
- contradictions of induced adhesion 709–713
- conventional liposomes 500–504
- corrected Young equation 711
- correlation function for percolation 324
- correlation length for percolation 324
- cortical actin network 836
- corticosteroids 503
- cosmetics 513
- cotransporters 26
- counterions 541, 543, 606, 614
- cream of liposomes 503
- critical behaviour of lipid mixtures 294
- critical behaviour of interacting membranes 557, 565, 575
- critical exponents for percolation 323
- critical exponents for unbinding 557, 565, 575
- critical micelle concentration, *see* critical monomer concentration
- critical monomer concentration 219, 525
- critical Hamaker constant 559
- crosslined lipids 269
- critical free area for diffusion 314
- critical points for monolayers 188
- critical transmembrane voltage, *see* threshold voltage
- crystalline phases of phospholipids 110, 225, *see also* gel phases
- crystalline vesicles 224–228
- cubic phases 87, 104, 119–122, 147, 942
- CURL (compartment of uncoupling of receptor and ligand) 45–48
- CURL-vesicle 45, 46, 48
- curvature elastic energy 129, 411, 412
- curvature elasticity 377, 407–416
- curvature models 409–413
- curvature of membranes 102, 281, 409, 469, 494, 920
- curvature-induced lateral phase segregation 444–446
- curved charged membrane 625
- cyclic adenosine monophosphate, *see* c-AMP
- cystic fibrosis 513
- cytochrome oxidase 56, 647
- cytoskeletal contraction 740, 741
- cytoskeletal-membrane interactions 812–831
- cytoskeletal-membrane interactions in erythrocytes 813–816, *see also* spectrin/actin network

- cytoskeletal-membrane interactions in lymphocytes 818
- cytoskeletal-membrane interactions in epithelial cells 818, 819
- cytoskeleton 7, 10, 74, 245, 807–838, 909
- cytoskeleton and diffusion 781–783
- cytoskeleton and electrofusion 877–879
- cytoskeleton and membrane asymmetry 819, 820
- cytosol of erythrocytes 31
- cytotoxic T lymphocytes (CTL) 758–761
- D-surface 104
- damping of bending undulations 429, 588
- DAG, *see* diacyl glycerol
- DAPE (diarachidic phosphatidyl ethanolamine) 658
- DDPE (didodecylphosphatidyl ethanolamine) 125, 658
- Debye–Hückel regime for bending rigidity 626
- Debye–Hückel regime for electrostatic forces 621
- Debye–Hückel screening length 251, 542, 610, 616, 618, 913
- Debye–Hückel theory 542, 610, 613, 680
- defects as attractive centers 258–261
- defects and enzymatic control 261, 262
- defects in bilayer membranes 254–264
- defects in bilayer phases 134
- deformability of cells, *see* cell deformability
- degree of dissociation 252
- dehydration 646, 647, 925–927
- dehydration of bilayers via cations 927
- dehydration of bilayers via polymers 926
- delay time of fusion 879
- densitometry 273
- density fluctuations, *see* fluctuations
- depletion attraction 545, 734, 737–740, 790, 921–925
- depletion flocculation 924
- depletion forces, *see* depletion attraction
- depth of liposome penetration 483
- Derjaguin approximation 527, 631, 653
- Derjaguin–Landau–Verwey–Overbeek (DLVO) theory 913
- dermis 89
- desmoplakins 831
- desmosomes 818, 819, 830, *see also* tight junctions
- destabilization by electric fields 855, 876, 887, 889, 890
- destabilization of bilayers 887, 888, 910, 930
- deuteration 236
- deuterium (^2H) NMR (unclear magnetic resonance) 80, 82, 84, 926
- dextran 923
- dextran sulfate 923
- dextrins 925
- DGDG (digalactosyl diglyceride) 573, 659, 660, 665, 694
- DHDAA (dihexadecyl dimethylammonium acetate) 659, 660
- DHPE (dihexadecyl phosphatidyl ethanolamine) 125
- di-ether lipid 77
- diabetes 55
- diacetylenic lipids 188, 269
- diacyl glycerols (DAG) 16, 139
- diacyl phospholipids 223
- didodecylphosphate vesicles 934
- dielectric relaxation measurements 925
- dielectrophoresis 855, 856, 867–869, 927
- differential scanning calorimetry 936
- differentiation of cells 30
- diffraction from monolayers 179
- diffuse double layer 540, 606, 913
- diffusion and cytoskeleton, *see* cytoskeleton
- diffusion coefficient 176, 309, 328, 329, 781, 882
- diffusion coefficient in two dimensions 309–312
- diffusion coefficient in the two-phase region 316
- diffusion coefficients of integral membrane proteins 328
- diffusion coefficients of lipids 329
- diffusion controlled process 55, 312, 346
- diffusion in a lattice 318
- diffusion in an archipelago 332
- diffusion in heterogeneous systems, theory 315–318
- diffusion in homogeneous bilayers, experiment 326
- diffusion in homogeneous systems, theory 309
- diffusion in mitochondrial membranes 345, 346
- diffusion in photosynthesis membranes 346–348

- diffusion in two-fluid bilayers 331
diffusion in two-fluid systems, theory 316
diffusion of a tracer 332
diffusion of membrane-spanning molecules 336, 337
digalactosyl diclyceride, *see* DGDG
dihexadecyl dimethylammonium acetate, *see* DHDAA
dimensionality 55, 325, 548
dioctadecenoyl-PE (phosphatidyl ethanolamine) 222
dipole moment in monolayers 168
dipole potential in bilayers 682
direct current pulses 857
direct interaction of membranes 529, 537–546
disclinations 257
discocytes 418
discontinuous shape transformations 419
discontinuous unbinding transitions 560–563
disjoining pressure 529, 533, 553, 582, 630
disjoining transition, *see* unbinding transition
dislocations 257
dispersion forces 539, 652
dispersive phase 713
dissociation constant 252
distribution of chain conformations 392
disulfide bonds 37
divalent cations 915
divalent ions 251, 609
DLPC (dilauroyl phosphatidyl choline) 177, 415, 658
DLPE (dilauroyl phosphatidyl ethanolamine) 112, 113, 171, 183, 184, 658
DMPC (dimyristoyl phosphatidyl choline) 112, 415, 658
DMPC/cholesterol mixtures 199, 275–277, 283, 341, 343
DMPC/DSPC mixtures 274, 295, 341, 343
DNA 512, 645
DOG (dioleoyl glycerol) 667
domain shapes in membranes 172, 173, 263, 342
domain structure 191, 195, 280, 281
domain-induced budding 437–443
domains in photosynthetic membranes 347, 348
donor fluorescence 911
DOPC (dioleoyl phosphatidyl choline) 658
DOPS (dioleoyl phosphatidyl serine) 659
double bonds, *see* unsaturated lipids
down regulation of signal transduction 60, 61
doxorubicin 507, 511, 512
doxorubicin HCl 502
DPPC (dipalmitoyl phosphatidyl choline) 165, 226, 229, 658
DPPG (dipalmitoyl phosphatidyl glycerol) 659
drug delivery, *see* liposomes in medicine
DSPC (distearoyl phosphatidyl choline) 658
dynamic surface roughness, *see* roughness
dynamic coarsening of bending undulations 589
dynamics of adhesive failure 745
E-cadherin 817
ecology 515
edge-active molecules 220, 471, 472, 474
edge energy 219, 437, 866, 886
edge tension, *see* line tension
effect of bounding fluid on diffusion 330
effect of integral proteins on lipid diffusion 335
effective contact angle 451, 452, 536, 729, 750
egg-sperm fusion 937
eggPC (phosphatidyl choline) 655, 658, 663
eggPE (phosphatidyl ethanolamine) 658
eggPEt 658, 663
eggPEt-Me 663
egg yolk PC (phosphatidyl choline) 694, 696, 697, 699, 714
Einstein model 568
elastic bilayer properties 240–245, 373–388, 407–413, 469, 526
elastic moduli 243, 380, 414–416, 623
elasticity of mixed bilayers 472, 474
electric breakdown 857
electric charges induced by curvature 250
electric double layer 540, 606
electric double layer repulsion 540–544, 685, 736, 917
electrochemical potential 609
electrochemical equilibrium 30
electrofusion 855, 872–893, 906
electrofusion and cytoskeleton, *see* cytoskeleton
electrofusion device 859, 874
electrofusion of cell membranes 890–892
electrofusion of erythrocyte ghosts 873, 976

- electrolyte composition 914
- electrolyte solutions 542, 606–608, 611
- electron density across monolayers 194
- electron density maps for multilayers 651
- electron donors 918
- electron microscopic binding area 775
- electron optical studies 187
- electron-spin resonance (ESR) spectroscopy 230, 290
- electron transport chain 347
- electroosmotic flow 861
- electroporation 855–866
- electroporation, models of 855–866
- electroporation threshold, *see* threshold voltage for electroporation
- electrostatic boundary conditions 541, 624, 625
- electrostatic contribution to bending rigidities 625–629, 635–639
- electrostatic correlation length 631
- electrostatic effects and phase transitions 249
- electrostatic forces 540–544, 614–622, 647, 734, 736, 785–787, 913, 915
- electrostatic forces and ion-ion correlations 544, 611, 685
- electrostatic forces, large screening length 543, 613, 617–622
- electrostatic forces, small screening length 542, 612, 615–617
- electrostatic forces, small surface separations 544
- electrostatic forces versus undulation forces, *see* superposition of intermembrane forces
- electrostatic free energy 610
- electrostatic interactions, *see* electrostatic forces
- electrostatic lateral pressure 251
- electrostatic pressure 610, 611, 615
- ellipsometry 177
- emulsions 514, 884
- endocytosis 41, 45–47, 89, 497, 498, 907, 908
- endoplasmic reticulum (ER) 6, 34
- endosomes 41, 46
- energy barriers for fusion 885, 891
- entropic tension 248, 428
- entropies of coexisting phases 166
- entropy of ions 611
- entropy-driven repulsion, *see* fluctuation-induced interactions
- enzymatic control 261
- enzymatic processes 258
- enzyme activity 264, 265
- epidermis 89–91
- epirubicin 507
- epithelial sheets 87
- equilibrium spreading pressure for monolayers 191
- ER, *see* endoplasmic reticulum
- ergosterol 82
- erythroblast 9
- erythrocyte birth 8
- erythrocyte plasma membrane 7–14, 24, 453–455, 935
- erythrocytes 19, 25, 53, 248, 813, 819
- erythrocytes, adhesion of 739, 742, 748
- erythrocytes, life data of 10
- erythropoietin 57
- ESR, *see* electron spin resonance
- essential fatty acids 92
- ether-linked lipids 76, 77
- eubacteria 72, 74
- eucaryotes 72, 74
- eucaryotic cells 6, 67, 72, 81, 84, 497
- eutectic system 273, 339, 340
- evolution of cells 67, 72–76
- evolution of membranes 67–77
- excess free energies in lipid/protein mixtures 286
- exclusion processes of polymers 921
- exocytosis 41, 89, 497, 906, 908
- extracellular matrix 7, 823
- extravasation 500
- EYPC, *see* egg yolk PC
- F-actin 12, 809
- failure of molecular attachments 745, 746
- F-surface 104
- fat digestion 143
- fatty acids 19, 92, 139
- fermentation via liposomes 514
- filamin, *see* ABP
- finite size effects in percolation 324
- first order transitions in monolayers 188
- fission 41, 283, 497
- fixed point of renormalization 553, 556
- flat charged membranes, no added electrolyte, *see* electrostatic forces, large screening length

- flat charged membranes, added electrolyte, *see*
 electrostatic forces, small screening length
 flexible membranes 521, 622
 flickering, *see* shape fluctuations
 flip-flop 24, 381, 408, 426
 flippase 24
 fluctuations and coalescence 885
 fluctuations and hydration, *see* protrusions
 fluctuation-induced interactions 546–550, 579–
 586, 593, 623, 678, 683, 684, 706–708,
 736
 fluctuations in lateral membrane density 267
 fluctuations in the membrane thickness 266,
 550, 866
 fluctuations of membrane shape, *see* shape fluc-
 tuations
 fluidity of biomembranes 78, 145, 526
 fluid lamellar phase 111
 fluid membranes 78, 436, 526, 622
 fluid phases 115
 fluid-phase domains 339, 343, 436
 fluid-fluid coexistence 82–85, 276, 436
 fluid-fluid miscibility gap, *see* fluid-fluid coex-
 istence
 fluid-mosaic model 86
 fluorescence dyes, *see* fluorescence probes
 fluorescence fusion assays 873, 912, 929
 fluorescence microscopy 172, 261, 879
 fluorescence probes 879, 911
 fluorescence recovery after photobleaching (FRAP)
 175, 334, 338, 339, 781
 fluorescence spectroscopy 175, 176
 fluorescence-labeled vesicles 911
 foams 884
 focal adhesions 816, 823, 824
 focal bonds between membranes 727, 742–746,
 750, 792, 793
 fodrin 14
 force measurements 527–536, 647–655, 686
 forces between membranes, *see* interactions be-
 tween membranes
 forces mediated by macromolecules, *see* polymer-
 induced steric forces
 formamide 670, 671
 fossil record 73
 Fourier-Transform infrared (FTIR) spectroscopy
 186, 290, 293
 fractional recovery fluorescence 338, 339
 fracture energies, *see* peeling tension
 fracture of adhesive contacts, *see* adhesive fail-
 ure
 FRAP, *see* fluorescence recovery after photo-
 bleaching
 free energy of chains, *see* chain free energy
 free energy of curved bilayer 377–379, *see also*
 bending energy
 free energy of electropores 866, 884, 891
 free energy of planar bilayers 364–367
 free energy of mixtures 268
 free exchange model for bending 381, 385, 386
 free volume model for diffusion 239, 314, 327
 freeze fracture electron microscopy 226, 227,
 277, 937
 freezing point depression 286
 frustration in lipid structures 126–128
 FTIR, *see* Fourier transform infrared spectroscopy
 functional renormalization of membrane interac-
 tions 551, 556
 fungal infections 501
 fusion and non-lamellar structures 145
 fusion channel between bilayers 134
 fusion intermediates, *see* inverted micellar inter-
 mediates or stalk formation
 fusion, molecular mechanisms of 884–892, 940–
 947
 fusion of intracellular vesicles 53, 144, 145,
 906, 907, 913
 fusion of membranes 497, 498, 589, 854, 872–
 893, 906–909, 927–947
 fusion of vesicles, *see* vesicle fusion
 fusion peptide 892
 fusion pore 880
 fusion rate constant 939
 fusion threshold, *see* threshold concentration for
 cation-induced fusion
 fusion yields 883
 fusogenic state 891
 G-proteins 23, 57
 G-surface 104
 gangliosides 15, 35
 Gauss–Bonnet theorem 109, 411
 Gaussian bending rigidity 382, 409
 Gaussian curvature 101, 409
 gel adjacent to membranes 812

- gel phases 112, 221, 224, 237, *see also* crystalline phases
- gelsolin 835–837
- gene therapy 513
- gene transfer 857
- generalized neck condition 443
- generic interactions of membranes 537–565, 614–622, 655–670, 677–686, 705–709, 734–740, 785–790
- genetic defects 44
- genetic disease 55
- genus of surfaces 108
- genus of vesicles 411
- giant cells 854, 879
- Gibbs dividing surface 650
- glues 701
- glycerol 670
- glycocalix 5–8, 778–780
- glycolipids 17, 37, 930, *see also* DGDG or gangliosides
- glycophorin A 14
- glycophorins 22, 814
- glycoproteins 5, 908
- glycosaminoglycans 935
- glycosilation 37
- Golgi apparatus 34
- Gouy–Chapman length 612, 616, 618
- Gouy–Chapman–Stern theory 169, 249, 616, 620, 631, 916
- grainy membranes 714
- granulocytes, 761–764
- gtg-kink 237
- GTP (guanosine triphosphate) 41, 811
- gyroid 104
- Hamaker constant 539, 913
- haptens 502
- hard wall interaction 537, 553–555, 570–572
- head group 15, 77, 137, 185
- head group area 365
- heat of transition 224, 272
- heat shock proteins 38
- Helfrich interactions, *see* undulation forces
- Helmholtz layers, *see* Stern layers
- hemagglutinin 909
- hemidesmosomes 818, 830
- hemoglobin 647
- heparin 935
- hexagonal phases 87, 100, 108, 669–676, 942
- hexatic phases 189, 257
- hexokinase 647
- histamines 42
- HIV infection 501, 935
- Hook's law 241
- Hookean stretching 710
- hopanoids 82
- hormone signal transduction 57–61
- hormones 57, 906
- hybrid cells 906
- hydration 249, 582, 645–647, 872, 917, 926
- hydration attraction 919
- hydration dependence of vesicle penetration 478
- hydration-dominated regime of intermembrane forces 583
- hydration forces 14, 240, 537, 538, 578–585, 652, 656, 677–682, 735, 915–918
- hydration water 181, 925–927
- hydrocarbon chains 15, 77, 237
- hydrodynamic resistance 885
- hydrogen-bonds 111
- hydrophilic pores 867
- hydrophobic attraction 667, 919, 920
- hydrophobic core 365
- hydrophobic effect 218, 361, 525
- hydrophobic index, *see* hydrophobicity plot
- hydrophobic mismatch for membrane proteins 79–81, 389–395
- hydrophobic point defects 943
- hydrophobic pores 867
- hydrophobic thickness of protein 388
- hydrophobicity 20, 875, 930
- hydrophobicity plot for membrane protein 20
- hydrophobicity of the membrane surface 920
- hypernetted chain approximation 611
- hysteresis effects in mixed bilayers 253, 254
- ideal adhesion 726, 740
- ideal neck 419
- ideal-gas regime for electrostatic forces 616, 618
- Ig superfamily 726
- immune system 499
- immunisation 502

- immunoglobulins 505
 immunoliposomes 500
 impingement pressure during peeling 751
 incoherent QENS (quasielastic neutron scattering) 237
 incomplete bud 439
 'independent membrane piece' approximation 706
 infections 512
 infectious entry 909
 infinite cluster in percolation 323
 infinite periodic minimal surfaces 104
 inflammations 503, 512
 influenza virus 907
 infrared spectroscopy 186, 290, 293, 926
 inhalation of liposomes 503, 504
 insertion of protein segments 940
 insulin 906
 integral membrane proteins 19–23, 78, 328
 integrins 725, 823, 824
 interactions of membranes, *see* generic or specific interactions
 interdigitated bilayer 114, 408
 interfacial area per molecule 110
 interfacial curvature 101
 interfacial polarity 168–170, 918, 930
 interfacial tension 101, 918, 930
 interlamellar attachment during fusion 942
 intermediate filaments 809, 811, 825
 intermediate filament/membrane interactions 829–831
 intermediates in fusion 879, 944
 intermembrane $\text{Ca}(\text{PS})_2$ complex 917
 intermixing of vesicle contents 910, 912
 intermonolayer friction 429
 intramembrane interactions 887, 940
 invagination length 438
 ion transport, *see* ion pumps
 isobar measurements for monolayers 165
 isothermal compressibility of monolayers 164
 isotropic solution phases 122
 jaundice 503
 Kaposi sarcoma 511, 512
 keratinocytes 91
 keratins 829
 ketocholestanol 667
 kinetic restrictions for cell adhesion 727
 kinetics of aggregation 915
 kinetics of electrofusion, experiments 879–883
 kinetics of electrofusion, theory 884–890
 kinetics of lyotropic transitions 141–143
 kinetics of vesicle transport 484
 kissing condition for vesicles, *see* neck condition
 Krafft point 219
 L_α -phase 225, 228–230, 237, 314
 $L_\alpha \rightarrow P_{\beta'}$ transition 224, 294
 L_β -phases 114, 225–227
 $L_\beta \rightarrow L_\alpha$ transition 239
 $L_{\beta'}$ -phases 114, 225–227
 L_c -phases, *see* L_β -phases
 lag time for fusion 879
 lamellar phases 87, 594–596, 629, 669, 673, 942, *see also* stacks of membranes
 laminar shear flow 763
 Landau theory for $L_\beta \rightarrow L_\alpha$ transition 231
 Landau–Peierls singularities 596
 Langmuir equation 617
 lanosterol 81
 large unilamellar vesicle (LUV) 217, 218, 406, 530, 532, 928
 lateral compressibility modulus 735 741 762_

- lateral tension 131, 531, 536, 549, 861, 864, 886
- Lawson surface 432
- leishmaniasis and liposomes 501
- leucocytes 758–764, 769
- Lewis acid-base interaction 918
- light driven ion pumps 27
- ligand receptor bonds between membranes, *see* focal bonds
- limiting hydration of lipids 479
- line tension 173, 220, 437, 866, 932
- linolenic acid 513
- lipid anchors 23
- lipid bilayer 14–24, 267, 468, 525
- lipid composition and diseases 55
- lipid composition of biomembranes 16–19
- lipid/cholesterol mixtures, *see* cholesterol/lipid mixtures
- lipid diffusion 314, 326–340
- lipid diversity 86
- lipid fluorescent probes, *see* fluorescence of labelled lipids
- lipid mediated protein-protein interaction 266
- lipid mixtures 138, 267–298, 340–343, 436–446, 470, 472, 911, 927
- lipid molecules 15, 77, 112–114, 165, 229
- lipid order parameter 230
- lipid packing 933
- lipid phase transitions 221–235, 686
- lipid polymorphism 87–89, 99–142, 221
- lipid/protein bilayer 8, 14–24
- lipid-protein interactions 78–81, 200, 286–293, 359, 388–396
- lipid/protein mixtures 146, 198, 271, 286–293
- lipid-protein selectivity 286
- lipid segregation 272, 443–446
- lipid synthesis 16, 34
- lipid vesicles, *see* vesicles
- liposome interaction with cells 498
- liposomes 467–487, 493–516, 821
- liposomes in agro-food industry 514
- liposomes in anticancer therapy 502
- liposomes in bioengineering 512
- liposomes in cosmetics 513
- liposomes in medicine 480–487, 498–512
- liposomes in pharmaceutical industry 494
- liquid disordered phase 84, 85, 316, 327, 329
- liquid expanded phase 192
- liquid ordered phase 84, 85, 316, 327, 329
- liquid-crystalline phase, *see* L_{α} phase
- local analgetics 484
- local anesthetic 486
- long range depletion attraction, *see* depletion attraction
- long range forces between membranes, *see* interactions between membranes
- long range interactions between proteins, *see* protein-protein interactions
- long-lived fusogenic states 874
- long-time tails in hydrodynamics 311
- lymphocytes 8, 758–761, 818
- lymphoma 507
- lyotropic liquid crystals 87, 105–123, 594–596, *see also* lamellar or hexagonal or cubic phases
- lyotropic structures 100, 105–123
- lyotropic transitions, *see* phase transitions
- lysis of bilayers, *see* rupture of bilayers
- lysosomal enzymes 44, 45
- lysosomal vesicles 46
- lysosomes 41, 44
- lysozyme 514, 940
- macrolipids, *see* crosslinked lipids
- macromolecular networks, *see* cytoskeleton or spectrin/actin network or extracellular matrix
- macrophages and liposomes 499, 502
- magnetite (Fe_3O_4) 69
- magnetosomes 70
- magnetotaxis 68, 69
- main transition, *see* chain melting transition
- mannose-6-phosphate 44
- Marangoni effect 885
- material flow across the intact skin 480
- material flow during metabolism and secretion 39–48
- mattress model, *see* hydrophobic mismatch for membrane proteins
- mean curvature 101, 409
- mean square amplitudes of bending undulations 427
- mechanical energy threshold for adhesion, *see* threshold energy
- mechanical limits for peeling tension 752

- mechanical strength of cell membranes 773
 mechanics of adhesion 728
 mechanochemical enzymes 831
 medium-Golgi 41
 membrane area 525
 membrane-bound motor molecules, 831–833
 membrane curvature, *see* curvature
 membrane-cytoskeletal interactions, *see* cytoskeletal-membrane interactions
 membrane as 2D-solvent 267–269
 membrane destabilization, *see* destabilization
 membrane electrostatics, *see* electrostatic
 membrane fluidity, *see* fluidity
 membrane fusion, *see* fusion
 membrane permeability 857
 membrane potential 30, 32, 250, 541, 612
 membrane proteins 19–23, 35–39, 77–81, 267–298, 645, 725, 760, 820–827, 831–834, 945–947
 membrane rigidity, *see* bending rigidity
 membrane rupture, *see* rupture
 membrane spanning proteins 21, 336
 membrane superstructure 114, 225, 691, 713–717
 membrane synthesis, *see* synthesis of biomembranes
 membrane tension, *see* lateral tension
 merging of membranes, *see* fusion
 mesoscale fracture, *see* adhesive failure
 mica surfaces 527, 920
 micellar cubic phase 121
 microfilaments, *see* actin filaments
 micropipette aspiration 530, 531, 648, 654, 666, 864
 microroughness of bilayers, *see* anomalous roughness
 microtubules 809–811, 828, 834
 microtubule-membrane interactions 827–829
 microvilli 775
 microviscosity 82
 minimal surfaces 104, 409
 mitochondria 6, 34, 38
 mitochondrial membranes 38, 345
 modular design of cells 5, 6, 24
 molecular architecture of biomembranes 5, 7–14
 molecular phylogeny, *see* phylogenetic tree
 molecular dynamics of bilayers 236–239
 molecular filters 47
 molecular fossils 82
 molecular mechanisms of fusion, *see* fusion
 monoacylglycerols 139
 monocaprylin 659
 monoelaidin 659
 monoglycerides 664, 682
 monolayers 109, 163–202, 278, 884, 930
 monolayers, experimental methods 163–188
 monolayers, theories 188–191
 ‘monopolarity’ of interfaces 918
 monotectic system 340, 343
 mono-unsaturated lipids 84
 morphology of vesicles 405–452
 motor molecules bound to membranes 831–833
 multi drug transporters 27
 multilamellar liposomes, *see* multilamellar vesicles
 multilamellar vesicles (MLV) 225, 926, 928
 multilayer systems, *see* stacks of membranes
 muramyl tripeptide 502
 myoblast fusion 937
 myosin I 831

N-state model for unbinding 576
 Na⁺/K⁺-ATPase 25, 26, 29
 Na⁺/K⁺-pump, *see* Na⁺/K⁺-ATPase
 nascent proteins 35
 natural permeability barriers for vesicles 480
 NBD-PE (N-(7-nitro-2,1,3-benzoxadiazol-4-yl) phosphatidyl ethanolamine) 911
 NBD-Rh probe dilution assay 934
 neck condition for vesicles 419, 443
 neurotransmitters 497, 906
 neutral surface 101, 380, 456
 neutron diffraction 228, 925
 neutron scattering 185
 neutron surface scattering 228, 534
 neutrophils, *see* granulocytes
 niosomes 513
 NMR, *see* nuclear magnetic resonance
 non-axisymmetric shapes of vesicles 432, 449
 non-bilayer structures 100, 105–111, 117–124, 645, 930, 942
 non-fusogenic cations 917

- non-lamellar phases 99, 100, 105–111, 941
- non-lamellar phases in biology 143
- non-local bending rigidity 412
- non-occlusive application of liposomes 483, 485
- non-saturated bonds, *see* unsaturated lipids
- nuclear magnetic resonance (NMR) spectroscopy 78, 80, 84, 230, 273, 926
- nucleation in monolayers 173
- nucleus 6

- obstacles for tracer diffusion 318
- occlusive application of liposomes 483, 488
- oligosaccharides 37, 44, 45
- optical microscopy of membrane bunches 536, 699, 701–703
- optical microscopy of monolayers 173, 175
- optical microscopy of vesicles 217, 218, 406, 530, 532, 697
- optimization via evolution 67–70
- order parameters for lipid chains 231, 266, 369, 370, *see also* orientational order
- order parameters for hydration 538, 679, 682
- orientation of water 918
- orientational defects in bilayers 259, 260
- orientational order of chains 80, 188, 231, 370, 371
- orientational order parameter of chains 80, 230, 332, 369, 370
- origin of life 70
- Ornstein–Zernicke theory 265, 294
- osmotic equilibrium 25–34
- osmotic forces 864
- osmotic pressure 482, 534, 615
- osmotic stress method 533, 534, 645–653, 660, 661, 664, 669–671, 920, 941
- osmotic stress method, different chain states 661, 662
- osmotic stress method, different polar groups 660
- osmotic stress method, different solvents 533, 667, 671
- osmotic stress method, lipid mixtures 662, 670
- osmotic stress method, surface methylation 662, 664
- osmotic swelling of cells 834
- osmotically controlled induced adhesion 696, 697
- out-of-plane fluctuations, *see* shape fluctuations

- PDO (1,3-propanediol) solvent 533, 670, 671
- $P_{\beta'}$ -phases 114, 224, 226
- P-surface 104
- P450 reductase 264
- packing constraints for lipids 364, 367, 372, 377, 382, 392
- packing density of lipids 224
- packing geometry of lipids 126
- paints 515
- palmitic acid 23
- parasitic diseases and liposomes 501
- partial bilayers 529
- passive targeting of liposomes 499
- PC/cholesterol mixtures, *see* cholesterol/lipid mixtures
- PC (phosphatidyl choline) 14, 15, 24, 77, 112, 165, 222, 229, 658, 682
- PC-cholesterol vesicles 283
- PE 16, 24, 222
- pearl chain of cells 867, 869
- peeling tension 729, 749, 750, 752
- PEG, *see* polyethylene glycol
- peptidoglycan cell wall 74
- percolation in two dimensions 322–326, 338
- percolation threshold 323, 338, 341–343
- peristaltic mode of bilayer, *see* fluctuations in membrane thickness
- peristaltic mode of two membranes 634, 637
- peritectic system 274, 340
- permeability barriers for vesicles 476–484
- permeation of mixed lipid vesicles, *see* vesicle permeation
- persistence length of membranes 416, 526
- persistence length of polymers 545
- perturbative renormalization for membrane interactions 588
- PG (phosphatidyl glycerol) 15, 628
- pH-induced fusion of acidic vesicles 940
- phagocytosis 49–52, 907
- pharmacology, *see* liposomes in medicine
- phase coexistence in monolayers 164
- phase diagrams for cholesterol/lipid mixtures 85, 199, 200, 275, 277, 343
- phase diagrams for lipid mixtures, experiment 274, 278, 343

- phase diagrams for lipid mixtures, theory 278, 279
- phase diagrams for lipid monolayers 192, 193
- phase diagrams for lipid water systems 123–125
- phase diagrams for vesicle shapes 419–426, 441, 442, 448, 451
- phase identification for lipid water systems 105
- phase metastability in lipid water systems 141
- phase separation in mixed membranes 272–286, 436
- phase transitions in bilayers 221–224
- phase transitions between lyotropic phases 136–143
- phase transitions in monolayers 164–168, 188, 194
- phosphatidyl cholines, *see* PC
- phosphatidyl ethanolamines, *see* PE
- phosphatidyl glycerol, *see* PG
- phosphatidyl serine, *see* PS
- phosphatidyl choline/cholesterol mixtures, *see* cholesterol/lipid mixtures
- phosphatidyl inositol 15, 23, 835
- phospholipase 261
- phospholipid composition in fusion 939
- phospholipid monolayers 191–196
- phospholipid vesicles, *see* vesicles
- phospholipids 14, 658, 875
- phosphorylation 28, 29
- photosynthesis 497
- photosynthesis membranes 54, 346–348
- phylogenetic tree 72–76
- π , *A*-isotherms for monolayers 164
- pinned state of adhering vesicles 450
- pinocytosis 907
- PIP₂ (phosphatidyl inositol 4,5 bis phosphate) 814, 820, 823, 835–837
- pipette aspiration, *see* micropipette aspiration
- plasma membranes 5, 8, 67, 81, 84, 777–783, *see also* erythrocyte plasma membrane
- plasmid 512
- platelet activating factor 933
- platelets 816, 828, 837
- Poisson equation 608
- Poisson–Boltzmann equation 541, 608, 913
- Poisson–Boltzmann theory 540, 607–639
- polar repulsion, *see* hydration forces
- polarity of interfaces, *see* interfacial polarity
- polarization of membranes 624, 625, 855–857, 868
- poly-unsaturated fatty acyl chains 16, 92
- polyamines 928
- polyanion-induced fusion 935
- polyelectrolytes 544, 623, 763, 809
- polyethylene glycol (PEG) 505–507, 906, 933–935
- polyhistidine 938
- polylysine-induced aggregation 922
- polylysine-induced fusion 937
- polymer adsorption 545, 546, 921, 936
- polymer-induced steric forces 545, 546, 787–790, 921–923
- polymerization of actin 809, 835
- polymerized membranes 454, 587
- polymers 545, 778, 903, 921
- polymorphism 87–89, 105–135, 221–235, 406, 416–426, 645, 697–703
- polyoxyethylene-containing surfactants 922
- polypeptides 512
- polysaccharides 646, 679, 763, 779, 923
- ponticulin 827
- POPC (palmitoyl oleoyl phosphatidyl choline) 77, 84
- POPE (palmitoyl oleyl phosphatidyl ethanolamine) 658, 660
- POPE/SOPC mixtures 663, 664
- pore reseal after electroporation 861
- pores induced by electric fields, *see* electroporation
- potential barrier of intermembrane interactions 560–563, 578
- PPetPC (palmitoyl petroselinoyl phosphatidyl choline) 84
- prebiotic membranes 70, 71
- preparation of model membranes 590
- pressure on membrane stacks, *see* disjoining pressure
- primary minimum of membrane interactions 914
- principal curvatures 101, 102, 361, 409
- probability density for adhesive failure 745
- probability distribution of chain conformations, *see* chain conformations
- probe mixing assay for fusion 911
- procaryotic cells 70, 72, 81, 497
- processing of nascent proteins 36, 37

- protein diffusion 312, 328
protein diffusion in crowded systems 321
protein reconstitution 268, 497
protein-induced aggregation of vesicles 937
protein-protein interactions 265, 294
protein/lipid mixtures, *see* lipid/protein mixtures
proteins in bilayers, *see* lipid/protein bilayer
protein transport into mitochondria 38
proteins solubilized in bilayers 268
proton acceptors 918
proton donors 918
protrusion-dominated regime 582
protrusions 578–585, 684, 918
protrusions versus bending undulations 585
PS (phosphatidyl serine) 14, 15, 24, 222
pumps, *see* ion pumps
putrescine²⁺ 916
- quadrupolar splitting of NMR signal 926
quasicrystalline array of membrane proteins 54
quasi-equilibrium in phosphosynthetic membranes 347, 348
quasi-spherical vesicles 427
quasielastic light scattering 177, 178
quasielastic neutron scattering (QENS) 236
QENS, *see* quasi elastic neutron scattering
- Raman infrared spectroscopy 186
random collision model for electron transport 345
random interactions between membranes 587
random process for adhesive failure 745
random walks 344
Raoult's law 167
rate constant for vesicle aggregation 915, 939
receptor-mediated endocytosis 45–47, 907
recycling of biomembranes 39, 40, 46
red blood cell, *see* erythrocyte
reflection interference contrast microscopy 531, 532
reflectivity, *see* surface reflectivity
regular solution theory 268–272, 279
renormalized interactions of membranes 550–564
repulsive hydration forces, *see* hydration forces
resonance energy transfer 911
restricted diffusion, theory 318–321
restricted diffusion of lipids 318, 332, 334, 345
restricted diffusion of membrane proteins 345–348, 781–783
reticulocyte 52
Rh-PE (N-(lissamine rhodamine B sulfonyl) phosphatidyl ethanolamine) 911
rhombohedral phase 116
ribosomal (r) RNA 72
ribosomes 35
ripple phase 113, 114, 224
rolling phenomenon in cell adhesion 763
'rough' cells 731
roughness exponent 587
roughness of bilayer surface 239, *see also* protrusions
roughness of cell surface 746, 747, 773–776, 782, 794
roughness of membrane bunches 565
roughness of membranes 547, 591–593
rupture of adhesive contacts, *see* adhesive failure
rupture of bilayers 452, 453, 857, 864
- saddle splay deformation 103, 285, 379
saddle splay modulus, *see* Gaussian bending rigidity
saddle surface 103
SANS, *see* small angle neutron scattering
saturated straight chain 196
scaling laws of induced adhesion 694, 708
scanning tunneling microscopy 186
schizophrenia 55
screening effects 542, 613, 915
secondary minimum of membrane interactions 914
secretion of proteins 35, 42, 52
second order transitions, *see* critical behavior or critical points
selectins 725
selective lipid-protein interaction, *see* lipid-protein interaction
'self' adhesion 732
self-assembly of lipids 218, 219, 525
semifusion of bilayers 887, 910
Sendai virus 906
sequence of unbinding transitions 578

- serum lipoproteins 907
- SFA, *see* surface force apparatus
- shape fluctuations 532, 547–550, 557, 569, 580, 736
- shape fluctuations and fusion 888, 945
- shape fluctuations of vesicles 246–248, 426–429
- shape of solid phase clusters, *see* domain shapes in membranes
- shapes of erythrocytes 33, 53
- shapes of leucocytes 770–773
- shapes of mixed vesicles 436–446
- shapes of vesicles 405–452, 495
- shape transformations of vesicles 416–426, 430–452
- shear elastic modulus 240, 526
- short range repulsion forces, *see* hydration forces
- signal sequence receptor 35
- simple vesicle shapes of minimal energy 413
- single crystal studies 110
- single particle tracking (SPT) 344
- single protrusion modes 579, 580
- site percolation 322
- skin as a permeability barrier 480–485
- skin creams 513
- skin lipids 89–91, 514
- skin structure 90, 481
- small angle neutron scattering (SANS) 273, 276
- small unilamellar vesicle (SUV) 928
- small-angle X-ray scattering 925
- solid-phase domains 335
- solid-solid miscibility 294
- solubility of drugs 499
- solubility of amphiphiles 467, 525
- solute effects on lipid polymorphism 139
- solvent perturbation models for hydration 679, 680
- SOPC (stearyl oleyl phosphatidyl choline) 246, 658, 660
- sorting of biomembranes 34–48
- space groups 106
- special conformal transformation 431
- specific interactions of membranes 742–746, 758–764, 792, 793
- specific targeting of liposomes 499
- spectrin 10, 13, 322, 813, 817
- spectrin/actin network 10–14, 322, 453, 813–816, 828
- spectrin/actin network coupled to bilayer 12, 814
- spectrofluorimetric assays 883
- spectrofluorometer 879
- specular reflection 178, 534
- spermidine³⁺ 916
- spermine⁴⁺ 916
- sphingomyelins (SPHM) 14, 17, 659, 682
- SPHM, *see* sphingomyelin
- spin-labelled lipids 230
- spinodal decomposition 279, 437
- splay modulus, *see* bending rigidity
- sponge phases 122, 123
- spontaneous adhesion 693, 694, 739
- spontaneous curvature 129, 220, 362, 382, 410, 472, 623, 945
- spontaneous-curvature model 411
- spreading by cytoskeletal contraction 740
- SPT, *see* single particle tracking
- squalene 81
- stacked bilayers from fusion 910
- stacks of charged membranes 543, 578, 629–638, 660
- stacks of membranes 533–536, 565–578, 629–638, 648–653, 656, 716
- stalk formation 944–946
- static distribution of membrane molecules 781
- stationary shapes of vesicles 417
- steady state fluorescence depolarization 82
- stealth liposomes, *see* sterically stabilized liposomes
- stearylamine 935
- steric forces from polymers, *see* polymer-induced steric forces
- steric forces from shape fluctuations, *see* fluctuation-induced interactions
- steric stabilization 787, 921
- sterically stabilised liposomes 505, 507–511
- Stern layers 544, 612
- sterols 74, 76, 81–85
- sterols and microviscosity 83
- Stokes' paradox 310, 311
- stomatocytes 418
- strains in packing 645
- stratum corneum 91, 480–482

- strength of focal attachment 742, 743
strength of the infinite percolation cluster 323
stress profile, *see* lateral stress profile
stretching elasticity 374, 526, 549
stretching of undulations 549, 550, 710
strings 548, 554, 561, 575
strong adhesion 447, 728
structural phase transitions in bilayers, *see* phase transitions in bilayers
sub-transition in bilayers 221
superlattices in monolayers 172
superposition of intermembrane forces 551, 553, 556, 630–633
superstructure of bilayers 713–715
surface area of cells 815, 834
surface charges 250, 540, 612, 628, 914
surface curvature, *see* curvature
surface dielectric constant and vesicle fusion 930, 931
surface force apparatus (SFA) 186, 527–530, 648, 653, 654, 918
surface methylation 662
surface polarity, *see* interfacial polarity
surface potential 168–172, 541, 611, 613, 637, 860, 913
surface reflectivity 178, 182, 534, 535
surface roughness, *see* roughness
surface texture of vesicles 226, 227
surfactant monolayers 163, 920
surfactants 467, 474
sustained release from liposomes 499
synaptic vesicles 497
synexin (annexin VII) 937, 939
synexin-facilitated fusion 939
synthesis of biomembranes 34–39
synthesis of membrane proteins 35–37
synthesis of membrane receptor 36
- tail, *see* chain
tail ordering, *see* orientational order of chains
talin 823, 825
targeting of liposomes 500, 503
targeting of proteins 45
target membranes 36
temperature-induced budding 424–426
temperature of chain-melting transition 222–224, 252, 253
temperature trajectories for vesicles 422
tension-induced adhesion, experiments 695–705
tension-induced adhesion, theory 564, 705–709
terbium/dipicolinic acid assay 934
ternary mixture of lipids 340
'tethered' membranes, *see* polymerized membranes
tethers 414, 713, 716
tetragonal phase 116
therapeutic window for drugs 498
therapeutic efficacy of transfersomes 485–487
thermal expansion coefficient 416
thermal expansivity 164
thermal fluctuations, *see* fluctuations
thermomechanical properties of vesicles 240
threshold concentrations for aggregation 916
threshold concentration for cation-induced fusion 927–929
threshold energy for adhesion 448, 733, 741
threshold voltage for electroporation 861–864
thrombocyte 14
thylakoid membranes, *see* photosynthesis membranes
tight junctions 87–89, *see also* desmosomes
tilt angle of chains 189, 232
tilt azimuth of chains 189
topographical roughness, *see* roughness
topology 107, 109, 143, 430–435
torus-shaped vesicle 218, 430–432
toxins 502
'tracer' membrane within stack 565
trafficking via vesicles, *see* vesicle exchange
transdermal gradient of hydration pressure 481
transepidermal osmotic pressure profile 481
transfection of genes 512
transferrin 46
transferrin receptor 46
transfersomal insulin 486, 487
transfersome biodistribution 485
transfersomes 472–475
transformation, due to Derjaguin, *see* Derjaguin approximation
trans-Golgi 40
transition enthalpy, *see* heat of transition

- transition kinetics, *see* kinetics
 transitions, *see* phase transitions or shape transformations
 translocation of proteins 38, 39
 transmembrane proteins 21, 822
 transmembrane receptors and cytoskeleton 833, 847
 transmembrane voltage 859–861
 transport, *see* diffusion or flip-flop or ion pumps
 triterpenes 82
 tropomyosin 12
 tubulin 810, 827
 tumour and liposomes 507, 510, 511
 tunneling of interacting membranes 563
 turbidity and vesicle aggregation 923, 924
 two-dimensionality of membranes 55–57, 407
 two-membrane approximation for stacks 568
 two-state model for unbinding 557

 ultraflexible membranes 471
 ultraflexible vesicles 475
 unbinding transition 555–559, 573, 693, 694
 undulation forces 248, 546–550, 683, 706–708, 888
 undulation forces versus electrostatic forces, *see* superposition of intermembrane forces
 undulations, *see* bending undulations
 unduloids 413
 anhydrous complexes of stacked bilayers 936
 uniform density constraint for bilayer 368
 uniform tilt of chains 189
 unsaturated bond, *see* unsaturated lipids
 unsaturated lipids 15, 16, 86, 196, 222, 224

 vaccination 502
 Van der Waals forces between membranes 539, 540, 686, 735, 785, 886, 913
 Van der Waals forces between molecules 84
 vasculature 508
 vectorial organisation of cells 39–48
 vesicle budding, *see* budding
 vesicle exchange between biomembranes 41–44
 vesicle fission, *see* fission
 vesicle formation 496
 vesicle fusion 452, 864, 909–947
 vesicle fusion, experimental methods 910–913
 vesicle fusion, induced by cations 927–930
 vesicle fusion, induced by polyanions 935–937
 vesicle fusion, modulated by polyethylene glycol 933–935
 vesicle fusion, modulated by proteins 937–940
 vesicle fusion, molecular mechanism 940–947
 vesicle leakage 912
 vesicle permeation 476, 477
 vesicle stability 217
 vesicle transport across the living skin 483
 vesicles 217, 218, 240–247, 405, 416–452, 657, 875
 vesicles as material carriers 475
 vesicles with non-spherical topology 430–435
 vesiculation 494
 vimentin 829
 vinculin 824
 virosomes 909
 virus-cell fusion 892, 907–909
 viscoelastic liquids 834
 viscosity 429, 880
 vitamins 515
 volume changes of cells 834

 water activity 648
 water flow 812
 weak adhesion 447, 733
 white blood cells, *see* leucocytes
 Willmore problem 430

 X-ray diffraction 105, 106, 221, 650
 X-ray surface reflectivity, *see* surface reflectivity
 X-ray surface diffraction 178, 179
 xylans 925

 Young equation, *see* Young–Dupré equation
 Young–Dupré equation 451, 536, 695, 696, 729, 733, 765

 zwitterionic lipids 15, 138, 365, 639

This Page Intentionally Left Blank